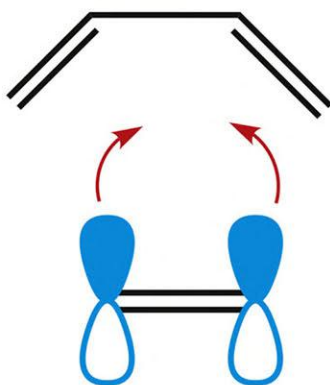
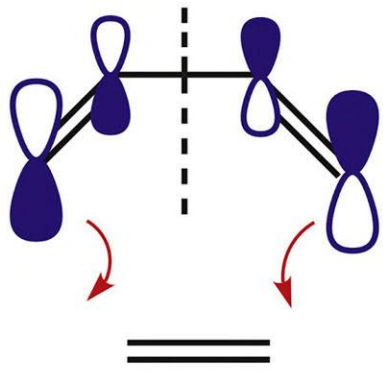


Pericyclic Chemistry

Orbital Mechanisms and Stereochemistry

Dipak K. Mandal



PERICYCLIC CHEMISTRY

PERICYCLIC CHEMISTRY

Orbital Mechanisms and Stereochemistry

DIPAK K. MANDAL

Formerly of Presidency College/University
Kolkata, India



Elsevier

Radarweg 29, PO Box 211, 1000 AE Amsterdam, Netherlands
The Boulevard, Langford Lane, Kidlington, Oxford OX5 1GB, United Kingdom
50 Hampshire Street, 5th Floor, Cambridge, MA 02139, United States

© 2018 Elsevier Inc. All rights reserved.

No part of this publication may be reproduced or transmitted in any form or by any means, electronic or mechanical, including photocopying, recording, or any information storage and retrieval system, without permission in writing from the publisher. Details on how to seek permission, further information about the Publisher's permissions policies and our arrangements with organizations such as the Copyright Clearance Center and the Copyright Licensing Agency, can be found at our website: www.elsevier.com/permissions.

This book and the individual contributions contained in it are protected under copyright by the Publisher (other than as may be noted herein).

Notices

Knowledge and best practice in this field are constantly changing. As new research and experience broaden our understanding, changes in research methods, professional practices, or medical treatment may become necessary.

Practitioners and researchers must always rely on their own experience and knowledge in evaluating and using any information, methods, compounds, or experiments described herein. In using such information or methods they should be mindful of their own safety and the safety of others, including parties for whom they have a professional responsibility.

To the fullest extent of the law, neither the Publisher nor the authors, contributors, or editors, assume any liability for any injury and/or damage to persons or property as a matter of products liability, negligence or otherwise, or from any use or operation of any methods, products, instructions, or ideas contained in the material herein.

Library of Congress Cataloging-in-Publication Data

A catalog record for this book is available from the Library of Congress

British Library Cataloguing-in-Publication Data

A catalogue record for this book is available from the British Library

ISBN: 978-0-12-814958-4

For information on all Elsevier publications
visit our website at <https://www.elsevier.com/books-and-journals>



Working together
to grow libraries in
developing countries

www.elsevier.com • www.bookaid.org

Publisher: John Fedor

Acquisition Editor: Emily McCloskey

Editorial Project Manager: Billie Jean Fernandez

Production Project Manager: Paul Prasad Chandramohan

Cover Designer: Mark Rogers

Typeset by SPi Global, India

Dedicated to the memory of my parents.

PREFACE

It is about 50 years since the appearance of the pioneering work of R. B. Woodward and R. Hoffmann on the theory of conservation of orbital symmetry in concerted reactions. The word pericyclic was introduced in 1969 and the application of the concept of orbital symmetry to pericyclic reactions proved to be a major turning point in understanding organic reaction mechanisms. The 1981 Nobel Prize in Chemistry was awarded to K. Fukui and R. Hoffmann for developing theories of pericyclic reactions (Woodward died in 1979 at the age of 62 and could not share this prize; however, he won the Nobel Prize in 1965 for his work on organic synthesis). Pericyclic reactions have a remarkable quality of being manifold, extremely elegant, and highly useful; they reveal stereochemical intricacies and idiosyncrasies and remain as an integral part of chemistry teaching and research.

Pericyclic chemistry is covered in every graduate course and in advanced undergraduate courses in organic chemistry. Ergo, this book is addressed principally to an audience of graduate and advanced undergraduate students. The purpose of writing this book is entirely pedagogic, keeping in view that our students crave understanding, not factual knowledge alone. The book evolves from a series of lecture notes and students' feedback during my teaching this course to graduate students for more than 20 years. The mechanistic descriptions and the stereochemistry resulting from orbital mechanisms are at the heart of this book; the synthesis of specific target molecules has been generally given short shrift.

The book contains eleven chapters. An introduction to molecular orbital theory (Chapter 1) and relevant stereochemical concepts (Chapter 2) have been provided as a background aid to follow the chapters on pericyclic chemistry. In the introductory chapter (Chapter 3), I have introduced all four classes of pericyclic reactions involving three mechanistic approaches linked through orbital picture representation. This unifying and integrated style would help enhance the pedagogy of this text. The qualitative perturbation molecular orbital theory has been incorporated as the most accessible and useful approach to understanding many aspects of reactivity and selectivity. Three chapters (Chapters 4–6) have been devoted to cycloadditions, the most versatile class, one to electrocyclic reactions (Chapter 7), two to sigmatropic rearrangements (Chapters 8 and 9), and one to group transfer reactions (Chapter 10). A separate chapter (Chapter 11) is included to

illustrate the construction of correlation diagrams in a practical, ‘how-to-do-it’ manner.

Besides the unifying approach of mechanistic discussion, the most important difference between this book and others is the emphasis on stereochemistry, specifically how to delineate the stereochemistry of products. I have found that students are not often quite comfortable to work stereochemistry for themselves. After all, reaction stereochemistry is not easy! Students need some more help. To address their concerns, I have always been looking for innovative approaches to stereochemical issues. My efforts have resulted in formulating simple stereochemical rules/guidelines, some of which have been published in the *Journal of Chemical Education*. These published (also some unpublished) rules/mnemonics have been used extensively in the relevant chapters as an aid to write quickly and correctly the product stereochemistry in pericyclic reactions.

Usually, the problem sets are given at the end of chapters without or with answer keys. One pedagogical decision I have made with respect to problem sets is that more than 130 problems are inserted within the chapters with detailed worked solutions, reinforcing the main themes in the text. It is hoped that students could test their learning immediately while reading through the chapters. These problem sets should be considered an integral part of the course. A list of selective references to primary and review literature is included at the end of each chapter. These references (about 550) would enable the students at the advanced levels to supplement the materials covered in the chapters.

The approach presented in this book is distinct and class-tested. I hope this book will be of value and interest to the students, teachers, and researchers of organic chemistry. I encourage the readers to contact me (dm.pcchem@gmail.com) with comments, corrections, and with suggestions that might be appropriate for future editions.

I would like to thank the reviewers for helpful suggestions. Special thanks are due to my undergraduate, graduate, and research students for their loving insistence, help, and encouragement in writing this book. I am grateful to the editorial members Emily M. McCloskey and Billie Jean Fernandez, production manager, and other people at Elsevier for their excellent support and cooperation. Finally, I thank my family, in particular my daughter Sudipta, for her continuous support and my son Tirtha for his active help in referencing.

Dipak K. Mandal

Kolkata, India

CHAPTER 1

Molecular Orbitals

A basic and pictorial knowledge of molecular orbitals (MOs) is essential for a mechanistic description of pericyclic reactions. In this context, a simplified and nonmathematical description of MO theory^{1–4} is presented in this chapter. We shall deal with three kinds of MOs— σ , π and ω with major emphasis on π MOs, and discuss their properties with reference to orbital symmetry, energy and coefficient.

1.1 ATOMIC ORBITALS

An atomic orbital (AO) is described by a wave function ϕ , where ϕ^2 denotes the probability of finding an electron at any point in a three-dimensional space. The algebraic sign of ϕ may be positive or negative, which indicates the phase of the orbital (cf. the peaks and troughs of a transverse wave). An orbital can have nodes where $\phi=0$. On opposite sides of a node, ϕ has opposite signs. An AO as a graphical description of ϕ shows lobes with a + or a – sign (the opposite signs of two lobes are also indicated by unshaded and shaded lobes). On the other hand, ϕ^2 is always positive whether ϕ is positive or negative. As such, the representation of AO in terms of ϕ^2 is made by drawing lobes without a phase sign. This drawing refers to the probability distribution of AOs, and is indicated in this text as simply orbital picture.

1.1.1 s, p and Hybrid Orbitals

1s orbital is spherically symmetrical about the nucleus and has a single sign of ϕ . It is represented as a circle, being one cross-section of the spherical contour. The 2s orbital is also spherically symmetrical but possesses a spherical node. The node is close to the nucleus and hence the inner sphere is not important for bonding overlap. The 2s orbital is usually drawn as a single circle with a single sign omitting the inner sphere.

Unlike an s orbital, the p orbitals are directional, and oriented along the x -, y - and z -axis. Each p orbital has two lobes with opposite signs and one node (nodal plane).

Carbon has four AOs ($2s$, $2p_x$, $2p_y$ and $2p_z$) that are available for bonding. Though this model of one s and three p orbitals is very useful, there is an alternative model of four AOs of carbon, based on Pauling's idea of hybridization. The hybridization involves mixing of $2s$ and $2p$ orbitals in various proportions to produce a new set of AOs. Mathematically, the mixing is taken to be the linear combination of atomic orbitals (LCAOs). Such LCAOs on the *same atom* are called hybrid orbitals. The combination of $2s$ with one, two or three p orbitals can be used in different ways to produce different sets of hybrid orbitals, designated as sp^n where n may be a whole number or a fraction. For example, a combination of $2s$ and three $2p$ orbitals can be used to generate four equivalent hybrid orbitals called sp^3 hybrids. Each sp^3 hybrid orbital has two lobes with opposite signs, but unlike a p orbital, the two lobes of a hybrid orbital have different sizes.

The schematic representations of s , p and sp^3 hybrid orbitals are shown in Fig. 1.1. In Fig. 1.1A, the orbitals are drawn as graphical description of wave function (ϕ) showing a phase sign while Fig. 1.1B shows the orbital picture in terms of ϕ^2 with no phase sign.

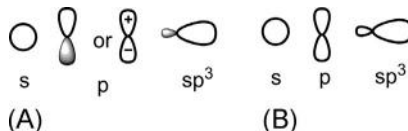


Fig. 1.1 (A) Sketch of atomic orbitals in terms of ϕ with a phase sign; (B) orbital picture in terms of ϕ^2 without a phase sign.

The unequal size of two lobes of a hybrid orbital, say sp , arises from the mixing of s orbital with a p orbital on the same atom (Fig. 1.2). The two lobes of p orbital have the same size, but opposite signs (unshaded and shaded), and the s orbital has a single sign (unshaded). The combination gives in-phase (same sign) mixing on one side of the nucleus and out-of-phase (different signs) mixing on the other side, leading to a large lobe on the left side and a small lobe on the right side of the hybrid orbital.

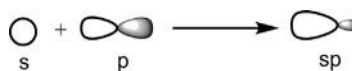


Fig. 1.2 Unequal size of two lobes of a hybrid orbital.

Table 1.1 Energies of s and p atomic orbitals

Atomic orbital	Orbital energy (eV)			
	H	C	N	O
1s	-13.6			
2s		-19.4	-25.6	-32.4
2p		-10.7	-12.9	-15.9

1.1.2 Atomic Orbitals of Nitrogen and Oxygen

Nitrogen and oxygen have similar sets of s, p and hybrid orbitals as for carbon. However, the energies are different. The relative energies of an AO on different atoms follow their pattern of electronegativity. An orbital on a more electronegative atom will have lower energy ([Table 1.1](#)).⁵

1.2 MOLECULAR ORBITALS

An MO is also described by a wave function ψ which can be expressed as an LCAOs. The set of AOs chosen for the linear combination is called the *basis set*. The total number of MOs will be equal to the total number of AOs combined. The calculation of MOs using all AOs of a molecule presents massive computational problems. However, the essential qualitative features of bonding can be understood if the basis set is restricted just to those AOs that are involved in a particular type of bonding. MOs are designated by the symbols σ , π and ω reflecting the type of bonding that occurs.

Now consider the linear combination of two AOs ϕ_1 and ϕ_2 on atoms 1 and 2. (Note that the linear combination uses only the first power of wave function; cf. equation of a straight line.) Two MOs ψ_1 and ψ_2 are produced which are expressed as

$$\psi_1 = c_1\phi_1 + c_2\phi_2$$

$$\psi_2 = c_1\phi_1 - c_2\phi_2$$

where c_1 and c_2 are the mixing coefficients which denote the relative contributions of the AOs ϕ_1 and ϕ_2 to an MO. The coefficients may be positive, negative or even zero.

The geometry of approach of the two AOs leads to different types of MOs. This is illustrated below taking, for example, the overlap of two p AOs centred on two identical atoms (homonuclear), when $c_1=c_2$.

End-on approach: End-on overlap of two p orbitals gives two MOs (ψ_1 and ψ_2) that are cylindrically symmetrical about the internuclear axis ([Fig. 1.3](#)).

These are called σ MOs. Here, ‘+’ combination signifies in-phase (same sign) overlap when ψ_1 has no node. In contrast, ‘−’ combination denotes out-of-phase (opposite sign) overlap leading to a node (nodal plane) in ψ_2 . The MO ψ_1 has lower energy than p AO and is called bonding σ orbital (symbolized σ), while ψ_2 has higher energy and is called an antibonding σ orbital (σ^*).

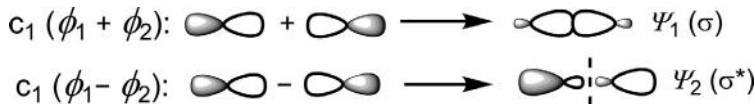


Fig. 1.3 End-on overlap of two p orbitals to produce σ MOs.

Side-on approach: Side-on (lateral) overlap of two p orbitals produces two MOs (ψ_1 and ψ_2) that are not cylindrically symmetrical about the internuclear axis, and are called π MOs (Fig. 1.4). ψ_1 has lower energy with no node and is a bonding MO (π), while ψ_2 with one node (nodal plane) is of higher energy and is an antibonding MO (π^*).

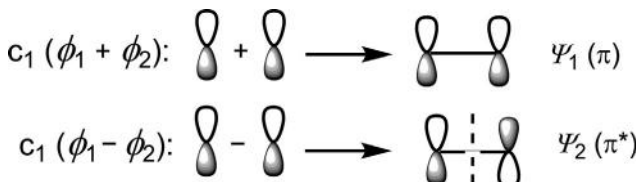


Fig. 1.4 Side-on (lateral) overlap of two p orbitals to produce π MOs.

Orthogonal approach: For orthogonal (perpendicular) approach of two p orbitals, bonding overlap of the same sign is cancelled by an antibonding overlap of the opposite sign (Fig. 1.5). The net interaction is therefore nonbonding. ψ_1 and ψ_2 have the same energy and are equivalent to individual p orbitals. These nonbonding MOs are called ω MOs.

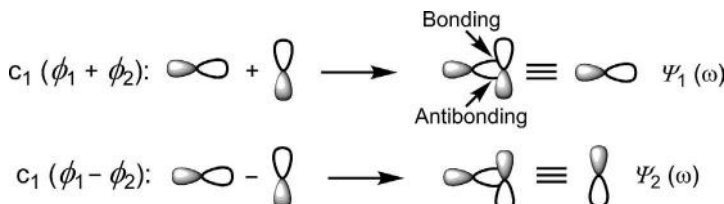


Fig. 1.5 Orthogonal approach of two p orbitals to produce ω MOs.

It may be mentioned here that besides nonbonding ω MOs, there are also nonbonding π MOs that can arise in conjugated π systems (see later).

1.2.1 Energy Diagram

In general, the interaction of two AOs leads to a pair of bonding and antibonding MOs. Consider the formation of σ and σ^* MOs for hydrogen molecule. From quantum mechanical calculation, the energy (E) of an electron in σ and σ^* orbital is expressed in terms of three integrals (α , β and S) as

$$E(\sigma) = \frac{\alpha + \beta}{1 + S} \quad (1.1)$$

$$E(\sigma^*) = \frac{\alpha - \beta}{1 - S} \quad (1.2)$$

where α is the Coulomb integral which denotes the energy of an electron in an isolated AO; β is the resonance integral which represents the energy of interaction between two AOs; and S is the overlap integral which indicates the extent of overlap of the AOs.

Now we focus on the numerator and denominator terms in Eqs (1.1), (1.2). α and β are negative quantities. Therefore, $(\alpha + \beta) < \alpha$ (indicating lowering of energy of σ) and $(\alpha - \beta) > \alpha$ (raising of energy of σ^*). The overlap integral S is a function of internuclear distance and the value of S ranges from 0 to 1. For two interacting orbitals, $S > 0$. Hence, the denominator $(1 + S) > (1 - S)$. Thus, the energy increase associated with antibonding σ^* orbital is slightly greater than the energy decrease for bonding σ orbital. These results are presented qualitatively in the MO energy diagram (Fig. 1.6).

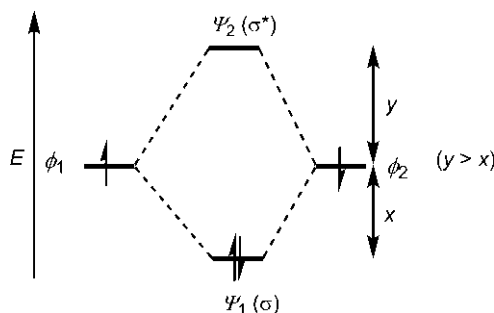


Fig. 1.6 MO energy diagram for a two-orbital interaction. x and y indicate, respectively, the energy decrease for the bonding orbital and energy increase for the antibonding orbital.

For π and π^* orbitals, a similar pattern follows; however, the value of S for π overlap is much smaller. If we assume $S=0$, we obtain

$$E(\pi) = \alpha + \beta; \quad E(\pi^*) = \alpha - \beta$$

where α is the energy of an electron in an isolated p orbital and β represents the energy of interaction between two adjacent p orbitals.

1.2.1.1 Remarks

The above MO energy diagram serves qualitatively a general pattern for a two-orbital interaction that may involve any AOs or MOs. It can be seen from Fig. 1.6 that if each interacting orbital is completely filled providing a total of four electrons, both bonding and antibonding orbitals would be completely filled. The net interaction would thus be repulsive because the increase in energy in the antibonding combination is greater than the decrease in energy in a bonding combination. This repulsive filled orbital/filled orbital interaction is the underlying reason for the steric strain (repulsion between closed-shell molecules or groups), and is included in the first term of the Salem–Klopman equation (see Section 4.1).

1.2.2 C—H and C—C σ Bonds

A C—H bond is formed by the interaction of a hybrid orbital (say, sp^3) of carbon with the 1s orbital of hydrogen. This two-orbital interaction leads to bonding σ_{CH} and antibonding σ^*_{CH} as shown in Fig. 1.7A. Note that the energy of sp^3_C (-16.1 eV) is somewhat lower than that of $1s_H$ (-13.6 eV). A C—C σ bond is formed by the end-on overlap of two hybrid orbitals, one from each carbon. Fig. 1.7B shows the formation of a bonding σ_{CC} and an antibonding σ^*_{CC} from two sp^3 hybrid orbitals. (Note the conventional MO sketches with the AOs instead of the delocalized sketches of MOs.) The bonding σ MO has no node between lobes of the same sign, but anti-bonding σ^* MO has one node between lobes of opposite sign (shaded and unshaded).

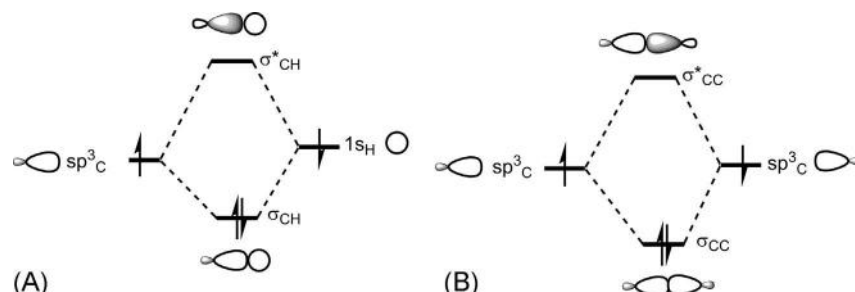


Fig. 1.7 Bonding and antibonding MOs for (A) C—H bond and (B) C—C bond.

We shall see later that the more important orbitals in connection with reactivity are the highest occupied molecular orbital (HOMO) and the lowest unoccupied molecular orbital (LUMO). These are called the frontier MOs. Thus, for the σ component (C—H or C—C), the HOMO is σ and the LUMO is σ^* .

Besides MOs, orbital picture representation (without phase sign) of a σ -component is used in the mechanistic analysis of pericyclic reactions. Fig. 1.8 shows the orbital pictures of C—H and C—C σ components. The σ component is labelled as σ_2 (2 is the number of electrons in the component).

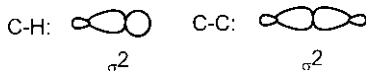


Fig. 1.8 Orbital pictures of C—H and C—C σ components.

1.3 HÜCKEL MOLECULAR ORBITAL (HMO) THEORY FOR ACYCLIC CONJUGATED π SYSTEMS

Hückel theory^{1,6} treats a π system independently of the σ framework (the π and σ orbitals being orthogonal to each other). The HMO theory assumes the following:

- (1) Each Coulomb integral (α) has the same value.
- (2) The resonance integral (β) is same for any two adjacent atoms but zero for two atoms not directly bonded.
- (3) The overlap integral (S) is zero for the interaction between two p orbitals.

It might be surprising that S is assumed to be zero, while the whole concept of chemical bonding is based on the overlap of orbitals (!). In fact, overlap is not really neglected because it is implicitly included in other parameters such as β which is roughly proportional to S . The assumption that $S=0$ greatly simplifies the calculation.

The π MO wavefunction (ψ_j) is described by a linear combination of p AO's (ϕ_r) as

$$\psi_j = \sum_{r=1}^n c_{jr} \phi_r \quad (1.3)$$

where n is the total number of p orbitals involved and $j=1, 2, 3, \dots, n$.

Here, we shall consider the linear conjugated systems and obtain their π MOs and energies using Coulson equations⁷ as follows:

$$c_{jr} = \sqrt{\frac{2}{n+1}} \sin\left(\frac{jr\pi}{n+1}\right) \quad (1.4)$$

$$E_j = \alpha + 2\beta \cos\left(\frac{j\pi}{n+1}\right) \quad (1.5)$$

1.3.1 Linear Conjugated System With Even Number of p Orbitals

1.3.1.1 Ethylene

The simplest system is ethylene in which two p orbitals ($n=2$) are conjugated to each other in forming a π bond. According to Eq. (1.3), the MO wavefunctions are

$$\psi_1 = c_{11}\phi_1 + c_{12}\phi_2$$

$$\psi_2 = c_{21}\phi_1 + c_{22}\phi_2$$

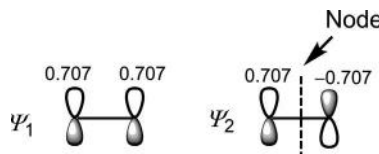
The coefficients are evaluated using Eq. (1.4). Thus $c_{11} = \sqrt{\frac{2}{3}} \sin \frac{\pi}{3} = 0.707$. Similarly, $c_{12} = c_{21} = 0.707$, $c_{22} = -0.707$. Substituting these values, we obtain

$$\psi_1 = 0.707\phi_1 + 0.707\phi_2$$

$$\psi_2 = 0.707\phi_1 - 0.707\phi_2$$

(Note that the signs of coefficients are arising from the calculation using Eq. 1.4.)

The wavefunctions (π MOs) can now be sketched as



The relative magnitudes of the coefficients are usually indicated by the relative sizes of the lobes. Here the two coefficients have the same size for both ψ_1 and ψ_2 . For ψ_1 , the coefficients have the same sign indicating in-phase (bonding) overlap. For ψ_2 , the coefficients have opposite signs indicating out-of-phase (antibonding) overlap which creates a node (nodal plane).

The energies of the π MOs are estimated using Eq. (1.5) as

$$E_1 = \alpha + 2\beta \cos \frac{\pi}{3} = \alpha + \beta$$

$$E_2 = \alpha + 2\beta \cos \frac{2\pi}{3} = \alpha - \beta.$$

Fig. 1.9 shows the MO energy diagram where ψ_1 is a bonding MO (π) as it has lower energy than the energy of p orbital (α) and ψ_2 is an antibonding MO (π^*) having an energy higher than α .

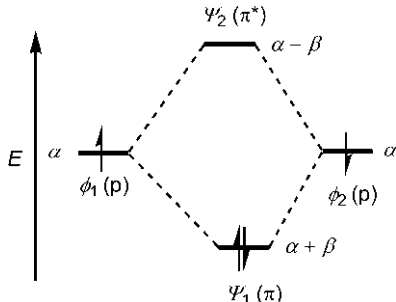


Fig. 1.9 MO energy diagram of ethylene.

The ground state π electron configuration of ethylene is $\pi^2\pi^{*0}$. Therefore, π is HOMO and π^* is LUMO. A thermal pericyclic reaction is a ground state process whereas a photochemical reaction is a first excited state process. On photochemical excitation by absorption of light, one electron is promoted from π (HOMO) to π^* (LUMO) with the conservation of spin, and the resulting excited state is a singlet with singly occupied π (formerly HOMO) and singly occupied π^* (formerly LUMO) (Fig. 1.10).

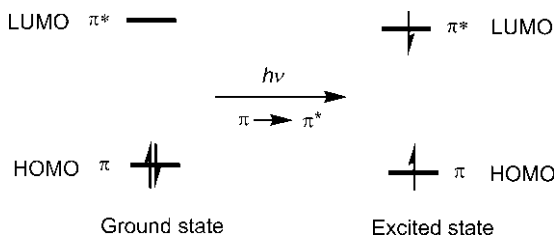


Fig. 1.10 Frontier orbitals in the ground state and in the excited state of ethylene.

A useful convention⁸ is to designate the singly occupied excited state orbitals of a molecule by its former ground state HOMO/LUMO labels. This excited state frontier orbital convention as shown in Fig. 1.10 will be used while dealing with the frontier orbital analysis of photochemical reactions. (An alternative excited state nomenclature that specifies π^* as HOMO and π as NHOMO, next lower HOMO, will not be used in this text.)

At the instant of excitation, the nuclei retain the planar ground state geometry (Frank–Condon principle). The π bond order [$\frac{1}{2}$ (no. of bonding electrons – no. of antibonding electrons)] in the excited state is zero. The initial planar excited state then quickly relaxes to the minimum energy geometry in which the two sp^2 carbons are twisted by about 90 degrees when there is no π overlap (Fig. 1.11). This twisted, excited state, sometimes called the *p state*, permits the possibility of returning to either *E* or *Z* configuration of the ground state alkene.

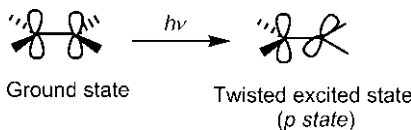


Fig. 1.11 Orbital pictures of the ground state and excited state of ethylene.

We shall see later that the phase relationship of terminal p orbitals in HOMO/LUMO is important in the mechanistic analysis of pericyclic reactions. This phase relationship is characterized by orbital symmetry. Fig. 1.12 shows the orbital symmetries of HOMO and LUMO of ethylene. The HOMO (π) has the same phase at the two ends and possesses a plane of symmetry (symbolized by *m*) since a lobe (labelled *) reflects to a lobe of the same sign. Note that the mirror plane (*m*) bisects the C–C bond and is perpendicular to the plane of the molecule. On the other hand, the LUMO (π^*) has opposite phases at the two ends and is characterized by C_2 symmetry as the C_2 operation brings a lobe (labelled *) to a position of a lobe with the same sign. Note that the C_2 axis bisects the C–C bond and is lying in the plane of the molecule.

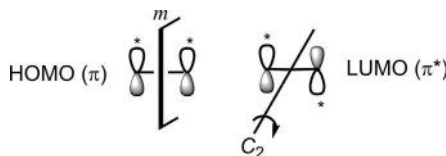


Fig. 1.12 Orbital symmetries of HOMO and LUMO of ethylene.

1.3.1.2 Butadiene

The basis set orbitals of butadiene (ϕ_1 – ϕ_4) are four p orbitals ($n=4$). The wavefunctions (ψ_1 – ψ_4) representing four π MOs are written as

$$\psi_1 = c_{11}\phi_1 + c_{12}\phi_2 + c_{13}\phi_3 + c_{14}\phi_4$$

$$\psi_2 = c_{21}\phi_1 + c_{22}\phi_2 + c_{23}\phi_3 + c_{24}\phi_4$$

$$\psi_3 = c_{31}\phi_1 + c_{32}\phi_2 + c_{33}\phi_3 + c_{34}\phi_4$$

$$\psi_4 = c_{41}\phi_1 + c_{42}\phi_2 + c_{43}\phi_3 + c_{44}\phi_4$$

Using Eq. (1.4), $c_{11} = \sqrt{\frac{2}{5}}\sin\frac{\pi}{5} = 0.371$, $c_{12} = \sqrt{\frac{2}{5}}\sin\frac{2\pi}{5} = 0.600$. The other coefficients are calculated similarly. We obtain

$$\psi_1 = 0.371\phi_1 + 0.600\phi_2 + 0.600\phi_3 + 0.371\phi_4$$

$$\psi_2 = 0.600\phi_1 + 0.371\phi_2 - 0.371\phi_3 - 0.600\phi_4$$

$$\psi_3 = 0.600\phi_1 - 0.371\phi_2 - 0.371\phi_3 + 0.600\phi_4$$

$$\psi_4 = 0.371\phi_1 - 0.600\phi_2 + 0.600\phi_3 - 0.371\phi_4$$

The wavefunctions (π MOs) of butadiene can be sketched in *s-trans* or *s-cis* conformation. Fig. 1.13 shows the butadiene π MOs in more stable *s-trans* conformation. (We shall see later that it is the *s-cis* form which is the reactive component in most pericyclic processes.) The relative sizes of the lobes indicate qualitatively the relative values of the coefficients. The number of nodes (indicated by dashed line) in ψ_1 , ψ_2 , ψ_3 and ψ_4 is 0, 1, 2 and 3, respectively. This indicates that an orbital ψ_j has $(j-1)$ nodes.

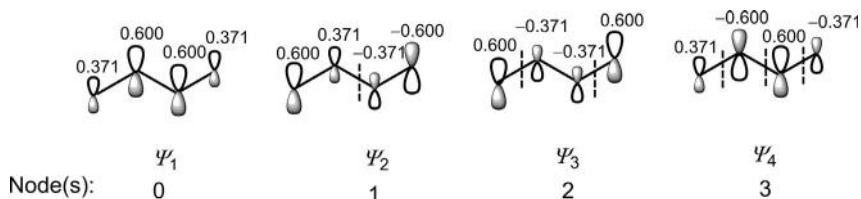


Fig. 1.13 Sketches of π MOs of butadiene in *s-trans* conformation.

As the number of nodes increases, the energy of the orbital increases in the order: $\psi_1 < \psi_2 < \psi_3 < \psi_4$. In another fashion, if we count the number of bonding/antibonding interactions between the adjacent p orbitals, it is seen that ψ_1 with three bonding overlaps and ψ_2 with two bonding and one antibonding interactions become bonding MOs whereas ψ_3 with two antibonding and one bonding interactions and ψ_4 with three antibonding interactions

become antibonding MOs. The MO energy therefore increases in the same order as shown above.

The energies of the π MOs can however be estimated using Eq. (1.5). For example, $E_1 = \alpha + 2\beta \cos \frac{\pi}{5} = \alpha + 1.618\beta$. The estimated energies of all π MOs are shown in the MO energy diagram (Fig. 1.14). Note that the more positive or less negative β values imply a decrease in energy; less positive or more negative β values indicate an increase in energy.

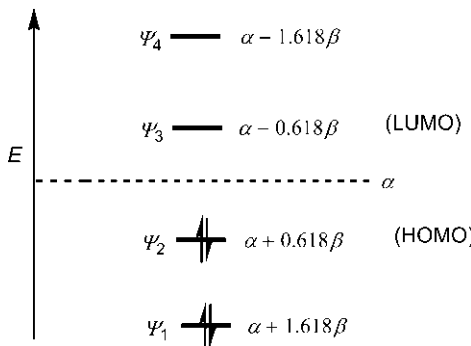


Fig. 1.14 MO energy diagram of butadiene.

The bonding/antibonding classification of the π MOs is now clearly evident. ψ_1 and ψ_2 have energies lower than the energy (α) of a p orbital and are therefore bonding MOs whereas ψ_3 and ψ_4 are antibonding MOs as their energies are higher than α .

(Since the decrease or increase in energy of an MO is considered relative to the energy of the AO, α can be arbitrarily assumed to be zero and the MO energy can be expressed in only β terms; however in this text MO energy is expressed in both α and β terms, as obtained from the energy expression.)

The ground state π electron configuration of butadiene is $\psi_1^2\psi_2^2$. Thus, ψ_2 is HOMO and ψ_3 is LUMO. In the first excited state, one electron is promoted from ψ_2 (HOMO) to ψ_3 (LUMO). As per the frontier orbital convention used in this text (see p. 10), the singly occupied ψ_2 and ψ_3 also represent HOMO and LUMO in the first excited state.

The HOMO/LUMO energies in *s-trans* and *s-cis* conformations of butadiene are not the same. In *s-cis* conformation, the HOMO energy is raised and the LUMO energy is lowered relative to those in the *s-trans* form (Fig. 1.15). Unlike the *s-trans* form, the *s-cis* conformation has a possible interaction between the two terminal p orbitals. An antibonding interaction raises the HOMO energy, while a bonding interaction lowers the LUMO energy in *s-cis* conformation.

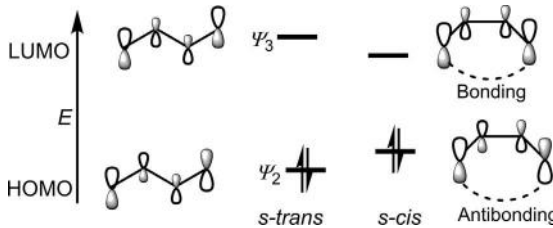


Fig. 1.15 Relative energies of frontier orbitals in *s-trans* and *s-cis* conformations of butadiene.

In frontier orbital analysis, the higher energy HOMO and lower energy LUMO would make the *s-cis*-butadiene more reactive than *s-trans*-butadiene in pericyclic reactions. It may be mentioned here that the lower HOMO/LUMO energy gap in *s-cis* conformation leads to UV absorption at a longer wavelength (253 nm) for a homoannular diene locked in *s-cis* conformation compared with a λ_{max} of 215 nm for an acyclic or a heteroannular diene existing predominantly or exclusively in *s-trans* conformation.

The orbital symmetry of frontier orbitals is important in the context of mechanism of pericyclic reactions. Fig. 1.16 shows that the HOMO has the opposite phase relationship at the two termini and is characterized by C_2 symmetry while the LUMO with the same phase relationship at the two ends exhibits m symmetry.



Fig. 1.16 Orbital symmetries of HOMO and LUMO of butadiene.

1.3.1.3 Hexatriene

1,3,5-Hexatriene is a conjugated π system of six p orbitals ($n=6$). Using Eqs (1.3), (1.4), the wavefunctions ($\psi_1 - \psi_6$) for six π MOs are obtained as follows:

$$\psi_1 = 0.232\phi_1 + 0.418\phi_2 + 0.521\phi_3 + 0.521\phi_4 + 0.418\phi_5 + 0.232\phi_6$$

$$\psi_2 = 0.418\phi_1 + 0.521\phi_2 + 0.232\phi_3 - 0.232\phi_4 - 0.521\phi_5 - 0.418\phi_6$$

$$\psi_3 = 0.521\phi_1 + 0.232\phi_2 - 0.418\phi_3 - 0.418\phi_4 + 0.232\phi_5 + 0.521\phi_6$$

$$\psi_4 = 0.521\phi_1 - 0.232\phi_2 - 0.418\phi_3 + 0.418\phi_4 + 0.232\phi_5 - 0.521\phi_6$$

$$\psi_5 = 0.418\phi_1 - 0.521\phi_2 + 0.232\phi_3 + 0.232\phi_4 - 0.521\phi_5 + 0.418\phi_6$$

$$\psi_6 = 0.232\phi_1 - 0.418\phi_2 + 0.521\phi_3 - 0.521\phi_4 + 0.418\phi_5 - 0.232\phi_6$$

Note the pattern in the size (not sign) of coefficients: the first three and last three values in each MO hold a mirror image relationship. The energies of the π MOs are estimated using Eq. (1.5). For instance, $E_3 = \alpha + 2\beta \cos \frac{3\pi}{7} = \alpha + 0.445\beta$. The sketches of six π MOs, their nodal properties and energies are shown in Fig. 1.17. It is evident that the six π MOs constitute three bonding and three antibonding MOs.

In the ground state, the π electron configuration of hexatriene is $\psi_1^2\psi_2^2\psi_3^2$. Thus, ψ_3 is HOMO and ψ_4 is LUMO. In the first excited state, ψ_3 and ψ_4 also represent HOMO and LUMO when each is half-filled. (Only HOMO and LUMO are labelled with coefficient values in the figure.)

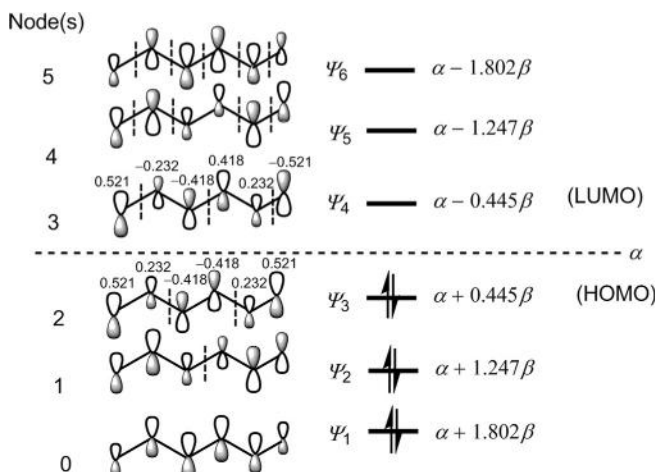


Fig. 1.17 MO energy diagram and sketches of the π MOs of 1,3,5-hexatriene.

In pericyclic reactions, the two termini of the hexatriene component ought to be generally close to each other. This is achieved when the middle double bond is *Z* and the molecule adopts *s-cis* conformation. The symmetry of the frontier orbitals of hexatriene is shown in Fig. 1.18. The HOMO has m symmetry while the LUMO is characterized by C_2 symmetry.

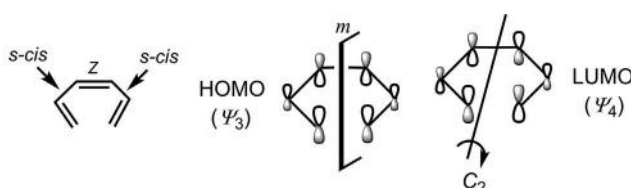
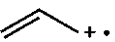


Fig. 1.18 Orbital symmetries of HOMO and LUMO of 1,3,5-hexatriene.

1.3.2 Linear Conjugated System With Odd Number of p Orbitals

We have seen that the π MOs of a conjugated system ($n = \text{even}$) comprise equal number of bonding and antibonding MOs. When $n = \text{odd}$, the conjugated π system is a reactive intermediate (carbocation, carbanion or carbon radical) when the π MOs will contain a nonbonding MO besides bonding and antibonding orbitals as described below.

1.3.2.1 Allyl System

The allyl system (cation, radical or anion)  represents a conjugated system of three p orbitals ($n = 3$). The wavefunctions ($\psi_1 - \psi_3$) for three π MOs are, according to Eq. (1.3), given by

$$\psi_1 = c_{11}\phi_1 + c_{12}\phi_2 + c_{13}\phi_3$$

$$\psi_2 = c_{21}\phi_1 + c_{22}\phi_2 + c_{23}\phi_3$$

$$\psi_3 = c_{31}\phi_1 + c_{32}\phi_2 + c_{33}\phi_3$$

The coefficients are evaluated using Eq. (1.4). For instance, $c_{21} = \sqrt{\frac{2}{4}}\sin\frac{2\pi}{4} = 0.707$; $c_{22} = \sqrt{\frac{2}{4}}\sin\frac{4\pi}{4} = 0$. With the calculated values of the coefficients, the wavefunctions are

$$\psi_1 = 0.500\phi_1 + 0.707\phi_2 + 0.500\phi_3$$

$$\psi_2 = 0.707\phi_1 - 0.707\phi_3$$

$$\psi_3 = 0.500\phi_1 - 0.707\phi_2 + 0.500\phi_3$$

In ψ_2 , the coefficient of ϕ_2 is zero which indicates that there is no contribution of ϕ_2 to ψ_2 . Physically, this implies that ϕ_2 is orthogonal to ϕ_1 and ϕ_3 in ψ_2 . The energies of the π MOs can be estimated using Eq. (1.5). The sketches of the MOs, their nodal properties and the estimated energies are shown in Fig. 1.19. The nodal properties indicate that ψ_j has again ($j - 1$) nodes, as observed for the system with even number of p orbitals. In case of ψ_2 , a node passes through the middle carbon C-2. The energy of ψ_2 is α , which is same as the energy of a p orbital, and hence ψ_2 is a nonbonding MO. It is seen that ψ_1 is bonding and ψ_3 is antibonding. Thus, the three π MOs of an allyl system comprise a bonding, a nonbonding and an antibonding MO.

The frontier orbitals of an allyl system depend on whether it is a cation, a radical or an anion. The number of π electrons in allyl cation, radical and anion is 2, 3 and 4, respectively. The frontier orbitals are given below:

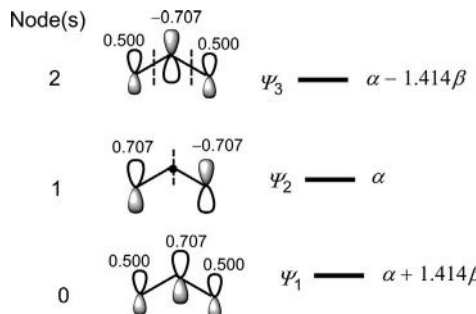


Fig. 1.19 The coefficients, nodal properties and energies of the π MOs of an allyl system.

Allyl cation (ψ_1^2)		Allyl radical ($\psi_1^2\psi_2^1$)	Allyl anion ($\psi_1^2\psi_2^2$)	
HOMO	LUMO	SOMO	HOMO	LUMO
ψ_1	ψ_2	ψ_2	ψ_2	ψ_3

The frontier orbital for an allyl radical is ψ_2 which is a singly occupied molecular orbital (SOMO). The symmetry properties of the π MOs are shown in Fig. 1.20.

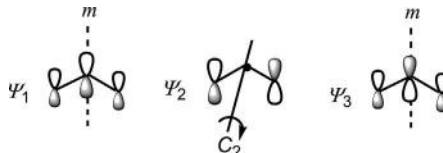


Fig. 1.20 Orbital symmetries of π MOs of an allyl system.

Problem 1.1

Derive the π MOs of a pentadienyl system using Coulson equations. Sketch the MOs in *s-cis* conformation of the molecule showing node(s). Indicate the frontier orbitals for cation, anion and radical species with symmetry.

Answer

The pentadienyl system (cation, radical or anion) is

The π MOs ($\psi_1 - \psi_5$) and their energies are derived as

$$\psi_1 = 0.288\phi_1 + 0.500\phi_2 + 0.576\phi_3 + 0.500\phi_4 + 0.288\phi_5 \quad E_1 = \alpha + 1.732\beta$$

$$\psi_2 = 0.500\phi_1 + 0.500\phi_2 - 0.500\phi_4 - 0.500\phi_5 \quad E_2 = \alpha + \beta$$

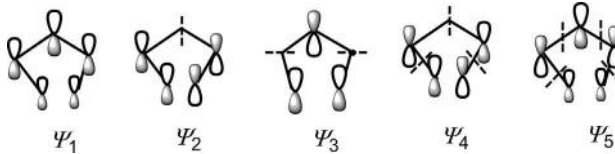
$$\psi_3 = 0.576\phi_1 - 0.576\phi_3 + 0.576\phi_5 \quad E_3 = \alpha$$

$$\psi_4 = 0.500\phi_1 - 0.500\phi_2 + 0.500\phi_4 - 0.500\phi_5 \quad E_4 = \alpha - \beta$$

$$\psi_5 = 0.288\phi_1 - 0.500\phi_2 + 0.576\phi_3 - 0.500\phi_4 + 0.288\phi_5 \quad E_5 = \alpha - 1.732\beta$$

The energies indicate that ψ_1 and ψ_2 are bonding MOs; ψ_3 is a nonbonding MO; and ψ_4 and ψ_5 are antibonding MOs.

The sketches of the π MOs are shown below. It is seen that an orbital ψ_j has $(j - 1)$ nodes.



The frontier orbitals for the pentadienyl cation, radical and anion, and their symmetry are given below:

Cation ($\psi_1^2\psi_2^2$)		Radical ($\psi_1^2\psi_2^2\psi_3^1$)	Anion ($\psi_1^2\psi_2^2\psi_3^2$)	
HOMO	LUMO	SOMO	HOMO	LUMO
ψ_2	ψ_3	ψ_3	ψ_3	ψ_4
Symmetry: C_2	m	m	m	C_2

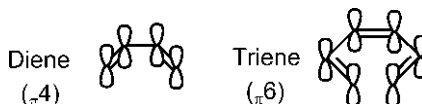
1.3.2.2 A Short-Cut Method for Sketching π MOs

The sketches of the π MOs can be simplified by ignoring the difference of coefficients, where the coefficients are not important in a mechanistic description of pericyclic reactions. A short-cut method to drawing such a simplified picture of π MOs is to use the nodal properties which indicate that an MO ψ_j has $(j - 1)$ nodes. The procedure is illustrated for the drawing of frontier orbitals in Fig. 1.21. Note that the nodes are to be placed in the most symmetrical manner in the prospective MO.

The symmetry properties of the π MOs can be summarized as follows:

$$\begin{aligned}\psi_j \ (j = \text{odd}) &\Rightarrow m \text{ symmetry;} \\ \psi_j \ (j = \text{even}) &\Rightarrow C_2 \text{ symmetry.}\end{aligned}$$

Besides the MOs, orbital picture representation (without phase sign) of the π components is also used in mechanistic analysis of pericyclic reactions. The orbital pictures of the diene and triene components are sketched as



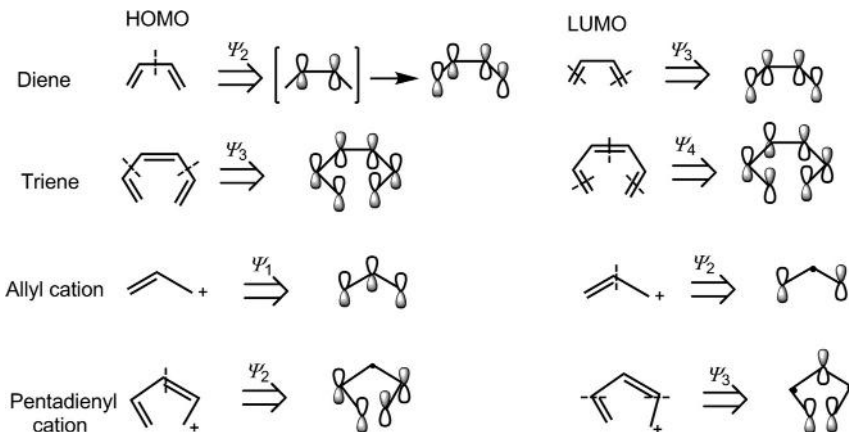
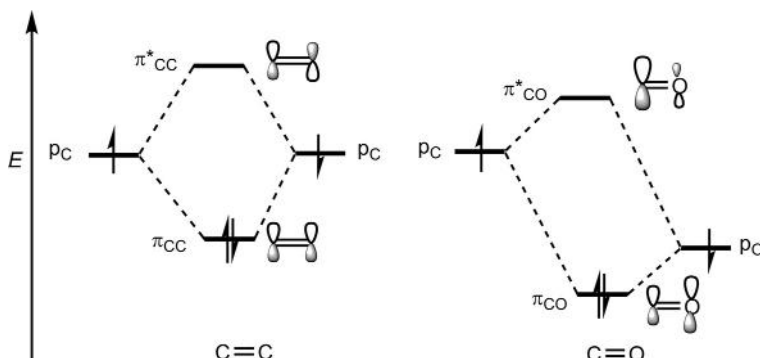


Fig. 1.21 Sketches of frontier orbitals from nodal properties.

1.4 CARBONYL π SYSTEM

The symmetry properties of π MOs of the carbonyl system are similar to those of alkenes; however, the energy and coefficient patterns differ. The energy of a p orbital on oxygen (-15.9 eV) is much lower than that on carbon (-10.7 eV) (see Table 1.1). This would lead to lowering of energy of both π_{CO} and π^*_{CO} compared with those for alkene (Fig. 1.22).

For the carbonyl group, the lower energy p_{O} would contribute more to the lower energy π_{CO} and the higher energy p_{C} would contribute more to the higher energy π^*_{CO} . As a result, there will be a larger coefficient on oxygen in π_{CO} and a larger coefficient on carbon in π^*_{CO} as shown in Fig. 1.22. π_{CO} is HOMO and π^*_{CO} is LUMO, the polarization of HOMO and

Fig. 1.22 Energy diagram of π MOs of carbonyl group vis-a-vis alkene π MOs.

LUMO being opposite. The presence of low-lying LUMO with a large coefficient on carbon makes the carbonyl group a particularly important electron-withdrawing substituent or a reactive component in pericyclic reactions.

1.5 EFFECT OF SUBSTITUENTS ON FRONTIER ORBITAL ENERGIES AND COEFFICIENTS OF π SYSTEMS

A qualitative picture of the perturbation effects of different types of substituents on the frontier orbital energies and coefficients of π systems is necessary to rationalize the features of reactivity and selectivity in cycloadditions and other pericyclic processes. The substituents are generally classified as follows:

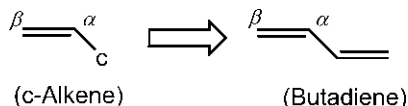
- c-Substituents: These are simple conjugating substituents such as vinyl, Ph etc. They can act as π donors or as π acceptors based on the electron demand of the parent π system.
 - z-Substituents: These indicate conjugating and electron-withdrawing substituents such as COR, CO₂R, CN, NO₂, SiR₃, BR₂ etc. They act as π acceptors.
 - x-Substituents: These denote the electron-donating substituents such as OR, NR₂, R (alkyl) etc. They act as π donors.

1.5.1 HOMO/LUMO Energies and Coefficients of Substituted Alkenes

The unsubstituted alkene (ethylene) is the reference or unperturbed alkene. A perturbed alkene system is represented by c-, z- or x-substituted alkene. The patterns of frontier orbital energies and coefficients for the perturbed systems vis-a-vis unperturbed alkene can be determined by choosing a reasonable model for each substituted alkene. An all-carbon model for which HMO energies and coefficients are known is the preferred choice to draw a qualitative inference.

1.5.1.1 Perturbation by c-Substituents

Since a c-substituent is a neutral conjugating substituent (e.g. $\text{CH}=\text{CH}_2$), a reasonable model for a c-substituted alkene is butadiene:



The energies and coefficients for HOMO and LUMO of butadiene and ethylene as shown earlier are

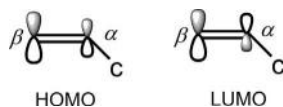
	Energy		Coefficient	
	HOMO	LUMO	HOMO	LUMO
Ethylene	$\alpha + \beta$	$\alpha - \beta$	<u>0.71</u> <u>0.71</u>	<u>0.71</u> <u>-0.71</u>
Butadiene	$\alpha + 0.62\beta$	$\alpha - 0.62\beta$	<u>0.60</u> <u>0.37</u> <u>-0.37</u> <u>-0.60</u>	<u>0.60</u> <u>-0.37</u> <u>-0.37</u> <u>0.60</u>

Comparing the HOMO/LUMO energies between butadiene (a model for *c*-alkene) and ethylene, we have

$$\begin{aligned} E_{\text{HOMO}} (\text{c-alkene}) &> E_{\text{HOMO}} (\text{alkene}) \\ E_{\text{LUMO}} (\text{c-alkene}) &< E_{\text{LUMO}} (\text{alkene}) \end{aligned}$$

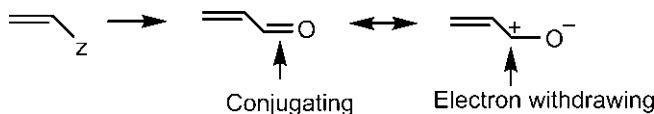
Therefore, a *c*-substituent raises HOMO energy and lowers LUMO energy. The HOMO and LUMO energies were estimated by Houk from the experimental data of ionization potential and electron affinity, respectively.⁹ These data indicating average or representative values will be shown later (see Fig. 1.23).

Now, to determine the effect of *c*-substituent on the frontier orbital coefficients, we consider the HOMO/LUMO coefficients of butadiene as a model for *c*-alkene. It is seen that there is a smaller coefficient (0.37) at the α -carbon carrying the substituent and a larger coefficient (0.60) at the unsubstituted β -carbon in both HOMO and LUMO. In the unsubstituted alkene, the coefficients are equal. Therefore, a *c*-substituent leads to a large coefficient at β -carbon and a small coefficient at α -carbon in both HOMO and LUMO. The coefficient pattern for a *c*-substituted alkene is represented as

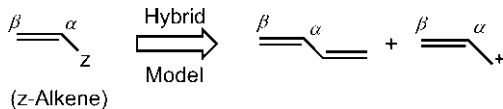


1.5.1.2 Perturbation by *z*-Substituents

A *z*-substituent such as a C=O group in a *z*-substituted alkene imparts both conjugating and electron-withdrawing character as a resonance hybrid:



Thus, a reasonable model of a *z*-substituted alkene is a hybrid model of butadiene (conjugating character) and allyl cation (electron-withdrawing character):



The frontier orbital energies and coefficients for the relevant π systems are

	Energy		Coefficient	
	HOMO	LUMO	HOMO	LUMO
Ethylene	$\alpha + \beta$	$\alpha - \beta$	<u>0.71</u>	<u>0.71</u>
Butadiene	$\alpha + 0.62\beta$	$\alpha - 0.62\beta$	<u>0.60</u> -0.37	<u>0.60</u> -0.37 0.60
Allyl cation	$\alpha + 1.41\beta$	α	<u>0.50</u> + <u>0.71</u> 0.50	<u>0.71</u> 0 -0.71

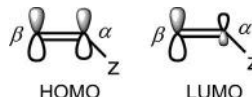
Comparing the energies, we see that the conjugating butadiene character in the *z*-substituted alkene tends to increase the energy of HOMO [$(\alpha + 0.62\beta) > (\alpha + \beta)$] but the electron-withdrawing allyl cation character tends to decrease it [$(\alpha + 1.41\beta) < (\alpha + \beta)$]. The two effects thus act in opposition leading to a very small effect on HOMO energy for *z*-alkene. In contrast, both butadiene and allyl cation characters act in concert to substantially lower the LUMO energy of *z*-substituted alkene [$(\alpha - 0.62\beta) < (\alpha - \beta)$, $\alpha < (\alpha - \beta)$]. Therefore,

$$\begin{aligned} E_{\text{HOMO}}(\text{z-alkene}) &\approx E_{\text{HOMO}}(\text{alkene}) \\ E_{\text{LUMO}}(\text{z-alkene}) &\ll E_{\text{LUMO}}(\text{alkene}) \end{aligned}$$

The Houk's data show that HOMO energy of *z*-substituted alkene (-10.9 eV) is slightly lower than that of unperturbed alkene (-10.5 eV), but the LUMO energy is substantially lowered from 1.5 to 0 eV. Therefore, a *z*-substituent *slightly lowers the HOMO energy and appreciably lowers the LUMO energy*.

Next, we examine the coefficient data. Butadiene HOMO contributes a small coefficient (0.37) at α -C and a large coefficient (0.60) at β -C, while the allyl cation HOMO contributes in opposite sense that is, a large coefficient (0.71) at α -C and a small coefficient (0.50) at β -C. The net effect is expected to

be a small difference in coefficient at the two termini in the HOMO of z -substituted alkene. As estimated by Houk, the coefficient at β -C is slightly larger than that at α -C. In contrast, for LUMO, both butadiene and allyl cation contribute larger coefficients at β -C reinforcing each other. Therefore, a z -substituent leads to a slightly larger coefficient at β -carbon in HOMO, but a much larger coefficient at β -carbon in LUMO. This pattern is represented as



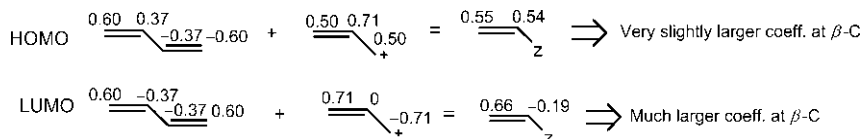
Problem 1.2

Assuming the model of z -substituted alkene to be a 1:1 mixture of butadiene and allyl cation, estimate its HOMO/LUMO energies and coefficients.

Answer

$E_{\text{HOMO}} (\text{z-alkene}) = [\frac{1}{2}(\alpha + 0.62\beta + \alpha + 1.41\beta)] = \alpha + 1.02\beta$. This energy is slightly smaller than that of ethylene.

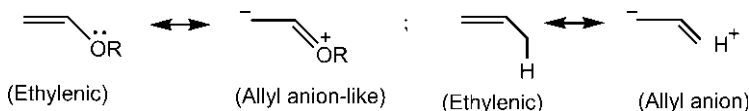
$E_{\text{LUMO}} (\text{z-alkene}) = [\frac{1}{2}(\alpha - 0.62\beta + \alpha)] = \alpha - 0.31\beta$. This LUMO energy is much smaller than that of ethylene.



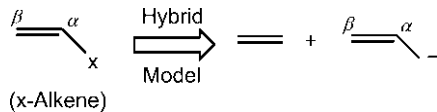
(The above coefficients estimated for z -substituted alkene are not true coefficients as the sum of the squares of coefficients on all atoms of z -alkene including z -substituent would not be unity. The estimated values show qualitatively a pattern of large/small coefficients.)

1.5.1.3 Perturbation by x -Substituents

An x -substituent is π donating through a lone pair on the heteroatom or through a σ bond (usually C—H):



Thus a reasonable model of x -substituted alkene is a hybrid model of ethylene and allyl anion:



The frontier orbital energies and coefficients for ethylene and allyl anion are

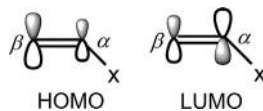
	Energy		Coefficient	
	HOMO	LUMO	HOMO	LUMO
Ethylene	$\alpha + \beta$	$\alpha - \beta$	0.71 0.71	0.71 -0.71
Allyl anion	α	$\alpha - 1.41\beta$	0.71 0	0.50 -0.71

It is seen that allyl anion component tends to increase the energy of HOMO [$\alpha > (\alpha + \beta)$] as well as the energy of LUMO [$(\alpha - 1.41\beta) > (\alpha - \beta)$] in proportion to its contribution to the hybrid. Thus

$$\begin{aligned} E_{\text{HOMO}}(\text{x-alkene}) &> E_{\text{HOMO}}(\text{alkene}) \\ E_{\text{LUMO}}(\text{x-alkene}) &> E_{\text{LUMO}}(\text{alkene}) \end{aligned}$$

Therefore, an x -substituent raises the energy of both HOMO and LUMO.

The coefficient values indicate that the allyl anion HOMO contributes zero coefficient at α -C and a large coefficient (0.71) at β -C. The resultant effect would be a larger coefficient at the β -C than at α -C in HOMO of an x -substituted alkene. For LUMO, allyl anion and ethylene contribute equal coefficient (0.71) at the α -C, but allyl anion contributes smaller coefficient (0.50) than ethylene (0.71) at β -C. The net effect would be a smaller coefficient at β -C in LUMO of an x -substituted alkene. Therefore, an x -substituent leads to a larger coefficient at β -carbon in HOMO and at α -carbon in LUMO. This coefficient pattern is represented as



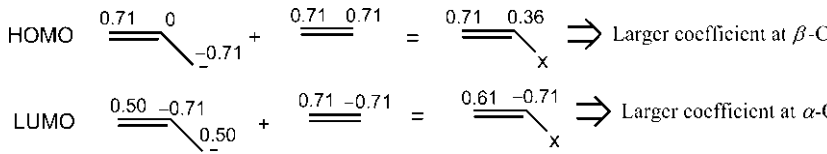
Problem 1.3

Assuming that the model for an x -substituted alkene is a 1:1 mixture of ethylene and allyl anion, estimate its HOMO/LUMO energies and coefficients. Compare the results with the unsubstituted alkene.

Answer

$$E_{\text{HOMO}} \text{ (x-alkene)} = [\frac{1}{2} (\alpha + \alpha + \beta) = (\alpha + 0.5\beta)] > E_{\text{HOMO}} \text{ (alkene)}$$

$$E_{\text{LUMO}} \text{ (x-alkene)} = [\frac{1}{2} (\alpha - 1.41\beta + \alpha - \beta) = (\alpha - 1.21\beta)] > E_{\text{LUMO}} \text{ (alkene)}$$



(The above coefficients calculated for x-alkene are not true coefficients, and indicate a qualitative pattern of large/small coefficients.)

1.5.1.4 Summary

The perturbation effects of c-, z- and x-substituents on frontier orbital energies and coefficients of alkene π system are summarized in [Table 1.2](#).

The energy diagram for the unsubstituted and c-, z- and x-substituted alkenes using Houk's data of frontier orbital energies and the coefficient pattern is shown in [Fig. 1.23](#).^{9,10}

Table 1.2 Perturbation effects of the substituents on frontier orbital energies and coefficients of alkene

Substituent	Energy	Coefficient
c	Raises HOMO energy	Larger coefficient at β -carbon in HOMO
	Lowers LUMO energy	Larger coefficient at β -carbon in LUMO
z	Slightly lowers HOMO energy	Slightly larger coefficient at β -carbon in HOMO
	Appreciably lowers LUMO energy	Much larger coefficient at β -carbon in LUMO
x	Raises HOMO energy	Larger coefficient at β -carbon in HOMO
	Raises LUMO energy	Larger coefficient at α -carbon in LUMO

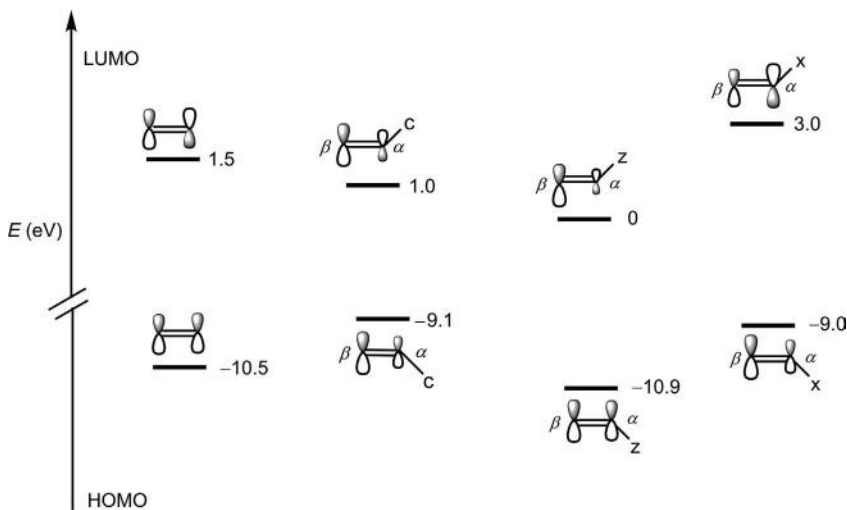


Fig. 1.23 Estimated frontier orbital energies and coefficient pattern for unsubstituted and c-, z- and x-substituted alkenes.

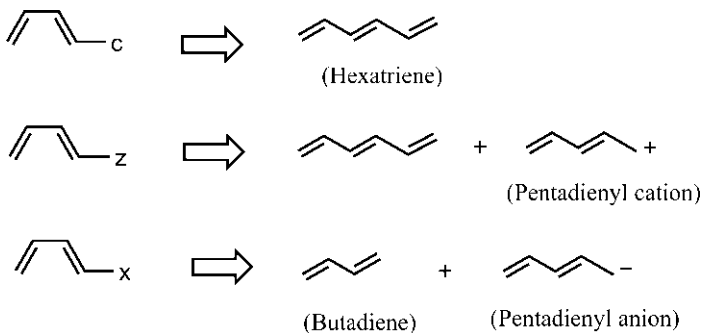
1.5.1.5 Alkyne π System

Alkynes have a shorter C—C bond length than alkenes, which results in a stronger overlap of p orbitals. Thus, the alkyne π system has a lower energy HOMO which is generally found to be 0.4–0.9 eV (\sim 0.7 eV on average) lower than the HOMO energy of alkene as measured by photoelectron spectroscopy. However, the LUMO energy of alkyne is almost same as that of alkene as shown by UV spectroscopy. The effects of c-, z- and x-substituents on the coefficients of alkyne are similar to those on alkene coefficients.

1.5.2 HOMO/LUMO Energies and Coefficients of Substituted Dienes

1.5.2.1 1-Substituted Dienes

The effects of c-, z- and x-substituents on the frontier orbital energies and coefficients of 1-substituted dienes can be determined using similar arguments as advanced for alkenes with the models given below.



The substituent effects on HOMO/LUMO energies and coefficients using the above models give similar trends as observed for alkenes (see Table 1.2). (The substituted dienes are drawn in an *s*-*cis* conformation; the pattern of change in *s*-*cis* and *s*-*trans* conformations is expected to be similar.) The Houk's data⁹ of estimated frontier orbital energies and the coefficient pattern at the terminal carbons C-1 and C-4 are shown in Fig. 1.24. The effect of the substituent at the unsubstituted terminal (C-4) of the dienes

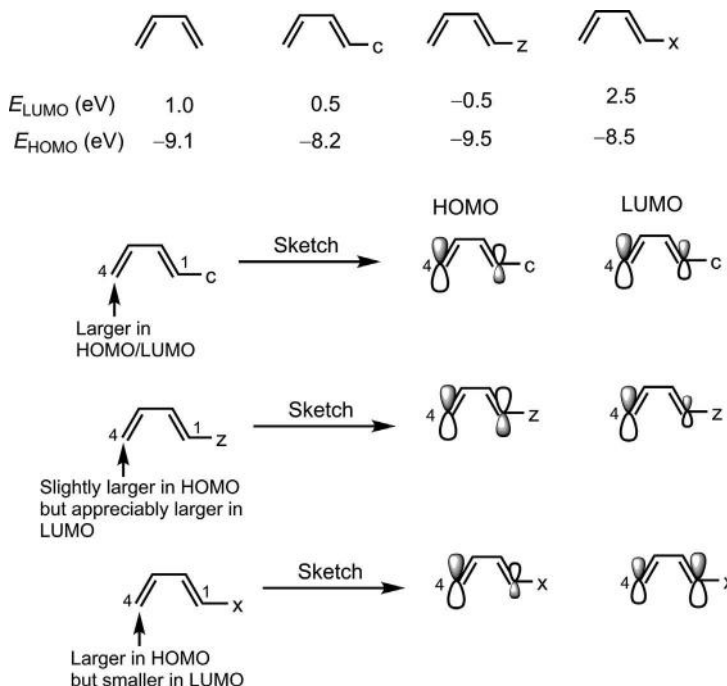


Fig. 1.24 Estimated frontier orbital energies and coefficient pattern of 1-substituted dienes.

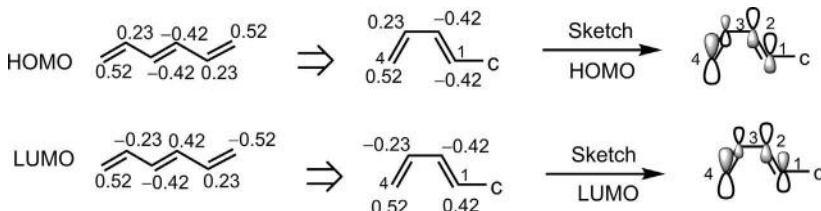
(cf. β -carbon in alkenes) is indicated. Remember that HOMO has opposite phase signs and LUMO has the same phase sign at C-1 and C-4.

Problem 1.4

Give the pattern of frontier orbital coefficients at C-1, C-2, C-3 and C-4 of 1-c-substituted diene.

Answer

For 1-c-substituted diene, the model is hexatriene. The pattern of coefficients as shown below is similar in HOMO and LUMO. Between two terminal carbons, C-4 has a large coefficient and C-1 has a small coefficient. Between the two internal carbons, C-2 has large and C-3 has small coefficients.



1.5.2.2 2-Substituted Dienes

The trends for frontier orbital energies and coefficients of dienes with c-, z- or x-substituent at C-2 can also be rationalized using the perturbation pattern for c-, z- or x-substituted alkene moiety present in a 2-substituted diene. To illustrate, let us consider a 2-c-substituted diene. In an unsubstituted diene, there are equal coefficients on the terminal atoms C-1 and C-4 in HOMO/LUMO. In a 2-c-substituted diene, a c-substituent on the alkene moiety tends to raise the coefficient at the β -carbon (i.e. C-1 of diene) in HOMO (or LUMO) as shown in Fig. 1.25. As a result, the coefficients at the terminal carbons of a 2-substituted diene become unequal, with a larger coefficient at C-1 in HOMO/LUMO. Similar arguments apply to other 2- substituted dienes.

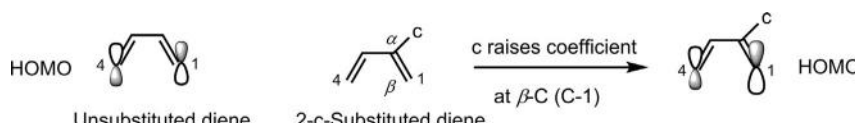


Fig. 1.25 Effect of the c-substituent on the frontier orbital coefficient of a 2-substituted diene.

Fig. 1.26 shows the frontier orbital energies and the coefficient pattern of 2-substituted dienes.⁹ Note that the substituted alkene moiety is placed in a box to highlight the substituent effect. It may be mentioned that the explicit models for 2-substituted dienes could also be formulated using similar arguments as used for alkenes (try for yourself), which would provide similar results as shown in Fig. 1.26.

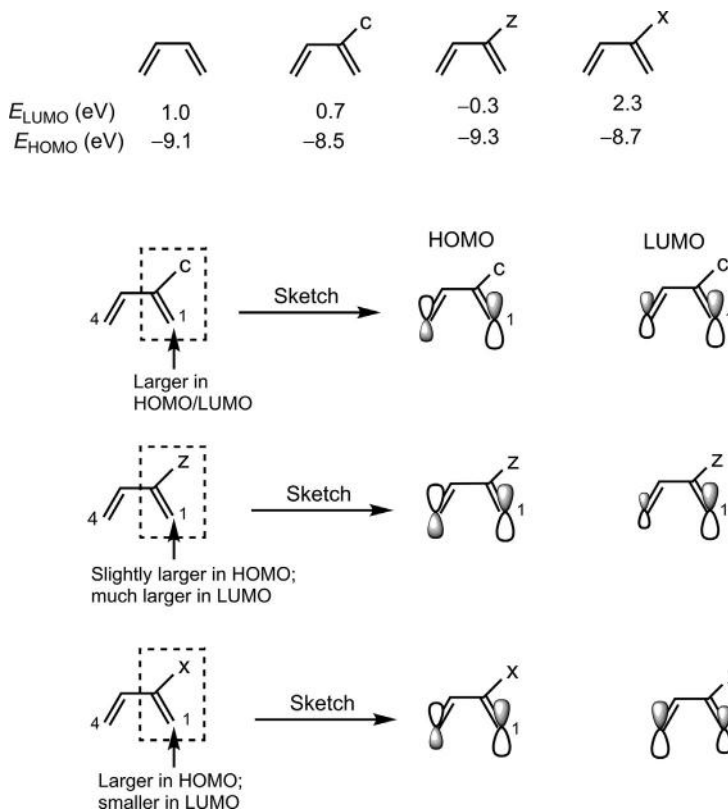
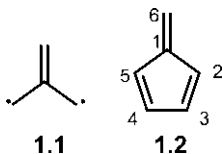


Fig. 1.26 Estimated frontier orbital energies and coefficient pattern of 2-substituted dienes.

1.6 TRIMETHYLENEMETHANE AND FULVENE SYSTEMS

Trimethylenemethane (TMM) **1.1** and fulvene **1.2** do not belong to linear conjugated π systems but represent cross-conjugated systems.



As shown, TMM is usually drawn as a diradical and is referred to as trimethylenemethane diradical (TMM diyl) which is a cross-conjugated system of four p orbitals. The energy diagram of its π MOs is shown in Fig. 1.27.¹¹ It is seen that ψ_1 is a bonding MO; ψ_2 and ψ_3 constitute a degenerate pair of nonbonding MOs; and ψ_4 is an antibonding MO.

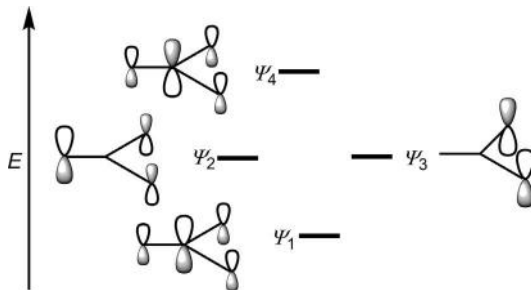


Fig. 1.27 The π MOs of TMM.

The TMM diyl is a reactive intermediate and can exist in triplet and singlet states. Triplet TMM with the π electron configuration $\psi_1^2\psi_2^1\psi_3^1$ behaves as a diradical. The singlet TMM has the π electron configuration $\psi_1^2\psi_2^2$ or $\psi_1^2\psi_3^2$. However, between ψ_2 and ψ_3 , ψ_2 as the HOMO can explain the course of pericyclic cycloadditions (see Chapter 4, Section 4.4). The LUMO is then ψ_3 .

Fulvene is a cross-conjugated system of six p orbitals. It can be formulated as a combination of butadiene and ethylene, and the perturbation analysis gives six π MOs of fulvene whose energies increase in the order $\psi_1 < \psi_2 < \psi_3 < \psi_4 < \psi_5 < \psi_6$ (Fig. 1.28).¹²

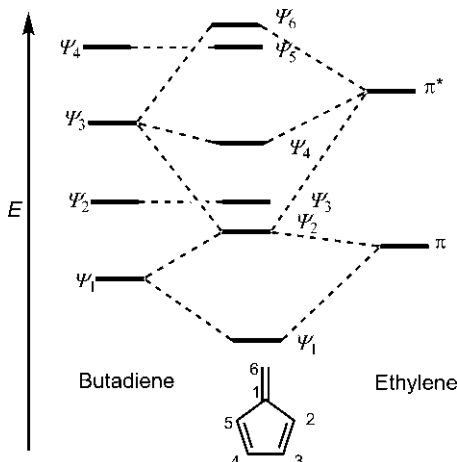


Fig. 1.28 The interaction energy diagram of fulvene.

Fulvene has six electrons. Therefore, HOMO is ψ_3 and LUMO is ψ_4 . The diagram suggests that fulvene HOMO (ψ_3) is the butadiene ψ_2 orbital, so the p orbitals at C-1 and C-6 of fulvene do not contribute to its HOMO. In contrast, all p orbitals contribute to fulvene LUMO (ψ_4). It is also seen that the NLUMO (next-lowest unoccupied molecular orbital) of fulvene is ψ_5 , and this orbital is the butadiene ψ_4 orbital, and so C-1 and C-6 have zero coefficient in NLUMO. Dimethylfulvene participates in a variety of pericyclic cycloadditions. The frontier orbital energies and coefficients of dimethylfulvene are shown in Fig. 1.29.^{13,14} (Note that only the front lobe of each p orbital is drawn.)

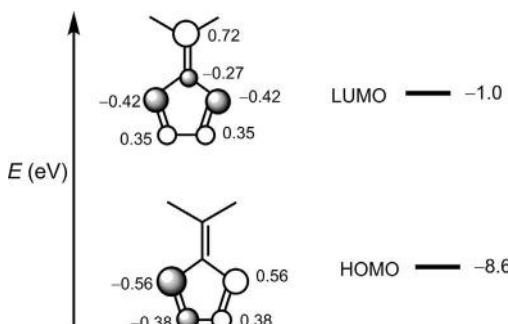


Fig. 1.29 Estimated frontier orbital energies and coefficients of dimethylfulvene.

1.7 CYCLIC CONJUGATED π SYSTEMS¹⁵

1.7.1 Hückel System

Hückel theory assumes that the cyclic π system is planar and a regular polygon with equal sides. The solution for the energies of π MOs of a monocyclic conjugated system is given by

$$E_j = \alpha + 2\beta \cos\left(2j\frac{\pi}{n}\right) \quad (j = 0, 1, 2, \dots, n-1) \quad (1.6)$$

where n is the total number of p orbitals.

First, we consider benzene as a cyclic conjugated system of six p orbitals ($n=6$). The possible j values are 0, 1, 2, 3, 4 and 5. Using Eq. (1.6), the energies of six π MOs ($\psi_0 - \psi_5$) of benzene are estimated as

$$E_0 = \alpha + 2\beta$$

$$E_1 = \alpha + 2\beta \cos\left(2\frac{\pi}{6}\right) = \alpha + \beta$$

$$E_2 = \alpha + 2\beta \cos\left(4\frac{\pi}{6}\right) = \alpha - \beta$$

$$E_3 = \alpha + 2\beta \cos\left(6\frac{\pi}{6}\right) = \alpha - 2\beta$$

$$E_4 = \alpha + 2\beta \cos\left(8\frac{\pi}{6}\right) = \alpha - \beta$$

$$E_5 = \alpha + \beta$$

It is seen that there is degeneracy in energy levels: $E_1 = E_5$ and $E_2 = E_4$. In general, $E_j = E_{n-j}$.

Since the cosine is a symmetric function [$\cos \theta = \cos(-\theta)$], the two degenerate energies can also be indicated as $E_j = E_{-j}$. Therefore, the possible values of j can also be given as $j = 0, \pm 1, \pm 2, \dots$ (up to a total of n values). The MO energy diagram of benzene is shown in Fig. 1.30 in which the wavefunctions are labelled by j values in both notations. The six π MOs of benzene are classified into three bonding and three antibonding MOs.

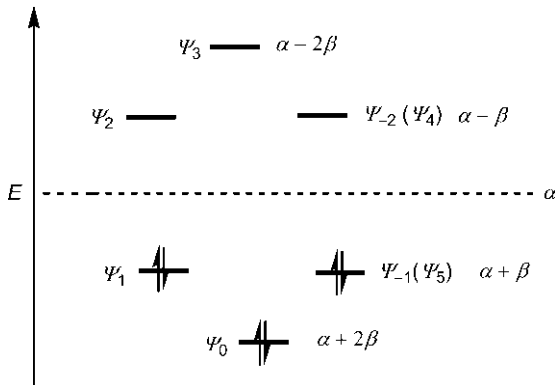


Fig. 1.30 Energy diagram for the π MOs of benzene.

The π electron configuration of benzene is $\psi_0^2\psi_1^2\psi_{-1}^2$ which indicates that all bonding orbitals are completely filled. This configuration represents a closed-shell system and hence is stable.

In general, the total number of electrons for a closed-shell system
 = no. of electrons in the filled lowest nondegenerate level + the total
 no. of electrons in filled degenerate bonding levels (n pairs)
 = $2 + 4n$.

(If any pair of degenerate levels is nonbonding, this may either be completely filled or completely vacant.)

These $(4n+2)\pi$ electron systems ($n=0, 1, 2, \dots$) with a closed-shell configuration are called aromatic. (Note that the same symbol n is used in

different contexts: in Eq. (1.6), n denotes the total number of p orbitals while for $4n+2$ electron system, n is zero or a positive integer.)

The π MO wavefunctions (ψ_j) for benzene as linear combinations of p AOs (ϕ_r) are obtained as

$$\psi_0 = \frac{1}{\sqrt{6}} (\phi_1 + \phi_2 + \phi_3 + \phi_4 + \phi_5 + \phi_6)$$

$$\psi_1 = \frac{1}{2\sqrt{3}} (2\phi_1 + \phi_2 - \phi_3 - 2\phi_4 - \phi_5 + \phi_6)$$

$$\psi_{-1} = \frac{1}{2} (\phi_2 + \phi_3 - \phi_5 - \phi_6)$$

$$\psi_2 = \frac{1}{2\sqrt{3}} (2\phi_1 - \phi_2 - \phi_3 + 2\phi_4 - \phi_5 - \phi_6)$$

$$\psi_{-2} = \frac{1}{2} (\phi_2 - \phi_3 + \phi_5 - \phi_6)$$

$$\psi_3 = \frac{1}{\sqrt{6}} (\phi_1 - \phi_2 + \phi_3 - \phi_4 + \phi_5 - \phi_6)$$

The π MOs of benzene are drawn schematically in Fig. 1.31. (Note that only the top lobe of each p orbital is shown.) A nodal plane perpendicular to the planar ring is indicated by a broken line. The number of nodes

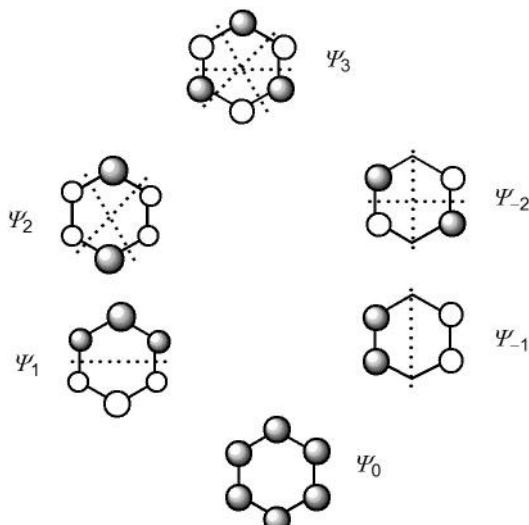


Fig. 1.31 Schematic drawing of the π MOs of benzene.

(nodal planes) increases with energy. The lowest energy bonding MO (ψ_0) has no node; the two degenerate bonding MOs (ψ_1, ψ_{-1}) have one node; the degenerate antibonding MOs (ψ_2, ψ_{-2}) have two nodes; and the highest energy antibonding MO (ψ_3) has three nodes.

Next, we consider cyclobutadiene with four p orbitals ($n=4$). The energies of the four π MOs ($j=0, 1, -1, 2$) are estimated as

$$\begin{aligned}E_0 &= \alpha + 2\beta \\E_1 &= \alpha + 2\beta \cos\left(2\frac{\pi}{4}\right) = \alpha, \\E_{-1} &= \alpha \\E_2 &= \alpha - 2\beta\end{aligned}$$

The MO energy diagram is shown in Fig. 1.32, which shows that ψ_0 is bonding, ψ_1 and ψ_{-1} are nonbonding and ψ_2 is antibonding.

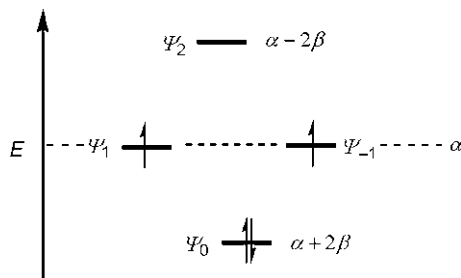


Fig. 1.32 Energy diagram for the π MOs of cyclobutadiene.

The ground state π electron configuration of cyclobutadiene is $\psi_0^2\psi_1^1\psi_{-1}^1$, which represents an open-shell system and also a triplet state. Cyclobutadiene is thus expected to be much less stable. In general, the total number of electrons for an open-shell system = $4n$ (2 less than $4n+2$, since the two orbitals in a degenerate level are half-filled). These $(4n)\pi$ systems ($n=1, 2, \dots$) with open-shell configuration are called antiaromatic.

The above results for Hückel π systems to be aromatic or antiaromatic are known as the Hückel rules and are summarized as

Number of electrons	Hückel system
$4n+2$	Aromatic
$4n$	Antiaromatic

1.7.1.1 Structure of Cyclobutadiene (Jahn–Teller Distortion)

The open-shell and triplet state configuration of cyclobutadiene is obtained using the Hückel's assumption of a square structure having equal bond length. However, both the experiments and theoretical calculations show that the ground state of cyclobutadiene is a singlet with a rectangular geometry showing alternating double and single bonds.^{16,17} The energy of the rectangular structure is predicted to be lower than that of the square by about 10 kcal mol⁻¹. Nevertheless, the singlet rectangular structure is still very unstable and extremely reactive. This is evident from the fact that cyclobutadiene dimerizes by Diels–Alder cycloaddition at an extremely low temperature (see Chapter 4, Problem 4.2).

The transformation of square cyclobutadiene to rectangular geometry causes splitting of the degenerate level as shown in Fig. 1.33.

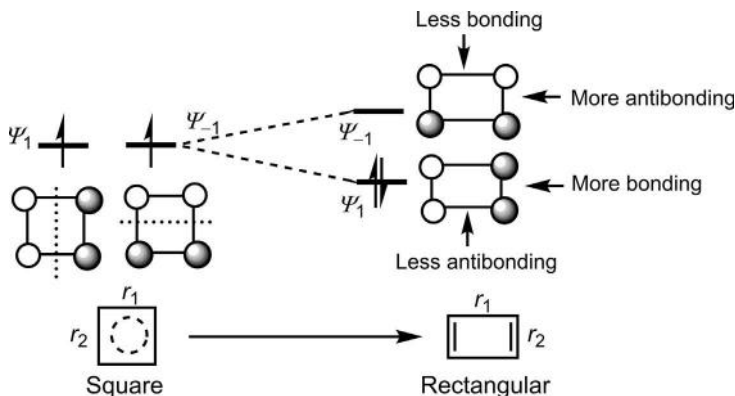


Fig. 1.33 Lifting of degeneracy from the transformation of square cyclobutadiene to a rectangular structure. The node in each π MO is indicated by a broken line. r_1 and r_2 denote horizontal and vertical bond distance, respectively.

The two degenerate π MOs (ψ_1 and ψ_{-1}) for square cyclobutadiene are shown on the left. Increasing r_1 and decreasing r_2 lead to a rectangular geometry. The overlap between two p orbitals is a function of bond distance. Therefore, there occurs more effective bonding overlap as well as less antibonding overlap in ψ_1 in a rectangular geometry, thereby lowering its energy. In contrast, there is less bonding overlap and more antibonding overlap in ψ_{-1} in a rectangular structure whose energy is therefore raised. The result is the splitting of the degenerate energy level in a rectangular geometry having less symmetry. This phenomenon is known as Jahn–Teller distortion. In a rectangular structure, two electrons occupy the lower energy

orbital ψ_1 . Thus, the rectangular cyclobutadiene is more stable than the square form, and is a singlet.

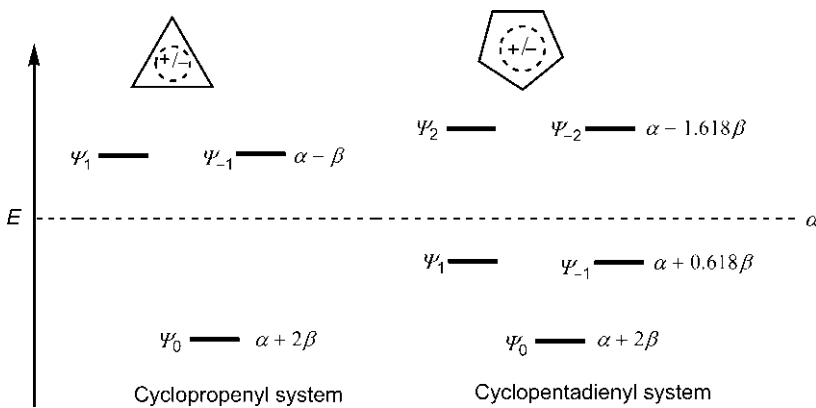
The π MOs of cyclobutadiene ($\psi_0, \psi_1, \psi_{-1}, \psi_2$) can be relabelled in a rectangular structure as ψ_1, ψ_2, ψ_3 and ψ_4 (cf. π MOs of butadiene). By this convention, the π electron configuration of singlet cyclobutadiene is $\psi_1^2\psi_2^2$. Therefore, ψ_2 is HOMO and ψ_3 is LUMO. The HOMO/LUMO energy separation is however very small.

Problem 1.5

Using the relevant Hückel expression, construct the energy diagram for the cyclopropenyl system and the cyclopentadienyl system. Hence predict whether the cationic and anionic species of each system is aromatic or antiaromatic.

Answer

For a cyclopropenyl system, $j=0, \pm 1$ and for a cyclopentadienyl system, $j=0, \pm 1, \pm 2$. Using Eq. (1.6), the energies of the π MOs for each system are determined, which are shown in the energy diagram below.



For a cyclopropenyl system, the cation has two electrons and its electron configuration is ψ_0^2 (closed-shell); hence it is aromatic. But the cyclopropenyl anion (4e system) has the open-shell configuration $\psi_0^2\psi_1^1\psi_{-1}^1$ and is therefore antiaromatic. For the cyclopentadienyl system, the cation having four electrons is antiaromatic as it has the open-shell configuration $\psi_0^2\psi_1^1\psi_{-1}^1$, whereas the anion (6e system) with the closed-shell configuration $\psi_0^2\psi_1^2\psi_{-1}^2$ is aromatic.

1.7.2 Möbius System

Heilbronner introduced the idea of Möbius π system in the MO description of a cyclic conjugated system.¹⁸ This π system is called Möbius in analogy with a Möbius strip described by the mathematician August Möbius. A simple model of a Möbius strip can be easily made by taking a narrow strip of paper, giving one of two ends a 180 degrees twist and then joining them together (try making a Möbius strip for yourself). If the two ends of the paper are simply joined without twisting, the resulting strip is a normal cycle with two-sided surfaces. In contrast, a Möbius strip has a single continuous surface. In a similar fashion, the topology of a cyclic array of p orbitals can be of Hückel type (normal cycle with two separate rings) or Möbius type (a single continuous ring), as shown in Fig. 1.34.

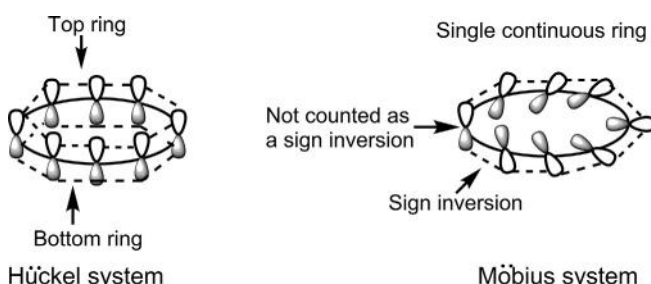


Fig. 1.34 Schematic drawing of Hückel and Möbius π systems.

The cyclic array representing Möbius topology involves a sign inversion (connecting lobes of opposite sign), while there is no sign inversion in Hückel topology. The intrinsic opposite signs of two lobes of a single p orbital must not be counted as a sign inversion in the cyclic orbital array.

In principle, one can consider any number of twists in the π system. The result is that zero or even number of twists gives Hückel system, and odd number of twists leads to Möbius system. Thus, the topology of a cyclic orbital array is classified as Hückel type or Möbius type based on the number of sign inversions in the cyclic array as given below:

Number of sign inversions	Topology of orbital array
Zero or even	Hückel-type
Odd	Möbius-type

1.7.2.1 Energy Diagram

The Heilbronner solution for the energies of Möbius π system is given by

$$E_j = \alpha + 2\beta \cos\left((2j+1)\frac{\pi}{n}\right) \quad (j=0, 1, 2, \dots, n-1) \quad (1.7)$$

where n is the total number of p orbitals (cf. Hückel system, Eq. 1.6).

Let us consider a Möbius system of four p orbitals ($n=4$). The energy levels are given by $j=0, 1, 2$ and 3 . Using Eq. (1.7), we have

$$E_0 = \alpha + 2\beta \cos\left(\frac{\pi}{4}\right) = \alpha + 1.414\beta$$

$$E_1 = \alpha + 2\beta \cos\left(3\frac{\pi}{4}\right) = \alpha - 1.414\beta$$

$$E_2 = \alpha + 2\beta \cos\left(5\frac{\pi}{4}\right) = \alpha - 1.414\beta$$

$$E_3 = \alpha + 2\beta \cos\left(7\frac{\pi}{4}\right) = \alpha + 1.414\beta$$

It is seen that the energy levels are degenerate: $E_0 = E_3$; $E_1 = E_2$. It is indeed a general pattern that the energy levels for $n=$ even are degenerate. The MO energy diagram for the system of four p orbitals ($n=4$) is shown in Fig. 1.35.

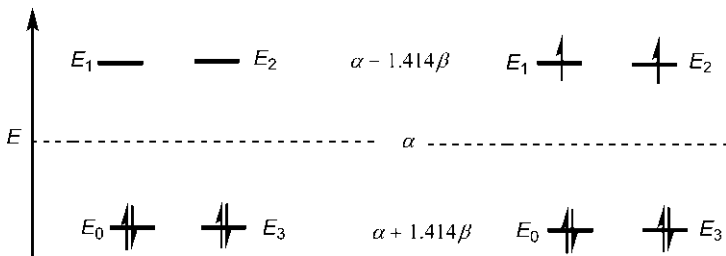


Fig. 1.35 MO Energy diagram for Möbius π electron system ($n=4$, even).

With 4 electrons (on the left side), the lowest degenerate levels are completely filled which indicate a closed-shell configuration. Hence the 4-electron system is aromatic. To generalize, the Möbius $(4n)\pi$ electron systems are aromatic. But with 6 electrons (on the right side), an open-shell configuration is obtained which predicts that Möbius $(4n+2)\pi$ electron systems are antiaromatic. These predictions are just the opposite to the predictions for Hückel π systems.

Next, we consider the pattern of energy levels when $n = \text{odd}$. For a system of five p orbitals ($n = 5$), the π MO energies estimated using Eq. (1.7) are shown in Fig. 1.36. It is seen that the energy levels except the highest level are degenerate. Thus, for $n = \text{odd}$, only the highest level is not degenerate.

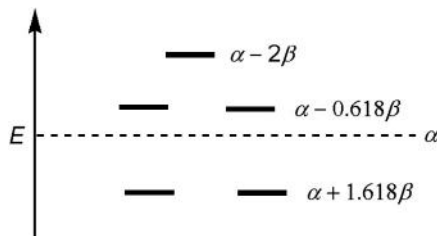


Fig. 1.36 MO Energy diagram for Möbius π electron system ($n = 5$, odd).

It is easy to see that this energy pattern for $n = \text{odd}$ also predicts that the 4-electron system is aromatic and the 6-electron system is antiaromatic.

The above results for the Möbius π electron systems to be aromatic or antiaromatic are summarized as given below:

Number of electrons	Möbius system
$4n$	Aromatic
$4n + 2$	Antiaromatic

1.7.2.2 Remarks

Molecules with Möbius topology has been synthesized.¹⁹ Large and flexible π systems appear to be more suitable for Möbius aromatic structures. In this text, we shall deal with Möbius transition structures, not molecules. The mechanistic approach involving Hückel/Möbius topology of pericyclic transition structures will be described in Chapter 3.

REFERENCES

1. Streitwieser, A., Jr. *Molecular Orbital Theory for Organic Chemists*. Wiley: New York, 1961.
2. Fleming, I. *Molecular Orbitals and Organic Chemical Reactions*; Student Edition; Wiley: Chichester, 2009. Reference Edition, 2010.
3. Jorgensen, W. L.; Salem, L. *The Organic Chemist's Book of Orbitals*; Academic Press: New York, 1973.
4. Atkins, P. W.; Friedman, R. S. *Molecular Quantum Mechanics*, 4th ed.; Oxford University Press: Oxford, 2005.

5. Slater, J. C. *Quantum Theory of Atomic Structure*. McGraw-Hill: New York, 1960; Vol. 1206.
6. Berson, J. A. *Angew. Chem. Int. Ed. Engl.* **1996**, *35*, 2751.
7. Coulson, C. A. *Proc. R. Soc. Lond.* **1939**, *A169*, 413.
8. Fleming, I. *Molecular Orbitals and Organic Chemical Reactions: Student Edition*; Wiley: Chichester, 2009; p. 301.
9. Houk, K. N. *J. Am. Chem. Soc.* **1973**, *95*, 4092.
10. Houk, K. N. *Acc. Chem. Res.* **1975**, *8*, 361.
11. Anh, N. T. *Frontier Orbitals: A Practical Manual*. Wiley: Chichester, 2007; p. 209.
12. Anh, N. T. *Frontier Orbitals: A Practical Manual*. Wiley: Chichester, 2007; p. 33.
13. Paddon-Row, M. N.; Gell, K.; Warrener, R. N. *Tetrahedron Lett.* **1975**, 1975.
14. Houk, K. N.; George, J. K.; Duke, R. E., Jr. *Tetrahedron* **1974**, *30*, 523.
15. Gleiter, R.; Haberhauer, G. *Aromaticity and Other Conjugation Effects*; Wiley-VCH: Weinheim, 2012.
16. Ermer, O.; Heilbronner, E. *Angew. Chem. Int. Ed. Engl.* **1983**, *22*, 402.
17. Borden, W. T.; Davidson, E. R.; Hart, P. *J. Am. Chem. Soc.* **1978**, *100*, 388.
18. Heilbronner, E. *Tetrahedron Lett.* **1964**, 1923.
19. Ajami, D.; Oeckler, O.; Simon, A.; Herges, R. *Nature* **2003**, *426*, 819.

CHAPTER 2

Stereochemical Concepts

A basic knowledge of static and dynamic stereochemistry¹ is a prerequisite for the study of pericyclic reactions. In this context, a brief introduction of some stereochemical representations, terms, descriptors and rules is presented in this chapter to facilitate the understanding and depiction of the stereochemical outcome of pericyclic reactions.

2.1 STEREOGENIC CENTRE

Most commonly, a stereogenic centre or stereocentre is a chiral centre, which is a tetrahedral sp^3 atom (usually C) attached to four different ligands. For the drawing of the tetrahedral structure, the following convention is adopted in this text: a bold bond in wedged form indicates a front (up) ligand, whereas a hashed bond in untapered form indicates a rear (down) ligand (see Fig. 2.1).

2.1.1 Stereocentre Configuration

The configuration at a stereocentre is defined by the *relationships* among any three ligands. Two ligands are connected by a *clockwise* (or *anticlockwise*) arrow through a tetrahedral angle when the third becomes a *front* (or *rear*) ligand.² Note that the geometry of the fourth ligand will be automatically fixed as front or rear in the tetrahedral space, i.e. if the third ligand is in front, the fourth ligand must be in rear. This definition of stereocentre configuration is represented in Fig. 2.1. 1, 2, 3 and 4 denote four ligands attached to the stereocentre, and any two of them can be chosen for the arrow relationship, as illustrated in Fig. 2.1. In Fig. 2.1A, 1→2 is clockwise when 3 is in front; equivalently, 3→4 can be drawn clockwise when 1 is in front as shown in Fig. 2.1B.

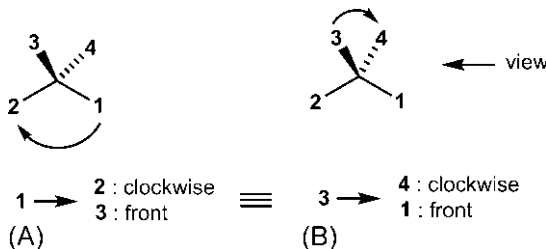
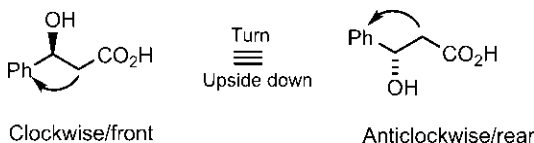


Fig. 2.1 Configuration defined at a stereocentre in terms of ligand relationships. (A) **1** and **2** are connected by a clockwise arrow when **3** is in front; (B) **3** and **4** are related by a clockwise arrow when **1** is in front. The configurations defined in (A) and (B) are equivalent.

For the set of three ligands, it is easy to see that
 clockwise/front \equiv anticlockwise/rear; clockwise/rear \equiv anticlockwise/
 front.

This is shown below with an example.



2.1.2 Relative Stereochemistry and Descriptors

The relative stereochemistry for diastereomers having two stereocentres can be designated by *threo/erythro* descriptors. Fig. 2.2 shows sawhorse representations of *threo* and *erythro* diastereomers for a general molecule $R^1CabCa'b'R^2$ in an eclipsed and a staggered conformation. $R^1-C-C-R^2$ is the main carbon chain; the ligand *a* being similar to *a'*, and *b* to *b'*. For the eclipsed conformation, the torsion angle (ϕ) for the bonds R^1-C and $C-R^2$ is 0 degrees, and $\phi=180$ degrees for the staggered conformation. In these representations when $\phi=0$ degrees (eclipsed) and $\phi=180$ degrees (staggered), the ligands in an antirelationship become *syn*, and vice versa on going from an eclipsed to a staggered conformation. When $R^1=R^2$, *erythro* becomes *meso*.

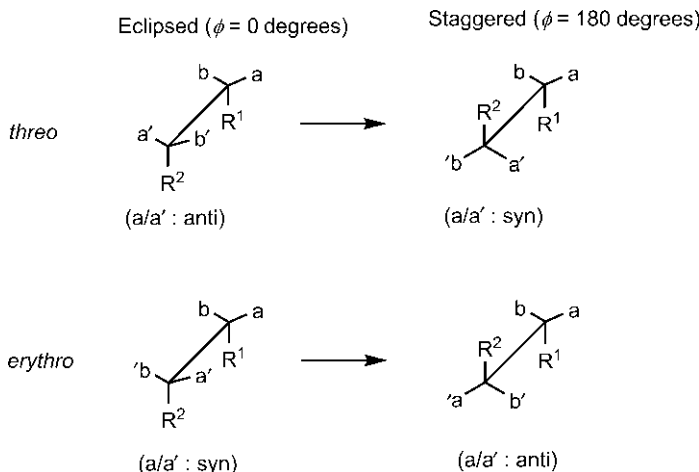


Fig. 2.2 Sawhorse representations of *threo* and *erythro* diastereomers.

The staggered conformation is more stable than an eclipsed conformation, and there are two more staggered conformations corresponding to $\phi = \pm 60$ degrees for each diastereomer (draw them).

In pericyclic reactions, the acyclic diastereomers are often drawn in eclipsed flying wedge and staggered zigzag representations. The diastereomers in the eclipsed wedge formula are designated as *threo/erythro* descriptors, whereas in a zigzag representation, *syn/anti* descriptors are used (the *syn/anti* as *descriptors* do not apply to an eclipsed formula, though two groups may hold a *syn* or *antirelationship* in an eclipsed structure). The translation of an eclipsed wedge formula to a staggered zigzag formula is shown in Fig. 2.3. Note that the main carbon chain (1-2-3-4) is eclipsed in the wedge formula and staggered in the zigzag formula. For the translation, consider any stereocentre, say 3 and its configuration defined by clockwise/rear as shown. Then draw a zigzag chain using a clockwise/rear or equivalent anticlockwise/front for the stereocentre 3. Write a final zigzag formula with Me/Me *syn* (descriptor) at the two stereocentres because the Me/Me relationship is *anti* (not descriptor) in the eclipsed formula. (The detailed procedure is only an aid to understanding; the translation can be done straightway.) It is important to note that the translation gives the correct absolute configuration that is, the same enantiomer of the chiral diastereomer.

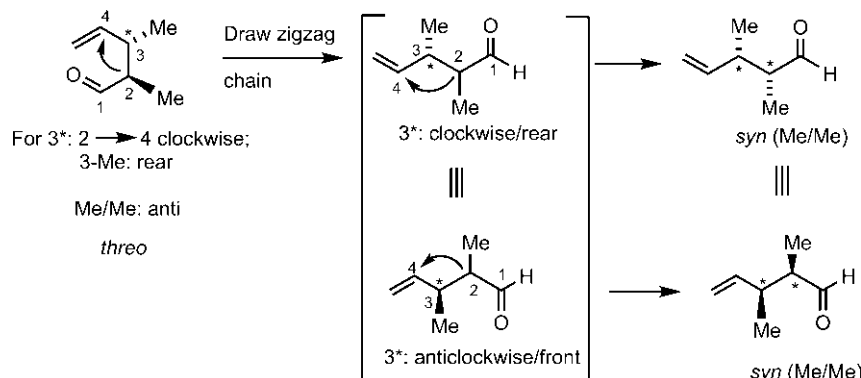
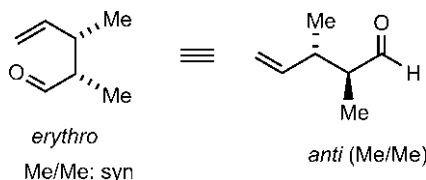


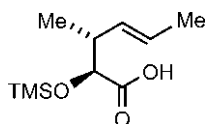
Fig. 2.3 Translation of the eclipsed flying wedge formula to the staggered zigzag formula and the consequent change in the descriptor.

Similarly, the *erythro* isomer corresponds to an *anti* diastereomer:



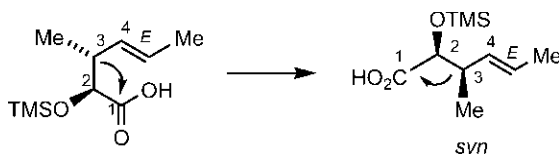
Problem 2.1

Draw the zigzag representation of the following optically active compound and designate it by a *syn/anti* descriptor.



Answer

The compound is a *syn* diastereomer as the following translation shows. The stereocentre configuration at 2 is defined by $3 \rightarrow 1$ clockwise with an OTMS front. The anti Me/OTMS changes to *syn* in the staggered zigzag formula. The stereochemistry of the double bond would remain the same.



2.1.3 Cyclic Conformation

The preferred cyclic conformation of a cyclohexane ring is chair conformation with axial (a) and equatorial (e) bonds (Fig. 2.4). The drawing of a chair indicates the joining of staggered sawhorse structures. Note the M- and W-shapes (highlighted in bold in a separate drawing) for equatorial bonds at C-6, C-2 and at C-5, C-3, respectively.

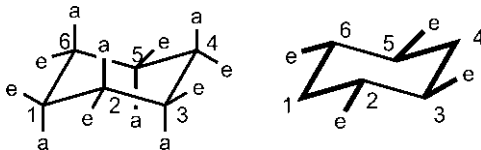


Fig. 2.4 Chair conformation of cyclohexane.

There are two possible chair conformations for a substituted cyclohexane as shown with a *trans*-1,2-disubstituted cyclohexane in Fig. 2.5. Note the up/down relationship of substituents which is maintained throughout. Here the two chair conformations are distinguishable as (a, a) and (e, e) conformations.

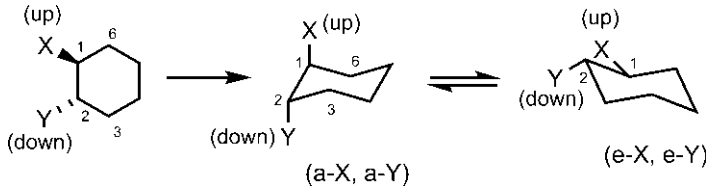
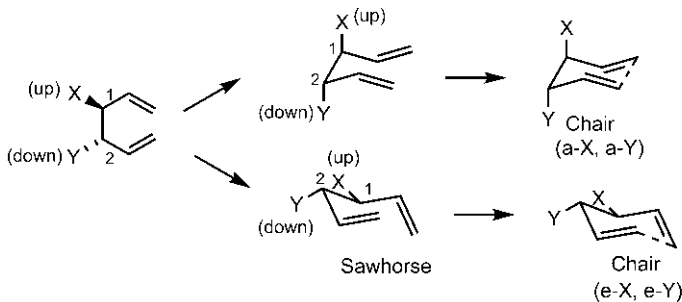


Fig. 2.5 Planar representation and chair conformations of *trans*-1,2 disubstituted cyclohexane.

Pericyclic reactions such as Cope and Claisen rearrangements usually involve a chair transition structure. The two possible chair transition structures from an acyclic substrate can be easily drawn by either Method 1 or Method 2 as delineated in Fig. 2.6. In each method, the eclipsed wedge formula is translated into a staggered sawhorse structure that straightway leads to the chair transition structure. The up/down substituents are maintained throughout the process.

Method 1



Method 2

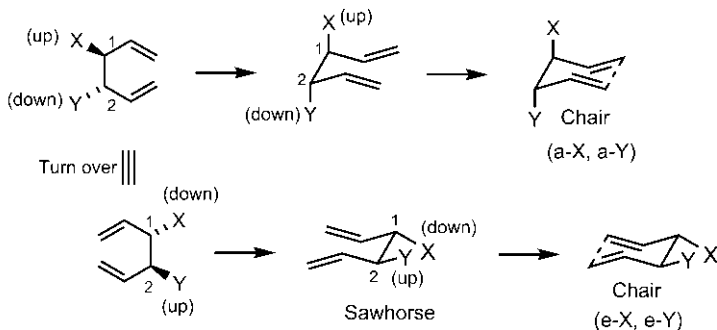


Fig. 2.6 Drawing of two possible chair transition structures starting from an acyclic substrate.

In the bicyclic decalin system, two chair conformations can be *trans* fused (cf. *trans*-1,2-dimethylcyclohexane) or *cis* fused (cf. *cis*-1,2-dimethylcyclohexane) (Fig. 2.7). Such a two-chair bicyclic transition structure is also involved in pericyclic processes.

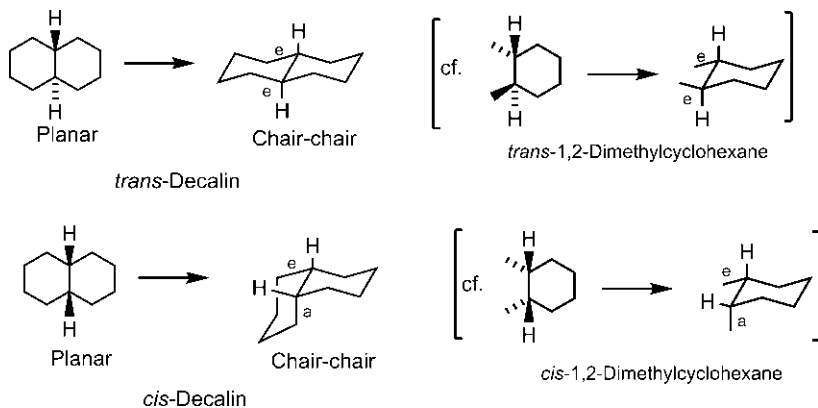


Fig. 2.7 Two-chair conformations of *trans*-decalin and *cis*-decalin.

Besides chair conformation, pericyclic reactions can also proceed through the boat transition structure. The boat conformation of cyclohexane is drawn in two equivalent representations in Fig. 2.8. a' and e' denote pseudoaxial and pseudoequatorial bonds, respectively. The flagpole bonds at C-1 and C-4 are indicated.

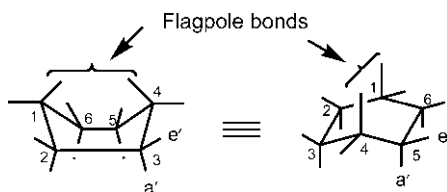


Fig. 2.8 Boat conformation of cyclohexane.

The two possible boat conformations of the transition structure from an acyclic substrate can be drawn as shown in Fig. 2.9 (cf. Method 2 of Fig. 2.6). The eclipsed wedge formula is translated into an eclipsed sawhorse representation that directly gives boat transition structures. The up/down substituents are maintained throughout.

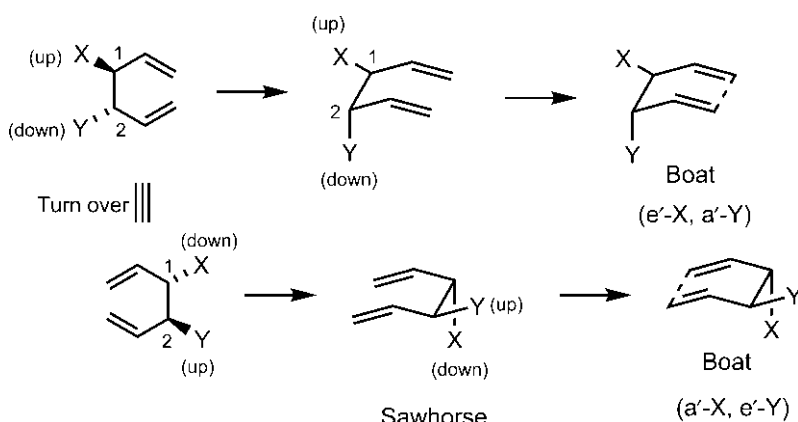


Fig. 2.9 Drawing of two possible boat transition structures from an acyclic substrate.

2.1.4 Relative Stereochemistry in Reactions

The reaction at a stereocentre generally involves the replacement of an old ligand with a new ligand, say 4 by $4'$ as



(Note that the new ligand in the product is labelled by affixing prime (') to the old number.) The relative stereochemistry of the product is described by retention or inversion of configuration at the stereocentre. If the spatial disposition of the ligands **1**, **2**, **3** and **4'** in the product is the same as that of **1**, **2**, **3** and **4** in the reactant, there is retention and, if different, there is inversion. The product stereochemistry as a result of retention or inversion of configuration could be easily delineated in terms of the number of changes in ligand relationships as indicated in Fig. 2.10.²

Change of relationship (reactant → product)	
I. Clockwise → anticlockwise (or anticlockwise → clockwise)	One change : inversion
II. Front → rear (or rear → front)	No change or both changes : retention

Fig. 2.10 Rule for determination of inversion or retention of configuration based on the number of changes of ligand relationship from a reactant to a product.

Pericyclic reactions can involve the migration of a group with inversion or retention at the migrating stereocentre. The product stereochemistry of such rearrangements is easily drawn using the above rule, as illustrated with the following examples.

Fig. 2.11 shows a thermal [1,3] sigmatropic rearrangement that occurs with inversion of configuration at the migrating centre (C^*). The bond to **1** is broken. For the reactant, $\text{H} \rightarrow \text{Me}$ is *clockwise* with **1** in the *front*. The stereochemistry of the product is depicted as: with **1'** in the *rear*, $\text{H} \rightarrow \text{Me}$ must be *clockwise* (inversion ⇒ one change). It should be noted that *exo*-Me in the reactant remains *exo*-Me in the product as a result of inversion of configuration.

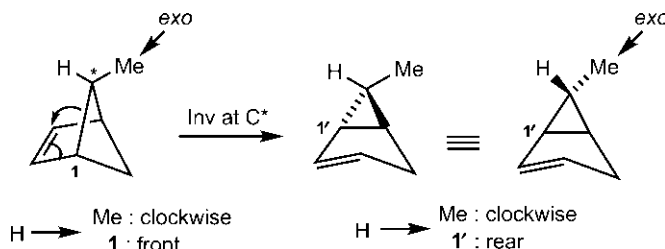


Fig. 2.11 Delineation of product stereochemistry as a result of inversion of configuration at a migrating stereocentre.

A thermal [1,5] sigmatropic rearrangement with retention of configuration is shown in Fig. 2.12. The bond to **1** is broken. For the reactant, X → Y is *clockwise* with **2** in the *rear*. The stereochemistry of the product is drawn as: with **2** in the *front*, X → Y must be *anticlockwise* (retention ⇒ both changes). Note that *endo*-X becomes *exo*-X in the product as a result of retention of configuration.

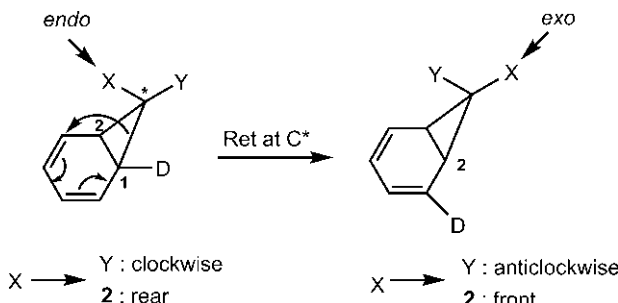


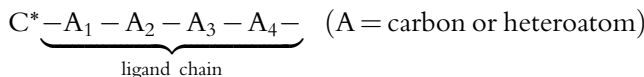
Fig. 2.12 Delineation of product stereochemistry as a result of retention of configuration at a migrating stereocentre.

2.1.5 Absolute Stereochemistry and Descriptors

The absolute stereochemistry to a stereocentre is specified by the *R* or *S* descriptor. The assignment of a descriptor requires a priority sequence of four ligands which is determined primarily by the CIP sequence rule: *higher atomic number precedes lower*. To apply this rule, several CIP subrules involving rather complicated schemes have been developed. Instead of those subrules, an alternative approach to determining ligand priority order is described here.³

2.1.5.1 Mandal's Approach to Determining Ligand Priority

The ligands are treated in their normal bonding connectivity. A ligand chain denotes a chain of the first atom (directly linked to stereocentre C*) and outward atom(s) as indicated below.



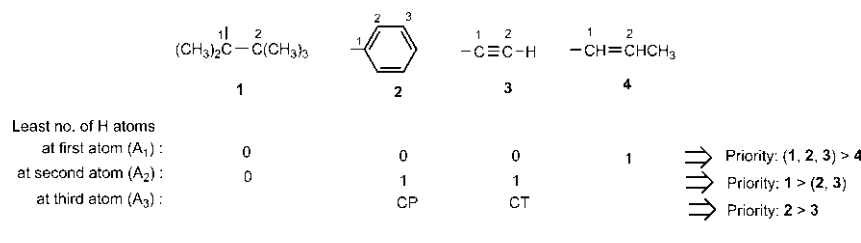
(A_1 = first atom, A_2 = second atom and so on)

A decision on ligand priority is reached at the earliest possible atom in a ligand chain based on the following ‘application rules.’

1. Count the number of C—O/C—N bonds at the first/similar outward carbon in the ligands, taking a double bond as two bonds and a triple bond as three bonds. The rule is: *greater number of bonds gives higher priority.* (C—O bond gets precedence over C—N bond).
2. Count the *least* number of H atoms attached to a similar atom in ligand chains. The rule is: *the fewer the number of H atoms, the higher is the priority.*
3. If the rule of H atoms cannot provide a decision, then compare as to whether a ligand possesses the next outward atom (chain propagation) or does not possess the next outward atom (chain termination). The rule is: *chain propagation (CP) precedes chain termination (CT).*

(If the ligand priority order can be obtained straightway on the basis of atomic number of the first/outward atom, no other rules need apply.)

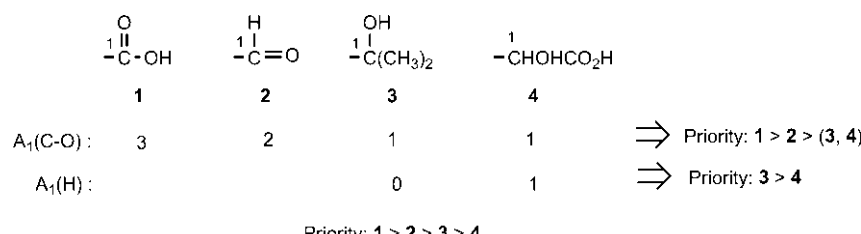
Let us now consider a set of four ligands given in Fig. 2.13. The priority order can be decided by the rule of hydrogen (rule 2) and the rule of CP vs CT (rule 3).



Priority: 1 > 2 > 3 > 4

Fig. 2.13 Ligand priority order using rule of hydrogen (rule 2) and rule of CP vs CT (rule 3).

Another set of ligands is shown in Fig. 2.14, for which the priority order is determined by rule 1 and rule 2.



Priority: 1 > 2 > 3 > 4

Fig. 2.14 Ligand priority order using rule 1 and rule 2.

(Figs 2.13 and 2.14 show a detailed illustration of the rules only as an aid to understanding; once understood, the ligand priority can be decided at a glance.)

In many cases, the ligand priority can be simply determined on the basis of the rule of hydrogen. Two examples are given in Fig. 2.15. Note that only one stereocentre (marked *) is considered in each case.

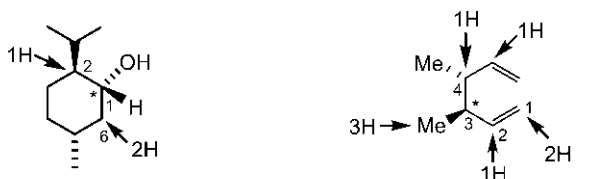


Fig. 2.15 Ligand priority order using rule of hydrogen (rule 2) only.

2.1.5.2 Assignment of the R/S Descriptor

If the priority order of four ligands (a, b, c and d) attached to a stereocentre is $a > b > c > d$, the absolute configuration (*R* or *S*) to the stereocentre is specified as follows. When the molecule is viewed away from the lowest priority ligand (d), the configuration is *R* if $a \rightarrow b \rightarrow c$ traces clockwise, and *S* if $a \rightarrow b \rightarrow c$ traces anticlockwise. Thus, as shown in Fig. 2.16A, the configuration at C-3 is *R*. The opposite is true when the molecule is viewed from the side of d; the descriptor is *R* if the array $a \rightarrow b \rightarrow c$ is anticlockwise, and *S* if $a \rightarrow b \rightarrow c$ traces clockwise. This is exemplified in Fig. 2.16B when the configuration at C-4 is *R*. Fig. 2.16C shows the absolute configuration at C-3 and C-4 determined as (3*R*, 4*R*) for an enantiomer of *trans*-3,4-dimethylhexa-1,5-diene.

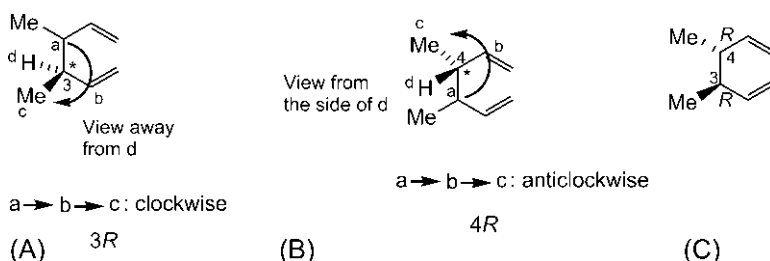
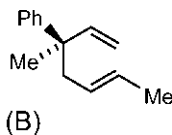
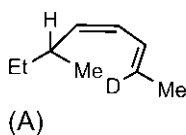


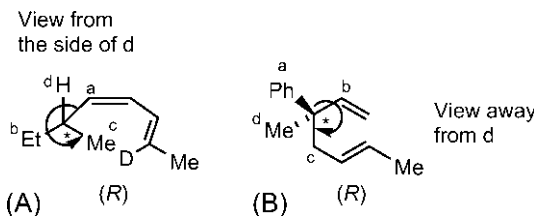
Fig. 2.16 Assignment of the *R/S* descriptor to an enantiomer of *trans*-3,4-dimethylhexa-1,5-diene. (A) Descriptor determined at C-3; (B) descriptor determined at C-4; (C) descriptors shown at C-3 and C-4 as determined.

Problem 2.2

Assign the *R/S* descriptor to the following molecules.

**Answer**

The descriptor is *R* in each case. The ligands are labelled a, b, c and d, with the priority $a > b > c > d$.



Since the stereocentres are represented in diverse projection or perspective formulas such as Fischer, flying wedge, zigzag, sawhorse, Newman, planar cyclic structure and cyclic conformation, the assignment of descriptors is often difficult. In this context, a unified method is described here for assigning descriptors to stereocentres in any stereochemical representation.³ In this method, a stereocentre in any stereochemical formula is transformed into an equivalent Fischer projection as shown in Fig. 2.17. (See Fig. 2.1 for stereocentre configuration.)

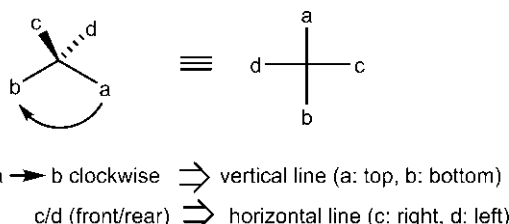


Fig. 2.17 Mandal's mnemonic for transformation of a 3D formula into a Fischer projection.

The assignment of an *R/S* descriptor is then straightforward and simple. If the lowest priority ligand is on the vertical line, the array of the remaining three in descending priority sequence gives the correct descriptor, *R* for clockwise and *S* for anticlockwise; but if the lowest priority ligand is on the horizontal line, the opposite assignment is correct.

This procedure is illustrated using four stereochemical representations, namely flying wedge (a), sawhorse (b), Newman (c) and planar cyclic structure (d) in Fig. 2.18. In (a), the three ligands H, D and T are isotopes and have the same atomic number. Their relative priority is therefore determined on the basis of mass number; higher mass number precedes lower. In (b), (c) and (d), there are two stereocentres of which one is assigned the descriptor. (Try for yourself to assign the descriptor to the other stereocentre.) Note that the ligands are labelled a, b, c and d, with the priority $a > b > c > d$.

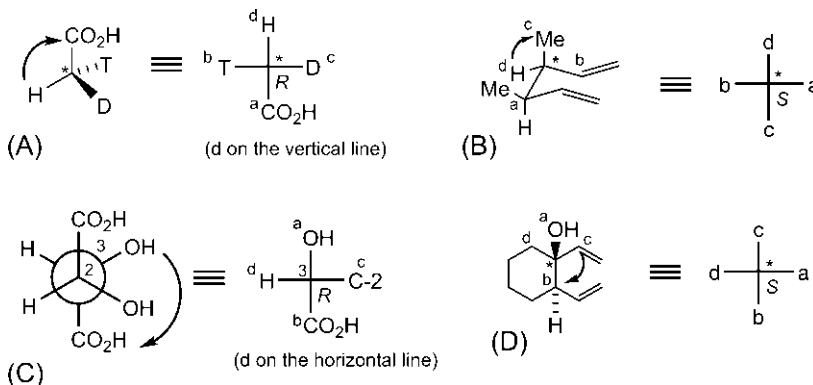
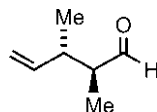


Fig. 2.18 Assignment of an *R/S* descriptor to a stereocentre using Mandal's mnemonic in (A) flying wedge, (B) sawhorse, (C) Newman, and (D) planar cyclic representations.

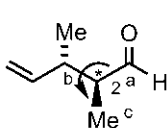
Problem 2.3

Assign an *R/S* descriptor to the following molecule directly from the zigzag structure, and also by using the Fischer projection method.



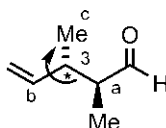
Answer

The descriptor is $2S, 3S$. The ligands are labelled a, b, c and d, with the priority $a > b > c > d$.



View away from rear H (d)

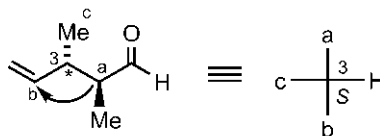
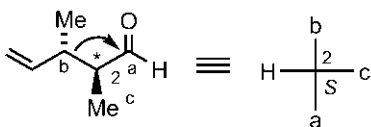
$a \rightarrow b \rightarrow c$: anticlockwise
2S



View from the side of front H (d)

$a \rightarrow b \rightarrow c$: clockwise
3S

R/S descriptor from zigzag formula



R/S descriptor using Fischer projection method

2.2 STEREOGENIC AXIS

A stereogenic axis or stereoaxis is a line connecting two atoms, each of which is linked to a pair of different ligands. Unlike four different ligands at a stereocentre, the two ligand pairs at the two ends of a stereoaxis may be the same or different.

A stereoaxis may be chiral or achiral. If the two ligand pairs are noncoplanar, and lie in orthogonal planes, the stereoaxis becomes chiral (Fig. 2.19A). The molecules such as allenes, biphenyls and related systems possessing a chiral axis exhibit enantiomerism depicting the axial *R*/axial *S* configuration. On the other hand, the two ligand pairs become coplanar for an achiral stereoaxis (Fig. 2.19B). The double-bond systems such as alkenes possessing an achiral axis exhibit diastereomerism depicting the *E/Z* configuration.

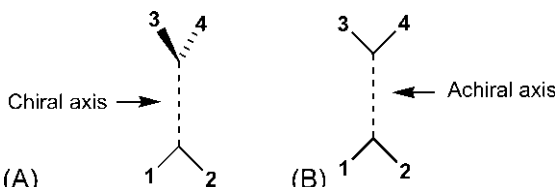


Fig. 2.19 (A) Chiral stereoaxis and (B) achiral stereoaxis. **1, 2, 3** and **4** denote ligands.

2.2.1 Chiral Axis Descriptors

For assigning a chiral axis configuration, a simple approach based on a directional relationship between two arrows, each joining two ligands at either end of the stereoaxis, is presented here.⁴ The procedure is depicted in Fig. 2.20. The chiral axis is defined by two atoms X and Y, each linked to a ligand pair (h, l) where h and l denote higher-priority and lower-priority ligands, respectively. A clockwise/anticlockwise h → l arrow is drawn through the bond angle for each (h, l) pair. As shown in Fig. 2.20, the arrow for the (h, l) pair in the perpendicular plane is to be drawn viewing from the right side.

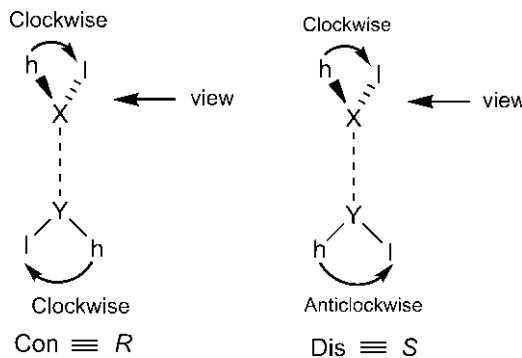


Fig. 2.20 Assignment of a chiral axis configuration.

The chiral axis configuration is specified as Con (when both arrows are clockwise or anticlockwise) or Dis (when one arrow is clockwise and the other anticlockwise). Con and Dis correspond, respectively, to the descriptors *R* and *S* for a chiral axis.

The drawing of the correct h → l arrow in the perpendicular plane might be difficult in some cases. To address this issue, the following mnemonic has been put forward:

h (front) ⇒ h → l clockwise

h (rear) ⇒ h → l anticlockwise

The above procedure is illustrated with an allene and a 2,2'-binaphthol (BINOL) in Fig. 2.21.

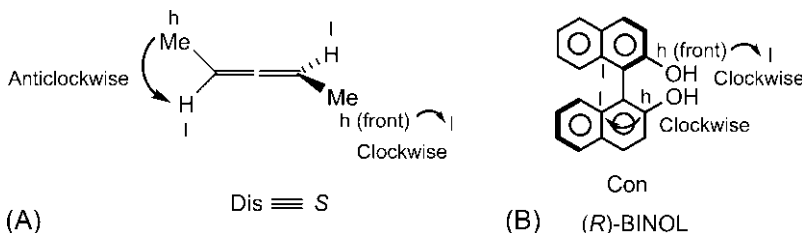


Fig. 2.21 Assignment of a chiral axis descriptor to (A) an allene and (B) a 2,2'-binaphthol. See the mnemonic.

2.2.2 Achiral Axis Descriptors

The assignment of *E/Z* descriptors for an achiral alkene axis is straightforward and simple. If two higher-priority ligands are on the same side of the double bond, the configuration is *Z*; otherwise, it is *E*. This is depicted with an example in Fig. 2.22.

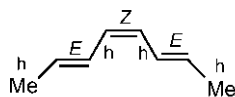
(2*E*,4*Z*,6*E*)-2,4,6-Octatriene

Fig. 2.22 Assignment of an *E/Z* descriptor to a triene.

2.3 ENANTIOTOPIC AND DIASTEREOTOPIC FACES

The two faces of a carbonyl double bond can be enantiotopic or diastereotopic if the carbonyl group is prochiral. A prochiral carbonyl group is attached to two unlike ligands and generates a chiral centre on addition to the trigonal carbon. If the addition to the two carbonyl faces gives enantiomeric products, the faces are enantiotopic, and if the products are diastereomeric, the faces are diastereotopic.

The two carbonyl faces are designated by *re/si* descriptors. A carbonyl face is a plane defined by three ligands, with priority $a > b > c$. If the sequence $a \rightarrow b \rightarrow c$ is clockwise, it is the *re* face, and if it is anticlockwise, it is the *si* face. This is illustrated with two carbonyl faces of benzaldehyde in Fig. 2.23. The descriptor for the front face is easy to assign: the sequence O → Ph → H is anticlockwise, and hence *si*. A direct view of the rear face is difficult; the molecule can be turned upside down and then viewing from the front gives an *re* descriptor for the rear face. It should be noted that the two faces must have opposite descriptors; easy assignment of a descriptor to one face automatically gives the opposite descriptor to the other face which may sometimes be difficult to observe directly.

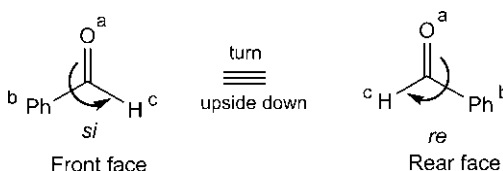


Fig. 2.23 Assignment of *re/si* descriptors to carbonyl faces of benzaldehyde.

Fig. 2.24 illustrates the enantiotopic and diastereotopic faces showing the products resulting from attack on the *re* face and *si* face. The *re/si* faces are enantiotopic when the carbonyl compound is achiral (**Fig. 2.24A**), and are diastereotopic for a chiral substrate (**Fig. 2.24B**). It is seen that the *si* face addition involves a nucleophilic attack on the front face and an *re* face addition on the rear face in both cases, creating a new chiral centre (*R* or *S*).

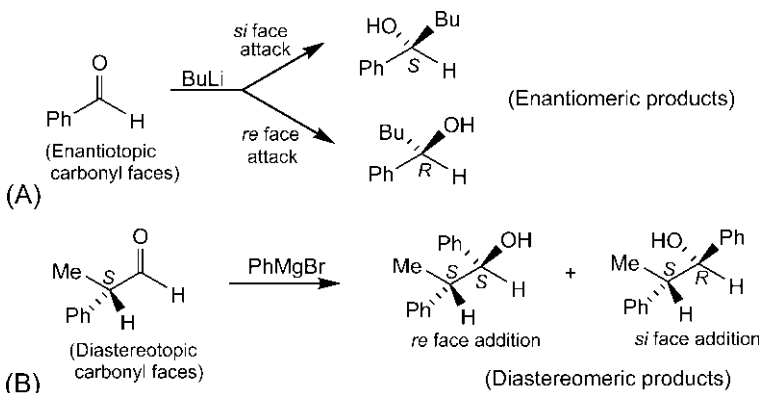


Fig. 2.24 Formation of a new chiral centre from the *re* face and *si* face addition to (A) enantiotopic carbonyl faces and (B) diastereotopic carbonyl faces.

Like carbonyl faces, the two faces of an alkene double bond can also be enantiotopic or diastereotopic. The *re/si* descriptors to the two alkene faces in respect of a trigonal α -carbon are shown in **Fig. 2.25A**. The top face or bottom face addition is indicated by a dashed line. Here the two faces are enantiotopic. The top face can be observed directly and its descriptor in respect of α -carbon is easily assigned as α -*si*. The bottom face is however difficult to observe directly but it holds a mirror image relationship to the top face and its descriptor must be opposite, i.e. α -*re*. If the ester group is chiral (CO_2R^*), the faces become diastereotopic. The *re/si* descriptors also apply to both trigonal carbons (α and β), as shown for the top face in **Fig. 2.25B**.

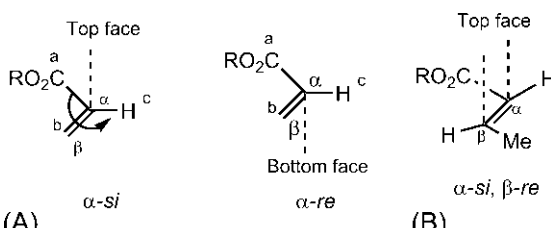


Fig. 2.25 *re/si* Descriptors to (A) top and bottom faces of an alkene with respect to α -carbon and (B) top face of another alkene with respect to α - and β -carbons.

2.4 STEREOSPECIFIC AND STEREOSELECTIVE REACTIONS

The terms ‘stereospecific’ and ‘stereoselective’ are often confusing, as these are defined in a number of ways. We shall use the terms on a mechanism basis as described below.

A reaction can take place by a mechanism which has a strict stereochemical requirement for an efficient, symmetry-allowed orbital overlap. If that mechanism leads to a single and specific product stereochemistry from a particular stereochemistry of the starting material, the reaction is stereospecific. For example, the supra/supra mechanism of the Diels–Alder reaction (supra-facial for both diene and dienophile) leads to its stereospecificity. A specific diastereomeric product is formed from a particular reactant stereochemistry: the (*E,E*) diene gives a *cis* product, whereas the (*E,Z*) diene yields a *trans* product as shown in Fig. 2.26. For details, see Chapter 5 and Section 5.1.1.

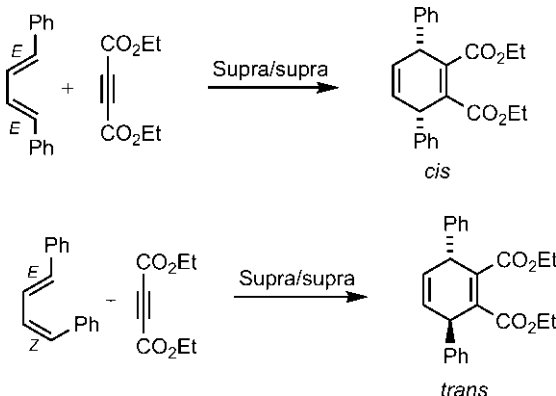


Fig. 2.26 Stereospecific Diels–Alder reactions.

In contrast, for a stereoselective reaction, the mechanism does not prevent the formation of two or more stereoisomeric products. This arises when the mechanism allows for two or more possible conformations/geometries of the transition structure. Usually one product predominates and the reaction becomes stereoselective. For example, the supra/supra mechanism of the Diels–Alder reaction can involve *endo* or *exo* geometry of the transition structure, and a mixture of *endo* and *exo* isomers are formed (Fig. 2.27). When $a = \text{NEt}_2$ and $b = \text{CO}_2\text{Et}$, the major product is an *endo* adduct. For details, see Chapter 5 and, Section 5.1.2. Note that the above definitions would allow many reactions to be described as both stereospecific and stereoselective, like the Diels–Alder reaction.

If the stereoisomeric products of a stereoselective reaction are diastereomeric, the reaction is said to be diastereoselective. If the stereoisomeric products are enantiomeric, and one of the enantiomers is formed in excess,

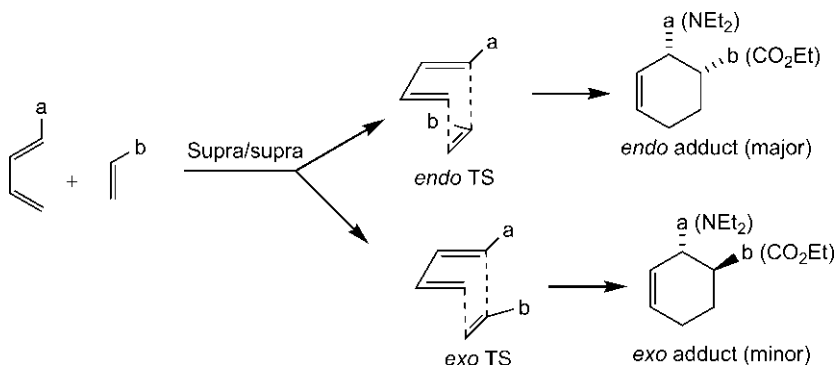


Fig. 2.27 Stereoselective Diels–Alder reaction.

the reaction is called enantioselective, also known as asymmetric synthesis. To put it more succinctly, diastereoselective synthesis is the synthesis of a diastereomer; asymmetric (or enantioselective) synthesis is the synthesis of an enantiomer.

2.4.1 Free Energy Diagram for Stereoselectivity

If the two possible transition structures of a reaction are enantiomeric, they are of equal energy and the two products are formed at the same rate. Under kinetic control, the two products would be obtained in equal amounts, and there is no selectivity. Thus, for a stereoselective reaction, the reaction must proceed through diastereomeric transition structures (TS_1 and TS_2) of differing energies as indicated in Fig. 2.28. Under kinetic control, the faster formed product (P_1) via a lower energy transition structure (TS_1) would be formed as a major product.

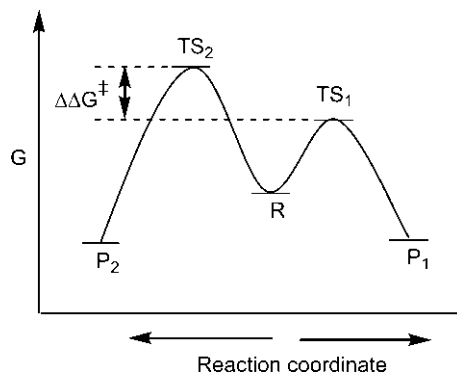


Fig. 2.28 Free energy diagram of a stereoselective reaction involving diastereomeric transition structures. R stands for reactant(s), P_1 and P_2 denote two products, and TS_1 and TS_2 indicate two transition structures. $\Delta\Delta G^\ddagger$ is the difference in free energy between TS_2 and TS_1 .

It is important to appreciate that both diastereoselective and enantioselective reactions must involve diastereomeric transition structures. For diastereoselective reaction, the diastereomeric transition structures directly lead to diastereomeric products. In case of enantioselective reaction, diastereomeric transition structures may either give diastereomeric compounds that are converted into enantiomeric products by a simple but separate cleavage reaction or give diastereomeric complexes which on dissociation lead to enantiomeric products.

The ratio of the two products $[P_1]/[P_2]$, is related to the difference in free energy between the two transition structures ($\Delta\Delta G^\neq$), and is given by

$$\frac{[P_1]}{[P_2]} = e^{\frac{\Delta\Delta G^\neq}{RT}} \quad (2.1)$$

For diastereoselective reaction, the extent of diastereoselectivity is given by the diastereomer ratio (dr), or by diastereomeric excess (de) which denotes the excess of one diastereomer over the other. In case of enantioselective reaction, enantioselectivity is expressed as enantiomeric excess (ee), that is, the excess of one enantiomer over the other.

The extent of diastereoselectivity or enantioselectivity in terms of $\Delta\Delta G^\neq$ values at 25°C (298 K), as estimated using Eq. (2.1), is given in Table 2.1. It is seen that a free energy difference of only 11.4 kJ mol⁻¹ or 2.72 kcal mol⁻¹ would favour the major product to the extent of 99:1 (de or ee 98%).

Table 2.1 Extent of stereoselectivity as a function of $\Delta\Delta G^\neq$ at 298 K

$\Delta\Delta G^\neq$ (kJ mol ⁻¹)	$P_1:P_2$ (dr)	de or ee (%)
0	1:1	0
2.72	3:1	50
5.44	9:1	80
7.30	19:1	90
11.4	99:1	98
17.1	999:1	99.8

Eq. (2.1) also indicates that the product ratio depends on temperature; lowering of temperature leads to an increase in selectivity (Table 2.2).

Table 2.2 Extent of stereoselectivity as a function of temperature

Temperature	$\Delta\Delta G^\neq$ (kJ mol ⁻¹)	$P_1:P_2$ (dr)
25°C (298 K)	8.0	25:1
-78°C (195 K)	8.0	139:1

REFERENCES

1. Eiel, E. L.; Wilen, S. H.; Mander, L. N. *Stereochemistry of Organic Compounds*; Wiley: New York, 1994.
2. Mandal, D. K. *J. Chem. Educ.* **2007**, *84*, 274.
3. Mandal, D. K. *J. Chem. Educ.* **2000**, *77*, 866.
4. Mandal, D. K. *Bull. Chem. Soc. Jpn.* **2002**, *75*, 365.

CHAPTER 3

Pericyclic Reactions: Introduction, Classification and the Woodward–Hoffmann Rules

3.1 INTRODUCTION

An elegant approach to classifying organic reactions is based on mechanism. Broadly, there are three mechanistic classes: ionic, radical and pericyclic. As such, pericyclic reactions^{1–7} constitute a separate and distinct mechanistic class of organic reactions. A pericyclic mechanism is characterized by *concerted* bond-breaking and bond-forming processes with *cyclic* movement of electrons in a *single* transition structure (TS).^{8–10} *Concerted* implies that bond-breaking and bond-forming events are simultaneous (at the same time) but not necessarily synchronous (to the same extent). In fact, most pericyclic reactions are asynchronous. *Cyclic* movement of electrons signifies a cyclic overlap of interacting orbitals (cf. cyclic orbital overlap in an aromatic/antiaromatic system). A *single* TS indicates that no intermediate is involved. The electrons move around in a cycle or ring; the word pericyclic (the prefix *peri* meaning around) was introduced by Woodward and Hoffmann in 1969¹¹ to christen this class of reactions. The Diels–Alder reaction provides a classic example of a pericyclic reaction. The basic or prototype Diels–Alder reaction between butadiene and ethylene to produce cyclohexene is represented in Fig. 3.1, which involves the breaking of three π bonds and formation of two σ bonds and one π bond.

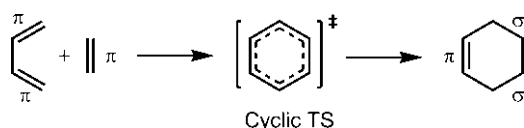
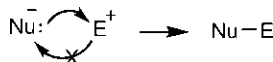


Fig. 3.1 A prototype Diels–Alder reaction between butadiene and ethylene.

Arrow formalism: It is usual to invoke arrow formalism to depict the mechanism of an organic reaction. An ionic mechanism is depicted by using curved (curly) arrows. For example, a bond-forming step between a nucleophile (Nu^-) and an electrophile (E^+) is represented as



Notice that a curved arrow in an ionic mechanism indicates two characteristics: the movement of an electron pair and the direction of electron flow. Now consider the curved arrow representation of the pericyclic mechanism of the Diels–Alder reaction as shown in Fig. 3.2.

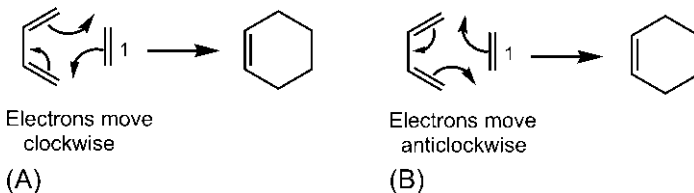


Fig. 3.2 Curved arrow representation of the Diels–Alder reaction. (A) Arrows move electrons clockwise and (B) arrows move electrons anticlockwise.

Clearly, unlike an ionic mechanism, an electron pair of a π bond (say, 1) can move in two possible directions, and overall the three arrows can move electrons clockwise (Fig. 3.2A) or anticlockwise (Fig. 3.2B) in a cyclic manner. Remember that this arrow representation is a formalism and electrons really do not rotate! Actually, the old bond orbitals are being transformed into new bond orbitals (see Chapter 11). Both curved arrow representations in Fig. 3.2 are valid, and imply that curved arrows in a pericyclic mechanism have no absolute sense of direction of electron flow. For this characteristic, the pericyclic reactions used to be called, somewhat flippantly, ‘no-mechanism reactions’.

There is more. If one component in the reaction is represented by a Lewis structure with a formal positive or negative charge on an atom, the curved arrow should begin from the negative charge and end on the positive charge. For example, consider a reaction between butadiene and the allyl cation to form a cycloheptenyl cation. The allyl cation canonical structure has a positive charge on C-1 or C-3, and any of the two canonicals can be used to draw a mechanism in which a curved arrow ends on a positive charge (Fig. 3.3). If the other canonical is chosen, the three arrows would move cyclically in the opposite direction.

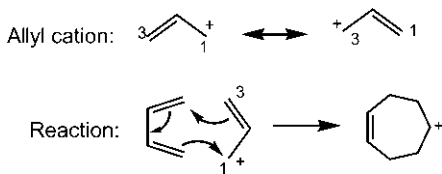


Fig. 3.3 Arrow representation of a reaction between butadiene and the allyl cation.

Another example is a reaction between a 1,3-dipole and ethylene to form a five-membered ring (Fig. 3.4). It makes sense if the arrows begin from the negative charge and end on the positive charge. Since the two ends of the dipole are electrophilic/nucleophilic, it is called a 1,3-dipole. Note that atom a or c bears the formal negative charge, and the arrows would move cyclically in the opposite direction if the other canonical is used.

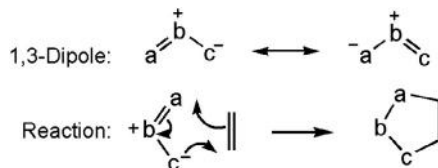


Fig. 3.4 Arrow representation of a reaction between a general 1,3-dipole and ethylene.

Notwithstanding the lack of directional sense of arrows in a pericyclic mechanism, the arrow formalism clearly indicates which old bonds are broken, and where new bonds are formed, and thus remains a useful tool to depict the pericyclic mechanism.

Number of curved arrows: In terms of the total number of electrons involved, pericyclic reactions fall into two types of electron systems:

$4n + 2$ electron system ($n = 0, 1, 2, \dots$) and a $4n$ electron system ($n = 1, 2, 3, \dots$).

Since each curved arrow involves 2 electrons, the number of curved arrows needed to write a mechanism = $\frac{1}{2}$ (total number of electrons).

The Diels–Alder reaction involves a total of 6 electrons ($4n + 2$, $n = 1$) and is therefore represented by three arrows (see Fig. 3.2). The 6-electron reactions in Figs 3.3 and 3.4 are also depicted by three arrows. (The 1,3-dipole in Fig. 3.4 is a 4-electron species.) On the other hand, the ring closing of butadiene to cyclobutene is a 4-electron ($4n$, $n = 1$) reaction, and hence is represented by two arrows (Fig. 3.5).

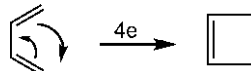


Fig. 3.5 Arrow representation of the ring closing of butadiene to cyclobutene.

3.1.1 A Pericyclic Versus Stepwise Ionic or Radical Mechanism

It is often not absolutely certain whether a reaction proceeds by a pericyclic or stepwise pathway. In the absence of theoretical and experimental evidences, one might write, besides a pericyclic mechanism, a *prima facie* reasonable stepwise ionic or radical mechanism for a reaction. For example, consider a Diels–Alder reaction between 1-methoxybuta-1,3-diene and acrolein (Fig. 3.6).

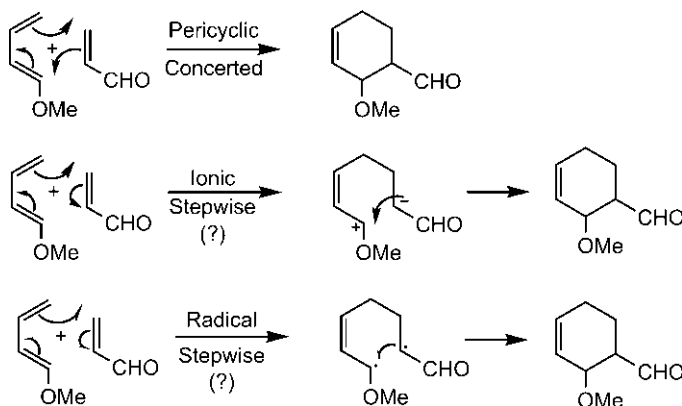


Fig. 3.6 Possible pericyclic, ionic and radical mechanisms of a Diels–Alder reaction.

It appears that the ionic mechanism could be reasonable as the cationic and anionic centres in the zwitterionic intermediate can be stabilized by an electron donating OMe and an electron withdrawing CHO substituent, respectively. The stepwise radical mechanism (notice the use of fishhook arrows for the movement of a single electron) by way of the diradical intermediate also seems to be reasonable as both electron donating and electron withdrawing groups can stabilize a radical centre. However, the Diels–Alder reaction proceeds by a pericyclic mechanism. The key to a pericyclic mechanism is the concertedness. It seems that the concerted process is highly favoured as this provides a pathway with the lowest energy barrier. This is supported by high-level molecular orbital calculations for the pericyclic TS.^{12–14}

The experimental evidences in favour of the concerted nature of the pericyclic reactions, especially Diels–Alder, have also been provided. The substituent and solvent effects on rates,^{15,16} kinetic isotope effect,¹⁷ and the estimate of very large negative entropy of activation¹⁸ support a concerted mechanism. The concertedness of bond-breaking and bond-forming events impose orbital symmetry restrictions that led to the development of the Woodward–Hoffmann rules for pericyclic reactions. For these reactions, these rules predict which reactions can take place and with what

stereochemistry. The stereochemical idiosyncrasies (thermodynamic/counter-thermodynamic stereochemistry) predicted by the concerted mechanism and supported by experiments provide fascinating aspects of pericyclic chemistry. These will be covered in the relevant chapters of this text.

The stepwise ionic pathway may be more competitive when the substituents can greatly stabilize the charges in the intermediate (Fig. 3.7A),¹⁹ and the radical pathway may get the preference if the radical centres in the intermediate are highly stabilized (Fig. 3.7B).²⁰ As shown in Fig. 3.7A, the positive charge is strongly stabilized by the powerful electron donating NMe₂ group while the negative charge resides on the electronegative oxygen atom. In Fig. 3.7B, the reaction does not proceed by the concerted pathway of a Diels–Alder reaction; rather, it takes the diradical pathway via a more stable diradical in which one radical centre is a stabilized allylic radical and the other centre is stabilized by α -chlorine and β -fluorine substituents (an α -chlorine can better stabilize a radical centre than an α -fluorine by p–p resonance and the stabilizing influence of β -fluorine is greater than that of β -chlorine by hyperconjugation). Butadiene exists mainly in the *s-trans* conformation, and since the diradical intermediates that could arise from *s-trans* and *s-cis* forms have similar stability, the radical pathway proceeds via the *s-trans* conformation without the energetic penalty associated with the *s-cis* form. Further, since bond rotations within the allyl unit are more

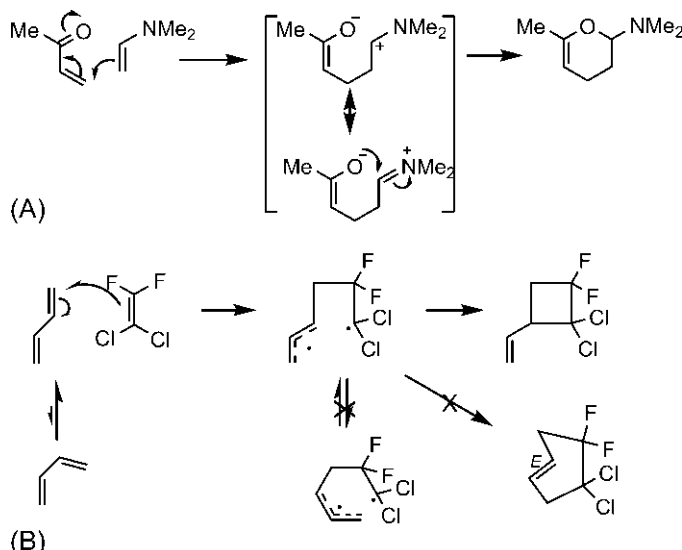


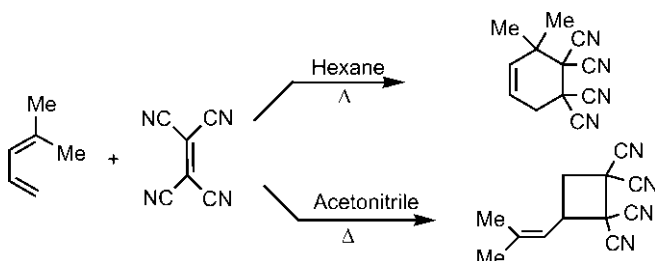
Fig. 3.7 Cycloaddition reaction via (A) ionic and (B) radical pathways.

restricted, the allyl radical is configurationally stable and the ring closing gives a four-membered ring instead of an impossibly strained six-membered ring with a *trans* double bond.

It is important to appreciate that pericyclic and stepwise pathways lie on a mechanistic spectrum linked by asynchronicity. At one extreme, there is a concerted and synchronous pathway with symmetrical TS, and at the other the stepwise mode. The pericyclic nature is retained with concertedness and some degree of asynchronicity. However, if the asynchronicity is too high so that one bond forms far ahead of the other, the concertedness breaks down and the pericyclic mechanism crosses over to the stepwise mode.

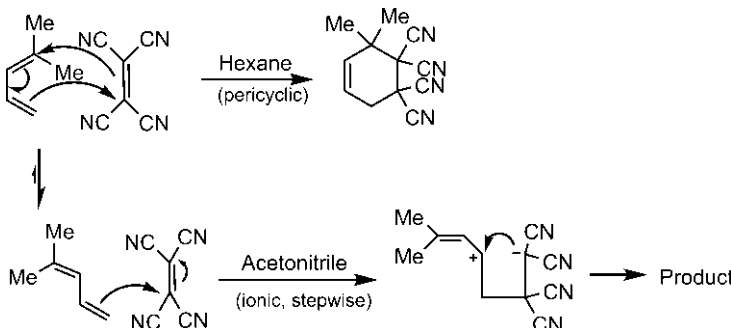
Problem 3.1

Account for the following observations.



Answer²¹

In the nonpolar solvent hexane, the Diels–Alder reaction is preferred and occurs by the pericyclic mechanism via the *s*-*cis* conformation of the diene. However, in the polar solvent acetonitrile, the stepwise ionic pathway is favoured via the *s*-*trans* conformation. The intermediate allyl cation is configurationally stable and the cyclization gives a four-membered ring instead of an impossibly strained *trans* cyclohexene. The solvent effect thus exhibits a delicately balanced, concerted and stepwise pathway for the reaction.



3.2 CLASSIFICATION

In a pericyclic reaction, the σ bond-breaking/-forming event is crucial as this determines the overall outcome of the reaction in terms of cyclization, ring opening or group migration. Pericyclic reactions are usually unimolecular or bimolecular, and fall into four major classes.⁴ Each class can be distinguished by the number of σ bonds formed or broken along with the molecularity of the reaction. The four classes of pericyclic reactions are cycloaddition reactions, electrocyclic reactions, sigmatropic rearrangements and group transfer reactions.

3.2.1 Cycloaddition Reactions

A cycloaddition reaction indicates the addition of two π reactants to form a cyclic adduct with formation of σ bonds at the ends of the π components and concomitant reduction in π length in each component. Cycloadditions are bimolecular as shown in the Diels–Alder reaction (Fig. 3.8) in which two π systems interact to form two σ bonds and a new π bond in the cycloadduct. In terms of change in the number of σ bonds, $\Delta\sigma$ (no. of σ bonds formed in the product—no. of σ bonds broken in the reactant), the cycloaddition is characterized by $\Delta\sigma=2$. (Cycloadditions involving more than two π components are relatively few when $\Delta\sigma > 2$.)

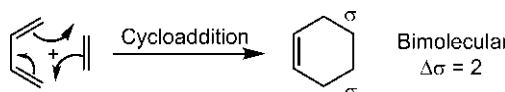


Fig. 3.8 Characteristics of a cycloaddition reaction.

Cycloaddition reactions are reversible, and it is possible to carry out the reverse reaction by a suitable choice of substrates and reaction conditions. The reverse cycloaddition is called retro-cycloaddition or cycloreversion. Retro-cycloaddition is unimolecular and commonly, $\Delta\sigma = -2$.

The cycloadditions are designated by electron and atom conventions.

Electron convention: By electron convention, a cycloaddition is designated as $[l+m]$ cycloaddition, where l and m denote the number of electrons involved in the two components.

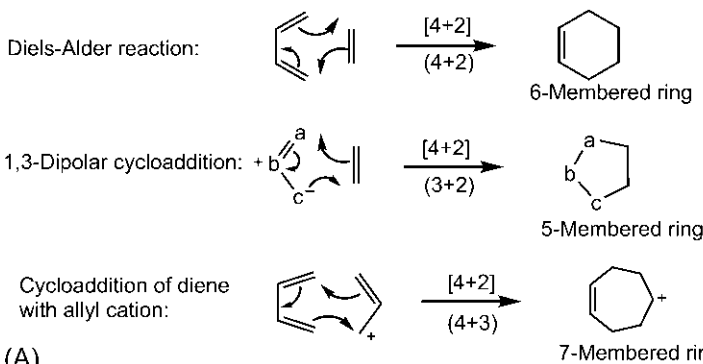
Atom convention: By atom convention, a cycloaddition is designated as $(l+m)$ cycloaddition wherein l and m indicate the number of atoms involved in the two components.

Thus, the designation $[l+m]$ describes the number of electrons participating in the cycloaddition, while $(l+m)$ indicates the number of atoms.

The electron convention is more important as it relates to the mechanism of the reaction. The atom convention, however, identifies the ring size of the product.

These designations of cycloadditions are illustrated with some examples in Fig. 3.9.

Cycloadditions involving 6 electrons ($4n+2$, $n = 1$)



Cycloadditions involving 4 electrons ($4n$, $n = 1$)

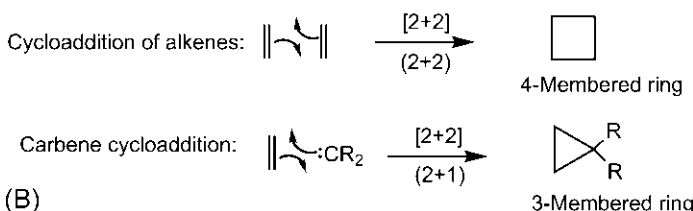


Fig. 3.9 Designations of cycloadditions by electron convention and atom convention. (A) 6-electron cycloadditions and (B) 4-electron cycloadditions.

By electron convention, all three examples of 6-electron cycloadditions in Fig. 3.9A are $[4+2]$ cycloadditions, one component providing 4 electrons and the other 2 electrons. By atom convention, the Diels–Alder reaction is a $(4+2)$ cycloaddition producing a six-membered ring, 1,3-dipolar cycloaddition is a $(3+2)$ cycloaddition giving a five-membered ring, and cycloaddition of butadiene with an allyl cation is a $(4+3)$ cycloaddition forming a seven-membered ring. In cycloadditions involving a total of 4 electrons in Fig. 3.9B, both examples indicate a $[2+2]$ cycloaddition. However, the cycloaddition of two alkenes is a $(2+2)$ cycloaddition giving a four-membered ring, and carbene cycloaddition is a $(2+1)$ cycloaddition forming

a cyclopropane ring. Cycloaddition reactions are most versatile and numerous among the four pericyclic classes.

3.2.2 Electrocyclic Reactions

An electrocyclic reaction denotes a ring closing process in which a new σ bond is formed between the ends of a conjugated π system to give a cyclic system with shorter conjugation, or the reverse ring opening process when a σ bond of a cyclic system is broken to give a longer conjugated π system. Both electrocyclic ring closing (cyclization) and ring opening reactions are unimolecular and are characterized by $\Delta\sigma = \pm 1$ (Fig. 3.10). As shown, the ring closing of hexatriene leads to a reduction of one π bond to form cyclohexadiene while the ring opening of cyclobutene causes an increase of one π bond to give butadiene. Electrocyclic reactions are reversible, and involve the transformation of one π bond into one σ bond, or the reverse.

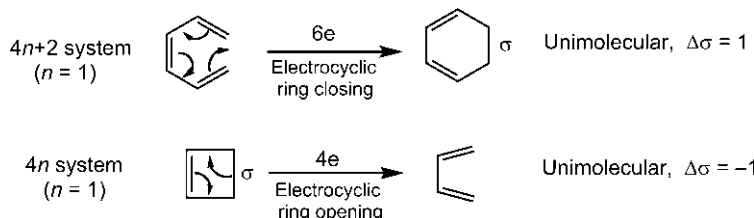


Fig. 3.10 Characteristics of electrocyclic reactions.

3.2.3 Sigmatropic Rearrangements

A sigmatropic rearrangement indicates the migration of a σ bond (adjacent to one or two π components) from one position to another in a molecule with concomitant reorganization of the π system(s). In this process, an old σ bond is broken and a new σ bond is formed. The reaction is therefore inherently reversible; the direction in which the rearrangement is favoured is determined by thermodynamics. A sigmatropic rearrangement is evidently unimolecular, and is characterized by $\Delta\sigma = 0$ (Fig. 3.11). Note that one end of the migrating σ bond is next or adjacent to a p orbital of the π component.

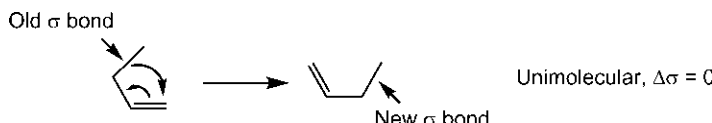


Fig. 3.11 Characteristics of a sigmatropic rearrangement.

A sigmatropic rearrangement is designated by its *order* $[i,j]$ where i and j are positive integers. The order is subclassified into two types: $[1,j]$ ($j > 1$) when one π component is involved, and $[i,j]$ ($i \neq 1$) when two π components are involved. In place of a π component, a single p orbital (i.e., a ω component) may also be involved in sigmatropic rearrangements.

The order is determined as follows. The migrating σ bond is labelled by number 1 at each end (bond 1-1). The numbering is then continued through π component(s) to each end of the new σ bond. The numbers (i,j) at the two ends of the new σ bond gives the order.

The assignment of order is illustrated with two examples of $[1,j]$ sigmatropic rearrangements (also called $[1,j]$ sigmatropic shifts) in Fig. 3.12. For a total electron count of $4n$ or $4n+2$, a σ component contributes 2 electrons and the rest comes from the π component. As shown in Fig. 3.12, the order for the 4-electron rearrangement in an alkene is $[1, 3]$, whereas for the 6-electron shift in a diene the order is $[1, 5]$. Note that one end of the new σ bond remains attached to the same R/H of the old bond, and hence the number 1 is retained for that end.

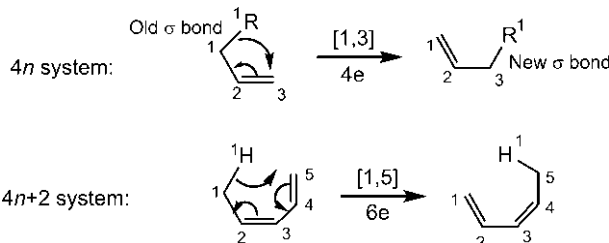


Fig. 3.12 Determination of order of two $[1,j]$ sigmatropic rearrangements.

The above $[1, 3]$ and $[1, 5]$ sigmatropic shifts indicate, respectively, the migration of a group (R) and an atom (H) in the molecule.

The $[i,j]$ rearrangements involving 6 electrons are most common. The well-known reactions are the Cope, Claisen and Wittig rearrangements. The order determined for each is shown in Fig. 3.13. In the Cope rearrangement, a C—C σ bond migrates and a new C—C σ bond is formed. The two ends of the migrating σ bond are adjacent to two π bonds so that the two ends of the new σ bond get the numbers 3, 3. The order is therefore $[3,3]$. Similarly, the order of the Claisen rearrangement is also $[3,3]$; however, the migrating σ bond is C—O and the new σ bond formed is C—C in this case. For the Wittig rearrangement, the carbon end of the

migrating C—O σ bond is adjacent to a π bond while the oxygen end is next to a filled p orbital. The two ends of the new C—C σ bond then get the numbers 2, 3 and hence the order is [2, 3].

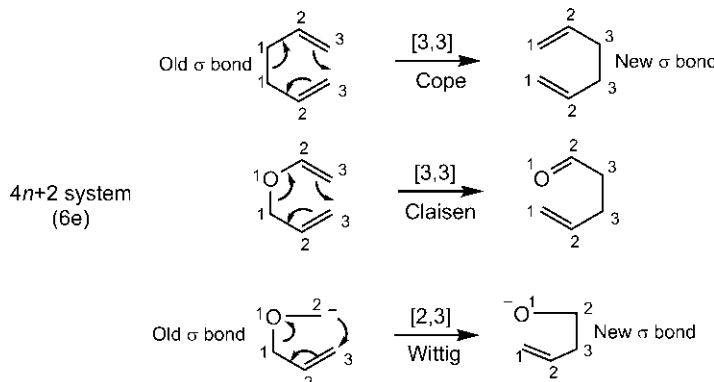


Fig. 3.13 Determination of order of $[i,j]$ sigmatropic rearrangements.

3.2.4 Group Transfer Reactions

A group transfer reaction denotes a pericyclic transfer of one or two groups from one molecule to another. This occurs by breaking and forming of σ bonds with associated changes in π systems. The group transfer reactions are bimolecular; however, $\Delta\sigma$ is variable (1 or 0). Not many pericyclic reactions belong to this class; the two well-known examples are ene reaction and diimide reduction (Fig. 3.14). In the ene reaction, an allylic hydrogen of an alkene (ene component) is transferred to another π system (called enophile). A single product is, however, obtained because of the simultaneous formation of a new σ bond at the ends of two π units of the ene component and enophile. The ene reaction thus has some characteristics of a cycloaddition.

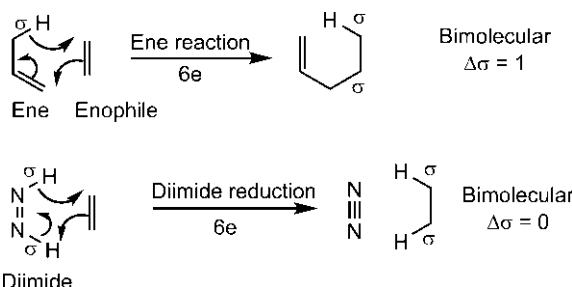


Fig. 3.14 Characteristics of group transfer reactions.

However, $\Delta\sigma=1$ and no cyclic product is formed, and hence the ene reaction does not fit into the cycloaddition class. Further, a σ bond moves from the ene component to enophile showing some characteristics of a sigmatropic rearrangement, but the bimolecular ene reaction with $\Delta\sigma=1$ cannot belong to the sigmatropic class. The dimide reduction shown in Fig. 3.14 is a double group transfer reaction since two hydrogens are transferred from the diimide to a π system. Here $\Delta\sigma=0$ and the reaction is bimolecular.

The ene reaction can be reversible, and retro-ene reactions are known (see Chapter 10). Retro-ene reactions are unimolecular with $\Delta\sigma=-1$. A retro group transfer reaction is shown in Fig. 3.15 which involves 1,4-cycloelimination of a stable R-R molecule. When R=H, the 1,4-cycloelimination refers to dehydrogenation by retro group transfer. The 6-electron 1,4-cycloelimination is unimolecular with $\Delta\sigma=-1$.

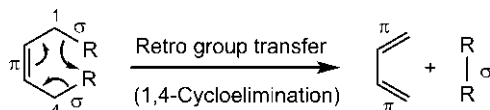


Fig. 3.15 A retro group transfer reaction involving 1,4-cycloelimination.

Summary: The characteristics of four classes of pericyclic reactions in terms of their molecularity and σ bond changes ($\Delta\sigma$) are summarized in Table 3.1. Retro-cycloadditions and retro group transfer reactions which are unimolecular with negative $\Delta\sigma$ are not included.

Table 3.1 Characteristics of four classes of pericyclic reactions

Class **Characteristics**

Cycloadditions	Bimolecular, $\Delta\sigma=2$ (usually)
Electrocyclic reactions	Unimolecular, $\Delta\sigma=\pm 1$
Sigmatropic rearrangements	Unimolecular, $\Delta\sigma=0$
Group transfer reactions	Bimolecular, $\Delta\sigma=1$ or 0

$\Delta\sigma = \text{no. of } \sigma \text{ bonds formed} - \text{no. } \sigma \text{ bonds broken.}$

3.3 MECHANISMS AND THE WOODWARD–HOFFMANN RULES

There are three principal mechanistic approaches to analysing pericyclic reactions. Molecular orbital theory is the basis for all three. These are

Orbital symmetry correlation approach—developed by Woodward and Hoffmann¹¹

TS aromaticity approach—developed independently by Zimmerman²² and Dewar²³

The Frontier molecular orbital (FMO) approach—developed first by Woodward and Hoffmann,²⁴ and then by Fukui²⁵

3.3.1 The Woodward–Hoffmann Generalized Rules

Woodward and Hoffmann used the orbital symmetry correlation approach to a wide variety of concerted processes for their development of the theory of pericyclic reactions. This approach is the most rigorous of the three, and requires consideration of all participating reactant and product molecular orbitals. The correlation diagrams have been covered in a separate chapter (Chapter 11). On the basis of their results, Woodward and Hoffmann put forward the *generalized rules* applicable to all classes of pericyclic reactions. These rules are concise, and predict easily whether a pericyclic reaction is symmetry-allowed or symmetry-forbidden.

There are two rules, one for thermal reactions and the other for photochemical reactions. A thermal reaction occurs from the electronical ground state of the reactants, and is referred to as a ground state process. A photochemical reaction involves the electronically first excited singlet state of a reactant, and is called an excited state process. The generalized rules are

- A thermal pericyclic reaction is symmetry-allowed when the total number of $(4q+2)_s$ and $(4r)_a$ components is odd.
- A photochemical pericyclic reaction is symmetry-allowed when the total number of $(4q+2)_s$ and $(4r)_a$ components is zero or even.
($q, r=0, 1, 2, 3\dots$; the subscripts s and a stand for suprafacial and antarafacial, respectively)

A $(4q+2)_s$ component indicates a suprafacial component with $4q+2$ electrons, and a $(4r)_a$ component is an antarafacial component having $4r$ electrons. A component can be a π system, a σ bond or a single p orbital, that is, a π , σ or ω component. Now the question is: how would a component be designated as suprafacial or antarafacial? The terms suprafacial (in shortened form, supra or s) and antarafacial (in short, antara or a) denote two distinct *geometric* ways by which new bonds can develop to a component in the TS.

The suprafacial and antarafacial designations for the π , σ and ω components are described below.

π component: If the new bonds develop on the same face of a π component, it is suprafacial, and when the new bonds develop on opposite faces, the π component is antarafacial. Fig. 3.16 shows orbital picture representations for suprafacial and antarafacial π components.

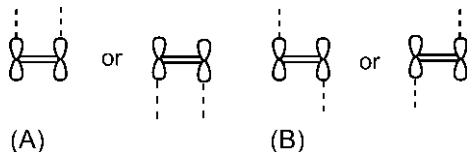


Fig. 3.16 (A) Suprafacial π component and (B) antarafacial π component.

σ component: If the new bonds develop through two inner or two outer lobes of a σ orbital, the σ component is suprafacial. An antarafacial σ component involves developing overlaps through the inner and outer lobes (Fig. 3.17).

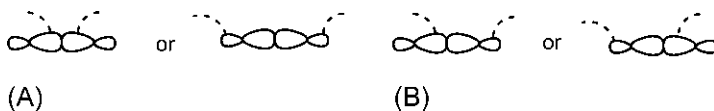


Fig. 3.17 (A) Suprafacial σ component and (B) antarafacial σ component.

ω component: If the new bonds develop through the same lobe of a p orbital on a heteroatom, carbocation or carbanion centre, the ω component is suprafacial, and if overlaps occur through opposite lobes, it is antarafacial (Fig. 3.18).

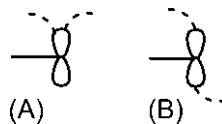


Fig. 3.18 (A) Suprafacial ω component and (B) antarafacial ω component.

Note: The identification of a component as suprafacial or antarafacial depends solely on the geometric sense of developing new bonds and orbital drawing is not a necessity. However, the orbital representation as shown in Figs 3.16–3.18 is more useful as it not only identifies the component easily but also relates to the orbital mechanism of the pericyclic reaction.

3.3.2 Analysis of Cycloaddition Reactions and Selection Rules

In order to analyse cycloaddition reactions, the possible geometric or stereochemical modes in terms of suprafacial/antarafacial components are determined. To illustrate, we begin with the Diels–Alder reaction between

a diene and a dienophile. The diene is a π_4 component and the dienophile is a π_2 component. (Notice that the type of electron (π) is indicated as a subscript to the left of the electron number.) Assuming bond-formation on the same face or opposite faces of the diene and dienophile, there are four possible stereochemical modes of diene/dienophile interactions as shown in Fig. 3.19. These are designated as: (A) supra/supra or $[\pi_4s + \pi_2s]$, (B) supra/antara or $[\pi_4s + \pi_2a]$, (C) antara/supra or $[\pi_4a + \pi_2s]$ and (D) antara/antara or $[\pi_4a + \pi_2a]$. The developing new σ bonds clearly identify a diene or a dienophile component to be supra or antara. This is explicitly delineated in Figs 3.19A and B as an aid to understanding. A suprafacial or antarafacial component is specified by electron number, type of electron (left subscript to electron number) and suprafacial or antarafacial (s or a as right subscript to electron number). As such, the suprafacial diene component is designated as π_4s , and the suprafacial dienophile component is designated as π_2s . The supra/supra mode of the reaction is then represented as $[\pi_4s + \pi_2s]$. The other modes are designated similarly.

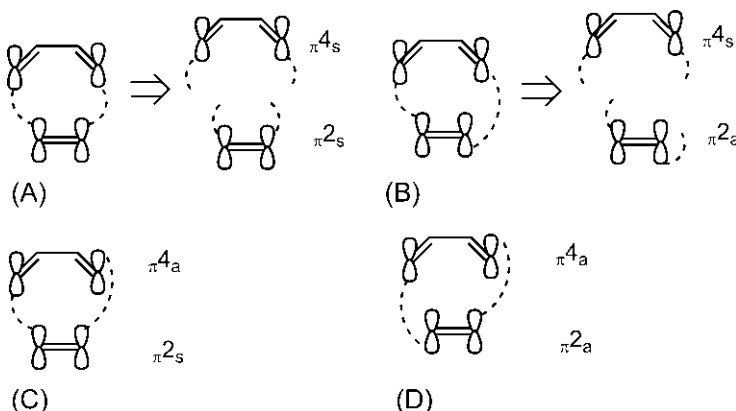


Fig. 3.19 Orbital picture representations of four possible stereochemical modes of the Diels–Alder reaction. (A) $[\pi_4s + \pi_2s]$, (B) $[\pi_4s + \pi_2a]$, (C) $[\pi_4a + \pi_2s]$ and (D) $[\pi_4a + \pi_2a]$.

In general, for any two-component cycloadditions, four stereochemical modes (supra/supra, supra/antara, antara/supra and antara/antara) are possible. Geometrically, a particular mode may be highly favourable, or difficult to achieve but not impossible, or very unfavourable. A symmetry-allowed but geometrically impossible mode of a pericyclic reaction would not occur in reality.

3.3.2.1 Application of the Woodward–Hoffmann Generalized Rules

We shall illustrate the application of the Woodward–Hoffmann generalized rules taking a representative case from $(4n+2)$ - and $(4n)$ -electron cycloadditions.

$4n+2$ Electron System: The Diels–Alder Reaction

Of the four possible stereochemical modes of the Diels–Alder reaction, the $[\pi 4_s + \pi 2_s]$ mode is most favourable geometrically as it requires an easy parallel approach of the diene and the dienophile. This parallel approach for the supra/supra mode leads to a boat geometry of the TS (Fig. 3.20). Note that the TS is drawn simply by showing the developing σ bonds (dashed lines) so as to complete the cycle.

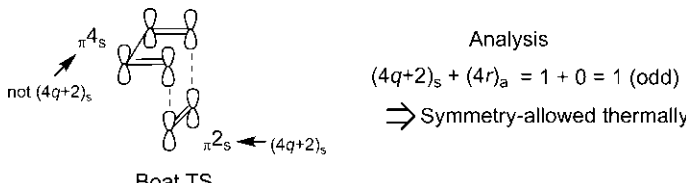


Fig. 3.20 Analysis of the $[\pi 4_s + \pi 2_s]$ Diels–Alder reaction using the Woodward–Hoffmann generalized rules.

For the purpose of analysis, we need to count only $(4q+2)_s$ and $(4r)_a$ components, and must not count $(4q+2)_a$ and $(4r)_s$ components, if any. Then we find the total number of $(4q+2)_s$ and $(4r)_a$ components, written here as $(4q+2)_s + (4r)_a$ (see Fig. 3.20). If the total is an odd number, the reaction is symmetry-allowed thermally, and when the total is zero or an even number, the reaction is symmetry-allowed photochemically.

It should be noted that the type of electrons (π , σ or ω) does not matter in the analysis. To avoid confusion, some countable and not countable components are given below.

Count	Do not count
$(4q+2)_s : 2_s, 6_s, 10_s, 14_s$	$(4q+2)_a : 2_a, 6_a, 10_a, 14_a$
$(4r)_a : 0_a, 4_a, 8_a, 12_a$	$(4r)_s : 0_s, 4_s, 8_s, 12_s$
(taking $q, r = 0, 1, 2, 3$)	

The analysis of the $[\pi 4_s + \pi 2_s]$ mode shows that $(4q+2)_s + (4r)_a = 1$ (odd number), and hence the process is symmetry-allowed thermally (Fig. 3.20). Almost all thermal Diels–Alder reactions proceed through this

symmetry-allowed and geometrically favourable $[\pi 4_s + \pi 2_s]$ mode. In general, the supra/supra mode is thermally allowed for cycloadditions involving $4n+2$ electrons.

The other modes of the Diels–Alder reaction can be analysed similarly. For the $[\pi 4_a + \pi 2_a]$ process, $(4q+2)_s + (4r)_a = 0 + 1 = 1$ (odd), and hence symmetry-allowed thermally. This antara/antara interaction is very difficult to achieve geometrically and examples are rare but known (see [Chapter 5, Section 5.1.6](#)). The $[\pi 4_s + \pi 2_a]$ mode gives $(4q+2)_s + (4r)_a = 0$, and is therefore symmetry-forbidden thermally but symmetry-allowed photochemically. The $[\pi 4_a + \pi 2_s]$ mode is also photochemically allowed because $(4q+2)_s + (4r)_a = 2$ (even number). These photochemically allowed modes are geometrically quite unfavourable and photochemical Diels–Alder reactions are indeed rare (see [Chapter 5, Section 5.1.5](#)).

4n Electron System: [2+2] Cycloaddition of Alkenes

The $[2+2]$ cycloaddition of two alkenes is a 4-electron cycloaddition that forms a cyclobutane (see [Fig. 3.9B](#)). For the prototype reaction between two ethylene molecules, supra/antara and antara/supra modes are equivalent. Therefore, there will be three distinct stereochemical modes (supra/supra, supra/antara and antara/antara) for the prototype reaction. The orbital picture representations of these modes and their analyses are shown in [Fig. 3.21](#).

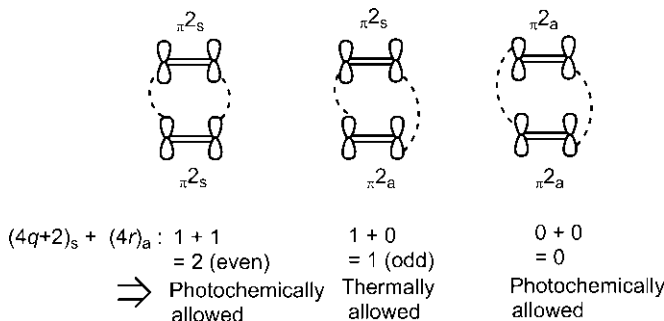


Fig. 3.21 Stereochemical modes of $[2+2]$ cycloaddition and their analyses.

It is seen that the $[\pi 2_s + \pi 2_s]$ and $[\pi 2_a + \pi 2_a]$ processes are symmetry-allowed photochemically. The $[\pi 2_s + \pi 2_a]$ mode is highly favourable geometrically by the parallel approach of the two components and allows photochemical cycloaddition of alkenes to take place readily (see [Chapter 5, Section 5.4.1](#)). In general, the supra/supra mode is photochemically allowed for cycloadditions involving $4n$ electrons. However, the antara/antara

interaction for two small π components is geometrically impossible to achieve and the photochemical cycloaddition of alkenes cannot occur through this mode. As shown in Fig. 3.21, the $[\pi_2s + \pi_2a]$ mode is symmetry-allowed thermally. The geometric requirement for this interaction is attained when the two components can approach in an orthogonal fashion and thermal $[\pi_2s + \pi_2a]$ cycloaddition can take place (see Chapter 5, Section 5.4.2).

Selection Rules for Cycloadditions

From the above analyses, the Woodward–Hoffmann selection rules for two-component cycloadditions are obtained as shown in Table 3.2. The selection rules clearly predict which cycloadditions are symmetry-allowed thermally or photochemically. A thermally allowed process is photochemically forbidden, and vice versa.

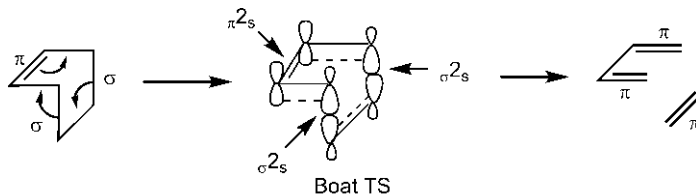
Table 3.2 Selection rules for two-component cycloadditions

Total no. of electrons	Thermally allowed	Photochemically allowed
$4n + 2$	Supra/supra Antara/antara	Supra/antara Antara/supra
$4n$	Supra/antara Antara/supra	Supra/supra Antara/antara

Analysis of Retro-Cycloaddition Reactions

So far, we have dealt with cycloadditions involving π components only. Analysis of a retro-cycloaddition includes σ components, besides the π component. To illustrate, we consider the retro-Diels–Alder reaction. Here the reactant cyclohexene possesses three components comprising two σ bonds and one π bond. As the microscopic reverse of the forward reaction, the retro-Diels–Alder reaction also proceeds through boat TS. The developing overlaps (dashed lines) in the boat TS with respect to formation of three new π bonds (two for diene and one for ene) are shown in Fig. 3.22.

Based on the developing overlaps, the two σ and one π components can be designated as supra or antara. As shown in Fig. 3.22, two inner lobes of both σ bonds are involved in the interactions, and hence both σ components are supra, that is, σ_2s and σ_2s . The π component is also supra (π_2s) as two lower lobes on the same face of the π bond are involved. The analysis then shows that the retro-Diels–Alder reaction is a thermally allowed $[\pi_2s + \sigma_2s + \sigma_2s]$ reaction.



$$(4q+2)_s + (4r)_a = 3 + 0 = 3 \text{ (odd)} \Rightarrow \text{Thermally allowed}$$

Fig. 3.22 Analysis of the retro-Diels–Alder reaction using the Woodward–Hoffmann generalized rules.

The lobe interactions in the TS may be depicted in multiple ways for the allowed retro-Diels–Alder reaction. Fig. 3.23A shows that lobe interactions for the formation of three π bonds involve two outer lobes of each σ bond and two upper lobes on the same face of the π bond. The designation is then also $[\pi_2s + \sigma_2s + \sigma_2s]$, as in Fig. 3.22. Another way of depicting lobe interactions is shown in Fig. 3.23B. In this drawing, the interactions involve two inner lobes of one σ bond, the inner and outer lobes of the other σ bond, and the upper and lower lobes on the opposite faces of the π bond in the same TS geometry. The designation is now $[\pi_2a + \sigma_2s + \sigma_2a]$, which is also thermally allowed. It should be noted that multiple versions of representation or designation can arise from more than one choice of lobe interactions in the same TS geometry, which do not indicate the different allowed pathways. A π bond orbital has four lobes (two upper and two lower) and a σ bond orbital too has four lobes (two inner and two outer). Out of four lobes, two lobes are needed to identify a component to be supra or antara, and therefore

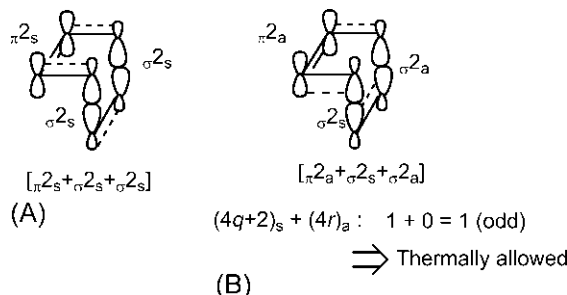


Fig. 3.23 Multiple representations of an allowed pathway of the retro-Diels–Alder reaction arising from more than one choice of lobe interactions. (A) $[\pi_2s + \sigma_2s + \sigma_2s]$ and (B) $[\pi_2a + \sigma_2s + \sigma_2a]$.

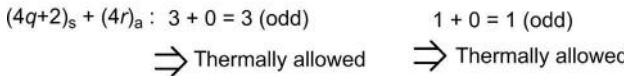
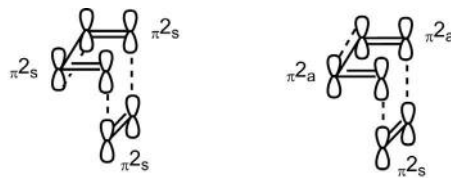
provide scope for multiple choices of two lobes in the interacting bond orbitals. The two designations $[\pi 2_s + \sigma 2_s + \sigma 2_s]$ and $[\pi 2_a + \sigma 2_s + \sigma 2_a]$ here indicate two representations or drawings of the same allowed pathway of the retro-Diels–Alder reaction. (Be careful to distinguish between multiple representations for the same pathway and different designations for different pathways.)

Problem 3.2

The $[\pi 4_s + \pi 2_s]$ Diels–Alder reaction can alternatively be represented as the $[\pi 2_s + \pi 2_s + \pi 2_s]$ or $[\pi 2_s + \pi 2_a + \pi 2_a]$ reaction. Explain.

Answer

In the $[\pi 4_s + \pi 2_s]$ description, the diene is regarded as a single $\pi 4$ component. However, for the purpose of analysis, each π bond of the diene can be artificially treated as a separate $\pi 2$ component. The analysis then involves three $\pi 2$ components (two from diene and one from dienophile), which provide alternative representations of the same supra/supra addition of diene and dienophile. The orbital interactions in this three-component analysis indicate developing overlaps in the TS for the formation of two σ bonds as well as one π bond as shown below.



The analyses show that $[\pi 2_s + \pi 2_s + \pi 2_s]$ and $[\pi 2_s + \pi 2_a + \pi 2_a]$ representations are symmetry-allowed thermally.

3.3.2.2 Transition Structure Aromaticity Approach

The TS aromaticity approach, developed independently by Dewar and Zimmerman, is based on the aromaticity/antiaromaticity of pericyclic TS. Cyclic TSs can be classified as aromatic or antiaromatic, just like the cyclic conjugated polyenes are (see Sections 1.7.1 and 1.7.2.1). Dewar used the perturbational molecular orbital (PMO) theory for aromaticity and antiaromaticity in cyclic conjugated Hückel or Möbius (anti-Hückel) system, and his

approach applied to the cyclic TS in concerted reaction is also called the PMO approach.²⁶ Zimmerman put forward the idea of Hückel or Möbius TS in concerted process using the Hückel molecular orbital method.²⁷

The TS aromaticity approach provides two simple rules, one for thermal reaction and the other for photochemical reaction, which are stated as follows.

1. A thermal pericyclic reaction proceeds via an aromatic TS.
 2. A photochemical pericyclic reaction proceeds via an antiaromatic TS.
- Now the question is: which TS is aromatic and which is antiaromatic? This can be easily decided in a practical manner using the following step-by-step procedure.

- Step 1.** Draw a cyclic orbital array in the TS using basis set orbitals (set of atomic orbitals) for each component for the pericyclic mode to be analysed.
- Step 2.** Classify the topology of the orbital array as the Hückel or Möbius system depending on the number of sign inversions in the cyclic array (see Section 1.7.2):

Number of sign inversions	Topology of orbital array
Zero or even	Hückel
Odd	Möbius

(It should be kept in mind that a sign inversion does not indicate an anti-bonding overlap with respect to bond formation; the counting of the number of sign inversions is simply a device to determine the Hückel/Möbius topology.)

- Step 3.** Determine the TS as aromatic or antiaromatic based on the total number of electrons involved:

Number of electrons	Hückel system	Möbius system
$4n + 2$	Aromatic	Antiaromatic
$4n$	Antiaromatic	Aromatic

To illustrate, we consider the $[\pi_4s + \pi_2s]$ Diels–Alder reaction. This process was analysed earlier by the Woodward–Hoffmann generalized rules (see Fig. 3.20). In order to build a common link in the analyses by different mechanistic approaches, the previous orbital picture representation is readily transformed into a cyclic orbital array of basis set orbitals (Step 1) as shown in Fig. 3.24. The basis set orbitals for the diene component is a set of four p atomic orbitals, and those for the dienophile component a set of two p

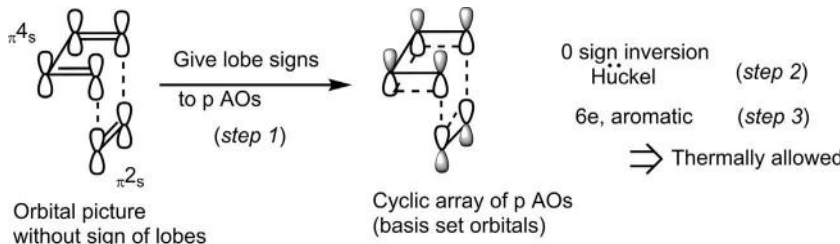


Fig. 3.24 Analysis of the $[\pi 4_s + \pi 2_s]$ Diels–Alder reaction using the TS aromaticity approach.

atomic orbitals. The choice of signs for lobes is arbitrary, with the proviso that a p orbital has two lobes of the opposite sign.

As shown in Fig. 3.24, the number of sign inversions is zero, and hence the topology of the orbital array is Hückel-type (Step 2). (Note that the choice of lobe signs is such that they minimize the number of sign inversions in the cyclic array; however, any other choice would give an equivalent even number of sign inversions.) The Hückel TS with 6 electrons is therefore aromatic (Step 3). Consequently, the $[\pi 4_s + \pi 2_s]$ mode is thermally allowed by Rule 1.

The other modes of the Diels–Alder reaction can be analysed similarly. To give one more illustration, Fig. 3.25 shows the analysis of the $[\pi 4_s + \pi 2_a]$ mode.

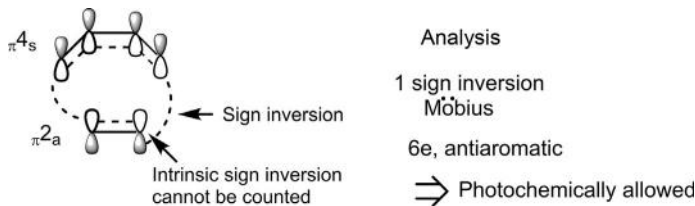


Fig. 3.25 Analysis of the $[\pi 4_s + \pi 2_a]$ Diels–Alder reaction.

Here the cycle includes both lobes of a p orbital for which the intrinsic sign change cannot be counted (see also Fig. 1.34, p. 36). The number of sign inversions is 1 and the orbital array is a Möbius system involving 6 electrons. Therefore, the Möbius TS is antiaromatic, and the $[\pi 4_s + \pi 2_a]$ mode is photochemically allowed by Rule 2.

Next, we consider the $[2+2]$ cycloaddition of alkenes. The analyses of $[\pi 2_s + \pi 2_s]$ and $[\pi 2_s + \pi 2_a]$ modes are shown in Fig. 3.26. The $[\pi 2_s + \pi 2_s]$ process is photochemically allowed involving an antiaromatic Hückel TS (Fig. 3.26A). For the supra/antara mode, an orthogonal approach of the

two components is shown in Fig. 3.26B. Notice that only the front lobes of the two p orbitals of the alkene approaching from the rear are drawn. The $[\pi_{2s} + \pi_{2a}]$ process is thermally allowed as the Möbius TS is aromatic.

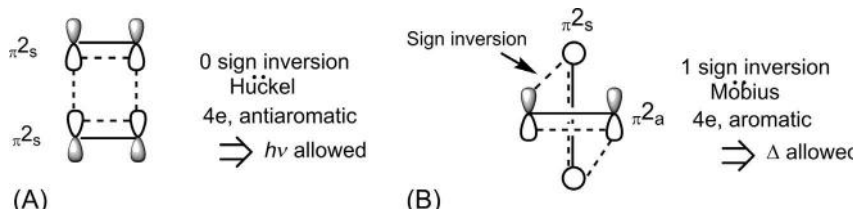


Fig. 3.26 Analysis of (A) $[\pi_{2s} + \pi_{2s}]$ and (B) $[\pi_{2s} + \pi_{2a}]$ cycloadditions.

The TS aromaticity approach gives the same predictions as obtained using the Woodward–Hoffmann generalized rules, and provides the same selection rules (Table 3.2).

3.3.2.3 Frontier Molecular Orbital (FMO) Approach

In a bimolecular process, all molecular orbitals of one component can interact with all molecular orbitals of the other component. Of these, the interaction of an occupied orbital with an unoccupied orbital leads to a net stabilization by lowering of energy (Fig. 3.27A). The extent of stabilization is greater when the energies of the interacting orbitals are closer; thus, the predominant contribution to stabilization is effected by the interacting orbitals with the lowest energy separation. Evidently, this dominant interaction is between the highest occupied molecular orbital (HOMO) of one component and the lowest unoccupied molecular orbital (LUMO) of the second component (Fig. 3.27B). This HOMO/LUMO interaction is called

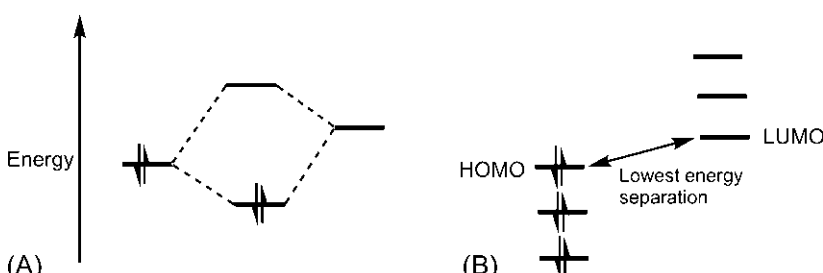


Fig. 3.27 (A) Interaction of an occupied orbital of one component with an unoccupied orbital of the second component and (B) HOMO/LUMO energy difference indicating lowest energy separation.

the FMO interaction. The frontier orbital theory developed and named by Fukui²⁸ is the most accessible theory to analysing organic chemical reactions. For the two interacting components A and B, there would be two frontier orbital pairs: HOMO_A/LUMO_B and HOMO_B/LUMO_A.

In terms of FMO interactions, a cycloaddition reaction is allowed when the orbital interactions at the ends of the components indicate bonding interactions with the in-phase (same sign) overlap. If any one of the interactions is antibonding with an out-of-phase (different sign) overlap, the concerted process is forbidden. It is the orbital symmetry (not the size of coefficients) of frontier orbitals that decides the bonding/antibonding interaction. The analysis of the thermal $[\pi 4_s + \pi 2_s]$ Diels–Alder reaction by the FMO approach is shown in Fig. 3.28. As described in the TS aromaticity approach, the orbital picture representation is now transformed into the frontier orbital pictures as HOMO_{diene}/LUMO_{dienophile} and LUMO_{diene}/HOMO_{dienophile} interactions.(Note that the transformation is just assigning proper lobe signs for HOMO/LUMO.)

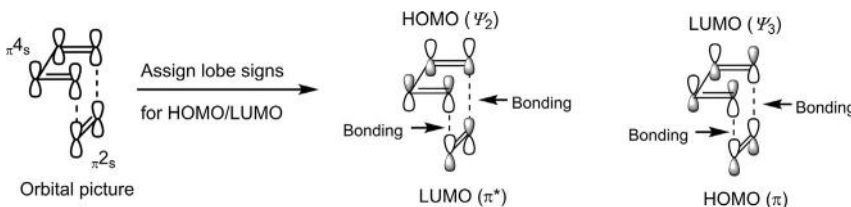


Fig. 3.28 FMO analysis of the $[\pi 4_s + \pi 2_s]$ Diels–Alder reaction.

It is clearly seen that both FMO interactions are bonding at the two ends of the diene and dienophile. The $[\pi 4_s + \pi 2_s]$ process is therefore thermally allowed. The other stereochemical modes of the Diels–Alder reaction can be analysed similarly.

The FMO analyses of thermal $[\pi 2_s + \pi 2_s]$ and $[\pi 2_s + \pi 2_a]$ cycloadditions are shown in Fig. 3.29. The $[\pi 2_s + \pi 2_s]$ process is thermally forbidden due to an antibonding interaction (Fig. 3.29A), whereas the $[\pi 2_s + \pi 2_a]$ process is thermally allowed (Fig. 3.29B).

We have previously seen that the $[\pi 2_s + \pi 2_s]$ process is photochemically allowed. We shall now see how the frontier orbital approach can provide an explanation for the allowed photochemical reaction. Since molecules in the excited singlet state have short lifetimes, the probability of two excited state molecules encountering one another is quite small. Photochemical cycloaddition therefore results from the interaction of an excited state molecule with a ground state molecule. As shown in Fig. 3.30, the most

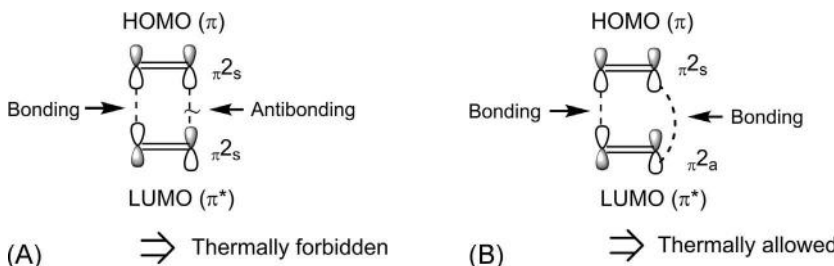


Fig. 3.29 FMO analyses for (A) $[\pi_{2s} + \pi_{2s}]$ and (B) $[\pi_{2s} + \pi_{2a}]$ cycloadditions.

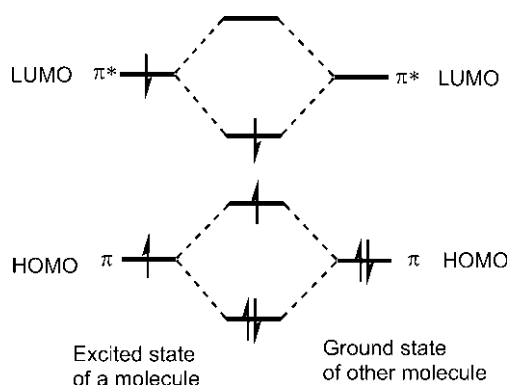


Fig. 3.30 Frontier orbital energy diagram for photochemical $[2+2]$ cycloaddition.

important interactions are π/π and π^*/π^* , each of which is energy-lowering. The π/π interaction is the HOMO/HOMO interaction, and π^*/π^* is the LUMO/LUMO interaction. It should be kept in mind that the excited state HOMO and LUMO are singly occupied (see p. 10 for frontier orbital convention). Thus, frontier orbital analysis for photochemical cycloaddition refers to HOMO/HOMO and LUMO/LUMO interactions.

Fig. 3.31 shows the FMO picture for the photochemical $[\pi_{2s} + \pi_{2s}]$ process.

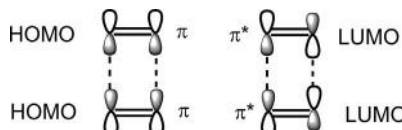


Fig. 3.31 FMO interactions for the photochemical $[\pi_{2s} + \pi_{2s}]$ reaction.

Both HOMO/HOMO and LUMO/LUMO interactions involve bonding interactions and the $[\pi_{2s} + \pi_{2s}]$ reaction is therefore allowed under photochemical conditions.

The FMO approach also gives the same predictions as obtained from other approaches, and leads to the same selection rules (Table 3.2).

3.3.3 Analysis of Electrocyclic Reactions and Selection Rules

For electrocyclic ring closing, the two parallel p orbitals at the ends of the conjugated π system must be rotated to allow their overlap in the σ sense (end-on fashion). On the other hand, electrocyclic ring opening requires rotation of the orbital lobes of the breaking σ bond to give two parallel terminal p orbitals of the resulting π system. According to the principle of microscopic reversibility, the ring closing and ring opening processes would proceed through the same TS. This is schematically shown in Fig. 3.32.

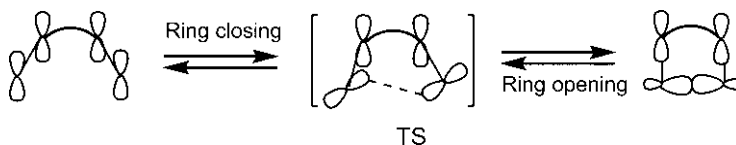


Fig. 3.32 Electrocyclic ring closing and ring opening via the same TS.

The terminal p orbitals in ring closing or the breaking σ orbital in ring opening can rotate in the same direction called the conrotatory (in short, con) motion, or in opposite directions called the disrotatory (in short, dis) motion. There are two possible con motions (clockwise/clockwise and anti-clockwise/anticlockwise) which may lead to different stereochemical consequences (see Chapter 7). Similarly, there are two possible dis motions (clockwise/anticlockwise and anticlockwise/clockwise).

Using the three mechanistic approaches as described earlier for cycloadditions, we shall analyse electrocyclic reactions involving $4n+2$ electrons and $4n$ electrons, taking a representative example from each system.

3.3.3.1 $4n+2$ Electron System: Ring Closing of Hexatriene

The ring closing of 1,3,5-hexatriene to cyclohexadiene is a 6-electron electrocyclic process (see Fig. 3.10). The analyses of the conrotatory ring closing process using the Woodward–Hoffmann generalized rules, TS aromaticity approach and FMO approach are shown in Fig. 3.33. The hexatriene is treated as a single π_6 component.

For the conrotatory process, the orbital picture representation 3.1 shows that hexatriene acts as an antarafacial component (π_{6a}). In terms of the Woodward–Hoffmann generalized rules, $(4q+2)_s + (4r)_a = 0$, and hence the conrotatory process is photochemically allowed. Transforming the

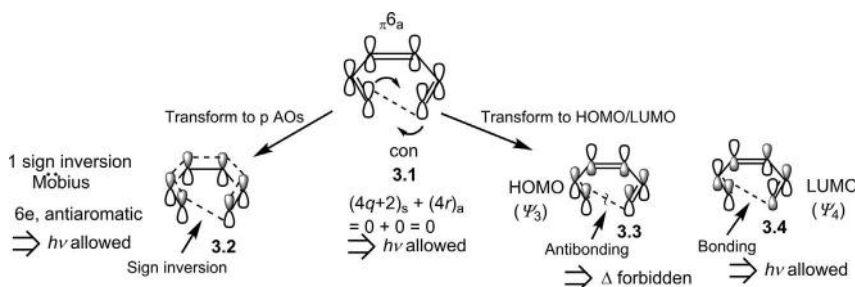


Fig. 3.33 Analysis of the conrotatory electrocyclic ring closing of hexatriene using the Woodward–Hoffmann generalized rules, TS aromaticity approach and FMO approach.

orbital picture 3.1 to a cyclic orbital array of basis set p orbitals, 3.2 gives a Möbius TS that is antiaromatic. The con mode is thus $h\nu$ allowed by the TS aromaticity approach.

The frontier orbital analysis of unimolecular electrocyclic cyclization is somewhat contrived. Recall that in a bimolecular cycloaddition, thermal reaction involves the HOMO/LUMO interaction, whereas photochemical reaction involves HOMO/HOMO and LUMO/LUMO interactions. However, for FMO analysis with a single component, one can only consider either HOMO or LUMO of the component. For thermal reaction, a filled ground state HOMO is a good choice while the singly occupied excited state LUMO is a reasonable choice for the photochemical process. Transforming the orbital picture 3.1 to HOMO (ψ_3) 3.3 and LUMO (ψ_4) 3.4 of hexatriene, the FMO analysis shows that thermal (Δ) reaction is forbidden as there is antibonding interaction for σ bond formation between the two ends of HOMO 3.3 but the photochemical reaction using LUMO 3.4 is allowed with the bonding interaction. (With a single frontier orbital, one can look at one TS interaction only for the developing σ bond. The intrinsic bonding/antibonding overlaps in HOMO or LUMO must not be confused with the TS interaction. To avoid confusion, HOMO or LUMO in this analysis may be drawn showing only the terminal p orbitals.)

In a similar manner, disrotatory ring closing of hexatriene can be analysed (Fig. 3.34). The analyses show that the dis mode is thermally allowed but photochemically forbidden. Notice that HOMO or LUMO shows only terminal p orbitals which can be easily drawn using the symmetry property. HOMO (ψ_3) of hexatriene has m symmetry (same phase relationship of terminal p orbitals) while LUMO (ψ_4) possesses C_2 symmetry (opposite phase relationship of terminal p orbitals). In general, $\psi_{\text{odd}} \Rightarrow m$; $\psi_{\text{even}} \Rightarrow C_2$ (see Section 1.3.2.2).

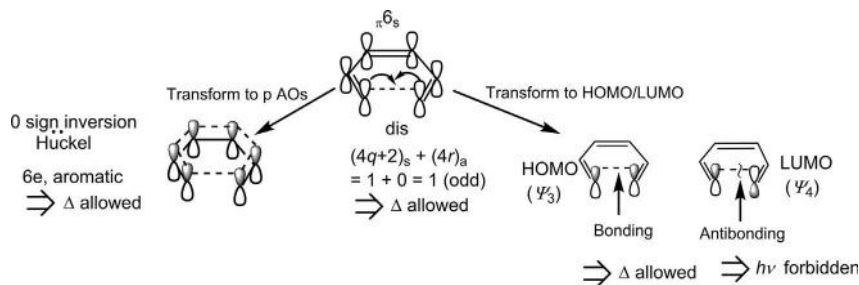


Fig. 3.34 Analysis of disrotatory electrocyclic ring closing of hexatriene using the Woodward–Hoffmann generalized rules, TS aromaticity approach and FMO approach.

3.3.3.2 4n Electron System: Ring Opening of Cyclobutene

The ring opening of cyclobutene to butadiene is a 4-electron electrocyclic process (see Fig. 3.10). The ring opening process can be analysed in terms of two components comprising the breaking σ bond (σ^2) and the π bond (π^2) of cyclobutene. Using the three mechanistic approaches, the analyses for conrotatory ring opening are shown in Fig. 3.35.

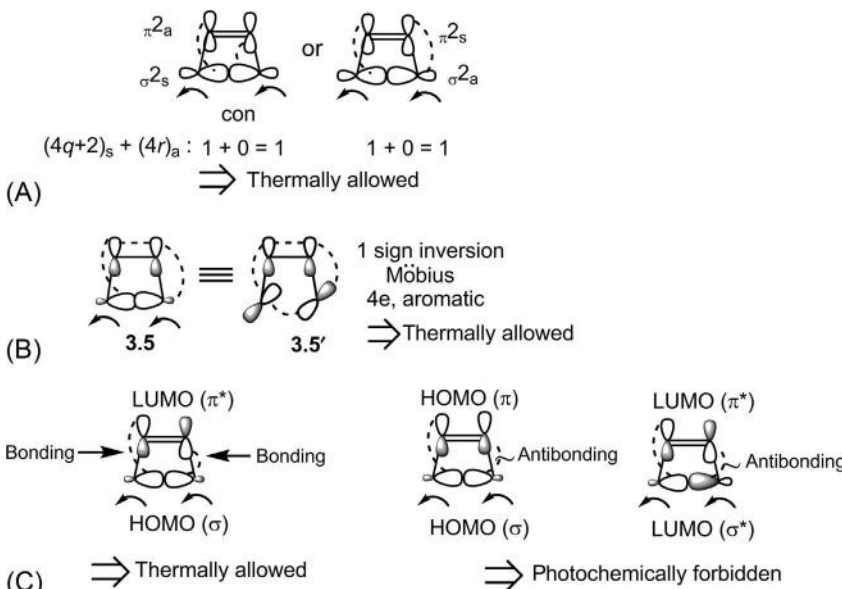


Fig. 3.35 Analysis of the conrotatory electrocyclic ring opening of cyclobutene using the (A) Woodward–Hoffmann generalized rules, (B) TS aromaticity approach and (C) FMO approach.

As shown in Fig. 3.35A, the con mode can be represented in two ways as $[\sigma_2s + \pi_2s]$ or $[\sigma_2a + \pi_2s]$ depending on the choice of lobe interactions and is thermally allowed in terms of the Woodward–Hoffmann generalized rules.

For the analysis by the TS aromaticity approach, the orbital picture in Fig. 3.35A is transformed into a cyclic array of four basis set orbitals (two p orbitals and two hybrid orbitals) 3.5 or the equivalent drawing 3.5' in which two forming p orbitals replace the hybrid orbitals (Fig. 3.35B). The TS has a Möbius topology with 4 electrons, and is aromatic. The con mode is therefore thermally allowed.

The frontier orbital analysis in terms of two components (σ and π) involves a HOMO/LUMO interaction for the thermal process, and HOMO/HOMO and LUMO/LUMO interactions for the photochemical process, as shown in Fig. 3.35C. The con mode is thermally allowed with bonding interactions but photochemically forbidden due to an antibonding interaction. Notice that, for the thermal reaction, the HOMO(σ)/LUMO(π^*) interaction is considered. [Check that the HOMO(π)/LUMO(σ^*) combination gives the same result.]

The analyses for the disrotatory ring opening of cyclobutene are shown in Fig. 3.36. The dis process is represented as $[\sigma_2s + \pi_2s]$ (draw the other $[\sigma_2a + \pi_2a]$ representation). As shown, the dis mode is thermally forbidden but photochemically allowed.

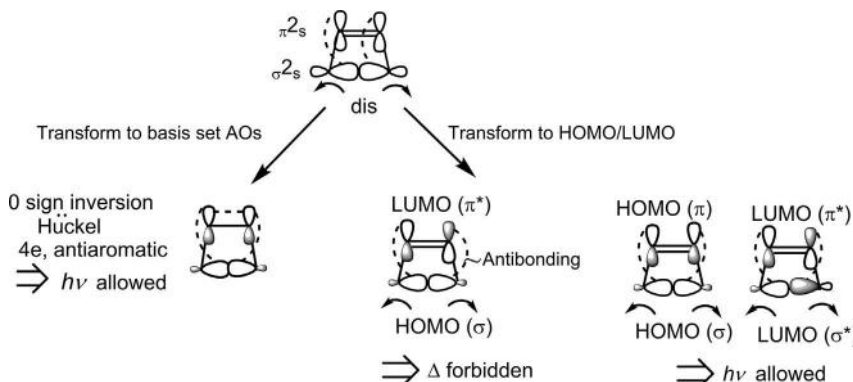


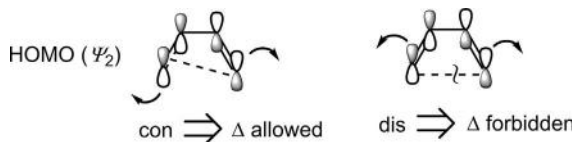
Fig. 3.36 Analysis of disrotatory electrocyclic ring opening of butadiene using the Woodward–Hoffmann generalized rules, TS aromaticity approach and FMO approach.

Problem 3.3

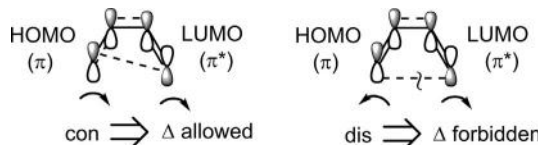
Perform one-component and two-component frontier orbital analyses of thermal ring closing of butadiene to cyclobutene.

Answer

In one-component analysis, butadiene is treated as a single π_4 component. For thermal reaction, the FMO analysis involves HOMO of butadiene. As shown below, the con mode is thermally allowed with bonding interaction for the developing σ bond while the dis mode is thermally forbidden with an antibonding interaction. The antibonding overlap between C-2 and C-3 is intrinsic to the HOMO, and must not be treated as a TS interaction.



The two-component analysis treats the diene artificially as two separate π_2 components, and involves a HOMO/LUMO interaction. For the con mode, the developing overlaps for new σ and π bonds are bonding for the thermally allowed reaction but the dis mode is thermally forbidden with the bonding and antibonding interactions.

**3.3.3.3 Selection Rules for Electrocyclic Reactions**

The Woodward–Hoffmann selection rules for electrocyclic reactions derived from the above analyses are given in [Table 3.3](#). The rules predict which stereochemical mode of an electrocyclic process is symmetry-allowed thermally or photochemically. A thermally allowed process is photochemically forbidden, and vice versa.

Table 3.3 Selection rules for electrocyclic reactions

Total no. of electrons	Thermally allowed	Photochemically allowed
$4n + 2$	Dis	Con
$4n$	Con	Dis

3.3.4 Analysis of Sigmatropic Rearrangements and Selection Rules

Sigmatropic rearrangements are subclassified into $[1,j]$ and $[i,j]$ rearrangements (see [Section 3.2.3](#)). We shall analyse $[1,j]$ rearrangements in two parts, namely $[1,j]$ hydrogen shifts and $[1,j]$ carbon shifts and then $[i,j]$ rearrangements.

3.3.4.1 Analysis of the $[1,j]$ Hydrogen Shifts

In the $[1,j]$ hydrogen shift, the migrating hydrogen has no stereochemistry. Here the only stereochemical consideration is whether migration of hydrogen occurs on the same face of the π component, called the suprafacial shift, or on the opposite face of the π component, termed the antarafacial shift. It should be noted carefully that the suprafacial/antarafacial *shift* is a distinct term in sigmatropic rearrangements, not to be equated with the suprafacial/antarafacial component. As before, the analyses are done for the $4n+2$ and $4n$ electron systems.

$4n+2$ Electron System: $[1, 5]$ Hydrogen Shift

A $[1, 5]$ hydrogen shift is a 6-electron sigmatropic rearrangement. The analyses of suprafacial H shift and antarafacial H shift based on the three approaches are shown in [Fig. 3.37](#).

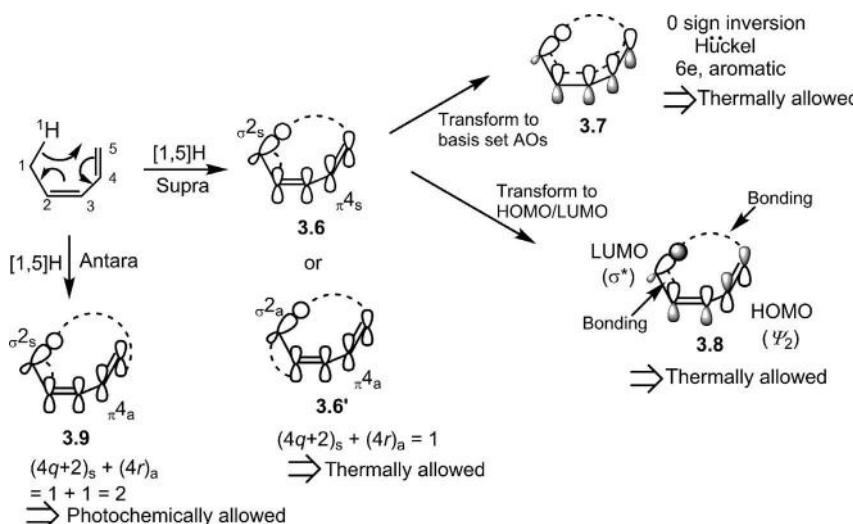


Fig. 3.37 Analysis of the $[1, 5]$ suprafacial H shift using the Woodward–Hoffmann generalized rule, TS aromaticity approach and FMO approach, and analysis of the $[1, 5]$ antarafacial H shift using the Woodward–Hoffmann generalized rules.

The analysis using the Woodward–Hoffmann generalized rule involves two components, a C—H σ bond and a diene unit. The suprafacial H shift can be represented in two ways: $[\sigma_2s + \pi_4s]$ 3.6 or $[\sigma_2a + \pi_4a]$ 3.6'. The total number of $(4q+2)_s$ and $(4r)_a$ components is 1 (odd), and hence the suprafacial H shift is thermally allowed. However, the designation $[\sigma_2s + \pi_4s]$ 3.6 makes more physical sense as the developing bonds are drawn on the same face of the diene where the hydrogen is moving, that is, when the diene is a suprafacial component (π_4s) for the suprafacial migration.

For the analysis using the TS aromaticity approach, 3.6 is transformed to a cyclic array of basis set orbitals 3.7, which indicates an aromatic Hückel TS for a thermally allowed reaction. For applying the FMO approach, 3.6 is transformed to a frontier orbital picture 3.8 which shows that both TS interactions are bonding for the HOMO (ψ_2)/LUMO (σ^*) interaction, and hence thermally allowed. (Check that the other HOMO/LUMO pair gives the same result.)

In Fig. 3.37, the antarafacial H shift is better represented as $[\sigma_2s + \pi_4a]$ 3.9. The total number of $(4q+2)_s$ and $(4r)_a$ components is 2 (even), and hence the antarafacial H shift is photochemically allowed.

An alternative FMO analysis in terms of the SOMO/SOMO interaction can also be performed. This is shown for the suprafacial H shift in Fig. 3.38. An inspection of the TS reveals that the molecule can be arbitrarily divided into two interacting radical components, pentadienyl radical and H atom. This is an artificial device for analysis; the reaction itself is concerted and does not involve radical intermediates. The frontier orbital for a radical component is its SOMO. The FMO analysis then involves the SOMO/SOMO interaction in general. For hydrogen, the relevant orbital is 1s and the SOMO for the pentadienyl radical is ψ_3 . As shown in Fig. 3.38, both interactions at the ends of the π system are bonding, and hence the suprafacial H migration is thermally allowed.

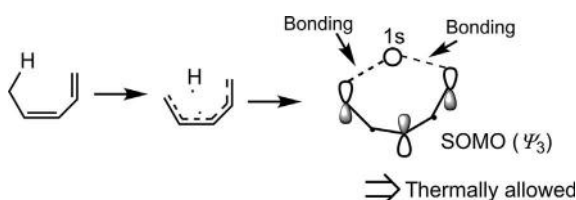


Fig. 3.38 An alternative FMO analysis of the [1, 5] suprafacial H shift in terms of the SOMO/SOMO interaction.

4n Electron System: [1, 3] and [1, 7] Hydrogen Shifts

The [1, 3] hydrogen shift is a 4-electron process. The analyses can be done in a similar manner as described for the [1,5]H shift. Fig. 3.39 shows the analysis of the [1, 3] suprafacial H shift and [1, 3] antarafacial H shift using the Woodward–Hoffmann generalized rules.

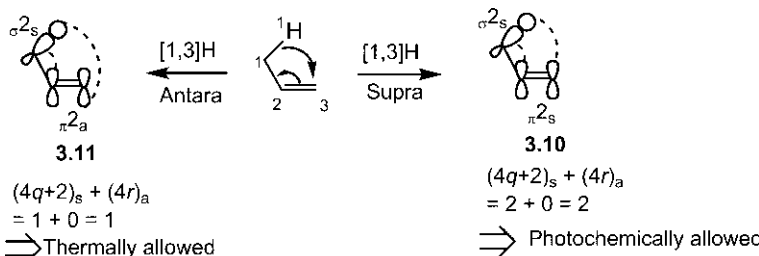


Fig. 3.39 Analysis of the [1, 3] suprafacial and antarafacial hydrogen shifts using the Woodward–Hoffmann generalized rules.

As shown, the suprafacial shift is photochemically allowed but thermally forbidden. On the other hand, the antarafacial hydrogen shift is thermally allowed. However, the orbital overlap necessary for antarafacial hydrogen migration across the very small π_2 component is geometrically impossible.

If the π component is large, the antarafacial migration is possible geometrically. Thus, for a triene system, the [1, 7] antarafacial migration of hydrogen can take place as the hydrogen atom can easily move from the upper face at C-1 to the lower face at C-7 for the flexible triene molecule (Fig. 3.40). Here the double bonds of the triene are in *s-cis* conformation with the middle double bond being *cis*. The antarafacial migration is depicted as $[\sigma_2s + \pi_6a]$ 3.12, which is thermally allowed according to the Woodward–Hoffmann generalized rule. (Draw the other $[\sigma_2a + \pi_6s]$ representation.) The $[\sigma_2s + \pi_6a]$ representation is, however, better as the hydrogen moves between the opposite faces of the triene. The TS aromaticity version of the

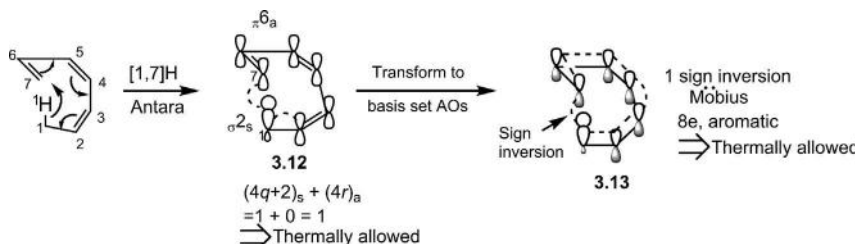


Fig. 3.40 Analysis of the [1, 7] antarafacial H shift using the Woodward–Hoffmann generalized rules and TS aromaticity approach.

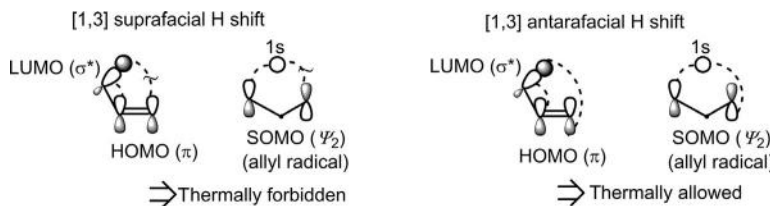
antarafacial migration is also shown in Fig. 3.40 by transforming 3.12 to a cyclic array of basis set orbitals 3.13 which gives an aromatic Möbius TS for the thermally allowed process.

Problem 3.4

Perform an FMO analysis of the thermal [1,3]H shift in terms of HOMO/LUMO and SOMO/SOMO interactions.

Answer

The suprafacial hydrogen shift is thermally forbidden with an antibonding interaction while the antarafacial shift is thermally allowed with bonding TS interactions as shown below.



Selection Rules for [1,j] Hydrogen Shifts

The selection rules for [1,j] hydrogen shifts are given in Table 3.4. The selection rules predict which [1,j] shift is allowed thermally or photochemically. A thermally allowed shift is photochemically forbidden, and vice versa.

3.3.4.2 Analysis of the [1,j] Carbon Shifts

Unlike the [1,j] hydrogen shift, in the [1,j] carbon shift the migrating carbon group can have stereochemistry. The migrating centre is usually a stereocentre. Besides the suprafacial and antarafacial nature of migration, an additional stereochemical consideration is necessary here. This refers to the relative change of configuration (retention or inversion) of the migrating group. The suprafacial or antarafacial migration in the [1,j] carbon shift is similar to that described for the [1,j] hydrogen shift. Now we shall see how the

Table 3.4 Selection rules for [1,j]H shifts

Total no. of electrons	Thermally allowed	Photochemically allowed
$4n + 2$	Supra	Antara
$4n$	Antara	Supra

retention or inversion of the migrating group leads to a symmetry-allowed suprafacial or antarafacial migration.

$4n+2$ Electron System: [1,5]C Shift

The analysis of the 6-electron [1,5]C shift based on the Woodward–Hoffmann generalized rules is shown in Fig. 3.41. It is seen that suprafacial migration with retention of configuration and antarafacial migration with inversion of configuration are symmetry-allowed thermally. Suprafacial migration is, however, geometrically much more favourable than antarafacial migration. For the supra/retention process, the TS 3.14 depicts a $[\sigma_2s + \pi_4s]$ process. Notice that at migrating carbon (*) the same lobe (labelled x) of breaking σ orbital is involved in interactions with the migration terminus and migration origin in the TS, thereby indicating retention of configuration at the migrating centre (cf. retention pathway in the S_N1 mechanism). The antara/inversion process is represented as $[\sigma_2a + \pi_4a]$ 3.15. Here two opposite lobes (x, y) at migrating carbon (*) are involved in interactions with the migration origin and migration terminus, indicating inversion of configuration of the migrating group (cf. inversion pathway in the S_N2 mechanism).

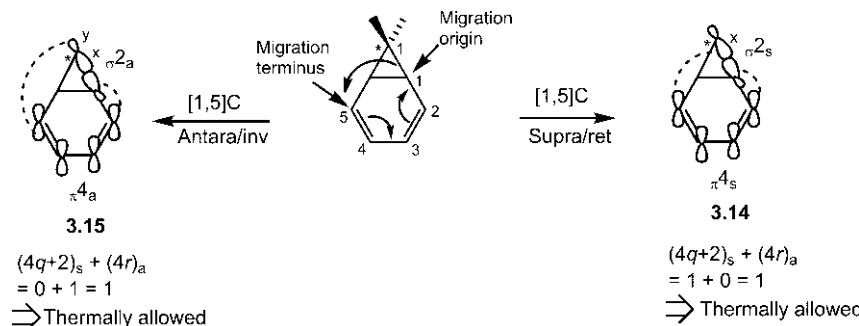


Fig. 3.41 Analysis of the [1,5]C shift for suprafacial/retention and antarafacial/inversion modes using the Woodward–Hoffmann generalized rules

(Verify that the suprafacial/inversion or antarafacial/retention mode is photochemically allowed.)

The FMO analysis of the [1,5]C shift in the suprafacial/retention pathway is shown in Fig. 3.42 in terms of HOMO/LUMO interaction 3.16 and SOMO/SOMO interaction 3.17. As shown, the interactions between HOMO (ψ_2) of the diene component and LUMO (σ^*) of the σ component

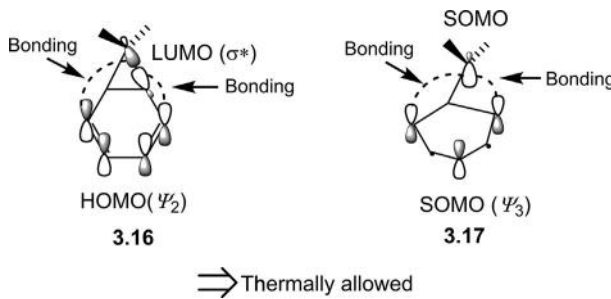


Fig. 3.42 FMO analysis of the [1,5]C shift in the suprafacial/retention pathway in terms of HOMO/LUMO interaction, and SOMO/SOMO interaction.

are bonding. The interactions of SOMO (ψ_3) of the pentadienyl radical and SOMO of the carbon radical are also bonding. Thus, the FMO analysis also indicates a thermally allowed supra/retention pathway in the [1,5]C shift.

4n Electron System: [1,3]C and [1,7]C Shifts

It was mentioned earlier that the 4-electron [1, 3] sigmatropic shift is geometrically constrained to be suprafacial but the [1, 3] suprafacial H shift is thermally forbidden. However, the [1,3]C shift in the suprafacial/inversion pathway is thermally allowed as shown in Fig. 3.43. The $[\sigma_{2_a} + \pi_{2_s}]$ TS 3.18 and the frontier orbital picture 3.19 depict a thermally allowed process.

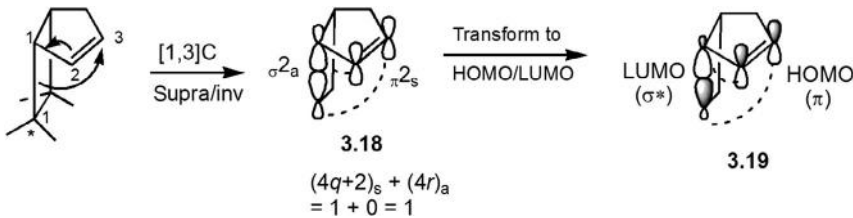


Fig. 3.43 Analysis of the [1,3]C shift in the suprafacial/inversion pathway using the Woodward–Hoffmann generalized rules and FMO approach.

The [1,7]C shift is an 8-electron process and is also allowed thermally under the suprafacial/inversion mode, as shown in Fig. 3.44. The TS aromaticity approach gives an aromatic Möbius TS for the thermally allowed reaction.

Selection Rules for [1,j] Carbon Shifts

The selection rules for [1,j]C shifts are given in Table 3.5. A thermally allowed shift is photochemically forbidden, and vice versa.

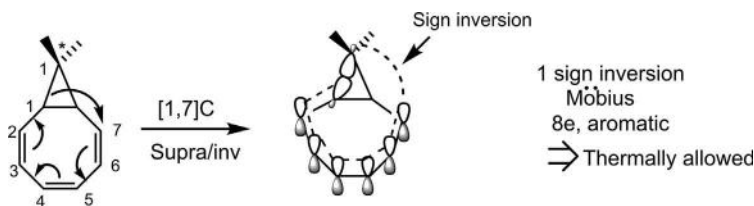


Fig. 3.44 Analysis of the $[1,7]C$ shift under the suprafacial/inversion mode using the transition structure aromaticity approach.

Table 3.5 Selection rules for $[1,j]C$ shifts

Total no. of electrons	Thermally allowed	Photochemically allowed
$4n + 2$	Supra/ret Antara/inv	Supra/inv Antara/ret
$4n$	Supra/inv Antara/ret	Supra/ret Antara/inv

inv, inversion; *ret*, retention.

3.3.4.3 Analysis of $[i,j]$ Rearrangements

The $[i,j]$ sigmatropic rearrangements involving 6 electrons ($4n + 2$, $n = 1$) are most common. The important rearrangements in this category are $[3,3]$ and $[2,3]$ sigmatropic rearrangements. The $[i,j]$ rearrangements with $4n$ electrons are rare.

[3,3] Sigmatropic Rearrangements

The most important $[3,3]$ sigmatropic rearrangements are the thermal Cope and Claisen rearrangements (see Fig. 3.13). The all-carbon version is Cope, and incorporation of one oxygen in the migrating σ bond gives a Claisen rearrangement. Fig. 3.45A shows an analysis of the Cope rearrangement of a 1,5-diene using the Woodward–Hoffmann generalized rule. Here the molecule is treated as a three-component system comprising one σ and two π bonds. As shown, an all-suprafacial $[\sigma_2s + \pi_2s + \pi_2s]$ process is symmetry-allowed thermally. (Show that the reaction can also be represented as an allowed $[\sigma_2s + \pi_2a + \pi_2a]$ by another choice of lobe interactions.) A two-component analysis of the $[3,3]$ rearrangement is shown in Fig. 3.45B. Inspection of the TS 3.20 reveals that three atoms (1,2,3) of the 1,5-diene remain bonded to each other in the TS, as do the other three atoms (4,5,6). The molecule can thus be artificially divided into two allyl components that interact suprafacially 3.21. An odd-electron allyl radical component cannot be considered for the purpose of the generalized rule,

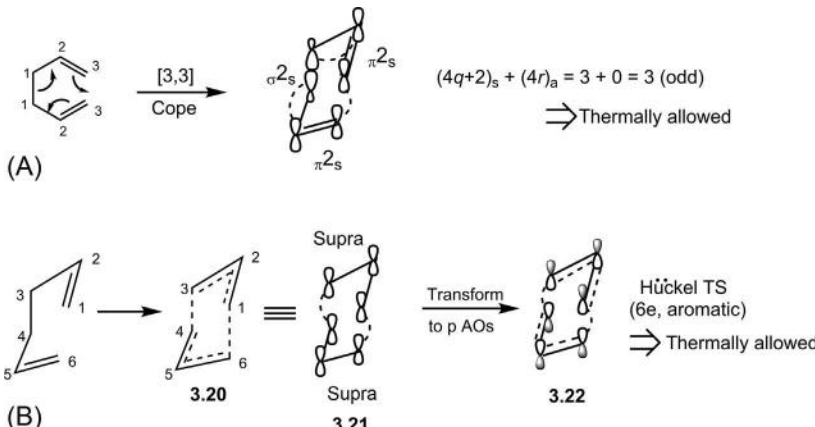


Fig. 3.45 Analysis of the [3,3] Cope rearrangement as (A) a three-component $[\sigma_{2s} + \pi_{2s} + \pi_{2s}]$ process and (B) a two-component supra/supra process.

but allyl cation/anion components are (see below). Here **3.21** is transformed to a cyclic array of basis set orbitals **3.22** which indicates an aromatic Hückel TS for a thermally allowed suprafacial/suprafacial process.

In the above analysis, the TS is drawn in chair conformation. We shall now consider other TS geometries using the two-component analysis. The two allyl units may be taken as either a radical/radical or cation/anion pair for the 6-electron reaction. This is an artificial device for analysis; the reaction itself is concerted and neither ionic nor radical. Since an allyl radical is an odd-electron component, the Woodward–Hoffmann generalized rule is not applicable to a radical/radical interaction. However, the FMO analysis can be applied which involves the SOMO (ψ_2)/SOMO (ψ_2) interaction. This is shown using three TS geometries, namely chair, boat and twist-boat in **Fig. 3.46**. For the chair TS **3.23** or boat TS **3.24**, the supra/supra mode is

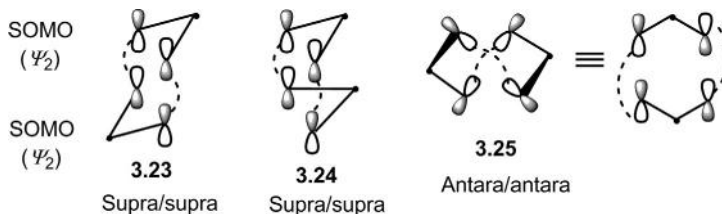


Fig. 3.46 Two-component FMO analysis of the Cope rearrangement involving the chair TS, boat TS and twist-boat TS.

thermally allowed with bonding interactions, whereas for the twist-boat TS **3.25** the antara/antara mode is allowed. Note that the supra/supra interaction involves lobes on the same face of each allyl component, whereas the antara/antara interaction involves lobes on opposite faces of each allyl unit.

The supra/supra interaction in the chair or boat TS is quite favourable geometrically but the effective antara/antara overlap in the twist TS is difficult to achieve. Thus, the Cope rearrangement proceeds mostly via the chair or boat TS; however, the chair TS is preferred (see below).

If we consider the allyl anion/allyl cation model, the FMO interaction is the $\text{HOMO}_{\text{allyl anion}}/\text{LUMO}_{\text{allyl cation}}$ interaction, in which the $\text{HOMO}_{\text{allyl anion}}$ is ψ_2 and $\text{LUMO}_{\text{allyl cation}}$ is also ψ_2 . Thus, in terms of both models, the FMO interaction represents the same pair of interacting MOs (ψ_2/ψ_2). The supra/supra interaction in the allyl anion/allyl cation model also refers to the allowed $[\pi 4_s + \pi 2_s]$ mode in terms of the generalized rule.

Chair TS vs Boat TS: When both chair and boat TSs in the Cope or Claisen rearrangement are geometrically accessible, the [3,3] sigmatropic rearrangement preferentially takes the chair route. This is because the chair TS is more stable than the boat TS. This is primarily attributed to the repulsive orbital interactions (steric repulsion) in chair and boat TSs (Fig. 3.47A). As shown, the repulsive interaction of the filled orbital (ψ_1) of one allyl component with the filled orbital (ψ_1) of the other, the first term of the Salem–Klopman equation (see Chapter 4, Section 4.1), will destabilize the boat conformation more than the chair due to an additional repulsion between the two p orbitals on C-2 carbons in the boat TS. (Note that the filled/filled repulsion is not related to whether we draw the ψ_1 MOs with lobes facing one another with the same sign or opposite sign.)

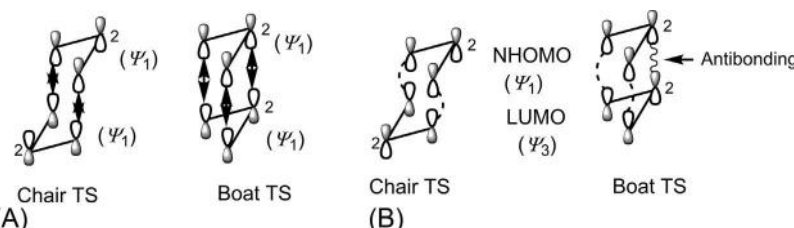


Fig. 3.47 Relative stability of chair and boat TS of the Cope rearrangement in terms of (A) a repulsive filled orbital (ψ_1)/filled orbital (ψ_1) interaction (double-headed arrows) and (B) a secondary orbital overlap (wavy line) in the NHOMO/LUMO interaction.

Furthermore, the secondary orbital interaction can also contribute to the destabilization of the boat TS as shown in Fig. 3.47B. Besides the dominant SOMO/SOMO interaction (ψ_2/ψ_2) (see Fig. 3.46), an interaction between a filled orbital (ψ_1) and a vacant orbital (ψ_3) can also play a role. This ψ_1/ψ_3 interaction is called the NHOMO/LUMO interaction (NHOMO indicating the next lower HOMO). As shown in Fig. 3.47B, besides the primary bonding interactions in both chair and boat TSs, an antibonding secondary orbital interaction (wavy line) involving lobes on C-2 carbons occurs in the boat TS, thereby destabilizing it relative to the chair TS where no secondary orbital interaction is present.

In sum, it is the repulsive interaction between the two p orbitals on C-2 carbons in the boat TS that makes it less stable than the chair TS.

[2, 3] Sigmatropic Rearrangements

An important 6-electron [2,3] sigmatropic rearrangement is the Wittig rearrangement (see Fig. 3.13). The geometry of a five-centre TS 3.26 has a likely envelope conformation (Fig. 3.48). The analysis, using the Woodward–Hoffmann generalized rule, in terms of three interacting components consisting of a σ bond, a lone pair and a π bond shows that the reaction is symmetry-allowed thermally as an all-suprafacial [$\sigma_{2s} + \omega_{2s} + \pi_{2s}$] process. The same process can also be regarded as a supra/supra interaction between two components, the allyl unit and O—C fragment. The TS aromaticity version 3.27 gives an aromatic Hückel TS for a thermally allowed reaction. The FMO analysis of the Wittig rearrangement in terms of the three components has been described later (see Chapter 6, Section 6.3.1, Problem 6.6).

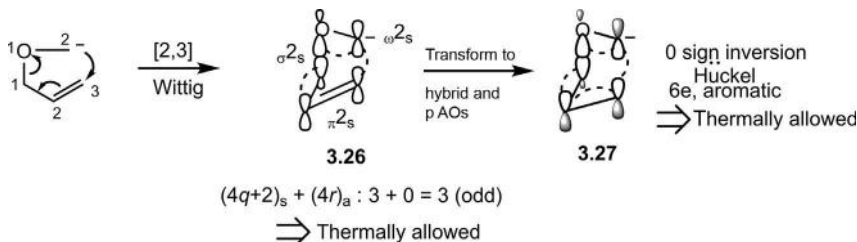


Fig. 3.48 Analysis of the [2, 3] Wittig rearrangement using the Woodward–Hoffmann generalized rule and TS aromaticity approach.

Selection Rules for $[i,j]$ Rearrangements

The selection rules for $[i,j]$ sigmatropic rearrangements in terms of two-component interactions are shown in Table 3.6.

Table 3.6 Selection rules for $[i,j]$ shifts

Total no. of electrons	Thermally allowed	Photochemically allowed
$4n+2$	Supra/supra Antara/antara	Supra/antara Antara/supra
$4n$	Supra/antara Antara/supra	Supra/supra Antara/antara

3.3.5 Analysis of the Group Transfer Reactions and Selection Rule

For the analysis of group transfer reactions, we shall consider an ene reaction and a diimide reduction, and also a 1,4-cycloelimination as a retro group transfer reaction.

3.3.5.1 Ene Reaction

The ene reaction is a thermal 6-electron process (see Fig. 3.14). Fig. 3.49 shows an analysis in terms of three components comprising a σ bond and two π bonds based on the Woodward–Hoffmann generalized rule. The reaction is symmetry-allowed thermally as an all-suprafacial $[\sigma_{2s} + \pi_{2s} + \pi_{2s}]$ process. The TS 3.28 involving an effective head-on orbital overlap for the C–H σ bond transfer has an envelope-like conformation, though the cyclic TS includes six atoms (five carbons and one hydrogen). The head-on overlap requires the three-atom chain (C … H … C) to lie on a single line of the envelope ring. For an analysis by the TS aromaticity approach, 3.28 is transformed to a cyclic array of basis set orbitals which gives an

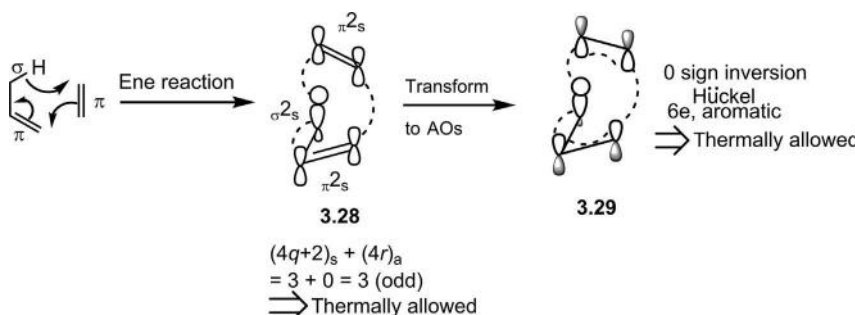


Fig. 3.49 Analysis of the ene reaction using the Woodward–Hoffmann generalized rule and TS aromaticity approach.

aromatic Hückel TS 3.29 for a thermally allowed process. The FMO analysis of the ene reaction has been described later (see Chapter 10, Fig. 10.4; Chapter 6, Problem 6.6).

3.3.5.2 Dimide Reduction

The analysis of diimide reduction using the Woodward–Hoffmann generalized rule is shown in Fig. 3.50. The transfer of two hydrogens from diimide to an alkene is symmetry-allowed thermally as an all-suprafacial $[\sigma_2s + \sigma_2s + \pi_2s]$ process.

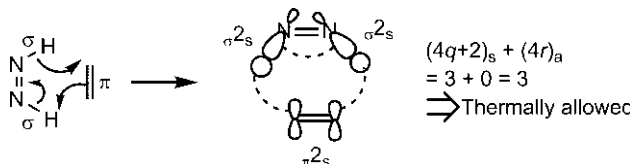


Fig. 3.50 Analysis of diimide reduction as a $[\sigma_2s + \sigma_2s + \pi_2s]$ process.

3.3.5.3 1,4-Cycloelimination

1,4-Cycloelimination is a 6-electron retro group transfer reaction (see Fig. 3.15). The analysis of a 1,4-dehydrogenation in terms of the TS aromaticity approach is shown in Fig. 3.51. The TS is a Hückel system which is aromatic, and hence the process is thermally allowed. The TS is boat-like, and the reaction represents a $[\sigma_2s + \sigma_2s + \pi_2s]$ process.

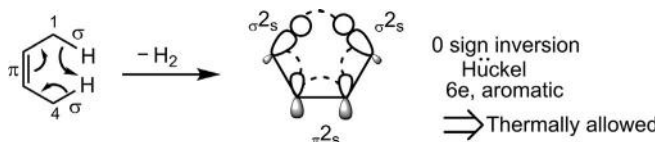


Fig. 3.51 Analysis of a 1,4-cycloelimination using the TS aromaticity approach.

3.3.5.4 Selection Rule for Group Transfer Reactions

Total no. of electrons	Thermally allowed
$4n + 2$	Supra/supra or all-supra

3.3.6 Concluding Remarks

The three mechanistic approaches are based on the molecular orbital theory. They are interrelated and provide the same selection rules. The analysis of the TS by the Woodward–Hoffmann generalized rules uses orbital picture representation (without phase sign), which has been linked to the analysis using the other two approaches by transforming the orbital picture to basis set orbitals in the TS aromaticity approach or frontier orbitals in the FMO approach. This unifying method of analysis has been described for all four classes of pericyclic reactions. Fig. 3.52 summarizes the idea, taking the Diels–Alder case.

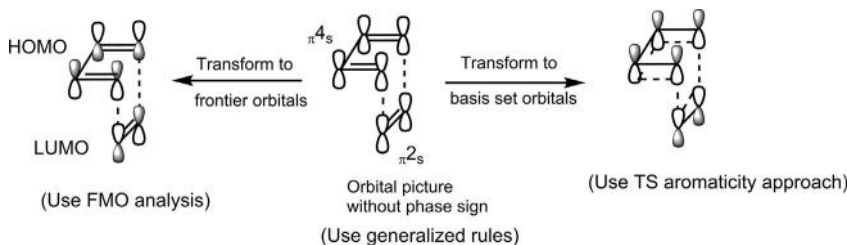


Fig. 3.52 Unifying method of analysis by three mechanistic approaches.

The generalized rules come as a handy tool to predict whether a pericyclic process is symmetry-allowed or symmetry-forbidden. These rules have their origin in the orbital symmetry correlation approach (see Chapter 11), which provides the most convincing orbital explanation. The mere application of the generalized rules, however, does not give a clear picture of the electronic interactions responsible for stabilization or destabilization of the TS. The description of the Hückel or Möbius TS as aromatic or antiaromatic immediately gives a picture on the relative stability of the TS. The frontier orbital approach describes bonding/antibonding interaction between the reactant frontier orbitals. This is an initial interaction which decides whether a concerted pathway is possible or not. If the initial interaction is bonding, the trend is assumed to be continued throughout the reaction. The bonding/antibonding interaction between the frontier orbitals thereby relates to the relative stability of a TS. The frontier orbital theory provides an extremely advantageous approach in dealing with the reactivity and different kinds of selectivity in pericyclic reactions (see later). The theory is so successful because pericyclic reactions in general have early TSs. However, it should

be borne in mind that the frontier orbital approach is an oversimplified procedure with the assumptions of disproportionate contributions of frontier orbitals to the interaction energy of the TS, and electrostatic, conformational and steric factors can override the frontier orbital effects in certain cases.

REFERENCES

1. Woodward, R. B.; Hoffmann, R. *The Conservation of Orbital Symmetry*; Verlag Chemie: Weinheim, 1971. Academic Press: New York, 1970.
2. Gilchrist, L.; Storr, R. C. *Organic Reactions and Orbital Symmetry*, 2nd ed.; Cambridge University Press: Cambridge, 1979.
3. Marchand, A. P.; Lehr, R. E., Eds. *Pericyclic Reactions*, Vols. 1 and 2; Academic Press: New York, 1977.
4. Fleming, I. *Pericyclic Reactions*, 2nd ed.; Oxford University Press: Oxford, 2015.
5. Sankararaman, S. *Pericyclic Reactions—A Textbook: Reactions, Applications and Theory*; Wiley-VCH: Weinheim, 2005.
6. Carey, F. A.; Sundberg, R. J. *Advanced Organic Chemistry, Part A*, 5th ed.; Springer: New York, 2007 (chapter 10).
7. Fleming, I. *Molecular Orbitals and Organic Chemical Reactions*, Student Edition; Wiley: Chichester, 2009. Reference Edition, 2010 (chapters 6 and 8).
8. Houk, K. N.; Gonzalez, J.; Li, Y. *Acc. Chem. Res.* **1995**, *28*, 81.
9. Rzepa, H. S. *J. Chem. Educ.* **2007**, *84*, 1535.
10. Arrieta, A.; de Cozar, A.; Cossio, F. P. *Curr. Org. Chem.* **2011**, *15*, 3594.
11. Woodward, R. B.; Hoffmann, R. *Angew. Chem. Int. Ed. Engl.* **1969**, *8*, 781.
12. Bernardi, F.; Bottoni, A.; Field, M. J.; et al. *J. Am. Chem. Soc.* **1988**, *110*, 3050.
13. Storer, J. W.; Raimondi, L.; Houk, K. N. *J. Am. Chem. Soc.* **1994**, *116*, 9675.
14. Beno, B. R.; Houk, K. N.; Singleton, D. A. *J. Am. Chem. Soc.* **1994**, *116*, 9984.
15. Tolbert, L. M.; Ali, M. B. *J. Am. Chem. Soc.* **1981**, *103*, 2104.
16. Desimoni, G.; Faita, G.; Righetti, P. P.; Toma, L. *Tetrahedron* **1990**, *46*, 7951.
17. Taagepera, M.; Thornton, E. R. *J. Am. Chem. Soc.* **1972**, *94*, 1168.
18. Sauer, J.; Sustmann, R. *Angew. Chem. Int. Ed. Engl.* **1980**, *19*, 779.
19. Fleming, I.; Karger, M. H. *J. Chem. Soc. C* **1967**, 226.
20. Bartlett, P. D. Q. *Rev. Chem. Soc.* **1970**, *24*, 473.
21. Stewart, C. A. *J. Am. Chem. Soc.* **1962**, *84*, 117.
22. Zimmerman, H. E. *Acc. Chem. Res.* **1971**, *4*, 272.
23. Dewar, M. J. S. *Angew. Chem. Int. Ed. Engl.* **1971**, *10*, 761.
24. Woodward, R. B.; Hoffmann, R. *J. Am. Chem. Soc.* **1965**, *87*, 395.
25. Fukui, K. *Acc. Chem. Res.* **1971**, *4*, 57.
26. Dewar, M. J. S.; Dougherty, R. C. *The PMO Theory of Organic Chemistry*. Plenum: New York, 1975.
27. Zimmerman, H. E. *Acc. Chem. Res.* **1972**, *5*, 393.
28. Fukui, K. *Angew. Chem. Int. Ed. Engl.* **1982**, *21*, 801.

CHAPTER 4

Cycloadditions 1: Perturbation Theory of Reactivity, Regioselectivity and Periselectivity

In Chapter 3 we have seen that the Woodward–Hoffmann selection rules govern whether a particular mode of cycloaddition is symmetry-allowed or symmetry-forbidden. If a symmetry-allowed mode gives a transition structure of favourable or reasonable geometry, the cycloaddition becomes a reality. For example, the geometrically favourable $[\pi 4_s + \pi 2_s]$ Diels–Alder cycloaddition is a popular and widely used reaction. However, the important features of reactivity, regioselectivity and periselectivity in cycloadditions cannot be accounted for by considering the selection rules alone. An approach to rationalize these features is obtained in perturbation molecular orbital theory. Using this theory, Klopman¹ and Salem² have derived a general perturbation expression to estimate chemical reactivity, which is known as the Salem–Klopman equation.

4.1 THE SALEM–KLOPMAN EQUATION

In general, three major forces operate as two molecules approach each other. The Salem–Klopman equation has the form of a sum of three terms for the three interactions.

The energy (ΔE) gained or lost due to the interactions of orbitals of one molecule with those of another is given by

$$\Delta E = \underbrace{- \sum_{ab} (q_a + q_b) \beta_{ab} S_{ab}}_{(1\text{st term})} + \underbrace{\sum_{k < l} \frac{Q_k Q_l}{\epsilon R_{kl}}}_{(2\text{nd term})} + \underbrace{\sum_r^{\text{occ.}} \sum_s^{\text{unocc.}} - \sum_s^{\text{occ.}} \sum_r^{\text{unocc.}} \frac{2 \left(\sum_{ab} c_{ra} c_{sb} \beta_{ab} \right)^2}{E_r - E_s}}_{(3\text{rd term})} \quad (4.1)$$

where q_a , q_b = electron populations in atomic orbitals a and b; β , S = resonance and overlap integrals; Q_k , Q_l = total charges on atoms k and l; ϵ = local dielectric constant; R_{kl} = distance between the atoms k and l; c_{ra} = coefficient of atomic orbital a in molecular orbital r; c_{sb} = coefficient of atomic orbital b in molecular orbital s; E_r , E_s = energy of molecular orbitals r and s.

The 1st term is positive as β is a negative energy quantity. Therefore the interactions represented by the 1st term are energy-raising and antibonding which would lead to destabilization of the interacting system. The 1st term describes the interactions of the occupied orbitals of one molecule with the occupied orbitals of the other (Eq. 4.2)

$$\text{1st term} = \sum_s^{\text{occ.}} \sum_r^{\text{occ.}} \frac{2 \left(\sum_{ab} c_{ra} c_{sb} \beta_{ab} \right)^2}{E_r - E_s} \quad (4.2)$$

This kind of interaction of a filled orbital with another filled orbital leads to a net antibonding effect (see Fig. 1.6, p. 5). The repulsive 1st term generally represents the steric effect in molecules and in molecular interactions.

The 2nd term denotes Coulombic repulsion between like charges or attraction between unlike charges, and thereby contributes to the destabilization or stabilization of the system.

The 3rd term is a second-order perturbation term and the whole term is negative as $E_{\text{occ}} < E_{\text{unocc}}$. This is therefore energy lowering and would lead to the stabilization of the interacting system. This term represents the interactions of all filled orbitals of one molecule with all unfilled orbitals of the other, and is a donor–acceptor orbital interaction term. The interaction of a filled orbital with an unfilled orbital leads to a net bonding effect, and the 3rd term therefore contributes to the stabilization energy of the reacting system.

The energy of activation of a reaction can be considered as being made up of the destabilization and stabilization energies contributed by the three terms of the equation.

4.1.1 Application of the Salem–Klopman Equation to Cycloadditions

The Salem–Klopman equation can be simplified in the case of cycloadditions using the following approximations:

- (a) The 1st term is neglected. For a particular kind of cycloaddition, it is generally the difference in reactivity and selectivity that is of interest. If a molecule is attacked at two possible sites or if there are two possible orientations, then the 1st term will be nearly the same for the two cases

of additions assuming that the substituents on the reactant sites are of constant size. It thus seems reasonable to neglect the 1st term for dealing with the differential reactivity and selectivity.

- (b) The 2nd term is neglected. For pericyclic cycloaddition, it is also reasonable to neglect the Coulombic term as the reactant molecules are not particularly polar.
- (c) In the 3rd term, the dominant interaction is arguably between orbitals with smallest energy separation ($E_r - E_s$) which is the denominator. These orbitals are the frontier orbitals (HOMOs and LUMOs). Thus the orbital interactions in the 3rd term can be approximated to HOMO/LUMO interactions.

With the above approximations, the Salem–Klopman equation in the case of cycloadditions can be simplified to a frontier orbital expression as described below.

Let us consider a cycloaddition of two hypothetical π systems A and B. The frontier orbital pairs are $\text{HOMO}_A/\text{LUMO}_B$ and $\text{HOMO}_B/\text{LUMO}_A$ (Fig. 4.1). Note that HOMO and LUMO for each π system have opposite symmetry or phase relationship at the terminal atoms.

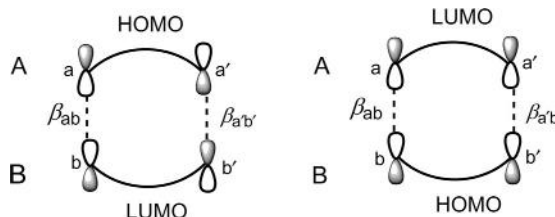


Fig. 4.1 Frontier orbital interactions involving the terminal atoms (a, b) and (a', b') of two π systems A and B. β_{ab} and $\beta_{a'b'}$ indicate the resonance integral with respect to the interaction between two p orbitals on atoms a, b and a', b', respectively.

Applying the above approximations, Eq. (4.1) is now simplified to a frontier orbital expression as

$$\Delta E_{\text{FMO}} = \frac{2 \left(\sum_{ab} c_{\text{HO}a} c_{\text{LU}b} \beta_{ab} \right)^2}{E_{\text{HO}(A)} - E_{\text{LU}(B)}} - \frac{2 \left(\sum_{ab} c_{\text{LU}a} c_{\text{HO}b} \beta_{ab} \right)^2}{E_{\text{LU}(A)} - E_{\text{HO}(B)}}$$

or,

$$\Delta E_{\text{FMO}} = - \frac{2 \left(c_{\text{HO}a} c_{\text{LU}b} \beta_{ab} + c_{\text{HO}a'} c_{\text{LU}b'} \beta_{a'b'} \right)^2}{E_{\text{LU}(B)} - E_{\text{HO}(A)}} - \frac{2 \left(c_{\text{LU}a} c_{\text{HO}b} \beta_{ab} + c_{\text{LU}a'} c_{\text{HO}b'} \beta_{a'b'} \right)^2}{E_{\text{LU}(A)} - E_{\text{HO}(B)}} \quad (4.3)$$

Clearly, ΔE_{FMO} is negative as $E_{\text{LU}} > E_{\text{HO}}$. Eq. (4.3) is to be employed when both HOMO/LUMO interactions are important. If one HOMO/LUMO interaction is more important than the other and the other can be ignored, Eq. (4.3) then further reduces to

$$\Delta E_{\text{FMO}} = -\frac{2(c_a c_b \beta_{ab} + c_{a'} c_{b'} \beta_{a'b'})^2}{E_{\text{LU}} - E_{\text{HO}}} \quad (4.4)$$

Eq. (4.4) represents the frontier orbital expression for a single or controlling HOMO/LUMO pair for a cycloaddition.

The features of reactivity, regioselectivity and periselectivity in cycloadditions can be rationalized by invoking Eqs (4.3) or (4.4), as applicable, using the energies and coefficients of the HOMO and LUMO of the interacting π systems.

4.2 THE DIELS–ALDER REACTION

The Diels–Alder cycloaddition of a diene with a dienophile is represented schematically in Fig. 4.2 (see Section 3.2.1).

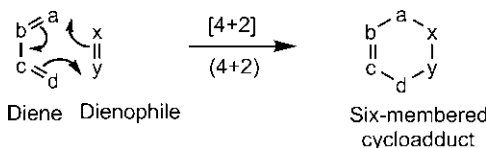


Fig. 4.2 Schematic representation of Diels–Alder reaction.

As two σ bonds are formed at the expense of two π bonds, the reaction is exothermic. Besides all-carbon diene systems, heterodienes with one or more heteroatoms (commonly N, O) also participate in Diels–Alder reactions. The dienophiles are usually alkenes ($\text{C}=\text{C}$) or alkynes ($\text{C}\equiv\text{C}$) but a variety of heterodienophiles such as $\text{C}=\text{O}$, $\text{N}=\text{O}$, $\text{N}=\text{N}$, $\text{O}=\text{O}$ (singlet) and $\text{C}\equiv\text{N}$ can also take part in Diels–Alder reactions. Such scope and versatility of the Diels–Alder reaction make the reaction most popular in mechanistic and synthetic studies.

The diene component of the Diels–Alder reaction cannot react in *s-trans* conformation as this introduces an impossibly strained *trans* double bond in the six-membered ring adduct (Fig. 4.3). Thus Diels–Alder reaction proceeds via a *s-cis* conformation which gives a stable *cis* double bond in the cycloadduct.

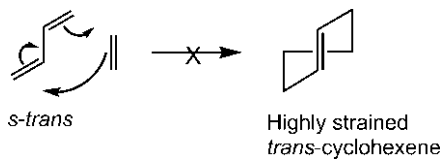


Fig. 4.3 No Diels–Alder reaction with *s-trans* diene.

The *s-trans* conformation of an acyclic diene has lower energy than *s-cis* conformation. Butadiene which exists in *s-trans* conformation (~99% at room temperature) must therefore take up the higher energy *s-cis* conformation to undergo the Diels–Alder reaction with a dienophile (Fig. 4.4A). On the other hand, cyclopentadiene that exists in locked *s-cis* conformation straightway undergoes the Diels–Alder reaction (Fig. 4.4B).

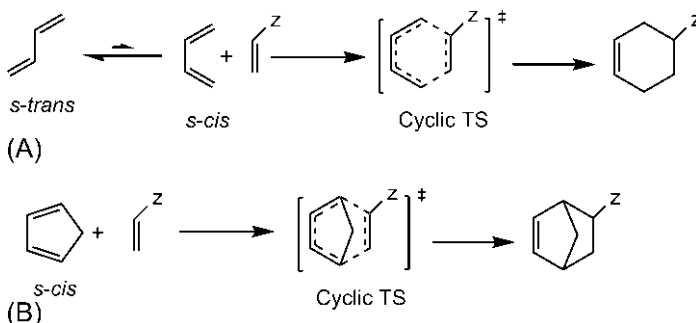


Fig. 4.4 Diels–Alder reaction with (A) butadiene and (B) cyclopentadiene.

For the acyclic butadiene, the free energy of activation is given by

$$\Delta G_{\text{acyclic}}^{\ddagger} = G_{\text{TS}} - G_{\text{reactants}} = G_{\text{TS}} - G_{\text{s-trans diene}} - G_{\text{dienophile}}$$

The free energy of ground state butadiene is a weighted sum of free energies of *s-trans* and *s-cis* forms but *s-cis* form contributes negligibly (1%). Therefore the free energy of butadiene is taken as that of *s-trans* diene.

In the case of cyclic diene, $\Delta G_{\text{cyclic}}^{\ddagger} = G_{\text{TS}} - G_{\text{reactants}} = G_{\text{TS}} - G_{\text{s-cis diene}} - G_{\text{dienophile}}$

Comparing ΔG^{\ddagger} for acyclic and cyclic cases, we get

$\Delta G_{\text{cyclic}}^{\ddagger} < \Delta G_{\text{acyclic}}^{\ddagger}$ because $G_{\text{s-cis diene}} > G_{\text{s-trans diene}}$.

Therefore the free energy difference between *s-cis* and *s-trans* forms raises the free energy barrier for the acyclic case, and a cyclic diene would react faster than acyclic diene in the Diels–Alder reaction.

The reactivity of cyclic dienes however diminishes with increasing ring size: cyclopentadiene \gg cyclohexadiene $>$ cycloheptadiene. This is because

the terminal carbons of the diene unit get further apart with increase in ring size resulting in progressively less effective overlap with the dienophile in the transition structure.

The dienes with exocyclic double bonds which are fixed in *s*-*cis* conformation react readily with dienophiles. Two important examples are *ortho*-quinonodimethanes and 1,2-dimethylenecyclohexane (Fig. 4.5A). On the other hand, cyclic dienes that are permanently in *s*-*trans* conformation and acyclic dienes which cannot adopt *s*-*cis* conformation due to steric reasons are unreactive (Fig. 4.5B).

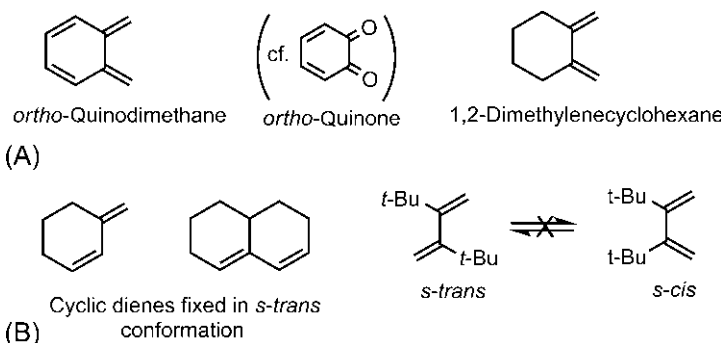


Fig. 4.5 Examples of dienes in (A) *s*-*cis* and (B) *s*-*trans* conformations.

The dienophiles with isolated double or triple bonds are usually unreactive; however, cyclic alkenes and alkynes with large angle strain are reactive dienophiles. For example, cyclopropene as a dienophile can react readily with cyclopentadiene (Fig. 4.6A).³ Cyclooctyne has a considerable ring strain but is isolable and undergoes Diels–Alder reaction rapidly with diphenylisobenzofuran to give the cycloadduct (Fig. 4.6B).⁴ The driving force for this reaction is attributed to the decrease in angle strain in the transition structure for the cycloaddition. The smaller cycloalkynes with increased angle strain are not isolable but can be trapped by Diels–Alder cycloaddition. Arynes are reactive intermediates and can act as powerful dienophiles. For example, benzyne reacts with a variety of dienes and even with benzene to give the cycloadducts (Fig. 4.6C).⁴

4.2.1 Frontier Orbital Control and Reactivity

There are three types of frontier orbital control that can operate on the Diels–Alder reaction based on whether a single HOMO/LUMO pair or both HOMO/LUMO pairs are involved. These are

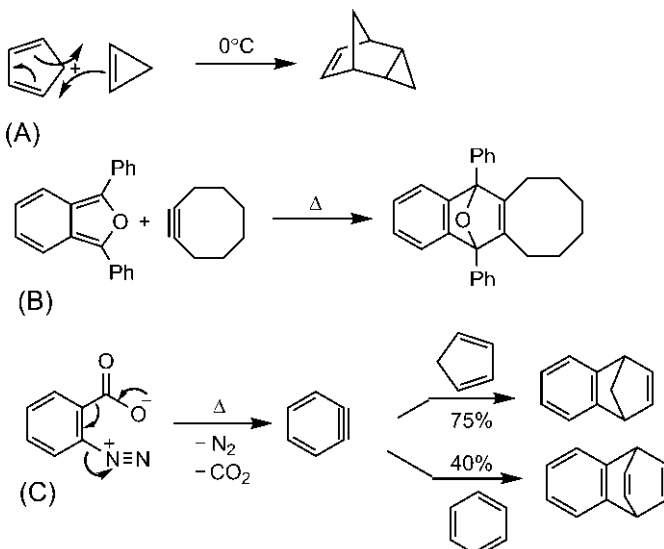


Fig. 4.6 Diels–Alder reactions with (A) cyclopropene, (B) cyclooctyne and (C) benzyne as dienophiles.

1. $\text{HOMO}_{\text{diene}}/\text{LUMO}_{\text{dienophile}}$ control
2. $\text{LUMO}_{\text{diene}}/\text{HOMO}_{\text{dienophile}}$ control
3. $\text{HOMO}_{\text{diene}}/\text{LUMO}_{\text{dienophile}}$ and $\text{LUMO}_{\text{diene}}/\text{HOMO}_{\text{dienophile}}$ control

The frontier orbital control can be determined using Eq. (4.3). The magnitude of ΔE_{FMO} is contributed largely by the denominator ($E_{\text{LUMO}} - E_{\text{HOMO}}$) which primarily decides the frontier orbital control. The smaller the denominator, the greater its contribution to ΔE_{FMO} . The denominator is calculated for each HOMO/LUMO pair using Houk's data for frontier orbital energies.^{5,6} The frontier orbital energies shown in Figs 1.23, 1.24 and 1.26 are combined in Fig. 4.7.

If the energy gaps for the two possible HOMO/LUMO interactions are closely balanced (~ 1 eV), both interactions become significant and the frontier orbital control is exercised by both HOMO/LUMO pairs. But, if the energy gap for one HOMO/LUMO pair is much smaller than the other complementary pair, the interaction with smaller energy separation becomes dominant and thereby determines the frontier orbital control. A HOMO/LUMO pair with a larger energy separation by 3 eV or more may practically be ignored.

E_{LUMO} (eV)	1.5	1.0	0	3.0
E_{HOMO} (eV)	-10.5	-9.1	-10.9	-9.0
E_{LUMO} (eV)	1.0	0.5	-0.5	2.5
E_{HOMO} (eV)	-9.1	-8.2	-9.5	-8.5
E_{LUMO} (eV)		0.7	-0.3	2.3
E_{HOMO} (eV)		-8.5	-9.3	-8.7

Fig. 4.7 Frontier orbital energies of unsubstituted and substituted alkenes and dienes. (For classification of substituents, see [Section 1.5](#), p. 19.)

We begin with a prototype Diels–Alder reaction of butadiene with ethylene. The denominator ($E_{\text{LUMO}} - E_{\text{HOMO}}$) in Eq. (4.3) is estimated as follows:

$$\begin{aligned}E_{\text{LUMO(ethylene)}} - E_{\text{HOMO(butadiene)}} &= 1.5 - (-9.1) \text{ eV} = 10.6 \text{ eV} \\E_{\text{LUMO(butadiene)}} - E_{\text{HOMO(ethylene)}} &= 1.0 - (-10.5) \text{ eV} = 11.5 \text{ eV}\end{aligned}$$

The two energy gaps are within 1 eV, and the frontier orbital control is operated by both $\text{HOMO}_{\text{diene}}/\text{LUMO}_{\text{dienophile}}$ and $\text{LUMO}_{\text{diene}}/\text{HOMO}_{\text{dienophile}}$ interactions. The prototype reaction is found to be extremely slow and requires rather forcing conditions (Fig. 4.8A).⁷

Let us now consider the Diels–Alder reactions when diene and dienophile are adorned with a c-, z- or x-substituent where c, z and x stand for conjugating, electron-withdrawing, and electron-donating substituent, respectively (see [Section 1.5](#), p. 19). It is observed experimentally that the introduction of a z-substituent (e.g., CHO) on the dienophile speeds up a Diels–Alder reaction quite remarkably when the reaction occurs under much milder conditions (Fig. 4.8B). The reaction of the z-substituted dienophile is more facile with a cyclic diene such as cyclopentadiene. The Diels–Alder reactions with electron-deficient z-substituted dienophiles are indeed most common.

The frontier orbital control with a z-substituted dienophile is obtained from the estimate of HOMO/LUMO energy separation ($E_{\text{LUMO}} - E_{\text{HOMO}}$).

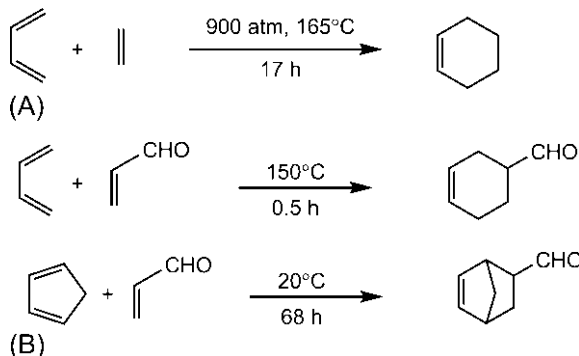


Fig. 4.8 (A) Diels–Alder reaction between butadiene and ethylene. (B) Diels–Alder reactions with acrolein (a α -substituted dienophile).

$$E_{\text{LUMO}(\alpha-\text{dienophile})} - E_{\text{HOMO}(\text{butadiene})} = 0 - (-9.1) \text{ eV} = 9.1 \text{ eV}$$

$$E_{\text{LUMO}(\text{butadiene})} - E_{\text{HOMO}(\alpha-\text{dienophile})} = 1.0 - (-10.9) \text{ eV} = 11.9 \text{ eV}$$

The energy separation for $\text{HOMO}_{\text{diene}}/\text{LUMO}_{\text{dienophile}}$ interaction is considerably smaller by 2.8 eV. The reaction is therefore mainly under $\text{HOMO}_{\text{diene}}/\text{LUMO}_{\text{dienophile}}$ control with an energy separation of 9.1 eV.

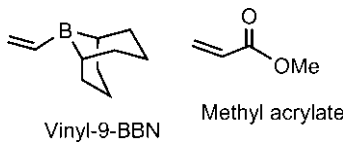
The reactivity pattern also follows from the HOMO/LUMO energy difference, the denominator in Eq. (4.3). *The smaller the HOMO/LUMO energy difference the higher is the reactivity.* For the prototype Diels–Alder reaction, both HOMO/LUMO pairs are important which give a weighted average value of ~ 11 eV for $(E_{\text{LUMO}} - E_{\text{HOMO}})$ whereas the reaction with a α -substituted dienophile gives a smaller energy difference of 9.1 eV. Thus a α -substituent on the dienophile increases the rate of the Diels–Alder reaction.

Problem 4.1

Explain the observation that butadiene reacts with vinyl-9-BBN at room temperature, and the reaction is 200 times faster than the reaction with methyl acrylate.

Answer⁸

The substituent 9-BBN in vinyl-9-BBN (shown below) is a strong π acceptor due to the presence of a vacant p orbital on B. It is a better electron-withdrawing α -substituent than CO₂Me of methyl acrylate. The LUMO of 9-BBN-substituted dienophile has lower energy than that of methyl acrylate and hence leads to the narrowing of the $\text{HOMO}_{\text{diene}}/\text{LUMO}_{\text{dienophile}}$ energy gap. The reaction of butadiene with vinyl-9-BBN thus occurs faster.

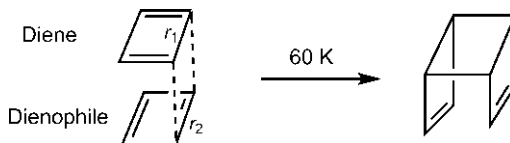


Problem 4.2

The dimerization of cyclobutadiene is an extremely fast Diels–Alder reaction which occurs even at 60 K. Explain.

Answer

The frontier orbital interaction for dimerization involves HOMO of one cyclobutadiene molecule with LUMO of another.



In rectangular cyclobutadiene, ψ_2 is HOMO and ψ_3 LUMO (see Section 1.7.1.1, p. 34). The HOMO/LUMO energy gap is very small which leads to very high reactivity. The extremely fast nature of the reaction is also contributed by the loss of antiaromaticity of cyclobutadiene. Further, more efficient orbital overlap is possible as the bond distances of single bond (r_1) and double bond (r_2) are close.

4.2.1.1 Normal Electron Demand Diels–Alder Reaction

The cycloaddition of butadiene with a z-substituted dienophile reveals complementary electron demand involving electron-rich (donor) diene and electron-deficient (acceptor) dienophile. This type of Diels–Alder reaction is known as normal electron demand Diels–Alder reaction. When the diene possesses a c- or x-substituent at C-1/C-2, it becomes even more electron rich and the reaction is expected to be more facile. The HOMO/LUMO energy separations ($E_{\text{LUMO}} - E_{\text{HOMO}}$) for cycloadditions of the c- and x-substituted dienes with z-substituted dienophile are shown in Fig. 4.9. The more important HOMO/LUMO interaction with a smaller energy separation in each case is indicated with the estimated value of ($E_{\text{LUMO}} - E_{\text{HOMO}}$) in bold.

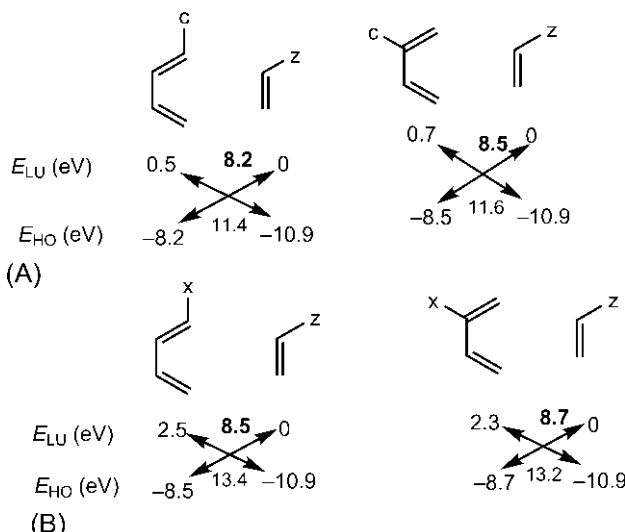


Fig. 4.9 HOMO/LUMO energy separations ($E_{LU} - E_{HO}$) for cycloaddition of z-substituted dienophile with (A) 1-c- and 2-c-substituted dienes and (B) 1-x- and 2-x-substituted dienes. The more important interaction is indicated with the estimated value in bold.

Clearly, for both c- and x-substituted dienes, the dominant frontier orbital interaction is $\text{HOMO}_{\text{diene}}/\text{LUMO}_{\text{dienophile}}$ interaction. The estimates of energy separations indicate that, in the case of c-substituted dienes (Fig. 4.9A), the dominant interaction is preferred over the other by a margin of 3.1–3.2 eV whereas for x-substituted dienes (Fig. 4.9B), the margin is still larger (4.5–4.9 eV).

The question of reactivity is then addressed as follows. The energy difference of the controlling $\text{HOMO}_{\text{diene}}/\text{LUMO}_{\text{dienophile}}$ interaction for c- and x-substituted dienes (as shown in Fig. 4.9) ranges from 8.2 to 8.7 eV, which is less than that for the unsubstituted diene (9.1 eV). Therefore both c- and x-substituted dienes react faster than the unsubstituted diene. This has been observed experimentally. For example, the reaction of 1-methoxybutadiene or 2-methoxybutadiene with acrolein is more facile and proceeds at lower temperature (Fig. 4.10B and C) than butadiene (Fig. 4.10A).

It follows that more than one z-substituent on the dienophile would further lower its LUMO energy leading to the narrowing of the HOMO/LUMO energy gap, and hence speed up the reaction further (Fig. 4.10D). The incorporation of electronegative N or O in the dienophile double bond can also provide a low-energy LUMO (see Section 1.4).

The triazolinedione dienophile in Fig. 4.10E has an extremely low-energy LUMO so that the reaction proceeds at a very low temperature. It is pertinent to mention here that the triazolinedione possesses both a high-energy HOMO (because of the combination of two adjacent nitrogen lone pairs) and a low-energy LUMO (because of the combination of p orbitals of two electronegative nitrogens), and is extremely reactive so that one bond forms far ahead of the other in the transition structure. The calculations suggest that the cycloaddition is concerted but highly asynchronous.⁹

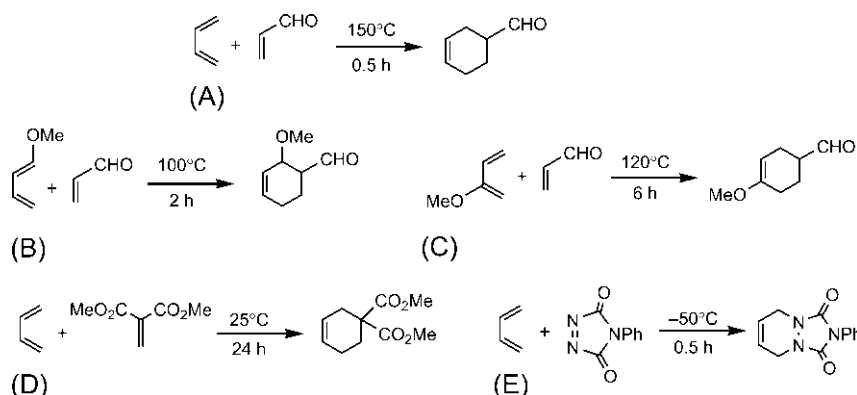


Fig. 4.10 Examples (A–E) of normal electron demand Diels–Alder reactions.

In summary, normal electron demand Diels–Alder reactions are $\text{HOMO}_{\text{diene}}/\text{LUMO}_{\text{dienophile}}$ controlled, and proceed at reasonable rates. Most Diels–Alder reactions belong to such type.

4.2.1.2 Inverse Electron Demand Diels–Alder Reaction

If the electron demands of the diene and dienophile are reversed using acceptor diene (electron deficient) and donor dienophile (electron rich), the reaction is called inverse electron demand Diels–Alder (IEDDA) reaction. The frontier orbital control and reactivity trend for IEDDA reaction can be determined from the estimation of $(E_{\text{LUMO}} - E_{\text{HOMO}})$ in a manner similar to that described before. This is illustrated with the combination of 1-z-substituted diene with x-substituted dienophile in Fig. 4.11.

Here the dominant interaction is $\text{LUMO}_{\text{diene}}/\text{HOMO}_{\text{dienophile}}$ interaction with a smaller energy separation of 8.5 eV which is favoured over the other interaction by a margin of 4 eV. The IEDDA reaction is therefore under $\text{LUMO}_{\text{diene}}/\text{HOMO}_{\text{dienophile}}$ control and has an energy separation similar to normal Diels–Alder reaction. The reaction with inverse electron demand is therefore expected to be facile. However, IEDDA reactions are

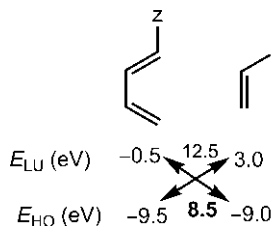


Fig. 4.11 HOMO/LUMO energy separations ($E_{\text{LU}} - E_{\text{HO}}$) for cycloaddition of 1-z-substituted diene with x-substituted dienophile. The more important interaction is indicated with the estimated value in bold.

much less common, and performing a reaction with inverse electron demand is often less effective compared with normal Diels–Alder reaction. In fact, when two dienes, one x-substituted and the other z-substituted, are allowed to react with each other, the normal Diels–Alder reaction takes place instead of IEDDA reaction as shown in Fig. 4.12.¹⁰

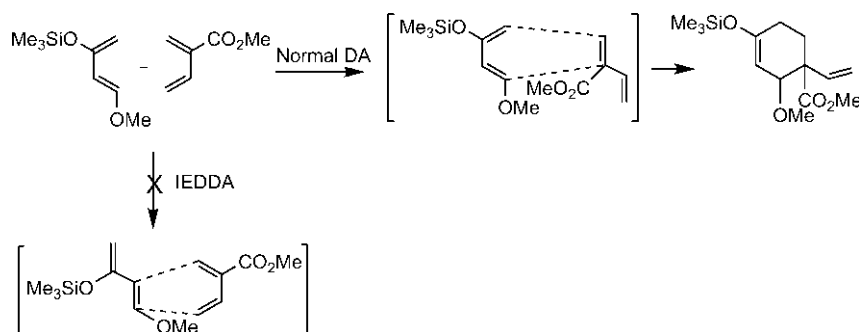


Fig. 4.12 Preference of normal Diels–Alder reaction over inverse electron demand Diels–Alder (IEDDA) reaction.

A simple frontier orbital explanation by Fukui¹¹ is described in Fig. 4.13, though other suggestions by perturbation calculation have been made.¹²

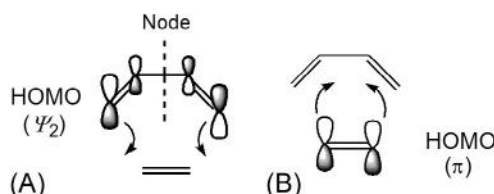
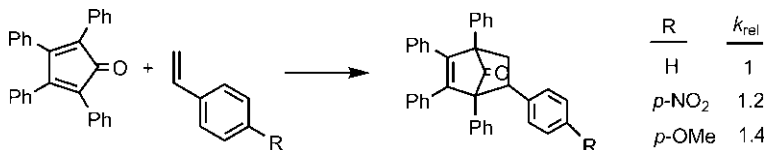


Fig. 4.13 Contrasting frontier orbital electron shift in (A) normal Diels–Alder reaction and (B) inverse electron demand Diels–Alder (IEDDA) reaction.

As the reaction proceeds, π electrons move into the space between the reactants to form σ bonds. In normal electron demand Diels–Alder reaction (Fig. 4.13A), the electrons flowing from the HOMO (ψ_2) of diene are not likely to be concentrated at the centre of the reacting system because of a node in the middle of the diene HOMO but are accumulated at the wings where new σ bonds will develop connecting the diene and the dienophile. This is consistent with orbital correlation diagram (see later Fig. 11.12, p. 476) which shows that electrons in ψ_2 move into a σ bond of the product cyclohexene. In sharp contrast, for IEDDA reaction (Fig. 4.13B), the electrons from HOMO (π) of dienophile having no node are likely to move towards the central part of the intermolecular region, and hence not involved in σ bond formation between the diene and the dienophile. The π orbital of dienophile is actually transformed into the π of cyclohexene, as shown by the correlation diagram. Although Fig. 4.13 does not give the whole picture of electronic reorganization along the reaction coordinate, the simple picture can account for the fact that normal Diels–Alder reaction involving HOMO of diene proceeds more satisfactorily than IEDDA involving HOMO of dienophile. For the reaction with inverse electron demand, it is usually necessary to strongly perturb and polarize the HOMO of dienophile by powerful donor substituent for interaction with the LUMO of diene also bearing strong electron-withdrawing group.

Problem 4.3

Explain the relative rates observed in the following Diels–Alder reactions.



Answer¹³

The relative rate data show that the cyclopentadienone (tetracyclone) as a diene reacts faster with a substituted styrene than with unsubstituted styrene ($R=H$) as a dienophile. It is immaterial whether the substituent R is electron withdrawing (p -NO₂) or electron donating (p -OMe). In tetracyclone, Ph is a *c*-substituent, and C=O is not so electron withdrawing as the polar carbonyl canonical structure would tend to make teracyclone antiaromatic. Therefore tetracyclone behaves more like a *c*-substituted diene. Styrene ($R=H$) is also a *c*-substituted dienophile.

The energy separations for the two HOMO/LUMO pairs in the reaction of *c*-substituted diene with *c*-substituted dienophile are close (check), and hence the reaction is $\text{HOMO}_{\text{diene}}/\text{LUMO}_{\text{dienophile}}$ and $\text{LUMO}_{\text{diene}}/\text{HOMO}_{\text{dienophile}}$ controlled.

When $\text{R} = p\text{-NO}_2$, the substituted styrene is an electron-deficient *z*-substituted dienophile. The reaction of tetracyclone (as a *c*-substituted diene) with *z*-substituted dienophile is $\text{HOMO}_{\text{diene}}/\text{LUMO}_{\text{dienophile}}$ controlled for a normal electron demand reaction. As the *z*-substituent ($p\text{-NO}_2$) lowers the energy of the styrene LUMO, the energy difference for $\text{HOMO}_{\text{diene}}/\text{LUMO}_{\text{dienophile}}$ in the case of $p\text{-NO}_2$ -substituted styrene is less than that in the case of styrene. The reaction with $p\text{-NO}_2$ -substituted styrene is thus faster.

When $\text{R} = p\text{-OMe}$, the substituted styrene acts as an electron-rich *x*-substituted dienophile which would preferentially use its HOMO. The more important frontier orbital interaction is therefore $\text{LUMO}_{\text{diene}}/\text{HOMO}_{\text{dienophile}}$ interaction for the reaction of *c*-substituted diene (tetracyclone) with *x*-substituted dienophile. Since the *x*-substituent ($p\text{-OMe}$) increases the energy of the dienophile HOMO, the energy gap for $\text{LUMO}_{\text{diene}}/\text{HOMO}_{\text{dienophile}}$ in the case of $p\text{-OMe}$ -substituted styrene is less than that in the case of unsubstituted styrene. Therefore, $p\text{-OMe}$ -substituted styrene reacts faster than styrene.

It is worth noting that this problem covers all three types of frontier orbital controls in Diels–Alder reaction.

4.2.1.3 Summary

The frontier orbital control is principally decided by smaller frontier orbital energy separation. The HOMO/LUMO energy gap becomes smaller if HOMO energy is raised or LUMO energy is lowered. The smaller energy separation also increases the rate of the reaction. An electron-rich component has a high-energy HOMO and therefore preferably uses its HOMO. An electron-deficient component on the other hand preferentially uses its low-energy LUMO. A normal electron demand Diels–Alder reaction is $\text{HOMO}_{\text{diene}}/\text{LUMO}_{\text{dienophile}}$ controlled while an IEDDA reaction is under $\text{LUMO}_{\text{diene}}/\text{HOMO}_{\text{dienophile}}$ control. Besides normal Diels–Alder and IEDDA reactions, some other combinations of diene and dienophile are also quite useful synthetically. If the diene and dienophile components bear similar type of substituents, no particular HOMO or LUMO is generally preferred and both HOMO/LUMO interactions become important. For example, the reaction of 1-*z*-substituted diene with a *z*-substituted

dienophile is $\text{HOMO}_{\text{diene}}/\text{LUMO}_{\text{dienophile}}$ and $\text{LUMO}_{\text{diene}}/\text{HOMO}_{\text{dienophile}}$ controlled (see Fig. 4.23). It can be easily seen that the combination of dienes with dienophiles, each carrying a single c-, z- or x-substituent, can lead to a total of 18 possible combinations comprising 9 combinations with 1-substituted dienes and 9 combinations with 2-substituted dienes.

4.2.2 Regioselectivity: 'Ortho/Para' Orientation

The Diels–Alder cycloaddition of an unsymmetrical diene with an unsymmetrical dienophile can occur in two different orientations to produce a mixture of two regioisomers (Fig. 4.14). As shown in Fig. 4.14A, 1-substituted diene combines with a substituted dienophile in two orientations to give 'ortho' (1,2-disubstituted) and 'meta' (1,3-disubstituted) adducts. Similarly, 2-substituted diene gives 'meta' (1,3-) and 'para' (1,4-) adducts (Fig. 4.14B). The 'ortho/meta/para' nomenclature applies to aromatic transition structure of the Diels–Alder reaction; however, this nomenclature is also retained and commonly used for the cycloadducts, though nonaromatic.

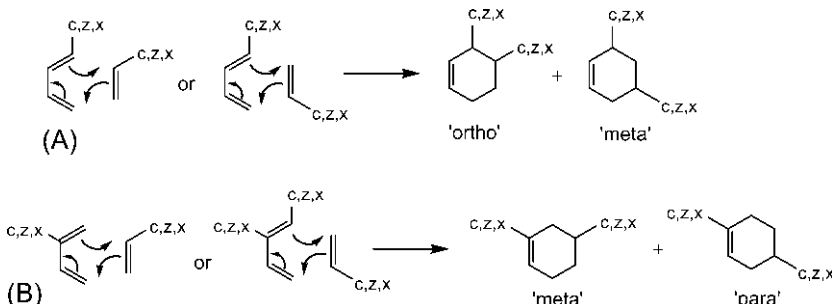


Fig. 4.14 Formation of regioisomers in the Diels–Alder reaction with (A) 1-substituted diene and (B) 2-substituted diene.

In general, the Diels–Alder reaction is highly regioselective with the predominant or exclusive formation of one regioisomer. The regioselectivity can be rationalized using frontier orbital theory as follows.

In two orientations of reactants, the same HOMO/LUMO pair is involved but interacting sites are different. Therefore we invoke Eq. (4.4) for a HOMO/LUMO pair when the denominator ($E_{\text{LU}} - E_{\text{HO}}$) remains constant in the two orientations. Further, $\beta_{ab} = \beta_{a'b'}$ because the interactions involve p orbitals of carbon at both ends, and β_{ab} is assumed to be constant in the two orientations. As such, Eq. (4.4) gets further reduced to

$$\Delta E_{\text{FMO}} = -\frac{2(c_a c_b \beta_{ab} + c_{a'} c_{b'} \beta_{a'b'})^2}{E_{\text{LU}} - E_{\text{HO}}} = -\frac{2\beta_{ab}(c_a c_b + c_{a'} c_{b'})^2}{E_{\text{LU}} - E_{\text{HO}}} \quad (4.5)$$

or,

$$\Delta E_{\text{FMO}} = \text{constant} \times (c_a c_b + c_{a'} c_{b'})^2$$

(It is of note that β depends on nuclear separation, and therefore may not be strictly same for asynchronous formation of two σ bonds.) The regioselectivity of the Diels–Alder reaction can be predicted and explained using Eq. (4.5). *The larger the coefficient term $(c_a c_b + c_{a'} c_{b'})^2$, the higher is the regioselectivity.*

We now consider a Diels–Alder reaction with 1-substituted diene and examine frontier orbital interactions in two orientations taking a HOMO_{diene}/LUMO_{dienophile} pair as shown in Fig. 4.15. Assuming a larger coefficient at the unsubstituted end of both diene and dienophile, let the magnitude of small and large coefficient be x and $(x + \Delta x)$ for the diene, and y and $(y + \Delta y)$ for the dienophile where Δx and Δy denote the difference of coefficient, that is, the extent of polarization in the diene HOMO and dienophile LUMO, respectively.

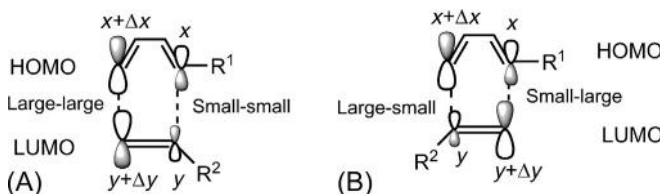


Fig. 4.15 Frontier orbital interactions in terms of coefficients in two orientations (A and B).

Qualitatively, the interactions involve large–large + small–small in Fig. 4.15A, and large–small + small–large interactions in Fig. 4.15B. Let us now evaluate the coefficient term for the two orientations.

In Fig. 4.15A,

$$(c_a c_b + c_{a'} c_{b'})^2 = (\text{large} - \text{large} + \text{small} - \text{small})^2 = [(x + \Delta x)(y + \Delta y) + xy]^2 \\ = (2xy + x\Delta y + y\Delta x + \Delta x\Delta y)^2$$

In Fig. 4.15B,

$$(c_a c_b + c_{a'} c_{b'})^2 = (\text{large} - \text{small} + \text{small} - \text{large})^2 = [(x + \Delta x)y + x(y + \Delta y)]^2 \\ = (2xy + x\Delta y + y\Delta x)^2$$

Comparing the values of the coefficient term for the two orientations, it is clearly seen that the coefficient term is greater for large–large + small–small interactions which would lead to the preferred regioisomer. Further, the extent of regioselectivity depends on the value of $\Delta x \Delta y$ which indicates that the stronger the polarization of the frontier orbital, the greater is the selectivity. For the reaction shown in Fig. 4.15, the preferred regioisomer is therefore ‘ortho’ adduct.

It is important to appreciate that large–large interaction provides the leading bond in the transition structure which is formed to a greater extent than the bond formed by small–small interaction. The transition structure is therefore unsymmetrical, and the reaction is concerted but asynchronous. The formation of leading σ bond decides the regioselectivity as it dictates the formation of the other σ bond.

In summary:

The regioselectivity is determined by large–large + small–small interactions. In other words, the leading σ bond from large–large interaction decides the regioselectivity as it directs the formation of the other σ bond.

The more the polarization of HOMO/LUMO, the higher is the regioselectivity.

The frontier orbital coefficient pattern shown in Figs 1.23, 1.24 and 1.26 are combined in Fig. 4.16.⁵

4.2.2.1 Illustrative Examples

We shall illustrate the regioselectivity of the Diels–Alder reactions in different cases of frontier orbital control taking the patterns of frontier orbital coefficients in Fig. 4.16.

First, we consider normal electron demand Diels–Alder reaction between a diene bearing x-substituent at C-1/C-2 and a dienophile carrying z-substituent. The reaction is governed by $\text{HOMO}_{\text{diene}}/\text{LUMO}_{\text{dienophile}}$ control. The coefficient patterns (Fig. 4.16) indicate that diene HOMO has larger coefficient at C-4 terminus of 1-x-substituted diene and at C-1 terminus of 2-substituted diene. For LUMO of z-substituted dienophile, there is a larger coefficient at β -C, the unsubstituted terminus. The frontier orbital interactions in two orientations with 1- and 2-substituted dienes are shown in Fig. 4.17. The regioselectivity is determined by more favourable large–large + small–small interactions. With 1-x-substituted

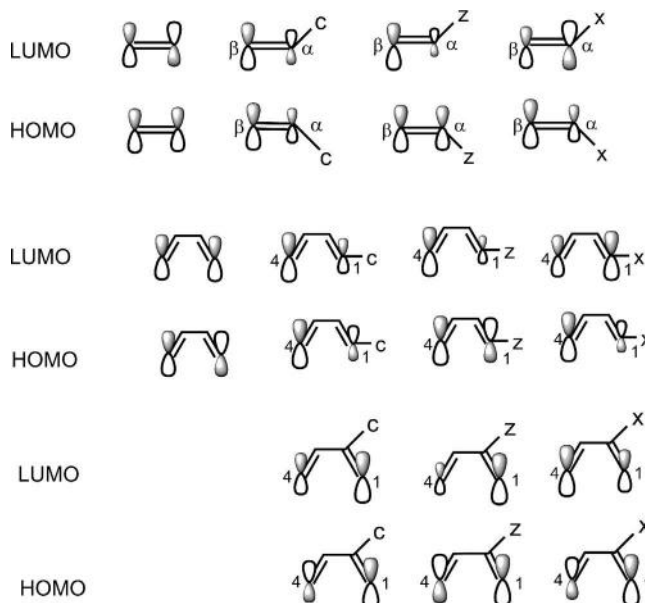


Fig. 4.16 Frontier orbital coefficient patterns of unsubstituted and substituted alkenes and dienes.

diene, the major regiosomer is ‘ortho’ adduct (Fig. 4.17A). The estimated HOMO/LUMO coefficients are indicated when $x = \text{OMe}$ and $z = \text{CHO}$. Fig. 4.17B shows that ‘para’ regiosomer is the major product in the case of 2-x-substituted diene. The estimated HOMO and LUMO coefficients are indicated for a case when $x = \text{OMe}$ and $z = \text{CO}_2\text{Me}$. Similar results are obtained with 1-c- and 2-c-substituted dienes as their patterns of HOMO coefficients are similar to those of x-substituted dienes (Fig. 4.16). This type of regioselectivity is expressed as ‘ortho/para’ rule.

Some examples of normal electron demand Diels–Alder reactions that conform to ‘ortho/para’ rule are shown in Fig. 4.18.

Danishefsky diene (1-methoxy-3-trimethylsilyloxy-1,3-butadiene) is an electron-rich diene and undergoes normal electron demand Diels–Alder reaction with enhanced reactivity and high regiochemical control. This is illustrated in Fig. 4.19 for the formation of an angularly substituted cyclohexenone intermediate in a synthesis of vernolepin.¹⁴ The electron-rich diene reacts readily with the z-substituted dienophile though it is relatively less electron deficient due to the presence of x-type alkyl substituents

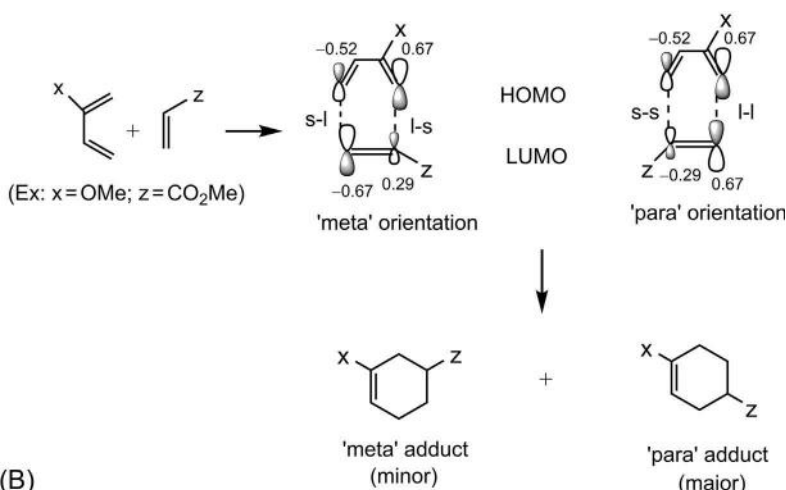
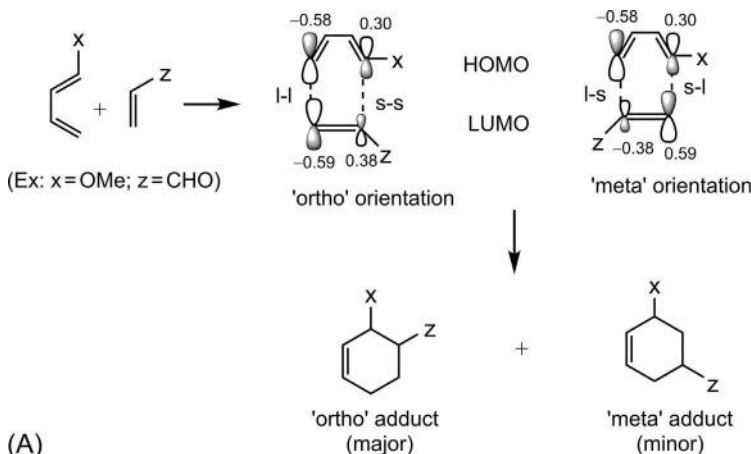


Fig. 4.17 Frontier orbital pictures of regioselectivity of Diels–Alder reaction between (A) 1-x-substituted diene and z-substituted dienophile and (B) 2-x-substituted diene and z-substituted dienophile. I–I = large–large, s–s = small–small, I–s = large–small, s–I = small–large.

	c/x	Δ	'ortho' + 'meta'		c/x	Δ	'para' + 'meta'
$c = \text{Ph}, z = \text{CHO}$	100 : 0			$c = \text{Ph}, z = \text{CN}$	85 : 15		
$x = \text{Me}, z = \text{CO}_2\text{Me}$	95 : 5			$x = \text{Me}, z = \text{CO}_2\text{Me}$	80 : 20		
$x = \text{OMe}, z = \text{CHO}$	100 : 0			$x = \text{OMe}, z = \text{CHO}$	100 : 0		
$x = \text{NEt}_2, z = \text{CO}_2\text{Et}$	100 : 0			$x = \text{OEt}, z = \text{CO}_2\text{Me}$	100 : 0		

Fig. 4.18 Examples of regioselective normal electron demand Diels–Alder reactions.

(ring residues). The regioselectivity arises from the influence of both x -substituents (OMe and OSiMe_3): the z -substituent (CO_2Me) is ‘ortho’ to OMe and ‘para’ to OSiMe_3 . (For stereochemistry of the cycloadduct, see Problem 5.4 in [Chapter 5](#).)

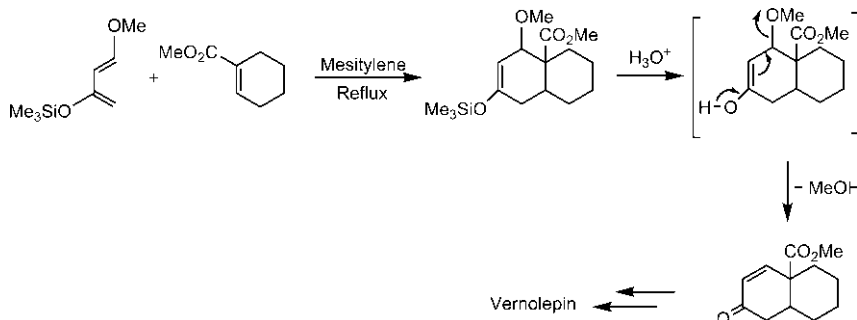


Fig. 4.19 Diels–Alder reaction with Danzig diene forming an angularly substituted cyclohexenone intermediate in a synthesis of vernolepin.

It may be mentioned that steric factor may sometimes disfavour the formation of ‘ortho’ adduct in the reaction with 1-substituted diene, and thereby causes the reversal of regioselectivity. For example, in the reaction of (*E*)-penta-1,3-diene with the sterically hindered vinyl-9-BBN, the predominant regiosomer is ‘meta’ adduct (98:2).

Next, we consider an IEDDA reaction of 1- z -substituted diene with x -substituted dienophile. The reaction is $\text{LUMO}_{\text{diene}}/\text{HOMO}_{\text{dienophile}}$ controlled. The frontier orbital interactions show that large–large + small–small interactions lead to the formation of ‘ortho’ adduct as the major regiosomer ([Fig. 4.20](#)). The ‘para’ adduct would be the preferred regiosomer in reaction with 2- z -substituted diene (verify). The IEDDA reaction therefore obeys the ‘ortho/para’ rule.

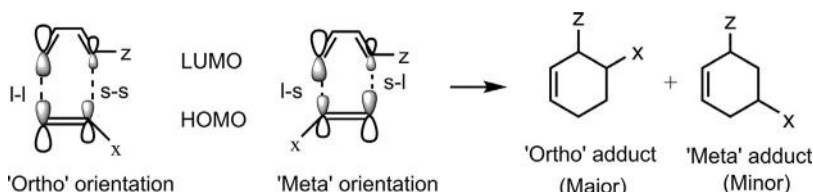


Fig. 4.20 Frontier orbital interactions for regioselectivity of the inverse electron demand Diels–Alder (IEDDA) reaction between 1- z -substituted diene and x -substituted dienophile.

Two examples of IEDDA reactions showing the formation of ‘ortho’ adducts are given in Fig. 4.21.

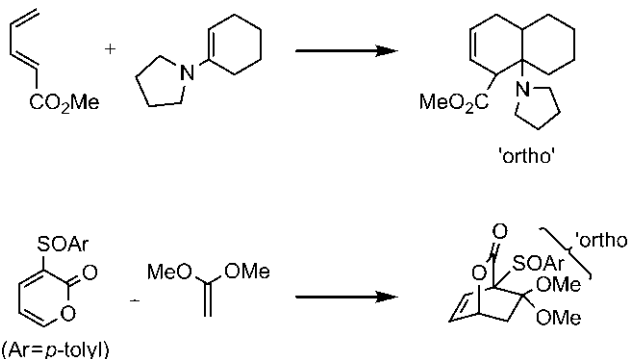


Fig. 4.21 Examples of regioselective inverse electron demand Diels–Alder (IEDDA) reactions.

Fig. 4.22 illustrates a synthesis¹⁵ involving an IEDDA reaction. The cycloaddition exhibits the expected regiochemistry. The nucleophilic enamine dienophile has larger HOMO coefficient at β -carbon. The pyrone acts as a strongly electrophilic diene due to the effect of ester group (as a 1-z-substituent) as well as ring carbonyl (as a 2-z-substituent). The formation of leading bond between large LUMO coefficient of pyrone and large HOMO coefficient of enamine leads to the preferred regioisomeric adduct which, after loss of pyrrolidine and opening of pyrone ring (shown in one step), gives the aromatic product.

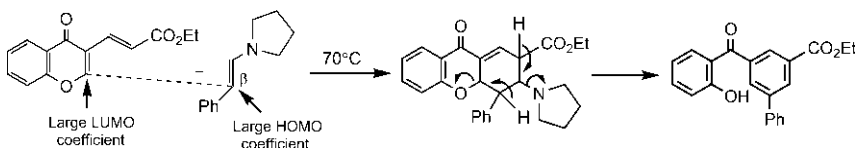
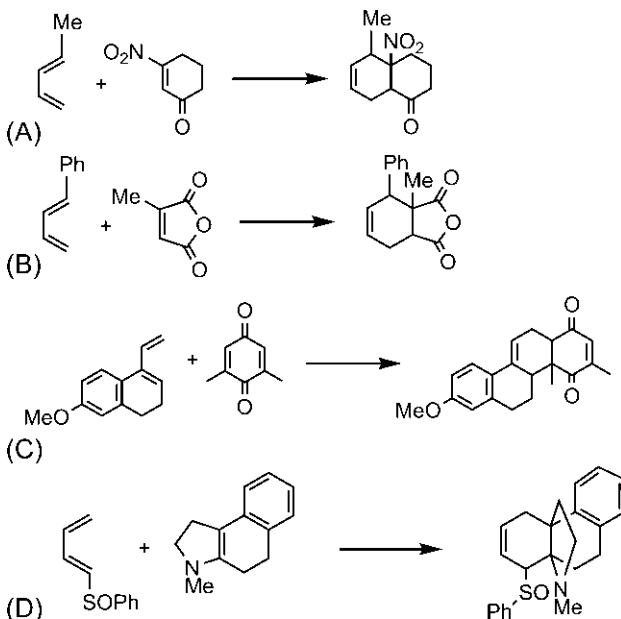


Fig. 4.22 Inverse electron demand Diels–Alder (IEDDA) reaction of a benzopyrone with an enamine leading to an aromatic product.

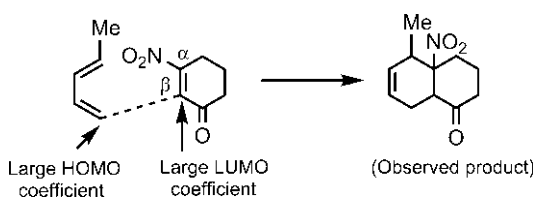
Problem 4.4

Explain the regioselectivity of the following Diels–Alder reactions.

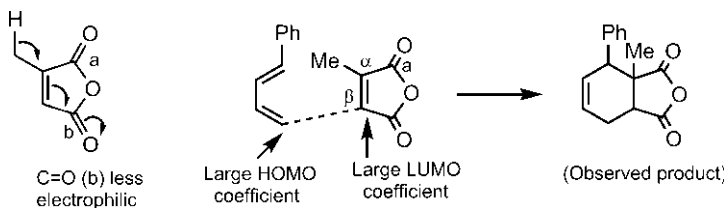
**Answer**

The reactions (A–C) involve electron-rich dienes (*c*- or *x*-substituted) and electron-deficient dienophiles (*z*-substituted), and are governed by $\text{HOMO}_{\text{diene}}/\text{LUMO}_{\text{dienophile}}$ interaction. In each dienophile, two electron-withdrawing *z*-substituents are present of which the more powerful *z*-substituent would control the regioselectivity. The formation of leading bond between two large coefficients gives the preferred regioisomeric product.

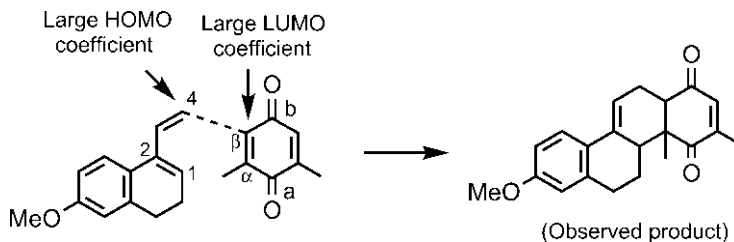
(A) NO_2 is a more powerful electron-withdrawing *z*-substituent than $\text{C}=\text{O}$, and hence controls the regioselectivity. The β -carbon with respect to NO_2 has larger coefficient in dienophile LUMO and is therefore involved in the formation of leading bond as shown below. (Note that the leading bond also fixes the formation of other σ bond to give the preferred regiosomer.)



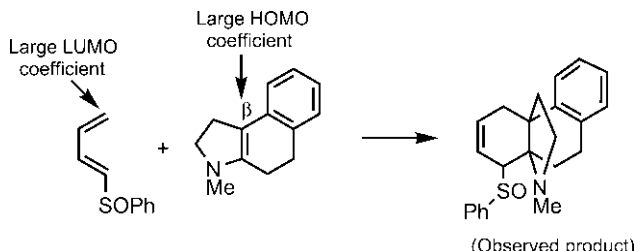
- (B)** As shown below, C=O (labelled a) is more electrophilic and electron withdrawing than C=O (labelled b) which is conjugated to electron-donating Me through C—H hyperconjugation. Therefore, C=O (a) controls the orientation. The β -carbon to C=O (a) has larger coefficient in LUMO.



- (C)** C=O (labelled a) is a better z-substituent due to similar reasoning as given above. The carbon β to C=O (a) has larger coefficient in LUMO. The diene is substituted at C-1 and C-2. Generally, a C-1 substituent is more effective in polarizing a frontier orbital than a C-2 substituent. Therefore C-4 of diene has larger coefficient.



- (D)** The reaction is an IEDDA reaction between 1-z-substituted diene ($z = \text{SOPh}$) and x-substituted dienophile (an enamine). The preferred regioisomer is ‘ortho’ adduct (SOPh and amine substituents being ‘ortho’) arising from the leading bond formed between two large coefficients.



Finally, we shall examine the regioselectivity of the Diels–Alder reaction when the diene and the dienophile bear similar type of substituent. To illustrate, we consider the cycloaddition of 1-z-substituted diene with a z-substituted dienophile (Fig. 4.23). The HOMO/LUMO energy separations estimated for the two HOMO/LUMO pairs are close (9.5 and 10.4 eV). The reaction is therefore under $HOMO_{\text{diene}}/LUMO_{\text{dienophile}}$ and $LUMO_{\text{diene}}/HOMO_{\text{dienophile}}$ control. To determine regioselectivity, we then need to examine frontier orbital interactions using both HOMO/LUMO pairs. Only the preferred large–large + small–small interactions are indicated in Fig. 4.23 which lead to ‘ortho’ adduct (see also Fig. 5.11 in Chapter 5). Note that the frontier orbital picture shows only the interacting lobe of each p orbital; other p orbital lobes are not drawn.

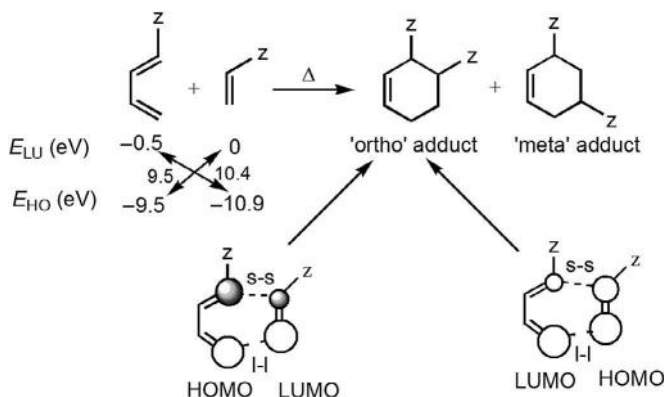


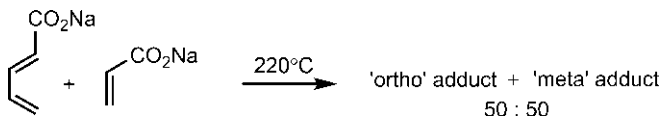
Fig. 4.23 Frontier orbital control and regioselectivity of the Diels–Alder reaction of a z-substituted diene with a z-substituted dienophile.

It has been found experimentally that ‘ortho’:‘meta’ = 90:10, when $z = \text{CO}_2\text{H}$.¹⁶ With a 2-z-substituted diene and a z-substituted dienophile, the preferred regiosomer would be ‘para’ adduct. For example, dimerization of 2-cyanobutadiene in which one molecule acts as a diene and the other as a dienophile gives ‘para’ isomer as only adduct (draw the scheme).

Note on drawings: Either two-lobe representation of p orbitals (see Figs 4.17 and 4.20) or one-lobe (interacting lobe) representation (see Fig. 4.23) can be used. Both representations indicate relative size of coefficients and symmetry of the frontier orbitals. The regioselectivity can also be addressed simply in terms of leading bond drawn between two large coefficients (see Fig. 4.22). However, the orbital representation is more explicit and informative.

Problem 4.5

Explain the following observation.

**Answer**

The CO_2^- is more like a c -substituent rather than a z -substituent. With the diene and dienophile, each bearing c -substituent, both $\text{HOMO}_{\text{diene}}/\text{LUMO}_{\text{dienophile}}$ and $\text{LUMO}_{\text{diene}}/\text{HOMO}_{\text{dienophile}}$ interactions are important. The frontier orbital picture would favour the formation of an ‘ortho’-adduct (check). But the strong repulsive interaction between the two adjacent negative charges in ‘ortho’ transition structure would tend to favour ‘meta’ adduct. The result is a 50:50 mixture of ‘ortho’ and ‘meta’ adducts.

Problem 4.6

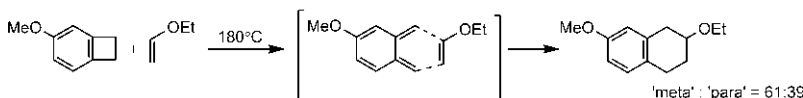
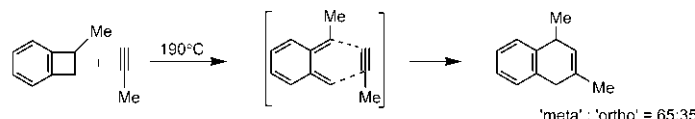
Predict the frontier orbital control and regioselectivity of the reaction between a diene bearing x -substituent at C-1/C-2 and a dienophile carrying x -substituent.

Cite examples using 1- x - and 2- x -substituted dienes in support of your prediction of the regioselectivity.

Answer

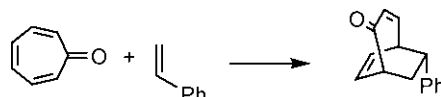
Analysis using HOMO/LUMO energy separations indicates that both $\text{HOMO}_{\text{diene}}/\text{LUMO}_{\text{dienophile}}$ and $\text{LUMO}_{\text{diene}}/\text{HOMO}_{\text{dienophile}}$ interactions are important. The HOMO/LUMO energy gap for the reaction with 1- or 2-substituted diene is found to be quite large (11.3–11.7 eV), which is even greater than the energy separation for the prototype Diels–Alder reaction (11 eV). The reaction would therefore be very slow. The major regioisomer based on coefficient analysis is predicted to be ‘meta’ adduct. This appears to be an exception to the ‘ortho/para’ rule.

Two examples¹⁷ are shown below in which 1- x - and 2- x -substituted dienes are extremely reactive *ortho*-quinodimethanes that are generated *in situ* by electrocyclic ring opening of the corresponding benzocyclobutenes (see Chapter 7). The cycloaddition with x -substituted dienophile proceeds by aromatization of the diene, thereby facilitating the otherwise slow reaction and gives ‘meta’ adduct as a major product.



Problem 4.7

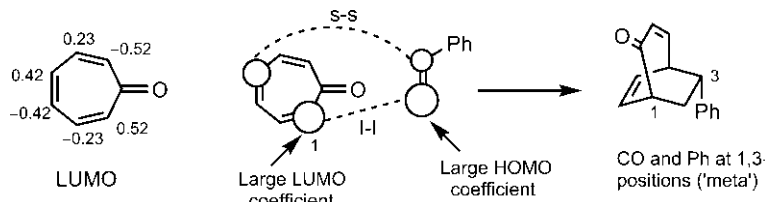
Explain the regioselectivity of the Diels–Alder reaction between tropone and styrene.



Answer¹⁸

The tropone reacts as a diene. Its C=O group is strongly electron withdrawing (the charged canonical structure gives a 6-electron aromatic system), and lowers appreciably the energy of the LUMO.

Therefore, tropone would preferably use its LUMO and the styrene dienophile with conjugating Ph would use its HOMO. The dominant frontier orbital interaction is LUMO_{diene}/HOMO_{dienophile} interaction. The diene component of tropone has a carbonyl group (*z*-substituent) at C-1 but, unlike a simple diene, it is symmetric and cross-conjugated. Therefore the frontier orbital coefficient pattern of tropone is not similar to that of 1-*z*-substituted diene. The calculated LUMO coefficients for tropone resemble those for 1,3,5-hexatriene and are given below. (The HOMO coefficients of tropone however do not resemble the pattern for either hexatriene or 1-*z*-substituted diene.) The observed product is the preferred regioisomer which results from large-large+small-small interactions. (Note that only the interacting lobe of each p orbital is drawn.)



4.2.2.2 Remarks

As an alternative to the frontier orbital arguments, simple valence bond (resonance) reasoning may be put forward for the formation of leading bond between electrophilic and nucleophilic centres of diene and dienophile, and hence regioselectivity. It indeed works, for example, in the reaction between 1-methoxybutadiene and acrolein for the formation of ‘ortho’ adduct as the observed product (Fig. 4.24A) but the valence bond reasoning fails, for instance, to account for the formation of the observed ‘ortho’ adduct in the reaction between butadiene carboxylic acid and acrylic acid (Fig. 4.24B).

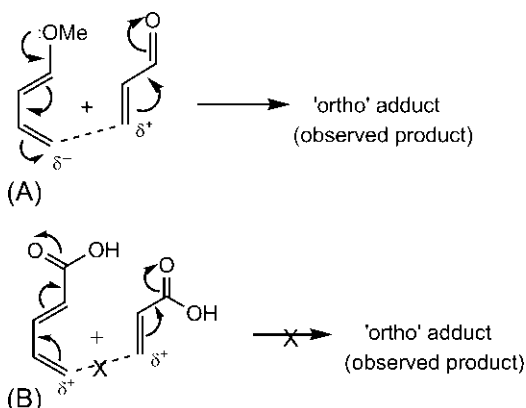


Fig. 4.24 Valence bond pictures of Diels–Alder reaction between (A) 1-methoxybutadiene and acrolein and (B) butadiene-1-carboxylic acid and acrylic acid.

Notwithstanding the simplifying assumptions and approximations, the frontier orbital theory thus appears to be a more promising and useful approach to predict and explain the regiochemical preferences.

4.2.3 Regioselectivity of Hetero Diels–Alder Reactions

Hetero Diels–Alder reactions involve a heterodiene or a heterodienophile where the heteroatom is a part of the π system (see Fig. 4.2). Here the two σ bonds being formed in the transition structure are usually different, C–C and C–X (X is a heteroatom). The resonance integral β for C–C bond (involving two carbon p orbitals) is not the same as for C–X bond (involving a carbon p orbital and a heteroatom p orbital).

For determining regioselectivity, we therefore need to consider coefficients as well as β , that is, the term $(c_a c_b \beta_{ab} + c_{a'} c_{b'} \beta_{a'b'})^2$ [cf. Eq. (4.5)] in the two orientations for a HOMO/LUMO pair.

4.2.3.1 Reaction With Heterodienophiles

Carbonyl compounds, nitroso compounds, imines and nitriles are some heterodienophiles that are commonly used in hetero Diels–Alder cycloadditions. The presence of a lower energy nitrogen or oxygen p orbital in a heterodienophile gives a low-energy LUMO. Therefore, a heterodienophile preferably uses its LUMO and the diene (usually electron rich) uses its HOMO. The dominant interaction is $\text{HOMO}_{\text{diene}}/\text{LUMO}_{\text{dienophile}}$ interaction which refers to a normal electron demand Diels–Alder reaction.

To illustrate, let us consider the cycloaddition of benzaldehyde with an electron-rich diene, 1-methoxy-3-trimethylsilyloxy-1,3-butadiene (Danishefsky diene) in the synthesis of a γ -pyrone (Fig. 4.25).¹⁹

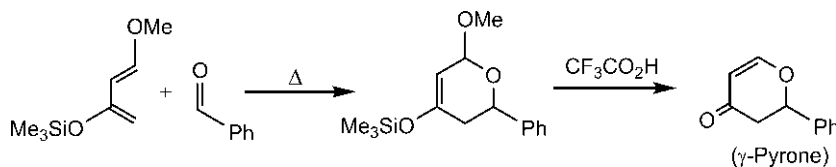


Fig. 4.25 Synthesis of a γ -pyrone via hetero Diels–Alder reaction between Danishefsky diene and benzaldehyde.

The regioselectivity of the reaction can be explained in terms of the leading bond arising from large–large interaction as well as the larger β for C–C bond (Fig. 4.26). The diene has large HOMO coefficient at C–4 due to the combined effects of electron-donating α -substituents OMe and OSiMe₃, and the dienophile has large LUMO coefficient on the carbonyl carbon.

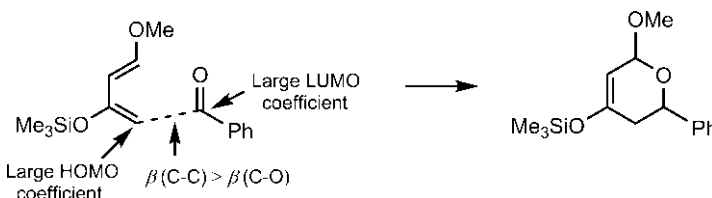
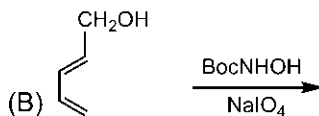
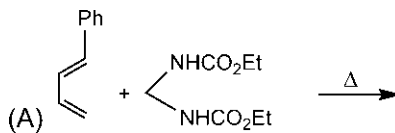


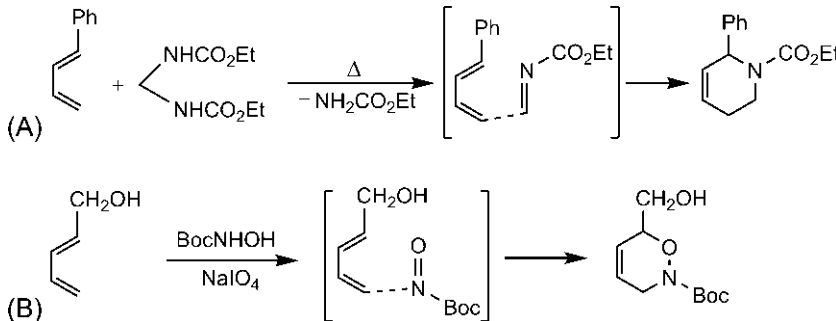
Fig. 4.26 Regioselectivity of the reaction in Fig. 4.25 in terms of leading bond arising from large–large interaction and larger β for C–C bond.

Problem 4.8

Predict the major product of each of the following reactions.

**Answer**

Each reaction represents a hetero Diels–Alder reaction with a heterodienophile generated in situ, and proceeds through a more important $\text{HOMO}_{\text{diene}}/\text{LUMO}_{\text{dienophile}}$ interaction. The major regioisomer results from the interaction between two large coefficients and a larger β for C–C bond in (a) and for C–N bond in (b). Like triazolinedione cycloaddition (see p. 118), the cycloaddition with nitroso compound is also highly asynchronous.

**4.2.3.2 Reaction With Heterodienes**

The α,β -unsaturated aldehydes, ketones and imines can act as heterodienes in hetero Diels–Alder reactions. An example of that involved in the synthesis of a α -pyrone is shown in Fig. 4.27.²⁰

Here the dominant frontier orbital interaction is between LUMO of heterodiene (the presence of electronegative oxygen in the π system gives a low-lying LUMO) and HOMO of dienophile that is electron rich.

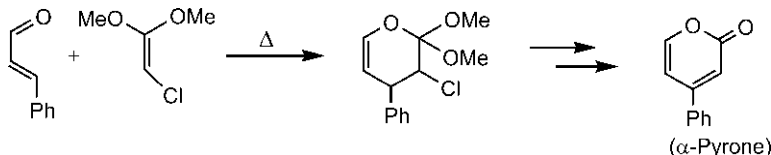


Fig. 4.27 Hetero Diels–Alder reaction with a heterodiene in a synthesis of a α -pyrone.

The reaction is an IEDDA reaction. The formation of major cycloadduct can be rationalized on the basis of large–large interaction and larger β as shown in **Fig. 4.28**. Note that the terminal carbon of heterodiene has larger coefficient in LUMO (see Problem 4.9).

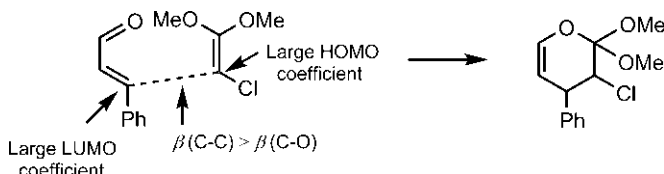


Fig. 4.28 Regioselectivity of the reaction in **Fig. 4.27** in terms of leading bond from large–large interaction and larger β for $C=C$ bond.

Two more examples of regioselectivity are shown in **Fig. 4.29**. In **Fig. 4.29A**, the initial adduct can act as a dienophile to undergo a second hetero Diels–Alder reaction. In each step, the regioselectivity is governed by large–large interaction and larger β for $C=C$ bond. In **Fig. 4.29B**, the initial adduct cyclizes by ionic mechanism to form the final product.

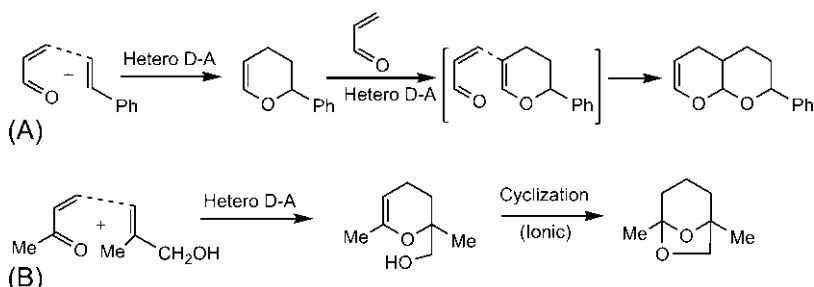
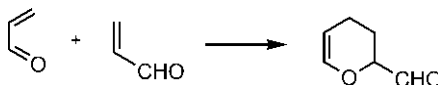


Fig. 4.29 Examples of regioselectivity of hetero Diels–Alder reactions: (A) two consecutive hetero Diels–Alder reactions, and (B) a hetero Diels–Alder reaction followed by ionic cyclization.

Problem 4.9

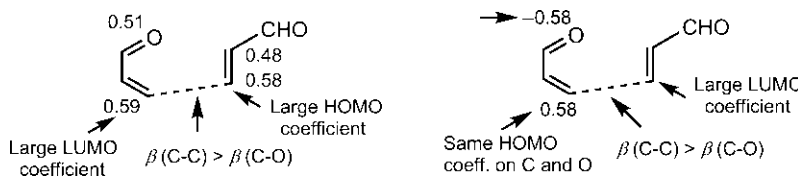
Explain the regioselectivity in the dimerization of acrolein.

**Answer²¹**

In dimerization, one molecule of acrolein acts as a heterodiene and the other as a dienophile. Therefore $\text{HOMO}_{\text{diene}} = \text{HOMO}_{\text{acrolein}}$, and $\text{LUMO}_{\text{dienophile}} = \text{LUMO}_{\text{acrolein}}$. Evidently, the energy gaps are same for $\text{HOMO}_{\text{diene}}/\text{LUMO}_{\text{dienophile}}$ and $\text{LUMO}_{\text{diene}}/\text{HOMO}_{\text{dienophile}}$ pairs, and both interactions are involved. The calculated HOMO and LUMO coefficients of acrolein²² are as shown below.



The $\text{LUMO}_{\text{diene}}/\text{HOMO}_{\text{dienophile}}$ interaction can account for the observed regiosomer in terms of the leading bond arising from large-large interaction and larger β for C–C bond as shown below. For $\text{HOMO}_{\text{diene}}/\text{LUMO}_{\text{dienophile}}$ interaction, though the HOMO coefficient of diene is same on terminal C and O, β is larger for C–C bond than for C–O bond. Therefore, C–C bond formation is preferred and gives the observed regiosomer.



4.2.4 Site Selectivity of Diels–Alder Reactions

Site selectivity is a special kind of regioselectivity that arises when multiple sites of diene or of dienophile are available for cycloaddition. In most cases, a diene interacts preferentially with one of the several alkene sites of an unsymmetrical dienophile. For example, in a normal electron demand

Diels–Alder reaction shown in Fig. 4.30, two alkene sites of a *p*-benzoquinone dienophile are available for cycloaddition; however, the reaction takes place preferentially with the alkene site bearing $\text{CH}_2\text{CH}_2\text{OBn}$ group, which is an early step in the synthesis of the plant hormone gibberellic acid.²³ (For stereochemistry of the cycloadduct, see Problem 5.4 in Chapter 5.)

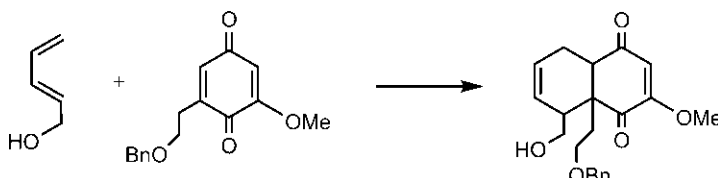


Fig. 4.30 Site selectivity in Diels–Alder reaction.

The site selectivity can be rationalized using frontier orbital theory as shown in Fig. 4.31. The two $\text{C}=\text{O}$ groups of the dienophile are different in their electron-withdrawing abilities: $\text{C}=\text{O}$ (labelled a) is more electron withdrawing than $\text{C}=\text{O}$ (labelled b) which is conjugated to electron-donating OMe and also to $\text{CH}_2\text{CH}_2\text{OBn}$ by C–H hyperconjugation. Therefore, $\text{C}=\text{O}$ (a) would determine the regioselectivity. In the dienophile LUMO, $\text{C}=\text{O}$ (a) would raise the coefficients on β and β' carbons but these LUMO coefficients would be somewhat diminished by the effects of electron-donating OMe and $\text{CH}_2\text{CH}_2\text{OBn}$ substituents. Since OMe is stronger electron donating than $\text{CH}_2\text{CH}_2\text{OBn}$, its diminishing effect on LUMO coefficient at β' carbon would be more. As a result β carbon would have larger LUMO coefficient than β' carbon. The observed regioselectivity thus arises from the leading bond between the two large coefficients of the diene and dienophile.

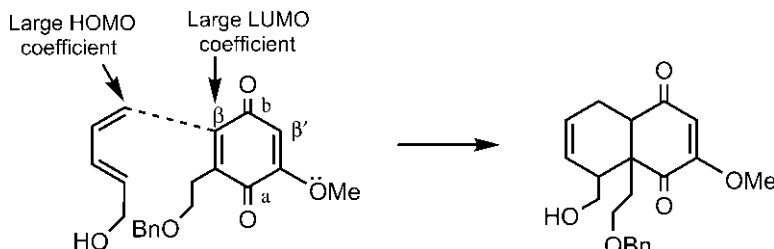


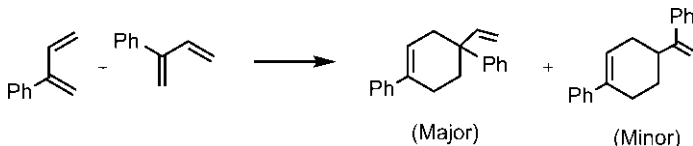
Fig. 4.31 FMO explanation of site selectivity of the reaction in Fig. 4.30.

Problem 4.10

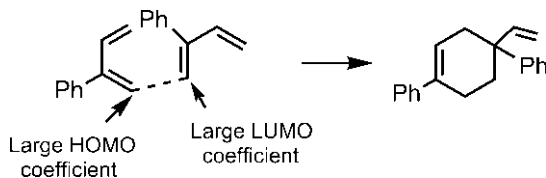
Give the products in the dimerization of 2-phenylbutadiene. Indicate the major product and explain the site selectivity involved.

Answer

The dimerization reaction gives two products from the interaction of 2-phenylbutadiene as a diene with two possible alkene sites of 2-phenylbutadiene dienophile.



The major dimer results from the leading interaction between large HOMO coefficient of diene and large LUMO coefficient of dienophile alkene site bearing two c-substituents (Ph and vinyl) as shown below.



4.2.5 Lewis Acid Catalysis of Diels–Alder Reactions

The Diels–Alder reaction between an electron-rich diene and an electron-deficient dienophile is governed by $\text{HOMO}_{\text{diene}}/\text{LUMO}_{\text{dienophile}}$ interaction. The effect of Lewis acid in the Diels–Alder reaction is attributed to its more pronounced effect on the LUMO of the dienophile. With electron-deficient α -substituted dienophile, Lewis acid forms a complex with electron-withdrawing group ($\text{C}=\text{O}$) making it more powerfully electron withdrawing because of the larger contribution of allyl cation-like canonical structure as shown in Fig. 4.32.

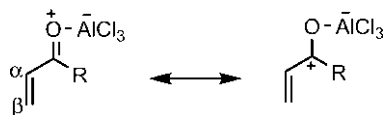


Fig. 4.32 Resonance representation of Lewis acid complex of a dienophile.

A α -substituted alkene can be modelled as a hybrid of butadiene and allyl cation (see [Section 1.5.1.2](#)). The Lewis acid increases the allyl cation character of α -substituted dienophile and perturbs the LUMO of dienophile on two counts. First, it lowers the energy of LUMO still further making the energy separation $E_{\text{LUMO(dienophile)}} - E_{\text{HOMO(diene)}}$ even smaller, thereby increasing the rate. Second, it leads to further polarization of the dienophile LUMO with enhanced coefficient on the β carbon and diminished coefficient on the α carbon. This stronger polarization of dienophile LUMO in the presence of Lewis acid leads to greater regioselectivity (see p. 124). [Fig. 4.33](#) illustrates the enhanced reactivity and regioselectivity of Diels–Alder reactions in the presence of Lewis acid. As shown in [Fig. 4.33A](#), the 2-substituted diene undergoes Diels–Alder reaction in the presence of SnCl_4 at much lower temperature giving higher proportion of ‘para’ adduct. In the case of 1-substituted diene, more ‘ortho’ adduct is obtained in the presence of AlCl_3 ([Fig. 4.33B](#)).

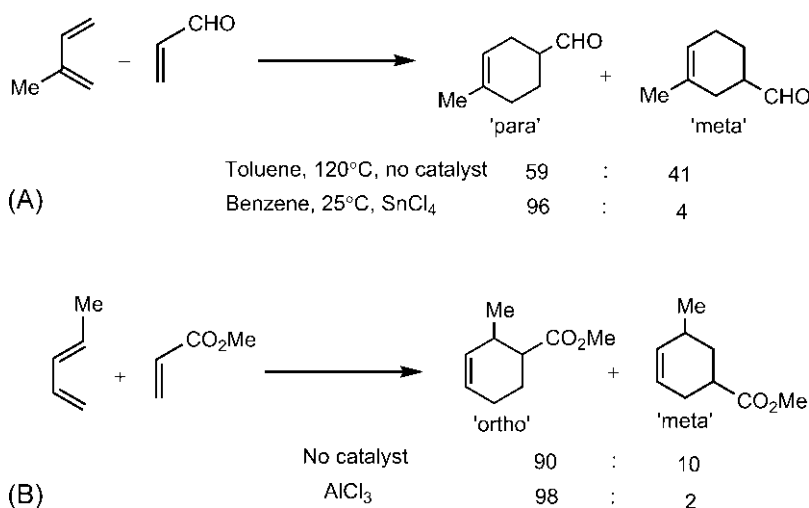
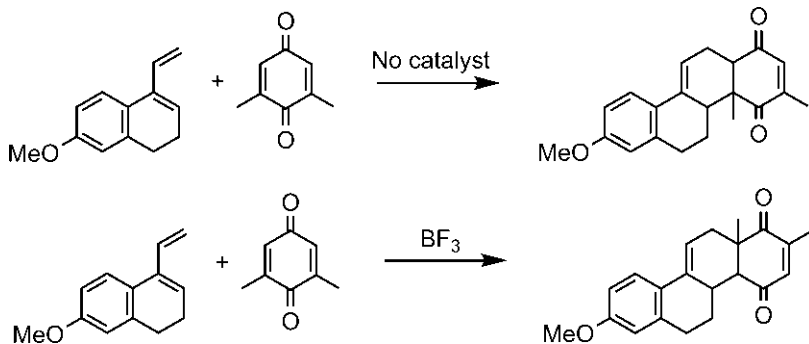


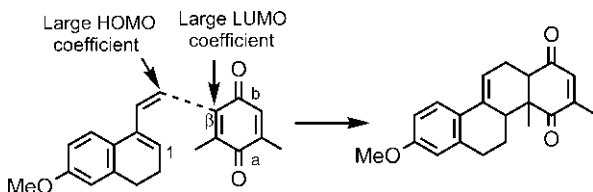
Fig. 4.33 Examples of enhanced reactivity and regioselectivity of Lewis acid-mediated Diels–Alder reactions.

Problem 4.11

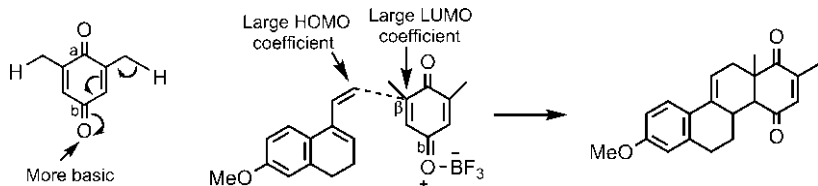
Explain the reversal of regioselectivity in the BF_3 -catalyzed Diels–Alder reaction.

**Answer²⁴**

Between two carbonyl groups of the dienophile, $\text{C}=\text{O}$ (labelled a) is more electron withdrawing than $\text{C}=\text{O}$ (labelled b) which is conjugated to electron-donating Me's through $\text{C}-\text{H}$ hyperconjugation. Therefore, $\text{C}=\text{O}$ (a), as a better α -substituent, influences the regioselectivity in the absence of Lewis acid. The carbon β to $\text{C}=\text{O}$ (a) has larger coefficient in LUMO, and the regioselectivity is determined by the leading interaction as shown below (see Problem 4.4C, p. 130).



In the presence of Lewis acid BF_3 , complexation with more basic carbonyl oxygen in $\text{C}=\text{O}$ (b) is highly favoured. The increased basicity is also ascribed to $\text{C}-\text{H}$ hyperconjugation. The complexation makes the $\text{C}=\text{O}$ (b) more electron withdrawing which then controls the regioselectivity. The dienophile LUMO gets strongly polarized with the carbon β to $\text{C}=\text{O}$ (b) having larger coefficient. The regioselectivity is determined by the leading interaction and is reversed in the presence of Lewis acid.



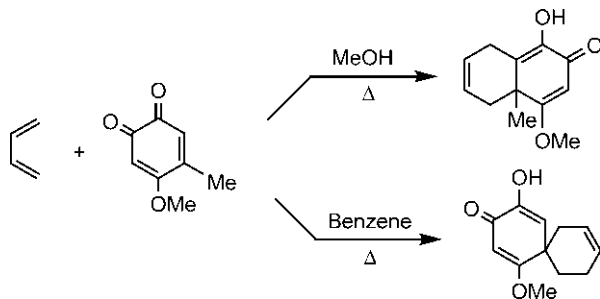
It is noteworthy that the regioselectivity effected in the presence of Lewis acid is appropriate for steroid synthesis. (For stereochemistry of the cycloadduct, see Problem 5.4 in [Chapter 5](#).)

4.2.5.1 Solvent Effect

The diene and dienophile substrates in Diels–Alder reaction are usually nonionic and the reaction is generally carried out in hydrocarbon solvents that dissolve the substrates or by simply mixing the diene and the dienophile. It is however interesting to observe that the Diels–Alder reaction could be speeded up by performing the reaction in water. For example, cyclopentadiene and methyl vinyl ketone react 740 times faster in water than in isooctane.²⁵ This is attributed to hydrophobic interaction which promotes the association of nonpolar parts of diene and dienophile under aqueous condition, thereby making the entropy factor more favourable for the cycloaddition to proceed rapidly. The stereoselectivity of the reaction in water is also higher (see [Section 5.1.2.5](#), p. 207).

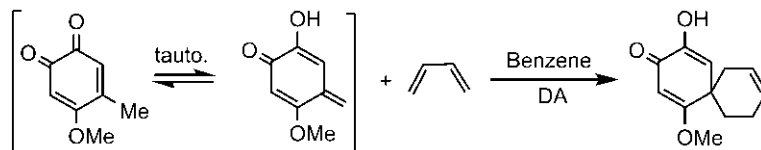
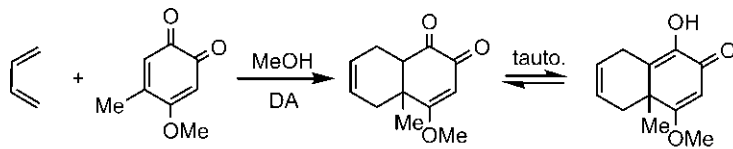
Problem 4.12

Account for the following observations:



Answer

In polar solvent (MeOH), the *o*-benzoquinone dienophile undergoes Diels–Alder reaction through keto form to give the product whereas in nonpolar solvent (benzene), it tautomerizes to enol form which then undergoes Diels–Alder reaction with butadiene. Note the site selectivity in each case: the more electron-deficient alkene site is involved.



4.2.6 Diels–Alder/Retro-Diels–Alder Strategy in Heterocyclic and Other Synthesis

The Diels–Alder reactions are reversible. Many Diels–Alder adducts at high temperature dissociate into their components in the reverse process. But the retro-Diels–Alder reaction is more important when two σ bonds that are not set up in the initial forward reaction are cleaved, thereby yielding a new diene or aromatic system. Moreover, the initial Diels–Alder adduct can be modified chemically, and the modified adduct can then undergo the retro-reaction to produce a new diene or dienophile. The retro-Diels–Alder reaction proceeds more easily when one or both of the dissociated components are particularly stable. The release of a nitrile, cyclopentadiene, N₂ or CO₂ by retro-reaction is most common. The Diels–Alder/retro-Diels–Alder sequence has been used successfully in a number of heterocyclic syntheses.²⁶

4.2.6.1 Heterocyclic Synthesis

The useful but otherwise relatively inaccessible 3-substituted and 3,4-disubstituted furans can be prepared via tandem Diels–Alder and retro-Diels–Alder reactions. These are shown in Fig. 4.34A and B^{27,28} using 4-phenyloxazole which provides an azadiene moiety for the Diels–Alder reaction. In retro-Diels–Alder step, the two σ bonds different from those formed in forward reaction are cleaved with elimination of benzonitrile.

In a similar manner, 3,4-disubstituted thiophene is formed from 4-phenylthiazole (Fig. 4.34C).²⁹

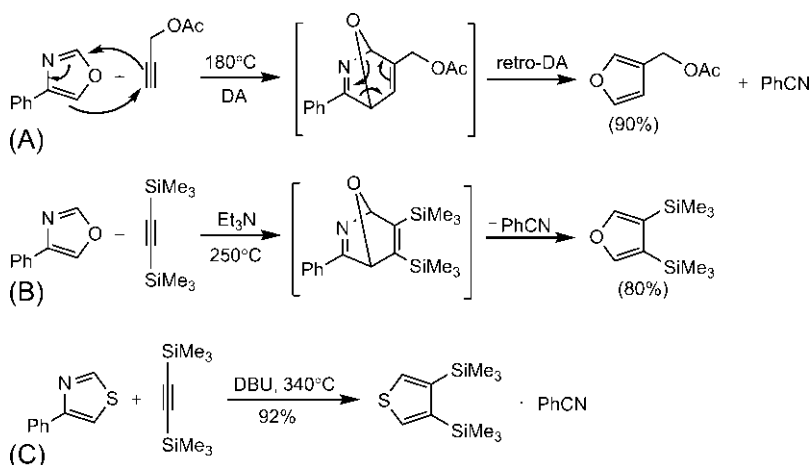


Fig. 4.34 Synthesis of (A) 3-substituted furan, (B) 3,4-disubstituted furan and (C) 3,4-disubstituted thiophene using Diels–Alder/retro-Diels–Alder sequence.

The 3,4-disubstituted furans can also be prepared from unsubstituted furan using a strategy that involves modification of initial Diels–Alder adduct followed by retro-Diels–Alder reaction (Fig. 4.35). Note that the less substituted double bond is preferentially reduced.

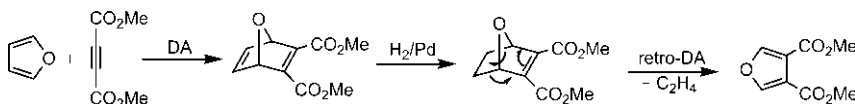


Fig. 4.35 Synthesis of a 3,4-disubstituted furan via modification of initial Diels–Alder adduct.

The Diels–Alder/retro-Diels–Alder sequence can also be used for the construction of six-membered heterocyclic systems. Fig. 4.36 shows that an oxazinone **4.1** can produce a pyridine derivative via Diels–Alder cycloaddition followed by retro-Diels–Alder reaction with extrusion of CO₂.³⁰

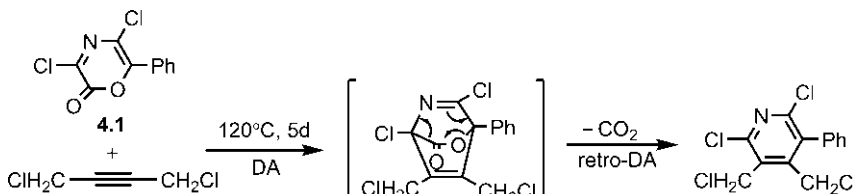


Fig. 4.36 Synthesis of a pyridine using Diels–Alder/retro-Diels–Alder sequence.

The triazines can act as inverse electron demand dienes. As shown in Fig. 4.37, a 1,3,5-triazine undergoes IEDDA reaction with an alkyne to give a pyrimidine derivative with loss of a nitrile in the retro-Diels–Alder step.³¹

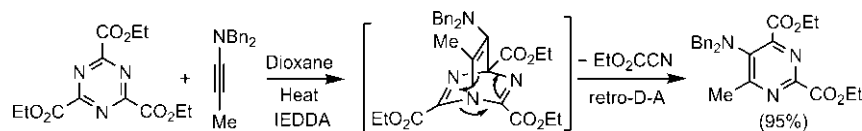


Fig. 4.37 Synthesis of a pyrimidine from a 1,3,5-triazine.

An enamine dienophile is considered as an alkyne equivalent because its amine fragment is lost finally to give an aromatic heterocycle, resembling a reaction with an alkyne dienophile. Fig. 4.38 shows that 1,2,4-triazine 4.2 undergoes IEDDA reaction with an enamine followed by loss of N₂ to give 4.3 which, after final loss of pyrrolidine, produces a pyridine derivative.³² The triazine 4.2 acts as a 2,3-diazadiene unit, and the preferred regioisomer has unreacted C=N moiety (1-z-substituent) ‘ortho’ to the amine fragment NR₂ (more powerful x-substituent of dienophile).

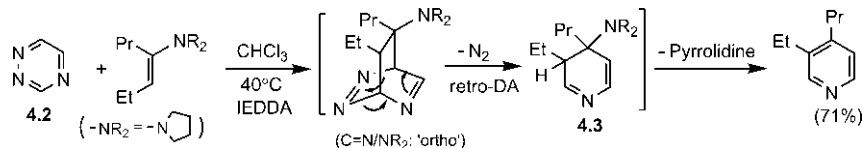


Fig. 4.38 Synthesis of a pyridine from a 1,2,4-triazine.

An example of a triazine synthesis is shown in Fig. 4.39. A 1,2,4,5-tetrazine undergoes IEDDA reaction with a nitrile bearing electron-donating NMe₂ substituent to give a 1,2,4-triazine after loss of N₂.

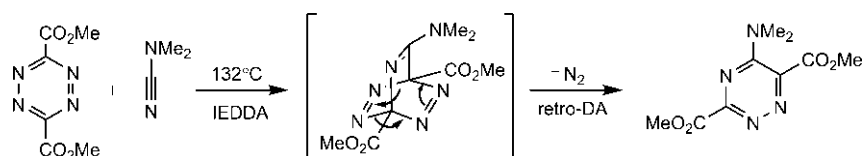
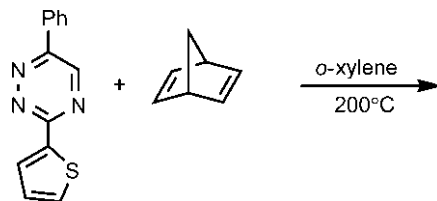


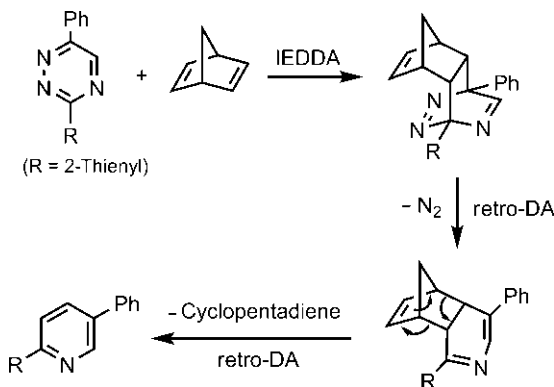
Fig. 4.39 Synthesis of a 1,2,4-triazine from a 1,2,4,5-tetrazine.

Problem 4.13

Predict the product formed in the following reaction.

**Answer**

The reaction proceeds through Diels–Alder reaction, then two successive retro-Diels–Alder reactions to form a pyridine derivative. Norbornadiene acts as an acetylene equivalent as cyclopentadiene is lost in the final retro-Diels–Alder step.



The forward Diels–Alder reaction followed by ionic elimination (not retro-Diels–Alder) of a small molecule is also used to construct heteroaromatic rings. For example, cycloaddition of acrylic acid with an oxazole leads to a pyridine derivative when the oxazole oxygen is lost as water (Fig. 4.40).³³ Note the regioselectivity: the terminal Me of azadiene moiety (5-Me of oxazole) is ‘ortho’ to CO₂H in the cycloadduct 4.4.

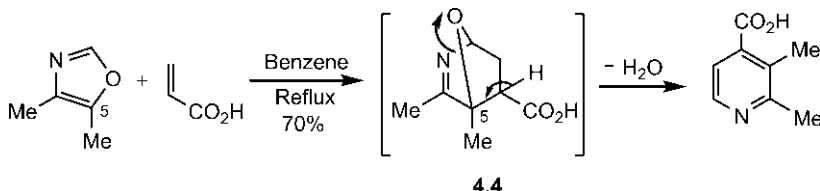


Fig. 4.40 Synthesis of a pyridine derivative via Diels–Alder reaction.

The *endo* adduct is formed; however, the stereochemistry is lost in the eventual formation of aromatic ring. As such, a planar representation without showing the *endo* stereochemistry is often drawn in aromatic heterocyclic synthesis.

Another pyridine synthesis is shown in Fig. 4.41 using an acyclic azadiene generated in situ. The azadiene **4.5** (obtained from an imide) reacts with dimethyl acetylenedicarboxylate (DMAD) to form a pyridine derivative after loss of *t*-butyldimethylsilanol. Subsequent desilylation with concentrated HCl gives a 2-pyridone.³⁴

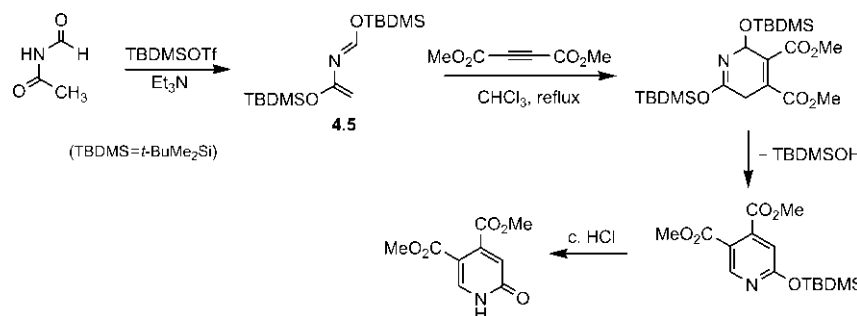
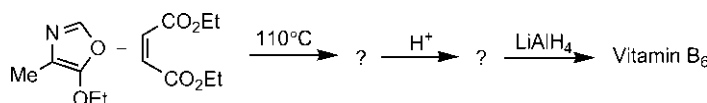


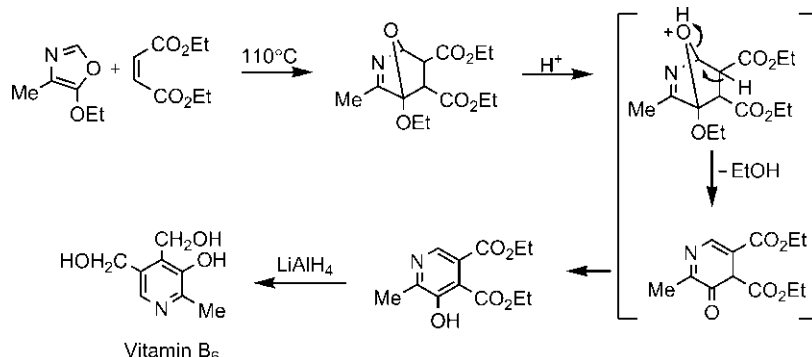
Fig. 4.41 Synthesis of a 2-pyridone via Diels–Alder reaction.

Problem 4.14

Complete the following scheme in a synthesis of vitamin B₆.



Answer



4.2.6.2 Other Synthesis

The Diels–Alder/retro-Diels–Alder sequence can be used for the synthesis of benzene derivatives. For example, 2-pyrone reacts with DMAD to give dimethyl phthalate after loss of CO₂ (Fig. 4.42A).³⁵ Note that both the diene (pyrone) and the dienophile (DMAD) are electron deficient (*z*-substituted).

The Diels–Alder/retro-Diels–Alder strategy can also be used to synthesize compounds that are difficult to obtain by other routes. For example, benzoquinone epoxide, which could not be obtained directly by the epoxidation of benzoquinone, is synthesized via Diels–Alder cycloaddition and retro-cycloaddition (Fig. 4.42B).³⁶ Another example is the synthesis of benzocyclopropene which involves Diels–Alder reaction of 1,6-methano[10]annulene with DMAD followed by retro-Diels–Alder reaction at a high temperature (Fig. 4.42C).³⁷ The 1,6-methano[10]annulene itself being aromatic is unreactive as a diene component; but it can undergo thermal electrocyclic ring closure to form its nonaromatic valence isomer in an equilibrium mixture. A cyclohexadiene unit of the valence isomer then serves as a reactive diene component in the Diels–Alder reaction.

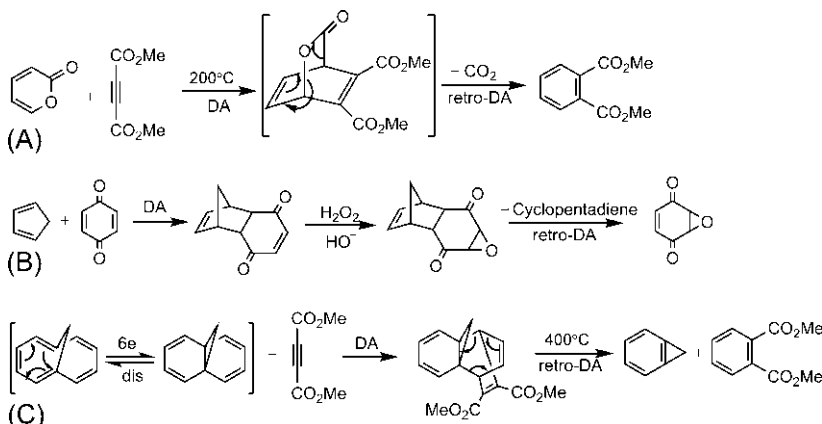
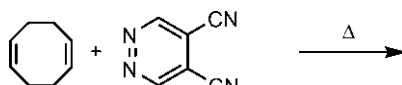


Fig. 4.42 Synthesis of (A) dimethyl phthalate, (B) benzoquinone epoxide and (C) benzocyclopropene by Diels–Alder and retro-Diels–Alder reactions.

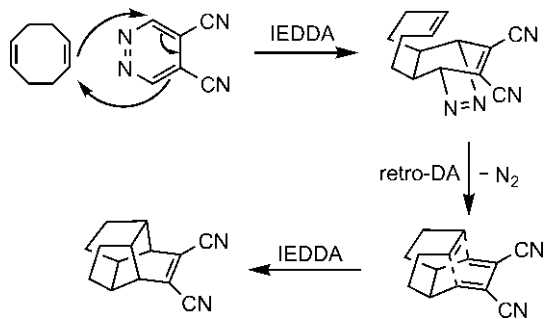
Problem 4.15

Predict the product of the following reaction.



Answer

The reaction proceeds through a sequence of IEDDA, retro-Diels–Alder with loss of N₂ and again IEDDA to give the product.



4.2.7 Dehydro-Diels–Alder Reactions

The Diels–Alder reaction is not limited to 1,3-dienes. If one or both double bonds in the diene component are replaced by a triple bond, the 4-atom component becomes an enyne or a diyne. The primary product is then a strained cyclic allene which can undergo further transformation (usually hydrogen migration) to reduce the ring strain and form a more stable aromatic isomer (Fig. 4.43). This ‘dehydrogenated’ variant of the Diels–Alder (DA) reaction with enynes or diarynes is called dehydro-Diels–Alder (DDA) reaction.³⁸ Relative to the Diels–Alder reaction between a diene and an alkene dienophile, enyne cycloaddition with an alkene is a didehydro-Diels–Alder, enyne cycloaddition with an alkyne or diyne cycloaddition with an alkene is a tetrahydro-Diels–Alder (TDDA), and diyne cycloaddition with an alkyne is a hexa-dehydro-Diels–Alder (HDDA) reaction.

Unlike the Diels–Alder reaction, the DDA cyclization is endothermic in most cases because of the ring strain arising from the cumulated double bonds. Theoretical computational studies indicate that the DDA reaction with simple enynes is concerted whereas diyne cycloaddition proceeds by competing concerted and stepwise diradical mechanisms.³⁹

Arylacetylenes can act as an enyne component where the double bond is part of an aromatic ring. The DDA dimerizations of phenylpropionic acid and its ester derivative are shown in Fig. 4.44. Historically these are the earliest DDA reactions. The DDA dimerization of the ethyl derivative upon

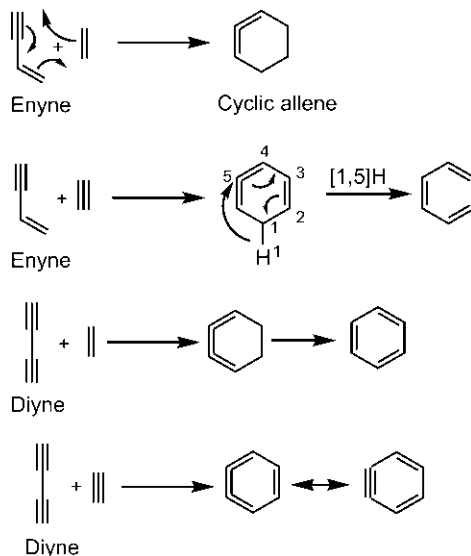


Fig. 4.43 Dehydro-Diels–Alder (DDA) reactions with enyne and diyne.

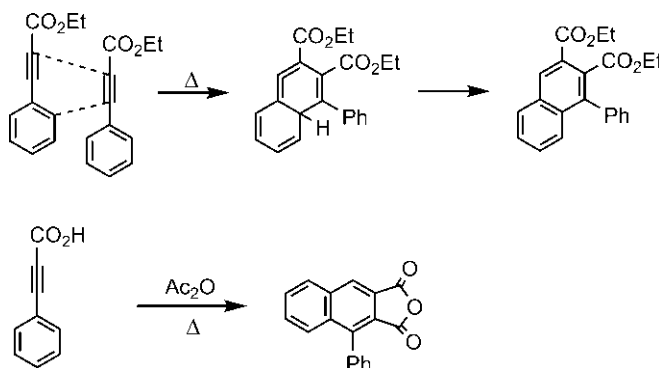
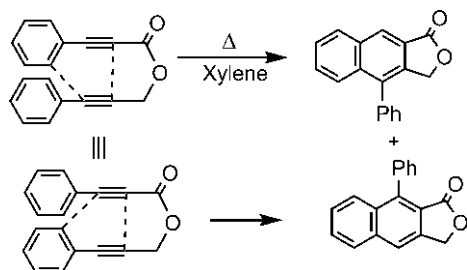


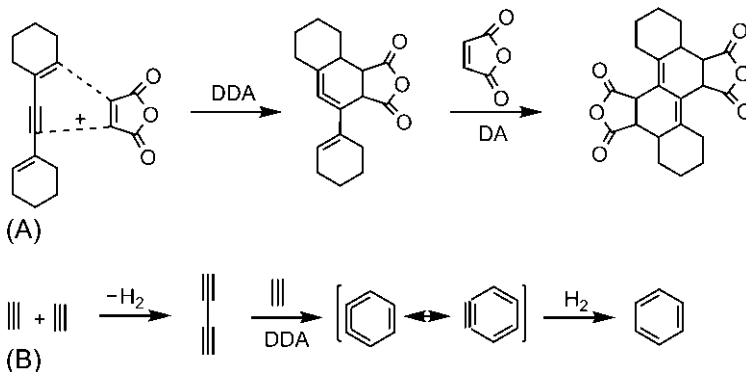
Fig. 4.44 DDA dimerization of phenylpropiolic acid and its ester.

heating produces the diester while the dimerization of the acid in the presence of acetic anhydride gives the anhydride.

If two arylacetylene moieties are linked by an ester or amide group, an intramolecular DDA reaction can take place, as shown in Fig. 4.45. Usually a mixture of isomeric lactones is obtained.

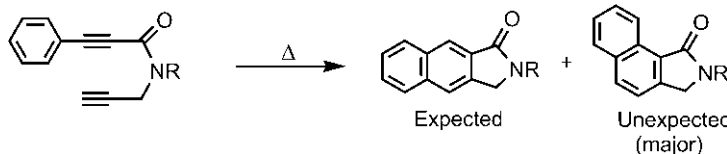
**Fig. 4.45** An intramolecular DDA reaction.

Unlike aryl acetylenes, the DDA reaction with an enyne or a diyne does not involve a temporary loss of aromaticity. Here, the initially formed cyclic allenenes are often more stable and can undergo intermolecular cycloaddition. This is illustrated with the reaction of a dienyne with maleic anhydride in Fig. 4.46A. As shown, the primarily formed cycloallene from DDA reaction undergoes DA reaction with the second molecule of maleic anhydride to form the product. The DDA reactions of diarynes are relatively few. An interesting example is the trimerization of acetylenes to benzene. The reaction proceeds by an oxidative dimerization of acetylene to butadiyne which undergoes the DDA reaction with another acetylene molecule (Fig. 4.46B).

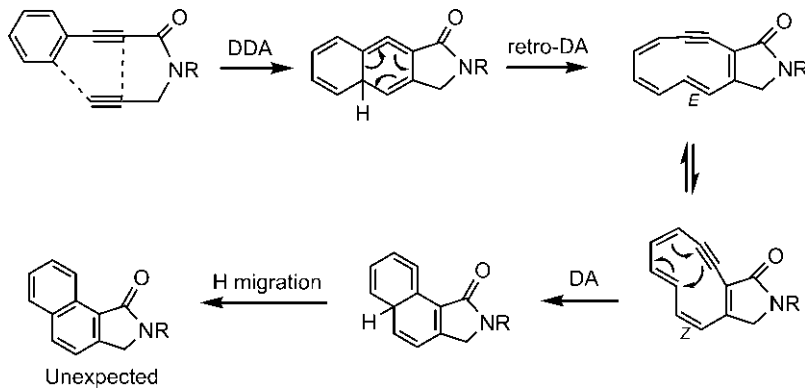
**Fig. 4.46** (A) DDA reaction with a dienyne and (B) trimerization of acetylene via DDA reaction with butadiyne.

Problem 4.16

Account for the formation of the unexpected product in the following dehydro-Diels–Alder (DDA) reaction.

**Answer⁴⁰**

The primarily formed cycloallene from the DDA reaction can undergo retro-Diels–Alder reaction followed by *E/Z* isomerization and Diels–Alder cyclization to form the rearranged cycloallene, which aromatizes via hydrogen migration to give the unexpected product.



4.3 1,3-DIPOLAR CYCLOADDITIONS

The 1,3-dipolar cycloaddition (1,3-DC) is also a [4 + 2] cycloaddition like Diels–Alder reaction, and proceeds thermally by geometrically favourable and symmetry-allowed $[\pi^4_s + \pi^2_s]$ mode. But structurally (by atom convention), unlike Diels–Alder, it is a (3 + 2) cycloaddition producing a five-membered heterocyclic ring (see Fig. 3.9A). The two reacting components for 1,3-dipolar cycloadditions are 1,3-dipoles (having a variety of structures) and dipolarophiles (usually substituted alkenes or alkynes, like dienophiles).

The 1,3-dipolar cycloadditions was first established as a major reaction-type by Huisgen⁴¹, and are often referred to as Huisgen cycloadditions.

1,3-Dipoles

The 1,3-dipole is a 3-atom π_4 system, and must contain at least one heteroatom (commonly N, O). The central atom of 1,3-dipole is always a heteroatom. There are 18 dipole structures with C, N and O that fall into two types (Fig. 4.47): allyl-type bent structure (12 dipoles) and propargyl-type linear structure (6 dipoles).

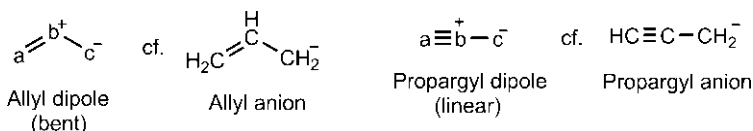


Fig. 4.47 Two types of 1,3-dipoles as allyl- and propargyl-type.

These 18 dipoles in terms of structural unit (C—N—C, C—N—N, etc.) are shown in Fig. 4.48.

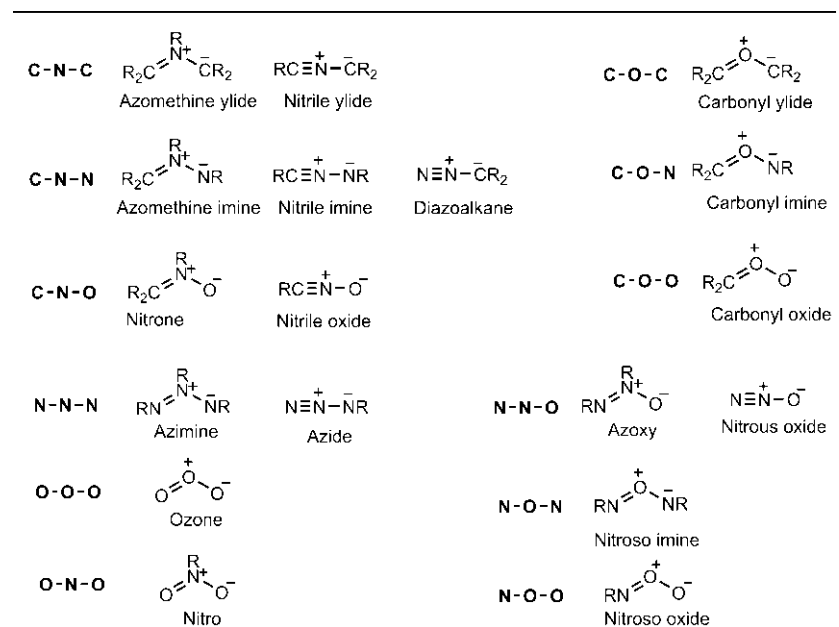


Fig. 4.48 Structures and names of allyl-type and propargyl-type 1,3-dipoles.

A number of canonical structures can be drawn for each dipole. Two propargyl dipoles, diazoalkanes and azides, are often represented as allenyl dipoles with reference to their allenyl anion-like canonical structure as shown in Fig. 4.49A. For a dipole, a canonical structure can show positive charge at one end and negative charge at the other end. But it does not imply that one end is electrophilic and the other end is nucleophilic because there is a canonical structure for the same dipole in which the formal charges are reversed. As such, most 1,3-dipoles have low dipole moment as the polarity implied by any single canonical structure is counterbalanced by other contributing structure. This is exemplified with diazomethane in Fig. 4.49B.

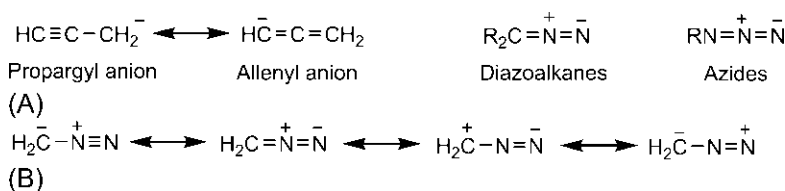


Fig. 4.49 (A) Diazoalkanes and azides represented as allenyl dipoles and (B) canonical structures of diazomethane.

4.3.1 Regioselectivity of 1,3-Dipolar Cycloadditions

The regiochemistry of 1,3-dipolar cycloaddition is particularly important when the reaction is utilized for the synthesis of aromatic heterocycles or their reduced forms. The transition structure for 1,3-dipolar cycloaddition is not quite polar, and the frontier orbital analysis is invoked to explain the regiochemistry of 1,3-dipolar cycloadditions in a manner similar to that described for the Diels–Alder reactions. Here the resonance integral β is to be taken into account as β is different for C–C, N–C and O–C bonds being formed. For this reason, Houk estimated frontier orbital coefficients of 1,3-dipoles as $(\phi\beta)^2/15$, instead of simple atomic orbital coefficients used for dienes. The division by 15 was made to bring the coefficient values close to 1. The Houk data for the frontier orbital energies and coefficients of some parent dipoles are listed in Table 4.1.^{42,43}

Table 4.1 Frontier orbital energies and coefficients of some parent 1,3-dipoles

Dipole	Energy (eV)	Coefficient $[(c\beta)^2/15]$		
HOMO	LUMO	HOMO	LUMO	
Dizomethane	−9.0	1.8	$\begin{array}{c} \bar{H}_2\bar{C}-\overset{+}{N}\equiv N \\ 1.57 \end{array}$ 0.85	$\begin{array}{c} \bar{H}_2\bar{C}-\overset{+}{N}\equiv N \\ 0.66 \end{array}$ 0.56
Hydrazoic acid (azide)	−11.5	0.1	$\begin{array}{c} \overset{+}{H}N-\overset{-}{N}\equiv N \\ 1.55 \end{array}$ 0.72	$\begin{array}{c} \overset{+}{H}N-\overset{-}{N}\equiv N \\ 0.37 \end{array}$ 0.76
Nitrile ylide	−7.7	0.9	$\begin{array}{c} HC\equiv\overset{+}{N}-CH_2 \\ 1.07 \end{array}$ 1.50	$\begin{array}{c} HC\equiv\overset{+}{N}-CH_2 \\ 0.69 \end{array}$ 0.64
Nitrile imine	−9.2	0.1	$\begin{array}{c} HC\equiv\overset{+}{N}-\overset{-}{NH} \\ 0.90 \end{array}$ 1.45	$\begin{array}{c} HC\equiv\overset{+}{N}-\overset{-}{NH} \\ 0.92 \end{array}$ 0.36
Nitrile oxide	−11.0	−0.5	$\begin{array}{c} HC\equiv\overset{+}{N}-O^- \\ 0.81 \end{array}$ 1.24	$\begin{array}{c} HC\equiv\overset{+}{N}-O^- \\ 1.18 \end{array}$ H ⁺ 0.17
Nitronate	−9.7	−0.5	$\begin{array}{c} H^+ \\ \\ H_2C=\overset{+}{N}-O^- \\ 1.11 \end{array}$ 1.06	$\begin{array}{c} H_2C=\overset{+}{N}-O^- \\ 0.98 \end{array}$ 0.32
Azomethine ylide	−6.9	1.4	$\begin{array}{c} H^+ \\ \\ H_2C=\overset{+}{N}-CH_2 \\ 1.28 \end{array}$ 1.28	$\begin{array}{c} H_2C=\overset{+}{N}-CH_2 \\ 0.73 \end{array}$ 0.73
Azomethine imine	−8.6	−0.3	$\begin{array}{c} H^+ \\ \\ H_2C=\overset{+}{N}-NH \\ 1.15 \end{array}$ 1.24	$\begin{array}{c} H_2C=\overset{+}{N}-NH \\ 0.87 \end{array}$ 0.49

4.3.1.1 Regioselectivity in Pyrazole/Pyrazoline/Pyrazolidine Synthesis

For the construction of pyrazole/pyrazoline/pyrazolidine rings using 1,3-dipolar cycloaddition, we shall first find the structural unit of the required 1,3-dipole by suitable disconnection as shown in Fig. 4.50.



Fig. 4.50 Disconnection for pyrazole/pyrazoline/pyrazolidine system.

Three useful dipoles for C—N—N unit are diazoalkanes, nitrile imines and azomethine imines (see Fig. 4.48).

Diazoalkane Cycloaddition

The diazoalkane dipole is most common. Let us consider a 1,3-dipolar cycloaddition of diazomethane with a z-substituted dipolarophile. The

frontier orbital control can be determined from HOMO/LUMO energy separations as shown in Fig. 4.51. For frontier orbital energies, see Table 4.1 for diazomethane and Fig. 4.7 for the dipolarophile.

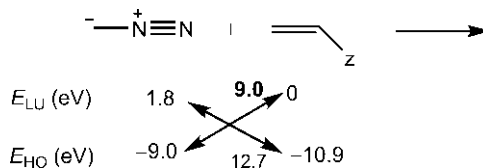


Fig. 4.51 HOMO/LUMO energy separations for 1,3-dipolar cycloaddition of diazomethane with z -substituted dipolarophile. The more important interaction is indicated with the estimated value in bold.

Clearly, the dominant frontier orbital interaction is $\text{HOMO}_{\text{dipole}}/\text{LUMO}_{\text{dipolarophile}}$ interaction ($E_{\text{LU}} - E_{\text{HO}} = 9.0$ eV) which is strongly favoured over the other by a large margin of 3.7 eV. The reaction is $\text{HOMO}_{\text{dipole}}/\text{LUMO}_{\text{dipolarophile}}$ controlled, and is expected to be quite facile.

The regioselectivity of the reaction can be analyzed in terms of interactions involving coefficients in two orientations (Fig. 4.52). The dipole coefficients (Table 4.1) and the coefficient pattern of the z -substituted alkene dipolarophile (Fig. 4.16) are indicated. Note that, as the dipole is isoelectronic with allyl anion, the dipole HOMO has the same symmetry as allyl anion HOMO (ψ_2).

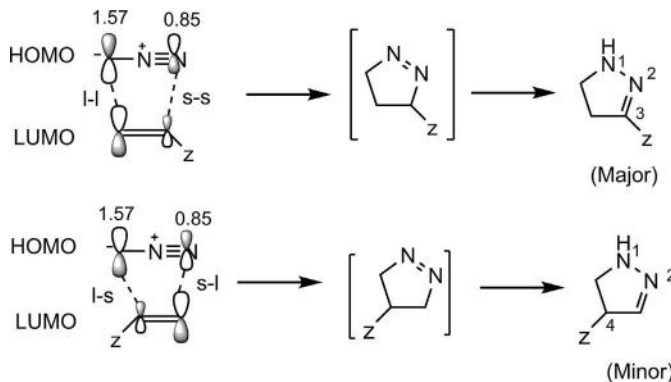


Fig. 4.52 Frontier orbital interactions for regioselectivity of 1,3-dipolar cycloaddition of diazomethane with z -substituted dipolarophile.

The major regiosomeric product arises from large–large + small–small interactions and is a 3-substituted pyrazoline. This regioselectivity is illustrated with two examples in Fig. 4.53.

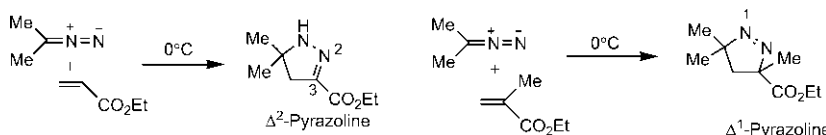


Fig. 4.53 Regioselectivity in pyrazoline synthesis using α -substituted alkenes.

The diazoalkane cycloaddition also exhibits site selectivity, as obtained for the Diels–Alder reaction. For example, diazomethane reacts with an unsaturated ester at the 4,5 double bond to give the product (Fig. 4.54).⁴⁴ The preferred bonding is between the two larger coefficients.

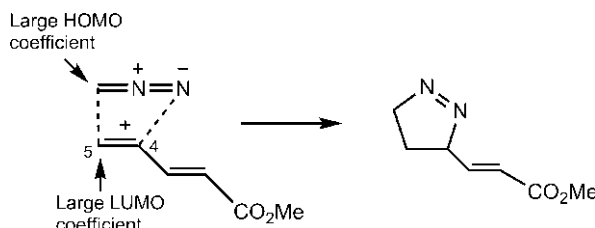


Fig. 4.54 Site selectivity of diazoalkane cycloaddition.

The reactions of diazomethane with α - and β -substituted alkenes with larger HOMO/LUMO energy gaps are quite slow, and not very common. The regioselectivity is however similar as for α -substituted alkenes giving a 3-substituted pyrazoline.⁴⁵ This is illustrated in Fig. 4.55 with an α -substituted alkene, ethyl vinyl ether. As the alkene dipolarophile preferably uses its HOMO, the frontier orbital control presumably changes to $\text{LUMO}_{\text{dipole}}/\text{HOMO}_{\text{dipolarophile}}$ control.

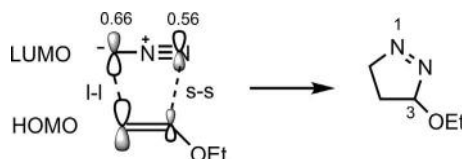
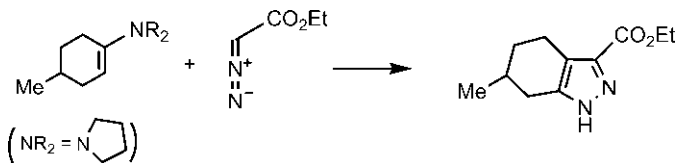


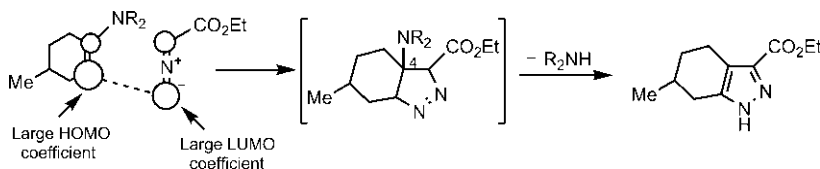
Fig. 4.55 Regioselectivity in pyrazoline synthesis using an α -substituted alkene.

Problem 4.17

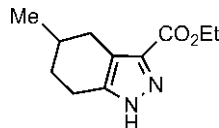
Account for the regioselectivity observed in the synthesis of pyrazole.

**Answer**

The electron-withdrawing CO_2Et group (α -substituent) in diazoacetic ester dipole will lower its LUMO energy. On the other hand, the alkene dipolarophile bears a strong, electron-donating NR_2 group (β -substituent) which will raise its HOMO energy. Thus the more important frontier orbital interaction is $\text{LUMO}_{\text{dipole}}/\text{HOMO}_{\text{dipolarophile}}$ interaction. The coefficients in the diazomethane LUMO are close (0.66 and 0.56), but the CO_2Et on carbon atom of the dipole would exert its effect to reduce appreciably the LUMO coefficient on carbon. Consequently, the leading bond between two large coefficients on nitrogen of dipole and alkene carbon β to NR_2 group of dipolarophile gives 4- NR_2 -substituted pyrazoline as intermediate, which loses R_2NH (pyrrolidine) to yield the aromatic pyrazole. The enamine dipolarophile acts as an alkyne equivalent.



The NR_2 group is involved in directing the cycloaddition but is lost in the final product. Therefore the regiochemistry of the reaction could not be ascertained from the product structure unless a ‘marker’ group is present somewhere. Here, Me on the cyclohexene ring of the dipolarophile acts as a ‘marker’ which differentiates the observed product from the other regioisomers as shown below.



Nitrile Imine Cycloaddition

The nitrile imines have been successfully employed in the synthesis of pyrazoles. An example is shown in Fig. 4.56.⁴⁶ The nitrile imine is generated *in situ* by eliminating benzenesulphonate, which then undergoes cycloaddition with an enamine dipolarophile. Nitrile imine has a low-energy LUMO (0.1 eV) (see Table 4.1). On the other hand, the enamine dipolarophile is electron rich and has a high-energy HOMO. The dominant frontier orbital interaction is therefore $\text{LUMO}_{\text{nitrile imine}}/\text{HOMO}_{\text{dipolarophile}}$ interaction. The regioselectivity arises from the interaction between the β carbon of enamine (large HOMO coefficient) and the carbon end of nitrile imine (large LUMO coefficient) (see Table 4.1). The enamine acts as an alkyne equivalent, morpholine being lost in the final aromatization step.

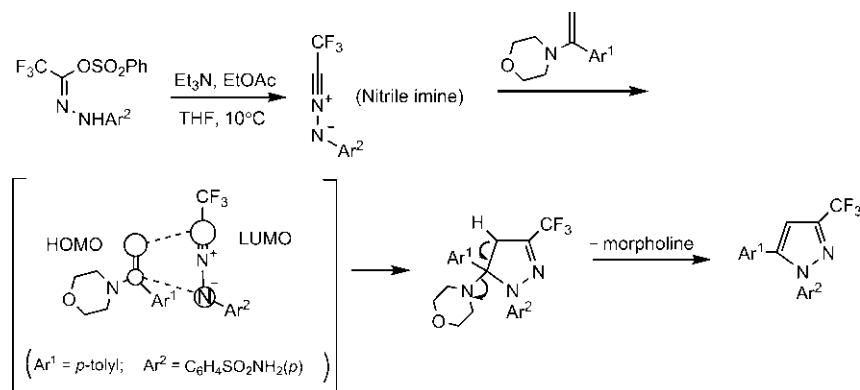


Fig. 4.56 Regioselectivity of nitrile imine cycloaddition in pyrazole synthesis.

Azomethine Imine Cycloaddition

Azomethine imines are useful in pyrazolidine synthesis. The common reagents have aryl group at each end of the azomethine imine dipole which raise the HOMO energy and lower the LUMO energy. With Ph at each end, Houk's data give that HOMO and LUMO energies are -5.6 and -1.4 eV, respectively (cf. parent dipole in Table 4.1). Azomethine imine cycloaddition with α -substituted alkene dipolarophile is $\text{HOMO}_{\text{dipole}}/\text{LUMO}_{\text{dipolarophile}}$ controlled (the energy separation being 5.6 eV as against 9.5 eV for the other) which explains the observed regioselectivity in cycloaddition of **4.6** with acrylonitrile to form a 4-substituted pyrazolidine (Fig. 4.57).^{41,47}

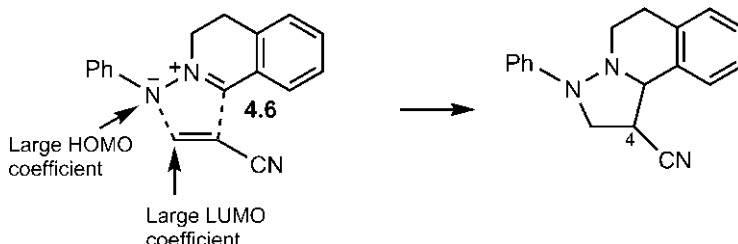
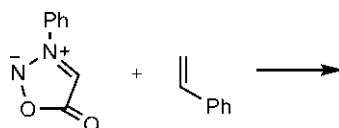


Fig. 4.57 Regioselectivity of azomethine imine cycloaddition with α -substituted dipolarophile in pyrazolidine synthesis.

With α -substituted alkene dipolarophile such as styrene, the $HOMO_{\text{dipole}}/LUMO_{\text{dipolarophile}}$ interaction is favoured by a small margin of 1.1 eV (6.6 eV as against 7.7 eV). The reaction produces a mixture of regioisomers with the 4-substituted isomer being the major product.^{41,47}

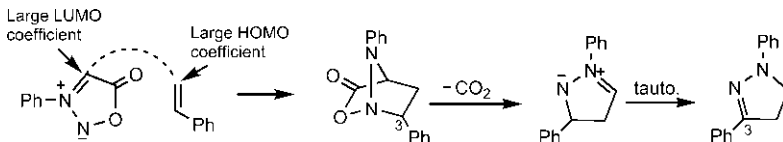
Problem 4.18

Explain the regioselectivity in the following synthesis of pyrazoline.



Answer⁴⁸

The sydnone represents an azomethine imine dipole bearing an electron-withdrawing carbonyl on the carbon atom, which lowers the energy of the dipole LUMO. This leads to $LUMO_{\text{dipole}}/HOMO_{\text{dipolarophile}}$ control. The coefficient on the carbon atom in dipole LUMO is larger, though somewhat reduced by the carbonyl group. The preferred regioisomer arises from the bonding between carbon atom of the dipole and the unsubstituted end of alkene (styrene). The 3-substituted regioisomer is formed as an intermediate which loses CO_2 by retro 1,3-dipolar cycloaddition followed by tautomerism to give the 3-substituted pyrazoline product. The sydnone acts as a nitrile imine equivalent.



4.3.1.2 Regioselectivity in Isoxazole/Isoxazoline/Isoxazolidine Synthesis

The disconnection for isoxazole and its reduced forms gives C—N—O dipole (Fig. 4.58).

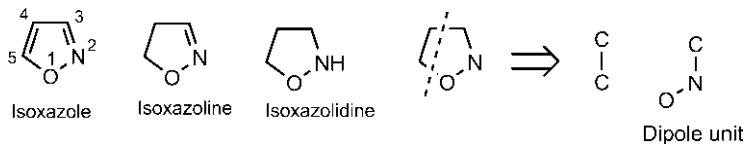


Fig. 4.58 Disconnection for isoxazole/isoxazoline/isoxazolidine system.

The dipoles for C—N—O unit are nitrile oxide and nitrone (see Fig. 4.48).

Nitrile Oxide Cycloaddition

Nitrile oxides **4.7** are generated in situ by dehydrohalogenation of α -halooximes or by dehydration of primary nitroalkanes (Fig. 4.59). (Draw a plausible mechanism for each.)

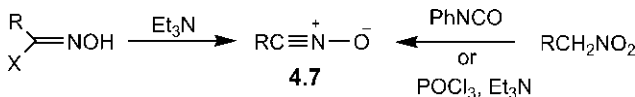


Fig. 4.59 Methods of generation of nitrile oxides.

Nitrile oxides have low-energy LUMOs, and their cycloadditions with electron-rich x- or c-substituted dipolarophiles are expected to be LUMO-dipole/HOMO_{dipolarophile} controlled. This can be easily seen from the HOMO/LUMO energy separations, for instance, with x-substituted alkene dipolarophiles:

$$E_{\text{LUMO(nitrile oxide)}} - E_{\text{HOMO(x-alkene)}} = [-0.5 - (-9.0)] \text{ eV} = 8.5 \text{ eV}$$

$$E_{\text{LUMO(x-alkene)}} - E_{\text{HOMO(nitrile oxide)}} = [3.0 - (-11.0)] \text{ eV} = 14 \text{ eV}$$

The LUMO_{dipole}/HOMO_{dipolarophile} interaction is therefore strongly favoured. These cycloadditions are highly regioselective, and lead to 5-substituted isoxazolines via preferred large-large + small-small interactions (Fig. 4.60). With phenyl nitrile oxide, the energy separation is reduced to 8.0 eV by the effect of Ph, which lowers the dipole LUMO energy from

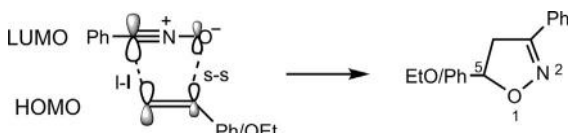


Fig. 4.60 Frontier orbital interactions for regioselectivity of 1,3-dipolar cycloaddition of phenyl nitrile oxide with c-/x-substituted dipolarophile.

-0.5 to -1.0 eV and the reaction is further facilitated. The parent nitrile oxide LUMO is highly polarized with much larger coefficient on carbon (1.18) than on oxygen (0.17) (see Table 4.1). As such, the carbon coefficient in phenyl nitrile oxide LUMO though somewhat reduced by conjugating Ph is expected to be larger.

For α -substituted alkene dipolarophiles, the prediction of regiochemistry is not quite straightforward. Based on energy separations, both HOMO/LUMO pairs seem to be important. The energy calculation shows that $\text{LUMO}_{\text{dipole}}/\text{HOMO}_{\text{dipolarophile}}$ energy separation is 10.4 eV while that between $\text{HOMO}_{\text{dipole}}$ and $\text{LUMO}_{\text{dipolarophile}}$ is 11 eV. The $\text{LUMO}_{\text{dipole}}/\text{HOMO}_{\text{dipolarophile}}$ interaction is thus slightly favoured. This preference is however reinforced by the stronger polarization of nitrile oxide LUMO compared with the polarization in HOMO (see Table 4.1). The more important $\text{LUMO}_{\text{dipole}}/\text{HOMO}_{\text{dipolarophile}}$ interaction then tends to favour the 5 -substituted regioisomeric product from the leading large-large interaction between dipole carbon and β -carbon of α -substituted dipolarophile. This has been observed in practice, for example, in cycloaddition with methyl acrylate (Fig. 4.61).⁴⁹

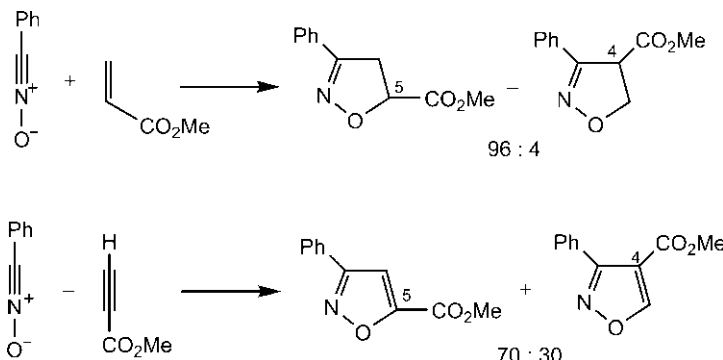


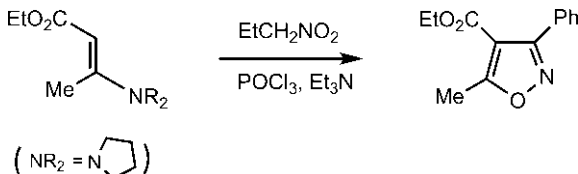
Fig. 4.61 Examples of regioselectivity in isoxazoline/isoxazole synthesis.

But interestingly, with alkyne dipolarophile, the regioselectivity falls⁵⁰, also shown in Fig. 4.61. The C—C bond length of alkyne is shorter than that in alkene, and therefore results in better p orbital overlap. As a consequence, alkyne HOMO is lower in energy by 0.4 – 0.9 eV than alkene HOMO but the LUMO energies are nearly same (see Section 1.5.1.5). This leads to increase in energy separation for $\text{LUMO}_{\text{dipole}}/\text{HOMO}_{\text{alkyne}}$. The coefficient patterns for substituted alkenes and alkynes are however similar. Consequently, the other $\text{HOMO}_{\text{dipole}}/\text{LUMO}_{\text{alkyne}}$ interaction becomes competitive which tends to favour 4 -substituted regioisomer (dipole oxygen

has larger coefficient in HOMO), and the regioselectivity diminishes with alkyne dipolarophile relative to alkene dipolarophile.

Problem 4.19

Account for the regioselectivity in the synthesis of isoxazole.

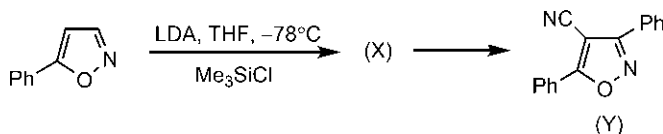


Answer⁵¹

The dipole generated is $\text{EtC}\equiv\text{N}^+—\text{O}^-$. The nitrile oxide uses its LUMO and the electron-rich enamine dipolarophile uses its HOMO. The dominant interaction is $\text{LUMO}_{\text{dipole}}/\text{HOMO}_{\text{dipolarophile}}$ interaction. The observed regioselectivity results from the leading bond formed between two large coefficients (C on dipole and β -C with respect to NR_2 in dipolarophile). NR_2 group is lost in the final aromatization step (cf. Problem 4.17).

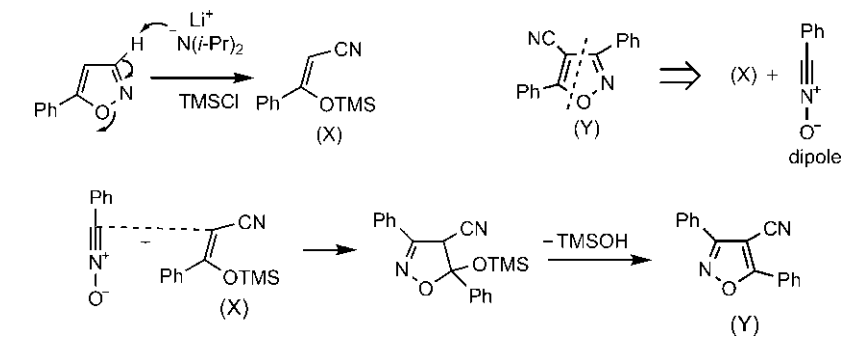
Problem 4.20

Identify (X) in the following scheme, and convert (X) into an isoxazole (Y) using 1,3-dipolar cycloaddition. Explain the regioselectivity of the cycloaddition reaction.



Answer

The (X) is formed by $\text{N}—\text{O}$ cleavage as shown below. It acts as an electron-rich dipolarophile (as a net effect of the substituents) in the second step. Retrosynthetic analysis for the nitrile oxide (Y) gives $\text{PhC}\equiv\text{N}^+—\text{O}^-$ dipole in cycloaddition. The reaction is $\text{LUMO}_{\text{dipole}}/\text{HOMO}_{\text{dipolarophile}}$ controlled. The regioselectivity results from the leading bond formed between two large coefficients (dipole carbon and dipolarophile carbon being β to stronger OTMS and Ph substituents). OTMS group is lost in the final aromatization step. The silyl enol ether (X) thus acts as an alkyne equivalent.



Nitronate Cycloaddition

Many nitrones are stable and isolable compounds. They are easily prepared by the oxidation of N,N-disubstituted hydroxylamine or by the condensation of N-alkylhydroxylamines with aldehydes or ketones (Fig. 4.62).

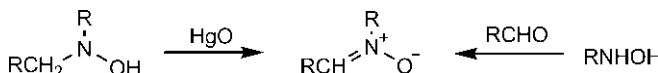


Fig. 4.62 Methods of generation of nitrones.

Like nitrone oxides, nitrones have low-energy LUMO (Table 4.1) and a similar $\text{LUMO}_{\text{dipole}}/\text{HOMO}_{\text{dipolarophile}}$ control operates in their cycloadditions with *x*- or *c*-substituted dipolarophiles producing a 5-substituted isoxazolidine as major product. With *z*-substituted alkene dipolarophile, the energy gap between $\text{LUMO}_{\text{dipole}}$ and $\text{HOMO}_{\text{dipolarophile}}$ is 10.4 eV whereas the energy difference between $\text{HOMO}_{\text{dipole}}$ and $\text{LUMO}_{\text{dipolarophile}}$ is 9.7 eV. Both interactions seem to be important with a slight edge in favour of the latter. But the nitrone LUMO is strongly polarized with carbon having much larger coefficient (0.98) than oxygen (0.32). In contrast, the nitrone HOMO coefficients at the two ends are almost equal (see Table 4.1). The net result is that $\text{LUMO}_{\text{dipole}}/\text{HOMO}_{\text{dipolarophile}}$ interaction controls regioselectivity even with *z*-substituted alkene dipolarophiles in a majority of cases. The patterns of regioselectivity of cycloadditions of nitrones with alkene dipolarophiles are similar to those of nitrone oxides and give 5-substituted isoxazolidine as a major regioisomer (Fig. 4.63A). These are illustrated in Fig. 4.63B with two examples.⁵²

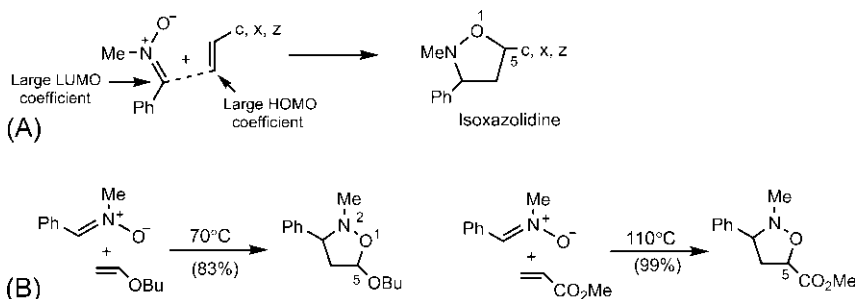


Fig. 4.63 (A) Frontier orbital interaction for regioselectivity of cycloaddition of a nitrone to c-, x- or z-substituted alkene. (B) Examples of regioselectivity of nitrone addition.

When the z-substituted alkene dipolarophile becomes highly electron deficient, its LUMO energy gets lowered so much that the $HOMO_{\text{dipole}}/LUMO_{\text{dipolarophile}}$ interaction tends to be competitive and even dominant. The HOMO coefficients of a simple nitrone are almost equal but introduction of a conjugating substituent such as Ph on nitrone carbon would tend to diminish its coefficient leading to a larger coefficient on oxygen in dipole HOMO, thereby inducing opposite polarization of dipole LUMO. In this situation, with highly electron-deficient dipolarophiles, the $HOMO_{\text{dipole}}/LUMO_{\text{dipolarophile}}$ interaction controls regioselectivity producing a 4-substituted isoxazolidine as the major product.⁵³ This is illustrated in Fig. 4.64 with cycloadditions of a C-phenyl-N-methylnitronone with two strongly electron-deficient dipolarophiles bearing NO_2 and two CO_2Me substituents, respectively.

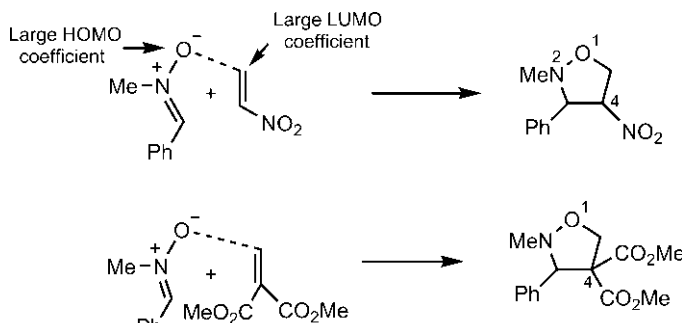
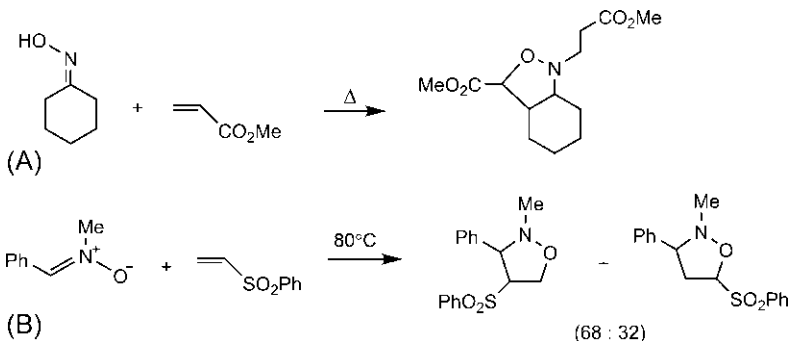


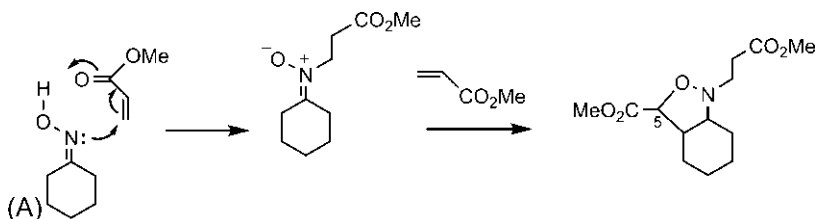
Fig. 4.64 Regioselectivity of cycloaddition of C-phenyl-N-methylnitronone to highly electron-deficient alkenes.

Problem 4.21

Account for the regioselectivity in the following nitrone cycloadditions.

**Answer**

(A) Nucleophilic addition of the oxime to methyl acrylate (conjugate addition) followed by abstraction of proton by the enolate produces a nitrone which then undergo 1,3-dipolar cycloaddition with a second molecule of methyl acrylate to give the adduct. Here the regioselectivity is governed by LUMO_{dipole}/HOMO_{dipolarophile} interaction which leads to a 5-substituted isoxazolidine product (see Fig. 4.63).



(B) The dipolarophile bearing SO₂Ph is highly electron deficient, and the nitrone carbon bears a conjugating Ph substituent. As such, HOMO_{dipole}/LUMO_{dipolarophile} control operates and 4-SO₂Ph-substituted isoxazolidine is obtained as the predominant product (cf. Fig. 4.64).

Intramolecular Nitrone Cycloaddition We shall describe here an intramolecular nitrone cycloaddition employed in a short and elegant synthesis of the alkaloid luciduline.⁵⁴ The synthesis involves an intermediate

nitrone (generated by the condensation of a hydroxyl amine with formaldehyde) which undergoes a highly regioselective intramolecular cycloaddition to an alkene double bond to give an isoxazolidine which is converted to luciduline by simple transformations (Fig. 4.65).

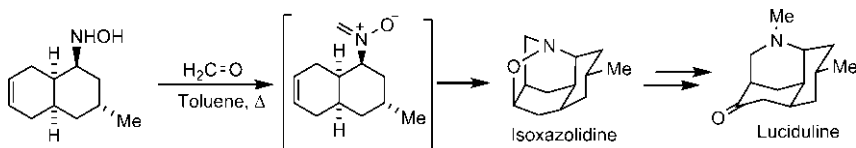


Fig. 4.65 Intramolecular 1,3-dipolar cycloaddition of nitrone in a synthesis of luciduline.

The regioselectivity of the reaction is explained as follows. The important frontier orbital interaction for the addition of a simple nitrone to an unactivated alkene double bond is $\text{LUMO}_{\text{dipole}}/\text{HOMO}_{\text{dipolarophile}}$ interaction. The 1,3-dipolar cycloaddition is quite asynchronous. Owing to the larger coefficient on carbon in nitrone LUMO and larger resonance integral β for C—C bond, formation of C—C bond is more advanced than O—C bond in the transition structure. Here the alkene double bond is essentially nonpolarized, and therefore does not provide a preference to C—C bond formation to one of the alkene carbons in terms of frontier orbital coefficient interaction. But the intramolecularity of the reaction plays a crucial role. Fig. 4.66 shows that the development of C—C bond by path (a) produces a six-membered ring whereas a seven-membered ring is formed by path (b). Path (a) is thus more favourable and leads to the intramolecular isoxazolidine adduct. Here the regiochemical preference is solely determined by the intramolecularity of the reaction.

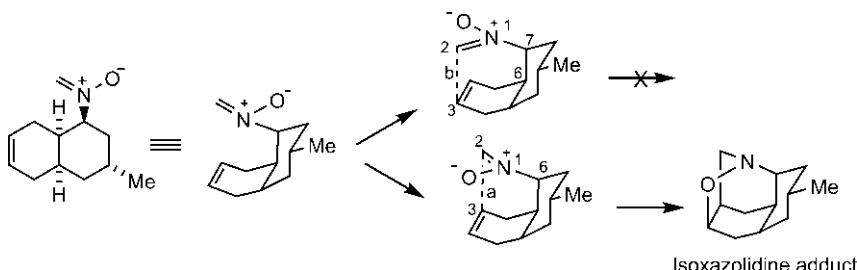


Fig. 4.66 Regioselectivity of intramolecular nitrone cycloaddition in luciduline synthesis.

4.3.1.3 Regioselectivity in 1,2,3-Triazole/Triazoline Synthesis

The disconnection for 1,2,3-triazole/triazoline gives N-N-N dipole (Fig. 4.67).

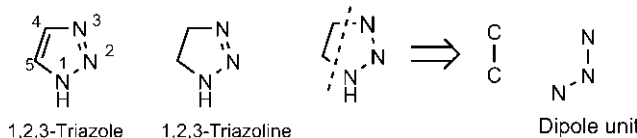


Fig. 4.67 Disconnection for 1,2,3-triazole/triazoline system.

The useful dipole for N-N-N fragment is a linear azide dipole (see Fig. 4.48). The dominant frontier orbital interaction for cycloaddition of an azide to c- or x-substituted alkene dipolarophile is LUMO_{dipole}/HOMO_{dipolarophile} interaction as obtained from the estimate of energy separations (verify). The parent hydrazoic acid is not the usual dipole; a common dipole is phenyl azide. The frontier orbital interaction leads to a 5-substituted triazoline as the predominant regiosomer (Fig. 4.68A). The azide dipole has larger coefficient at the unsubstituted terminal in the LUMO (see Table 4.1). The conjugating Ph on the dipole also enhances the coefficient at the unsubstituted terminal. The predicted regioselectivity is illustrated in Fig. 4.68B with the cycloaddition of phenyl azide to styrene, giving 1,5-diphenyltriazoline.⁵⁵

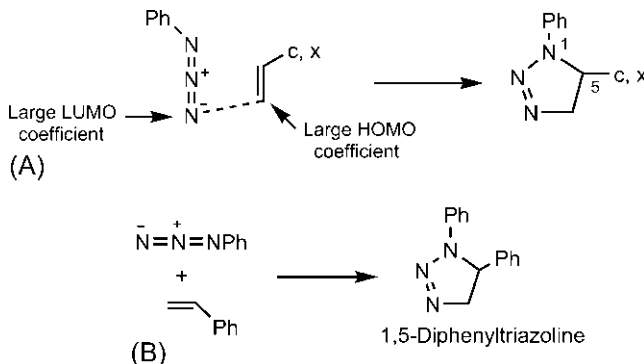
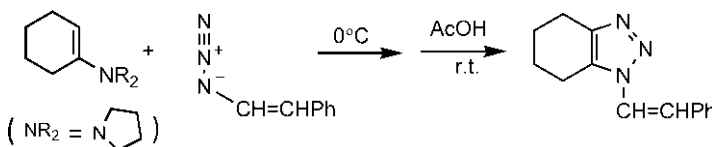


Fig. 4.68 (A) Regioselectivity of cycloaddition of phenyl azide to c- or x-substituted alkene and (B) example of regioselective cycloaddition between phenyl azide and styrene.

In contrast to α - or β -substituted alkene, the cycloaddition of a γ -substituted alkene dipolarophile such as methyl acrylate with phenyl azide usually gives 1,4-disubstituted triazoline.⁵⁶ The estimate of HOMO/LUMO energy differences (using Houk's data for PhN_3 , instead of HN_3 ; see below) favours $\text{HOMO}_{\text{dipole}}/\text{LUMO}_{\text{dipolarophile}}$ interaction from the other by a margin of only 1.2 eV (9.5 eV as against 10.7 eV). This tends to favour the formation of 4-substituted regioisomer (preferred bonding between phenyl substituted nitrogen with large HOMO coefficient and β -carbon of alkene with large LUMO coefficient) but cannot explain the high regioselectivity observed.

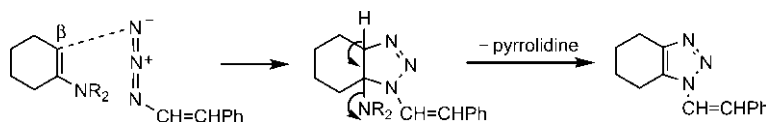
Problem 4.22

Account for the regioselectivity in the synthesis of 1,2,3-triazole.



Answer⁵⁷

The electron-rich enamine dipolarophile uses HOMO for interaction with azide LUMO. The regioselectivity results from the leading bond formed between two large coefficients at β carbon of enamine and unsubstituted nitrogen of azide. The enamine is an alkyne equivalent; NR₂ group being lost in the final aromatization step (cf. Problems 4.17, 4.19).



When an alkyne dipolarophile is used in place of alkene dipolarophile, the regioselectivity of azide cycloaddition is largely reduced (cf. Fig. 4.61). For example, the reaction of phenyl azide with phenylacetylene (in place of styrene, see Fig. 4.68B) yields approximately 1:1 mixture of 5- and 4-substituted triazoles (Fig. 4.69).⁵⁸

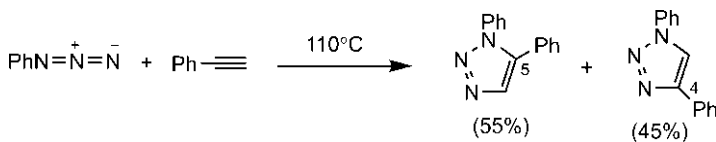


Fig. 4.69 Poor regioselectivity in azide–alkyne cycloaddition.

To rationalize the observation, we shall first determine the frontier orbital control by estimating the HOMO/LUMO energy separations. Alkyne HOMO is lower in energy by 0.4–0.9 eV (an average of 0.7 eV) than alkene HOMO but the LUMO energies are nearly the same (see [Section 1.5.1.5](#)). Using Houk’s data for PhN_3 (instead of HN_3) and the HOMO energy of c-substituted alkyne to be -9.8 eV ($E_{\text{HOMO(c-alkene)}} - 0.7$ eV), the energy separations are

$$E_{\text{LUMO(phenyl azide)}} - E_{\text{HOMO(c-alkyne)}} = [-0.2 - (-9.8)]\text{eV} = 9.6 \text{ eV}$$

$$E_{\text{LUMO(c-alkyne)}} - E_{\text{HOMO(phenyl azide)}} = [1.0 - (-9.5)]\text{eV} = 10.5 \text{ eV}$$

The energy differences for the two HOMO/LUMO pairs are within 1 eV, and both are important with $\text{LUMO}_{\text{dipole}}/\text{HOMO}_{\text{dipolarophile}}$ being slightly preferred. The polarizations of LUMO and HOMO of azide are opposite (see [Table 4.1](#)) whereas the polarizations of HOMO and LUMO of c-alkyne are similar. The $\text{LUMO}_{\text{dipole}}/\text{HOMO}_{\text{dipolarophile}}$ interaction gives a 5-substituted adduct (see [Fig. 4.68](#)) but $\text{HOMO}_{\text{dipole}}/\text{LUMO}_{\text{dipolarophile}}$ interaction would lead to a 4-substituted adduct as the polarization of HOMO of azide is reversed. The operation of both frontier orbital controls therefore gives a mixture of 5- and 4-substituted triazoles with poor regioselectivity.

Remarks

The thermal Huisgen 1,3-dipolar cycloaddition of azides to alkynes gives poor regioselectivity. However, the Huisgen cycloaddition can be catalyzed using copper(I) and ruthenium catalysts when the reaction becomes highly regioselective. The catalyzed version of azide–alkyne cycloaddition is a popular ‘click’ reaction. ‘Click chemistry’ is a term introduced by K. B. Sharpless to represent highly efficient and reliable general reactions that are simple to perform in easily removable or benign solvents. The catalyzed version of the azide–alkyne cycloaddition occurs by a different mechanism involving a

catalytic cycle^{59,60} but conform fully to the definition of ‘click chemistry.’ The copper-catalyzed cycloaddition can be conducted under aqueous conditions at room temperature, and provides easy synthesis of the 1,4-disubstituted triazoles specifically while a ruthenium-catalyzed reaction gives opposite regioselectivity with the formation of 1,5-disubstituted triazole (Fig. 4.70).

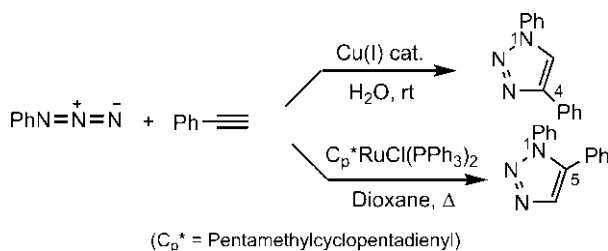


Fig. 4.70 Catalyzed azide–alkyne cycloadditions.

The classic uncatalyzed Huisgen azide–alkyne cycloaddition however fails as a true ‘click’ reaction as it requires elevated temperature and gives poor regioselectivity.

4.3.1.4 1,3-Dipolar Cycloaddition Route to Pyrrole Synthesis

As the central atom of 1,3-dipole is a heteroatom, the disconnection for pyrrole is made as shown in Fig. 4.71 to give C—N—C unit for the dipole.

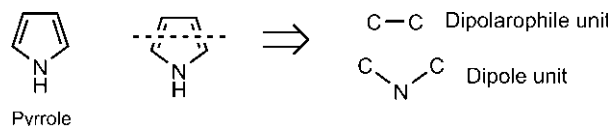


Fig. 4.71 Disconnection for pyrrole system.

Two dipoles for C—N—C unit are azomethine ylide and nitrile ylide (see Fig. 4.48). Here the terminal atoms of the dipoles are carbons and the resonance integral β will be similar. The frontier orbital coefficients at the terminal carbons are also similar in azomethine ylide or do not differ much in nitrile ylide (Table 4.1).

An azomethine ylide or a nitrile ylide is generated *in situ* as shown in Fig. 4.72 which then undergoes 1,3-dipolar cycloaddition with DMAD to give finally a pyrrole derivative.^{61,62}

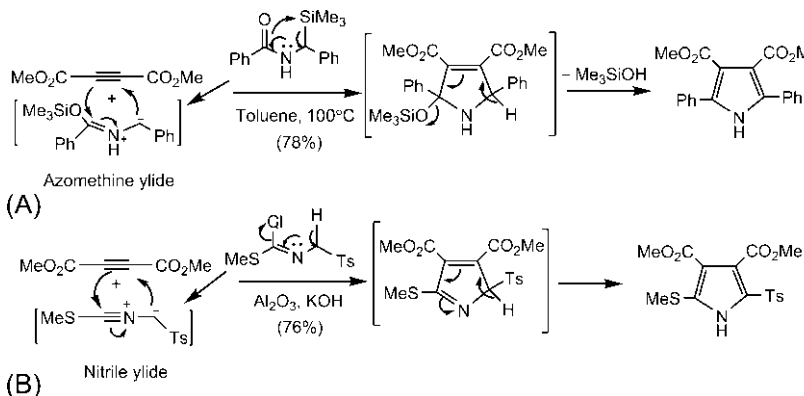


Fig. 4.72 Pyrrole synthesis using 1,3-dipolar cycloaddition involving (A) an azomethine ylide and (B) a nitrile ylide.

Mesoionic compounds can also act as a dipole.⁶³ For example, an azlactone exists in equilibrium with mesoionic oxido-oxazolium species that acts as an azomethine ylide dipole and undergoes cycloaddition with DMAD. Final loss of CO₂ by retro-Diels–Alder reaction produces a pyrrole (Fig. 4.73).

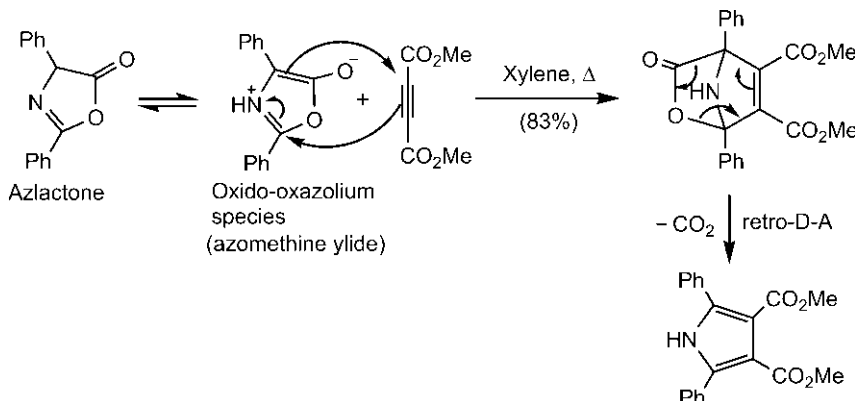


Fig. 4.73 Pyrrole synthesis via cycloaddition of a mesoionic species acting as a 1,3-dipole.

4.3.1.5 Conclusions

The foregoing discussion on the regiochemistry of 1,3-dipolar cycloadditions includes substituted alkenes or alkynes as dipolarophiles. The heterodipolarophiles such as carbonyl compounds, imines and nitriles also

undergo successful 1,3-dipolar cycloadditions with a range of 1,3-dipoles and show regioselectivity in agreement with the frontier orbital theory (e.g., see Fig. 4.90). However, the frontier orbital control to regioselectivity is not always straightforward; the energies and coefficients of the frontier orbitals need closer scrutiny to determine the dominant frontier orbital interaction under different situations. Though the frontier orbital approach, with its simplifying approximations and limitations, comes as a handy tool to explain most of the patterns of regioselectivity, its outcome does not always conform to experimental observations. Other forces like steric or polar factors might sometimes play the decisive role. As an example, let us consider a case of nitrile oxide cycloaddition. We have previously seen that $\text{PhC}\equiv\text{N}^+-\text{O}^-$ reacts with $\text{H}_2\text{C}=\text{CHCO}_2\text{Me}$, under $\text{LUMO}_{\text{dipole}}/\text{HOMO}_{\text{dipolarophile}}$ control, to produce predominantly 5-substituted isoxazoline (see Fig. 4.61). If the dipolarophile is replaced by $\text{Me}_2\text{C}=\text{CHCO}_2\text{Me}$, the 4-substituted regioisomer is obtained as the exclusive product. The frontier orbital theory cannot account for this. As Me is an electron-donating α -substituent, it would raise the energy of both HOMO and LUMO of alkene dipolarophile though LUMO energy is raised more. In effect, the frontier orbital control should remain more or less the same and 5-substituted isoxazoline is expected to be the major product but the experimental observation is just the opposite. The observed result may possibly be reasoned by steric effect. The carbon and oxygen ends of the nitrile oxide dipole as well as the two ends of the alkene dipolarophile differ drastically in their steric demand. The bond formation between sterically hindered ends of both nitrile oxide and alkene is extremely unfavourable. Therefore the interaction of the sterically congested end bearing two Me substituents of alkene dipolarophile with the unhindered oxygen end of the nitrile oxide dipole is favoured to give the 4-substituted isoxazoline.

4.4 DIYL CYCLOADDITIONS

We shall describe briefly the diyl cycloadditions using trimethylenemethane (TMM) as a diyl component.^{64,65} The TMM is generally represented as a diradical (TMM diyl) (see Section 1.6, p. 28), which can undergo pericyclic cycloaddition in its singlet state. The singlet TMM can be generated in situ by heating strained bicyclic hydrocarbons or the bridged diazenes (Fig. 4.74).

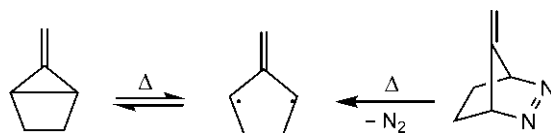


Fig. 4.74 Methods of generation of singlet trimethylenemethane (TMM).

The cycloaddition of the above singlet TMM with methyl acrylate gives a fused bicyclic product as shown in Fig. 4.75. The regioselectivity of the reaction can be explained using frontier orbital theory. The dominant frontier orbital interaction is presumably between HOMO_{TMM} and LUMO_{z-alkene}. The inspection of the frontier orbitals of TMM (see Fig. 1.27, p. 29) indicates that there is a large coefficient on the exocyclic methylene carbon in ψ_2 which is taken as HOMO.⁶⁴ The frontier orbital picture 4.7 shows that the leading bond is formed between exocyclic carbon (large HOMO coefficient) and β -carbon of methyl acrylate (large LUMO coefficient) which leads to a fused product.

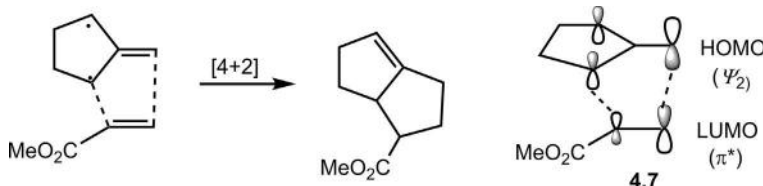


Fig. 4.75 Regioselectivity of a TMM cycloaddition with methyl acrylate.

Another example is the dimerization of the singlet TMM to give predominantly a fused-bridged product as shown in Fig. 4.76. The regioselectivity is governed by the frontier orbital interaction 4.8 between HOMO (ψ_2) and LUMO (ψ_3) of TMM.⁶⁴

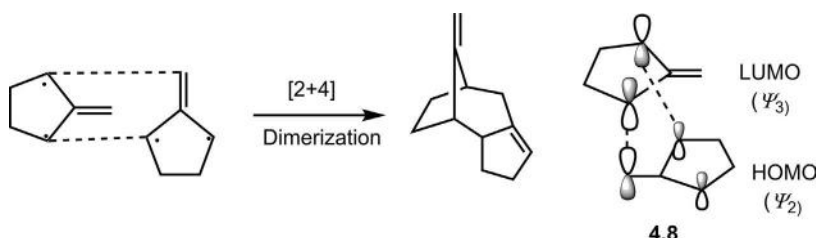


Fig. 4.76 Regioselectivity of a TMM dimerization.

4.5 PERISELECTIVITY IN CYCLOADDITIONS

The term ‘periselectivity’ refers to the preference of a pericyclic mode over the other belonging to the same pericyclic class. The possible modes ought to be geometrically reasonable and symmetry-allowed. For cycloaddition of two π systems, more than one cycloaddition mode is possible involving the whole or part of the conjugated systems. Periselectivity is thus a kind of site selectivity.

The periselectivity can be predicted and explained using frontier orbital theory in terms of the orbital coefficients involved. To illustrate, we first consider thermal dimerization of an azepine when two symmetry-allowed cycloadditions are possible: $[\pi 6_s + \pi 4_s]$ and Diels–Alder $[\pi 4_s + \pi 2_s]$ (Fig. 4.77). The two azepine molecules are labelled 1, 2.

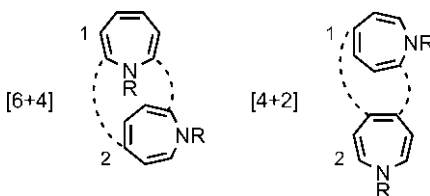


Fig. 4.77 Two possible symmetry-allowed cycloadditions in azepine dimerization.

The two frontier orbital pairs are $\text{HOMO}_{\text{azepine } 1}/\text{LUMO}_{\text{azepine } 2}$ and $\text{LUMO}_{\text{azepine } 1}/\text{HOMO}_{\text{azepine } 2}$. Clearly, the energy separations for the two pairs are identical, and hence both are equally important. Each HOMO/LUMO pair is involved in $[6 + 4]$ and $[4 + 2]$ processes, and $(E_{\text{LUMO}} - E_{\text{HOMO}})$ remains constant for the two cycloadditions. The resonance integral β representing interaction between carbon p orbitals is also constant in the two possible cycloadditions. Under these conditions, the frontier orbital expression is Eq. (4.5) (see p. 123), as obtained for the analysis of regioselectivity of Diels–Alder reaction. The periselectivity is therefore determined by the larger coefficient term $(c_a c_b + c'_a c'_b)^2$ for a cycloaddition. For azepine dimerization, since both HOMO/LUMO pairs are involved, we shall consider the expression $\sum (c_a c_b + c'_a c'_b)^2$ for each of the two possible cycloadditions.

The HOMO/LUMO coefficients of azepine ($R = \text{CO}_2\text{Et}$) are known (Fig. 4.78A).⁶⁶ Using these values, the coefficient terms for $[6 + 4]$ and $[4 + 2]$ cycloadditions are estimated as shown in Fig. 4.78B and C, respectively.

As the interacting atoms must have the same sign of coefficient for the symmetry-allowed mode, the product of coefficients is always positive.

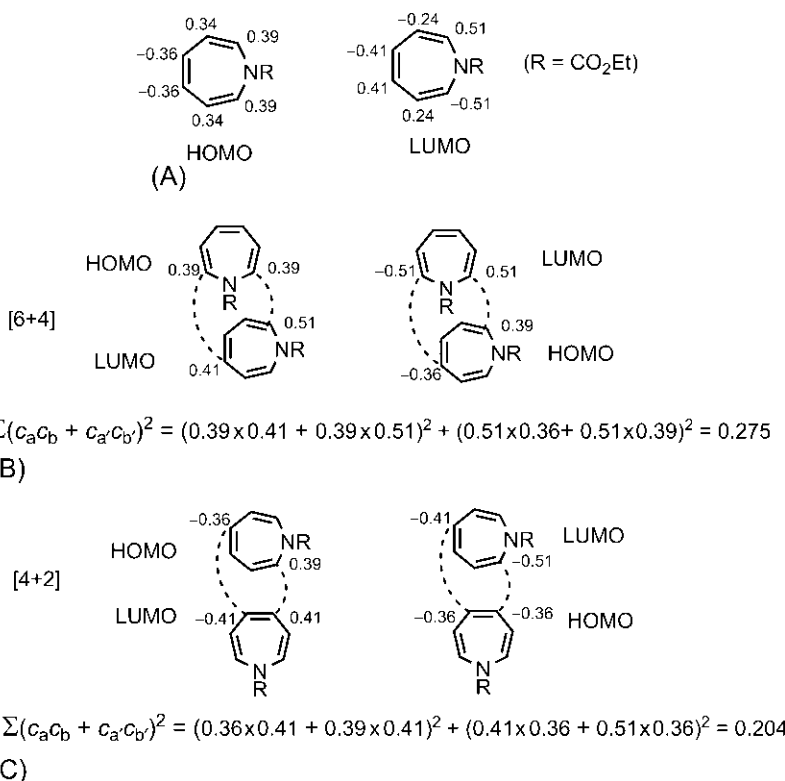


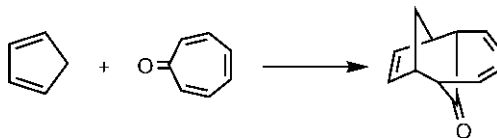
Fig. 4.78 (A) HOMO and LUMO coefficients of an azepine. Estimation of coefficient term for (B) [6+4] cycloaddition and (C) [4+2] cycloaddition.

It may be mentioned that, for the [4+2] cycloaddition, if the terminal double bond of azepine is considered as a π^2 component, the value of the coefficient term would be still less, 0.196 instead of 0.204.

As shown, the [6+4] cycloaddition has larger coefficient term (0.275) than that for the [4+2] process (0.204), and hence [6+4] cycloaddition is preferred. This result indicates that a periselective process uses longest or longest part of a conjugated system. Qualitatively, the longest conjugated system has largest coefficients on the terminal atoms which therefore provide the preferred bonding sites, if allowed by symmetry.

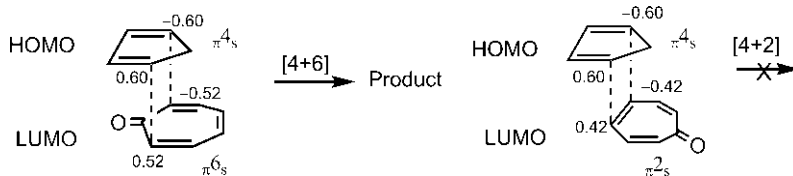
Problem 4.23

Account for the observed periselectivity in the cycloaddition between cyclopentadiene and tropone.

**Answer**

Tropone is electron deficient and has a low-energy LUMO (see Problem 4.7, p. 133), and cyclopentadiene is electron rich having a high-energy HOMO. The dominant frontier orbital interaction is therefore $\text{HOMO}_{\text{cyclopentadiene}}/\text{LUMO}_{\text{tropone}}$ interaction. The two possible cycloadditions are $[\pi 4_s + \pi 6_s]$ and $[\pi 4_s + \pi 2_s]$. As shown below, the $[4+6]$ cycloaddition involves bonding between the largest coefficients of both components. The coefficient term $(c_a q_b + c_a' q_b)^2$ is calculated to be 0.389. On the other hand, the $[4+2]$ cycloaddition involves bonding with smaller LUMO coefficients of tropone and gives a smaller value of coefficient term (0.254). It can be seen that $[4+2]$ combination of tropone ($\pi 4$) and cyclopentadiene ($\pi 2$) involves still smaller coefficients, and is not considered. The cycloaddition is periselective, and the observed product is the preferred $[4+6]$ cycloadduct.

(The HOMO coefficients of cyclopentadiene are taken as those of butadiene and the LUMO coefficients of tropone are as shown before.)

**4.5.1 Periselectivity in Fulvene Cycloadditions**

The periselectivity in fulvene cycloadditions is intriguing.^{6,67,68} First, we consider three examples of fulvene cycloadditions and their observed periselectivity as shown in Fig. 4.79.

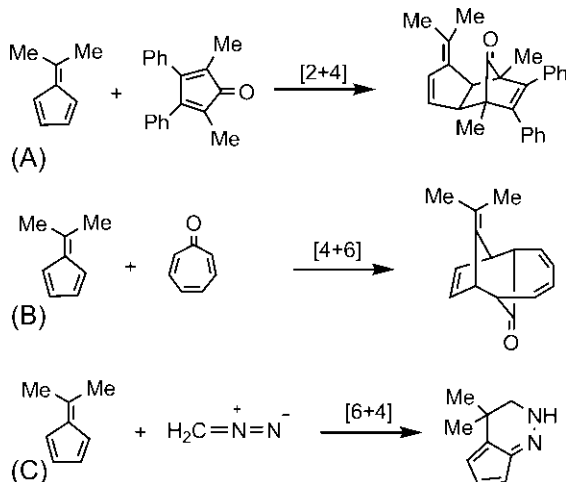


Fig. 4.79 Examples (A–C) of periselectivity in fulvene cycloadditions.

The periselectivities can be accounted for using frontier orbital theory as described below. The frontier orbital energies and coefficients of dimethylfulvene shown in Fig. 1.29 are repeated in Fig. 4.80.^{69,70}

Fulvene	Energy (eV)		Coefficient	
	HOMO	LUMO	HOMO	LUMO
	-8.6	-1.0	 	

Fig. 4.80 Frontier orbital energies and coefficients of dimethylfulvene.

The first example (Fig. 4.79A) depicts a [2 + 4] Diels–Alder reaction in which dimethylfulvene acts as a π_2 component and the cyclopentadienone acts as a π_4 component. The fulvene structure indicates that it could react as a π_2 or a π_6 system for the allowed cycloaddition pathways. However, the reaction proceeds by [2 + 4] pathway instead of the normal periselective [6 + 4] pathway. The cycloaddition thus shows abnormal periselectivity. Dimethylfulvene is electron rich and has a high-energy HOMO while cyclopentadienone (acting as a diene) is relatively electron deficient. The more important frontier orbital interaction therefore seems to involve

$\text{HOMO}_{\text{fulvene}}$ and $\text{LUMO}_{\text{cyclopentadienone}}$. If the fulvene is to react as a π_6 system, it must interact through C-2 and C-6 (see the numbering of carbons in Fig. 4.80). But the fulvene HOMO has a zero coefficient at C-6, and therefore fulvene does not act as a π_6 component in the cycloaddition. The fulvene then reacts as a π_2 component involving either C-2-C-3 or C-5-C-4 double bond and undergoes [2 + 4] Diels–Alder reaction.

In the second example (Fig. 4.79B), the reaction between electron-rich dimethylfulvene and electron-deficient tropone is under $\text{HOMO}_{\text{fulvene}}/\text{LUMO}_{\text{tropone}}$ control. Here fulvene can act as a π_4 component and tropone as a π_6 component. The frontier orbital interactions involving largest HOMO coefficients on C-2 and C-5 of fulvene and largest LUMO coefficient on the terminal carbons of tropone (see Problem 4.23) lead to the preferred [4 + 6] cycloadduct.

The third example (Fig. 4.79C) is a reaction between dimethylfulvene and diazomethane. In this case, diazomethane as a 1,3-dipole acts as a π_4 component and preferentially uses its HOMO to interact with the fulvene LUMO due to their smaller energy separation (8.0 eV) relative to the energy gap (10.4 eV) for the other HOMO/LUMO pair. Dimethylfulvene preferably acts as a π_6 component because its LUMO has two large coefficients on C-2 and C-6 (see Fig. 4.80), and [6 + 4] cycloaddition is preferred. The [6 + 4] cycloadduct tautomerizes to give the product shown in Fig. 4.79C.

Next, we consider the contrasting periselectivity of two fulvene cycloadditions shown in Fig. 4.81.

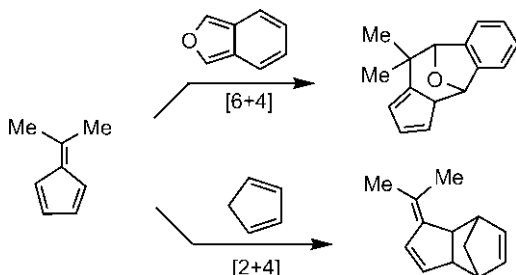


Fig. 4.81 Periselectivity in fulvene cycloadditions with isobenzofuran and cyclopentadiene.

The cycloaddition of dimethylfulvene with isobenzofuran exhibits the expected periselectivity. The electron-rich isobenzofuran uses its HOMO as a π_4 component (diene unit of furan ring) when the fulvene

uses its LUMO as a π_6 component. The more important $\text{LUMO}_{\text{fulvene}}/\text{HOMO}_{\text{diene}}$ interaction gives the normal [6 + 4] periselectivity forming the observed cycloadduct. The fulvene cycloaddition with cyclopentadiene is also expected to be dominated by $\text{LUMO}_{\text{fulvene}}/\text{HOMO}_{\text{diene}}$ interaction but the observed product is an unexpected [2 + 4] adduct. This contrasting behaviour has been explained by superjacent orbital interaction.⁶⁹ The superjacent fulvene orbital lies just above the LUMO, which is NLUMO of fulvene having zero coefficients on C-1 and C-6 (see Section 1.6, p. 30). Therefore, in $\text{NLUMO}_{\text{fulvene}}/\text{HOMO}_{\text{diene}}$ interaction, fulvene cannot act as a π_6 component, instead it would act as a π_2 component involving C-2-C-3 or C-5-C-4 double bond bearing two large coefficients (the coefficients being C-2: 0.49, C-3: -0.74, C-4: 0.74, C-5: -0.49).⁶⁹ The NLUMO coefficients thus determine the periselectivity. Though HOMO and LUMO are the most important frontier orbitals, the HOMO/NLUMO interaction can sometimes be proportionately greater which should be kept in the purview when dealing with the frontier orbital theory.

Finally, we consider fulvene cycloaddition between 6-dimethylaminofulvene and a sulphone in a synthesis of an azulene (Fig. 4.82).⁷¹

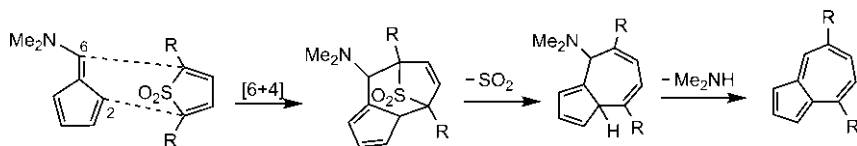


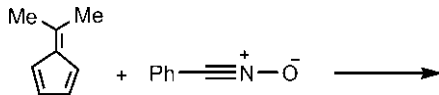
Fig. 4.82 Fulvene cycloaddition in azulene synthesis.

The fulvene bearing a strong, electron-donating α -substituent (NMe_2) has a high-energy HOMO and the sulphone as a γ -substituted diene has a low-energy LUMO. The dominant interaction is between $\text{HOMO}_{\text{fulvene}}$ and $\text{LUMO}_{\text{sulphone}}$. Here, due to the presence of a single powerful NMe_2 substituent at C-6, fulvene symmetry is lost which leads to a nonzero coefficient at C-6 in fulvene HOMO and the effect of NMe_2 also causes enhanced coefficient at C-2. Thus using HOMO, fulvene can now act as a π_6 component, interacting through C-2 and C-6 with the sulphone acting as a π_4 component. The cycloaddition gives a [6 + 4] adduct which on cheletropic extrusion of SO_2 (see Chapter 6) and loss of Me_2NH produces the aromatic azulene.

For periselectivity in ketene cycloadditions and carbene cycloadditions, see [Chapters 5 and 6](#), respectively.

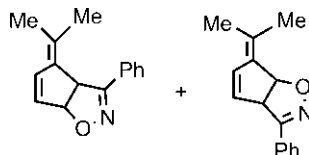
Problem 4.24

Predict the product(s) of the following fulvene cycloaddition. Explain the periselectivity involved.



Answer

Nitrile oxide dipole acts as a π^4 component and uses its low-energy LUMO. Consequently, $\text{HOMO}_{\text{fulvene}}/\text{LUMO}_{\text{nitrile oxide}}$ interaction favours [2 + 4] cycloaddition which gives a mixture of regioisomers as shown below.



4.6 CYCLOADDITIONS WITH SINGLET OXYGEN AND OZONE

We shall end this chapter with two useful cycloadditions involving all-oxygen species singlet oxygen and ozone. The molecular oxygen in the excited singlet state can participate as a reactive dienophile in the celebrated Diels–Alder reaction, and ozone can take part as a reactive dipole in a synthetically useful 1,3-dipolar cycloaddition.

Oxygen is a triplet diradical in the ground state (termed the ${}^3\Sigma$ state) in which two degenerate π^* orbitals contain one electron each with parallel spin ([Fig. 4.83](#)). Thus the ground state molecular oxygen cannot participate in concerted cycloaddition. Pairing of electrons in one of the π^* orbitals results in an excited singlet state (termed the ${}^1\Delta$ state), which can act as a π^2 component in pericyclic cycloaddition. Another excited singlet state of higher energy (termed the ${}^1\Sigma$ state) is possible with two degenerate π^* orbitals being singly occupied with opposite spins. It is the lower excited singlet oxygen (${}^1\Delta\text{O}_2$) that can serve as a suitable dienophile in concerted Diels–Alder reaction.

4.6.1 Diels–Alder Reactions With Singlet Oxygen

The singlet oxygen (${}^1\Delta O_2$) is readily obtained by the dye-sensitized irradiation of oxygen molecule (Fig. 4.83).⁷² The dye commonly used as a sensitizer is fluorescein, eosin or methylene blue. The energy difference between excited state and ground state (${}^1\Delta - {}^3\Sigma$) is estimated to be 22 kcal mol $^{-1}$.

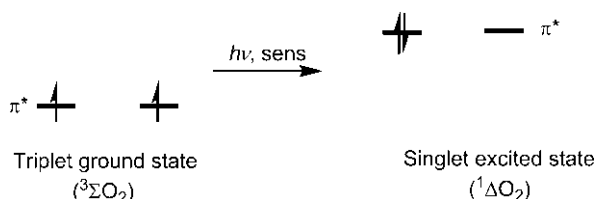


Fig. 4.83 Generation of singlet oxygen.

The process of sensitization is shown in Fig. 4.84. The sensitizer absorbs radiation and is promoted to a singlet excited state (${}^1\text{sens}$) which, after inter-system crossing (ISC), forms a triplet excited state (${}^3\text{sens}$). Collision of triplet state sensitizer with ground state oxygen results in energy transfer and formation of excited singlet oxygen (${}^1\Delta\text{O}_2$). Note that the energy transfer process obeys the spin conservation rule.

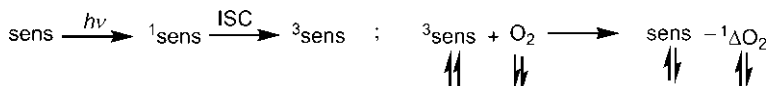


Fig. 4.84 Process of sensitized energy transfer.

The singlet oxygen (${}^1\Delta O_2$) with two electronegative oxygen atoms is a very electron-deficient heterodienophile, and uses its LUMO (the vacant π^* orbital in Fig. 4.83) in Diels–Alder reaction. The frontier orbital interaction between HOMO_{diene} and LUMO_{O=O} is depicted in Fig. 4.85A. However, the cycloaddition is highly asynchronous. The presence of a high-energy HOMO (π^*) and a low-energy LUMO (π^*) leads to extremely high reactivity of singlet oxygen and a bond can develop far ahead of the other bond so that the reaction might proceed via stepwise diradical pathway (Fig. 4.85B).⁷³ The calculations suggest that singlet oxygen cycloaddition takes a stepwise pathway with simple dienes but with aromatic substrate as a less reactive diene, it proceeds via asynchronous pericyclic pathway.

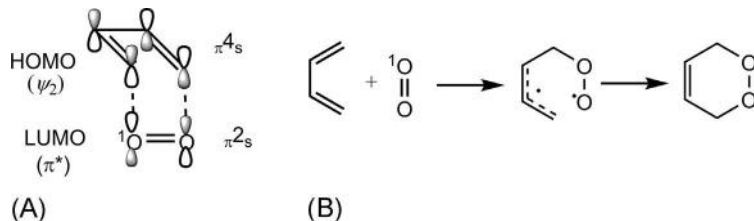


Fig. 4.85 Diels–Alder reaction with singlet oxygen: (A) frontier orbital picture for concerted pathway and (B) stepwise diradical pathway.

The Diels–Alder reaction with singlet oxygen indicates a photooxidation reaction and produces a cyclic 1,4-peroxide called endoperoxide.⁷⁴ This is illustrated with three examples in Fig. 4.86. Fig. 4.86A shows that a naturally occurring ascaridole can be synthesized from α -terpinene. The addition of singlet oxygen is also sensitive to steric effect. This is exemplified in Fig. 4.86B in which a steroidal diene forms an endoperoxide from the least hindered face of the molecule. An example of singlet oxygen addition to a polycyclic aromatic compound such as anthracene is shown in Fig. 4.86C. The reaction is regioselective forming a 9,10-endoperoxide involving the middle ring instead of a terminal ring. The cycloaddition across 9,10-positions is driven by the stability of two benzene rings being greater than a naphthalene ring. Here the hydrocarbon itself can act as a sensitizer, and no external sensitizer is needed.

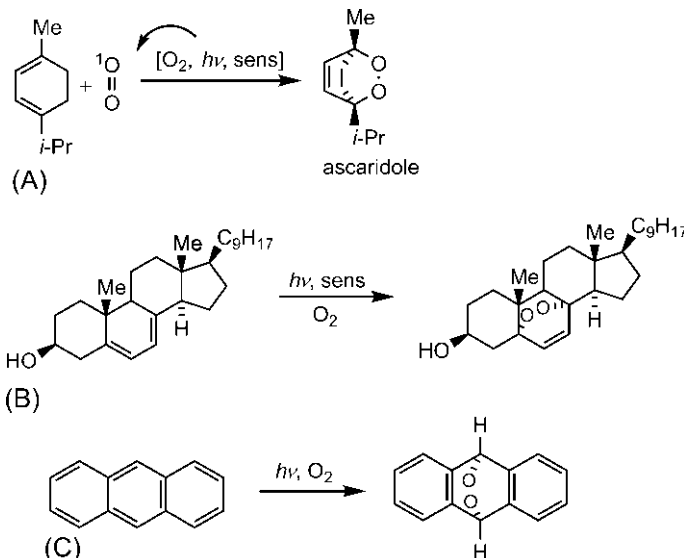


Fig. 4.86 Examples (A–C) of Diels–Alder reactions with singlet oxygen.

The endoperoxides formed in singlet oxygen cycloadditions can be easily converted to useful compounds. For example, cyclopentadiene gives an endoperoxide that can be reduced to a *cis*-1,4-diol (Fig. 4.87). As both oxygens add suprafacially to the diene, the diol produced is *cis*.

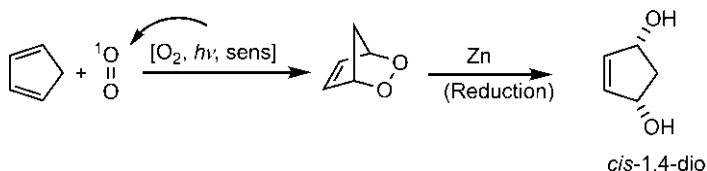


Fig. 4.87 Formation of a *cis*-1,4-diol via singlet oxygen cycloaddition.

4.6.2 1,3-Dipolar Cycloadditions With Ozone and Related Dipole

Ozone (O_3) is a symmetrical bent 1,3-dipole (see Fig. 4.48). As the highly electronegative oxygen has a low-energy p orbital, ozone has a very low-energy HOMO (-13.5 eV) as well as a low-energy LUMO (-2.2 eV).⁶⁸ The frontier orbital energy separations for 1,3-dipolar cycloaddition of ozone with ethylene (unsubstituted dipolarophile) are

$$E_{\text{LUMO}(\text{ozone})} - E_{\text{HOMO}(\text{ethylene})} = 8.3 \text{ eV}$$

$$E_{\text{LUMO}(\text{ethylene})} - E_{\text{HOMO}(\text{ozone})} = 15.0 \text{ eV}$$

The LUMO_{dipole}/HOMO_{dipolarophile} interaction is therefore strongly favoured. With c- or x-substituted alkene having higher energy HOMO, the energy gap will be further reduced from 8.3 eV. The z-substituted alkene has a slightly lower energy HOMO and gives a separation of 8.7 eV. These results indicate that 1,3-dipolar cycloadditions of ozone with alkenes are quite facile, and involve LUMO of ozone.

The reaction of ozone with an alkene gives an ozonide (Fig. 4.88). However, the ozonide is not usually isolated but is decomposed in situ and the whole process is known as ozonolysis.

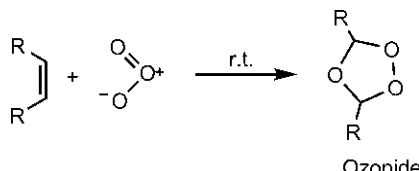


Fig. 4.88 Formation of ozonide.

The structure of ozonide indicates that it cannot result from a simple one-step cycloaddition of ozone. Mechanistic studies reveal that the ozonide is formed by a sequence of three pericyclic steps involving 1,3-dipolar cycloaddition, retro-1,3-dipolar cycloaddition and again 1,3-dipolar cycloaddition as shown in Fig. 4.89.

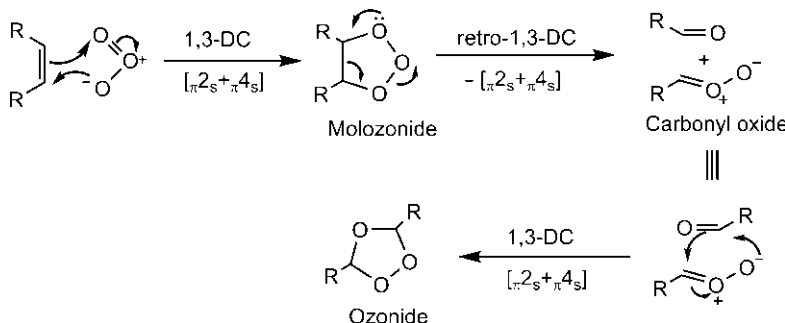


Fig. 4.89 Mechanism of ozonide formation.

The initial adduct, molozonide (1,2,3-trioxolane) is very unstable (note the presence of two weak O—O bonds) and collapses by retro-1,3-dipolar cycloaddition to a carbonyl compound (new dipolarophile) and a carbonyl oxide (new dipole). The final step is the 1,3-dipolar cycloaddition between carbonyl oxide dipole and carbonyl dipolarophile. This cycloaddition is highly regioselective and forms the favoured regioisomer, ozonide (1,2,4-trioxolane) as the product. Reforming molozonide (other regioisomer) is much less favourable. Both HOMO_{dipole}/LUMO_{dipolarophile} and LUMO_{dipole}/HOMO_{dipolarophile} interactions lead to the same regioisomer (ozonide) from large–large + small–small interactions as shown in Fig. 4.90. Note that carbonyl dipolarophile has larger coefficient on carbon in LUMO, and on oxygen in HOMO. A similar pattern is obtained for carbonyl oxide dipole.^{42,43}

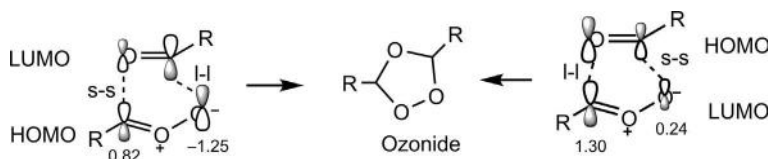


Fig. 4.90 Frontier orbital interactions for regioselectivity in 1,3-dipolar cycloaddition of carbonyl oxide dipole with carbonyl dipolarophile.

In ozonolysis, the ozonides can be decomposed in many ways. The reduction with dimethyl sulphide (Me_2S) or trimethyl phosphite [$(\text{MeO})_3\text{P}$] gives the aldehydes as valuable products (Fig. 4.91).

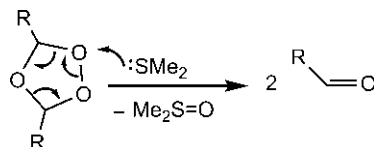
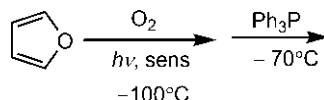


Fig. 4.91 Ozonide decomposition by dimethyl sulphide.

If necessary, the ozonides can be decomposed using NaBH_4 to form alcohols or H_2O_2 to give carboxylic acids. The process of ozonolysis involving oxidative cleavage of alkenes serves as a useful synthetic methodology.

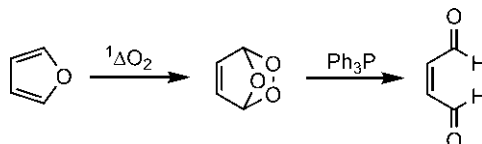
Problem 4.25

Predict the product in the following scheme.



Answer

Singlet oxygen cycloaddition gives an ozonide which is decomposed by Ph_3P to butenedial.



4.6.2.1 1,3-Dipolar Cycloaddition With Osmium Tetroxide

Osmium tetroxide (OsO_4) can act as a 1,3-dipole similar to ozone (Fig. 4.92) and can participate in 1,3-dipolar cycloaddition.

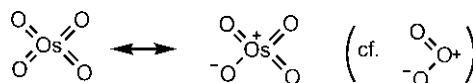


Fig. 4.92 Osmium tetroxide as a 1,3-dipole.

OsO_4 adds to an alkene to form a cyclic osmate ester⁷⁵ which, unlike molozonide, can be isolated. An example of 1,3-dipolar cycloaddition of OsO_4 to (*E*)-2-butene is shown in Fig. 4.93. The stereochemistry of the osmate ester is *trans* because the alkene stereochemistry is retained as a result of supra/supra mode of cycloaddition. But the osmate ester is not the desired product and is hydrolyzed to give a 1,2-diol. The diol produced from (*E*)-butene is a *syn* diastereomer.

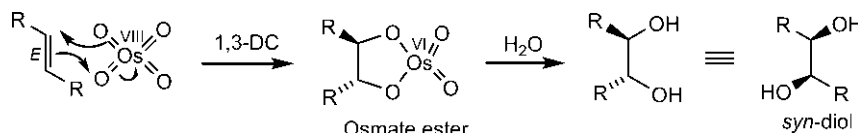


Fig. 4.93 Formation of a diastereomeric 1,2-diol via 1,3-dipolar cycloaddition of OsO_4 to an alkene.

OsO_4 is toxic and expensive. The cycloaddition is an oxidation and Os(VIII) is reduced to Os(VI) . In a suitable modification, OsO_4 is employed in catalytic amount along with a reagent that reoxidizes Os(VI) to Os(VIII) . This reagent is commonly N-methylmorpholine-N-oxide (NMO).

REFERENCES

1. Klopman, G. *J. Am. Chem. Soc.* **1968**, *90*, 223.
2. Salem, L. *J. Am. Chem. Soc.* **1968**, *90*, 543.
3. Deem, M. L. *Synthesis* **1972**, 675.
4. Wittig, G. *Angew. Chem. Int. Ed. Engl.* **1962**, *1*, 415.
5. Houk, K. N. *J. Am. Chem. Soc.* **1973**, *95*, 4092.
6. Houk, K. N. *Acc. Chem. Res.* **1975**, *8*, 361.
7. Joshel, L. M.; Butz, L. W. *J. Am. Chem. Soc.* **1941**, *63*, 3350.
8. Singleton, D. A.; Martinez, J. P. *J. Am. Chem. Soc.* **1990**, *112*, 7423.
9. Chen, J. S.; Houk, K. N.; Foote, C. S. *J. Am. Chem. Soc.* **1998**, *120*, 12303.
10. Spino, C.; Crawford, J. *Can. J. Chem.* **1993**, *71*, 1094.
11. Fujimoto, H.; Inagaki, S.; Fukui, K. *J. Am. Chem. Soc.* **1976**, *98*, 2670.
12. Sustmann, R.; Daute, P.; Sauer, R.; Sicking, W. *Tetrahedron Lett.* **1988**, *29*, 4699.
13. Konovalov, A. I.; Solomonov, B. N. *Dokl. Akad. Nauk SSSR, Ser. Kim.* **1973**, *211*, 1115 (*Chem. Abs.* **1973**, *79*, 125446n).
14. Danishefsky, S.; Kitahara, T.; Schuda, P. F.; Etheredge, S. *J. Am. Chem. Soc.* **1976**, *98*, 3028.
15. Bodwell, G. J.; Hawco, K. M.; da Silva, R. P. *Synlett* **2003**, 179.
16. Alder, K.; Schumacher, M.; Wolff, O. *Justus Liebigs Ann. Chem.* **1949**, *564*, 79.
17. Fleming, I.; Gianni, F. L.; Mah, T. *Tetrahedron Lett.* **1976**, 881.
18. Uyehara, T.; Kitahara, Y. *Chem. Ind.* **1971**, 354.
19. Danishefsky, S. J.; DeNinno, M. P. *Angew. Chem. Int. Ed. Engl.* **1987**, *26*, 15.
20. Belanger, A.; Brassard, P. *J. Chem. Soc. Chem. Commun.* **1972**, 863.
21. Toma, L.; Romano, S.; Quadrelli, P.; Caramella, P. *Tetrahedron Lett.* **2001**, *42*, 5077.

22. Houk, K. N.; Strozier, R. W. *J. Am. Chem. Soc.* **1973**, *95*, 4094.
23. Corey, E. J.; Danheiser, R. L.; Chandrasekaran, S.; Siret, P.; Keck, G. E.; Gras, J. L. *J. Am. Chem. Soc.* **1978**, *100*, 8031.
24. Dickinson, R. A.; Kubela, R.; MacAlpine, G. A.; Stojanac, Z.; Valenta, Z. *Can. J. Chem.* **1972**, *50*, 2377.
25. Rideout, D. C.; Breslow, R. *J. Am. Chem. Soc.* **1980**, *102*, 7816.
26. Foster, R. A. A.; Willis, M. C. *Chem. Soc. Rev.* **2013**, *42*, 63.
27. Rickborn, B. *Org. React.* **1998**, *53*, 223.
28. Song, Z. Z.; Ho, M. S.; Wong, H. N. C. *J. Org. Chem.* **1994**, *59*, 3917.
29. Ye, X.-S.; Wong, H. N. C. *J. Org. Chem.* **1997**, *62*, 1940.
30. Carly, P. R.; Cappelle, S. L.; Compernolle, F.; Hoornaert, G. J. *Tetrahedron* **1996**, *52*, 11889.
31. Boger, D. L. *Chem. Rev.* **1986**, *86*, 781.
32. Sainz, Y. F.; Raw, S. A.; Taylor, R. J. K. *J. Org. Chem.* **2005**, *70*, 10086.
33. Naito, T.; Yoshikawa, T.; Ishikawa, F.; Isoda, S.; Omura, Y.; Takamura, I. *Chem. Pharm. Bull.* **1965**, *13*, 869.
34. Sainte, F.; Serckx-poncin, B.; Hesbain-Frisque, A.-M.; Ghosez, L. *J. Am. Chem. Soc.* **1982**, *104*, 1428.
35. Afarinkia, K.; Vinader, V.; Nelson, T. D.; Posner, G. H. *Tetrahedron* **1992**, *48*, 9111.
36. Alder, K.; Flock, F. H.; Beumling, H. *Chem. Ber.* **1960**, *93*, 1896.
37. Vogel, E.; Grimme, W.; Korte, S. *Tetrahedron Lett.* **1965**, 3625.
38. Wessig, P.; Müller, G. *Chem. Rev.* **2008**, *108*, 2051.
39. Ajaz, A.; Bradley, A. Z.; Burrell, R. C.; et al. *J. Org. Chem.* **2011**, *76*, 9320.
40. Rodríguez, R.; Navarro-Vázquez, A.; Castedo, L.; Domínguez, D.; Saá, C. *J. Am. Chem. Soc.* **2001**, *123*, 9178.
41. Huisgen, R. *Angew. Chem. Int. Ed. Engl.* **1963**, *2*, 565.
42. Houk, K. N.; Sims, J.; Duke, R. E., Jr.; Strozier, R. W.; George, J. K. *J. Am. Chem. Soc.* **1973**, *95*, 7287.
43. Houk, K. N.; Sims, J.; Watts, C. R.; Luskus, L. *J. Am. Chem. Soc.* **1973**, *95*, 7301.
44. Martellii, J.; Tonnard, P.; Carrié, R.; Sustmann, R. *Nouveau. J. Chem.* **1978**, *2*, 609.
45. Firestone, R. A. *J. Org. Chem.* **1976**, *41*, 2212.
46. Oh, L. M. *Tetrahedron Lett.* **2006**, *47*, 7943.
47. Padwa, A., Ed. *1,3-Dipolar Cycloaddition Chemistry*, Vols. 1 and 2; Wiley: New York, 1984.
48. Gotthardt, H.; Huisgen, R. *Chem. Ber.* **1968**, *101*, 552.
49. Bast, K.; Christl, M.; Huisgen, R.; Mack, W.; Sustmann, R. *Chem. Ber.* **1973**, *106*, 3258.
50. Iddon, B.; Suschitzky, H.; Thompson, A. W.; Wakefield, B. J.; Wright, D. J. *J. Chem. Res.* **1978**, (S), 174; (M), 2038.
51. McMurray, J. E. *Org. Synth. Coll.* **1988**, *VI*, 592.
52. Padwa, A.; Fisera, L.; Koehler, K. F.; Rodriguez, A.; Wong, G. S. K. *J. Org. Chem.* **1984**, *49*, 276.
53. Sims, J.; Houk, K. N. *J. Am. Chem. Soc.* **1973**, *95*, 5798.
54. Oppolzer, W.; Petrzilka, M. *Helv. Chim. Acta* **1978**, *61*, 2755.
55. Huisgen, R.; Möbius, L.; Szeimies, G. *Chem. Ber.* **1965**, *98*, 1138.
56. Huisgen, R.; Szeimies, G.; Möbius, L. *Chem. Ber.* **1966**, *99*, 475.
57. Normura, Y.; Takeuchi, Y.; Tomoda, S.; Ito, M. M. *Bull. Chem. Soc. Jpn.* **1981**, *54*, 261.
58. Kirmse, W.; Horner, L. *Justus Liebigs Ann. Chem.* **1958**, *614*(1).
59. Himo, F.; Lovell, T.; Hilgraf, R.; Rostovtsev, V. V.; Noddleman, L.; Sharpless, K. B. *J. Am. Chem. Soc.* **2005**, *127*, 210.
60. Boren, B. C.; Narayan, S.; Rasmussen, L. K.; et al. *J. Am. Chem. Soc.* **2008**, *130*, 8923.
61. Ohno, M.; Komatsu, M.; Miyata, H.; Ohshiro, Y. *Tetrahedron Lett.* **1991**, *32*, 5813.

62. Berée, F.; Marchand, E.; Morel, G. *Tetrahedron Lett.* **1992**, *33*, 6155.
63. Padwa, A.; Burgess, E. M.; Gingrich, H. L.; Roush, D. M. *J. Org. Chem.* **1982**, *47*, 786.
64. Siemionko, R. K.; Berson, J. A. *J. Am. Chem. Soc.* **1980**, *102*, 3870.
65. Rule, M.; Mondo, J. A.; Berson, J. A. *J. Am. Chem. Soc.* **1982**, *104*, 2209.
66. Mok, K. L.; Nye, M. *J. J. Chem. Soc. Perkin I* **1975**, 1810.
67. Houk, K. N.; Luskus, L. J. *J. Org. Chem.* **1973**, *38*, 3836.
68. Houk, K. N.; Luskus, L. J. *Tetrahedron Lett.* **1970**, *4029*.
69. Paddon-Row, M. N.; Gell, K.; Warrener, R. N. *Tetrahedron Lett.* **1975**, 1975.
70. Houk, K. N.; George, J. K.; Duke, R. E., Jr. *Tetrahedron* **1974**, *30*, 523.
71. Mukherjee, D.; Dunn, L. C.; Houk, K. N. *J. Am. Chem. Soc.* **1979**, *101*, 251.
72. Gollnick, K. *Adv. Photochem.* **1968**, *6*, 1.
73. Bobrowski, M.; Liwo, A.; Oldziej, S.; Jeziorek, D.; Ossowski, T. *J. Am. Chem. Soc.* **2000**, *122*, 8112.
74. Frimer, A. A. *Chem. Rev.* **1979**, *79*, 359.
75. Jorgensen, K. A.; Hoffmann, R. *J. Am. Chem. Soc.* **1986**, *108*, 1867.

CHAPTER 5

Cycloadditions 2: Stereochemistry of [4+2] and [2+2] Cycloadditions

5.1 STEREOCHEMISTRY OF [4+2] DIELS–ALDER REACTIONS

The Diels–Alder (DA) reaction between a diene and an alkene dienophile can create a *maximum* of four new stereocentres in the cyclohexene adduct. The new double bond produced must be *cis* (*Z*) in a six-membered ring. The double bonds in the diene and dienophile can be *E* or *Z*. These are shown schematically in Fig. 5.1.

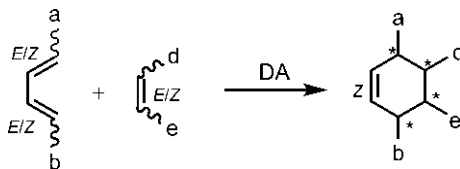


Fig. 5.1 Schematic representation of Diels–Alder reaction showing possible stereochemistry of reactant double bonds and potential stereocentres (*) in the product.

We shall describe the stereochemical features of the Diels–Alder reactions taking different cases in terms of the number of stereocentres formed. In the simplest case when just one stereocentre is formed, no diastereomer is possible and the chiral product from achiral diene and dienophile is obtained as a racemate. In general, if a chiral product is formed from achiral reactants or from chiral but racemic reactants (and catalysts etc.), then it is always obtained as a racemate. If a single enantiomer of the product is required, the preferred method is asymmetric (enantioselective) synthesis when this is possible (see Section 5.1.4).

5.1.1 Stereospecificity: The ‘*cis* Principle’

To illustrate stereospecificity, let us consider the Diels–Alder reactions that form two new stereocentres, contributed either by a diene or by a dienophile.

5.1.1.1 Diene Providing Two Stereocentres

The dienes having stereochemistry at both double bonds lead to two stereocentres in the product. In this case, the dienophile has no stereochemistry. The dienophile is then an alkyne or an alkene with no double bond stereochemistry. For example, consider the reaction between (*E,E*)-1,4-diphenylbutadiene and diethyl acetylenedicarboxylate (Fig. 5.2). The Diels–Alder reaction is a $[\pi^4_s + \pi^2_s]$ reaction, being suprafacial on both diene and dienophile. Clearly, as shown in Fig. 5.2, the suprafacial addition to the diene gives *cis* stereochemistry of two Ph groups in the cycloadduct. Here the *cis* product is achiral. Note that the two out-substituents (Ph/Ph) of the diene as a result of suprafacial attack become *cis*. This feature can be generalized to a mnemonic, *Mnemonic 1* (see below).

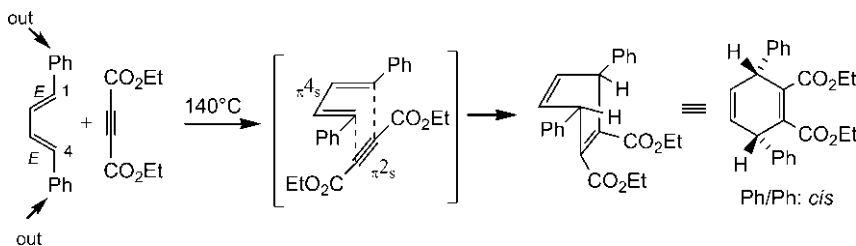


Fig. 5.2 Stereospecificity of Diels–Alder reaction with a (*E,E*) diene.

The supra/supra mechanism does not allow the formation of *trans* adduct. The mechanism thus leads to a specific diastereomeric product from a particular stereochemistry of the reactant diene. The reaction is therefore stereospecific (see Section 2.4). The general stereochemical outcome is that the relative stereochemistry of substituents at C-1 and C-4 of the diene is retained in the product. This is known as the ‘*cis* principle’. Understanding the stereochemical consequence of suprafacial addition to the diene, the product stereochemistry could be delineated easily using a mnemonic (*Mnemonic 1*) shown in Fig. 5.3 without the need for spatial imagination in each and every case.

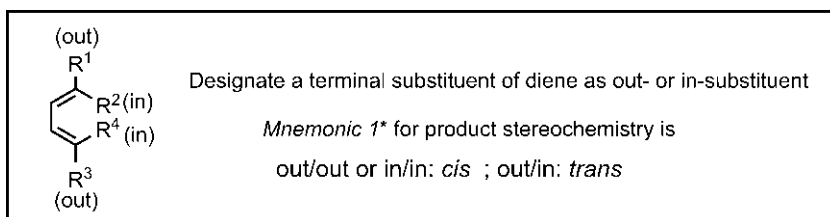


Fig. 5.3 *Mnemonic 1* for delineating stereospecificity with respect to a diene. (*Also applicable to 1,3-dipolar cycloaddition using a dipole instead of a diene.)

Fig. 5.4 shows the use of *Mnemonic 1* for delineating product stereochemistry. The reaction of a (*E,Z*) diene with dimethyl acetylenedicarboxylate (DMA) gives a *trans* adduct (**Fig. 5.4A**). Note that the *trans* diastereomer is chiral and is obtained as a raceme because the reactants are achiral. With cyclopentadiene, a *cis* adduct is formed (**Fig. 5.4B**).

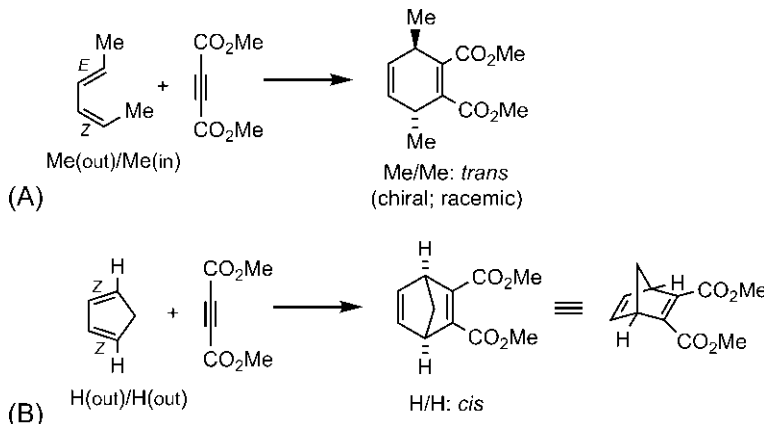


Fig. 5.4 Examples of stereospecific reactions with (A) acyclic and (B) cyclic dienes.

5.1.1.2 Dienophile Providing Two Stereocentres

In this case, the dienophile has stereochemistry but the diene has no stereochemistry. As a result of suprafacial addition to a dienophile, the relative stereochemistry of substituents in the dienophile is also retained in the product. This is another case of ‘*cis* principle’. Thus an alkene dienophile with *cis* substituents will form an adduct in which these substituents are also *cis*. Similarly, a *trans* alkene will give a *trans* adduct. The stereospecificity arising from dienophile geometry is illustrated with two examples in **Fig. 5.5**.

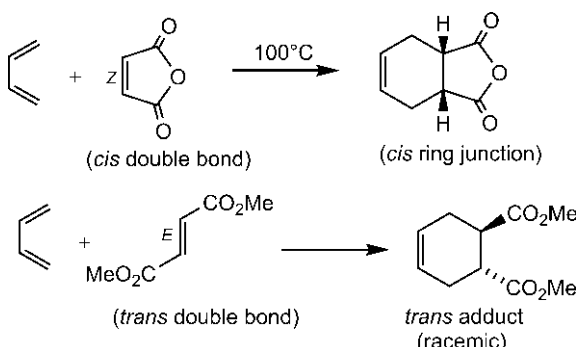
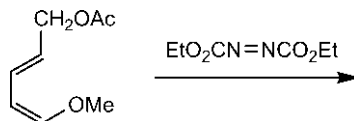


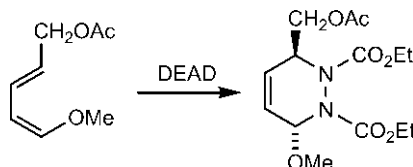
Fig. 5.5 Examples of stereospecific reactions with *cis* and *trans* dienophiles.

Problem 5.1

Predict the product of the following Diels–Alder reaction.

**Answer**

The dienophile diethyl azodicarboxylate (DEAD) exists predominantly as *E* isomer in the *E/Z* equilibrium mixture. However, the stereochemistry of DEAD will not be reflected in the product, as the two amide nitrogens in the product are sp^2 and planar. The (*E,Z*) stereochemistry of the diene with CH_2OAc (out)/ OMe (in) leads to a *trans* adduct.



5.1.2 Stereoselectivity: The *endo* Rule

5.1.2.1 Diene and Dienophile Each Providing a Stereocentre

In this case, both diene and dienophile are prochiral and the $[\pi 4_s + \pi 2_s]$ mechanism can now lead to two diastereomeric products known as *endo* and *exo* adducts, as shown in Fig. 5.6 in a general case. The ‘ortho’ regioselectivity is

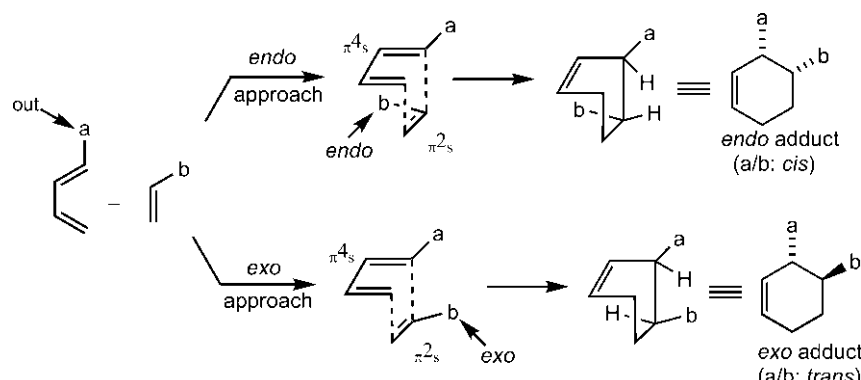


Fig. 5.6 *endo* and *exo* cycloaddition in Diels–Alder reaction.

assumed for the reaction. The dienophile can approach the diene in *endo* fashion (when the substituent b sits under the diene) or *exo* fashion (when the substituent b sits away from the diene).

Both *endo* and *exo* adducts are formed by supra/supra mechanism. Note that out-substituent (a) of the diene and *endo*-substituent (b) of the dienophile are *cis* in the *endo* adduct; if the dienophile substituent (b) is *exo*, then it is *trans* to the diene out-substituent (a) in the *exo* product. These relationships can lead to another mnemonic (*Mnemonic 2*) shown in Fig. 5.7 to delineate *endo* and *exo* stereochemistry easily.

Diene substituent: out / in ; dienophile substituent: b
*Mnemonic 2** for product stereochemistry is
endo-b \Rightarrow b/out: *cis* or b/in: *trans*
exo-b \Rightarrow b/out: *trans* or b/in: *cis*

Fig. 5.7 *Mnemonic 2* for delineating *endo/exo* stereochemistry of Diels–Alder reaction.
(*Also applicable to 1,3-dipolar cycloaddition and ene reaction using a dipole/dipolarophile and an ene/enophile, respectively, instead of the diene/dienophile.)

Now, the question is whether there is stereoselectivity as to which diastereomer is the major product. Although the *endo* diastereomer is more hindered and thermodynamically less stable than *exo* diastereomer, *endo* is often the major product under normal kinetic control of the Diels–Alder reaction. This is known as the Alder *endo* rule. An example of *endo* stereoselectivity is shown in Fig. 5.8. Note also ‘ortho’ regioselectivity of the reaction. Here the *endo* cycloadduct is chiral and racemic.

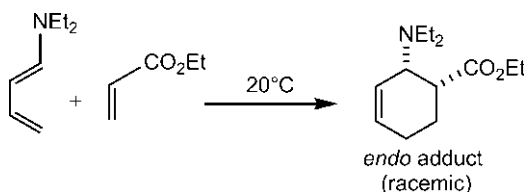


Fig. 5.8 Example of *endo* stereoselectivity of Diels–Alder reaction.

The preference for the *endo* adduct has been rationalized by Woodward and Hoffmann in terms of secondary orbital interactions.¹ This is illustrated below using the above example. In the *endo* approach, the carbonyl π system

(α -substituent) of the dienophile can be oriented over the residual π orbitals of the diene in the transition structure 5.1 (Fig. 5.9). (Note that the conjugated dienophile is in *s-trans* conformation.)

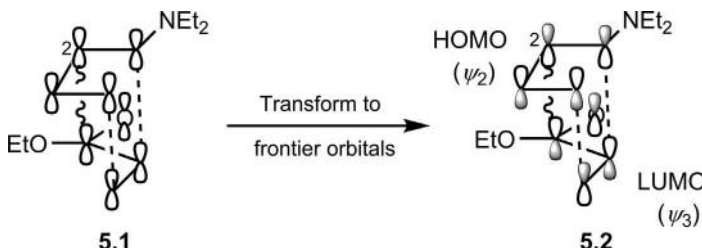
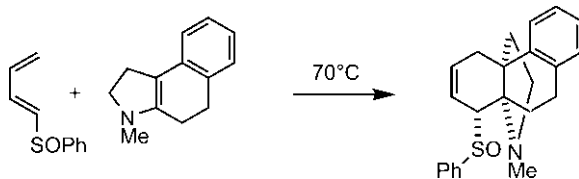


Fig. 5.9 Secondary orbital interaction (indicated by wavy line) for *endo* addition in Diels–Alder reaction.

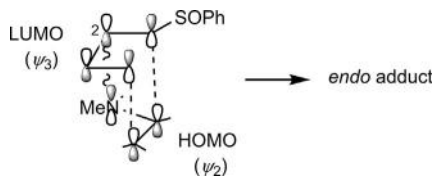
Clearly, apart from the primary bonding interactions (dashed lines), overlap is also possible between the p orbital on C-2 of the diene and the p orbital of the carbonyl carbon (wavy line). This interaction is called secondary orbital interaction. It should be understood that this secondary interaction does not lead to a full bond but may stabilize or destabilize the *endo* TS relative to *exo* TS where it must be absent. Now, to determine whether the secondary orbital interaction stabilizes or destabilizes the *endo* TS, the frontier molecular orbital (FMO) theory is invoked. The orbital picture representation (without lobe signs) 5.1 is transformed into a FMO picture 5.2. The dominant frontier orbital interaction in the normal electron demand Diels–Alder reaction is between $\text{HOMO}_{\text{diene}} (\psi_2)$ and $\text{LUMO}_{\text{dienophile}} (\psi_3)$. Note that $\text{LUMO} (\psi_3)$ of the conjugated dienophile π system ($\text{C}=\text{C}-\text{C}=\text{O}$) is considered to examine the secondary interaction; the LUMO (π^*) of $\text{C}=\text{C}$ π system of dienophile permits only to look at primary bonding interactions. Since the secondary interaction (wavy line) involves lobes with same sign, it is bonding and stabilizes the TS for *endo* addition. (For simplicity, the frontier orbitals are drawn without taking into consideration the size of the coefficients, as the bonding or antibonding interaction is determined by the sign of the coefficients.) The *endo* adduct is formed faster than *exo* adduct and hence becomes the major product under kinetic control of the reaction. The extent of diastereoselectivity is related to the difference in free energy between the *endo* and *exo* TSs, and is expressed as diastereomer ratio (dr) or diastereomeric excess (de) (see Section 2.4.1, p. 60).

Problem 5.2

Explain the diastereoselectivity of the following inverse electron demand Diels–Alder (IEDDA) reaction.

**Answer²**

The frontier orbital control is $\text{LUMO}_{\text{diene}}/\text{HOMO}_{\text{dienophile}}$ interaction. Secondary orbital interaction between p orbital on C-2 of diene and nitrogen p orbital of enamine is bonding in the *endo* addition as shown below. The HOMO of enamine (x-substituted alkene) resembles allyl anion HOMO but with orbital at the middle carbon. The *endo* adduct is the observed product.



The reaction between (*E*)-butadiene-1-carboxylic acid and acrylic acid at 75°C gives *endo* adduct exclusively (Fig. 5.10).

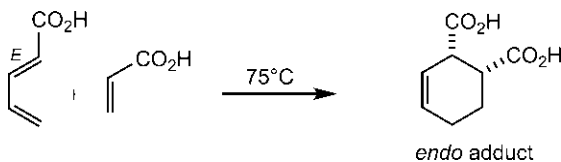


Fig. 5.10 Diastereoselectivity of the Diels–Alder reaction between (*E*)-butadiene-1-carboxylic acid and acrylic acid.

In this reaction, both diene and dienophile are z-substituted. The explanation for high regioselectivity of the reaction in favour of ‘ortho’ isomer as described previously (see Fig. 4.23, p. 131) might appear to be not quite convincing as HOMO of a z-substituted alkene or diene is slightly polarized. Here the secondary orbital interaction, besides explaining *endo*

selectivity, can provide further rationalization of the observed regioselectivity (Fig. 5.11).³ The HOMO of the *z*-substituted diene has a relatively large difference in coefficients at C-2 and C-3. Calculations suggest that the magnitude of HOMO coefficient at C-2 and C-3 is 0.384 and 0.314, respectively.³ (Recall that a 1-*z*-substituted diene is modelled as a hybrid of hexatriene and pentadienyl cation. However, as CO₂H is not very electron withdrawing, the coefficient pattern of the diene resembles more closely the pattern for a *c*-substituted diene (hexatriene model) which has a larger HOMO coefficient at C-2 and a smaller coefficient at C-3; see Problem 1.4). The secondary orbital interactions involving a larger lobe on C-2 favours formation of ‘ortho’/endo adduct rather than ‘meta’/endo adduct through a smaller lobe on C-3 (Fig. 5.11).

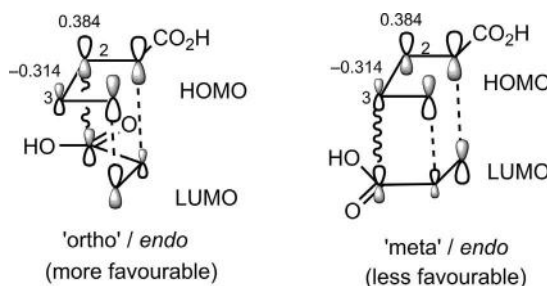


Fig. 5.11 Analysis of regioselectivity and stereoselectivity of the reaction in Fig. 5.10 using secondary orbital interaction.

5.1.2.2 Diene and Dienophile Providing Three or Four Stereocentres

The Diels–Alder reaction between (*E,E*)-1,4-diphenylbutadiene and acrylic acid generates three stereocentres, two from diene and one from dienophile, and gives *endo* adduct as a major product at room temperature (Fig. 5.12).

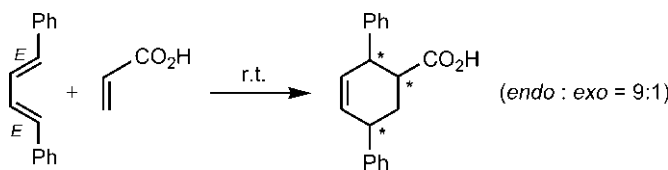


Fig. 5.12 Generation of three stereocentres in the Diels–Alder reaction.

The reaction is both stereoselective and stereospecific. The stereochemistry of *endo* adduct could be delineated easily using *Mnemonic 2* and *Mnemonic 1* successively as shown explicitly in Fig. 5.13.

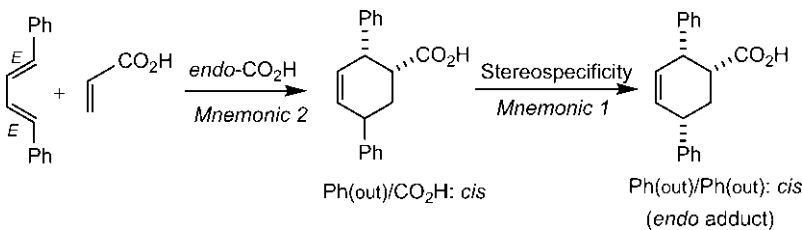


Fig. 5.13 Delineation of stereochemistry of *endo* adduct of the reaction in Fig. 5.12.

The stereochemistry of *exo* adduct is delineated similarly (Fig. 5.14).

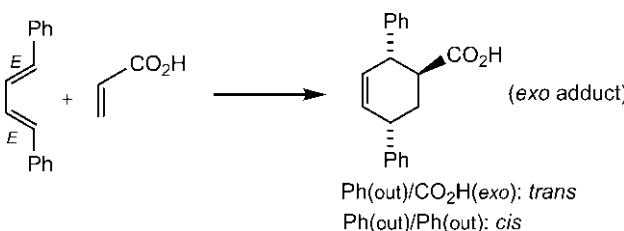


Fig. 5.14 Stereochemistry of *exo* adduct of the reaction in Fig. 5.12.

In the Diels–Alder reaction shown in Fig. 5.15, four stereocentres are formed, two each from diene and dienophile.

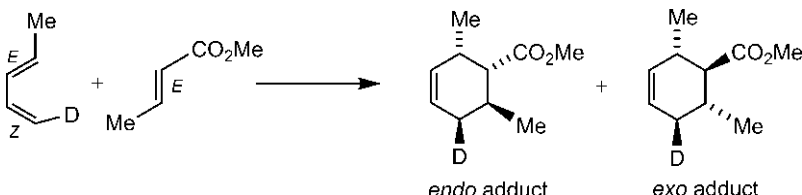


Fig. 5.15 Generation of four stereocentres in the Diels–Alder reaction.

The reaction exhibits all three features, namely, regioselectivity, stereoselectivity and stereospecificity. The *endo* adduct is drawn as shown in detail in Fig. 5.16. (The factorization into steps is only an aid to understanding; the product stereochemistry can be drawn straightway.)

In general, the product stereochemistry is easily delineated using the following sequence:

1. Regioselectivity: Use ‘ortho/para’ rule.
2. Stereoselectivity (*endo/exo*): Use *Mnemonic 2*.
3. Stereospecificity: Use *Mnemonic 1* for diene and *cis/trans* for dienophile.

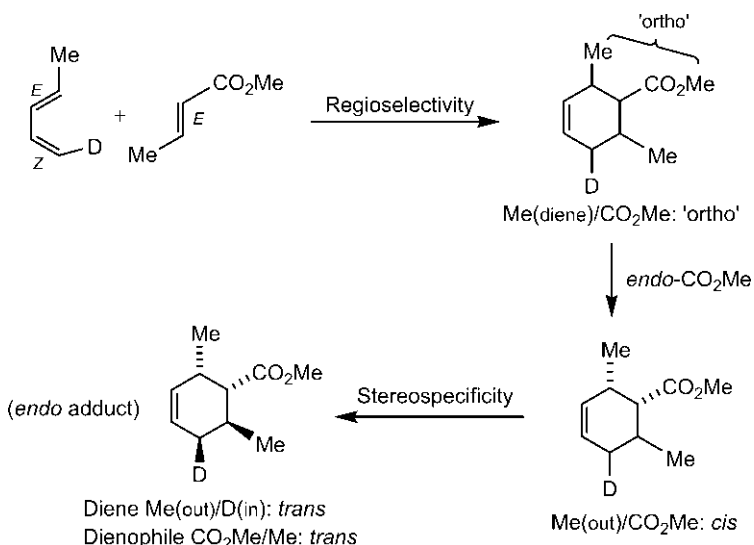


Fig. 5.16 Delineation of stereochemistry of *endo* adduct of the reaction in Fig. 5.15.

We shall now consider the Diels–Alder reaction with a cyclic diene. The addition of maleic anhydride to cyclopentadiene creates four stereocentres, and gives almost exclusively the *endo* adduct at room temperature (Fig. 5.17). The reaction is also stereospecific with respect to both diene and dienophile.

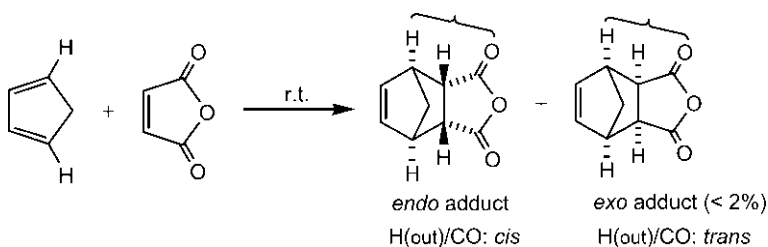


Fig. 5.17 Diels–Alder reaction between cyclopentadiene and maleic anhydride.

The secondary orbital interactions involve both carbonyls of maleic anhydride dienophile for *endo* addition (Fig. 5.18). The interactions are bonding and thereby favour the formation of *endo* adduct. Note that dienophile LUMO (ψ_4) refers to the extended π system (cf. hexatriene).

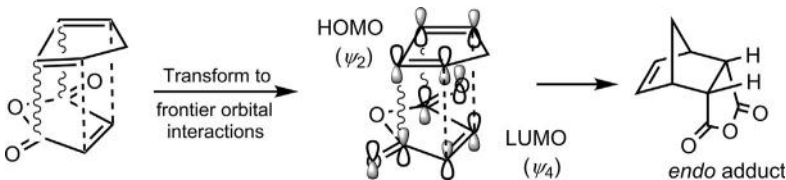


Fig. 5.18 Secondary orbital interactions (indicated by wavy lines) for *endo* addition of maleic anhydride to cyclopentadiene.

The Diels–Alder reaction involves a boat transition structure. In the case of cyclic diene, the product is also locked in boat conformation (Fig. 5.18), and cannot assume the preferred half-chair conformation of cyclohexene.

The dimerization of cyclopentadiene also favours the formation of *endo* adduct. The frontier orbital interactions in terms of coefficients and theoretical calculations provide more insight into the *endo* dimerization.^{4,5} As shown in Fig. 5.19, the developing overlaps in the TS indicate large–large interaction **1** and large–small interaction **2** for the formation of two σ bonds signifying an asynchronous process. The inspection of the TS reveals that a small–large interaction **3**, equivalent to **2**, can also take place. Calculations give a bond distance of 1.96 Å for the leading interaction **1** whereas the bond distance for **2** or **3** is 2.90 Å. Therefore, one interaction between **2** and **3** can develop into a full σ bond while the other is involved in secondary orbital interaction. The two pathways for σ bond formation involving (**1**, **2**) and (**1**, **3**), however, give the same *endo* structure (Fig. 5.19). The (**1**, **2**) pathway represents [4+2] pathway (top molecule π_4 , bottom π_2), and (**1**, **3**) indicates [2+4] pathway (top π_2 , bottom π_4).

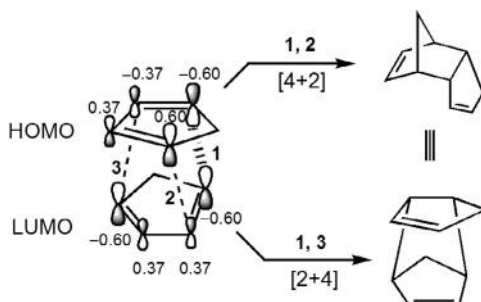


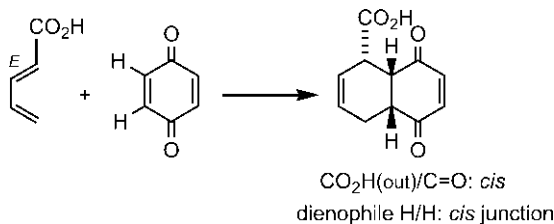
Fig. 5.19 Frontier orbital analysis of two pathways of *endo* dimerization of cyclopentadiene.

Problem 5.3

Woodward synthesis of reserpine⁶ started with the Diels–Alder reaction of (*E*)-pentadienoic acid with *p*-benzoquinone. Draw the structure of the exclusive cycloadduct.

Answer

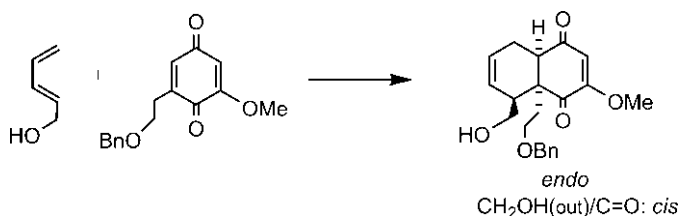
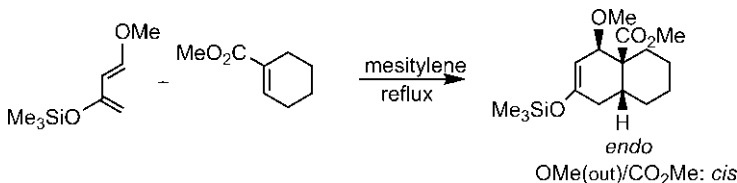
The reaction is stereospecific with respect to the quinone dienophile giving a *cis* ring junction and highly stereoselective forming an exclusive *endo* adduct.

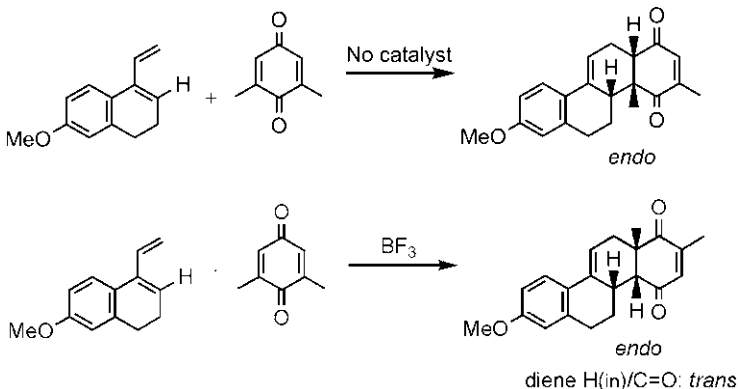
**Problem 5.4**

Give the stereochemistry of the cycloadduct in Fig. 4.19, Fig. 4.30 and Problem 4.11 in Chapter 4.

Answer

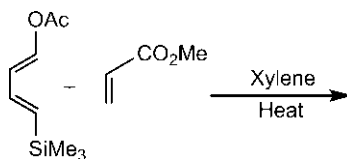
In each case, the reaction is stereospecific with respect to the dienophile giving *cis* ring junction for the *cis* substituents and stereoselective to give *endo* adduct.





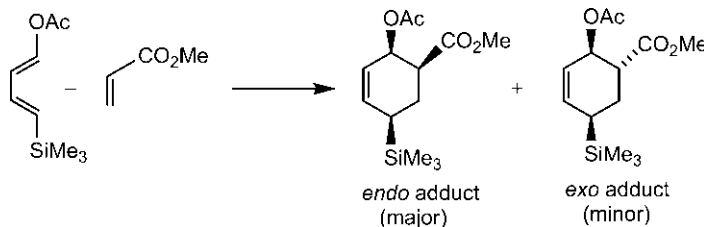
Problem 5.5

Give the products of the following reaction, indicating the major product.



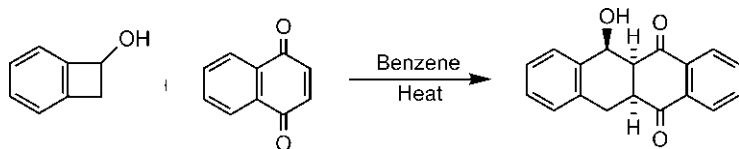
Answer

The reaction is regioselective, stereoselective and stereospecific. The products are *endo* and *exo* adducts, *endo* being major product. OAc being more powerful directing group than SiMe₃ would control regioselectivity: OAc/CO₂Me: 'ortho'. For *endo*-CO₂Me, OAc(out)/CO₂Me: *cis*; for *exo*-CO₂Me, OAc/CO₂Me: *trans*. For stereospecificity, OAc/SiMe₃: *cis*.

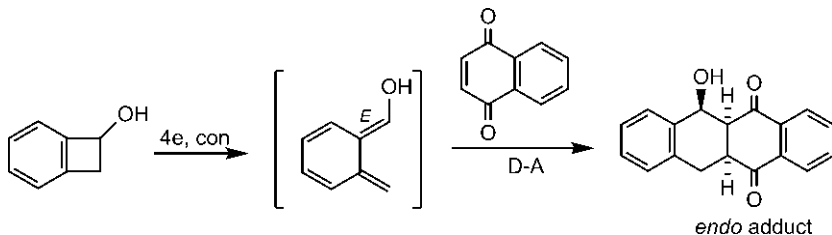


Problem 5.6

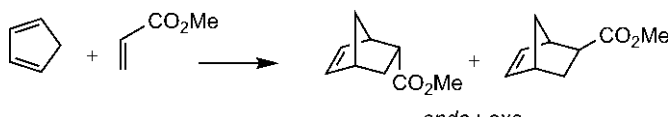
Account for the following observation.

**Answer**

Electrocyclic ring opening of cyclobutene ring would give *ortho*-quinonodimethane as a very reactive diene, with the substituent OH adopting *E* configuration (see [Section 7.1.2.2, Fig. 7.8](#)). The observed product results from the preferred *endo* addition. The reaction is also stereospecific with respect to the quinone dienophile. For *endo*-carbonyl, OH(out)/C=O: *cis*.

**5.1.2.3 Effect of Lewis Acids on Stereoselectivity**

We have seen earlier that Lewis acids can enhance the rate and regioselectivity of the Diels–Alder reaction (see [Section 4.2.5](#)). In addition, Lewis acids can also lead to enhanced stereoselectivity.⁷ This is illustrated with the reaction between cyclopentadiene and methyl acrylate in the absence or presence of Lewis acid ([Fig. 5.20](#)). The reaction in the presence of AlCl₃ gives higher proportion of *endo* adduct than without AlCl₃.



0°C, without AlCl₃ 82 : 18

0°C, AlCl₃ 93 : 7

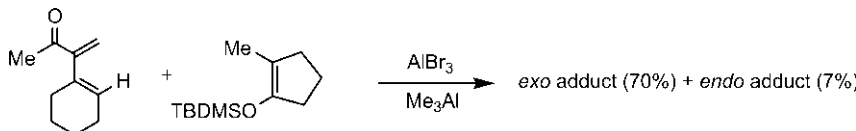
-80°C, AlCl₃ 97 : 3

Fig. 5.20 Stereoselectivity of the Diels–Alder reaction in the presence of Lewis acid.

The increased reactivity and regioselectivity were attributed to the effects of Lewis acid on the LUMO of the dienophile. The Lewis acid also tends to increase the LUMO coefficient on the carbonyl carbon which can lead to a stronger secondary orbital interaction and hence enhanced *endo* selectivity.

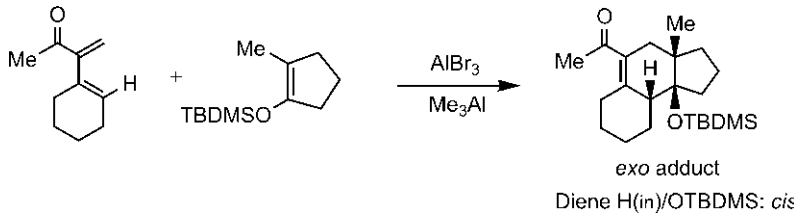
Problem 5.7

The following Lewis acid-catalyzed IEDDA reaction gives *exo* adduct as the major product.⁸ Draw the structure of the *exo* adduct.



Answer

The major product is thermodynamically more stable *exo* adduct in which the bulky OTBDMS group is *exo*. The regioselectivity gives OTBDMS and 2-substituent COMe to be ‘para’. For *exo*-OTBDMS, diene H(in)/OTBDMS: *cis*. The reaction is also stereospecific with respect to the dienophile forming a *cis* ring junction with Me/OTBDMS.



5.1.2.4 Thermodynamic Control

The Diels–Alder reaction is reversible. Under kinetic control, the retro-cycloaddition is not favourable and the reaction is essentially irreversible with the formation of less stable but fastly formed *endo* adduct as a major product. At higher temperature, the energy barrier of the reverse process is overcome. The reaction is then reversible and leads to equilibration between *endo* and *exo* adducts in favour of the more stable *exo* isomer. The reaction is said to be under equilibrium or thermodynamic control. The initial *endo* adduct dissociates by retro-cycloaddition followed by the re-addition which allows conversion of the kinetic *endo* adduct into the

thermodynamically more stable *exo* isomer. In some cases, prolonged reaction times may also lead to equilibration and formation of some *exo* adduct at the expense of the *endo* isomer. The formation of *exo* adduct as a major product at higher temperature is illustrated with two examples shown in Fig. 5.21.

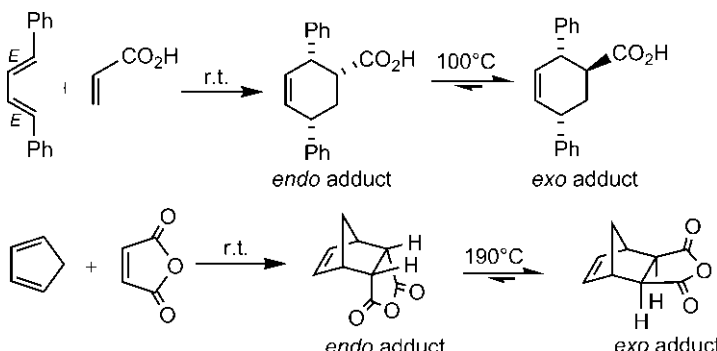


Fig. 5.21 Examples of thermodynamic control of the Diels–Alder reaction at higher temperature.

Problem 5.8

Explain the following observations.

- (a) The Diels–Alder reaction between cyclopentadiene and crotonic acid at -10°C gives 85% *endo* and 15% *exo* isomer but when carried out at 170°C , 40% *endo* and 60% *exo* adducts are obtained.⁹
- (b) Cyclopentadiene and maleic anhydride react at room temperature to give *endo* adduct whereas the reaction of furan with maleic anhydride at room temperature produces *exo* isomer.¹⁰

Answer

- (a) At low temperature (-10°C), kinetic control operates and the major product is *endo* adduct; however, at high temperature (170°C) thermodynamic control favours the more stable *exo* isomer.
- (b) For the reaction between cyclopentadiene and maleic anhydride, kinetically more favourable *endo* adduct is produced at room temperature when the reaction is essentially irreversible in nature. Furan, being aromatic, is a less reactive diene, and the initial *endo* adduct dissociates by retro-cycloaddition even at room temperature. The reversibility of the reaction at room temperature allows the conversion of *endo* adduct into more stable *exo* isomer.

5.1.2.5 Role of Other Forces in Stereoselectivity

So far, the *endo* stereoselectivity has been rationalized using frontier orbital theory in terms of secondary orbital interaction. Although the secondary orbital interaction remains the simple and most widely used explanation, it is not fully accepted. For some asynchronous reactions, the interacting atoms may be too far apart to have a significant secondary overlap. Other forces such as electrostatic interaction, hydrogen bonding and steric interaction can also play their part.¹¹ For example, as shown in Fig. 5.22A, electrostatic interaction may disfavour the *exo* transition structure because of repulsion between two partially positive charges on hydrogen (C—H bond being polarized to C) and carbonyl carbon, and the *endo* product would be preferred.

It was mentioned earlier (see Section 4.2.5.1) that the Diels–Alder reaction between cyclopentadiene and methyl vinyl ketone in water is not only faster than in isooctane but also exhibits higher stereoselectivity. The product ratio *endo*:*exo* = 96:4 compared with the ratio 80:20 in isoctane. This can be explained in terms of electrostatic repulsion between two partially positive charges, one on hydrogen of cyclopentadiene and the other on methyl group of methyl vinyl ketone in *exo* TS. The charge separation in a molecule is greater in ionizing water solvent leading to the development of more positive charges in cyclopentadiene and methyl vinyl ketone. The greater repulsion in *exo* TS in water thereby increases the *endo* selectivity.

In some reactions, the electrostatic effect may favour the *exo* adduct through attraction between opposite charges. In the reaction of furan with cyclopropenone, *exo* TS is stabilized by electrostatic attraction between partial negative charge on oxygen of furan and partial positive charge on carbonyl carbon, and leads to *exo* product (Fig. 5.22B).

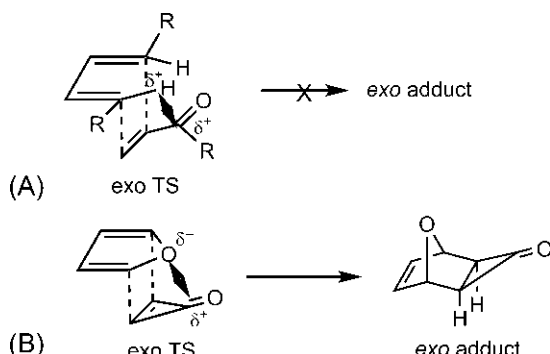


Fig. 5.22 Stereoselectivity of Diels–Alder reactions in terms of electrostatic interactions favouring (A) *endo* adduct and (B) *exo* adduct.

For some reactions, the introduction of alkyl group on the substituted atom of a α -substituted dienophile may cause reversal of stereoselectivity. Cyclopentadiene reacts with acrylic acid to give the major *endo* adduct. However, the *endo* preference is not obtained when α -substituted acrylic acids are used (Fig. 5.23). The reason for this is uncertain. A number of the above-mentioned factors may be responsible for this.

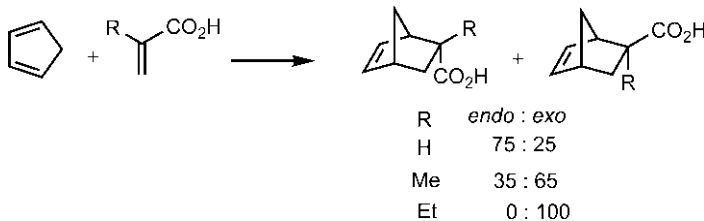


Fig. 5.23 Stereoselectivity in the reaction between cyclopentadiene and α -substituted acrylic acids.

The reactivity and *endo* selectivity can also be increased by the application of high pressure.¹² The rate of a reaction in solution is related to the activation volume, ΔV^\ddagger (the difference in molar volume between transition structure and reactants). Increasing pressure decreases ΔV^\ddagger and rate is accelerated. In other words, as the number of species decreases on going from reactants to cyclic transition structure, the rate increases at high pressure. Further, since *endo* TS is more compact than *exo* TS, it has a smaller volume. Therefore, *endo* selectivity increases with increase in pressure.

For *exo* lone pair effect in *endo* selectivity, see Fig. 7.26, p. 311.

5.1.3 Intramolecular Diels–Alder Reactions

In intramolecular Diels–Alder (IMDA) reaction, the diene and dienophile units are held together in the same molecule by a tether (connecting chain) and the intramolecular cycloaddition can provide easy access to polycyclic compounds with high regio- and stereoselectivity.^{13–15} There are two principal types of IMDA reactions based on the point of attachment of the tether to the diene unit in the substrate. In Type I substrate, the dienophile is tethered to a terminal atom of the diene whereas in Type II substrate, the tether is attached to an internal atom of the diene. *Two new rings* are created, and the stereochemistry of the reaction refers to the stereochemistry of the ring junction as well as the relative stereochemistry of the substituents. Intramolecular

reactions become more facile than intermolecular ones due to favourable entropy factor, and can occur with reasonable speed even in the absence of activating α -substituent. As for intermolecular reactions, the formation of *endo* adduct is often favoured. However, the absence of activating α -substituent or geometrical constraints can lead to the *exo* product. The IMDA reactions are illustrated below with some selected examples.

Fig. 5.24 shows a Type I reaction in which the dienophile moiety bears an activating electron-withdrawing carbonyl substituent. The intramolecular reaction takes place readily and the major product is *endo* adduct in which the ring fusion is *cis*. The *endo* TS **5.3** shows that the tether adopts a chair-like conformation and the ring junction is clearly *cis*, one H is axial (*up*) and the other H is equatorial (*up*). See also the use of *Mnemonic 2* to draw the *endo* adduct.

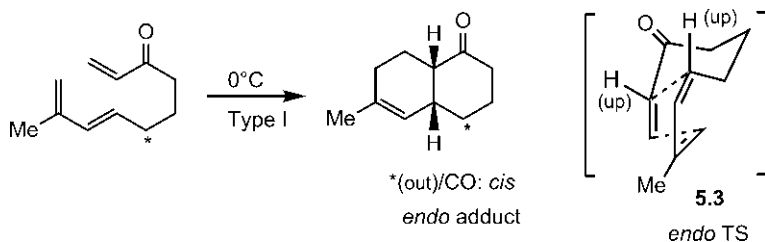


Fig. 5.24 Formation of *endo* adduct in a Type I intramolecular Diels–Alder reaction.

Fig. 5.25 shows a Type I reaction when there is no activating carbonyl substituent on the dienophile unit of the substrate **5.4** and a much higher temperature is required. The absence of secondary orbital interaction favours the sterically favourable *exo* TS **5.5** (the connecting chain to the dienophile being *exo*) which leads to *exo* adduct **5.6** with *trans* ring junction (H/H: *up/down* in the TS). See also the use of *Mnemonic 2* to draw the *exo* stereochemistry (box in **Fig. 5.25**).

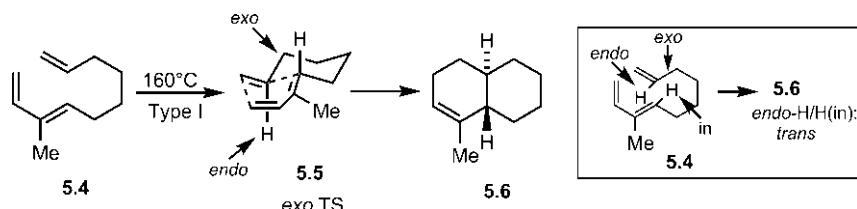


Fig. 5.25 Formation of *exo* adduct in a Type I intramolecular Diels–Alder reaction.

The Type I IMDA reaction shown in Fig. 5.26 gives *endo* adduct 5.7 (a *trans*-hydrindane) as a major product but the stereoselectivity is not high (*endo*:*exo*=60:40). However, Lewis acid catalysis can greatly improve the *endo* selectivity of the intramolecular reaction. The use of EtAlCl₂ permits the reaction to proceed at room temperature, and the *trans*-hydrindane 5.7 is formed exclusively.¹⁶

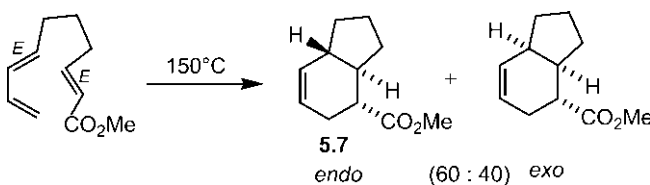


Fig. 5.26 Type I intramolecular Diels–Alder reaction of (*E,E*)-dienyl-acrylate producing a *trans*- and a *cis*-hydrindanes.

The regiochemistry and stereochemistry of the reaction are rationalized as follows. The reaction represents a cycloaddition of 1-x-substituted diene (x=alkyl chain) with z-substituted dienophile (z=CO₂Me). The preferred regioisomer is then expected to be 1,2-isomer ('ortho'). However, the observed regioisomer for the intramolecular reaction is 1,3-isomer ('meta'), a fused-ring product instead of a bridged-ring system for 1,2-isomer. For this tethered Diels–Alder reaction, the geometric factor becomes dominant over electronic effects. The formation of internal bond is presumably more advanced than the peripheral bond because of the proximity (entropic) effect as shown in a schematic drawing 5.8. The leading internal bond then gives rise to 1,3-isomer (Fig. 5.27). The stereochemistry of the major product follows from the normal *endo* selectivity and stereospecificity with respect to dienophile.

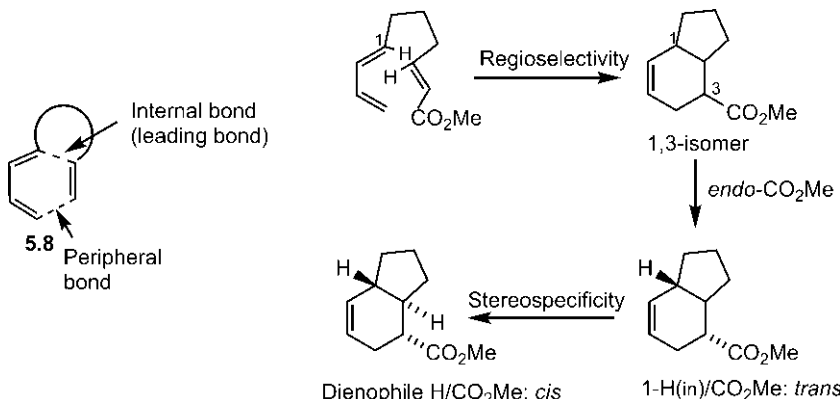


Fig. 5.27 Regioselectivity and stereochemistry of the IMDA reaction in Fig. 5.26.

Electrocyclic ring opening of a benzocyclobutene **5.9** produces a *ortho*-quinonodimethane **5.10** as a diene unit. Intramolecular reaction with the alkene dienophile moiety lacking an activating α -substituent proceeds preferably through *exo* TS giving the steroid estrone as *exo* adduct **5.11** (Fig. 5.28).¹⁷

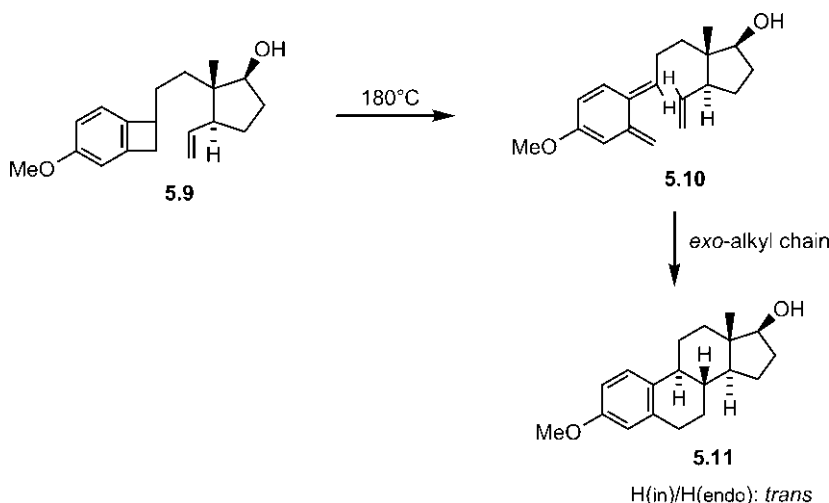


Fig. 5.28 Intramolecular Diels–Alder reaction giving an *exo* steroid product.

The Type II intramolecular reaction with a 2-substituted diene necessarily gives a bridged-ring compound (Fig. 5.29). The molecule folds up in the right conformation to undergo the reaction. The product can accommodate a bridge-head double bond in a nine-membered ring and its stereochemistry reflects the *trans* stereochemistry of the dienophile unit exhibiting stereospecificity.¹⁸

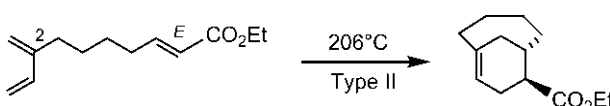
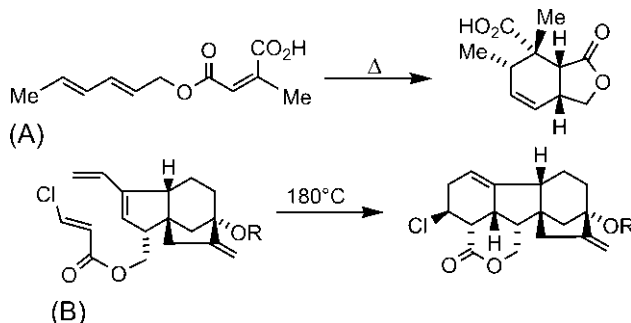


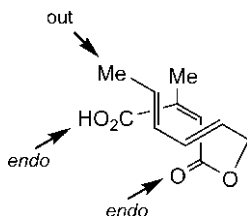
Fig. 5.29 Type II intramolecular Diels–Alder reaction producing a bridged-ring system.

Problem 5.9

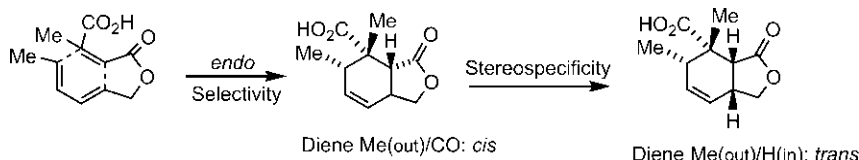
Explain the stereoselectivity in the following intramolecular Diels–Alder reactions.

**Answer**

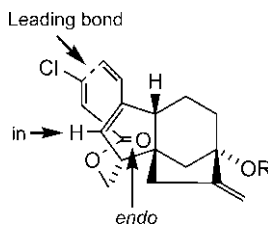
(A) Inspection of the product shows that two C=O substituents (acid and ester) of the dienophile are *cis* to Me (out-substituent) of the diene. The product is therefore *endo*. The stereoselectivity is determined by electronic effect of the two C=O groups that favour *endo* TS by secondary orbital interaction. The attainment of *endo* geometry is also not impeded by the intervening linkage between the diene and dienophile as shown below.



The product stereochemistry is delineated as follows:



(B) The product is *endo* as C=O is *trans* to diene H (in). The dienophile bears activating C=O substituent and the *endo* TS is favoured by secondary orbital interaction. The short tether controls the regiochemistry to form the fused-ring adduct and also allows the formation of *endo* geometry as shown below.



The stereochemistry of the reaction is worked out as follows:



Remarks: There is no general rule or pattern for the stereoselectivity of intramolecular Diels–Alder reaction because the geometry or conformational effects of the tether connecting the two reacting moieties may be the deciding factor. The controlling structural features can be ascertained by molecular modelling.¹⁹ Intramolecular reactions with the dienophiles bearing a α -substituent do not always give the *endo* adduct.²⁰ For example, a cycloaddition in which the diene and dienophile are tethered by silicon atom, produced a single *exo* adduct (Fig. 5.30). The reaction is stereospecific with respect to both diene and dienophile.

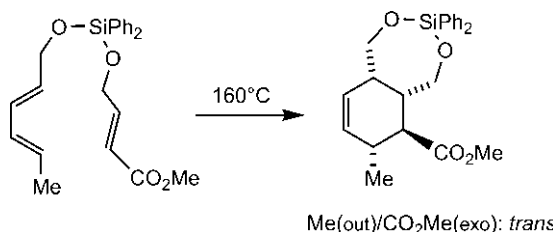


Fig. 5.30 Formation of *exo* adduct in an intramolecular reaction with dienophile bearing a α -substituent.

5.1.4 Asymmetric Diels–Alder Reactions

Asymmetric synthesis is the synthesis of an enantiomer. Asymmetric Diels–Alder reaction gives an enantiopure or enantiomerically enriched cycloadduct. The extent of enantioselectivity is expressed as enantiomeric excess (ee), an excess of one enantiomer over the other (see Section 2.4.1).

So far, we have described the diastereoselective Diels–Alder reactions when the diene and dienophile are achiral. The product cycloadduct, if chiral, is then necessarily racemic. This is now explained for *endo*-cycloaddition in Fig. 5.31. The addition of diene (in *endo* fashion) can take place equally on the top and bottom face of the dienophile as the two prochiral faces (*re* face and *si* face) of the achiral dienophile are enantiotopic (for *re/si* descriptor, see Fig. 2.25). The product is then a 1:1 mixture of enantiomers.

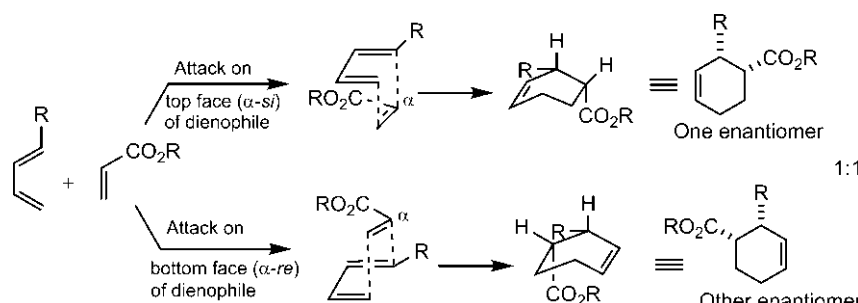


Fig. 5.31 Formation of a racemic *endo* adduct through diene attack on two enantiotopic faces of a dienophile.

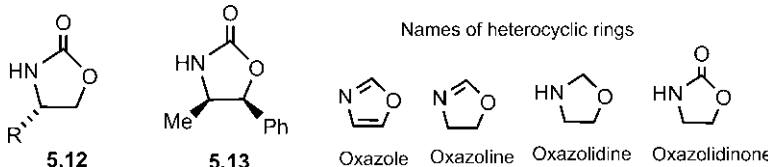
For the cycloaddition to be enantioselective, the diene has to distinguish between the two faces of the dienophile. This happens when the two faces of the dienophile become diastereotopic with the alkene double bond being covalently or noncovalently linked to a chiral moiety. Importantly, the chiral moiety must be nonracemic, preferably a single enantiomer because racemic chiral reactant leads to a racemic chiral product. The reaction then proceeds through diastereomeric transition structures of different energies, and the more stable TS leads to a major diasteromer still attached to the chiral moiety. The predominant enantiomeric product is obtained by simple chemical cleavage of covalently attached chiral unit or by the dissociation of noncovalently or coordinatively linked chiral moiety. (The asymmetric synthesis gives optically active product when the reacting system contains at least one optically active component. The use of chiral but optically inactive racemic reactant leads to optically inactive racemic product. You cannot create optical activity out of optically inactive starting materials!)

A detailed discussion of this important topic is beyond the scope of this book, but a brief description follows with two main approaches of asymmetric Diels–Alder reactions using chiral auxiliaries and chiral catalysts.^{21–23}

5.1.4.1 Chiral Auxiliaries

There are many chiral auxiliaries²⁴ available; however, we will restrict ourselves to the particularly useful chiral oxazolidinones developed by Evans.²⁵

Two examples **5.12** and **5.13** are shown below. Note the nomenclature of the heterocyclic rings.



These oxazolidinones can easily be prepared as a single enantiomer from naturally occurring and readily available enantiomerically pure amino acids or amino alcohols (Fig. 5.32).

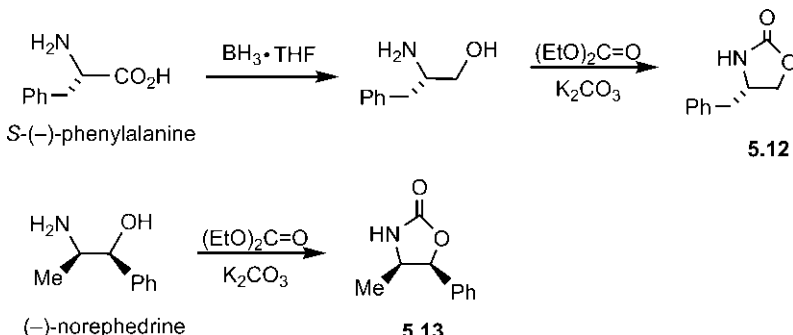


Fig. 5.32 Preparation of two oxazolidinone chiral auxiliaries.

The chiral auxiliary strategy involves three steps: (1) covalent attachment of auxiliary to a starting material (usually dienophile), (2) diastereoselective reaction and (3) removal of auxiliary by simple chemical cleavage. This is illustrated with an example in Fig. 5.33.²⁶

After attachment of auxiliary, the chiral dienophile **5.14** undergoes diastereoselective reaction via a cationic complex **5.15** in the presence of Lewis acid Et_2AlCl at low temperature (-100°C). The rigid aluminium chelate **5.15**, because of restricted orientation of the dienophile, provides high levels of diastereofacial selectivity which is crucial to the success of the asymmetric Diels–Alder reaction. The cycloaddition with 2-methylbutadiene is highly regioselective ('para') and *endo*-selective. Attack of diene occurs preferentially on the less hindered top face (*si* face) of dienophile to give *endo*

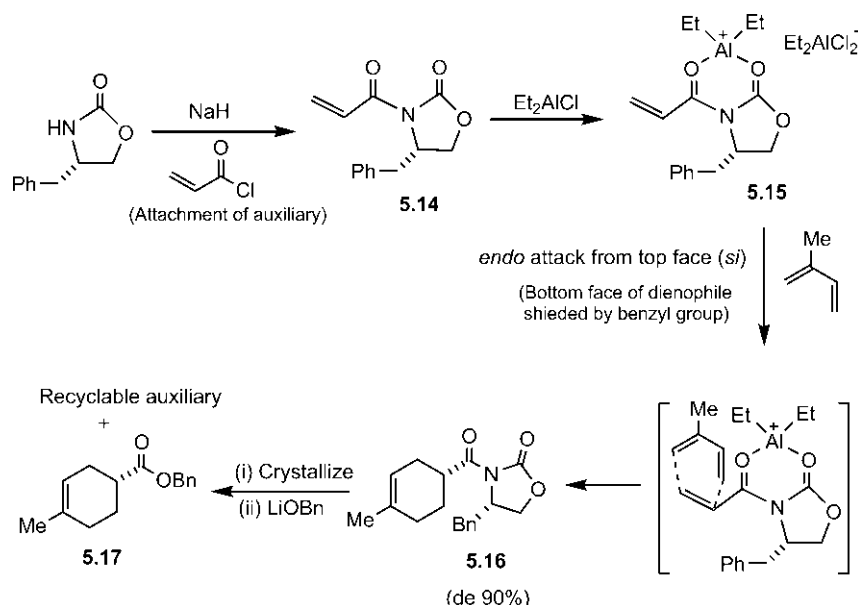


Fig. 5.33 Asymmetric Diels–Alder reaction using chiral auxiliary strategy.

diastereomer **5.16** (de 90%). Subsequent purification and removal of auxiliary yields the enantiomeric product **5.17**. Note that the chiral auxiliary can be recycled.

Stereochemistry is often confusing! It needs to appreciate that the same diastereoselective reaction can also be represented as *endo* attack from the bottom face of dienophile as shown in Fig. 5.34. In whatever way the scheme is drawn, the attacking face of the dienophile remains *si* face, as shown in Figs 5.33 and 5.34.

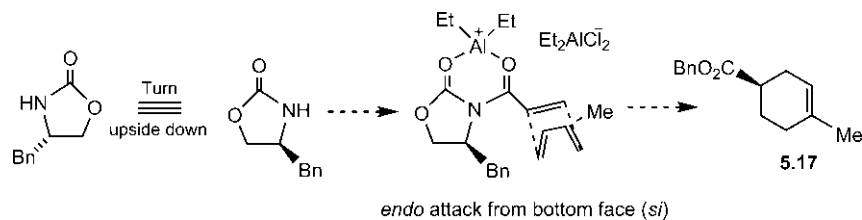


Fig. 5.34 Alternative representation of the scheme shown in Fig. 5.33.

The synthetic utility of this asymmetric Diels–Alder reaction is demonstrated by the conversion of **5.17** into *(R)*–(+)- α -terpineol by Grignard reaction (Fig. 5.35).²⁶

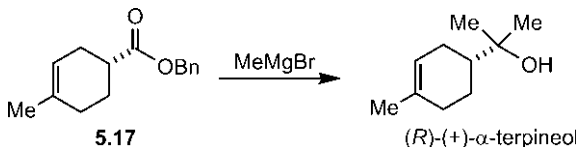


Fig. 5.35 Synthesis of (R)-(+)- α -terpineol via asymmetric Diels–Alder reaction shown in Fig. 5.33.

To delineate the absolute stereochemistry of the product enantiomer easily from *endo* addition, a third mnemonic (*Mnemonic 3*) is formulated as shown in Fig. 5.36.

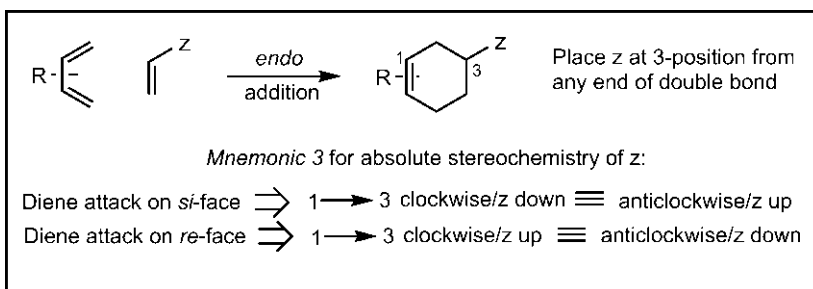


Fig. 5.36 *Mnemonic 3* for delineating absolute *endo* stereochemistry in asymmetric Diels–Alder reaction.

It is easy to assign *si* or *re* as the descriptor for the top face of a dienophile. The bottom face is then given the opposite descriptor. To illustrate the application of *Mnemonic 3*, let us predict the stereochemistry of the product (**P**) of an asymmetric Diels–Alder reaction shown in Fig. 5.37. Here the diene attacks the top face (*re* face) of dienophile attached to a chiral auxiliary (X_c) **5.18**, since the bottom face is shielded by benzyl group. The regiochemistry is ‘ortho’ relationship between R^1 and COX_c . Using *Mnemonic 3*, the stereochemistry of COX_c (z) is 1 \rightarrow 3 clockwise/up **5.19** or equivalently 1 \rightarrow 3 anticlockwise/down **5.20**. The stereochemistry of the product (**P**) is then delineated easily by considering *endo*- COX_c (COX_c/R^1 (out): *cis*) and stereospecificity with respect to dienophile (COX_c/R^2 : *trans*).

In summary, the final product structure is obtained by applying the sequence: regioselectivity (‘ortho/para’) \rightarrow stereochemistry of z-substituent (*Mnemonic 3*) \rightarrow *endo* stereochemistry (*Mnemonic 2*) \rightarrow stereospecificity with respect to diene (*Mnemonic 1*) and with respect to dienophile. (The step-by-step assignment is only an aid to understanding.)

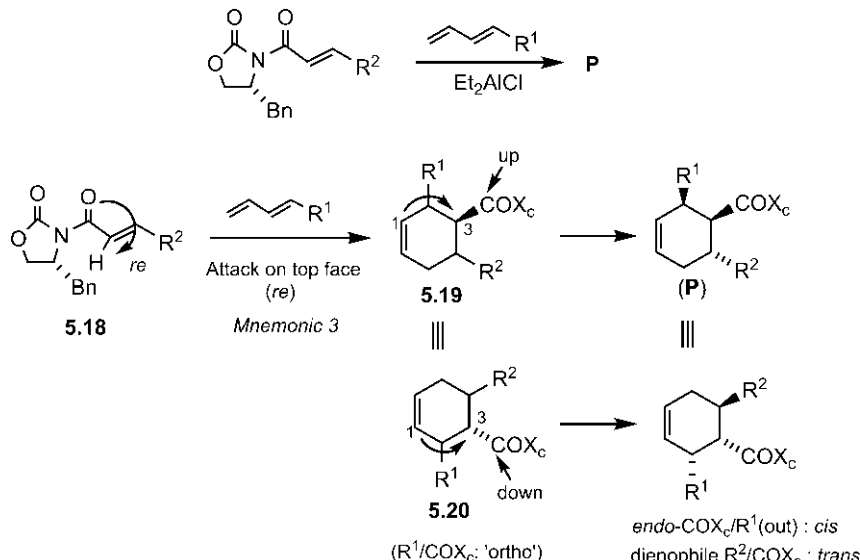
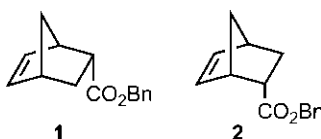


Fig. 5.37 Delineation of stereochemistry of an asymmetric Diels–Alder reaction with the help of mnemonics.

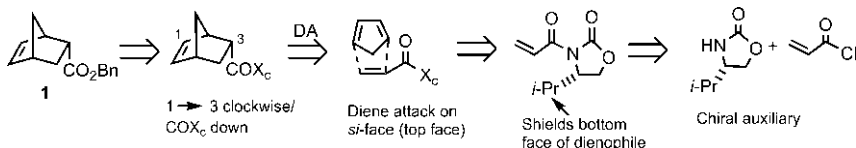
Problem 5.10

Suggest a suitable oxazolidinone chiral auxiliary for the synthesis of enantiomer **1** and enantiomer **2** of a bicyclic compound.

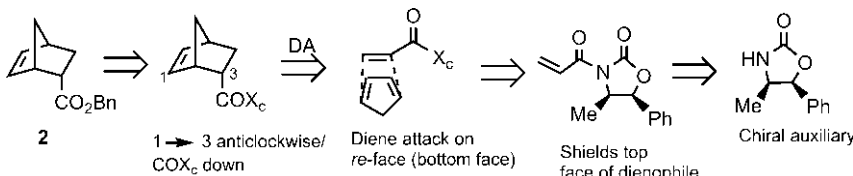


Answer

Retrosynthetic analysis with the help of *Mnemonic 3* provides the chiral auxiliary.



The chiral auxiliary is easily prepared from a chiral pool starting material, (S)-(+)-valine.

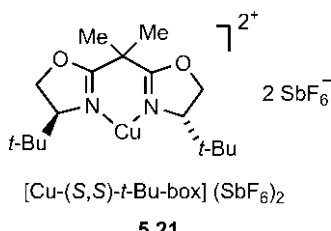


Here the auxiliary is derived from a chiral pool starting material, (−)-norephedrine. The top Me substituent reinforced by top Ph directs the cyclopentadiene to attack from the bottom face of the dienophile.

Remarks: The chiral auxiliary strategy has the advantage that the diastereomeric products are easily separated and purified. The final product enantiomer can thus be obtained in essentially pure state (~100% ee). Further, the chiral auxiliary is recyclable; thus although stoichiometric quantities are needed, there is no waste. However, a major disadvantage is that the methodology requires additional steps for the initial preparation of chiral substrate using the auxiliary and the final removal of chiral auxiliary.

5.1.4.2 Chiral Catalysts

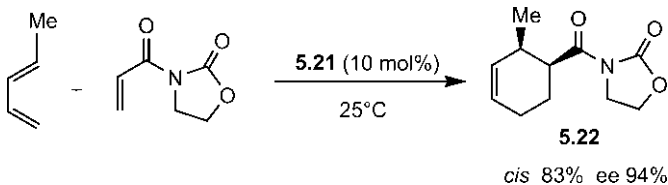
Over several years, some efficient chiral catalysts have been developed which give highly enantiomerically enriched cycloadduct from a variety of dienes and dienophiles. Here we shall describe only the catalyst system known as box catalysts,²⁷ the copper(II) complex of chiral **bis-oxazolines** such as **5.21**.



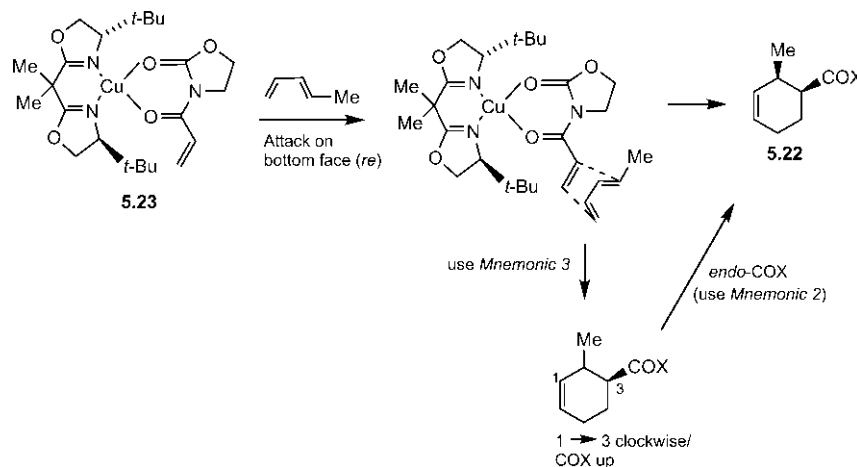
The metal ion (Cu²⁺) acts as a Lewis acid, and coordinates (or chelates) with the carbonyl group(s) of the dienophiles.

To illustrate the asymmetric Diels–Alder reactions using **5.21**, we first consider the reaction shown in Fig. 5.38.^{28,29}

The formation of the observed product **5.22** is rationalized as follows. The dienophile bears two carbonyl groups which could chelate with the copper forming a well-defined catalyst-substrate complex **5.23** of

**Fig. 5.38** Asymmetric Diels–Alder reaction using a chiral box catalyst.

square-planar geometry (**Fig. 5.39**). Clearly, the diene would attack on the bottom face (*re* face) of the dienophile (top face being sterically shielded by bulky *t*-Bu group) to give the product **5.22** after dissociation of catalyst from the catalyst–product complex. (Note that, as can be seen, the top face of the dienophile is *si*; therefore the bottom face is *re*.) See also the use of mnemonics to delineate the product enantiomer.

**Fig. 5.39** Mechanism of catalytic asymmetric Diels–Alder reaction in **Fig. 5.38** (X = oxazolidinone ring).

It is of note that the catalyst **5.21** has C_2 symmetry. Therefore, the alternative orientation of the dienophile, in which the alkene double bond is on the side of the other oxazoline ring which has below the plane *t*-Bu, would give the same enantiomeric product **5.22** (check).

Next, we consider an asymmetric Diels–Alder reaction with furan as a key step in the synthesis of an unnatural enantiomer of shikimic acid (**Fig. 5.40**).³⁰

Attack of furan as a cyclic diene takes place from the bottom face (*re*) of the dienophile of catalyst–dienophile complex (cf. **5.23**) to yield the *endo*

enantiomer **5.24** ($1 \rightarrow 3$ anticlockwise/COX down). The cycloadduct **5.24** is of very high enantiomeric purity which was converted into an unnatural enantiomer of shikimic acid. The reaction is carried out at very low temperature (-78°C) to favour the formation of *endo* adduct (see Problem 5.8b).

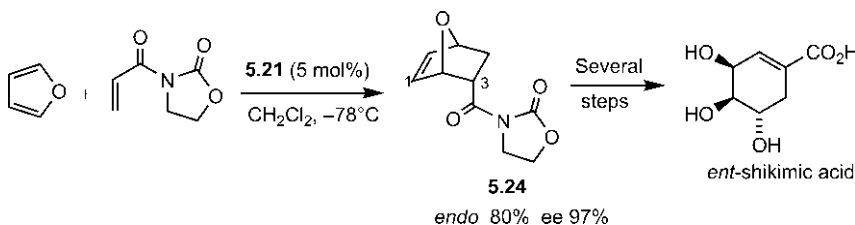


Fig. 5.40 Asymmetric Diels–Alder reaction as a key step in the synthesis of *ent*-shikimic acid.

5.1.5 Photochemical Diels–Alder Reaction

The $[\pi 4_s + \pi 2_s]$ Diels–Alder reaction is symmetry-forbidden in the excited state and not observed photochemically. However, the $[\pi 4_s + \pi 2_a]$ and $[\pi 4_a + \pi 2_s]$ modes (Fig. 5.41) are symmetry-allowed under photochemical condition but steric considerations make these geometries quite unfavourable.

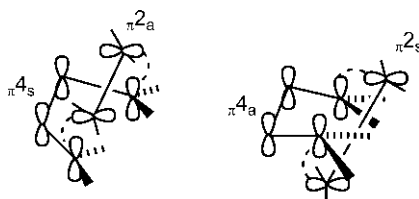


Fig. 5.41 Allowed $[\pi 4_s + \pi 2_a]$ and $[\pi 4_a + \pi 2_s]$ modes of photochemical Diels–Alder reaction.

The photochemical Diels–Alder reactions are indeed rare, and observed particularly as intramolecular cycloadditions. The intramolecular photochemical reaction represents a crossed cycloaddition as shown in the conversion of a triene to a bicyclo[3.1.0]hexene (Fig. 5.42A).^{31,32} Note that the bicyclohexene can only be *cis*-fused. The stereochemical outcomes of $[\pi 4_s + \pi 2_a]$ and $[\pi 4_a + \pi 2_s]$ modes are delineated in Fig. 5.42B. Note that the relative stereochemistry of substituents for suprafacial component is retained in the product; for antarafacial component, it is reversed.

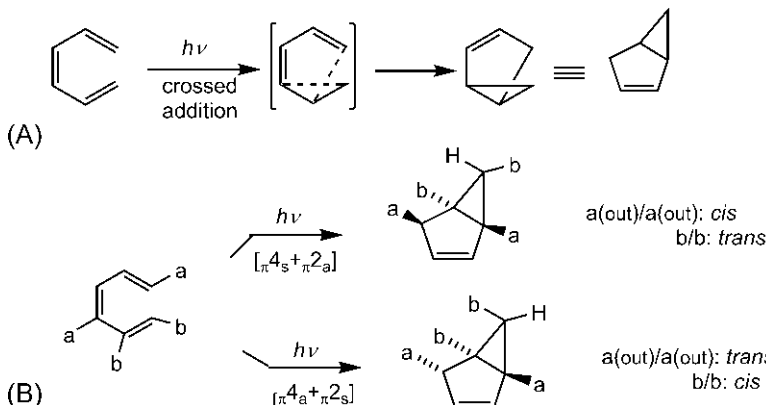


Fig. 5.42 (A) Intramolecular photochemical reaction as a crossed cycloaddition; (B) stereochemical outcomes of $[\pi 4_s + \pi 2_a]$ and $[\pi 4_a + \pi 2_s]$ modes.

An interesting example of photochemical Diels–Alder reaction is the intramolecular cycloaddition of vitamin D₂ **5.25** to give suprasterol I and suprasterol II, which result from the allowed $[\pi 4_s + \pi 2_a]$ cycloaddition (Fig. 5.43).³³

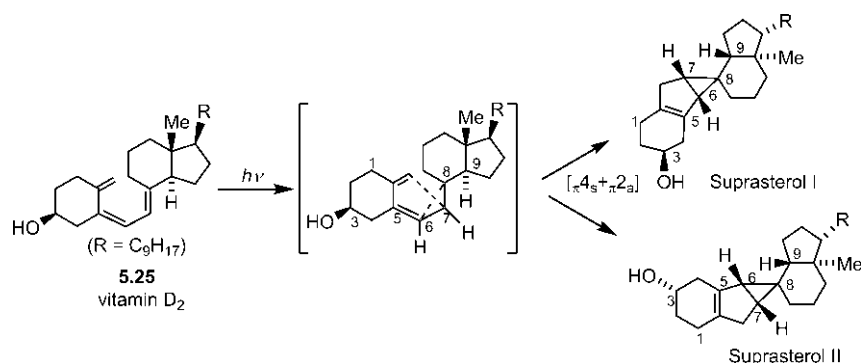


Fig. 5.43 Intramolecular photochemical Diels–Alder reaction of vitamin D₂.

The antarafacial addition to C₇–C₈ double bond causes rotation of the bicyclic unit to the other side leading to C₇–H/C₉–H: *cis* in the products. The bicyclohexene produced is favourably *cis*-fused (C₆–H/C₇–H: *cis*). The relative stereochemistry of substituents in the bicyclic unit (Me/C₉–H: *trans*; Me/R: *cis*) remains the same in the products. Suprasterol I and suprasterol II arise from the attack involving two opposite faces of diene unit in **5.25**; the former from the top face and the latter from the bottom face, being the same as obtained by turning the top face down.

5.1.6 $[\pi 4_a + \pi 2_a]$ Diels–Alder Reaction

The $[\pi 4_a + \pi 2_a]$ Diels–Alder cycloaddition, though symmetry-allowed thermally, is unlikely to take place as this process requires severe twisting of the reacting molecules in the transition structure (Fig. 5.44A). Only a few intramolecular reactions are known as crossed cycloadditions. An example is the conversion of a cyclooctatetraene into a semibullvalene (Fig. 5.44B).³⁴ The use of base protects the substrate from the acid-catalyzed side reaction.

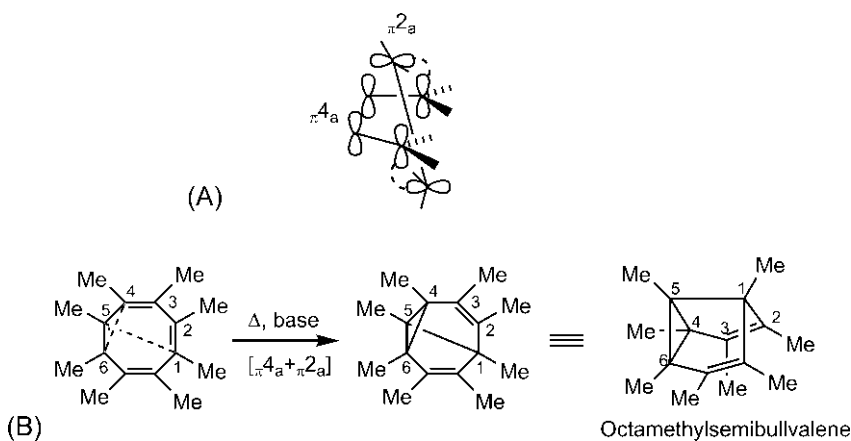


Fig. 5.44 (A) Orbital interactions for $[\pi 4_a + \pi 2_a]$ Diels–Alder reaction and (B) thermal conversion of a cyclooctatetraene into a semibullvalene by $[\pi 4_a + \pi 2_a]$ mode.

Antarafacial addition of a diene unit to $C_5—C_6$ double bond gives $C_5—Me/C_6—Me$: *trans* in the product. Further, as a result of antarafacial addition to the diene unit, $C_1—Me(\text{out})/C_4—Me(\text{out})$ becomes *trans* in the semibullvalene.

5.2 STEREOCHEMISTRY OF 1,3-DIPOLAR CYCLOADDITIONS

1,3-Dipolar cycloaddition (1,3-DC) of a 1,3-dipole (three-atom four-electron component) with an alkene or alkyne dipolarophile (two-atom two-electron component) produces a five-membered heterocyclic ring with one or more heteroatoms, and can create a *maximum* of four carbon stereocentres (Fig. 5.45). (Remember that the middle atom of a dipole is a heteroatom.)

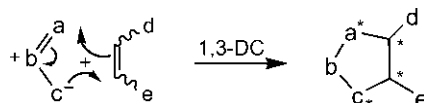


Fig. 5.45 Schematic representation of 1,3-dipolar cycloaddition showing potential stereocentres in the product (b is always a heteroatom).

Like the Diels–Alder (DA) reaction, we will describe the stereochemical features of 1,3-DC in terms of stereospecificity and stereoselectivity of the reactions. As the DA and 1,3-DC proceed by the similar supra/supra mechanism, the stereospecificity with respect to a dipole and *endo/exo* stereochemistry in 1,3-DC could be delineated using *Mnemonic 1* (see p. 192) and *Mnemonic 2* (see p. 195), respectively, considering a dipole instead of a diene.

5.2.1 Stereospecificity of 1,3-Dipolar Cycloadditions

1,3-Dipolar cycloaddition is a $[\pi 4_s + \pi 2_s]$ reaction. For most 1,3-dipolar cycloadditions, stereospecificity refers to the stereochemistry of the alkene dipolarophiles. As a result of suprafacial addition, the relative stereochemistry of substituents in the alkene is retained in the product. An alkene dipolarophile with *cis* substituents gives a *cis* adduct, and a *trans* dipolarophile produces a *trans* product. These are illustrated using nitrile oxide as a 1,3-dipole in Fig. 5.46.³⁵ The isoxazoline adducts **5.26** and **5.27** are sometimes not the final target and are used as suitable intermediates in synthetic schemes. As shown in Fig. 5.46, the isoxazolines **5.26**

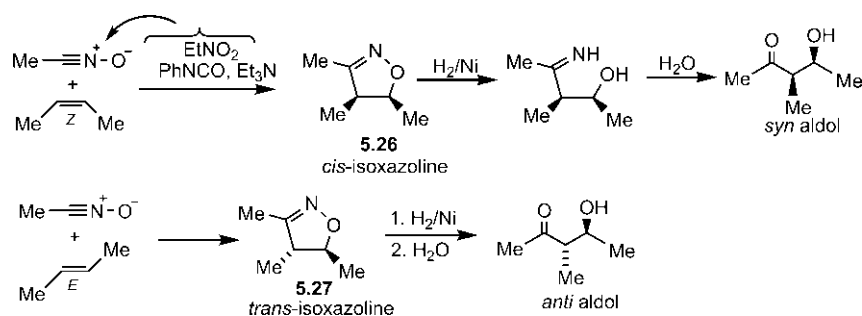


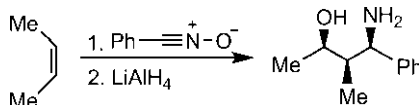
Fig. 5.46 Stereospecificity of nitrile oxide cycloadditions with (*Z*)- and (*E*)-butenes, and conversion of isoxazoline adducts into diastereomeric aldols.

and **5.27** are converted into diastereomeric *syn* and *anti* aldols, respectively, on hydrolytic reduction with Raney nickel in aqueous acid. If necessary, the isoxazolines can be converted into diastereomeric β -amino alcohols by successive reductive cleavage and reduction by catalytic hydrogenation.

Stereospecificity is also observed with respect to 1,3-dipoles which can create two new stereocentres. Two such dipoles are azomethine ylide and carbonyl ylide (see Fig. 4.48). Fig. 5.47 shows that electrocyclic ring opening of *cis*- and *trans*-disubstituted aziridines by conrotatory or disrotatory mode (see Fig. 7.66) generates diastereomeric azomethine ylides in situ, which are trapped by an alkyne dipolarophile DMAD.³⁶ The electron-withdrawing CO₂Me group stabilizes the negative charge in the azomethine ylide, thereby facilitates its formation by the ring opening process. Under thermal condition, *cis* aziridine gives the ylide **5.28** whereas the *trans* isomer gives **5.29**. On photolysis, *cis* aziridine gives **5.29**, and *trans* aziridine gives **5.28**. As a result of suprafacial addition to the ylide dipole, the relative stereochemistry of substituents in the ylide is retained in the cycloadduct. Thus **5.28** leads to a *trans* Δ^3 -pyrroline product **5.30**, and **5.29** yields a *cis* pyrroline product **5.31**. See also the use of *Mnemonic 1* to delineate the product stereochemistry.

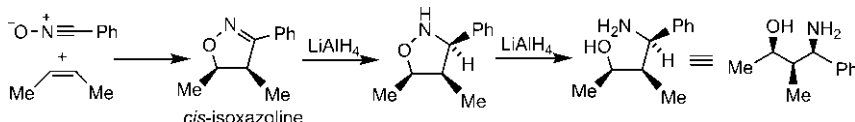
Problem 5.11

Account for the formation of product in the following reaction.



Answer

cis-2-Butene produces a stereospecific *cis* diastereomer of 1,3-dipolar cycloadduct. LiAlH₄ reduces the imine unit (hydride attack takes place from the bottom face of the ring as the top face is sterically shielded by methyl substituents) to give an intermediate which then undergoes reductive cleavage of N—O bond to yield the product.



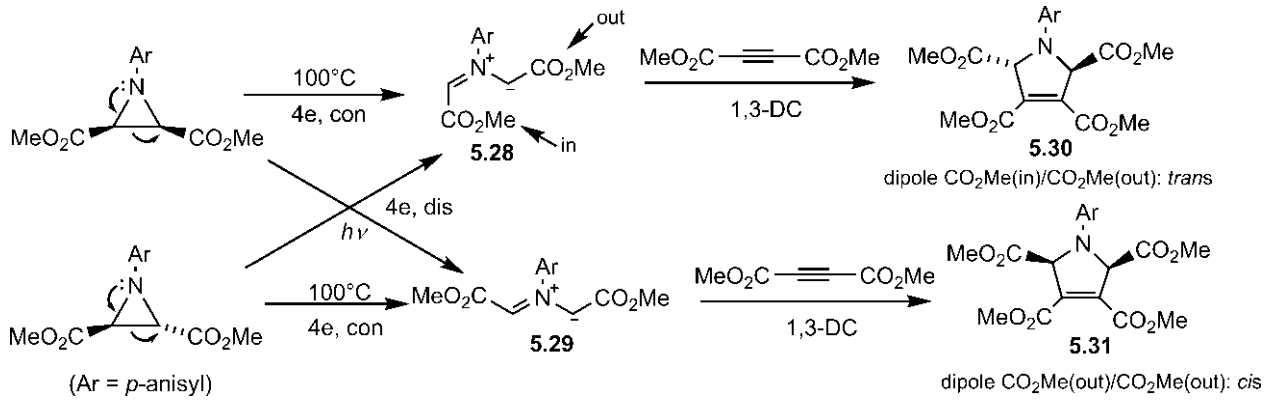
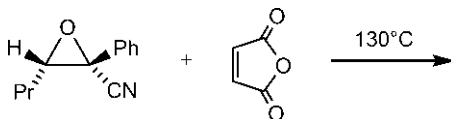


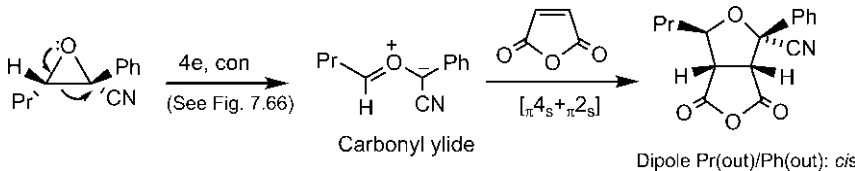
Fig. 5.47 Stereospecificity of 1,3-dipolar cycloaddition with respect to azomethine ylide dipole generated from suitably substituted aziridines by electrocyclic ring opening.

Problem 5.12

Predict the stereochemistry of the product of the following reaction.

**Answer**

The conrotatory ring opening of the oxirane produces a carbonyl ylide dipole (negative charge being stabilized by CN) which undergoes a 1,3-dipolar cycloaddition with maleic anhydride dipolarophile to give the cycloadduct. The cycloaddition is stereospecific as a result of suprafacial addition to the dipole making Pr/Ph *cis* in the product. The ring junction is also *cis* as a result of suprafacial addition to the dipolarophile.



5.2.2 Stereoselectivity of 1,3-Dipolar Cycloadditions

In contrast to Diels–Alder reactions, stereoselectivity of 1,3-dipolar cycloadditions varies considerably. The selectivity is often low, though some reactions can give largely the *endo* adduct while some others are *exo* selective. Let us first examine the frontier orbital effects. The dipole HOMO (ψ_2) is similar to allyl anion HOMO but with a small coefficient at the central atom. The small central lobe in dipole HOMO cannot give rise to any significant *endo* effect by secondary orbital interaction. However, the secondary overlap involving the central lobe of dipole LUMO (ψ_3) and carbonyl p orbital of dipolarophile HOMO (ψ_2) can give a favourable bonding effect for *endo* addition. However, the dipolar cycloaddition is quite asynchronous and the observed stereoselectivities do not always conform to *endo* rule. The steric factor tends to favour *exo* addition, and it appears that both electronic and steric factors influence the stereoselectivity of 1,3-dipolar cycloadditions. To illustrate, we consider the following examples.

The cycloaddition of methyl acrylate to C,N-diphenylnitrone gives a mixture of *endo* and *exo* adducts (Fig. 5.48). The regioselectivity is in favour of 5-substituted isoxazolidine (see Fig. 4.63). The *endo* addition gives a *trans*

adduct while the *exo* addition leads to a *cis* adduct. The stereoselectivity is low, the *exo* (*cis*) isomer is somewhat favoured (de 14%). See also the use of *Mnemonic 2* to delineate *endo/exo* stereochemistry.

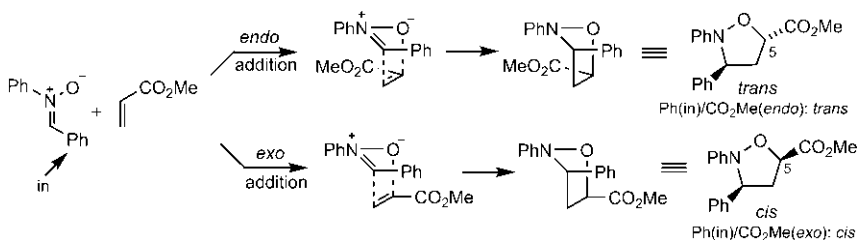


Fig. 5.48 Formation of *endo* and *exo* adducts in cycloaddition of methyl acrylate to *C,N*-diphenylnitrone.

The cycloaddition of an azomethine ylide (generated from an imine by the addition of a metal salt and a base) to methyl acrylate is largely *endo* selective (Fig. 5.49).^{37,38} The stereochemistry of the *endo* pyrrolidine product is delineated explicitly using *endo* stereochemistry (*Mnemonic 2*), then stereospecificity with respect to the dipole (*Mnemonic 1*).

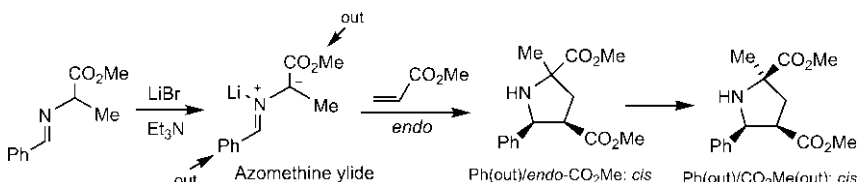


Fig. 5.49 *endo* selectivity in cycloaddition of an azomethine ylide to methyl acrylate.

The reaction between a cyclic nitrone and propene (an x-substituted dipolarophile) gives mainly the sterically favoured *exo* product. The preferred regioisomer is 5-substituted isoxazolidine. The cycloadduct can produce the alkaloid sedridine by reductive N—O cleavage (Fig. 5.50).³⁹

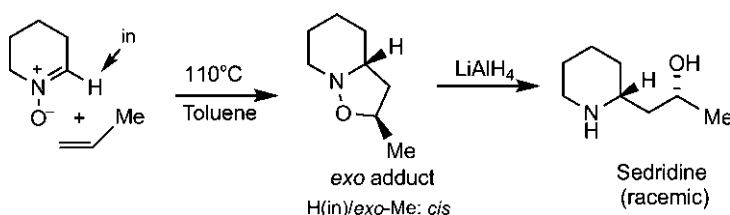


Fig. 5.50 *exo* selectivity of cycloaddition of a cyclic nitrone in a synthesis of sedridine.

5.2.2.1 Intramolecular 1,3-Dipolar Cycloadditions

Intramolecular cycloadditions of nitrones are especially useful in synthesis.^{40,41} The alkenylnitron 5.32 is generated by the condensation of (*E*)-5-heptenal with *N*-methylhydroxylamine, which undergoes intramolecular cycloaddition to give a *cis* bicyclic isoxazolidine 5.33 (Fig. 5.51).

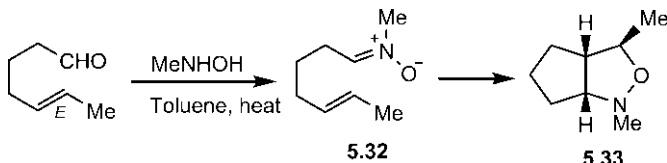


Fig. 5.51 Intramolecular 1,3-dipolar cycloaddition of an unsaturated nitrone.

Here the intramolecularity of the reaction determines the stereochemical outcome (Fig. 5.52). The alkene unit is tethered to the carbon atom of the nitrone dipole and involves *endo*-Me TS 5.34. Clearly, two H's at the ring junction and Me are all *cis* in the product 5.33.

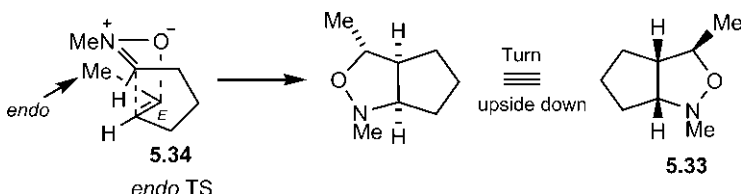


Fig. 5.52 Rationalization of product stereochemistry of the reaction in Fig. 5.51.

5.2.2.2 Asymmetric 1,3-Dipolar Cycloadditions

The asymmetric 1,3-dipolar cycloadditions can be performed using a variety of approaches including chiral substrates and chiral catalysts.^{42,43} First, we consider an example using a chiral catalyst. The cycloaddition of crotonaldehyde to a nitrone in the presence of chiral secondary amine catalyst **5.35** gives predominantly an *endo* adduct **5.36** [Ph(in)/CHO: *trans*] with high enantioselectivity (ee 94%) (Fig. 5.53).⁴⁴

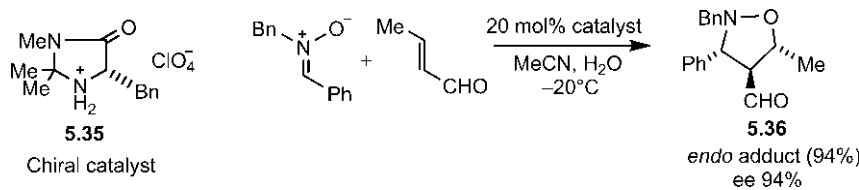


Fig. 5.53 Catalytic asymmetric 1,3-dipolar cycloaddition of a nitrone to crotonaldehyde.

The cycloaddition is believed to proceed through the reactive iminium ion **5.37** formed by the condensation of the catalyst with the dipolarophile. The alkene faces of the chiral iminium ion species **5.37** become diastereotopic, and the nitrone attacks preferentially from the top face of the alkene (bottom face being sterically shielded by benzyl group) in *endo* fashion to yield the enantioselective product **5.36** after workup (Fig. 5.54). As the dipolarophile bearing iminium ion moiety in **5.37** is highly electron deficient, the nitrone addition is regioselective in favour of 4-substituted regioisomer (see Fig. 4.64).

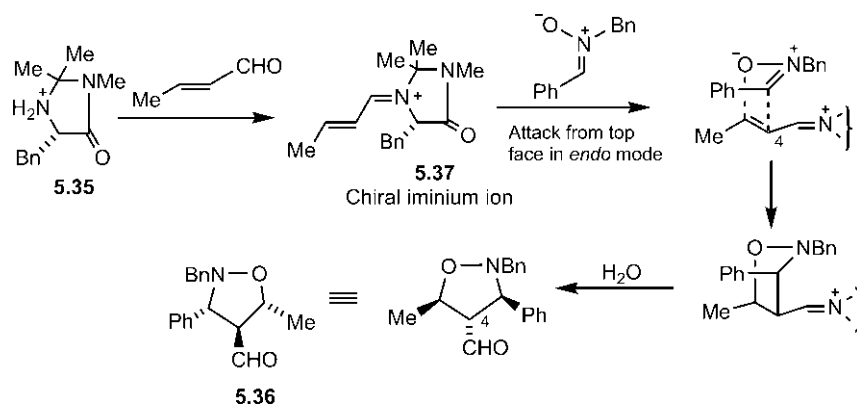


Fig. 5.54 Mechanism of asymmetric dipolar cycloaddition in Fig. 5.53.

Next, we consider an asymmetric dipolar cycloaddition with a chiral reactant. Vinyl sulphoxides are chiral and can act as a chiral alkene dipolarophile. Fig. 5.55 shows an asymmetric 1,3-dipolar cycloaddition of a cyclic nitrone with an enantiomerically pure chiral sulphoxide. The *exo*-approach of the nitrone takes place preferentially to the face of the alkene anti to the bulky *p*-tolyl substituent. The *exo* adduct (de = 82%) has been applied in the synthesis of the natural product (+)-sedridine⁴⁵ (cf. Fig. 5.50).

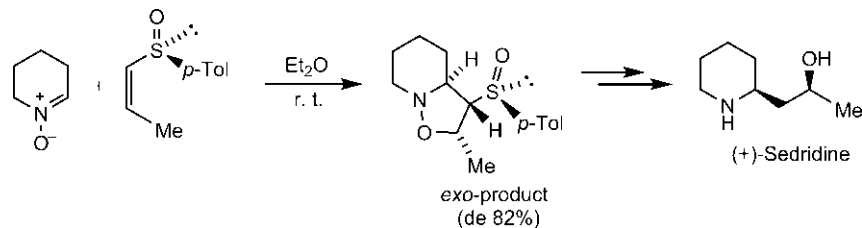


Fig. 5.55 Asymmetric dipolar cycloaddition using a chiral vinyl sulphoxide in the synthesis of (+)-sedridine.

5.3 STEREOCHEMISTRY OF [4+2] CYCLOADDITIONS WITH CATIONS AND ANIONS

In comparison to Diels–Alder and 1,3-dipolar cycloadditions, [4+2] cycloaddition reactions with cations and anions are much less common. There are three cases involving (a) allyl cation (three-atom, π_2), (b) pentadienyl cation (five-atom, π_4) and (c) allyl anion (three-atom, π_4) components (Fig. 5.56).^{1,46} The symmetry-allowed and geometrically favourable process for all three cases is $[\pi_4 + \pi_2]$.

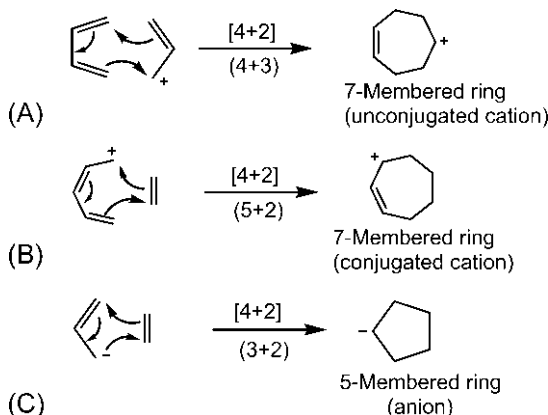


Fig. 5.56 Three cases of [4+2] cycloadditions with cations and anion. For the designations of cycloadditions, see p. 69.

5.3.1 Cycloadditions With Allyl Cations

Cycloaddition of allyl cations to dienes provides a convenient synthetic route to seven-membered rings.^{47,48} Allyl cations are generated *in situ* in the presence of dienes. Cyclic dienes are better than acyclic dienes for intermolecular cycloadditions. For example, cyclopentadiene and methylallyl cation (derived from its iodide) gives bicyclo[3.2.1]octadiene **5.38** (Fig. 5.57).

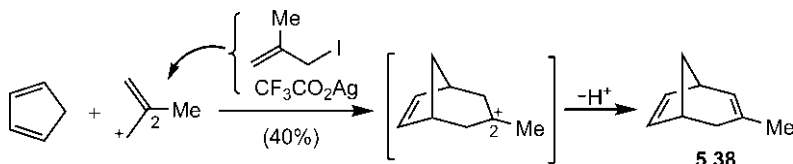


Fig. 5.57 [4+2] Cycloaddition of an allyl cation with cyclopentadiene.

With acyclic dienes, electrophilic allyl cations may react with the nucleophilic diene in *s-trans* conformation by stepwise ionic mechanism before the diene assumes *s-cis* conformation for concerted cycloaddition. But the cyclic dienes are usually locked in *s-cis* conformation necessary for pericyclic cycloaddition, although stepwise ionic pathways are not ruled out in some cycloadditions.

As can be seen from Fig. 5.57, C-2 of allyl cation unit accommodates a positive charge in the adduct cycloheptenyl cation. Therefore a substituent at C-2 of allyl cation, which would stabilize the cationic centre in the product, promotes the cycloaddition. 2-Oxyallyl cations are one such important species which have been applied to both intermolecular and intramolecular cycloadditions. Different methods have been used to generate 2-oxyallyl cations. The electrocyclic ring opening of cyclopropanone (see Fig. 7.54) gives 2-oxyallyl cation which can undergo cycloaddition with furan to give a bicyclic ketone (Fig. 5.58).

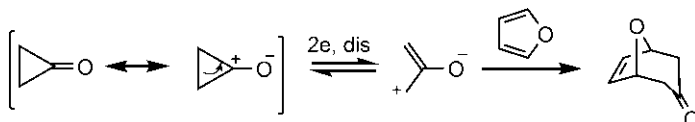


Fig. 5.58 Cycloaddition of cyclopropanone with furan via 2-oxyallyl cation.

α,α' -Dibromoketone on treatment with Zn–Cu couple produces a 2-oxyallyl cation **5.39** (draw a mechanism), which reacts with furan to give a *cis* product (Fig. 5.59). The *cis* stereochemistry of two Me's in the product reflects the stereospecificity with respect to the allyl cation.

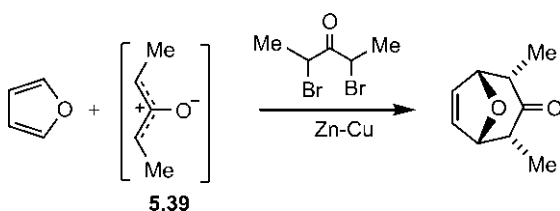


Fig. 5.59 Stereospecificity of cycloaddition of a 2-oxyallyl cation with furan.

An intramolecular cycloaddition of 2-oxyallyl cation with furan in the species **5.40** (generated from the corresponding ketone) gives an *exo* adduct **5.41** as a major product (Fig. 5.60).

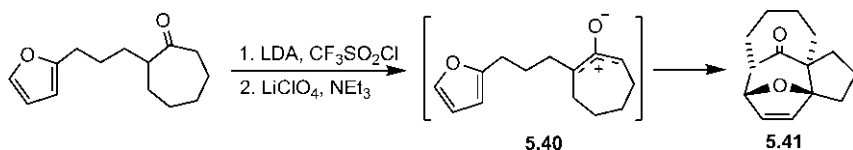


Fig. 5.60 Stereoselectivity of an intramolecular cycloaddition with a 2-oxyallyl cation.

The mechanism of the reaction is shown in Fig. 5.61. On treatment with lithium diisopropylamide (LDA) and $\text{CF}_3\text{SO}_2\text{Cl}$, an intermediate α -chloroketone is formed, which then transforms into **5.40** with LiClO_4 and base. The intramolecular cycloaddition yields the *exo*-carbonyl adduct **5.41**.

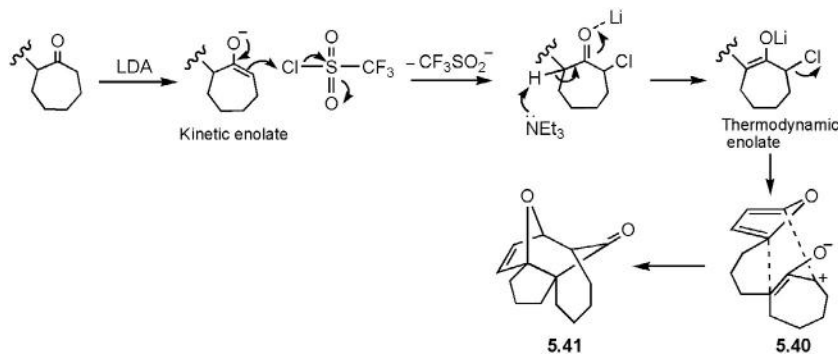


Fig. 5.61 Mechanism of the intramolecular cycloaddition in Fig. 5.60.

The 2-oxyallyl cation **5.42**, generated from 1,1,3-trichloroacetone on treatment with base, undergoes cycloaddition with furan ring of the substrate to give a mixture of two regioisomeric adducts, which are reduced to the same ketone product by zinc (Fig. 5.62).⁴⁹

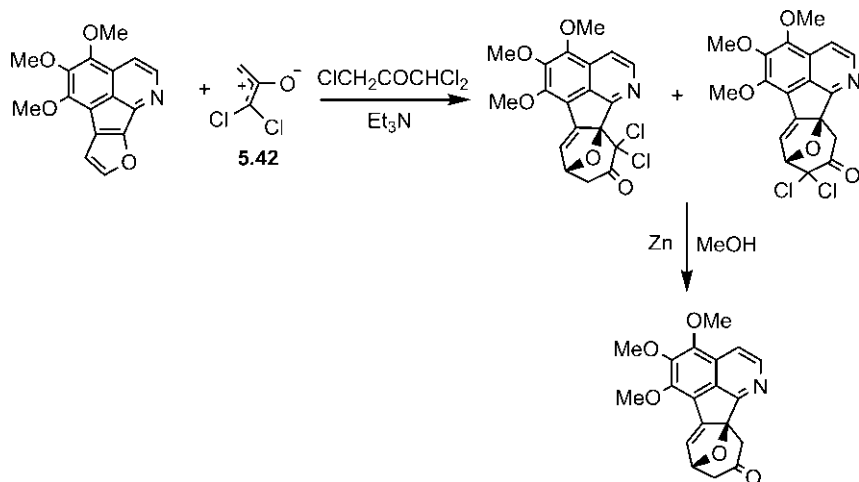
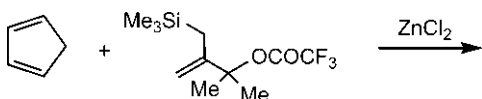


Fig. 5.62 Formation of regioisomeric adducts in 2-oxyallyl cation cycloaddition.

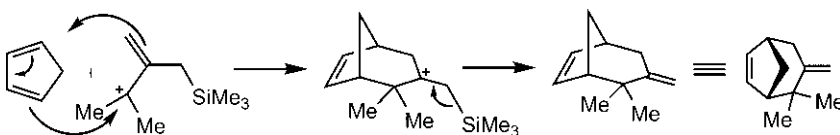
Problem 5.13

Draw the structure of the product and explain its formation.



Answer

An allyl cation is generated after departure of CF₃CO₂⁻ (ZnCl₂ coordinates with oxygen lone pair and assists dissociation). Cyclopentadiene reacts with the allyl cation to give a cationic cycloadduct, which loses the silyl group to yield the product with exocyclic double bond. The cycloaddition is facilitated by the presence of the β-silyl substituent which stabilizes the cationic centre in the cycloadduct. The silyl group serves two purposes: it stabilizes the cationic centre by σ-p hyperconjugation and, after doing so, loses itself in preference to H⁺ to form the exocyclic methylene group in the product.



5.3.2 Cycloadditions With Pentadienyl Cations

Cycloaddition with a pentadienyl cation is not so common. Two examples, one for intermolecular and the other for intramolecular cycloaddition, are illustrated below.

The pentadienyl cation **5.43** (generated in situ by the ionization of an acetal in the presence of a Lewis acid SnCl_4) undergoes an intermolecular cycloaddition with 1,2-dimethylcyclopentene to form the cycloadduct **5.44**, in a synthesis of a tricyclic sesquiterpenoid gymnomitrol (Fig. 5.63).⁵⁰ The cycloaddition is facilitated by the stabilization of allyl cation moiety in **5.44** by electron-donating OMe substituent.

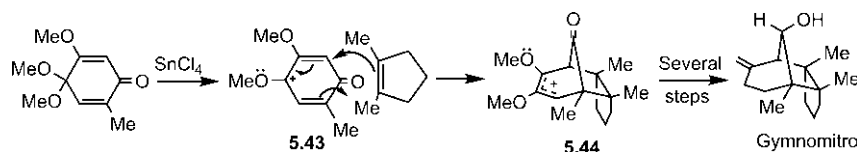


Fig. 5.63 Intermolecular cycloaddition with a pentadienyl cation in a synthesis of gymnomitrol.

Fig. 5.64 shows an intramolecular cycloaddition with a pentadienyl cation to form a tricyclic sesquiterpene pipitzol from perezone.⁵¹ In perezone, the quinone part (tethered to an alkene) is in equilibrium with isomeric pentadienyl cation moiety which undergoes an intramolecular cycloaddition to give the pipitzol.

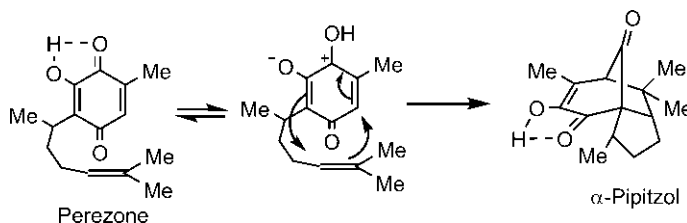


Fig. 5.64 Intramolecular cycloaddition with a pentadienyl cation in perezone–pipitzol conversion.

5.3.3 Cycloadditions With Allyl Anions

Allyl anions are usually associated with metal ion, and are not well defined as a conjugated system. Unlike allyl cations, the scope of allyl anion cycloadditions is limited and some cycloadditions may be stepwise instead of concerted process.⁵² The allyl anion cycloaddition with an alkene gives a

cyclopentyl anion with the negative charge on C-2 of allyl unit. An anion stabilizing substituent at C-2 or an electronegative atom at 2-position would facilitate the reaction.

2-Phenylallyl anion (generated in situ by abstraction of methyl proton of α -methylstyrene by LDA) reacts with (*E*)-stilbene to produce a *trans* cyclopentane after workup (Fig. 5.65). The reaction is stereospecific with respect to the alkene. The Ph substituent at C-2 in the adduct stabilizes the negative charge and thereby favours the cycloaddition.

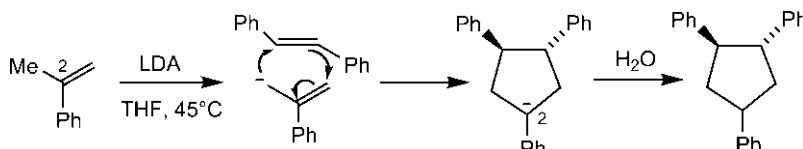


Fig. 5.65 Stereospecificity of allyl anion cycloaddition with an alkene.

2-Aza-allyl anions (in which electronegative nitrogen atom replaces C-2 in the allyl anion) undergo cycloadditions with alkenes to form pyrrolidine products.⁵³ For example, 2-aza-allyl anion **5.45** (prepared in situ from an imine and a base) undergoes cycloaddition with an alkene to give a *trans* pyrrolidine **5.46** as a major product after workup (Fig. 5.66).

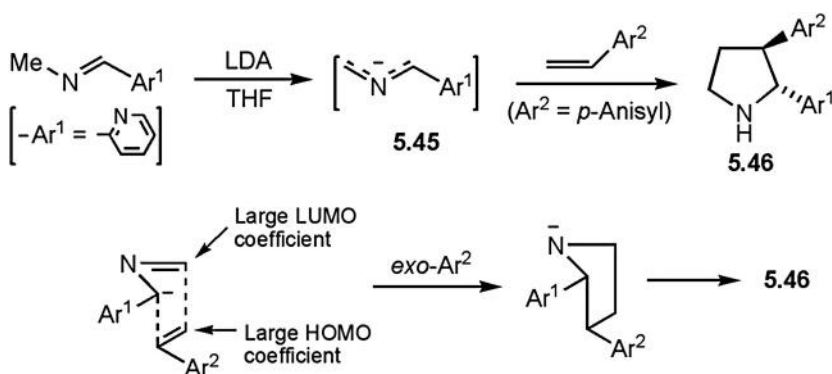


Fig. 5.66 Regioselectivity and stereoselectivity of a 2-aza-allyl anion cycloaddition.

The preferred regioisomer is a 1,2-disubstituted isomer. The 2-aza-allyl anion bears an electron-withdrawing 2-pyridyl substituent while the alkene is attached to an electron-donating *p*-anisyl substituent. The dominant frontier orbital interaction is between $LUMO_{\text{allyl anion}}$ and $HOMO_{\text{alkene}}$. The major 1,2-isomer results from the interaction between the large LUMO coefficient at the more electron-deficient methylene end of 2-aza-allyl anion

and large HOMO coefficient at the more electron-rich methylene carbon of alkene (Fig. 5.66). The steric factor makes the *exo* transition structure more favourable than *endo*, and the *exo* adduct (*trans* isomer) **5.46** is the major product.

5.4 STEREOCHEMISTRY OF [2+2] CYCLOADDITION REACTIONS

5.4.1 Photochemical [2+2] Cycloadditions

The $[\pi_{2s} + \pi_{2s}]$ cycloaddition is symmetry-forbidden thermally, but symmetry-allowed photochemically. The supra/supra mode is geometrically highly favourable with two small π systems approaching easily in parallel planes. In the FMO picture (see Figs 3.30 and 3.31), HOMO/HOMO and LUMO/LUMO interactions are presumably strong as the interacting orbitals are very close in energy. This may also lead to the formation of an exciplex (**excited complex**) or excimer (**excited dimer**) as an intermediate and lead to a stepwise photochemical pathway. The concerted bonding can result only from a singlet excited state. The triplet excited state [obtained by intersystem crossing (ISC) or by sensitization] would involve a spin inversion barrier to concerted addition, and hence the triplet state reactions would follow a stepwise mechanism.

The [2+2] cycloaddition of alkenes provides a cyclobutane with a maximum of four stereocentres. The dimerization of (*Z*)- and (*E*)-2-butenes are shown in Fig. 5.67.⁵⁴

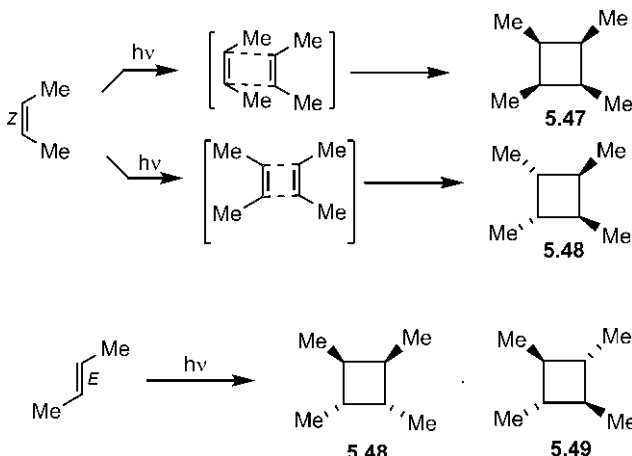


Fig. 5.67 [2+2] Dimerization of (*Z*)-2-butene and (*E*)-2-butene.

(*Z*)-2-Butene gives **5.47** and **5.48** while (*E*)-2-butene yields **5.48** and **5.49**. The cycloaddition is stereospecific for a $[\pi_{2s} + \pi_{2s}]$ mechanism. However, the stereospecificity is observed at low conversions (short reaction times). At longer reaction times, *E*-*Z* isomerization is involved and leads to a mixture of all stereoisomeric cyclobutanes **5.47–5.50** (Fig. 5.68).⁵⁴

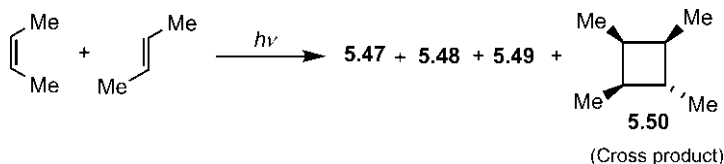


Fig. 5.68 [2+2] Cycloaddition between (*Z*)-butene and (*E*)-butene.

The mechanism of a photochemical cycloaddition is not quite simple. The observation of stereospecificity indicates that the reaction is most likely to be concerted; however, it is not certain, the reaction may be stepwise. For example, a cross addition of (*E*)-stilbene to tetramethylethylene gives a *trans* product showing high stereospecificity (Fig. 5.69).⁵⁵ However, the reaction is not concerted. It has been shown that the cycloaddition proceeds through the formation of a singlet exciplex. Collapse of the exciplex either to the cycloadduct directly or to a diradical which subsequently undergoes ring closing faster than bond rotation, can explain the observed stereospecificity.

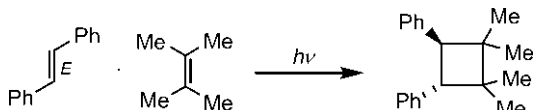


Fig. 5.69 Photocycloaddition of (*E*)-stilbene with tetramethylethylene.

The photochemical retro-cycloaddition can also proceed stereospecifically, as shown in Fig. 5.70. It is seen that *cis* and *trans* stereochemistry at the ring junction of the substrates are retained in the 12-membered ring products. It is likely that the cycloreversion proceeds through a concerted $[\sigma_{2s} + \sigma_{2s}]$ mechanism.⁵⁶ Note that the large 12-membered ring can accommodate a triple bond and *E* or *Z* double bond.

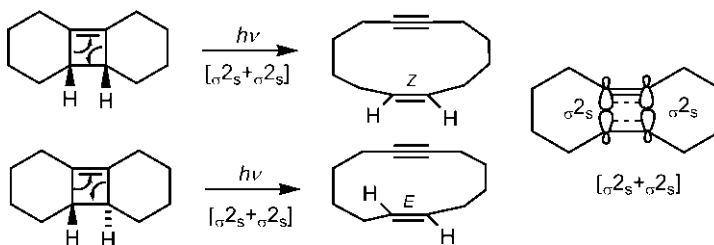


Fig. 5.70 Stereospecificity of photochemical [2+2] retro-cycloaddition.

Intramolecular photocycloadditions are very useful synthetically.^{57,58} These can give highly strained polycyclic and cage systems, which are not easily obtainable by other routes.^{59,60} Some examples of intramolecular photocycloadditions are shown in Fig. 5.71. The cycloaddition is facilitated by the molecular geometry imposing an interaction between the π orbitals on the bottom face of the molecules.

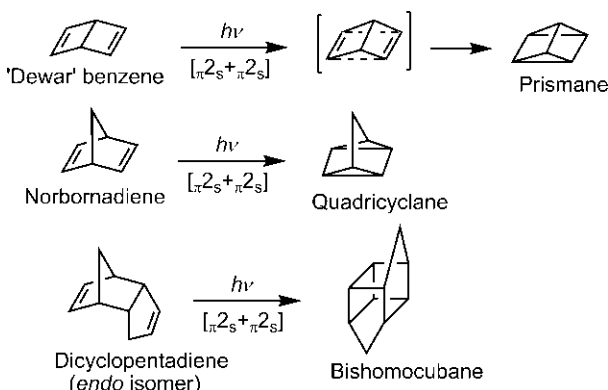


Fig. 5.71 Examples of intramolecular [2+2] photocycloadditions.

The cage structures are regarded as energy stores since catalytic or thermal cleavage regenerates starting materials with the release of energy. The trivial names of three cage structures 5.51–5.53 are given below.



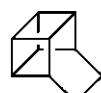
5.51

Cubane
(cf. cube)



5.52

Homocubane
(higher homologue)



5.53

Basketane
(cf. basket)

The synthesis of cage molecules can be performed via intramolecular [2+2] photocycloaddition. A synthesis of cubane is shown in Fig. 5.72.⁶¹ The dibromoquinone undergoes a Diels–Alder reaction with cyclobutadiene generated in situ by the oxidative decomposition of its iron complex (see Fig. 7.15B) with ceric ion to form an *endo* adduct in which the two alkene units are suitably oriented one above the other for efficient [2+2] photocycloaddition. The photoadduct is converted to cubanedicarboxylic acid by the Favorskii rearrangement. Thermal decarboxylation via *t*-butyl perester gives cubane. The decarboxylation of the perester proceeds by a radical mechanism and cubane is formed by the abstraction of hydrogen from solvent (cumene).

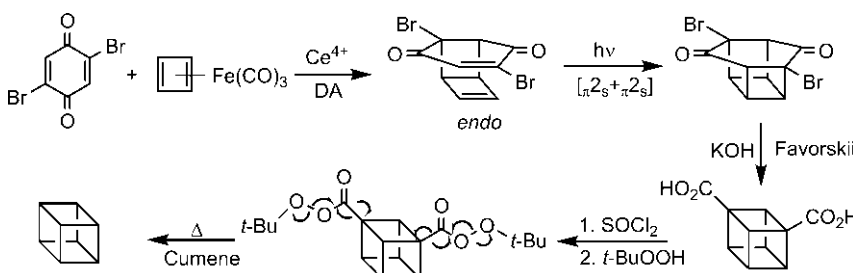


Fig. 5.72 A synthesis of cubane.

A synthesis of basketene from cyclooctatetraene is shown in Fig. 5.73.⁶² The synthesis involves three key pericyclic steps: electrocyclic ring closing, Diels–Alder reaction and [2+2] photocycloaddition. The photocycloadduct

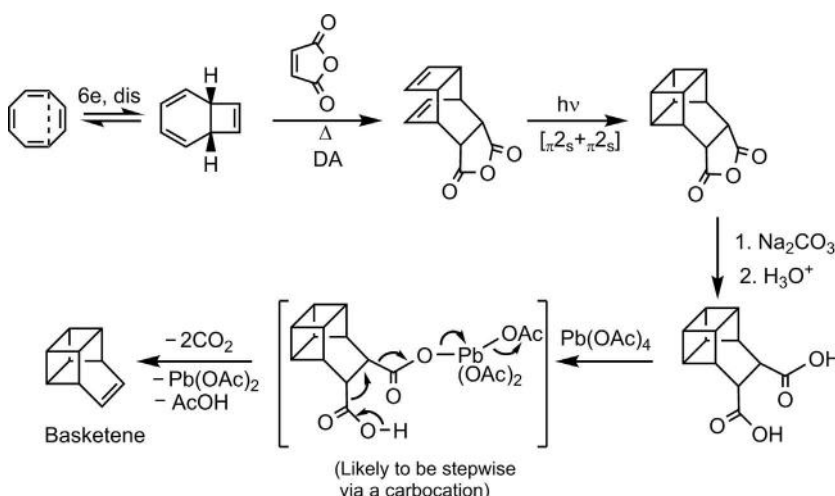


Fig. 5.73 Synthesis of basketene starting from cyclooctatetraene.

on hydrolysis and bis-decarboxylation with $\text{Pb}(\text{OAc})_4$ gives basketene. It is seen that the decarboxylation makes the maleic anhydride cycloaddition the synthetic equivalent of an acetylene addition.

Nonconjugated alkenes absorb light in the far-ultraviolet (far-UV) region ($\sim 190\text{--}220\text{ nm}$) which is not readily accessible experimentally. In the presence of sensitizer, the photocycloaddition can be carried out in more accessible UV region near 300 nm. The sensitized cycloaddition proceeds through a triplet excited state, and follows a stepwise radical pathway. For example, dimerization of norbornene in the presence of acetone as a sensitizer gives dimers (Fig. 5.74A).⁶³ If benzophenone is used instead of acetone, no sensitized cycloaddition takes place and a [2+2] photocycloaddition between benzophenone and norbornene gives an oxetane (Fig. 5.74B). The photocycloaddition of aldehydes or ketones with alkenes to produce oxetanes is known as Paterno–Büchi reaction.⁶⁴

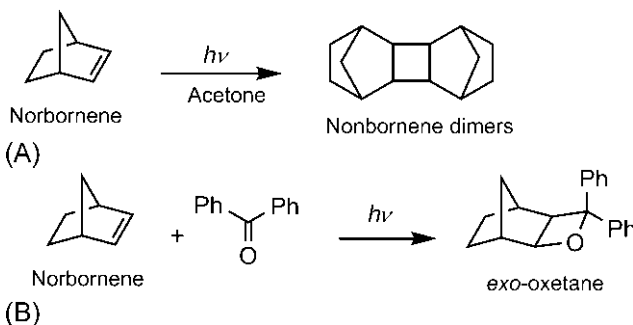


Fig. 5.74 (A) Photosensitized dimerization of norbornene; (B) Paterno–Büchi reaction between benzophenone and norbornene.

The mechanisms of the above reactions are shown in Fig. 5.75. Acetone as a sensitizer absorbs radiation and is excited to $n-\pi^*$ singlet state which by ISC goes to $n-\pi^*$ triplet state. The triplet excited state then excites the ground state norbornene to its $\pi-\pi^*$ triplet state by energy transfer when the excited acetone returns to its ground state. The combination of excited state norbornene with the ground state norbornene gives the norbornene dimer via a 1,4-diradical 5.54 (Fig. 5.75A). With benzophenone, a $n-\pi^*$ triplet state is readily obtained by the absorption of radiation and an efficient ISC but the triplet benzophenone instead of energy transfer combines with the ground state norbornene to give predominantly the *exo*-oxetane as approach from this side is less sterically hindered (Fig. 5.75B). The reaction proceeds via a diradical which may be preceded by the formation of an exciplex. If the triplet energy

of a ketone is comparable to or exceeds the triplet energy of an alkene, triplet energy transfer by the ketone to the ground state alkene can occur. An aliphatic ketone acetone has a high triplet energy ($E_T \sim 78 \text{ kcal mol}^{-1}$) and therefore transfers triplet energy to norbornene ($E_T \geq 74 \text{ kcal mol}^{-1}$) whereas the triplet energy of benzophenone ($E_T = 69 \text{ kcal mol}^{-1}$) is significantly less than that of norbornene and energy transfer does not occur. It may be mentioned that aliphatic ketones such as acetone can react with alkenes to form oxetanes but the picture is much more complicated owing to the significance of singlet state cycloaddition of acetone.

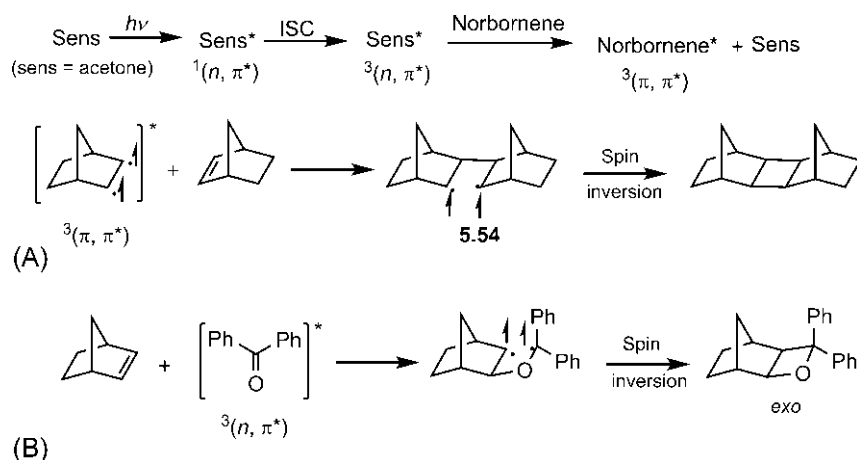
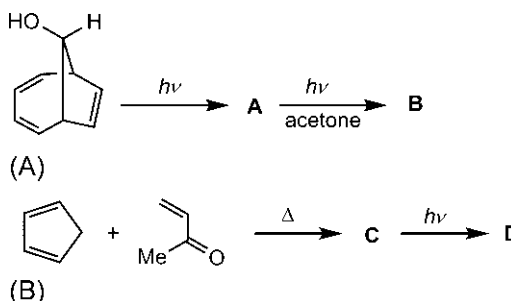


Fig. 5.75 Mechanism of (A) photodimerization of norbornene and (B) Paterno–Büchi reaction between benzophenone and norbornene in Fig. 5.74. ISC=intersystem crossing; $^1(n,\pi^*)$ and $^3(n,\pi^*)$ indicate singlet and triplet $n-\pi^*$ excited state, respectively, $^3(\pi,\pi^*)$ denotes triplet $\pi-\pi^*$ excited state.

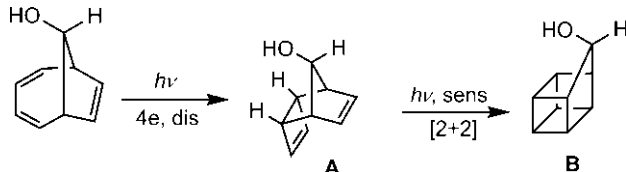
Problem 5.14

Give structures of **A–D** in the following schemes, and suggest mechanisms for their formation.

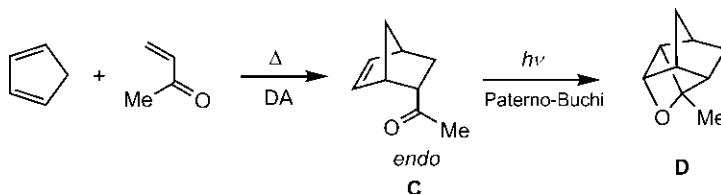


Answer

- (A) 4-Electron electrocyclic ring closing by disrotatory mode produces **A** which undergoes a sensitized photocycloaddition to give **B**.



- (B) The Diels–Alder reaction gives **C** which then undergoes an intramolecular Paterno–Büchi reaction to give **D**.



5.4.1.1 Photocycloadditions of α,β -Unsaturated Carbonyl Compounds

Photocycloadditions of α,β -unsaturated carbonyl compounds are particularly valuable in synthesis. As these compounds can absorb light at longer wavelengths (greater than 300 nm), sensitizers are not normally required in their reactions. In general, these cycloadditions are not pericyclic but stepwise, and involve triplet excited enones formed by ISC of the initial (n,π^*) singlet.^{65,66} The triplet excited state may be (n,π^*) and/or (π,π^*) depending on the substrate and the conditions employed. The reaction may involve an exciplex and/or a diradical intermediate as shown mechanistically in Fig. 5.76.

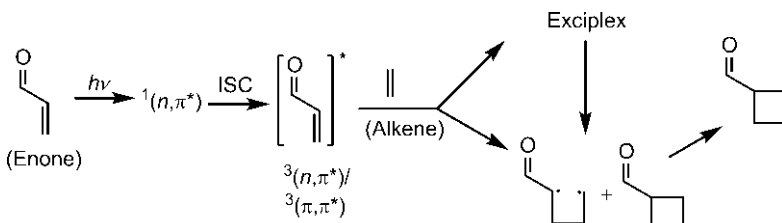


Fig. 5.76 Mechanism of triplet state photocycloaddition of an enone with an alkene.

These reactions can give regioisomeric products which are often termed as head-to-head and head-to-tail isomers. For example, photochemical dimerization of cyclopentenone gives a mixture of head-to-head and head-to-tail dimers (Fig. 5.77).⁶⁷

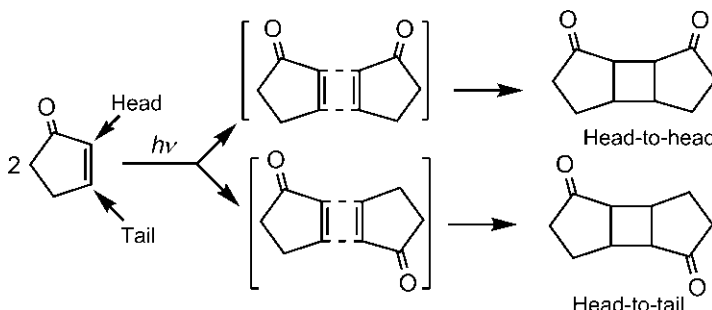


Fig. 5.77 Formation of regioisomers in photodimerization of cyclopentenone.

The [2 + 2] cycloaddition of an enone with an alkene is often regioselective and stereoselective. An electron-rich alkene generally produces a head-to-tail isomer as major product while head-to-head isomer is preferred with an electron-deficient alkene. The regioselectivity and stereoselectivity of the photocycloadditions of α,β -unsaturated carbonyl compounds are illustrated with the following examples.

First, we consider a cycloaddition of cyclohexenone with isobutene. This is the first step in Corey's synthesis of caryophyllene.^{68,69} The major product is a head-to-tail regioisomer with *trans* ring fusion (Fig. 5.78).

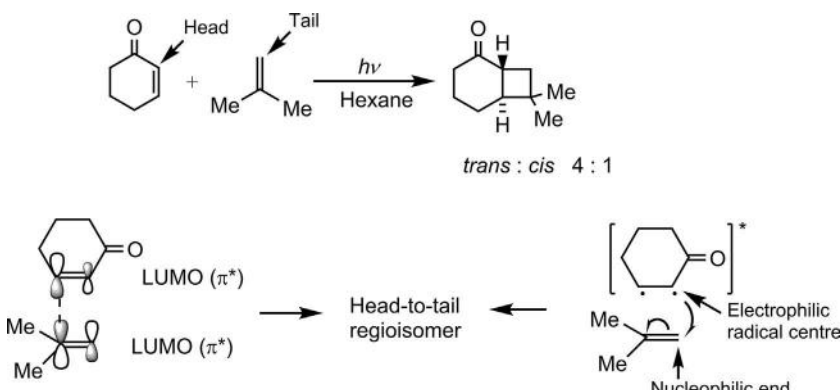


Fig. 5.78 Regioselectivity and stereoselectivity in photocycloaddition of cyclohexenone with isobutene.

The regioselectivity can be explained in terms of large/large interaction in the appropriate frontier orbitals. In photochemical reaction, the frontier orbital interactions involve HOMO/HOMO and LUMO/LUMO interactions (see Fig. 3.30). The enone is a *z*-substituted alkene, for which HOMO is slightly but LUMO is strongly polarized. The regioselectivity would therefore be governed more by the LUMO/LUMO interaction. As shown in Fig. 5.78, large/large interaction leads to a head-to-tail adduct as a major regioisomer. Note that isobutene, being an *x*-substituted alkene, has large LUMO coefficient at the substituted carbon. It is pertinent to mention that the regioselectivity is determined primarily by the leading bond formed between two atoms with large coefficients; therefore, it may not be important whether the other bond is formed at the same time (pericyclic cycloaddition) or at a different time (stepwise cycloaddition). The arguments for regioselectivity based on coefficients seem to work for both pericyclic and stepwise cycloadditions. Further, the excited state of the cyclohexenone seems to be a (π, π^*) triplet. The excited state with twisted geometry (see Fig. 1.11) behaves like a diradical. The radical centre attached to the carbonyl group (head) is electrophilic and would preferably bond with the nucleophilic end (tail) of the alkene giving preferentially a head-to-tail adduct (Fig. 5.78). The stereoselectivity of the reaction can also arise from the twisted excited state of cyclohexenone. It is possible that an exciplex with a highly twisted character, which may approach to assume a *trans* structure, is involved and leads to the preferential formation of the *trans*-fused product.

Next, we consider a photocycloaddition of a cyclohexenone with a cyclobutene bearing CN substituent. The major product is *exo* diastereomer of a head-to-head regioisomer (Fig. 5.79).⁷⁰ Note that in *exo* isomer, the terminal six-membered and four-membered rings are *anti* to the middle cyclobutane ring formed.

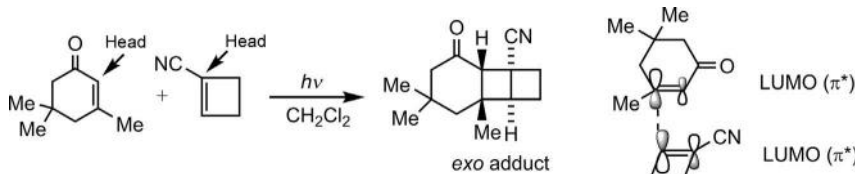


Fig. 5.79 Photocycloaddition of a cyclohexenone with a cyclobutene and FMO interaction for its regioselectivity.

As before, the preferential formation of a head-to-head isomer is obtained from the leading bond formed between two large LUMO coefficients (Fig. 5.79). The observed regioselectivity can also be accounted for by the preferred interaction between the nucleophilic radical centre (tail) of the

excited cyclohexenone with the electrophilic β end (tail) of cyclobutene (Fig. 5.80). The cycloaddition is stepwise through a diradical intermediate, and bond rotation can occur before spin inversion to produce a mixture of diradical species **5.55** and **5.56** for *exo* and *endo* ring closures (Fig. 5.80). The stereoselectivity is in favour of thermodynamically more stable *exo* (*anti*) cyclobutane derivative.

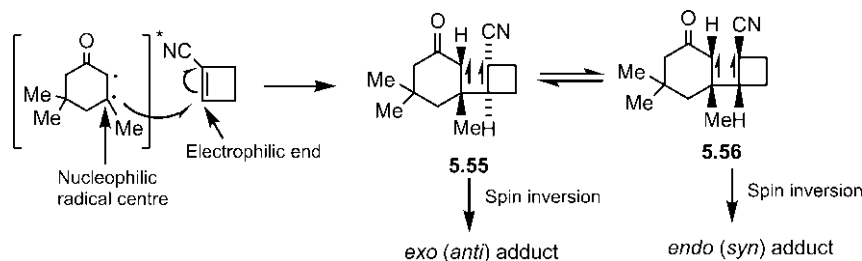


Fig. 5.80 Mechanism of photocycloaddition in Fig. 5.79.

In intramolecular photocycloadditions, conformational constraints would determine the regioselectivity with the initial C—C bond formed between the nearer ends of the two components. For example, an intramolecular enone–alkene photocycloaddition of **5.57** involves a five-membered ring (not a six-membered) to give an *exo* product **5.58** (Fig. 5.81).^{71,72}

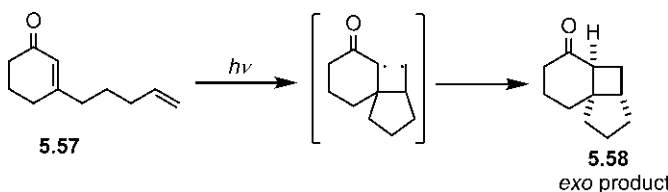
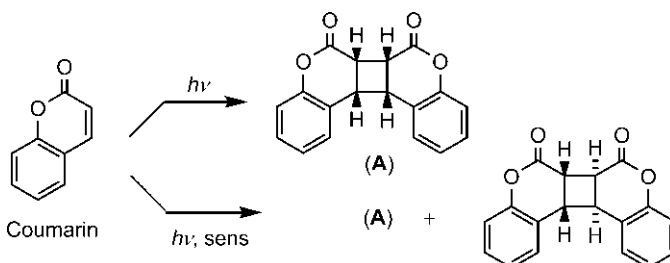


Fig. 5.81 An intramolecular [2+2] photocycloaddition.

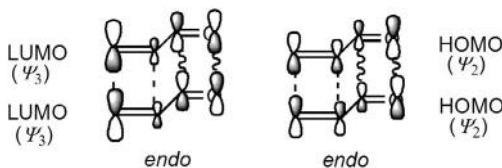
Problem 5.15

Account for the following observations.



Answer⁷³

On direct irradiation, coumarin dimerizes to give only head-to-head isomer with *endo* (*syn*) stereochemistry of the cyclobutane (**A**). However, in sensitized reaction, a mixture of *endo* (*syn*) and *exo* (*anti*) head-to-head dimers are obtained. Coumarin behaves as an enone. The important frontier orbitals for coefficient interaction involve LUMO/LUMO, and the large/large interaction leads to the preferential formation of a head-to-head (equivalently, tail-to-tail) regioisomer in both direct and sensitized reactions. A single stereoisomeric product in direct photochemical reaction could result if a singlet excited state is involved. The reaction may take a concerted pathway or proceed through a singlet exciplex leading to the cycloadduct directly or via a diradical when the cyclization is much faster than bond rotation. The formation of *endo* adduct (**A**) can be rationalized in terms of bonding secondary orbital interactions (wavy lines) in both LUMO/LUMO and HOMO/HOMO interactions as shown below. (See frontier orbital coefficients for the reference α,β -unsaturated carbonyl system acrolein in Problem 4.9.)



The sensitized cycloaddition is a stepwise triplet state reaction. Here the cyclization step involves a spin inversion barrier. Consequently, bond rotation would lead to a mixture of both *endo* and *exo* stereoisomers.

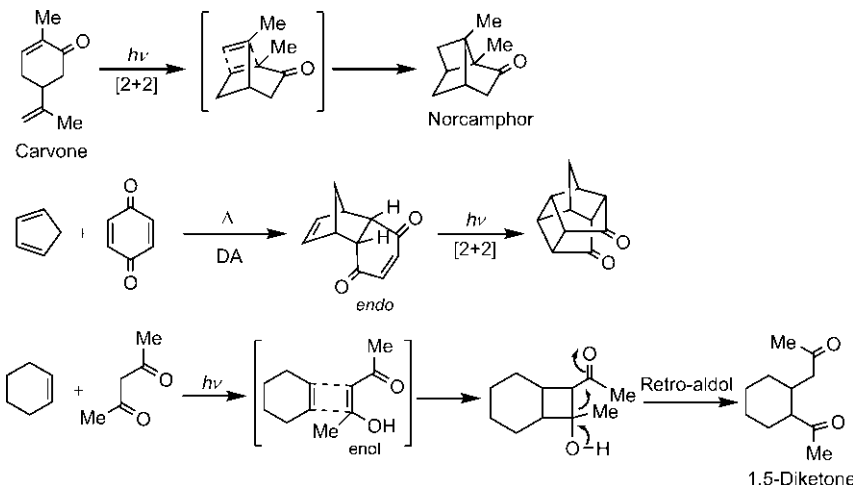


Fig. 5.82 Examples of [2+2] photocycloadditions in synthesis.

The photocycloadditions of α,β -unsaturated carbonyl compounds are quite useful in synthesis^{74–76} as illustrated with some examples in Fig. 5.82.

5.4.2 Thermal [2+2] Cycloadditions

The [2+2] cycloaddition is symmetry-allowed thermally under supra-antara mode but for two small alkene π components, this geometric approach is difficult to obtain. Owing to the forbidden nature of supra/supra cyclization and steric problems of supra/antara pathway, most thermal [2+2] cycloadditions are not concerted, and proceed by stepwise radical pathway^{77,78} or ionic pathway.^{79,80}

However, if the double bond is sufficiently twisted about its axis, the orbital overlap for $[\pi 2_s + \pi 2_a]$ process is possible. An example with twisted π bonds is illustrated in Fig. 5.83.^{1,81} The $[\pi 4_s + \pi 4_s]$ cycloaddition of *s-trans* butadiene to benzene is a symmetry-allowed photochemical reaction [total number of $(4q+2)_s$ and $(4r)_a$ components is zero] which gives, among others, a cycloadduct **5.59** in which the *trans* (*E*) double bond is necessarily twisted by constraints within the molecule. This *trans*-alkenic adduct **5.59** dimerizes spontaneously by $[\pi 2_s + \pi 2_a]$ process to give the dimer **5.60**, and also undergoes Diels–Alder reaction with butadiene to give **5.61**. The dimerization is stereospecific. A molecule of *trans* alkene as a $\pi 2_s$ component leads to *trans* H's, and the other molecule as a $\pi 2_a$ component gives rise to *cis* H's in the ring junctions of the dimeric adduct **5.60**. The *trans* alkene also produces a *trans* ring junction in the Diels–Alder adduct **5.61**.

The thermal retro-cycloaddition can also proceed stereospecifically. The *exo*, *exo*-2,4-dimethylbicyclobutane gives (*E,Z*)-2,4-hexadiene while *exo*,

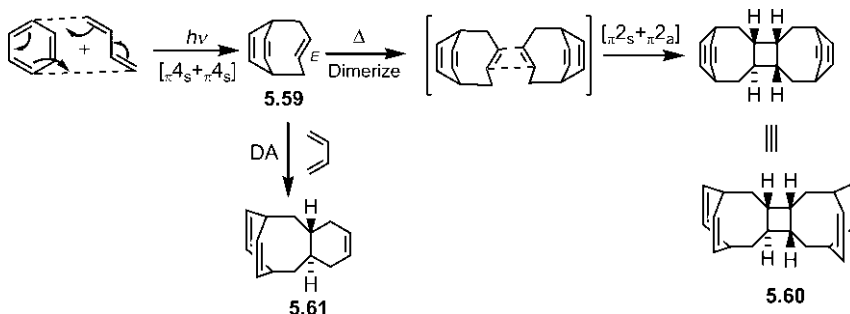


Fig. 5.83 $[\pi 2_s + \pi 2_a]$ Dimerization in a photocycloaddition of benzene and butadiene.

endo isomer produces (*E,E*) isomer of hexadiene (Fig. 5.84).⁸² These results suggest that the reactions proceed by a concerted [$\sigma_2s + \sigma_2a$] mechanism.

The bicyclobutane system allows suprafacial and antarafacial interactions of the breaking σ bonds in the transition structure (Fig. 5.85). (Use of the

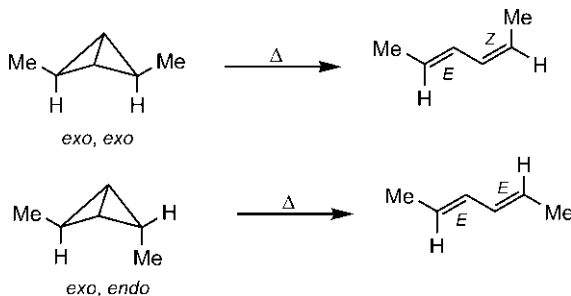


Fig. 5.84 $[\sigma_2s + \sigma_2a]$ Retro-cycloaddition of stereoisomeric bicyclobutanes.

molecular model would be helpful.) The σ_{2a} and σ_{2s} components (2–3 and 1–4 bonds) lead to inversion at C-2 (old bond cleavage and new bond formation involve different lobes, cf. S_N2 mechanism) and retention at C-4 (old bond cleavage and new bond formation involve same lobe, cf. S_Ni mechanism), respectively. For the *exo, exo* isomer, inversion at C-2 (Me/bond a: *cis*) leads to (Me/bond a: *trans*) to form *E* double bond whereas retention at C-4 (Me/bond a: *cis*) gives (Me/bond a: *cis*) to produce *Z* double bond. In a similar fashion, *exo, endo* isomer gives *E, E* double bonds.

The $[\pi_{2s} + \pi_{2a}]$ cycloaddition is possible when the two alkenes approach in orthogonal fashion (Fig. 5.86).

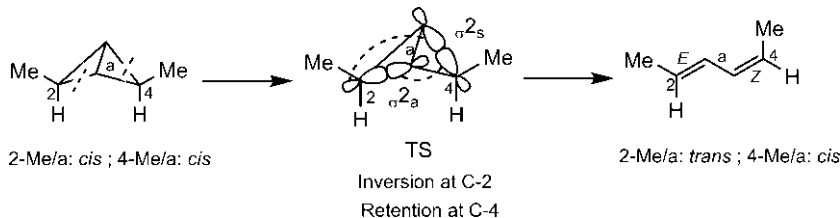


Fig. 5.85 Mechanism of retro-cycloaddition in Fig. 5.84. The 1–3 bond at the ring fusion in the bicyclobutane is labelled a.

However, inefficient orbital overlap and steric crowding in the crossed transition structure would not make this process quite favourable. If the TS

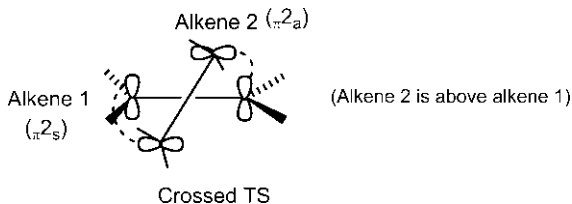
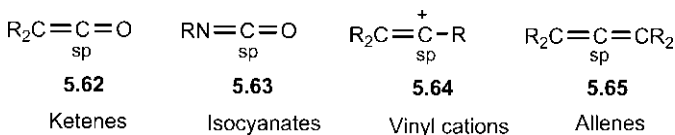


Fig. 5.86 Crossed transition structure for orthogonal approach of two alkenes.

for orthogonal approach could be stabilized by reducing steric strain and by better orbital overlaps, concerted addition might occur. This happens when one end of an alkene is a sp carbon (sterically less demanding), and the alkene has an orthogonal π bond or p orbital for more effective orbital interactions. Such alkene π systems are cumulenes or related systems such as ketenes **5.62**, isocyanates **5.63**, vinyl cations **5.64** and allenes **5.65**.



5.4.2.1 Cycloadditions of Ketenes

Cycloadditions of ketenes with alkenes yield cyclobutanone products.⁸³ Similar to a dienophile in Diels–Alder reaction, the alkene component in ketene cycloaddition is referred to as a ketenophile.

Mechanistic Analysis

Many ketene cycloadditions are pericyclic in which the alkene acts as a π^2_s component and the ketene as a π^2_a component. The favourable frontier orbital interaction is $LUMO_{\text{ketene}}/\text{HOMO}_{\text{alkene}}$ interaction. It has been suggested by Woodward and Hoffmann¹ that the transition structure would be further stabilized by the bonding secondary orbital interactions (wavy lines) between the lobes of alkene HOMO and the orthogonal p orbital of $C=O$ (π^*) in ketene LUMO (Fig. 5.87). The reaction will be faster when ketene is more electron deficient (lower energy LUMO) and the alkene is more electron rich (higher energy HOMO).

The ketene cycloaddition can also be treated as a [2 + 2 + 2] cycloaddition in which both ketene π bonds are involved. In this analysis, the reaction is represented as a symmetry-allowed $[\pi^2_s + \pi^2_s + \pi^2_s]$ or $[\pi^2_s + \pi^2_a + \pi^2_a]$.

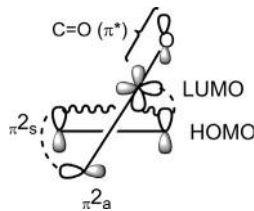


Fig. 5.87 FMO interactions between HOMO of alkene and LUMO of ketene. Wavy lines indicate secondary orbital interactions.

cycloaddition (Fig. 5.88).⁸⁴ The alkene approaches at an angle to the ketene, and the transition structure is similar to that for $[\pi_{2s} + \pi_{2a}]$ mode but less tight. The TS shows the developing overlaps for the formation of two σ bonds and a π bond. Note that the old $\text{C}=\text{O}$ π bond changes to a new $\text{C}=\text{O}$ π bond (marked *) using a central carbon p orbital originally involved in $\text{C}=\text{C}$ bond of ketene.

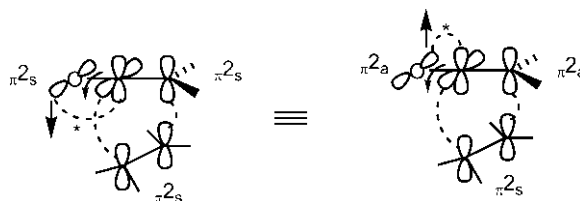


Fig. 5.88 Ketene cycloaddition as a $[\pi_{2s} + \pi_{2s} + \pi_{2s}]$ or $[\pi_{2s} + \pi_{2a} + \pi_{2a}]$ cycloaddition.

Stereospecificity of Ketene Cycloaddition

The suprafacial addition to the alkene (ketenophile) in ketene cycloaddition leads to its stereospecificity. The relative stereochemistry of alkene substituents is retained in the product. This is illustrated with the cycloadditions of dichloroketene with (*Z*)- and (*E*)-cyclooctenes (Fig. 5.89).⁸⁵ The (*Z*) alkene leads to a *cis* ring junction while the (*E*) alkene produces a *trans* ring fusion.

Dichloroketene is generated *in situ* by dehydrohalogenation of dichloroacetyl chloride with a hindered base triethylamine. The elimination reaction proceeds by E1cB mechanism (draw the mechanism). Dichloroketene is particularly reactive as the C—Cl bonds exert electron-withdrawing effects by negative hyperconjugation with $\text{C}=\text{O}$ (C—Cl σ bond and carbonyl π orbitals are in the same plane) and thereby lowers the energy of LUMO of the ketene.

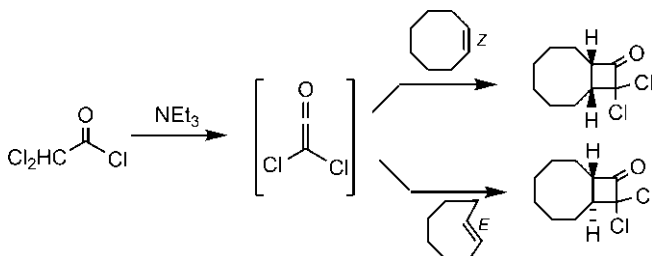


Fig. 5.89 Stereospecificity of ketene cycloaddition with (*Z*)- and (*E*)-cyclooctenes.

The cycloadducts can be reduced by zinc and acetic acid to give cyclobutanones, which are the products of addition of ketene itself.

Regioselectivity of Ketene Cycloaddition

The cycloaddition of dimethylketene with a (*Z*)-enol ether shows regioslectivity in favour of the regioisomer **5.66** (Fig. 5.90).⁸⁶ The reaction is also stereospecific with respect to the alkene.

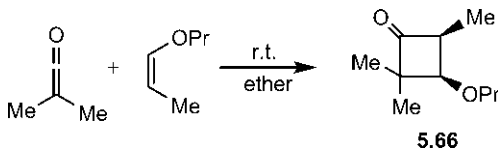


Fig. 5.90 Regioselectivity of ketene cycloaddition.

The regioselectivity can be explained using frontier orbital theory. The frontier orbital energies for ketene⁸⁷ are: HOMO – 12.4 eV, LUMO 3.8 eV. The alkene is electron rich (α -substituted). The frontier orbital energy separations between a ketene and an α -substituted alkene are estimated to be 12.8 eV for $\text{LUMO}_{\text{ketene}}/\text{HOMO}_{\text{alkene}}$ pair and 15.4 eV for the other pair. The more important interaction is therefore $\text{LUMO}_{\text{ketene}}/\text{HOMO}_{\text{alkene}}$ interaction. The formation of leading bond (labelled 1) between large LUMO coefficient on the central carbon of ketene and large HOMO coefficient on the alkene carbon β to a stronger electron-donating OPr substituent gives **5.66** (Fig. 5.91A). Note that the ketene LUMO with the terminal carbon bearing a very small coefficient is primarily the LUMO (π^*) of C=O.

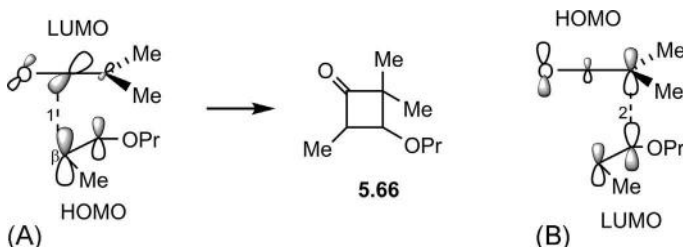


Fig. 5.91 FMO picture in terms of (A) $\text{LUMO}_{\text{ketene}}/\text{HOMO}_{\text{alkene}}$ and (B) $\text{HOMO}_{\text{ketene}}/\text{LUMO}_{\text{alkene}}$ interactions for regioselective ketene cycloaddition in Fig. 5.90.

Ketene cycloaddition is quite asynchronous. Calculations indicate that C—C bonding to the carbonyl carbon is more advanced ($1.71\text{--}1.78\text{ \AA}$) than the other C—C bond ($2.43\text{--}2.47\text{ \AA}$).⁸⁸ As the terminal carbon in ketene LUMO has a very small coefficient, its contribution to the formation of the second C—C bond appears to be minimal. It is suggested that the second C—C bond (labelled 2) develops mainly from the other frontier orbital interaction between $\text{HOMO}_{\text{ketene}}$ and $\text{LUMO}_{\text{alkene}}$ due to more effective coefficient interaction (Fig. 5.91B). Note that ketene HOMO resembles HOMO (Ψ_2) of allyl anion as ketene $\text{C}=\text{C}$ is conjugated to a lone pair on oxygen ($\text{C}=\text{C}-\ddot{\text{O}}$).

Fig. 5.92 shows two more examples of the regioselectivity of ketene cycloadditions with an α -substituted alkyne ketenophile⁸⁹ and a γ -substituted doubly vinylogous alkene ketenophile.⁹⁰ The regioselectivity arises from the leading bond formed between large LUMO coefficient on

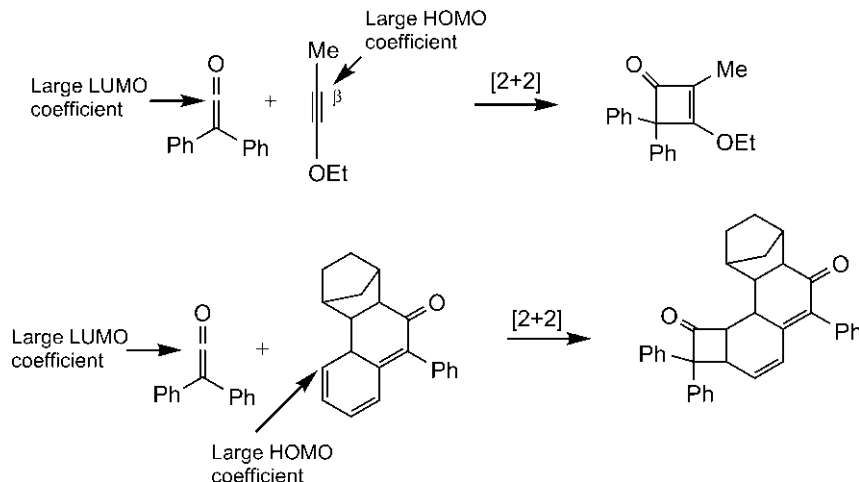


Fig. 5.92 Regioselectivity of ketene cycloaddition with an α -substituted alkyne and a γ -substituted doubly vinylogous alkene ketenophiles.

the central carbon of ketene and large HOMO coefficient on the alkyne β -carbon with respect to stronger electron-donating OMe group in x-substituted ketenophile, and on the terminal carbon of the conjugated chain of the z-substituted ketenophile.

Ketenes can undergo cycloadditions with carbonyl compounds to produce β -lactones⁹¹ with expected regioselectivity as illustrated with benzoquinone in Fig. 5.93A. Ketene itself forms a dimer (β -lactone)^{92,93} easily; one molecule acts as an alkene component and the other as a carbonyl component (Fig. 5.93B). The substituted ketenes dimerize to give cyclobutane-1,3-dione when two alkene units undergo cycloaddition as shown also in Fig. 5.93B.⁹⁴ Here the head-to-tail regioselectivity is as expected from the frontier orbital interaction.

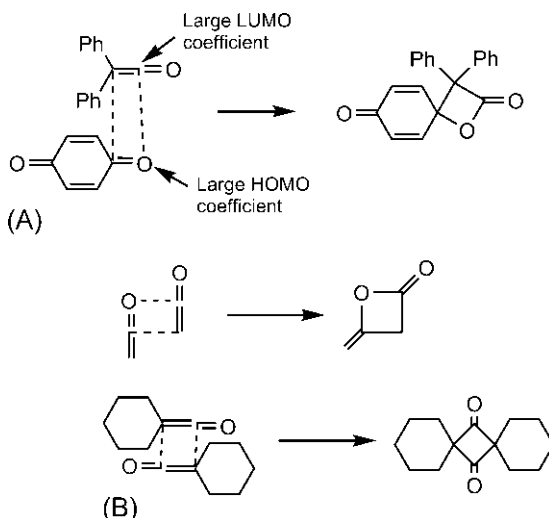
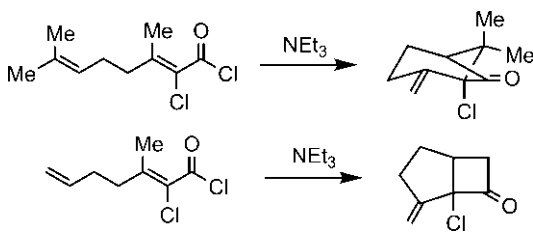


Fig. 5.93 Regioselectivity of ketene cycloadditions: (A) with benzoquinone and (B) in dimerization of ketene itself and a substituted ketene.

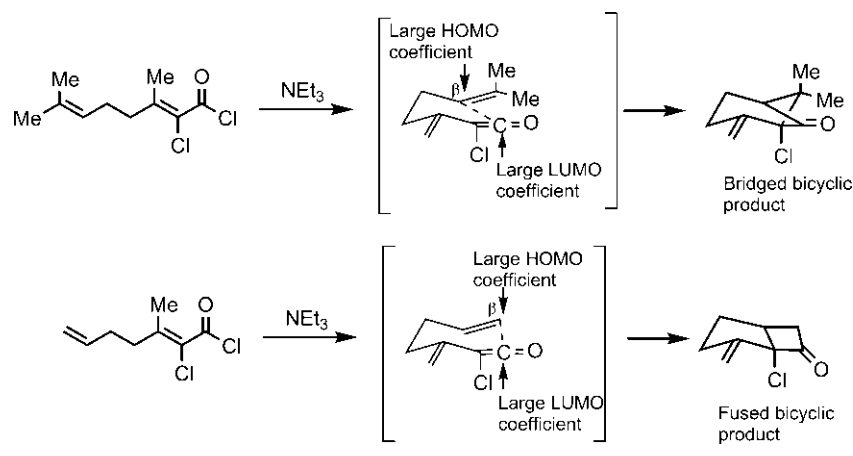
Problem 5.16

Intramolecular ketene cycloadditions⁹⁵ are synthetically very useful. Account for the regioselectivity of the following intramolecular cycloadditions.



Answer

Treatment of the acid chloride with a base (NEt_3) produces a chloroketene. Intramolecular cycloaddition of chloroketene takes place with the tethered alkene unit. The regioselectivity is governed by C—C bonding between the central carbon (large LUMO coefficient) of the ketene and the alkene end with larger HOMO coefficient. Electron-donating alkyl substituent raises HOMO coefficient on the β carbon.

**Stereoselectivity of Ketene Cycloaddition**

The cycloaddition of an unsymmetrical ketene with an unsymmetrical alkene gives predominantly the product in which bulky substituents are *cis* to each other.⁹⁶ For example, the reaction between ethoxyketene and a monosubstituted alkene produces the *cis* cyclobutanone **5.67** (Fig. 5.94). The reaction is also regioselective (R is vicinal to OEt).

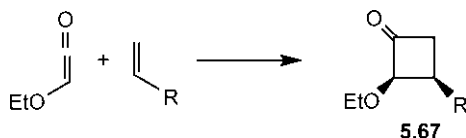


Fig. 5.94 Stereoselectivity of ketene cycloaddition.

The stereoselectivity of the reaction arises from the more stable crossed transition structure in which OEt and R are maximally separated (Fig. 5.95). As the twisted cyclobutanone ring moves to nearly planar form, R and OEt end up on the same face of the ring (use a model to see this). The reaction is under kinetic control and gives thermodynamically less stable *cis* product.

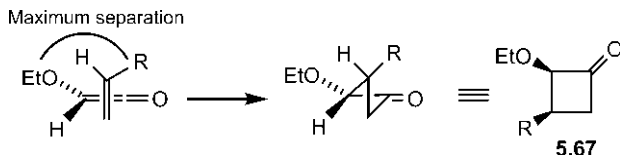


Fig. 5.95 Mechanism of stereoselective ketene cycloaddition in Fig. 5.94.

Another example is a cycloaddition of ethylketene with cyclopentadiene which yields the cyclobutanone **5.68** with Et in the more hindered *endo* position (Fig. 5.96).⁹⁷ The lower energy [2+2+2] transition structure **5.69** has larger Et pointing away from the diene. As the product is reached, Et moves to the *endo* position.

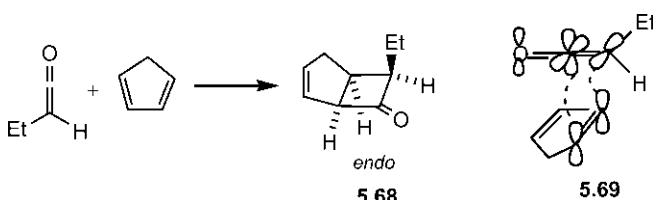
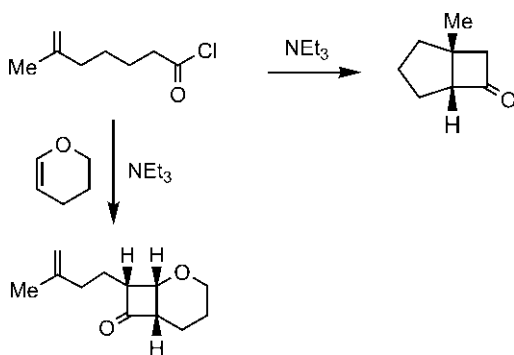


Fig. 5.96 Formation of *endo* product in cycloaddition of ethylketene with cyclopentadiene.

Problem 5.17

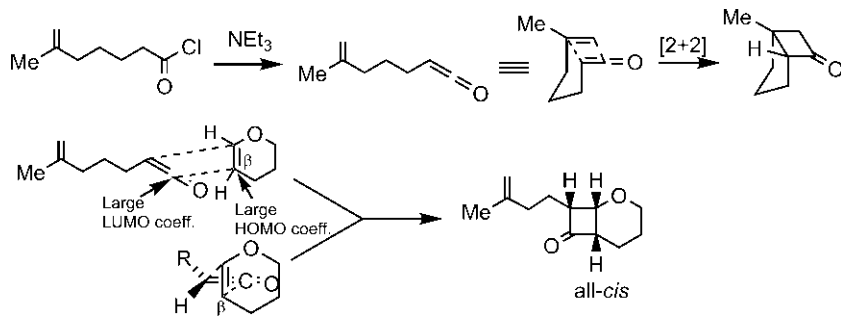
Explain the following observations.



Answer⁹⁸

Treatment of the acid chloride with base (NEt₃) produces a chloroketene. In the absence of other alkene, intramolecular cycloaddition takes place producing a bicyclic ketone with *cis* (Me/H) ring junction. However, in

the presence of a reactive alkene (an enol ether), intermolecular ketene cycloaddition occurs. The regioselectivity is governed by C—C bonding between the central carbon (large LUMO coefficient) of the ketene and the alkene end with larger HOMO coefficient. Electron-donating oxygen raises coefficient on the β carbon in the enol ether. The reaction is stereospecific with respect to the alkene and also stereoselective forming all-*cis* product (the large alkyl group and six-membered ring end up on the same face of the middle cyclobutanone ring).



Periselectivity in Ketene Cycloaddition

Two symmetry-allowed pathways are possible for cycloaddition reaction between a diene and a ketene, namely, $[\pi 2_s + \pi 2_a]$ and $[\pi 4_s + \pi 2_s]$ (Diels–Alder) as shown, for example, with the reaction between cyclopentadiene and dichloroketene in Fig. 5.97. However, the ketene cycloaddition exhibits periselectivity, the $[2+2]$ reaction is favoured over $[4+2]$ reaction.⁹⁹ Note also the regioselectivity arising from the preferred bonding between the large LUMO coefficient on the central carbon of ketene and the larger HOMO coefficient at C-1 of the diene.

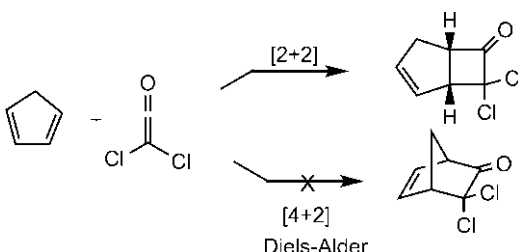


Fig. 5.97 Possible $[2+2]$ and $[4+2]$ pathways for cycloaddition of cyclopentadiene to dichloroketene.

The periselectivity of ketene cycloaddition can be explained using FMO theory. The Diels–Alder reaction between cyclopentadiene and dichloroketene requires HOMO of diene to interact with LUMO of ketene. However, the alkene unit in ketene is a poor dienophile because it is not only orthogonal to C=O but also conjugated to the oxygen lone pair (C=C— $\ddot{\text{O}}$), thereby resembles an α -substituted alkene with relatively high-energy LUMO. Therefore the Diels–Alder reaction of cyclopentadiene with ketene as alkene dienophile is not favourable. The orthogonal C=O unit in ketene on the other hand has low-energy LUMO with large LUMO coefficient on carbonyl carbon which favours the formation of [2+2] adduct (see Fig. 5.91).

It is possible that ketene C=O would act as a heterodienophile in the Diels–Alder reaction but no hetero-Diels–Alder product is observed in the above reaction. However, in the reaction between diphenylketene and cyclopentadiene, there is evidence that a hetero-Diels–Alder adduct is formed which can subsequently undergo a [3,3] Claisen rearrangement to give the [2+2] product (Fig. 5.98).¹⁰⁰

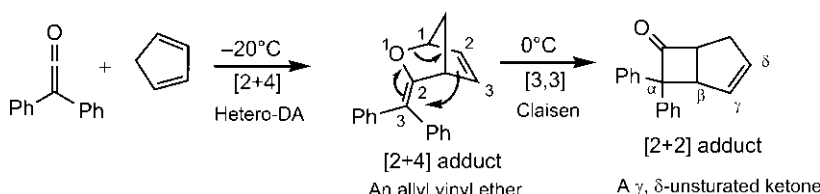


Fig. 5.98 Formation of [2+2] product via a Claisen rearrangement of [2+4] adduct.

Interestingly, an initial [2+2] adduct can also transform into a [4+2] product by a [3,3] retro-Claisen rearrangement.¹⁰¹ For example, as shown in Fig. 5.99, 1-methoxybutadiene and diphenylketene undergo a [2+2] cycloaddition at 0°C to give an adduct, which on warming to 25°C forms a [4+2] hetero-Diels–Alder product by a retro-Claisen rearrangement being facilitated by relief of ring strain and formation of a stable double bond.

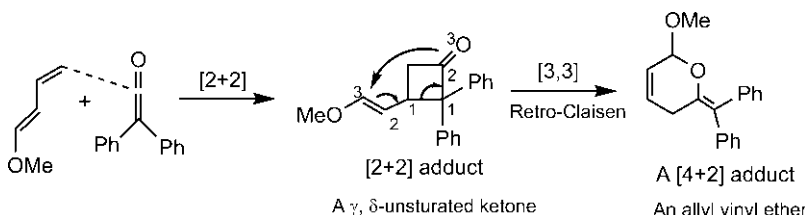
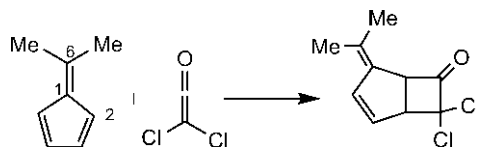


Fig. 5.99 Formation of a [4+2] product via a retro-Claisen rearrangement of [2+2] adduct.

Problem 5.18

Rationalize the periselectivity of the following cycloaddition of ketene.

**Answer**

Two possible symmetry-allowed pathways are $[\pi_{6s} + \pi_{2a}]$ and $[\pi_{2s} + \pi_{2a}]$. Dichloroketene acts as a π_{2a} component and uses its LUMO. Dimethylfulvene might then act as a π_{6s} or π_{2s} component, using its HOMO. If the fulvene is to react as a π_6 system, it must interact through C-2 and C-6. But the fulvene HOMO has a zero coefficient at C-6 (see Fig. 4.80). Therefore fulvene acts as a π_{2s} component in the cycloaddition with ketene, and forms a [2+2] adduct.

Stepwise Mechanism of Ketene Cycloaddition

Many but not all ketene cycloadditions are concerted. Some cycloadditions may be stepwise involving a zwitterionic intermediate. For example, cycloaddition of an imine with a ketene (referred to as Staudinger reaction) is stepwise (Fig. 5.100).¹⁰² This reaction provides a convenient approach to β -lactam antibiotics.

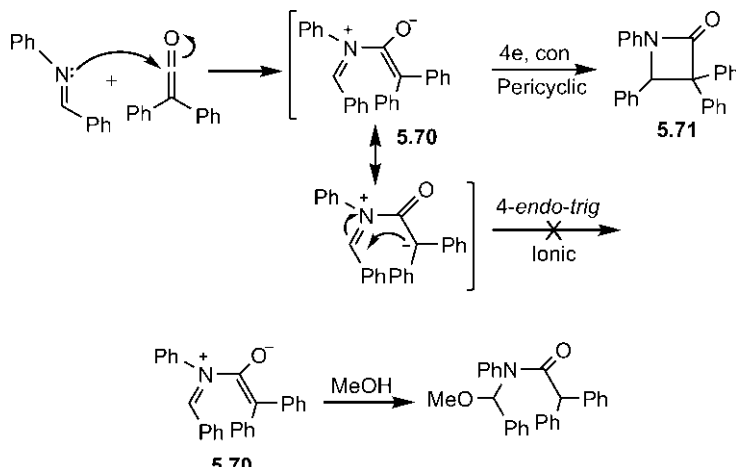


Fig. 5.100 Stepwise ketene cycloaddition with an imine in a Staudinger reaction.

The imine acts as a nucleophile with a lone pair on nitrogen, and attacks readily the electrophilic carbonyl group of ketene to form an intermediate **5.70**. Subsequent electrocyclic ring closure gives the β -lactam product **5.71**. The intermediate can be trapped by methanol providing evidence for its formation.¹⁰³ The cyclization step is pericyclic, and not ionic because the ionic bonding between nucleophilic and electrophilic carbons entails unfavourable 4-*endo-trig* ring closure. The pericyclic mechanism is not subject to such restriction of Baldwin rules.

The stereochemistry of the β -lactam formed in a Staudinger reaction is also consistent with the conrotatory electrocyclization step, as shown in Fig. 5.101. Attack of nitrogen lone pair on the carbonyl group of ketene takes place preferentially from the less hindered side opposite to OMe group and the resultant intermediate undergoes a conrotatory ring closure to give a *cis* β -lactam.

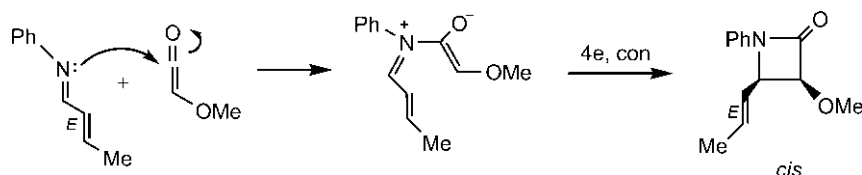


Fig. 5.101 Stereochemistry of a β -lactam formed in the Staudinger reaction.

5.4.2.2 Cycloadditions of Isocyanates, Vinyl Cations and Allenes

Isocyanates are similar to ketenes. The cycloaddition of an alkene with an isocyanate gives a β -lactam ring.^{104,105} For example, the reaction of cyclopentadiene with chlorosulphonyl isocyanate produces a β -lactam **5.72**. The isocyanate bearing an electron-withdrawing SO₂Cl group has a lower energy LUMO and interacts quite favourably with relatively high energy HOMO of cyclopentadiene. The regioselectivity arises from the large/large combination of electron-deficient carbonyl carbon of the isocyanate with more electron-rich end of the alkene unit of cyclopentadiene. After cycloaddition, the SO₂Cl group can be easily removed by mild hydrolysis to sulphonic acid followed by desulphonation to give the β -lactam **5.73** (Fig. 5.102).

In vinyl cations, the cationic centre (sp carbon) with two orthogonal p orbitals is similar to carbonyl carbon of ketenes. The vacant p orbital of vinyl cation LUMO could stabilize the crossed transition structure by secondary orbital overlaps (wavy lines) (Fig. 5.103) in a manner similar to ketene

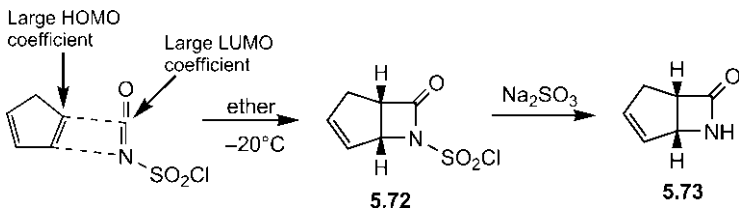


Fig. 5.102 Formation of a β -lactam by [2+2] cycloaddition of an isocyanate with cyclopentadiene.

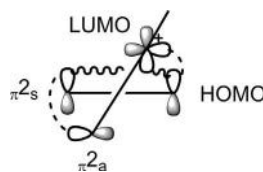


Fig. 5.103 FMO interactions between HOMO of alkene and LUMO of vinyl cation.

cycloaddition (see Fig. 5.87). The vinyl cation acts as a π^2_a component and alkene as a π^2_s component.

Vinyl cations, as reactive intermediates, can be generated by electrophilic addition to an alkyne or an allene. The cycloadditions of vinyl cations are illustrated in Fig. 5.104. Fig. 5.104A shows a Smirnov–Zamkow reaction which gives the cyclobutene product from 2-butyne and chlorine in the presence of a Lewis acid.¹⁰⁶ In Fig. 5.104B, a cyclobutane is formed from allene and HCl.¹⁰⁷

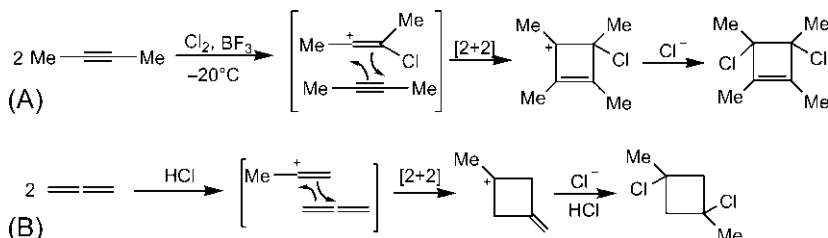


Fig. 5.104 Examples of vinyl cation cycloaddition with (A) an alkyne and (B) an allene.

Like ketenes, cycloaddition of allenes can also proceed by a concerted pathway, though a stepwise process involving diradical intermediate seems likely in some cases.¹⁰⁸ As the two C=C π bonds are orthogonal, an allene has a pair of HOMOs and a pair of LUMOs. The HOMO and LUMO energies of parent allene¹⁰⁹ are -8.8 and 8.7 eV, respectively, and relatively high.

With α -substituted allene (higher energy HOMO) and β -substituted alkene (lower energy LUMO), the cycloaddition is more favourable. The cycloaddition of dimethylallene with dimethyl maleate gives mainly *cis* isomer of a methylenecyclobutane while that with dimethyl fumarate yields mainly *trans* isomer (Fig. 5.105).¹¹⁰ The reaction shows a high level of stereospecificity and indicates a concerted mechanism with suprafacial addition to alkene. The reaction is also regioselective. The major regioisomer may arise from the interaction of unsubstituted end of allene possessing larger HOMO coefficient (Me group diminishes HOMO coefficient at the substituted end). It is also possible that steric factor plays a dominant role.

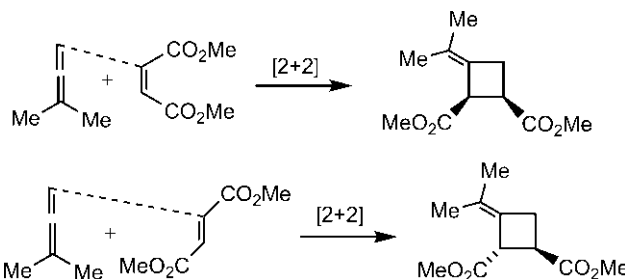


Fig. 5.105 Stereospecificity and regioselectivity of [2+2] allene cycloadditions.

Allenes can be chiral (see Section 2.2.1). Cycloaddition of optically active (*R*)-1,3-dimethylallene with acrylonitrile gives optically active adducts with (*R*) configuration (Fig. 5.106).¹¹¹ Similarly, (*S*)-1,3-dimethylallene gives optically active adducts with opposite configuration (*S*). These reactions reveal stereospecificity with respect to the allyl component; the two enantiomeric allenes lead to opposite configurations at the specified stereocentre of the product.

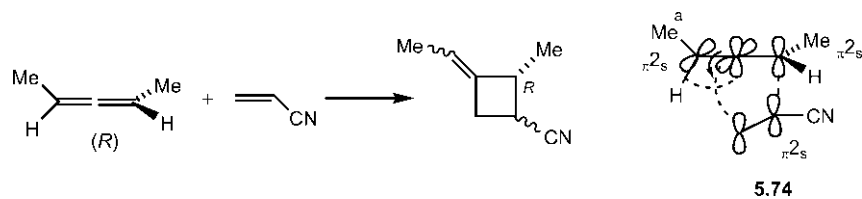


Fig. 5.106 Cycloaddition of optically active allene with acrylonitrile.

The formation of (*R*) product (Fig. 5.106) arises from the preferred (sterically favourable) $[\pi 2_s + \pi 2_s + \pi 2_s]$ transition structure 5.74 obtained by the approach of acrylonitrile to the allene from the side opposite to Me (marked a).

5.4.2.3 Cycloaddition of Singlet Vinyl Carbenes

Singlet vinyl carbene is a π -delocalized system with an orthogonal filled sp^2 orbital, and can act as a three-atom π_2 component in [2+2] cycloaddition with an alkene to produce a cyclopentene (Fig. 5.107). Note that singlet vinyl carbenes are 1,1-/1,3-dipoles without octet stabilization; the [2+2] cycloadditions of singlet vinyl carbenes ought not to be confused with the [4+2] 1,3-dipolar cycloadditions described earlier.



Fig. 5.107 [2+2] Three-atom + two-atom cycloaddition of singlet vinyl carbene.

Singlet vinyl carbenes can be generated by reversible thermal ring opening of cyclopropene ketals, and (3+2) cycloaddition is very efficient with electron-deficient alkenes bearing two geminal electron-withdrawing substituents (Fig. 5.108).¹¹² Since the π -delocalized singlet vinyl carbene possesses a 2π three-carbon backbone, it may be suited for participation as a π_{2a} component in cycloaddition with an alkene acting as a π_{2s} component, as shown in $HOMO_{\text{vinyl carbene}}/LUMO_{\text{alkene}}$ interaction 5.75.¹¹¹ The HOMO of singlet vinyl carbene is similar to that of allyl cation. The regioselectivity of the reaction is governed by the leading bond formed between the alkene β -carbon (large LUMO coefficient) and the unsubstituted end (large HOMO coefficient) of π -delocalized singlet vinyl carbene.

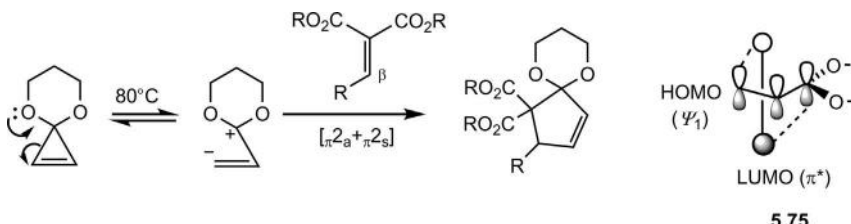


Fig. 5.108 $[\pi_{2a} + \pi_{2s}]$ Cycloaddition of a singlet vinyl carbene with an electron-deficient alkene, and the frontier orbital interaction.

The stereochemistry of the reaction shows that alkene geometry is maintained in the major cycloaddition product (Fig. 5.109). However, further experimental investigations suggest an alternative single-electron transfer/anion-radical and cation-radical combination mechanisms.¹¹³

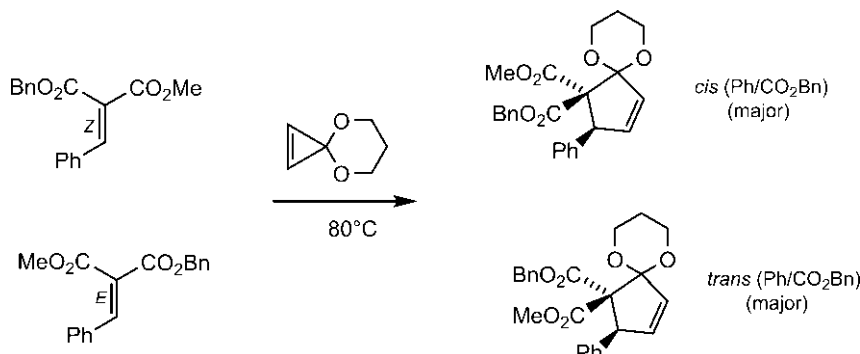


Fig. 5.109 Cycloadditions of a singlet vinyl carbene with electron-deficient *E* and *Z* alkenes.

5.4.2.4 Cycloaddition of Metal Alkylidenes

A transition metal alkylidene possesses a metal–carbon double bond. In contrast to alkene π bond, the metal–carbon π bond involves a d orbital on the transition metal. The cycloaddition of a metal alkylidene with an alkene gives a metallacyclobutane as the [2+2] adduct (Fig. 5.110).¹¹⁴

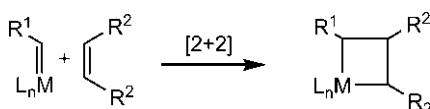


Fig. 5.110 [2+2] Cycloaddition of metal alkylidene.

The $[\pi_{2s} + \pi_{2s}]$ cycloaddition of two alkene π systems is symmetry-forbidden thermally but such cycloaddition of metal alkylidenes with alkenes is an allowed reaction (Fig. 5.111).¹¹⁵ Frontier orbital analysis shows that the metal d orbital makes the HOMO/LUMO interactions bonding at both ends because its lobes are alternating in phases due to an extra orbital

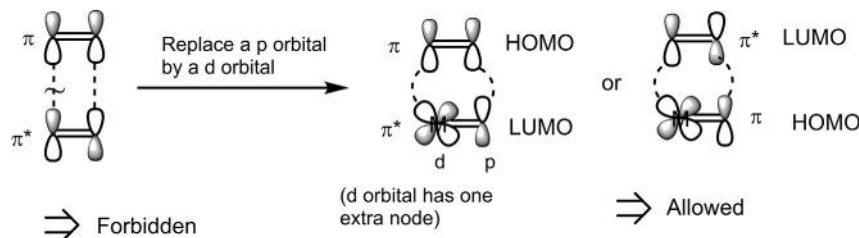


Fig. 5.111 Frontier orbital interaction for [2+2] cycloaddition of metal alkylidene.

node. An extra node transforms a forbidden reaction into an allowed reaction of far-reaching synthetic importance!

The transition metal alkylidenes are usually carbene complexes which act as catalysts in alkene metathesis. Metal carbene complexes of ruthenium such as **5.76** (Grubbs-type) are efficient catalysts.¹¹⁶ The alkene metathesis is a reaction in which the alkylidene fragments of two alkenes are swapped (Fig. 5.112).¹¹⁷

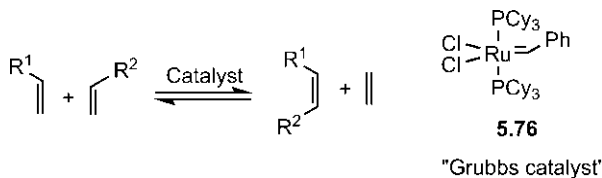


Fig. 5.112 An alkene metathesis.

The metathesis proceeds by a series of [2+2] cycloadditions and retro-cycloadditions (Fig. 5.113).¹¹⁸ The reaction steps are reversible and it is possible to drive the equilibrium in one direction. Theoretical calculations show that the frontier orbital interaction for the [2+2] cycloaddition involves preferably HOMO of alkene and LUMO of catalyst.

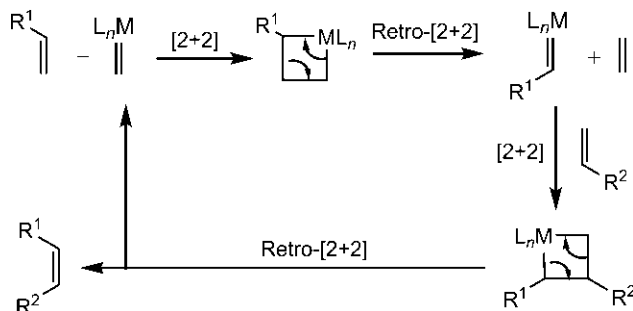


Fig. 5.113 Mechanism of metathesis reaction in Fig. 5.112 involving [2+2] cycloadditions and retro-cycloadditions.

REFERENCES

- Woodward, R. B.; Hoffmann, R. *Angew. Chem. Int. Ed. Engl.* **1969**, *8*, 781.
- Evans, D. A.; Bryan, C. A.; Sims, C. L. *J. Am. Chem. Soc.* **1972**, *94*, 2891.
- Alston, P. V.; Ottenbrite, R. M. *J. Org. Chem.* **1975**, *40*, 1111.

4. Caramella, P.; Quadrelli, P.; Toma, L. *J. Am. Chem. Soc.* **2002**, *124*, 1130.
5. Leach, A. G.; Houk, K. N. *Chemtracts Org. Chem.* **2002**, *15*, 611.
6. Woodward, R. B.; Bader, F. E.; Bickel, H.; Frey, A. J.; Kierstead, R. W. *Tetrahedron* **1958**, *2*, 1.
7. Sauer, J. *Angew. Chem. Int. Ed. Engl.* **1967**, *6*, 16.
8. Jung, M. E.; Davidov, P. *Angew. Chem. Int. Ed. Engl.* **2002**, *41*, 4125.
9. Alder, K.; Gunzl, W.; Wolff, K. *Chem. Ber.* **1960**, *93*, 809.
10. Millward, D. B.; Sammis, G.; Waymouth, R. M. *J. Org. Chem.* **2000**, *65*, 3902.
11. García, J. I.; Mayoral, J. A.; Salvatella, L. *Acc. Chem. Res.* **2000**, *33*, 658.
12. Asano, T.; le Noble, W. J. *Chem. Rev.* **1978**, *78*, 407.
13. Roush, W.R. In Trost, B. M.; Fleming, I., Eds.; *Comprehensive Organic Synthesis*, Vol. 5; Pergamon Press: Oxford, 1991; p 513.
14. Winkler, J. D. *Chem. Rev.* **1996**, *96*, 167.
15. Fallis, A. G. *Acc. Chem. Res.* **1999**, *32*, 464.
16. Roush, W. R.; Gillis, H. R.; Ko, A. I. *J. Am. Chem. Soc.* **1982**, *104*, 2269.
17. Funk, R. L.; Vollhardt, K. P. *C. J. Am. Chem. Soc.* **1979**, *101*, 215. *1980*, *102*, 5253.
18. Shea, K. J.; Wise, S.; Burke, L. D.; Davis, P. D.; Gilman, J. W.; Greeley, A. C. *J. Am. Chem. Soc.* **1982**, *104*, 5708.
19. Raimondi, L.; Brown, F. K.; Gonzalez, J.; Houk, K. N. *J. Am. Chem. Soc.* **1992**, *114*, 4796.
20. Bols, M.; Skrydstrup, T. *Chem. Rev.* **1995**, *95*, 1253.
21. Oppolzer, W. *Angew. Chem. Int. Ed. Engl.* **1984**, *23*, 876.
22. Kagan, H. B.; Riant, O. *Chem. Rev.* **1992**, *92*, 1007.
23. Corey, E. J. *Angew. Chem. Int. Ed. Engl.* **2002**, *41*, 1650.
24. Rück-Braun, K.; Kunz, H. *Chiral Auxiliaries in Cycloadditions*; Wiley-VCH: Weinheim, 1999; p. 30.
25. Evans, D. A. *Aldrichim. Acta* **1982**, *15*, 23.
26. Evans, D. A.; Chapman, K. T.; Bisaha, J. *J. Am. Chem. Soc.* **1984**, *106*, 4261. *J. Am. Chem. Soc.* **1988**, *110*, 1238.
27. Johnson, J. S.; Evans, D. A. *Acc. Chem. Res.* **2000**, *33*, 325.
28. Evans, D. A.; Miller, S. J.; Lectka, T.; von Matt, P. *J. Am. Chem. Soc.* **1999**, *121*.
29. Evans, D. A.; Barnes, D. M.; Johnson, J. S.; et al. *J. Am. Chem. Soc.* **1999**, *121*, 7582.
30. Evans, D. A.; Barnes, D. M. *Tetrahedron Lett.* **1997**, *38*, 57.
31. Meinwald, J.; Mazzocchi, P. H. *J. Am. Chem. Soc.* **1966**, *88*, 2850.
32. Chow, Y. L.; Joseph, T. C.; Quon, H. H.; Tam, J. N. S. *Can. J. Chem.* **1970**, *48*, 3045.
33. Dauben, W. G.; Philips, R. B. *J. Am. Chem. Soc.* **1982**, *104*, 355. *104*, 5781.
34. Criegee, R.; Askani, R. *Angew. Chem. Int. Ed. Engl.* **1968**, *7*, 537.
35. Caramella, P.; Grünanger, P. In Padwa, A., Ed.; *1,3-Dipolar Cycloaddition Chemistry*, Vol. 1; Wiley: New York, 1984; p 291.
36. Huisgen, R.; Scheer, W.; Huber, H. *J. Am. Chem. Soc.* **1967**, *89*, 1753.
37. Tsuge, O.; Kanemasa, S.; Yoshioka, M. *J. Org. Chem.* **1988**, *53*, 1384.
38. Barr, D. A.; Grigg, R.; Gunaratne, H. Q. N.; Kemp, J.; McMeekin, P.; Sridharan, V. *Tetrahedron* **1988**, *44*, 557.
39. Tufariello, J. J.; Ali, S. A. *Tetrahedron Lett.* **1978**, *4647*.
40. LeBel, N. A.; Post, M. E.; Whang, J. *J. Am. Chem. Soc.* **1964**, *86*, 3759.
41. Mulzer, J. In *Organic Synthesis Highlights*; Mulzer, J.; Altenbach, H.-J.; Braun, M.; Krohn, K.; Reissig, H.-U., Eds.; VCH: New York, 1991; p 77.
42. Gothelf, K. V.; Jørgensen, K. A. *Chem. Rev.* **1998**, *98*, 863.
43. Pellissier, H. *Tetrahedron* **2007**, *63*, 3235.
44. Jen, W. S.; Wiener, J. J. M.; MacMillan, D. W. C. *J. Am. Chem. Soc.* **2000**, *122*, 9874.
45. Louis, C.; Hootelé, C. *Tetrahedron: Asymmetry* **1997**, *8*, 109. *1995*, *6*, 2149.
46. Houk, K. N. *Acc. Chem. Res.* **1975**, *8*, 361.

47. Hoffmann, H. M. R. *Angew. Chem., Int. Ed. Engl.* **1984**, *23*, 1.
48. Rigby, J. H.; Pigge, F. C. *Org. React.* **1997**, *51*, 351.
49. Lee, J. C.; Cha, J. K. *J. Am. Chem. Soc.* **2001**, *123*, 3243.
50. Buchi, G.; Chu, P.-S. *J. Am. Chem. Soc.* **1979**, *101*, 6767.
51. Walls, F.; Padilla, J.; Joseph-Nathan, P.; Giral, F.; Romo, J. *Tetrahedron Lett.* **1965**, *1577*.
52. Neumann, F.; Lambert, C.; Schleyer, P.v.R. *J. Am. Chem. Soc.* **1998**, *120*, 3357.
53. Kauffmann, T. *Angew. Chem., Int. Ed. Engl.* **1974**, *13*, 627.
54. Yamazaki, H.; Cvetanovic, R. *J. J. Am. Chem. Soc.* **1969**, *91*, 520.
55. Chapman, O. L.; Adams, W. R. *J. Am. Chem. Soc.* **1968**, *90*, 2333.
56. Saltiel, J.; Ng Lim, L.-S. *J. Am. Chem. Soc.* **1969**, *91*, 5404.
57. Becker, D.; Haddad, N. *Org. Photochem.* **1989**, *10*, 1.
58. Crimmins, M. T. *Chem. Rev.* **1988**, *88*, 1453.
59. Hammond, G. S.; Turro, N. J.; Fischer, A. *J. Am. Chem. Soc.* **1961**, *83*, 4674.
60. Schenck, G. O.; Steinmetz, R. *Chem. Ber.* **1963**, *96*, 520.
61. Barborak, J. C.; Watts, L.; Pettit, R. *J. Am. Chem. Soc.* **1966**, *88*, 1328.
62. Masamune, S.; Cuts, H.; Hogben, M. G. *Tetrahedron Lett.* **1966**, *1017*.
63. Arnold, D. R.; Trecker, D. J.; Whipple, E. B. *J. Am. Chem. Soc.* **1965**, *87*, 2596.
64. Arnold, D. R. *Adv. Photochem.* **1968**, *6*, 301.
65. Turro, N. J. *Modern Molecular Photochemistry*; Benjamin/Cummings, Menlo Park, CA, 1978.
66. Schuster, D. I.; Lem, G.; Kaprinidis, N. A. *Chem. Rev.* **1993**, *93*, 3.
67. Eaton, P. E. *Acc. Chem. Res.* **1968**, *1*, 50.
68. Corey, E. J.; Mitra, R. B.; Uda, H. *J. Am. Chem. Soc.* **1964**, *86*, 485.
69. Corey, E. J.; Bass, J. D.; LeMahieu, R.; Mitra, R. B. *J. Am. Chem. Soc.* **1964**, *86*, 5570.
70. Wender, P. A.; Lechleiter, J. C. *J. Am. Chem. Soc.* **1978**, *100*, 4321.
71. Agosta, W. C.; Wolff, S. J. *Org. Chem.* **1980**, *45*, 3139.
72. Pirrung, M. C. *J. Am. Chem. Soc.* **1981**, *103*, 82.
73. Hoffman, R.; Wells, P.; Morrison, H. *J. Org. Chem.* **1971**, *36*, 102.
74. Büchi, G.; Goldman, I. M. *J. Am. Chem. Soc.* **1957**, *79*, 4741.
75. Winkler, J. D.; Bowes, C. M.; Liotta, F. *Chem. Rev.* **1995**, *95*, 2003.
76. Crimmins, M. T.; Reinhold, T. L. *Org. React.* **1993**, *44*, 297.
77. Roberts, J. D.; Sharts, C. M. *Org. React.* **1962**, *12*, 1.
78. Bartlett, P. D. *Science* **1968**, *159*, 833.
79. Gompper, R. *Angew. Chem. Int. Ed. Engl.* **1969**, *8*, 312.
80. Bartlett, P. D. Q. *Rev.* **1970**, *24*, 473.
81. Kraft, K.; Koltzenburg, G. *Tetrahedron Lett.* **1967**, *4357*, 4723.
82. Closs, G. L.; Pfeffer, P. E. *J. Am. Chem. Soc.* **1968**, *90*, 2452.
83. Brady, W. T. In: *The Chemistry of Ketenes, Allenes and Related Compounds*; Patai, S., Ed.; John Wiley: Chichester, 1980; p 279 (chapter 8).
84. Valenti, E.; Pericas, M. A.; Moyano, A. *J. Org. Chem.* **1990**, *55*, 3582.
85. Montaigne, R.; Ghosez, L. *Angew. Chem. Int. Ed. Engl.* **1968**, *7*, 221.
86. Huisgen, R.; Feiler, L. A.; Binsch, G. *Chem. Ber.* **1969**, *102*, 3460.
87. Houk, K. N.; Strozier, R. W.; Hall, J. A. *Tetrahedron Lett.* **1974**, *897*.
88. Deubel, D. V. *J. Phys. Chem. A* **2002**, *106*, 431.
89. Hurd, C. D.; Kimbrough, R. D., Jr. *J. Am. Chem. Soc.* **1960**, *82*, 1373.
90. Feiler, L. A.; Huisgen, R.; Koppitz, P. J. *J. Am. Chem. Soc.* **1974**, *96*, 2270.
91. Chick, F.; Wilsmore, N. T. M. *J. Chem. Soc.* **1908**, 946.
92. Andreades, S.; Carlson, H. D. *Org. Synth.* **1973**, *V*, 679.
93. Seidl, E. T.; Schaeffer, H. F., III *J. Am. Chem. Soc.* **1991**, *113*, 5195.
94. Huisgen, R.; Otto, P. *J. Am. Chem. Soc.* **1968**, *90*, 5342.
95. Snider, B. B. *Chem. Rev.* **1988**, *88*, 793.

96. Sustmann, R.; Ansmann, A.; Vahrenholt, F. *J. Am. Chem. Soc.* **1972**, *94*, 8099.
97. Rey, M.; Roberts, S. M.; Dreiding, A. S.; et al. *Helv. Chim. Acta* **1982**, *65*, 703.
98. Bisceglia, R. H.; Cheer, C. J. *J. Chem. Soc. Chem. Commun.* **1973**, 165.
99. Fleming, I. *Molecular Orbitals and Organic Chemical Reactions: Student Edition*. Wiley: Chichester, 2009;:265.
100. Yamabe, S.; Dai, T.; Minato, T.; Machiguchi, T.; Hasegawa, T. *J. Am. Chem. Soc.* **1996**, *118*, 6518.
101. Machiguchi, T.; Hasegawa, T.; Ishiwata, A.; Terashima, S.; Yamabe, S.; Minato, T. *J. Am. Chem. Soc.* **1999**, *121*, 4771.
102. Cossio, F. P.; Arrieta, A.; Sierra, M. A. *Acc. Chem. Res.* **2008**, *41*, 925.
103. Kagan, H. B.; Luche, J. C. *Tetrahedron Lett.* **1968**, 3093.
104. Rasmussen, J. K.; Hassner, A. *Chem. Rev.* **1976**, *76*, 389.
105. Singh, G. S. *Tetrahedron* **2003**, *59*, 7631.
106. Criegee, R.; Moschel, A. *Chem. Ber.* **1959**, *92*, 2181.
107. Griesbaum, K.; Naegele, W.; Wanless, G. G. *J. Am. Chem. Soc.* **1965**, *87*, 3151.
108. Alcaide, B.; Almendros, P.; Aragoncillo, C. *Chem. Soc. Rev.* **2010**, *39*, 783.
109. Rastelli, A.; Bagatti, M.; Gandolfi, R. *Tetrahedron* **1994**, *50*, 5561.
110. Kiefer, E. F.; Okamura, M. Y. *J. Am. Chem. Soc.* **1968**, *90*, 4187.
111. Baldwin, J. E.; Roy, U. V. *J. Chem. Soc. D. Chem. Commun.* **1969**, 1225.
112. Boger, D. L.; Brotherton, C. E. *J. Am. Chem. Soc.* **1986**, *108*, 6695.
113. Boger, D. L.; Wysocki, R. J., Jr. *J. Org. Chem.* **1988**, *53*, 3408.
114. Judy, W. A. *Angew. Chem. Int. Ed. Engl.* **1976**, *15*, 401.
115. Alabugin, I. V. *Stereoelectronic Effects: A bridge between Structure and Reactivity*. John Wiley: Chichester, 2016; (chapter 1).
116. Scholl, M.; Ding, S.; Lee, C. W.; Grubbs, R. H. *Org. Lett.* **1999**, *1*, 953.
117. Ivin, K. J. *Olefín Metathesis*. Academic Press: New York, 1983.
118. Grubbs, R. H. *Prog. Inorg. Chem.* **1978**, *24*, 1.

CHAPTER 6

Cycloadditions 3: Cheletropic, Higher Order and Multicomponent Cycloadditions

6.1 CHELETROPIC REACTIONS

A cheletropic reaction¹ denotes a cycloaddition of a 2-electron 1-atom component ($\omega 2$) to a π system (πm) or the reverse process. By electron convention, the cheletropic cycloaddition is a $[m+2]$ reaction whereas by atom convention, this is a $(m+1)$ reaction (when π system contains m atoms). Two σ bonds are formed to the same atom in cycloaddition or broken from the same atom in cycloreversion (Fig. 6.1). As shown in the figure, the πm component is a diene; however, m is usually 2, 4 or 6. The 1-atom component is generally represented as Xab which is a singlet carbene or a small molecule such as SO₂, N₂ and CO.

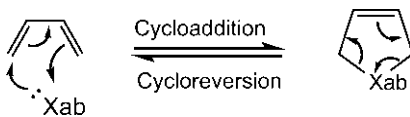


Fig. 6.1 A representative cheletropic reaction.

The forward cycloaddition is important for singlet carbenes, and also for sulphur dioxide to some extent. However, the cycloreversions are more common when these involve extrusion of highly stable N₂, CO or SO₂ molecules.

In the general component Xab, the atom X has a lone pair orbital lying in the plane of the molecule and a vacant p orbital perpendicular to it (Fig. 6.2). The orbital pictures of singlet carbene and SO₂ are also shown alongside.

Like parallel and orthogonal approaches of two components in the cycloadditions described earlier, there are also two geometries of approach of Xab to the π system in a cheletropic reaction, called linear and nonlinear cheletropic processes. These are shown in Fig. 6.3. In the linear process, the line (z -axis) of approach or departure of Xab is same as the axis of the lone pair

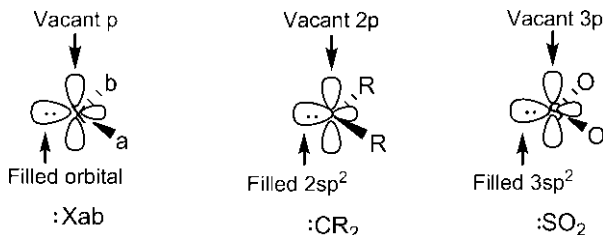


Fig. 6.2 Orbital pictures of Xab, singlet carbene and sulphur dioxide.

with a, b lying in the yz -plane (Fig. 6.3A). In the nonlinear process, the line of approach or departure of Xab is orthogonal to the axis of lone pair with a, b lying in the xy -plane (Fig. 6.3B). Note that p orbitals of π_m system lie in the plane of the paper (xz -plane). The orbital interactions show that the two linear modes are represented as $[\pi m_s + \omega 2_s]$ and $[\pi m_a + \omega 2_s]$ while the two nonlinear modes are $[\pi m_s + \omega 2_a]$ and $[\pi m_a + \omega 2_a]$. It is of note that Xab is a suprafacial component ($\omega 2_s$) in linear process and an antarafacial component ($\omega 2_a$) in nonlinear process.

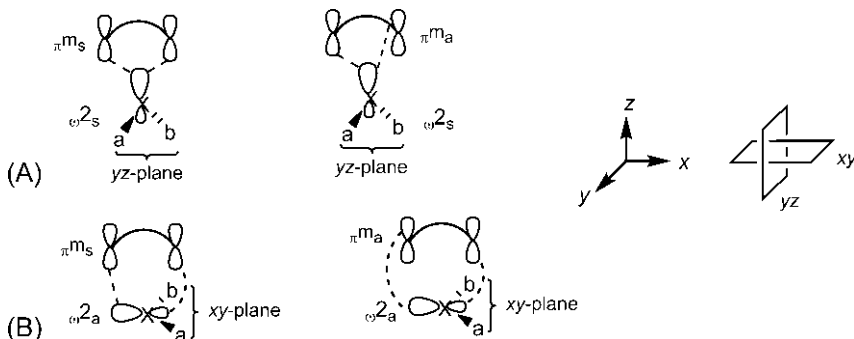


Fig. 6.3 (A) Linear process: Xab approaches or departs along z-axis (axis of the lone pair). (B) Nonlinear process: Xab approaches or departs along z-axis (perpendicular to the lone pair x-axis).

The symmetry-allowed modes under thermal or photochemical condition can be easily determined using the Woodward–Hoffmann generalized rules.

Using a diene component ($m=4$), linear $[\pi 4_s + \omega 2_s]$ (supra/supra) and nonlinear $[\pi 4_a + \omega 2_a]$ (antarafacial/antarafacial) modes are thermally allowed [total number of $(4q+2)_s$ and $(4r)_a$ components = 1]. The other linear $[\pi 4_a + \omega 2_s]$ and nonlinear $[\pi 4_s + \omega 2_a]$ modes are photochemically allowed (check).

Similarly, with an alkene component ($m=2$) or a triene component ($m=6$), linear antara/supra process ($[\pi 2_a + \omega 2_s]$ or $[\pi 6_a + \omega 2_s]$) and nonlinear supra/antara process ($[\pi 2_s + \omega 2_a]$ or $[\pi 6_s + \omega 2_a]$) are thermally allowed.

Since stereochemistry is not associated with Xab component, the stereochemical outcome of cheletropic reactions can be defined in respect of only π system (similar to electrocyclic reactions) using conrotatory (con)/disrotatory (dis) motions. The suprafacial addition to a polyene involves dis motion of its terminal substituents while antarafacial addition leads to con motion of the termini. Therefore $\pi 4_s$ or $\pi 6_s$ component refers to dis motion whereas $\pi 4_a$ or $\pi 6_a$ component implies con rotation. The con/dis motion is not relevant for alkene π system. The selection rules² for thermally allowed cheletropic reactions in terms of con/dis rotation of a polyene system are given in Table 6.1. The rules for photochemical reactions are reversed (not shown). The con/dis formulation of selection rules allows easy determination of the stereochemical outcome of cheletropic reactions.

Table 6.1 Selection rules for $[m+2]$ cheletropic reactions

m (no. of π electrons)	Thermally allowed	
	Linear	Nonlinear
$4n$	Dis	Con
$4n+2$	Con	Dis

6.1.1 Cheletropic Reactions With Singlet Carbenes

The cycloaddition of a singlet carbene with an alkene gives a cyclopropane. The (*Z*)-2-butene on reaction with dichlorocarbene gives a *cis* cyclopropane whereas (*E*)-2-butene yields a *trans* cyclopropane (Fig. 6.4). The reaction is stereospecific and clearly suprafacial on the alkene.^{3,4}

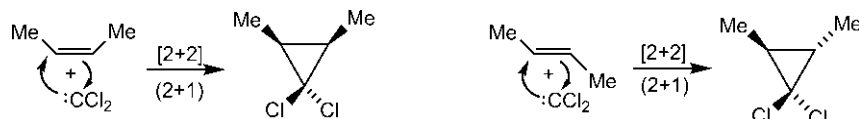


Fig. 6.4 Stereospecific addition of dichlorocarbene to (*Z*)- and (*E*)-butenes.

The linear $[\pi 2_s + \omega 2_s]$ process is thermally forbidden but the nonlinear $[\pi 2_s + \omega 2_a]$ process is thermally allowed (see above). Therefore, suprafacial addition to the alkene by a nonlinear mode⁵ gives the stereospecificity. The cheletropic cycloaddition of a singlet carbene to an alkene can also be examined using frontier orbital theory. The HOMO for singlet carbene

is a filled sp^2 orbital and the LUMO is a vacant p orbital (see Fig. 6.2). The frontier orbital interactions using two possible HOMO/LUMO pairs for the linear and nonlinear processes with (Z)-butene are shown in Fig. 6.5. As shown in Fig. 6.5A, the linear process involving bonding/antibonding interactions is thermally forbidden while the nonlinear process is thermally allowed with bonding interactions occurring at both ends (Fig. 6.5B). In the context of the Woodward–Hoffmann generalized rule, a carbene using LUMO (vacant p orbital) is regarded as a ω_0^0 component. So for $HOMO_{\text{alkene}}/LUMO_{\text{carbene}}$ combination, the linear $[\pi_{2s} + \omega_0^0]$ description is symmetry-forbidden thermally while the nonlinear $[\pi_{2s} + \omega_0^0]$ is thermally allowed.

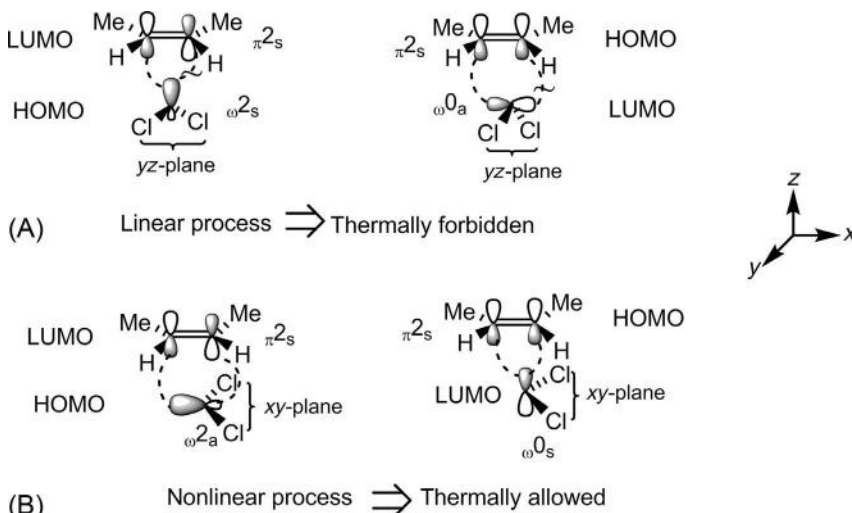


Fig. 6.5 Frontier orbital interactions of cheletropic addition of a singlet carbene to (Z)-butene by (A) linear mode and (B) nonlinear mode.

As the carbene carbon becomes nearly tetrahedral in the cyclopropane product, the carbene with Cl substituents lying in the xy -plane in the allowed nonlinear process would have to swing around 90 degrees to the yz -plane as the product is formed (Fig. 6.6). (Note that, if the process were linear, the carbene substituents in the yz -plane would remain in the yz -plane in the product.)

The frontier orbital analysis also suggests that both filled and vacant orbitals of the singlet carbene might be involved in the formation of two σ bonds. This is also in accord with the presence of both nucleophilic and electrophilic sites on carbene (see the curved arrows in Fig. 6.4).

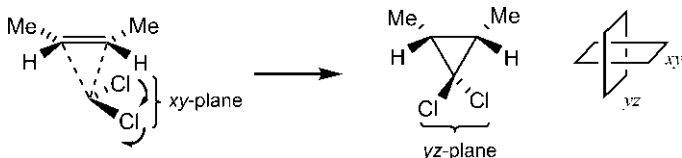


Fig. 6.6 Nonlinear pathway of carbene cycloaddition.

Thus the concerted nonlinear reaction can also be described in terms of the transition structure **6.1**⁶ involving interactions of all three components (π^2 , ω_2 and ω_0) shown in Fig. 6.7, similar to ketene cycloaddition. This indicates an allowed $[\pi^2_s + \omega_2_s + \omega_0_a]$ process, total number of $(4q+2)_s$ and $(4r)_a$ components being 3 (odd). The equivalent frontier orbital analysis involves both HOMO and LUMO of carbene, and LUMO of alkene (see Section 6.3.1), and indicates bonding interactions for an allowed process (Fig. 6.7).

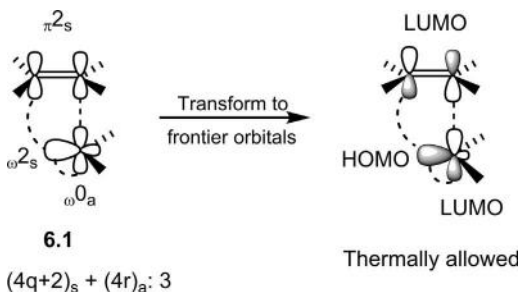


Fig. 6.7 Three-component analysis of carbene cycloaddition.

6.1.1.1 Periselectivity and Site Selectivity

Carbene cycloaddition exhibits periselectivity.^{7,8} With conjugated acyclic or cyclic polyenes dichlorocarbene undergoes [2+2] reactions to produce (2+1) cyclopropane products. For example, a diene reacts with dichlorocarbene to give a cyclopropane and does not undergo [4+2] reaction to produce a cyclopentene though [4+2] reaction via linear pathway also seems reasonable (Fig. 6.8A). Likewise, cycloheptatriene also gives a cyclopropane product (Fig. 6.8B).

The reasons for the periselectivity are not quite clear. Carbenes are reactive species, and the periselectivity appears to be governed primarily by a favourable entropic effect or proximity factor. The two ends of an alkene are much closer than those for a diene or a triene, and therefore interact easily with a relatively small carbon atom of carbene. Further, a carbene can interact straightway with the *s-trans* form of the diene and thereby avoids

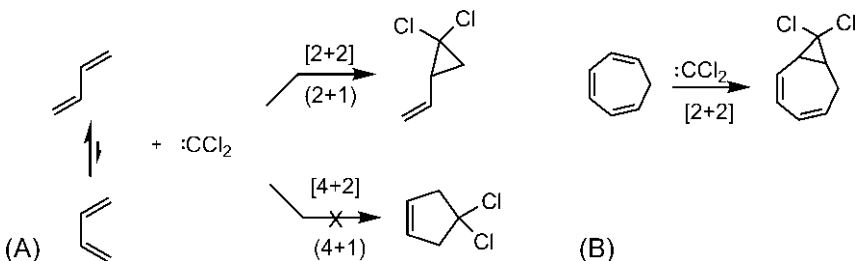


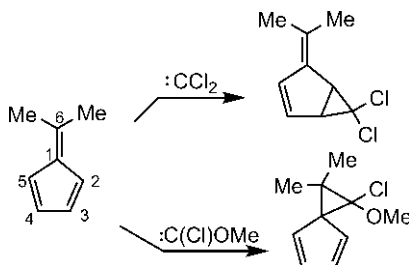
Fig. 6.8 (A) Periselectivity and (B) site selectivity in carbene cycloaddition.

the energetic penalty associated with the *s-cis* form required for a $[4 + 2]$ reaction. For cycloheptatriene, which is locked in *s-cis* form, two ends of the triene are still far apart for interaction with carbene, and with smaller cyclic diene such as cyclopentadiene, a $[4 + 2]$ cycloaddition leads to a more strained bicyclic product. Furthermore, the calculations indicate that the linear $[4 + 2]$ addition in *s-cis* form of a diene suffers from filled/filled repulsion between carbene lone pair orbital and NHOMO, the next lower HOMO (ψ_1) of diene which tends to offset the attractive frontier orbital interactions.⁹

The carbene cycloaddition with cycloheptatriene in Fig. 6.8B also shows site selectivity (a kind of regioselectivity) when a terminal double bond of the triene instead of central double bond is involved. Dichlorocarbene is an electrophilic carbene. Therefore the more important frontier orbital interaction is between LUMO of carbene and HOMO of triene. The coefficient pattern of a hexatriene (see Fig. 1.17) indicates largest HOMO coefficient on the terminal carbons. The nonlinear cheletropic cycloaddition of carbene is quite asynchronous, and the largest coefficient on a terminal carbon determines the formation of the leading bond and hence regioselectivity.

Problem 6.1

Explain the difference in site selectivity in the following carbene cycloadditions.



Answer¹⁰

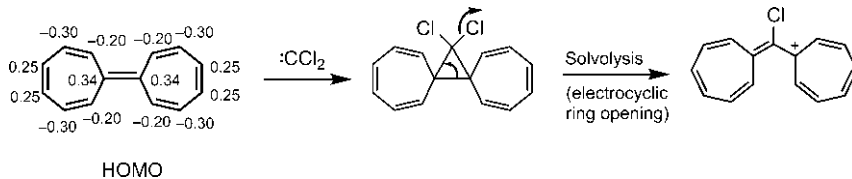
With dichlorocarbene, 2-3 double bond of dimethylfulvene is involved in cycloaddition. Dichlorocarbene is an electrophilic carbene and preferably uses its LUMO to interact with the largest HOMO coefficient (0.56) at C-2 or C-5 of dimethylfulvene (see Fig. 4.80) leading to the observed product (2-3 and 5-4 double bonds are equivalent). Methoxychlorocarbene has a stronger electron donating OMe substituent and therefore prefers to use its HOMO. The site selectivity in this case is therefore controlled by the interaction of carbene HOMO with the largest LUMO coefficient (0.72) at C-6 of dimethylfulvene (see Fig. 4.80). The product is formed by carbene addition to 6-1 double bond.

Problem 6.2

Predict the product in the following scheme.

**Answer⁸**

The dichlorocarbene generated from CHCl_3/KOH adds to the central double bond of heptafulvalene with highest HOMO coefficients. Solvolysis of the adduct involves 2-electron electrocyclic ring opening with departure of one of two Cl's (see Section 7.2.1). The ring opening is driven by the formation of a tropylidium cation moiety which is aromatic.

**6.1.2 Cheletropic Reactions With Sulphur Dioxide**

Unlike carbene cycloaddition, SO_2 can undergo [2 + 4] reaction with a diene to produce a five-membered ring sulphone, and [2 + 6] reaction with a triene to give a seven-membered ring sulphone. SO_2 is a stable molecule, and is less reactive than carbene. The two large frontier orbital coefficients at the terminal carbons of a diene or a triene now appear to favour the [4 + 2] or

[6 + 2] cycloaddition. Further, S is larger in size than C and can interact easily with the end atoms of diene or triene. There are two linear and two nonlinear pathways possible for any cheletropic reaction (see Fig. 6.3). These processes are shown in Fig. 6.9 for the cheletropic reaction of SO_2 with (2E,4E)-hexadiene using con/dis terminology. It bears recall that suprafacial addition to a diene involves disrotatory movement of its terminal substituents whereas antarafacial addition leads to conrotatory motion.

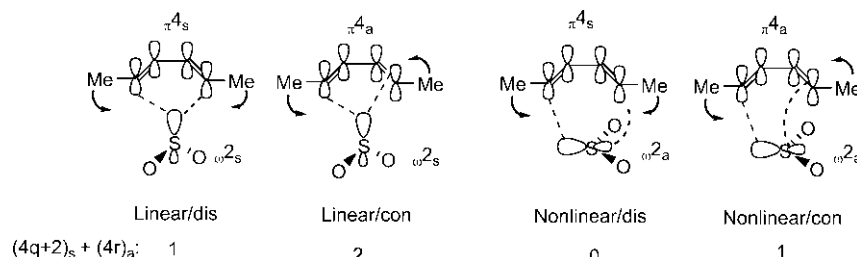


Fig. 6.9 Four possible modes of cheletropic reaction between (2E,4E)-hexadiene and sulphur dioxide.

Under thermal condition, linear/dis and nonlinear/con modes are symmetry-allowed (see also Table 6.1) while linear/con and nonlinear/dis modes are allowed photochemically.

The linear cheletropic reaction is found to be more favourable than nonlinear reaction. This is due to better orbital overlap and less steric crowding in the linear pathway. A frontier orbital description of thermally allowed linear/dis reaction with a diene is shown in Fig. 6.10. For SO_2 , HOMO is a filled 3sp^2 orbital and LUMO is a vacant 3p orbital (see Fig. 6.2).

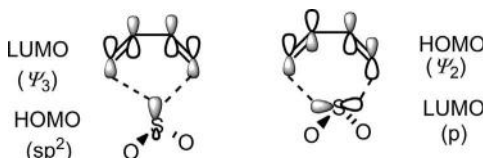


Fig. 6.10 FMO picture of cheletropic reaction of SO_2 with a diene by linear/dis pathway.

Cheletropic reactions with SO_2 are reversible, and both cycloaddition and cycloreversion can be performed under appropriate conditions. The prototype reaction between butadiene and SO_2 has been carried out at 100°C in an yield of 80%–85%.¹¹ The cheletropic reactions with SO_2 are highly stereospecific, as illustrated with (E,E)- and (E,Z)-2,4-hexadiene (Fig. 6.11).¹²

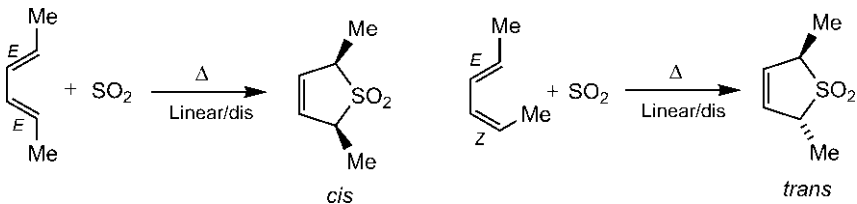


Fig. 6.11 Stereospecificity of cheletropic cycloadditions of SO_2 with (E,E) and (E,Z) dienes.

The (E,E) isomer produces a *cis* sulphone whereas the (E,Z) isomer gives a *trans* sulphone as the reactions proceed through a favourable linear/dis pathway. The stereochemistry of the product arises from the dis rotation of terminal Me substituents of the diene (see also Fig. 7.5, p. 297). The reaction with (E,E) diene is faster than with (E,Z) diene due to steric effect. The reverse process, that is, cycloreversions of the above sulphones with extrusion of SO_2 have also been shown to be highly stereospecific.¹³

The cheletropic extrusions of the above sulphones can also be carried out under photochemical condition. The photochemical reaction also manifests stereospecificity, and largely proceeds through a linear/con mode (Fig. 6.12).¹⁴

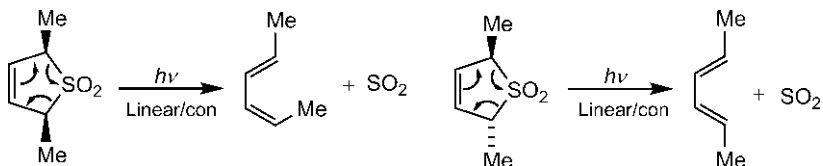


Fig. 6.12 Photochemical extrusions of five-membered ring sulphones.

As shown, the *cis* sulphone gives (E,Z) -diene, and the *trans* sulphone forms predominantly (E,E) -diene from the less hindered transition structure.

The thermal cheletropic extrusion reactions of seven-membered ring sulphones are also stereospecific, and occur by a favourable linear/con mode (see Table 6.1). As shown in Fig. 6.13, a *cis* sulphone gives $(2E,4Z,6Z)$ -hexatriene whereas a *trans* sulphone produces (E,Z,E) isomer.¹⁵

Cycloreversion (extrusion) is the microscopic reverse of the forward cycloaddition reaction. A simple analysis of the linear/con transition structure for the extrusion of SO_2 can be performed by invoking a forward linear/con, that is, $[\pi_6a + \omega_2]$ cycloaddition 6.2. The reverse extrusion reaction is then formally represented as a retro- $[\pi_6a + \omega_2]$ process. The π_6 component is antarafacial involving conrotatory movement of its termini. (Draw an equivalent frontier orbital picture.)

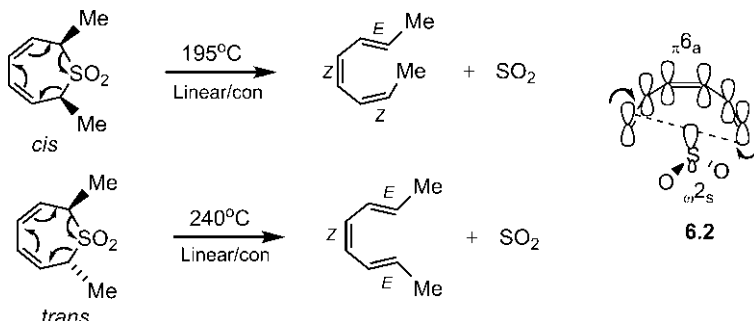


Fig. 6.13 Thermal cheletropic extrusions of seven-membered ring sulphones.

It should be noted that the forward cycloaddition of SO_2 to the triene is periselective involving longest conjugated system (in which the ends have the largest coefficients) to produce a seven-membered ring instead of a five-membered ring involving a shorter diene component.

The thermal elimination of SO_2 from a three-membered ring sulphone has also been performed. The reactions are stereospecific and suprafacial with respect to the alkene (Fig. 6.14).¹⁶

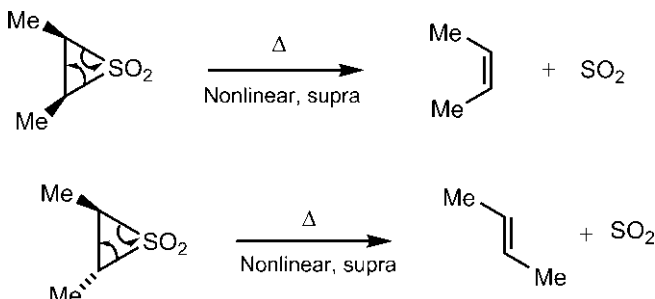


Fig. 6.14 Thermal extrusions of three-membered ring sulphones.

Using the principle of microscopic reversibility, the extrusion can be analysed by invoking a forward nonlinear $[\pi 2_s + \omega 2_a]$ addition, similar to carbene cycloaddition.

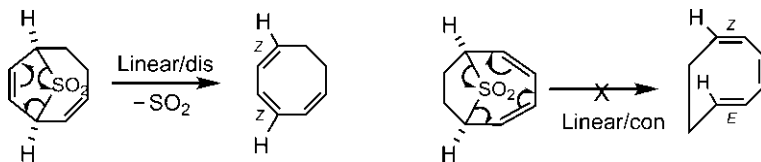
Arrow formalism: The extrusion reactions of saturated three-ring system (Fig. 6.14), unsaturated five-ring system with one double bond (Fig. 6.12) and unsaturated seven-ring system with two double bonds (Fig. 6.13) involve a total of 4, 6 and 8 electrons, respectively, and therefore represented by 2, 3 and 4 arrows.

Problem 6.3

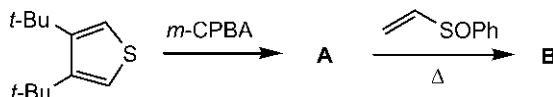
Compare the relative rates of the following cheletropic extrusions.

**Answer¹⁷**

The first reaction involves cheletropic extrusion of a five-membered ring sulphone by linear/dis pathway and gives an unstrained (*Z,Z*)-diene in the product, and hence is facile. In contrast, in the second reaction, extrusion of seven-membered ring sulphone by linear/con mode would give an *E* double bond leading to a highly strained triene product. The other allowed nonlinear/dis mode can give all-*Z* double bonds but the nonlinear process is much less favourable than a linear process. Therefore, the first reaction occurs much faster. The relative rate data show that the first reaction is 60,000 times faster than second reaction at 180°C. (In practice, the second reaction requires much higher temperature, and experimental evidence indicates a stepwise pathway.)

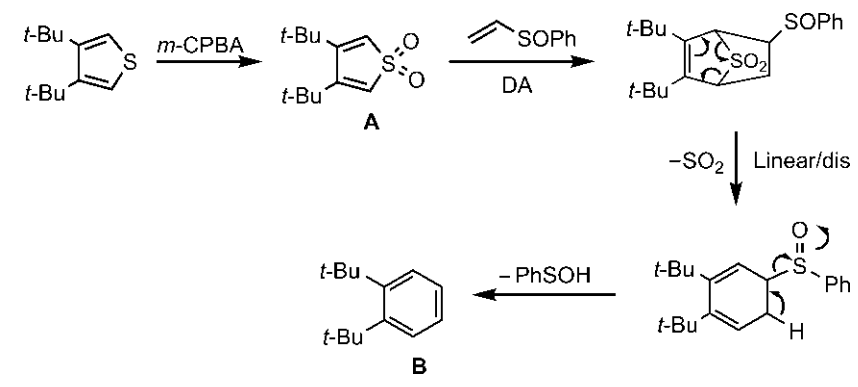
**Problem 6.4**

Identify **A** and **B** in the following scheme. Suggest mechanism for the formation of **B** from **A**.

**Answer**

A is a sulphone. The mechanism for **A** to **B** conversion is shown below. Unlike a thiophene, the sulphone **A** is not aromatic, and hence

undergoes Diels–Alder reaction readily. The resulting adduct loses SO_2 by cheletropic extrusion, then elimination of PhSOH gives **B**.



6.1.3 Cheletropic Extrusions of Nitrogen and Carbon Monoxide

Cheletropic extrusion of nitrogen from a cyclic diazene (generated *in situ* from a 3-pyrroline or a cyclic hydrazine) is spontaneous and stereospecific. For example, *cis* and *trans* isomers of a 3-pyrroline give diastereomeric dienes by cheletropic extrusion of N_2 from the corresponding cyclic diazenes (Fig. 6.15A).¹⁸ A synthesis of a *cis* benzocyclobutene is shown in Fig. 6.15B.¹⁹ Extrusion of N_2 from a cyclic diazene (generated by oxidation of a cyclic hydrazine) gives an unstable *o*-quinonodimethane which undergoes electrocyclic ring closing to form the *cis* benzocyclobutene and regain the aromaticity.

The thermal cheletropic elimination of carbon monoxide (decarbonylation) constitutes an important step in synthesis, particularly in the synthesis of aromatic compounds from substituted cyclopentadienones.²⁰ For example, a synthesis of hexaphenylbenzene is shown in Fig. 6.16.

6.2 HIGHER ORDER CYCLOADDITIONS

The cycloadditions involving more than 6 electrons are called higher order cycloadditions. If concerted, the higher order cycloadditions are also governed by the Woodward–Hoffmann selection rules (see Table 3.2). We shall consider here the following cases.

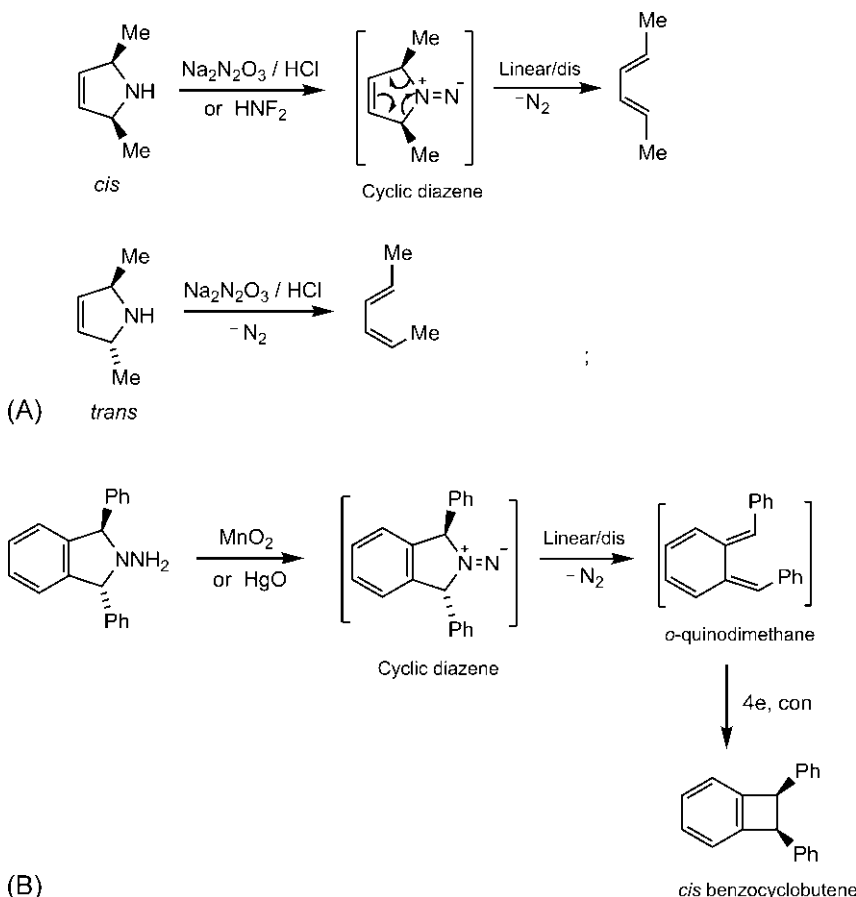


Fig. 6.15 (A) Stereospecific extrusion of N_2 from cyclic diazenes obtained from 3-pyrrolines; (B) synthesis of a *cis* benzocyclobutene from a cyclic hydrazine via extrusion of N_2 followed by electrocyclic ring closing.

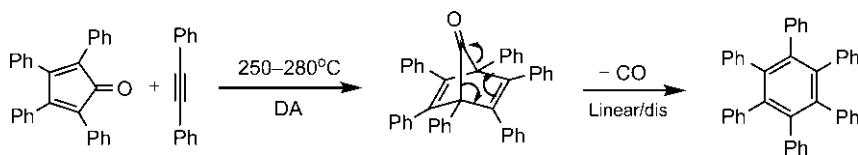


Fig. 6.16 Synthesis of hexaphenylbenzene via cheletropic extrusion of CO.

6.2.1 Cycloadditions involving 8 Electrons

The [4 + 4] cycloadditions involving two π components refer to 8-electron cycloadditions. The geometrically favourable $[\pi 4_s + \pi 4_s]$ mode is thermally forbidden, but symmetry-allowed under photochemical condition. The addition of butadiene to benzene as a $[\pi 4_s + \pi 4_s]$ cycloaddition has been shown earlier (see Fig. 5.83). The photochemical dimerization of anthracene²¹ indicates a $[\pi 4_s + \pi 4_s]$ cycloaddition, as shown in Fig. 6.17A. The cycloaddition occurs across the 9,10-positions of two anthracene molecules creating two benzene rings from each to form a more stable dimer. The photodimerization of 9-substituted anthracenes could lead to a mixture of head-to-head and head-to-tail dimers. However, 9-bromoanthracene forms a head-to-tail dimer which can undergo transannular debromination since the two Br's are *anti* (Fig. 6.17B).²²

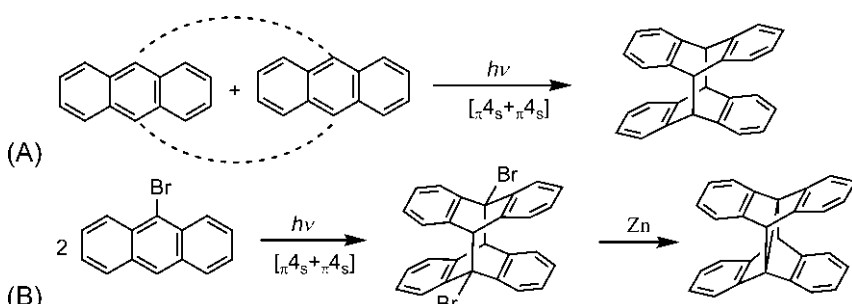


Fig. 6.17 (A) [4+4] Photodimerization of anthracene; (B) head-to-tail dimerization of 9-bromoanthracene and subsequent Zn-induced transannular debromination.

2-Pyridones and 2-pyrone also undergo $[\pi 4_s + \pi 4_s]$ dimerization to form head-to-tail dimers (Fig. 6.18).^{23,24}

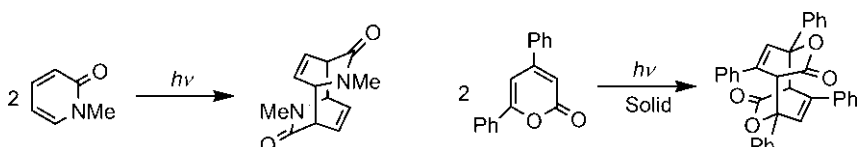


Fig. 6.18 [4+4] Photodimerization of a 2-pyridone and a 2-pyrone.

Intramolecular [4 + 4] photocycloaddition can also take place, as illustrated with *cis*-9,10-dihydronaphthalene in Fig. 6.19.²⁵

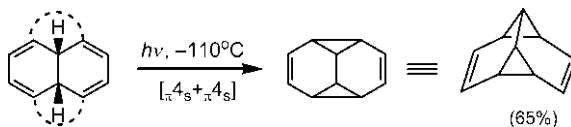


Fig. 6.19 Intramolecular [4+4] photocycloaddition of *cis*-9,10-dihydronaphthalene.

6.2.2 Cycloadditions Involving 10 Electrons

6.2.2.1 [6+4] Cycloadditions

[6+4] Cycloadditions of two π components belong to 10-electron cycloadditions. The $[\pi_6s + \pi_4s]$ reaction is thermally allowed, and several examples are known. The reaction is highly stereoselective forming predominantly the *exo* adduct (cf. Diels–Alder reaction which is *endo* selective). For example, cycloaddition of cyclopentadiene with tropone gives the [4+6] *exo* adduct in quantitative yield (Fig. 6.20)²⁶ (see also Problem 4.23).

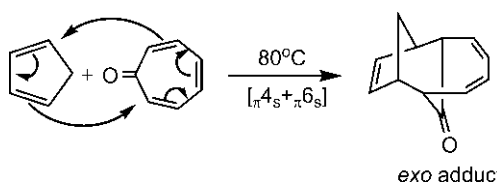


Fig. 6.20 Stereoselective [4+6] cycloaddition of cyclopentadiene with tropone.

The preference for *exo* adduct can be rationalized as follows. As shown in Fig. 6.21, the secondary orbital interactions disfavour the *endo* transition structure 6.3 by antibonding overlap (wavy lines) whereas the *exo* TS 6.4 does not involve any secondary orbital overlap. The *endo* TS is also unfavourable by steric effect. Thus the *exo* adduct is preferred both kinetically and thermodynamically.

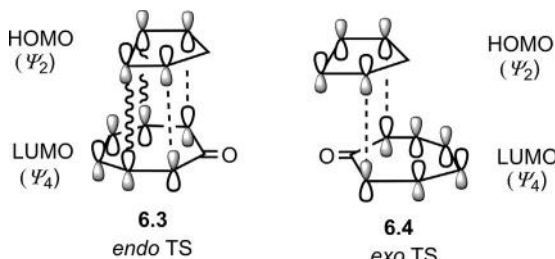


Fig. 6.21 FMO analysis of *endo* and *exo* addition in [4+6] cycloaddition in Fig. 6.20. Wavy lines in *endo* TS indicate antibonding secondary orbital interactions.

Two more examples of *exo* selectivity are shown in Fig. 6.22.^{26,27}

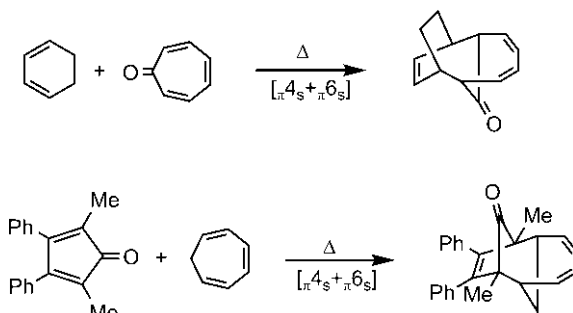


Fig. 6.22 Examples of *exo* selectivity in [4+6] cycloadditions.

Thermal dimerization of azepines provides interesting results. At 130°C, *N*-carbethoxyazepine produces predominantly the *exo* [6 + 4] adduct along with a small amount of [6 + 6] adduct; however, at higher temperature (200°C), the product is a [6 + 6] dimer (Fig. 6.23).²⁸

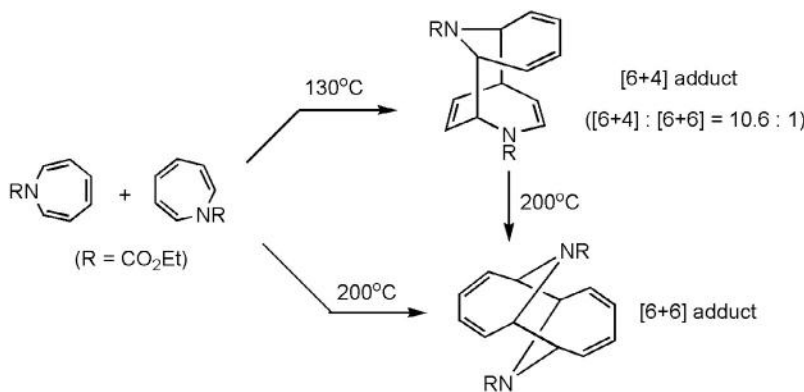


Fig. 6.23 Low-temperature and high-temperature dimerization of *N*-carbethoxyazepine.

The formation of [6 + 6] adduct by concerted $[\pi 6_s + \pi 6_s]$ cycloaddition is thermally forbidden. The high-temperature [6 + 6] product is not formed directly but possibly results from the rearrangement of the [6 + 4] dimer by a suprafacial [1,3]C shift (Fig. 6.24). The transition structure for a concerted [1,3]C shift is distorted (see Section 8.3.2); in contrast, a highly stabilized diradical intermediate **6.5** can be involved in the radical pathway and the migration is preferably stepwise.²⁸

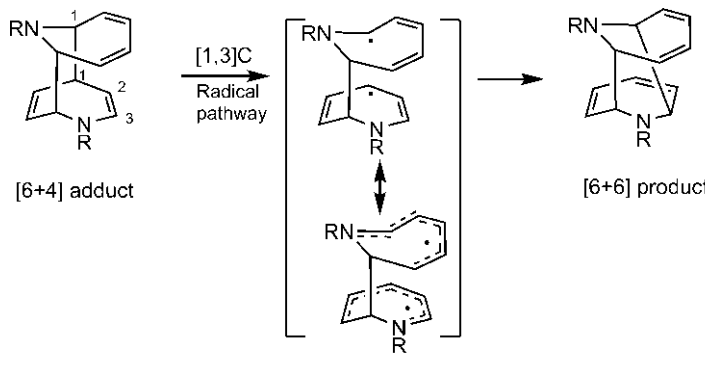


Fig. 6.24 Conversion of [6 + 4] dimer into [6 + 6] dimer by [1, 3] shift via radical pathway.

6.2.2.2 [8 + 2] Cycloadditions

The [8 + 2] cycloadditions between two π systems also involve 10 electrons. The $[\pi 8_s + \pi 2_s]$ mode is thermally allowed but the two ends of a large conjugated π_8 polyene need to be close enough to interact with a small alkene or alkyne component. This can be achieved by introducing a cyclic moiety in the π_8 component. For example, cycloaddition of 5,7-dimethylenecyclohepta-1,3-diene with dimethyl azodicarboxylate gives a bridged bicyclic adduct (Fig. 6.25)²⁹ (see also Problem 5.1).

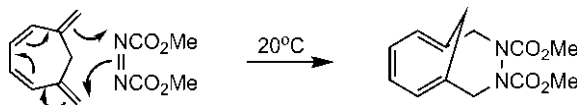


Fig. 6.25 [8 + 2] Cycloaddition of 5,7-dimethylenecyclohepta-1,3-diene with dimethyl azodicarboxylate.

The [8 + 2] cycloadditions are also useful in synthesis. Fig. 6.26A shows a cycloaddition of heptafulvene with dimethyl acetylenedicarboxylate (DMAD) to give a dihydroazulene derivative which is converted to a more stable azulene by dehydrogenation *in situ* with Pd/C.³⁰ In Fig. 6.26B, cycloaddition of indolizine with DMAD gives an [8 + 2] adduct which on dehydrogenation produces an aromatic cyclazine.³¹

6.2.3 Cycloadditions Involving More Than 10 Electrons

Cycloadditions involving more than 10 electrons are not common. A 12-electron $[\pi 6_s + \pi 6_s]$ cycloaddition is thermally forbidden but

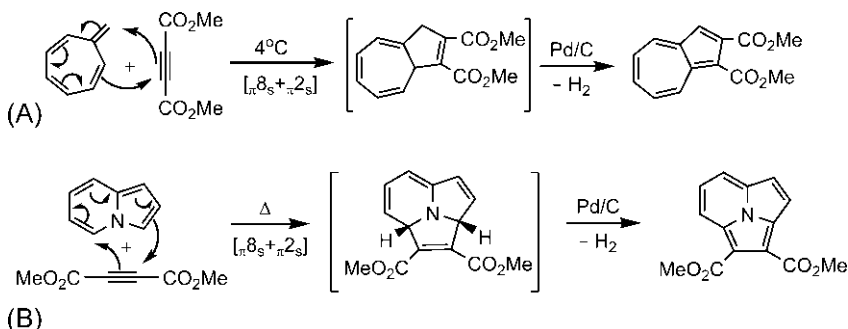


Fig. 6.26 Synthesis of (A) an azulene and (B) a cyclazine via $[8+2]$ cycloaddition.

photochemically allowed. Irradiation of a dilute acid solution of tropone gives a $[6+6]$ dimer (Fig. 6.27).³² The yield is quite low (7.5%) and the photodimerization may well be stepwise.

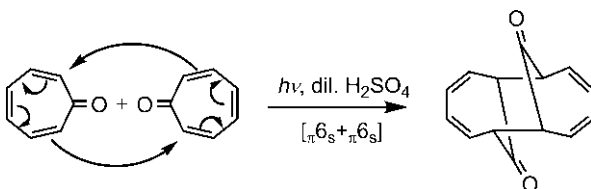


Fig. 6.27 $[6+6]$ Photodimerization of tropone.

Cycloadditions with progressively higher orders become rarer. An example of a 14-electron thermal $[\pi 12_s + \pi 2_s]$ cycloaddition is shown in Fig. 6.28.³³ The stereochemistry of two H's at ring junctions is *cis* as a result of suprafacial addition to the sesquifulvene.

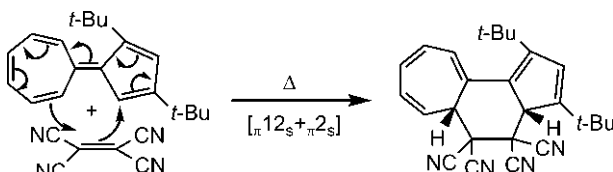


Fig. 6.28 A thermal $[12+2]$ cycloaddition.

The cycloaddition of heptafulvene with tetracyanoethylene produces a $[14+2]$ adduct (Fig. 6.29). The stereochemistry of the two hydrogens at the ring junctions has been shown to be *trans* by X-ray crystallography. This indicates that heptafulvene acts as an antarafacial component. The cycloaddition is thus concerted and proceeds by thermally allowed $[\pi 14_a + \pi 2_s]$.

pathway.¹ The twisted shape of heptafulvene allows its antarafacial overlap involving a lower lobe and an upper lobe of π_{14} system in the transition structure **6.6**.

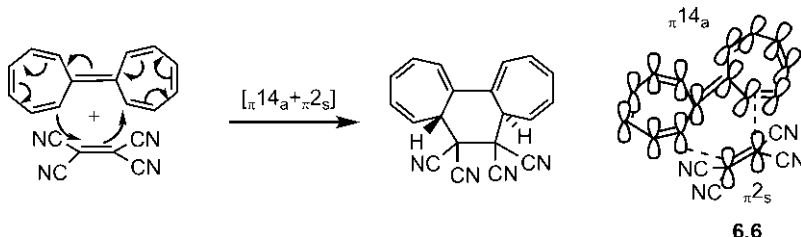


Fig. 6.29 Thermal $[\pi_{14a} + \pi_{2s}]$ cycloaddition between heptafulvene and tetracyanoethylene.

This cycloaddition demonstrates a spectacular success of the Woodward–Hoffmann rules on the concerted reactions.

The thermal reaction between pentafulvene and dicyanoacetylene does not proceed by an allowed $[\pi_{10a} + \pi_{2s}]$ pathway. It appears that a smaller pentafulvene fails to act as a π_{10a} component as it is not flexible enough to allow antarafacial overlap. However, pentafulvene undergoes a Diels–Alder reaction with dicyanoacetylene to give a 1:2 adduct (Fig. 6.30).

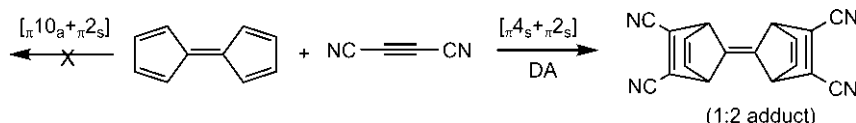


Fig. 6.30 Thermal cycloaddition between pentafulvene and dicyanoacetylene.

6.3 MULTICOMPONENT CYCLOADDITIONS

Concerted three- or four-component cycloadditions requiring collisions of three or four molecules simultaneously are very improbable, and suffer from an extremely unfavourable entropy factor. This problem could be redressed by reducing the many-body collision to a two-body collision when two of the components are built in one reacting molecule.

The $[2 + 2 + 2]$ cycloaddition of three π systems to form a cyclohexane (Fig. 6.31A) is thermally allowed as an all-suprafacial $[\pi_{2s} + \pi_{2s} + \pi_{2s}]$ process [total number of $(4q + 2)_s$ and $(4r)_a$ components is 3, an odd number]. This type of three-component cycloaddition can be designed successfully taking

two reacting partners, for example, norbornadiene (in which two π components are held together) and tetracyanoethylene as shown in Fig. 6.31B.³⁴ The geometry of two π components in norbornadiene is also favourable for all-suprafacial interactions in the transition structure **6.7**. This reaction is sometimes called homo-Diels–Alder reaction (when cyclopropane ring replaces the π bond of Diels–Alder cyclohexene adduct).

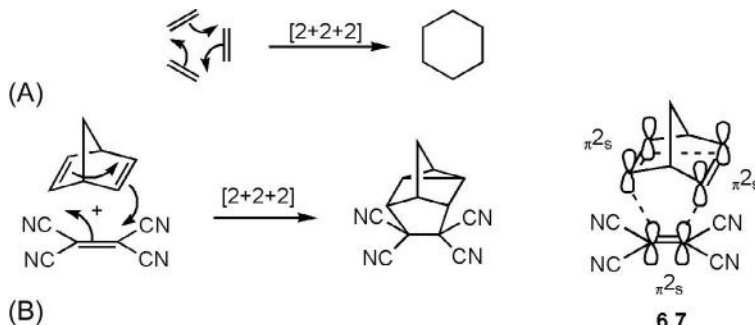


Fig. 6.31 (A) Prototype [2 + 2 + 2] cycloaddition of three ethylene π systems. (B) [2 + 2 + 2] cycloaddition as a bimolecular collision between norbornadiene and tetracyanoethylene.

Another example of [2 + 2 + 2] cycloaddition of 1,3,5,7-tetramethylenecyclooctane with tetracyanoethylene is shown in Fig. 6.32.³⁵ The tetramethylenecyclooctane adopts a boat conformation and two methylene units at relative 1,5-positions participate in the cycloaddition.

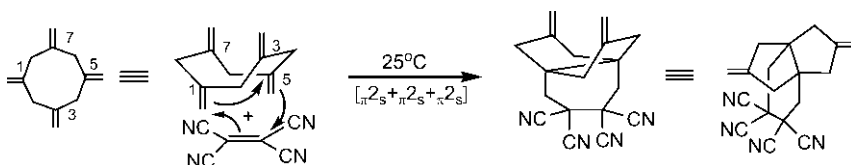


Fig. 6.32 [2 + 2 + 2] cycloaddition of tetramethylenecyclooctane with tetracyanoethylene.

The four-component [$\pi_2 + \pi_2 + \pi_2 + \pi_2$] cycloaddition is thermally forbidden but photochemically allowed [total number of $(4q + 2)_s$ and $(4r)_a$ components is 4, an even number]. This is illustrated with the photocycloaddition of dihydrophtalic anhydride with 2-butyne (Fig. 6.33).^{36,37} Two π components are held together in dihydrophtalic anhydride and the other two comprise the orthogonal π bonds of butyne. The reaction

proceeds through a boat conformation of dihydrophtalic anhydride for all-suprafacial interactions in the transition structure **6.8**. Note that at each end of alkyne two orthogonal p orbitals are involved to form a cyclopropane ring (cf. carbene cycloaddition).

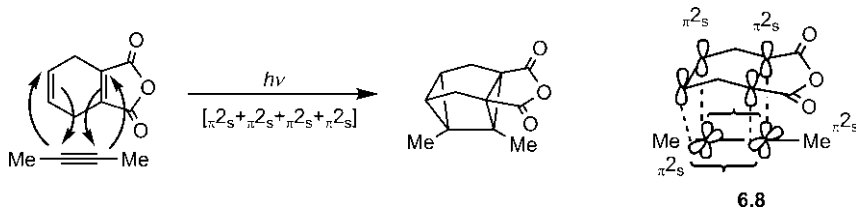


Fig. 6.33 [2 + 2 + 2 + 2] Photocycloaddition of dihydrophtalic anhydride with 2-butyne.

6.3.1 Frontier Orbital Analysis of Multicomponent Systems

Frontier orbital analysis of a concerted process involving more than two components is not straightforward as for a two-component HOMO/LUMO interaction. For the purpose of analysis, the frontier orbital interactions of a multicomponent system are reduced to HOMO/LUMO interaction of an equivalent two-component system. To illustrate, we consider the frontier orbital analysis of $[\pi_{2s} + \pi_{2s} + \pi_{2s}]$ process (Fig. 6.34).

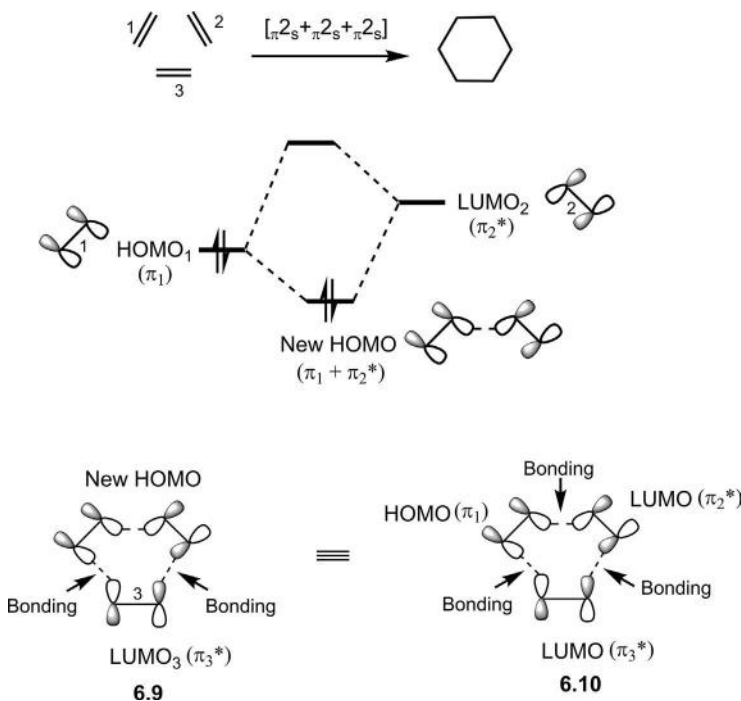


Fig. 6.34 Frontier orbital analysis of three-component [2 + 2 + 2] cycloaddition.

The three π components and their MOs are labelled 1, 2 and 3. Taking any pair of π components, say, 1 and 2 as shown in the figure, combination of HOMO_1 with LUMO_2 in bonding fashion creates a new HOMO ($\pi_1 + \pi_2^*$). The frontier orbital analysis of the three-component process then reduces to the interaction of the new HOMO with LUMO_3 . The bonding interactions at the ends of new HOMO and LUMO_3 in the transition structure 6.9 indicate an allowed reaction. In effect, this analysis is equivalent to the interactions 6.10 involving one HOMO (π_1) and two LUMOs (π_2^* and π_3^*) for the three components when all three interactions are bonding.

Another frontier orbital analysis is shown in Fig. 6.35.

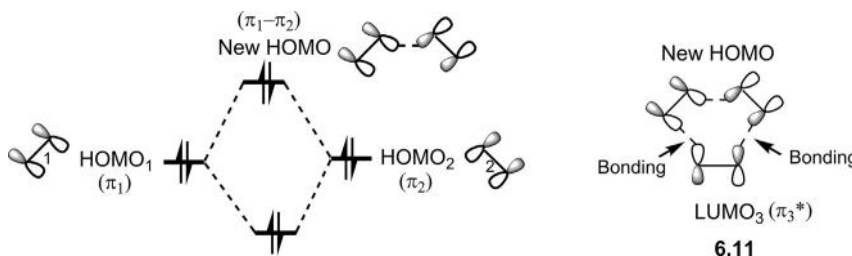


Fig. 6.35 Another frontier orbital analysis of [2+2+2] cycloaddition.

Combining HOMO_1 with HOMO_2 in antibonding (out-of-phase) sense creates a new HOMO ($\pi_1 - \pi_2$). The bonding interactions at the ends of new HOMO and LUMO_3 in the transition structure 6.11 indicate an allowed reaction.

The above frontier orbital analyses are applicable to any three-component concerted reaction irrespective of the nature of electrons (σ , π or ω) involved.

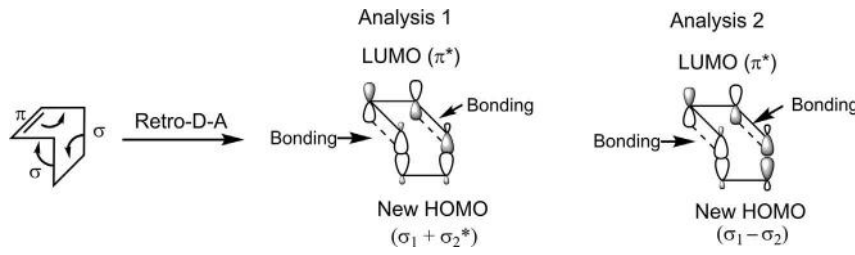
Problem 6.5

Give frontier orbital analysis of retro-Diels–Alder [$\sigma_{2s} + \sigma_{2s} + \pi_{2s}$] reaction (see Fig. 3.22).

Answer

As a microscopic reverse of forward reaction, retro-Diels–Alder reaction proceeds through boat transition structure. Two frontier orbital analyses are shown below. The two σ components are nearly parallel, and their mixing with each other is geometrically reasonable. In analysis 1, a new HOMO is created by bonding combination of HOMO (σ_1) and LUMO

(σ_2^*) of two σ components (cf. Fig. 6.34), and in analysis 2, a new HOMO is obtained from antibonding combination of HOMO (σ_1) and HOMO (σ_2) (cf. Fig. 6.35). The frontier orbital interaction between the new HOMO and LUMO of the π component in each case is bonding, and hence the reaction is thermally allowed.

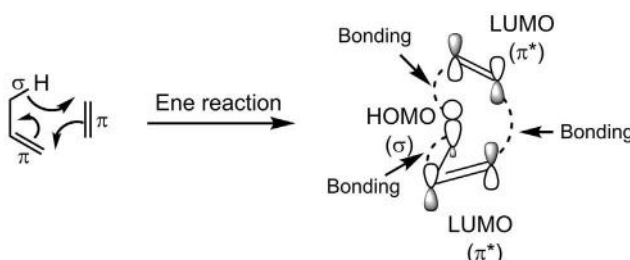
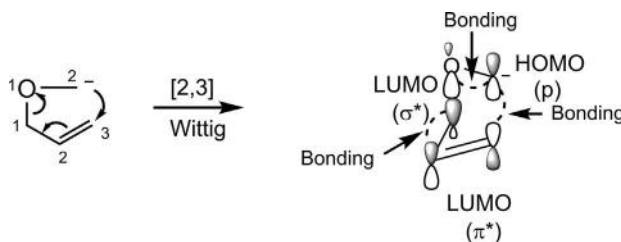


Problem 6.6

Perform three-component frontier orbital analysis of Wittig rearrangement (see Fig. 3.48) and ene reaction (see Fig. 3.49).

Answer

The three-component analysis is performed using three frontier orbitals, that is, one HOMO and two LUMOs (cf. TS 6.10 in Fig. 6.34). All interactions are bonding and hence indicate an allowed reaction.



REFERENCES

1. Woodward, R. B.; Hoffmann, R. *Angew. Chem. Int. Ed. Eng.* **1969**, *8*, 781.
2. Woodward, R. B.; Hoffmann, R. *The Conservation of Orbital Symmetry*; Academic Press: New York, 1970; p.152.
3. Skell, P. S.; Woodworth, R. C. *J. Am. Chem. Soc.* **1956**, *78*, 4496.
4. Moore, W. R.; Moser, W. R.; LaPrade, J. E. *J. Org. Chem.* **1963**, *28*, 2200.
5. Skell, P. S.; Garner, A. Y. *J. Am. Chem. Soc.* **1956**, *78*, 5430.
6. Fleming, I. *Molecular Orbitals and Organic Chemical Reactions: Student Edition*; Wiley: Chichester, 2009; p.214.
7. terBorg, A. P.; Bickel, A. F. *Rec. Trav. Chim.*, **1961**, *80*, 1217.
8. Fleming, I. *J. Chem. Soc. Perkin Trans.* **1973**, *1*, 1019.
9. Schoeller, W. W.; Yurtsever, E. *J. Am. Chem. Soc.* **1978**, *100*, 7548.
10. Moss, R. A.; Young, C. M.; Perez, L. A.; Krogh-Jespersen, K. *J. Am. Chem. Soc.* **1981**, *103*, 2413.
11. Grummitt, O.; Ardis, A. E.; Fick, J. *J. Am. Chem. Soc.* **1950**, *72*, 5167.
12. Mock, W. L. *J. Am. Chem. Soc.* **1975**, *97*, 3666.
13. Mock, W. L. *J. Am. Chem. Soc.* **1966**, *88*, 2857.
14. Saltiel, J.; Metts, L. *J. Am. Chem. Soc.* **1967**, *89*, 2232.
15. Mock, W. L. *J. Am. Chem. Soc.* **1969**, *91*, 5682.
16. Paquette, L. A.; Wittenbrook, L. S. *J. Am. Chem. Soc.* **1967**, *89*, 4483.
17. Mock, W. L. *J. Am. Chem. Soc.* **1970**, *92*, 3807.
18. Lemal, D. M.; McGregor, S. D. *J. Am. Chem. Soc.* **1966**, *88*, 1335.
19. Carpino, L. A. *J. Am. Chem. Soc.* **1962**, *84*, 2196.
20. Ogliaruso, M. A.; Romanelli, M. G.; Becker, E. I. *Chem. Rev.* **1965**, *65*, 261.
21. Dauben, W. G.; Philips, R. B. *J. Am. Chem. Soc.* **1982**, *104*, 355. *104*, 5781.
22. Applequist, D. E.; Little, R. L.; Friedrich, E. C.; Wall, R. E. *J. Am. Chem. Soc.* **1959**, *81*, 452.
23. Nakamura, Y.; Kato, T.; Morita, Y. *J. Chem. Soc. Perkin Trans.* **1982**, *1*, 1187.
24. Taylor, E. C.; Kan, R. O.; Paudler, W. W. *J. Am. Chem. Soc.* **1961**, *83*, 4484.
25. Masamune, S.; Seidner, R. T.; Zenda, H.; Wiesel, M.; Nakatsuka, N.; Bigam, G. *J. Am. Chem. Soc.* **1968**, *90*, 5286.
26. Cookson, R. C.; Drake, B. V.; Hudec, J.; Morrison, A. *J. Chem. Soc. Chem. Commun.* **1966**, *15*.
27. Houk, K. N.; Woodward, R. B. *J. Am. Chem. Soc.* **1970**, *92*, 4143.
28. Paquette, L. A.; Barrett, J. H.; Kuhla, D. E. *J. Am. Chem. Soc.* **1969**, *91*, 3616.
29. Farrant, G. C.; Feldman, R. *Tetrahedron Lett.* **1970**, 4979.
30. Doering, W.v.E.; Wiley, D. W. *Tetrahedron* **1960**, *11*, 183.
31. Galbraith, A.; Small, T.; Barnes, R. A.; Boekelheide, V. *J. Am. Chem. Soc.* **1961**, *83*, 453.
32. Mukai, T.; Tezuka, T.; Akasaki, Y. *J. Am. Chem. Soc.* **1966**, *88*, 5025.
33. Prinzbach, H.; Knöfel, H. *Angew. Chem. Int. Ed. Eng.* **1969**, *8*, 881.
34. Blomquist, A. T.; Meinwald, Y. C. *J. Am. Chem. Soc.* **1959**, *81*, 667.
35. Williams, J. K.; Benson, R. E. *J. Am. Chem. Soc.* **1962**, *84*, 1257.
36. Askani, R. *Chem. Ber.* **1965**, *98*, 3618.
37. Takahashi, M.; Kitahara, Y.; Murata, I.; Nitta, T.; Woods, M. C. *Tetrahedron Lett.* **1968**, 3387.

CHAPTER 7

Electrocyclic Reactions: Stereochemistry and Torquoselectivity

7.1 ELECTROCYCLIC REACTIONS IN NEUTRAL SYSTEMS

Electrocyclic reactions¹ in neutral systems involve conjugated polyenes that can mobilize $4n$ or $4n+2$ electrons. The simplest electrocyclic process in neutral systems is a 4-electron ($4n$, $n=1$) butadiene–cyclobutene interconversion. In an electrocyclic ring closing (ERC), a more stable σ bond is formed at the expense of a weaker π bond. However, thermodynamics predicts that the electrocyclic ring opening (ERO) of cyclobutene would be more favourable because of the relief of ring strain. In contrast, for a 6-electron ($4n+2$, $n=1$) hexatriene–cyclohexadiene interconversion, the ring closing process forming a relatively unstrained six-membered ring is thermodynamically more favourable. However, with a proper choice of substrates, the thermodynamic balance can be tilted in favour of either a ring closing or ring opening.

The stereochemical idiosyncrasies (thermodynamic or contrathermodynamic stereochemistry) of the electrocyclic reactions stem from the operation of either the conrotatory (con) or disrotatory (dis) mode of ring closing and ring opening processes (see Table 3.3). It bears recall that there are two possible con and two possible dis modes. Two con modes may lead to the same or different diastereomeric products. The same is true for two dis modes. One of the two con (or dis) modes can get preference when it entails a more stable transition structure that leads to a major diastereomer. This kind of selectivity of one con (or dis) mode over an alternative one is called torquoselectivity.

We begin with the thermal ERO of a cyclobutene to a butadiene² taking 3,4-disubstituted cyclobutenes (Fig. 7.1). The *cis* isomer gives stereospecifically a (*E,Z*) diene, whereas the *trans* isomer yields exclusively the (*E,E*) diene.

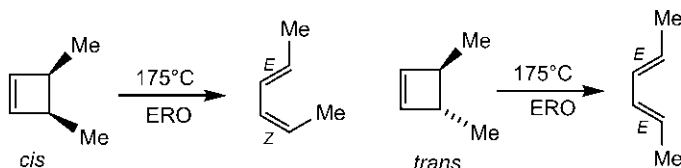


Fig. 7.1 Thermal electrocyclic ring opening of *cis*- and *trans*-3,4-dimethylcyclobutene.

The products arise from the thermally allowed conrotatory pathway as shown in Fig. 7.2.

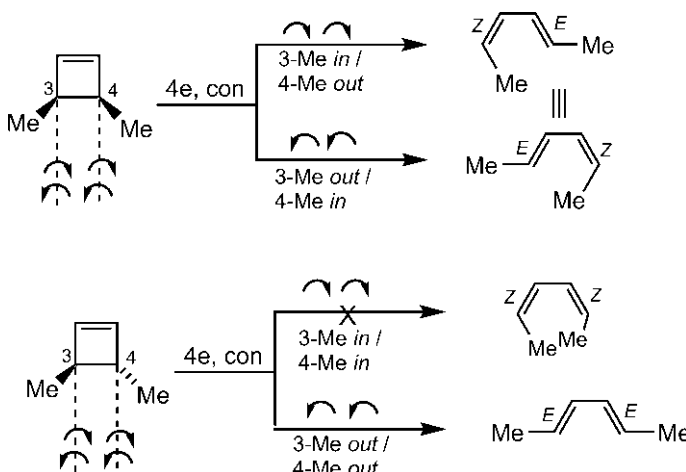


Fig. 7.2 Mechanism of electrocyclic ring opening reactions in Fig. 7.1.

For the *cis* isomer, two con motions give the same diastereomeric (*E,Z*) diene, whereas in case of the *trans* isomer, (*E,E*) and (*Z,Z*) dienes could form; however, only the (*E,E*) diene is obtained since the transition structure for the formation of the (*Z,Z*) diene is severely crowded. Thus, the con motion leading to the (*E,E*) isomer is preferred over the other con motion, that is, a torque selectivity operates due to a steric effect. It is also seen that the *cis* cyclobutene gives a thermodynamically less stable (*E,Z*) isomer, not the most stable (*E,E*) isomer. This indicates that under the symmetry control in a pericyclic mechanism, the electrocyclic product is rather counter-thermodynamic. If the mechanism were stepwise radical, the (*E,E*) diene would be expected to be the major product even from the *cis* isomer.

7.1.1 Mandal's Stereochemical Rule for Electrocyclic Reactions

The stereochemistry of electrocyclic reactions in the conrotatory or disrotatory pathway results from the rotation of substituents in the same or

opposite directions. It is often difficult particularly in a complex system to depict product stereochemistry resulting from such movements of substituents. To address the issue, a simple and straightforward rule has been developed.³

For the purpose of the rule, the stereochemical properties of the reactant and product are designated as syn (**S**) or anti (**A**) based on a directional sense as shown in Fig. 7.3. There are two possible syn (**S**) and two possible anti (**A**) relationships between the substituents X and Y at the two ends of a conjugated π system (Fig. 7.3A) or at the two ends of a σ bond broken or formed in a cyclic system (Fig. 7.3B). Notice that, in the plane of the π system, a terminal substituent (X or Y) is either on the right side or left side when viewed along the respective terminal double bond.

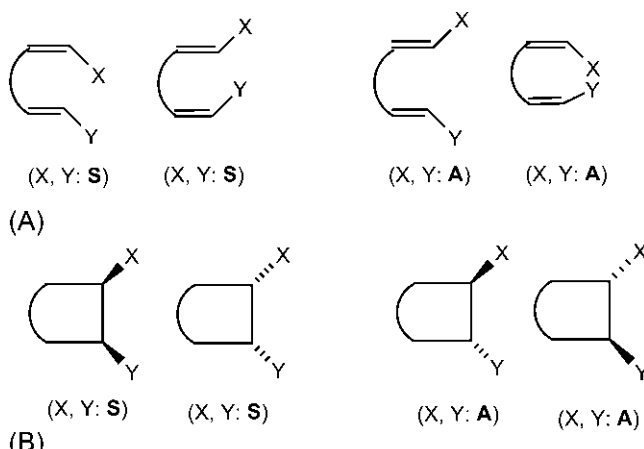
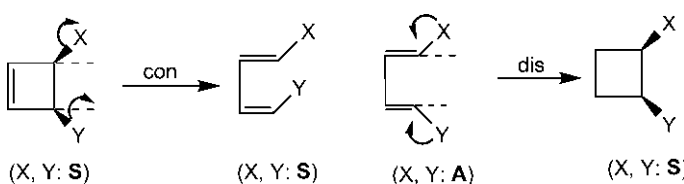


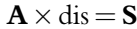
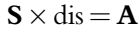
Fig. 7.3 (A) Two possible syn (**S**) and two possible anti (**A**) relationships of substituents X and Y at the ends of a conjugated π system; (B) two possible syn (**S**) and two possible anti (**A**) relationships of X and Y at the ends of the σ bond broken or formed in a cyclic system.

Applying the syn/anti designation in the conrotatory and disrotatory electrocyclic process as shown below, it is seen that a syn reactant forms a syn product under the con mode while an anti reactant gives a syn product under the dis mode.



The above results are generalized to obtain the following rule.

The rule is



where the reactant stereochemistry undergoes the specified process to give the product stereochemistry.

The designated property **S** or **A** remains the same in a conrotatory process, whereas it becomes the opposite in a disrotatory reaction. Since a directional sense is integrated in the definition of syn or anti, the movement of substituents in the same direction (con motion) causes the syn or anti to remain unchanged, whereas the movement of substituents in the opposite direction (dis motion) makes the syn or anti to become opposite. The rule provides a useful supplement to delineate product stereochemistry in a straightforward manner without the need for spatial imagination of the movement of substituents in each and every case.

As a simple illustration of the rule, we consider again the ERO reactions described in Fig. 7.1. Using the rule, the product stereochemistry is delineated as shown in Fig. 7.4. The two Me substituents, which are syn (**S**) in *cis*-cyclobutene, remain syn (**S**) in the product diene (Fig. 7.4A) as **S** × con = **S**.

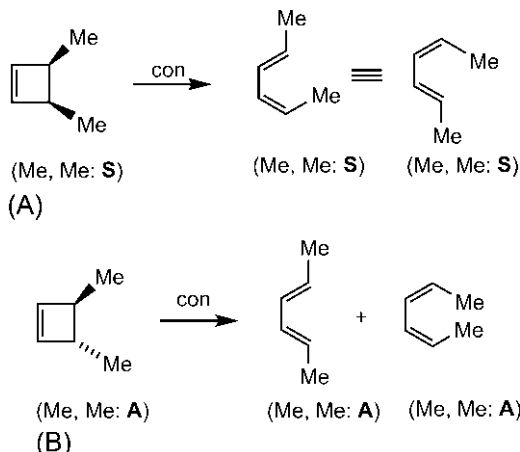


Fig. 7.4 Delineation of product stereochemistry, using Mandal's rule, in the electrocyclic ring opening of (A) *cis*-3,4-dimethylcyclobutene and (B) *trans*-3,4-dimethylcyclobutene.

Note that the two syn stereochemistries of diene are equivalent and represent the (*E,Z*) isomer. Similarly, the anti (**A**) relationship of two Me's in *trans*-cyclobutene is retained in the product diene ([Fig. 7.4B](#)) as **A** × con = **A**. Notice that the two anti stereochemistries of the diene are not equivalent and indicate (*E,E*) and (*Z,Z*) isomers; however, formation of the (*Z,Z*) diene is unfavourable due to steric factors.

We have previously seen in [Chapter 6](#) that the stereochemical course of cheletropic cycloadditions could be determined based on the conrotatory or disrotatory process with respect to the conjugated polyene. The above rule is also applicable to cheletropic reactions to delineate product stereochemistry. This is illustrated in [Fig. 7.5](#) with the cheletropic addition of SO₂ to a diene (see [Fig. 6.11](#)) and cheletropic extrusion of SO₂ from a seven-membered ring sulphone (see [Fig. 6.13](#)).

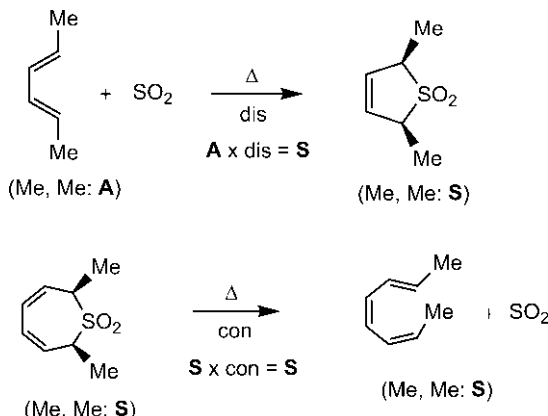


Fig. 7.5 Delineation of product stereochemistry, using Mandal's rule, in cheletropic cycloaddition and extrusion reactions.

7.1.2 4-Electron Electrocyclic Process

7.1.2.1 Relative Rates

The cyclobutene ring opening is accelerated when there is an electron donating *x* or an electron withdrawing *z* substituent at C-3 of the cyclobutene ring. For example, a benzocyclobutene **7.1** undergoes a ring opening at 180°C to give an *ortho*-quinodimethane which undergoes an intramolecular Diels–Alder (IMDA) reaction ([Fig. 7.6](#)).⁴ In contrast, when a much more powerful electron donating oxy anion substituent is present at C-3 of the cyclobutene **7.2**, the ring opening takes place at 0°C.⁵ In this case, the *ortho*-quinodimethane is trapped by benzyne as a Diels–Alder adduct.

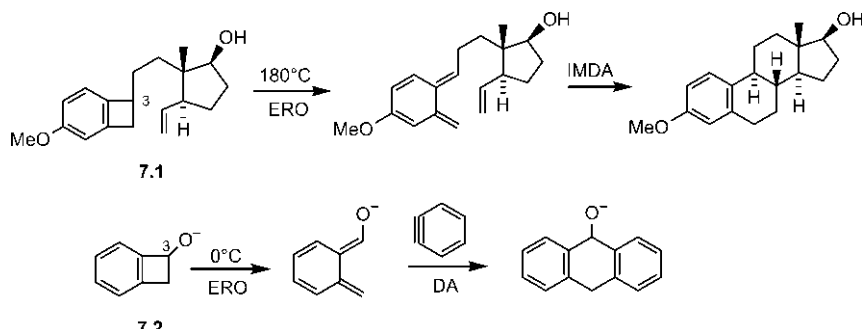


Fig. 7.6 Relative reactivity of the ring opening of a cyclobutene and an oxyanion derivative.

The conrotatory ring opening of a cyclobutene involves an aromatic Möbius transition structure (see Fig. 3.35B). The electron donating x or the electron withdrawing z substituent in a 3-substituted cyclobutene is not conjugated to the double bond and therefore not stabilizing; however, the x- or z-substituent is conjugated with the aromatic transition structure and stabilizes it. Thus, the rate of the electrocyclic reaction is increased in the presence of the electron donating or electron withdrawing 3-substituent.⁶

The substituent effect on the rate has been explained⁶ by estimating the π -energy difference for the conrotatory ring opening of the unsubstituted cyclobutene and the x- or z-substituted cyclobutene. As model systems, x- and z-substituents can be considered as carbanion and carbocation centres, respectively.

For both unsubstituted and substituted cyclobutene,

$$\begin{aligned}\pi - \text{energy} &= \text{energy of two electrons in an isolated } \pi \text{ system (ethylene)} \\ &= 2(\alpha + \beta).\end{aligned}$$

The π -energy of Möbius TS in the unsubstituted system

$$\begin{aligned}&= \text{energy of completely filled lowest degenerate levels (see Fig. 1.35)} \\ &= 4(\alpha + 1.414\beta) = 4\alpha + 5.656\beta.\end{aligned}$$

The π -energy of Möbius TS for the substituted cyclobutene⁶

$$= 4\alpha + 6.293\beta$$

These π -energies are shown in an energy diagram (Fig. 7.7). (Remember that a more positive β indicates decreased energy.) Clearly, the π -energy difference between the reactant and Möbius TS for the x- or z-substituted cyclobutene is less than that for the unsubstituted system by 0.637β (in units of β) (Fig. 7.7), and hence the increase in rate.

The rate also increases when a c-substituent is present on C-3 of cyclobutene when the π -energy of the Möbius TS is $(4\alpha + 8.055\beta)$.⁶

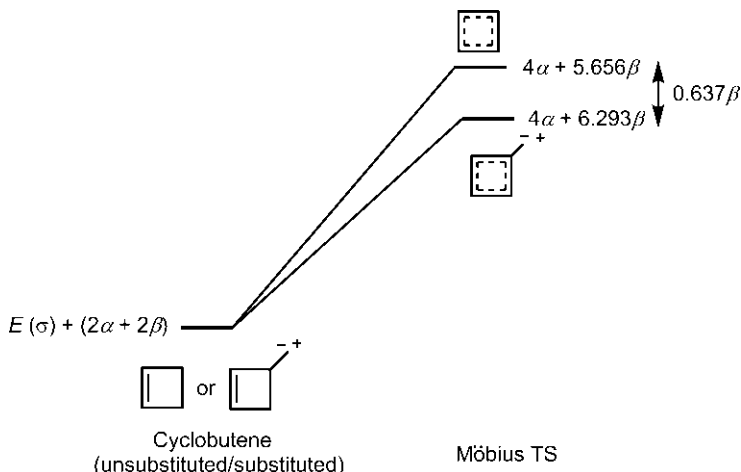


Fig. 7.7 π -Energies of unsubstituted and x- or z-substituted cyclobutenes and their corresponding Möbius transition structures in the conrotatory ring opening reactions.

7.1.2.2 Torquoselectivity

We have already seen that torquoselectivity operates in the ring opening of the *trans*-3,4-dimethylcyclobutene, which is attributed to steric effects. Now, we consider the thermal ring opening of 3-x- and 3-z-substituted cyclobutenes (Fig. 7.8). It has been observed that an x-substituent (π donor) preferentially moves outwards to give the (E) diene,⁷ whereas a z-substituent (π acceptor) preferentially moves inwards to give the (Z) diene.⁸

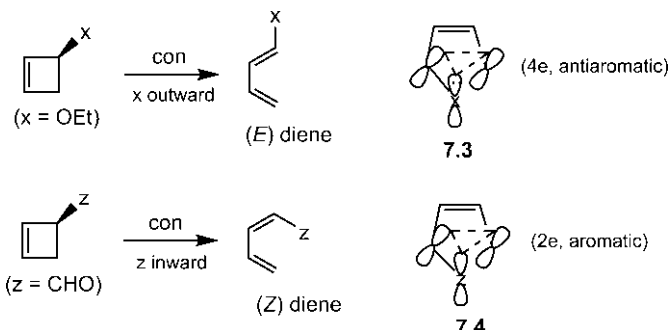
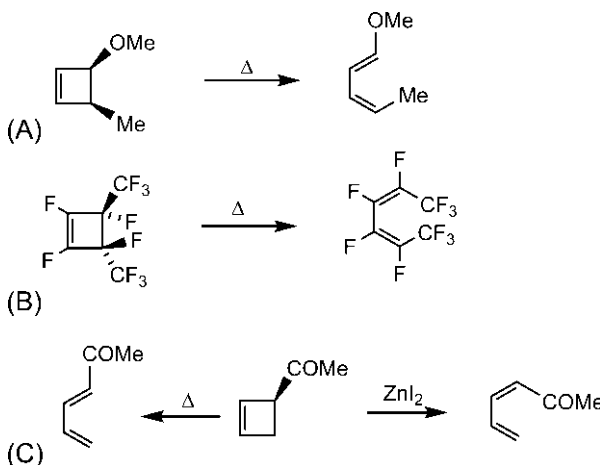


Fig. 7.8 Torquoselectivity in the electrocyclic ring opening of 3-x and 3-z-substituted cyclobutenes. Secondary cyclic overlaps during the inward movement of x- and z-substituents are indicated in **7.3** and **7.4**.

The observed torque selectivity cannot be understood by steric effects alone. A simple explanation⁹ is that the electronic effect of the substituent operates in the form of a secondary cyclic orbital overlap when the substituent moves inwards as shown in 7.3 and 7.4. Only the lobes of the breaking σ bond with 2 electrons are involved in the secondary overlap (the involvement of p orbitals of the π bond is negligible as indicated by Houk's calculation). An x-substituent provides a filled orbital, and consequently the Hückel-type secondary cyclic overlap involving 4 electrons contributes an antiaromatic character to the transition structure. Therefore, an x-substituent does not move inwards but prefers to move outwards. However, a z-substituent provides a vacant orbital and the secondary cyclic overlap involving 2 electrons contributes an aromatic character to the transition structure. Thus, a z-substituent moves inwards.

Problem 7.1

Explain the torque selectivity observed in the following electrocyclic reactions.



Answer

Each reaction involves a conrotatory ring opening of a cyclobutene.

- (A) OMe is a much stronger π donor than Me. Hence, OMe controls torque selectivity and moves outwards because its inward movement would contribute a more antiaromatic character to the transition structure by way of a secondary cyclic overlap. Consequently, Me must rotate inwards as a result of the con motion.
- (B) F is a π donor, though it has an opposing inductive trend. The π donating property of F destabilizes the transition structure by an

antiaromatic secondary cyclic overlap in its inward movement, and hence F's on C-3 and C-4 move outwards. This is reinforced by the preference for the inward movement of CF_3 groups which are electron withdrawing via the C—F hyperconjugation.¹⁰

(C) Torquoselectivity results from the balance between electronic and steric effects. In the absence of Lewis acid, the steric effect seems to be dominant and the large *z*-substituent (COMe) moves outwards, yielding an (*E*) isomer. However, in the presence of Lewis acid, the complexed COMe is strongly electron withdrawing, and the electronic factor becomes dominant even though the complexed COMe is a larger substituent. In the presence of ZnI_2 , COMe moves inwards to produce a (*Z*) isomer.¹¹

(It is mentioned in this context that when both OMe and *t*-Bu substituents are present on C-3 of cyclobutene, it is the bulky *t*-Bu that moves inwards to the more hindered position because of the dominant preference of electron donating OMe to move outwards.¹²)

The torquoselectivity is also observed in the thermal ring opening of a bicyclic system as shown in Fig. 7.9.¹³

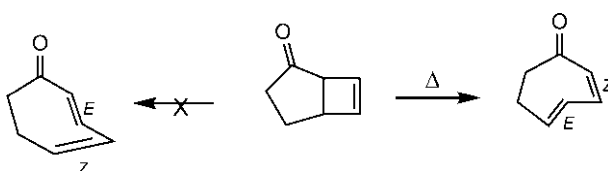


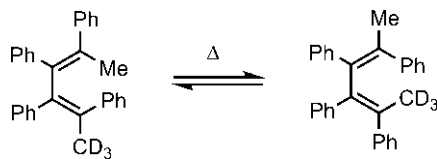
Fig. 7.9 Torquoselectivity in the thermal ring opening of bicyclo[3.2.0]hept-6-en-2-one.

The cyclobutene ring is substituted by an electron donating alkyl chain and an electron withdrawing carbonyl group. The outward rotation of the alkyl chain gives an *E* double bond and inward rotation of carbonyl forms a *Z* double bond in the product.

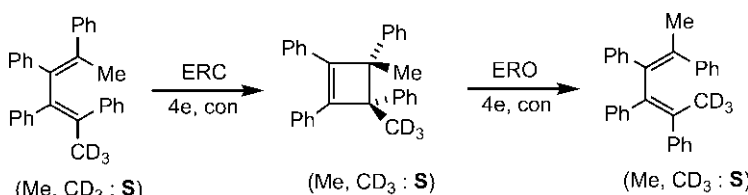
7.1.2.3 Stereochemistry

The stereochemistry of a 4-electron electrocyclic reaction arises from the conrotatory process under thermal conditions, and disrotatory process under photochemical conditions. Let us consider the thermal isomerization of two dienes as shown in Fig. 7.10.¹⁴

Apparently, the interconversion indicates as if there were rotation about double bonds in the diene! This is definitely not so. The isomerization has been explained by the successive ERC and ERO reactions as shown

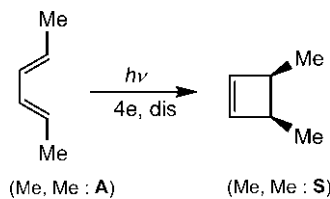
**Fig. 7.10** Thermal isomerization of two dienes.

in Fig. 7.11. The product stereochemistry at each step is delineated using the stereochemical rule: any two substituents, say Me and CD₃, which are syn (**S**), remain syn (**S**) throughout as **S** × con = **S**.

**Fig. 7.11** Mechanism of thermal isomerization of the dienes in Fig. 7.10.

Note that the cyclobutene intermediate is chiral, and two possible syn stereochemistries for CD₃ and Me refer to two enantiomers, one of which is drawn. The ring opening of the intermediate could give the product diene or revert to the starting diene. No product by symmetry-forbidden dis mode was formed even after 51 days at 124°C.

The photochemical ring closing of the (E,E)-2,4-hexadiene gives a *cis* cyclobutene, which arises from the allowed disrotatory pathway (Fig. 7.12).¹⁵ See the use of the rule: **A** × dis = **S**.

**Fig. 7.12** Photochemical electrocyclic ring closing of the (E,E)-2,4-hexadiene.

The ERC of stereochemically different diene units in a nine-membered ring has been studied thermally and photochemically (Fig. 7.13).¹⁶ The product is the same bicyclic system with *cis* stereochemistry at the ring junction. See the use of the rule: **S** × con = **S**; **A** × dis = **S**.

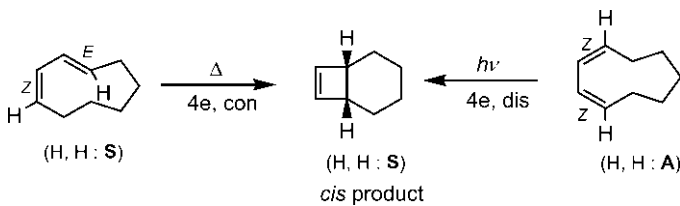


Fig. 7.13 Thermal ring closing of the (E,Z) diene and photochemical ring closure of the (Z,Z) diene in a nine-membered ring.

The thermal conversion of Dewar benzene to benzene involves a ring opening of a cyclobutene unit. Dewar benzene is thermodynamically much less stable than benzene, and its conversion to benzene is highly exothermic by 71 kcal mol^{-1} . Surprisingly, Dewar benzene converts to benzene with a half-life of about 2 days at 25°C .¹⁷ This is attributed to the relatively high kinetic stability ($\Delta H^\ddagger = 23 \text{ kcal mol}^{-1}$) of Dewar benzene. The high kinetic barrier arises because the allowed con mode does not lead to benzene but proceeds through a highly strained cyclohexatriene **7.5** with a *trans* (E) double bond (Fig. 7.14A). On the other hand, the dis mode that leads directly to benzene is symmetry-forbidden (Fig. 7.14B).

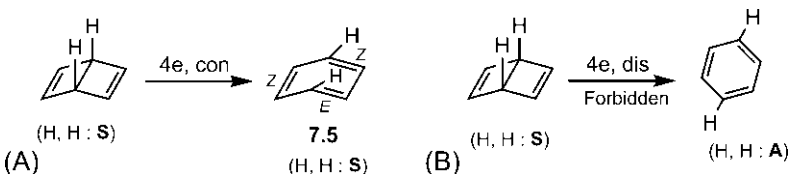


Fig. 7.14 Electrocyclic ring opening of Dewar benzene by the (A) con mode and (B) dis mode.

Theoretical calculations¹⁸ have shown that the TS for the conrotatory process could lead to benzene without the intermediate formation of **7.5**. The TS for the conrotatory process is of lower energy than that for the disrotatory process by $6.6 \text{ kcal mol}^{-1}$.¹⁹

Photochemical 4-electron ERC has been used in synthesis.²⁰ Dewar benzene was synthesized via a photochemical ring closure followed by bis-decarboxylation with lead tetraacetate (Fig. 7.15A). A similar reaction sequence is involved in a synthesis of cyclobutadiene from an unsaturated lactone (Fig. 7.15B). Here the final decarboxylation is done photochemically in the presence of iron pentacarbonyl to give the cyclobutadiene iron tricarbonyl. The photochemical decarboxylation is probably a retro-cycloaddition by the $[\sigma_2 + \sigma_2]$ mechanism.

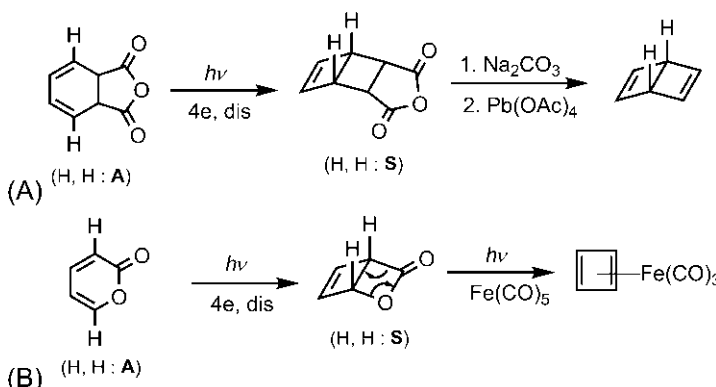
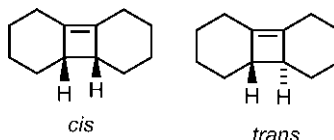


Fig. 7.15 Synthesis of (A) Dewar benzene and (B) cyclobutadiene iron tricarbonyl via a photochemical electrocyclic reaction.

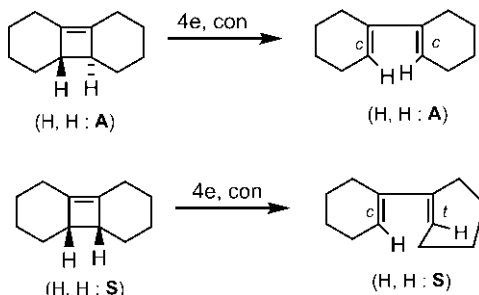
Problem 7.2

Of the following cyclobutenes, the *trans* isomer undergoes ring opening much faster ($k = 10^{-4}$ at 87°C) than the *cis* isomer ($k = 10^{-4}$ at 261°C). Explain.



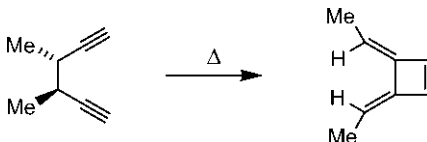
Answer²¹

The symmetry-allowed conrotatory ring opening of the *trans* isomer can produce a favourable *cis* double bond in each six-membered ring of the product and hence proceeds rapidly. In contrast, the conrotatory ring opening of the *cis* isomer leads to an impossibly strained *trans* double bond in a six-membered ring. Thus, the reaction is extremely slow and requires a very high temperature; it may even be stepwise. (Note that the ring opening of the *trans* isomer is completely *torquoselective* since the other con mode would result in a highly strained *trans* double bond in each ring.)

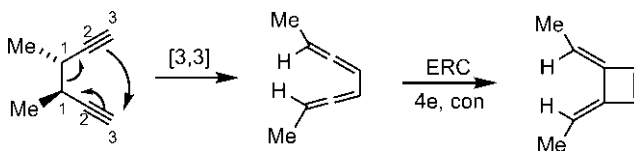


Problem 7.3

Suggest a mechanism for the following transformation.

**Answer²²**

The reaction proceeds through a [3,3] sigmatropic shift to form a bisallene which then undergoes a 4-electron ERC by the con mode to give the product.



7.1.3 6-Electron Electrocyclic Process

For the 6-electron hexatriene–cyclohexadiene interconversion,²³ ERC is favourable. The middle double bond of the triene must be *cis* (*Z*), and the molecule must adopt *s-cis* conformation so that the two ends can come closer to form a σ bond (Fig. 7.16).

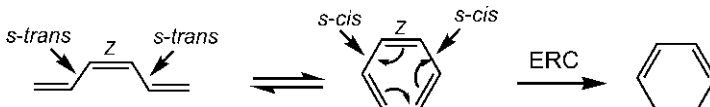


Fig. 7.16 Electrocyclic ring closing of hexatriene to cyclohexadiene.

The 6-electron electrocyclic reaction proceeds through a disrotatory pathway thermally, and occurs by the conrotatory mode photochemically (see Table 3.3). The stereochemical outcomes of some ring closing and ring opening reactions are illustrated in Fig. 7.17. In each case, the product stereochemistry is delineated using the stereochemical rule. Fig. 7.17A shows thermal ring closing reactions: (2*E*,4*Z*,6*E*)-octatriene gives almost exclusively *cis*-5,6-dimethylcyclohexadiene, whereas (2*E*,4*Z*,6*Z*)-octatriene produces *trans*-5,6-dimethylcyclohexadiene as a major product (see also Fig. 8.21, p. 353). The *trans* isomer is chiral, and the two possible diis modes lead to a racemic product. The stereochemistry of the photochemical ring opening of *cis* and *trans* isomers of a substituted cyclohexadiene is shown in Fig. 7.17B.

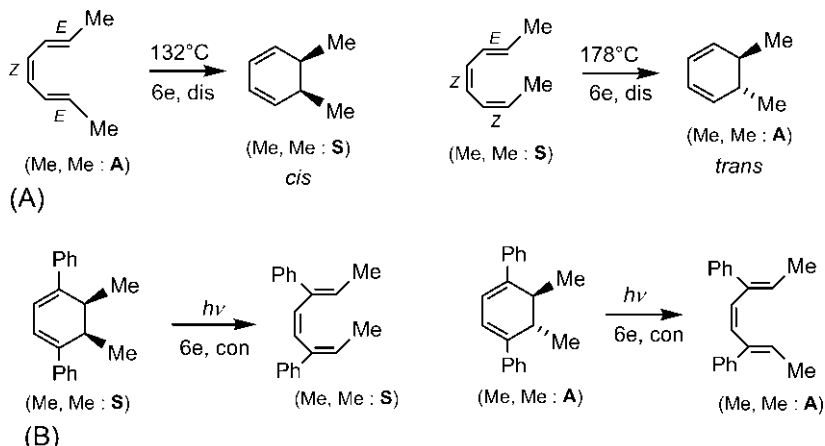


Fig. 7.17 (A) Stereochemistry of thermal ring closing reactions and (B) stereochemistry of photochemical ring opening reactions.

Dimethyldihydropyrene exhibits photochromism by a photochemical 6-electron ring opening and the reverse process. A reversible phototransformation of a species between two states of different absorption spectra is called photochromism.²⁴ Under visible light, dimethyldihydropyrene undergoes a ring opening by the con mode to form metacyclophadiene and the reverse ring closing occurs on UV irradiation (Fig. 7.18). The closed form (dimethyldihydropyrene) is dark green while the open form (metacyclophadiene) is colourless.²⁵

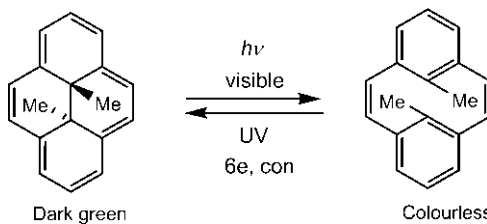


Fig. 7.18 Photochromism of dimethyldihydropyrene by electrocyclic isomerization.

Problem 7.4

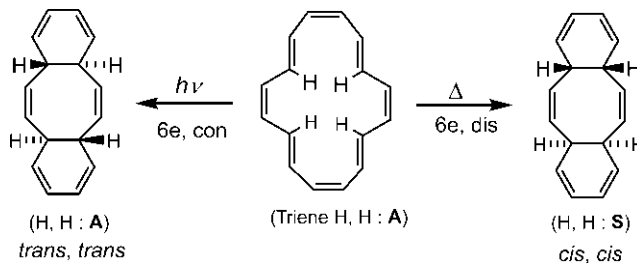
Predict the products of the following reactions.



Answer²⁶

The thermal 6-electron ERC by the disrotatory process gives a *cis*, *cis* product while the photochemical conrotatory ring closing produces a

trans, trans product. The *cis, cis* isomer in which the two terminal rings are on opposite sides of the central ring is sterically more stable, and is the observed product. Similarly, a sterically more favourable *trans, trans* isomer is formed.



trans-9,10-Dihydronaphthalene can be converted into *cis*-9,10-dihydronaphthalene, and vice versa by a sequence of thermal and photochemical

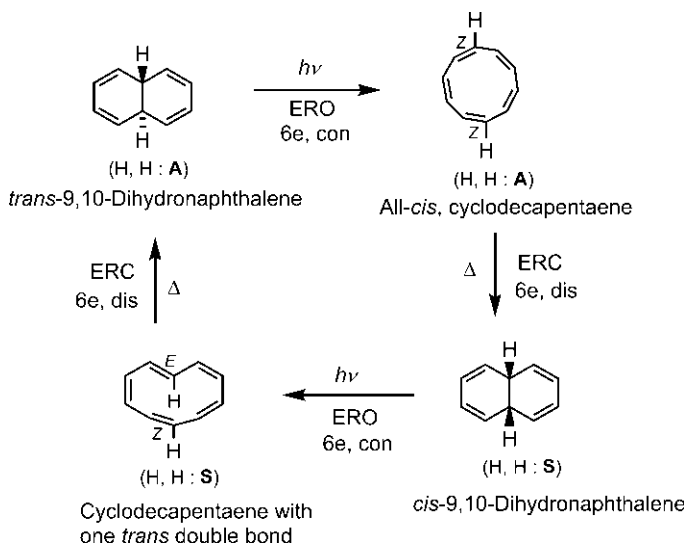
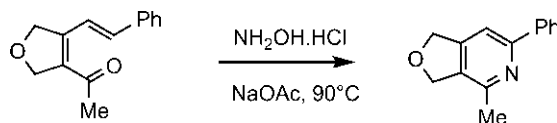


Fig. 7.19 Transformation of *trans*-9,10-dihydronaphthalene into *cis*-9,10-dihydronaphthalene and vice versa.

6-electron electrocyclic reactions, as shown in Fig. 7.19.²⁷

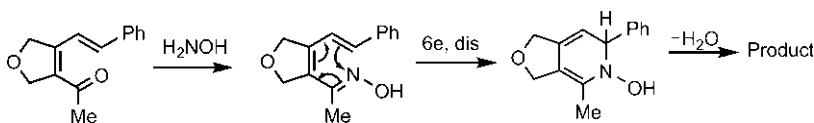
Problem 7.5

Suggest a mechanism for the following pyridine synthesis.



Answer²⁸

The reaction proceeds via a thermal 6-electron ring closing as shown below.



Photochemical cyclization of (*Z*)-stilbene gives *trans*-dihydrophenanthrene (Fig. 7.20). The dihydrophenanthrene has lost the aromaticity of stilbene; however, once formed, it cannot revert to stilbene by the thermal ring opening because the allowed dis mode would produce a highly strained *trans* cyclohexatriene ring (cf. Fig. 7.14A). The dihydrophenanthrene on oxidation by air or iodine gives phenanthrene. The photochemical reaction is useful for the synthesis of angularly fused polycyclic compounds and natural products.²⁹

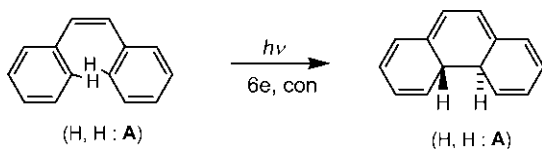


Fig. 7.20 Photochemical cyclization of (*Z*)-stilbene to *trans*-dihydrophenanthrene.

7.1.3.1 Cyclic Hexatrienes: Valence Tautomerism

Monocyclic hexatriene can undergo ERC to give a bicyclic system and an equilibrium is rapidly established between the monocyclic and bicyclic systems by the disrotatory pathway. The cyclic triene system thus exhibits valence tautomerism (a process that involves reorganization of bonding electrons). Since the bicyclic system is generally more strained, the equilibrium lies essentially in favour of the monocyclic triene. However, with a larger ring size as in the case of cyclononatriene, the equilibrium favours the bicyclic form. Fig. 7.21 shows some examples in which the equilibrium favours the triene form.

The valence tautomerism is of more interest with respect to cycloheptatriene–norcaradiene interconversion.³⁰ Cycloheptatriene and its alkyl derivatives exist predominantly in the triene form because of the strain involved in the 6–3 fused bicyclic norcaradiene. However, the

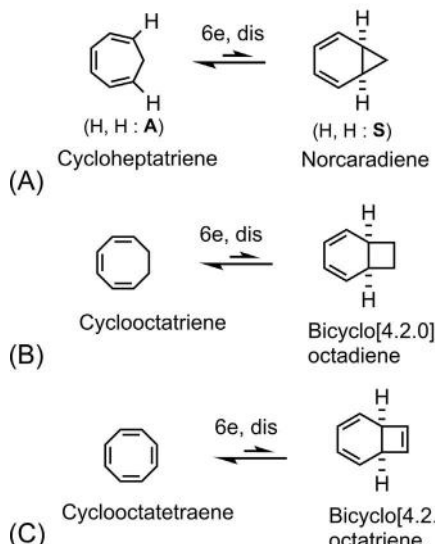


Fig. 7.21 Valence tautomerism in (A) cycloheptatriene (B) cyclooctatriene and (C) cyclooctatetraene systems.

norcaradiene structure is strongly favoured with cycloheptatriene bearing electron withdrawing substituents such as CN or BR_2 (Fig. 7.22).^{31,32}

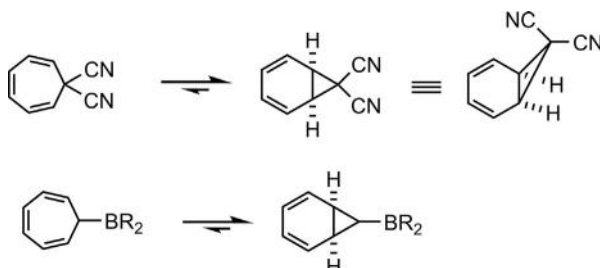


Fig. 7.22 Preference of the norcaradiene structure in the valence tautomerism of a dicyano or boron derivative of cycloheptatriene.

Here the norcaradiene structure is stabilized by the frontier orbital interaction of a *Walsh*-type cyclopropyl σ orbital (HOMO) with the vacant π^* or p orbital (LUMO) of the electron withdrawing substituent (Fig. 7.23). The cyclopropyl ring possesses two degenerate high-energy σ orbitals (HOMOs); however, the σ orbital in the bisected conformation as shown in Fig. 7.23 can overlap efficiently with the vacant π^* or p orbital (LUMO) of the CN or BR_2 substituent. This type of interaction is also

described as $\sigma-\pi^*$ (or $\sigma-p$) hyperconjugation. (Note that this frontier orbital interaction refers to the ground state stability of a molecule, not its reactivity. The interaction is similar to the strong hyperconjugation of the cyclopropyl ring with the vacant carbon p orbital of cyclopropylcarbinyl cation accounting for its stability.)

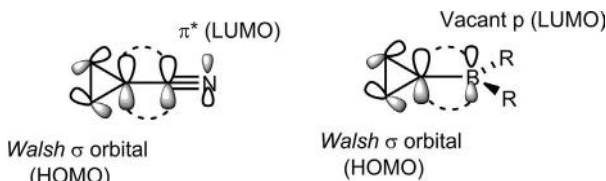
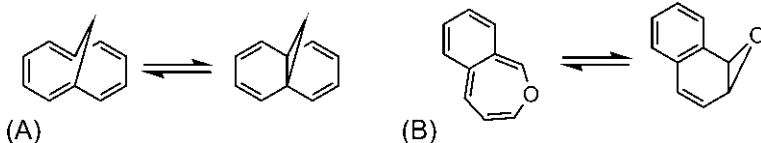


Fig. 7.23 Frontier orbital interaction stabilizing the norcaradiene structure in Fig. 7.22.

Problem 7.6

To which side would the following valence equilibria lie? Explain.



Answer

- (A) The hexatriene form on the left is more stable as it is aromatic with nearly planar 10 π electrons (Hückel system). It is a [10] annulene. The ring closed form on the right is nonaromatic. The equilibrium therefore lies to the left side.
- (B) The equilibrium favours the ring closed naphthalene oxide on the right, which is aromatic. The open triene (oxepin) structure is nonaromatic.

Cyclooctatetraene is a useful starting material in organic synthesis (see Figs. 5.73, 9.22A and 10.51; Problem 9.5) and the reaction usually proceeds through its valence tautomer. When bromocyclooctatetraene is heated to 80°C, (*E*)- β -bromostyrene is obtained in quantitative yield (Fig. 7.24).³³

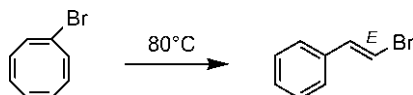


Fig. 7.24 Thermal conversion of bromocyclooctatetraene into (*E*)- β -bromostyrene.

Bromocyclooctatetraene can give four valence isomers (**7.6–7.9**) by the disrotatory ring closing, but the isomer **7.6** can only lead to the product (Fig. 7.25).

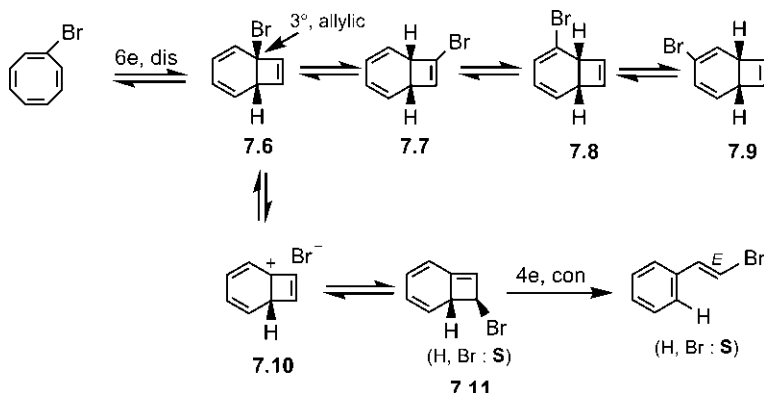


Fig. 7.25 Mechanism of thermal conversion of bromocyclooctatetraene in Fig. 7.24.

The reactive isomer **7.6** is a tertiary as well as an allylic bromide which can readily dissociate to form a stabilized carbocation **7.10**. Re-addition of Br^- can form an isomeric bromide **7.11** which undergoes ERO to give the product. The formation of intermediate carbocation **7.10** is consistent with the following experimental results: (a) the rate of the reaction is solvent dependent, being 600 times faster in polar solvent acetonitrile than in cyclohexane; (b) in the presence of LiI, the product is (*E*)- β -iodostyrene, although (*E*)- β -bromostyrene is unaffected by LiI under the reaction conditions.

The valence isomers can be trapped by the Diels–Alder reaction with a very reactive dienophile, 4-phenyl-1,2,4-triazoline-3,5-dione. The Diels–Alder *endo* adduct with the reactive valence isomer **7.6** is shown in Fig. 7.26. Here the strong *endo* preference arises from the presence of two nitrogen lone pairs on the dienophile. A lone pair in the *endo* orientation is strongly repelled by the antibonding interaction with the diene orbitals and therefore takes up the *exo* orientation. This is known as the *exo* lone pair effect for *endo* selectivity.

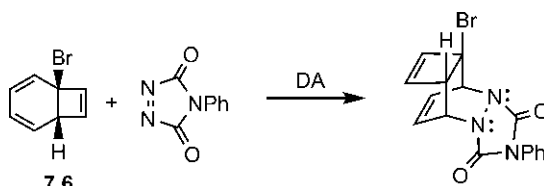


Fig. 7.26 Trapping of valence isomer **7.6** in Fig. 7.25 by the Diels–Alder reaction.

1,4-Dibromocyclooctatetraene, on heating at 180°C, follows a pathway similar to bromocyclooctatetraene (Fig. 7.27).

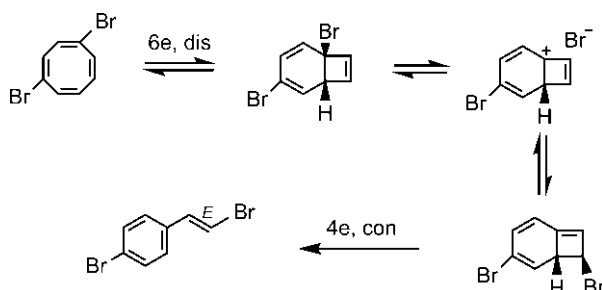


Fig. 7.27 Thermal transformation of 1,4-dibromocyclooctatetraene.

7.1.4 4-Electron versus 6-Electron Electrocyclic Process

7.1.4.1 Photocyclization of Cycloheptatrienes

In contrast to the 6-electron thermal reaction, cycloheptatriene undergoes a 4-electron disrotatory ring closing under photochemical conditions. This is because a photochemical 6-electron reaction by the conrotatory process would lead to an impossibly strained *trans* fused 6–3 bicyclic structure 7.12. The 4-electron reaction, on the other hand, gives a favourably *cis* fused 5–4 bicyclic system 7.13 (Fig. 7.28).

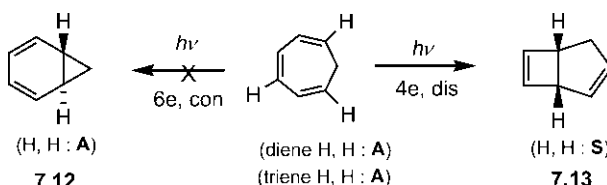


Fig. 7.28 Photochemical ring closing of cycloheptatriene.

Photocyclization of Substituted Cycloheptatrienes and Regioselectivity

The nature of the substituent (x-type or z-type) on a double bond of cycloheptatriene influences the regioselectivity of the ring closing process. The electron donating x-substituent at the 1-, 2- or 3-position of the triene directs the ring closing as shown in Fig. 7.29.³⁴

The regioselectivity has been explained by considering the geometry and sudden polarization in the excited state of a cycloheptatriene.³⁵ Recall that the excited state of an alkene has a twisted, perpendicular (*p*) geometry (see Fig. 1.11). Similarly, a triene on excitation loses a π bond [bond order = $(5 - 1)/2 = 2$] and the excited state adopts a geometry in which a

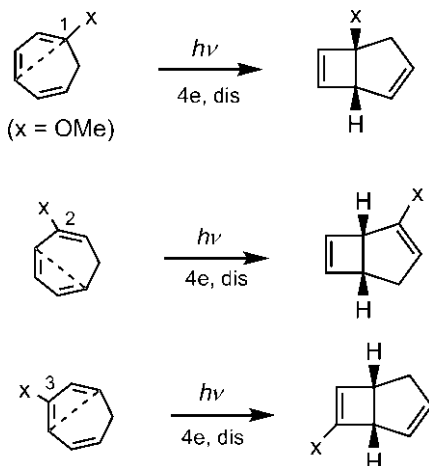


Fig. 7.29 Regioselectivity of photocyclization of the 1-x-, 2-x- and 3-x-substituted cycloheptatriene.

terminal p orbital is orthogonal to the pentadienyl unit (Fig. 7.30). Calculations indicate that the orthogonal p orbital carries a partial positive charge while the pentadienyl unit accommodates a partial negative charge.

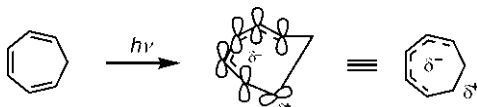


Fig. 7.30 Geometry and sudden polarization in the excited state of cycloheptatriene.

Since an ERC requires a rotation of terminal p orbitals, it is likely that the orthogonal p orbital in the excited state of the triene is ready to participate in the ring closing process. An x-substituent stabilizes a positive charge; therefore, the excited state of the 1-x-substituted triene has the orthogonal p orbital at the 1-position which would participate in the 1–4 ring closing to give the observed product (Fig. 7.31A). When an x-substituent is at the 2- or 3-position of the triene, it necessarily resides in the pentadienyl anion unit in the excited state because a terminal carbon of the triene would possess the orthogonal p orbital. Since an x-substituent destabilizes a negative charge, it would make the least destabilization if x is at the node of the HOMO (ψ_3) of the pentadienyl anion (Fig. 7.31B and C). Therefore, for a 2-x-substituted triene, the orthogonal p orbital is at the 6-position which participates in the 6–3 closing to give the product (Fig. 7.31B). For the 3-x-substituted triene, the orthogonal p orbital is evidently at the 1-position which leads to the product via the 1–4 closing (Fig. 7.31C).

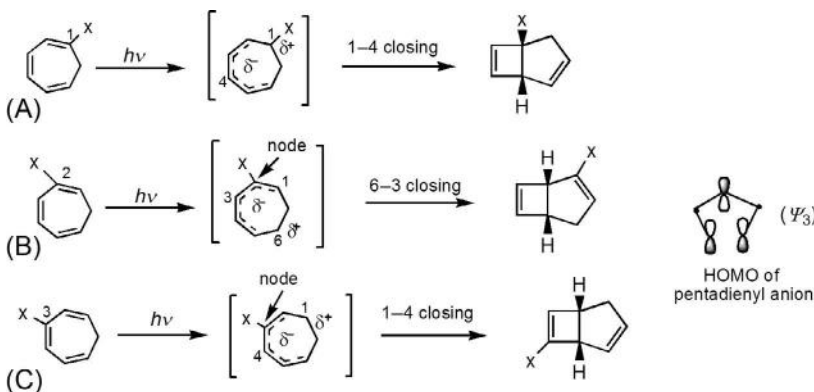


Fig. 7.31 Mechanism of regioselectivity of photocyclization of the (A) 1-*x*-substituted, (B) 2-*x*-substituted and (C) 3-*x*-substituted cycloheptatrienes in Fig. 7.29.

The different pattern of regioselectivity of ring closing of cycloheptatriene with the *z*-substituent at the 1-, 2- or 3-position has been explained similarly (Fig. 7.32).³⁴ An electron withdrawing *z*-substituent stabilizes a negative charge and therefore prefers to reside in the pentadienyl anion unit on a carbon having a large coefficient in HOMO. (Note that the size of the coefficient is the same at C-1, C-3 and C-5 of the pentadienyl anion HOMO.) The ring closing is effected involving the orthogonal p orbital on the respective carbon.

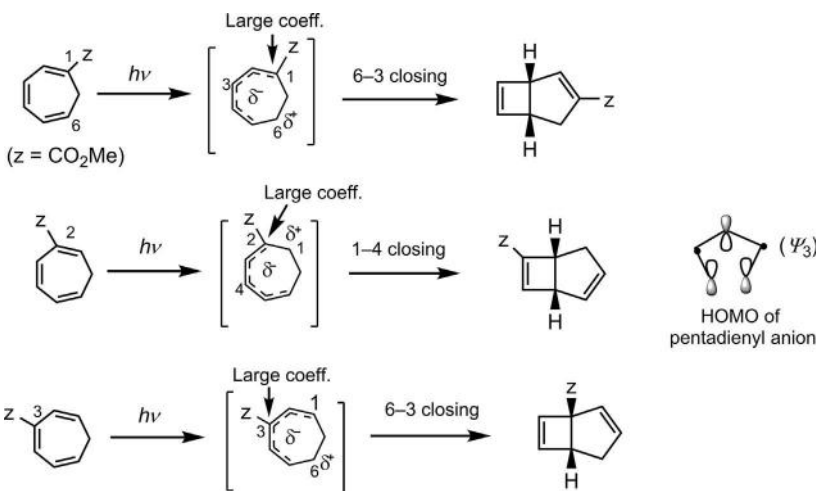


Fig. 7.32 Regioselectivity of photocyclization of the 1-*z*-, 2-*z*- and 3-*z*-substituted cycloheptatrienes.

Cyclooctatetraene also undergoes a 4-electron photocyclization to give a bicyclic product (Fig. 7.33), which is interestingly the same as that obtained from the 6-electron thermal reaction (see also Fig. 7.21C).

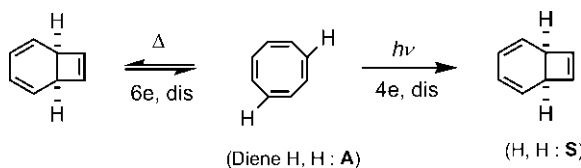


Fig. 7.33 Photocyclization of cyclooctatetraene.

7.1.4.2 Electrocyclic Reactions in Natural Products

Like the photocyclization of cycloheptatriene, the stereochemical constraints can govern the feasibility or otherwise of a 4-electron or 6-electron electrocyclic process. These stereochemical constraints are found in many electrocyclic reactions in the field of natural products. A beautiful illustration from the vitamin D series is presented in Fig. 7.34.³⁶ The stereochemistry at each step is delineated using the stereochemical rule. Ergosterol and lumisterol on photolysis undergo a 6-electron ring opening to give the same product precalciferol (previtamin D₂). The photochemical ring opening is torquoselective. The reaction is also reversible, and precalciferol is in photochemical equilibrium with ergosterol and lumisterol. Precalciferol, on heating to 150–200°C, produces a mixture pyrocalciferol and isopyrocalciferol by a 6-electron ring closing. On irradiation, pyrocalciferol and isopyrocalciferol cannot undergo a photochemical 6-electron ring opening as the process introduces a *trans* double bond in a six-membered ring, but gives photopyrocalciferol and photoisopyrocalciferol by a 4-electron ring closing with favourable *cis* fusions for four-membered rings.

It will be shown later (see Fig. 8.20, p. 352) that precalciferol spontaneously isomerizes to calciferol (vitamin D₂) by a reversible [1,7] sigmatropic H shift.

7.1.4.3 Consecutive Ring Opening and Ring Closing Reactions

First, we consider a thermal transformation as shown in Fig. 7.35.

Here 2-electrocyclic reactions proceed in tandem: a 4-electron ring opening by the conrotatory process followed by a 6-electron ring closing by the disrotatory pathway (Fig. 7.36). The two possible con modes lead to two intermediates. The intermediate triene with a *trans* double bond in the middle cannot undergo a 6-electron ring closing reaction. However,

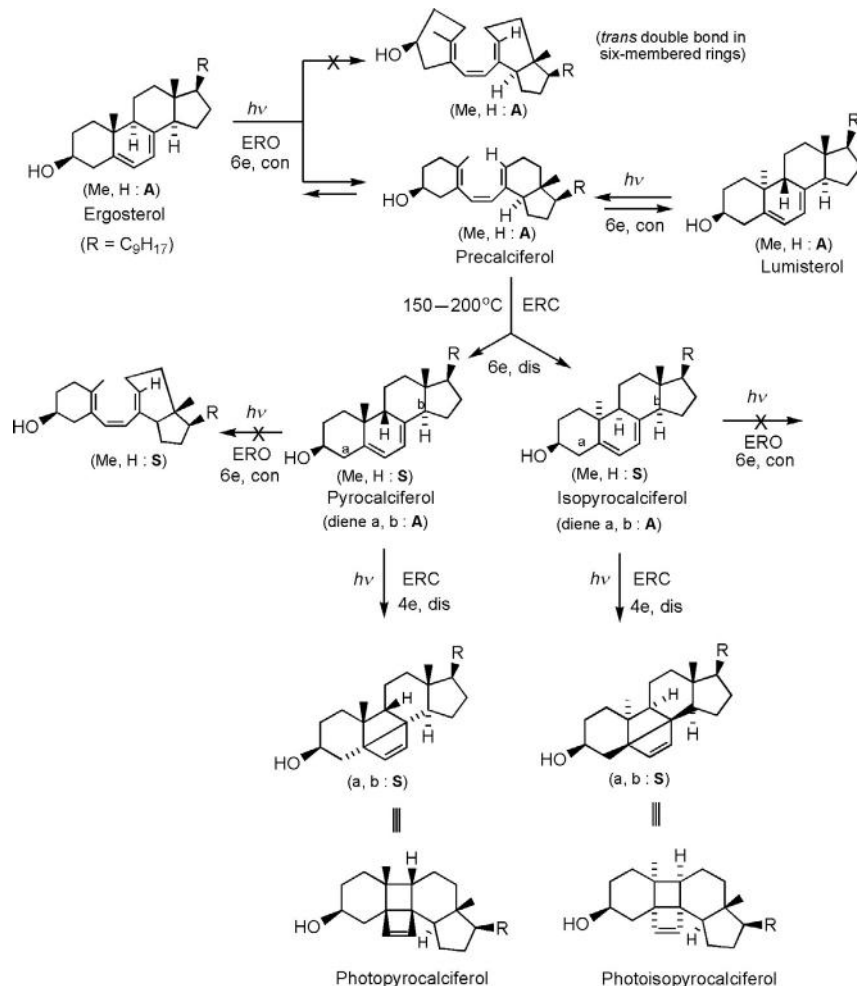


Fig. 7.34 Electrocyclic reactions in the vitamin D series.

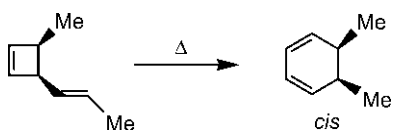


Fig. 7.35 Thermal transformation of a four-membered ring into a six-membered ring.

the other intermediate with a *cis* geometry of the middle double bond does and gives the *cis* product.

Next, we consider a reaction in which a *cis* fused 4–8 bicyclic system **7.14** is thermally transformed into a *trans* fused 6–6 bicyclic system **7.15** (Fig. 7.37).

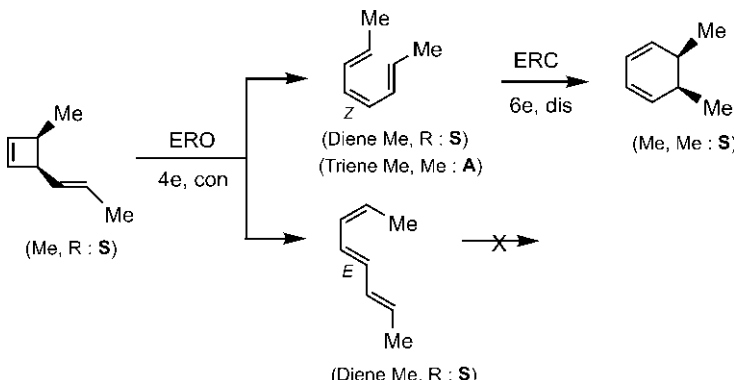


Fig. 7.36 Mechanism of thermal transformation in Fig. 7.35.

The reaction also proceeds through a conrotatory 4-electron ring opening followed by a disrotatory 6-electron ring closure. The intermediate triene with *cis* geometry of the middle double bond undergoes the ring closing to give the *trans* product **7.15**. (The product is chiral, and the two possible dis modes give a racemate, one enantiomer of which is drawn.)

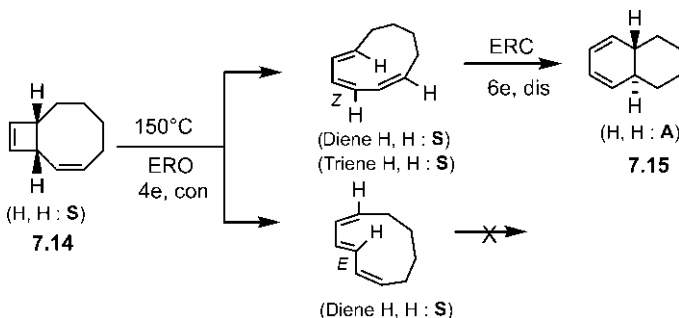


Fig. 7.37 Thermal conversion of a *cis* fused 4–8 bicyclic system into a *trans* fused 6–6 bicyclic system.

In contrast, thermal transformation of an analogous *cis* fused 4–6 bicyclic system takes a different course, as shown with the deuterium labelled compound **7.16** (Fig. 7.38). In this case, the intermediate triene with *cis* stereochemistry of the middle double bond **7.17** cannot undergo a 6-electron disrotatory ring closure as the process would lead to a highly strained *trans* fused 6–4 bicyclic system. The formation of the triene with *trans* geometry of the middle double bond in an eight-membered ring **7.18** is possible, though not quite favourable. Thus, **7.18** can either return to the starting material or can undergo an alternative 4-electron ring closing via **7.19** to

give the product **7.20**. The *s*-*cis* diene unit in **7.18** equilibrates to the *s*-*trans* diene unit in **7.19**. (In the absence of labelling, the reactant and product would be indistinguishable.)

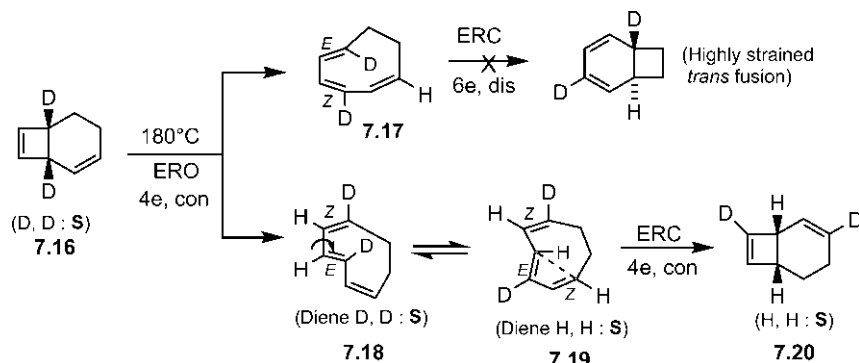


Fig. 7.38 Thermal reaction of a deuterium labelled *cis* fused 4–6 bicyclic system.

The 4-electron ring opening/6-electron ring closing sequence is involved in a variety of transformations. Fig. 7.39 shows the transformation of a formyl derivative of benzocyclobutene to a pyran derivative³⁷ via an *ortho*-quinodimethane intermediate. The 4-electron ring opening is torquoselective when the formyl group moves inwards.

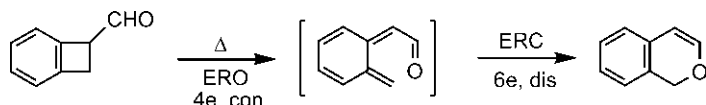
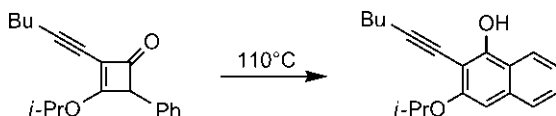


Fig. 7.39 Synthesis of a pyran from a formyl derivative of benzocyclobutene.

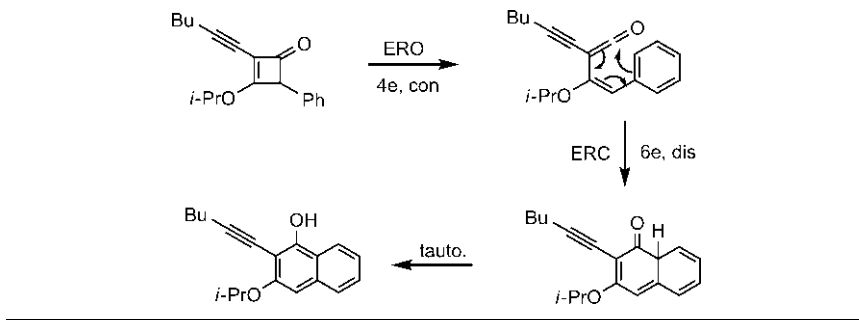
Problem 7.7

Account for the following observation.



Answer³⁸

The reaction involves a 4-electron ring opening to produce a ketene intermediate which then undergoes a 6-electron ring closure followed by tautomerization to give a naphthol.



7.1.5 8-Electron Electrocyclic Process

The 8-electron ($4n, n=2$) electrocyclic process represents the octatetraene–cyclooctatriene reaction.^{39,40} For the ring closing to take place, two inner double bonds must be *cis* (*Z*), and the molecule will adopt the *s-cis* conformation (Fig. 7.40).

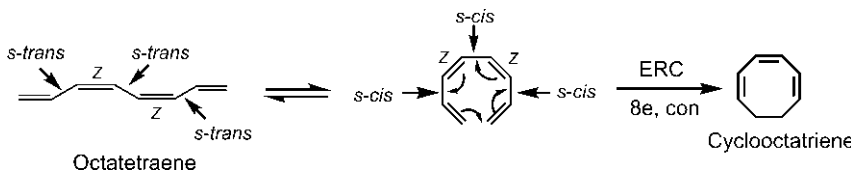


Fig. 7.40 Electrocyclic ring closing of octatetraene to cyclooctatriene.

The reaction proceeds thermally by an allowed conrotatory pathway. The product is a hexatriene which can undergo a second ERC by the disrotatory process to yield a bicyclic diene. This is illustrated with two examples in Fig. 7.41. The stereochemistry of the product is delineated using the stereochemical rule.

The ring closing of the substrate tetraene proceeds by an 8-electron process rather than by a 6-electron reaction, thereby demonstrating periselectivity involving the longest conjugated system. The 8-electron electrocyclic process occurs at a lower temperature and the reaction can be stopped at this stage. With an increase in temperature, a subsequent 6-electron reaction takes place. This indicates that an 8-electron reaction is faster than a 6-electron process. This has been rationalized as follows.⁴¹ The 8-electron component is antarafacial (π_{8_a}) for the conrotatory mode and the transition structure 7.21 is largely unstrained as the p orbital overlap can develop easily by a spiral approach because of the conformational

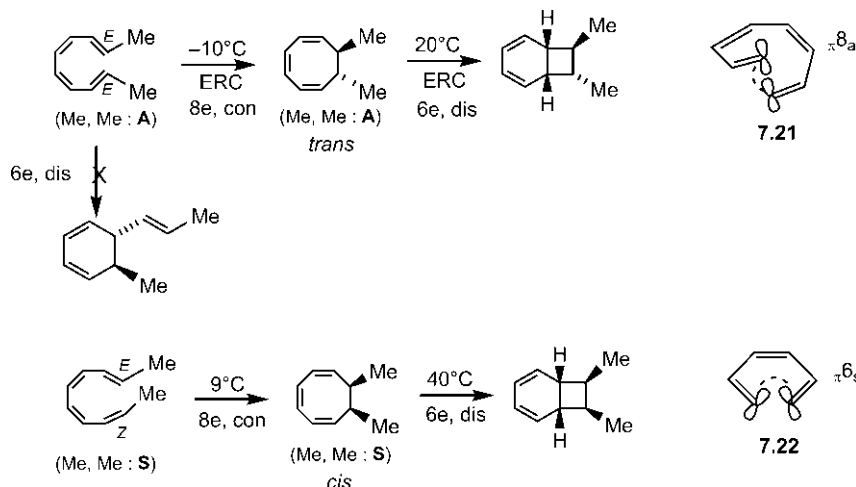


Fig. 7.41 Electrocyclic reactions of stereoisomeric octatetraene systems.

flexibility of the large $\pi 8$ system. In comparison, the transition structure 7.22 for the 6-electron reaction in the disrotatory pathway involves a suprafacial overlap and requires pushing of lobes on the same face towards each other in the smaller $\pi 6$ system, which appears to be geometrically more strained, and hence the reaction is relatively slower.

Problem 7.8

Predict the product of the following reaction.



Answer

A 12-electron conrotatory ERC gives a *trans* tricyclic product. The 12-electron electrocyclic ring closure of a very long π system is feasible here as four π bonds are constrained in two rings when the two ends of the π system can come closer in the *s-cis* conformation of the diene unit outside the rings.



7.1.6 Mixed Electrocyclic and Cycloaddition Reactions

A combination of an electrocyclic reaction and cycloaddition (mostly Diels–Alder) is an important strategy in synthetic schemes which have been described in different chapters of this text. Here we describe two examples.

A benzocyclobutene **7.23** reacts with methyl acrylate to give the product **7.24** (Fig. 7.42). The reaction involves a Diels–Alder cycloaddition with an *ortho*-quinodimethane generated by the ERO of **7.23**.

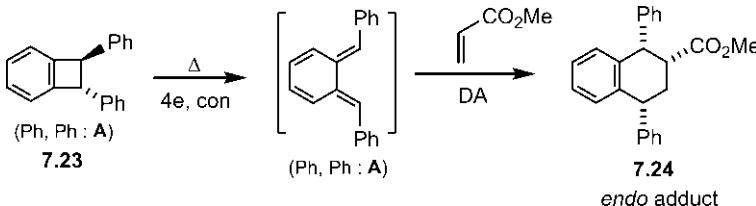


Fig. 7.42 Reaction of a benzocyclobutene with methyl acrylate.

Next, we consider a reaction of an octatetraene with dimethylacetylene dicarboxylate (Fig. 7.43).

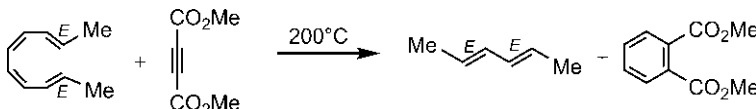


Fig. 7.43 Reaction of an octatetraene with dimethylacetylene dicarboxylate.

The reaction proceeds through a number of electrocyclic processes and cycloadditions as shown in Fig. 7.44. Note that all three (4e, 6e and 8e) electrocyclic processes are involved.

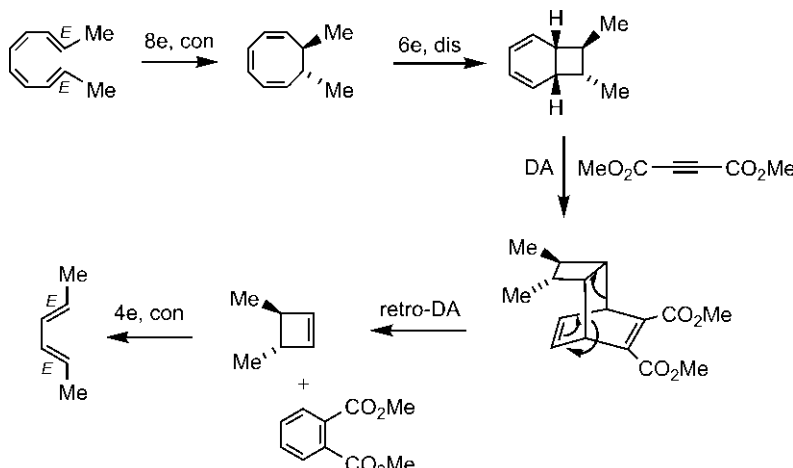


Fig. 7.44 Mechanism of the reaction in Fig. 7.43.

7.2 ELECTROCYCLIC REACTIONS IN CHARGED SYSTEMS

The Woodward–Hoffmann rules for electrocyclic reactions apply equally to the charged species.

7.2.1 2-Electron Electrocyclic Process in Cations

The 2-electron ($4n + 2$, $n=0$) electrocyclic process^{42,43} is the simplest case of an electrocyclic reaction, and is thermally allowed by the disrotatory mode. The process represents a prototype allyl cation–cyclopropyl cation reaction (Fig. 7.45). (Note that only one arrow is needed for a 2-electron process.)

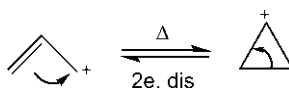


Fig. 7.45 2-Electron allyl cation–cyclopropyl cation reaction.

The ring opening process is thermodynamically more favourable because of the relief of ring strain. Let us consider the solvolysis of cyclopropyl tosylate in acetic acid (Fig. 7.46).⁴⁴ The product is allyl acetate instead of cyclopropyl tosylate.

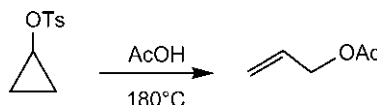


Fig. 7.46 Solvolysis of cyclopropyl tosylate.

It might appear that cyclopropyl tosylate ionizes to form a cyclopropyl cation (cf. the S_N1 mechanism) which then undergoes ERO followed by a nucleophilic attack by acetic acid to give the allyl acetate. However, there is no evidence that a free cyclopropyl cation is involved. Moreover, a cyclopropyl cation is not easy to form because dissociation introduces more cyclopropyl ring strain associated with change of hybridization ($sp^3 \rightarrow sp^2$). Theoretical computations⁴⁵ also suggest that a cyclopropyl cation encounters no barrier to its ERO and is not an intermediate.

The relative rates of solvolysis of the cyclopropyl tosylates 7.25 and 7.26 in AcOH/NaOAc are shown in Fig. 7.47.

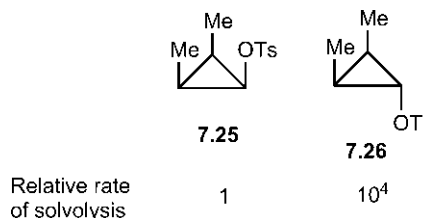


Fig. 7.47 Relative rates of solvolysis of *cis*- and *trans*-2,3-dimethylcyclopropyl tosylates.

If ionization to the cyclopropyl cation is involved in the r/d step, **7.25** should be more reactive because of the greater relief of steric strain as ionization occurs. The result shows the opposite: **7.26** is much more reactive and undergoes solvolysis 10^4 times faster than **7.25** (cf. anchimeric assistance).

The observed rates can be explained if the ring opening and ionization are concerted.⁴⁶ In this case, the electron density of the breaking σ bond can provide assistance to the departure of the leaving group. The assistance will be maximum when the electrons of the σ bond move from the back side of the leaving group (cf. the S_N2 mechanism). Nevertheless, the reaction will remain pericyclic in nature and obey the Woodward–Hoffmann rule of the disrotatory electrocyclic process. There are two possible dis modes. However, the requirement of the backside approach of the σ electrons to the leaving group dictates that only one of the two dis modes could operate, that is, the ring opening reaction is highly torquoselective. The orbital interactions for the ring opening of **7.25** and **7.26** are shown in Fig. 7.48. In Fig. 7.48A, the inner lobes of the breaking σ bond interact with a lobe of the vacant p orbital **7.27** and **7.28**, assuming the C-OTs bond pair being completely transferred to the departing group (OTs). The reaction is a $[6]2_s + \omega 0_s$ process, the sum of $(4q+2)_s$ and $(4r)_a$ components being 1 (odd) for the thermally allowed reaction. Fig. 7.48B shows the FMO pictures **7.31** and **7.32** in terms of the HOMO (σ_{C-C})/LUMO (σ_{C-O}^*) interaction for the *cis* tosylate **7.25** and *trans* tosylate **7.26**, respectively.

For the *cis* tosylate **7.25**, the torquoselective dis mode involves an inward movement of two methyl groups. This gives a U-shaped allyl cation **7.29** with a *cis* double bond when there is a severe steric strain in the transition structure. In contrast, for the *trans* tosylate **7.26**, the required dis mode moves two methyl groups outwards forming a sterically favourable W-shaped allyl cation **7.30** containing a *trans* double bond. Thus, solvolysis of **7.26** becomes much faster than that of **7.25**.

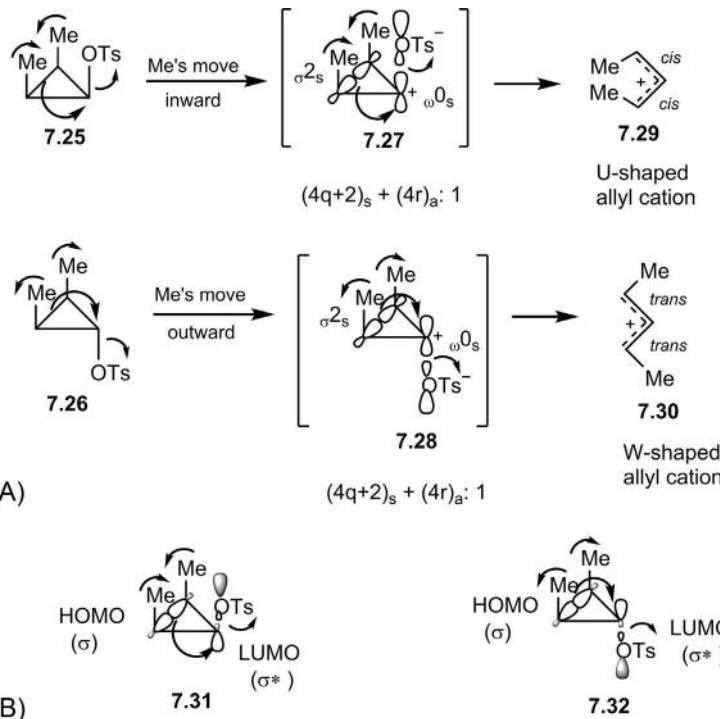


Fig. 7.48 Torquoselectivity in the ring opening of *cis* and *trans* cyclopropyl tosylates in solvolysis. Analysis of the transition structure by (A) generalized rules and (B) FMO interactions.

The ring opening of cyclopropyl cations or its equivalent can give rise to three possible configurations of allyl cations. For example, the diastereomers of the 2,3-dimethyl-1-chlorocyclopropane in a super acid medium produce U-shaped, Z-shaped (or sickle-shaped) and W-shaped allyl cations (Fig. 7.49),⁴⁷ which have been characterized by ¹H NMR spectroscopy. The configuration of an allyl cation is maintained by a continuous bonding overlap (there is no node in the filled molecular orbital ψ_1) and is retained at low temperature.

Evidently, for acyclic allyl cations, the stability decreases in the order W-shaped > Z-shaped > U-shaped due to steric factors.

If the allyl cation is part of a ring, the U-shaped cation with *cis* double bonds is most favourable in a six- or seven-membered ring (a *trans* double bond will be highly strained). However, an eight-membered or a larger ring with a *trans* double bond will be preferred. To illustrate, we shall now consider 2-electron electrocyclic reactions in bicyclic cyclopropane systems.

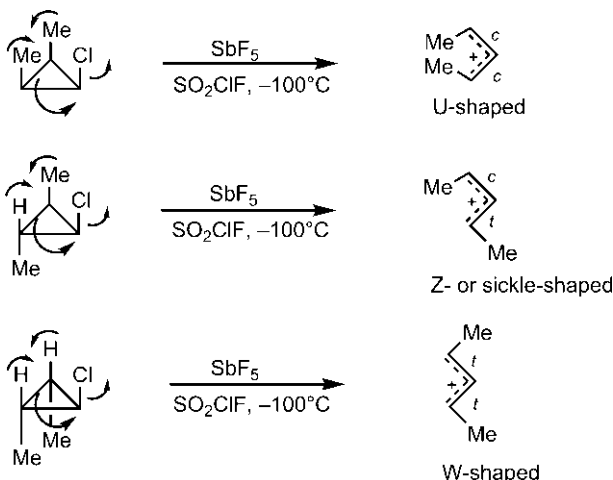


Fig. 7.49 Generation of U-shaped, Z- or sickle-shaped and W-shaped allyl cations in a super acid medium.

The relative rates of solvolysis of *endo* 7.33 and *exo* 7.34 isomers of fused 5–3 bicyclic cyclopropyl tosylates^{42,43} are shown in Fig. 7.50 vis-à-vis the relative rates for *cis* 7.25 and *trans* 7.26 isomers of cyclopropyl tosylates. Note the difference in the pattern of relative rates in the two cases.

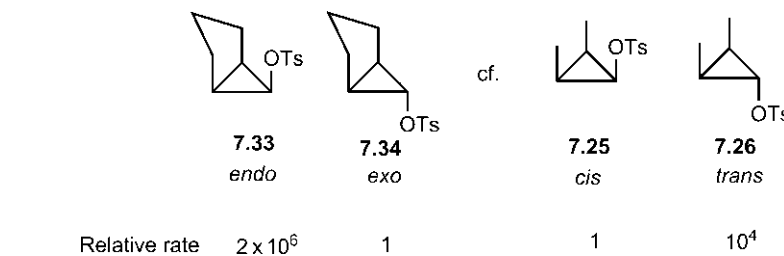


Fig. 7.50 Relative rates of solvolysis of *endo* and *exo* isomers of 5–3 fused bicyclic cyclopropyl tosylates vis-à-vis *cis* and *trans* cyclopropyl tosylates.

The ring opening of bicyclic tosylates 7.33 and 7.34 gives an allyl cation in a six-membered ring. For the *endo* tosylate, the torquoselective dis mode produces a U-shaped allyl cation with a favourable *cis* double bond in a six-membered ring as shown in Fig. 7.51A (cf. the U-shaped allyl cation from 7.25, see Fig. 7.48). However, in case of the *exo* tosylate, the torquoselective dis mode gives a W-shaped cation with an impossibly strained *trans* double bond as shown in Fig. 7.51B (cf. the W-shaped allyl cation from 7.26, see Fig. 7.48). Hence, the *endo* tosylate reacts much faster.

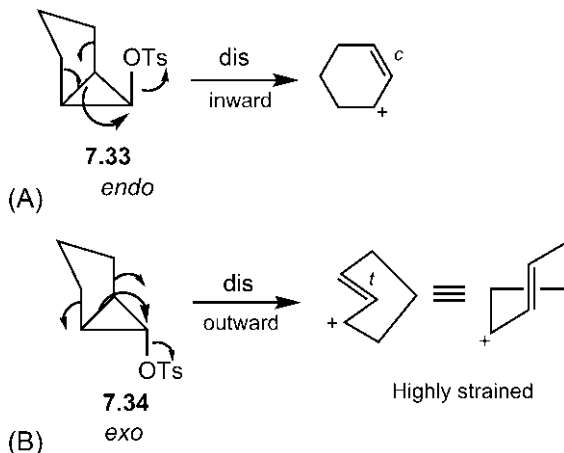


Fig. 7.51 Torquoselectivity in the ring opening of the (A) *endo* and (B) *exo* 5–3 fused bicyclic tosylates.

For similar reasons, the *endo* chloride of a fused 5–3 bicyclic system readily isomerizes to 3-chlorocyclohexene on heating at 125°C, whereas the *exo* isomer remains unchanged even at a much higher temperature of 250°C (Fig. 7.52).

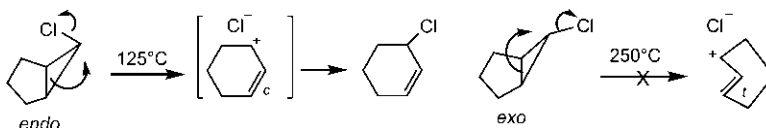


Fig. 7.52 Thermal isomerizations of *endo* and *exo* chlorides of a 5–3 fused bicyclic system.

In a fused 7–3 bicyclic cyclopropyl system, the relative rate pattern is opposite. It is the *exo* bromide **7.36** that undergoes hydrolysis faster than the *endo* isomer **7.35** (Fig. 7.53).⁴⁸ This is because a *trans* double bond in the eight-membered ring is sterically more stable than a *cis* double bond. The torquoselective dis mode in case of the *exo* isomer produces a *trans* double bond, and hence the *exo* bromide **7.36** reacts faster.

(Note that, in the bicyclic system *as drawn*, if the breaking σ bond moves downwards, an allyl cation with a *cis* double bond results, and if it moves upwards, a *trans* double bond forms, see also Figs. 7.51 and 7.52.)

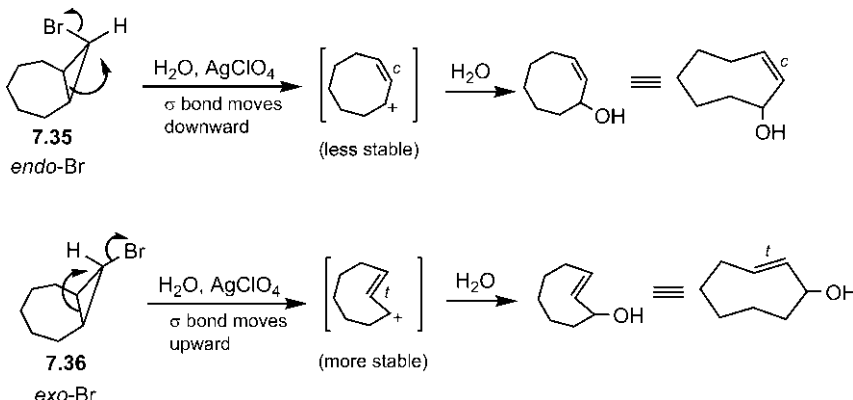
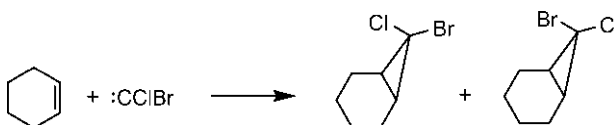


Fig. 7.53 Torquoselectivity in the ring opening of *endo* and *exo* 7–3 fused bicyclic bromides in hydrolysis.

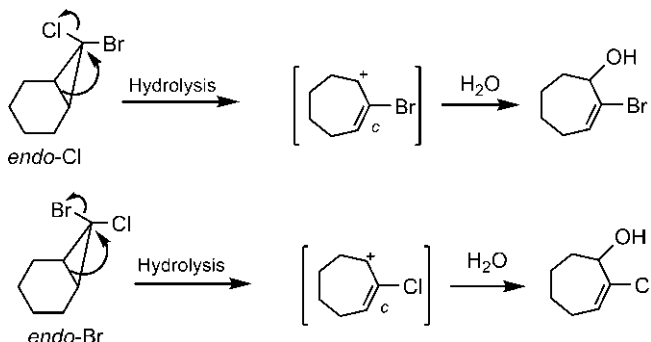
Problem 7.9

How would you establish the stereochemistry of Cl in each product by solvolysis?



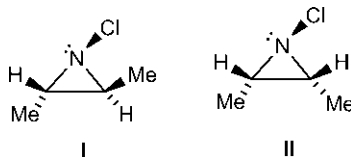
Answer

The hydrolysis of the 6–3 fused bicyclic products gives different compounds. The characterization of the hydrolysis products would determine the stereochemistry of Cl in the bicyclic molecules. The *endo*-Cl isomer gives bromocycloheptenol, whereas the *endo*-Br isomer yields chlorocycloheptenol, each via the formation of a favourable *cis* double bond in a seven-membered ring by the torquoselective *dis* mode of ring opening. Notice that the concerted ring opening of the *endo*-Cl isomer leads to loss of Cl instead of Br though Br is a better leaving group.

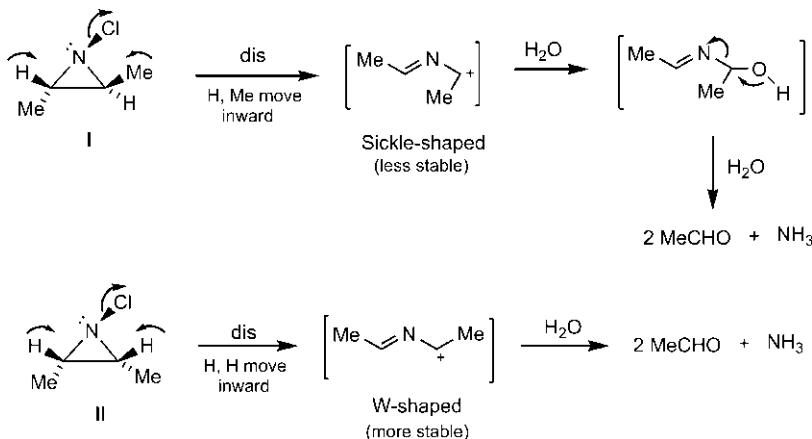


Problem 7.10

Which of the following diastereomeric *N*-chloroaziridines undergoes hydrolysis faster? Predict the products.

**Answer⁴⁹**

Aziridine is a heterocyclic analogue of the cyclopropyl system. The stereochemistry of Cl in *N*-chloroaziridine is preserved because there is a high-energy barrier to pyramidal inversion. Similar to the cyclopropyl system, the ring opening of *N*-chloroaziridine also proceeds by the torquoselective dis mode as shown below. In each case, the breaking σ bond would move downwards to provide assistance to the departure of Cl pointing upwards. Since a W-shaped cation is sterically more favourable than a Z- or sickle-shaped cation, the aziridine II undergoes hydrolysis faster than I. (The relative rate is found to be 100:1.) The ionic cleavage of the initial hydrolysis products gives the same final products for the two aziridines.



The cyclopropyl cation–allyl cation reaction is also observed in cyclopropanones (Fig. 7.54). Here no leaving group is to be lost to obtain a potential cyclopropyl cation, and hence the stereoelectronic requirement for the backside approach of the breaking σ bond is not operative.

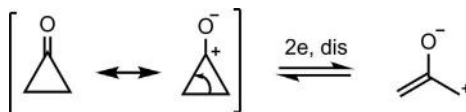


Fig. 7.54 2-Electron disrotatory ring opening of cyclopropanone.

To illustrate, we consider a thermal racemization of optically active *trans*-2,3-di-*t*-butylcyclopropanone at 80°C. The racemization occurs by consecutive ring opening and ring closing processes (Fig. 7.55).⁵⁰ The two possible dis modes for ring opening give the same sickle-shaped allyl cation, but for ring closing they yield two enantiomers of the chiral *trans* isomer.

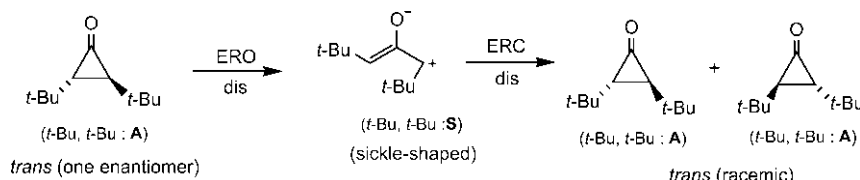
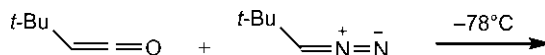


Fig. 7.55 Thermal racemization of the optically active *trans*-2,3-di-*t*-butylcyclopropanone.

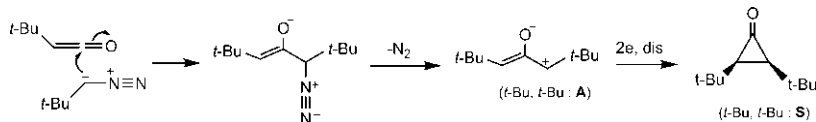
Problem 7.11

Predict the product of the following reaction. Explain mechanistically.



Answer 51

The nucleophilic attack by the diazoalkane to ketene carbonyl takes place from the side opposite to the *t*-Bu group of the ketene followed by the loss of nitrogen to produce a more stable W-shaped allyl cation. The allyl cation then undergoes ring closing by the disrotatory mode to give a counter-thermodynamic product, *cis*-di-*t*-butylcyclopropanone. The ring closing and the departure of the nitrogen may also be concerted without the intermediary of the carbocation.



The ring closing of diastereomeric α -chloro enolates **7.37** and **7.38** (obtained from the corresponding diastereomeric α -chloro ketones with base) to cyclopropanones **7.39** and **7.40** by the disrotatory process is involved in the Favorskii rearrangement (Fig. 7.56). Here the stereoelectronic requirement of the backside approach of the π bond to provide assistance to the departure of the leaving group (Cl) is operative. The π bond approaches from the axial side in **7.37**, and from the equatorial side in **7.38** in the disrotatory ring closing. If the mechanism were not pericyclic, the ionic mechanism would entail a 3-*endo*-trig ring closure at C-3' which is forbidden by Baldwin's rules. Pericyclic reactions are not subject to Baldwin's rules. The cyclopropanones are transformed into esters by alkoxide under the reaction conditions.

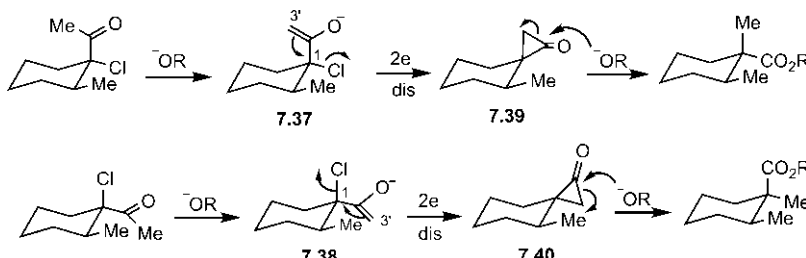


Fig. 7.56 Disrotatory ring closing of α -chloro enolates to cyclopropanones in the Favorskii rearrangement.

7.2.2 4-Electron Electrocyclic Process in Cations

The 4-electron electrocyclic process in cations represents a pentadienyl cation-cyclopentenyl cation reaction (Fig. 7.57). The process is allowed thermally by the con mode, and photochemically by the dis mode.

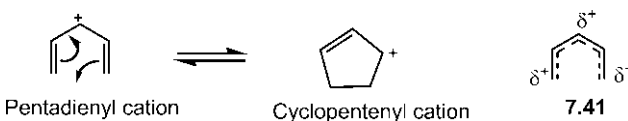


Fig. 7.57 A 4-electron pentadienyl cation-cyclopentenyl cation reaction.

The forward ring closing process is thermodynamically more favourable, and is estimated to be exothermic by 18 kcal mol^{-1} .⁵² It may be surprising to observe that the σ bond is formed between the two electrophilic centres of pentadienyl cation **7.41**. Again, it is the orbital interaction (not the ionic bonding) that is crucial in the pericyclic mechanism.

The cyclopentenyl cations formed by the ring closing can be characterized at low temperature by ^1H NMR spectroscopy. Fig. 7.58 shows the formation of stereoisomeric cyclopentenyl cations by the conrotatory ring closing of pentadienyl cations generated from the corresponding alcohols at low temperature in a super acid. ⁵³ A frontier orbital picture 7.42 using HOMO (ψ_2) of the pentadienyl cation shows that the thermal reaction is allowed by the con mode.

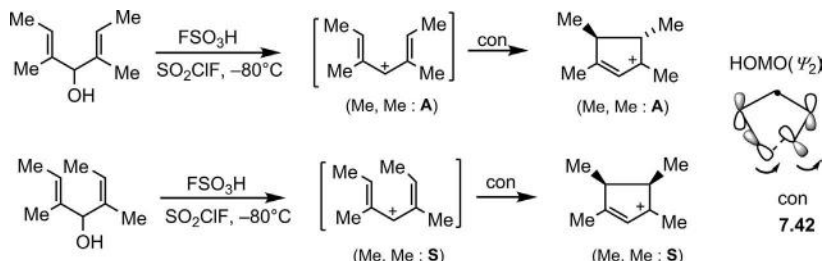


Fig. 7.58 Formation of stereoisomeric cyclopentenyl cations at low temperature; FMO picture for thermally allowed cyclization.

A synthetically useful electrocyclization of pentadienyl cations is the Nazarov cyclization of divinyl ketones.^{54,55} Fig. 7.59 shows an acid-catalysed Nazarov cyclization of a divinyl ketone under thermal and photochemical conditions.⁵⁶ The stereochemistry of the cyclopentenone products results from the conrotatory and disrotatory ring closure, respectively. See also the use of the stereochemical rule.

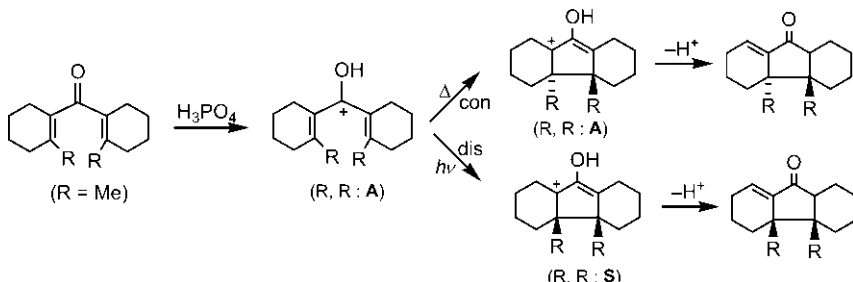


Fig. 7.59 Thermal and photochemical electrocyclizations of a cross-conjugated dienone.

In the above reaction, if $R = H$, the proton is lost preferentially from a ring junction of the cyclopentenyl cation and the product stereochemistry at

the ring junctions could not be observed. However, with allyl silane **7.43**, the silyl group is lost in the final step (Me_3Si^+ is a better leaving group than H^+) and the stereochemistry at the ring junction remains intact in the cyclopentenone product (Fig. 7.60). The product is chiral and the two possible con modes lead to a racemate.

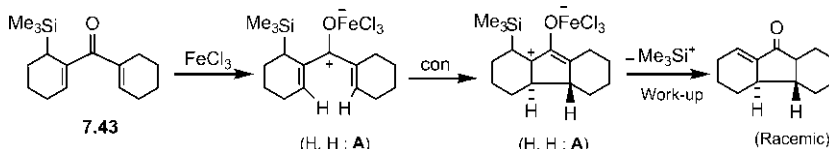


Fig. 7.60 Stereochemistry of a silicon-directed Nazarov cyclization.

If optically active divinyl ketone **7.44** is employed, torque selectivity operates to give the optically active product **7.45** (Fig. 7.61).⁵⁷

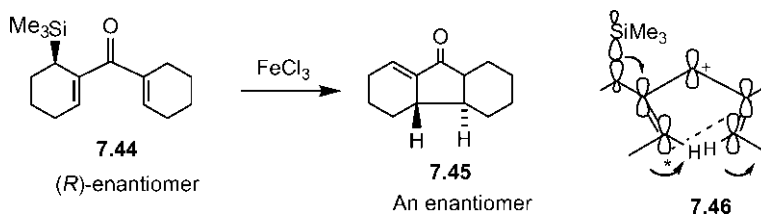


Fig. 7.61 Asymmetric synthesis using Nazarov cyclization.

Me_3Si is a donor substituent through C—Si hyperconjugation and directs the lobe (*) of a terminal p orbital anti to SiMe_3 for developing the σ bond in the transition structure **7.46**. Therefore, an anticlockwise con mode operates, resulting in the formation of an enantiomer **7.45**. This is an asymmetric synthesis using Nazarov cyclization.

The silicon-directed cyclization can also be used to control the regioselectivity of Nazarov cyclization.⁵⁸ The divinyl ketone **7.45** ($R = \text{H}$) on treatment with a Lewis acid SnCl_4 forms the cyclopentenyl cation **7.47**, a 3° carbocation, which loses a proton to give a more stable regioisomeric product **7.48** (Fig. 7.62). In contrast, the divinyl ketone **7.46** ($R = \text{SiMe}_3$) gives the cyclopentenyl cation **7.49** which is a β -silyl carbocation, strongly stabilized by C—Si hyperconjugation. The β -silyl-stabilized cation **7.49** eliminates the silyl group in preference to a proton to yield the less stable regioisomeric product **7.50**.

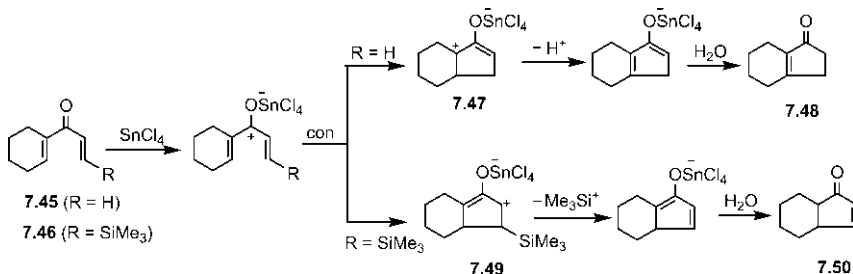
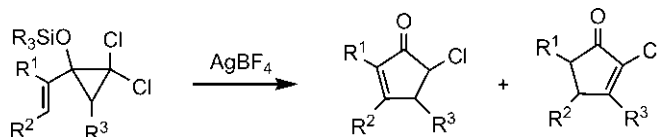


Fig. 7.62 Regioselectivity of Nazarov cyclization.

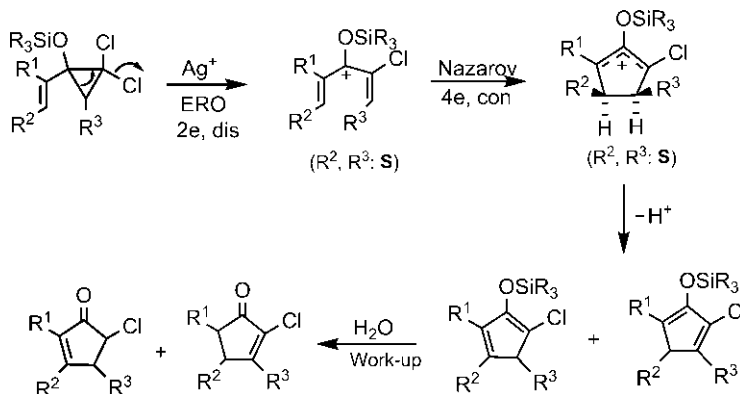
Problem 7.12

Explain the following observation.



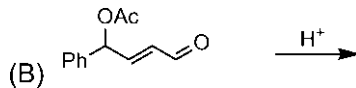
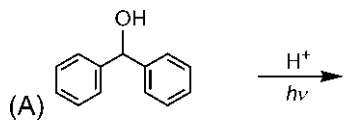
Answer⁵⁹

The reaction proceeds through the ERO of a cyclopropyl cation followed by a Nazarov cyclization to give the products. The *cis* stereochemistry is lost on elimination of a proton.

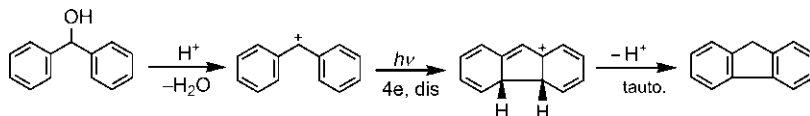


Problem 7.13

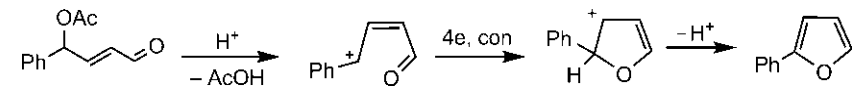
Predict the product of each of the following reactions.

**Answer**

(A) The product is fluorene.



(B) The product is 2-phenylfuran.



7.2.3 4-Electron Electrocyclic Process in Anions

In an anionic system, a 4-electron process represents an allyl anion-cyclopropyl anion reaction (Fig. 7.63). The ring opening will be more favourable because of the relief of cyclopropyl ring strain.



Fig. 7.63 A 4-electron allyl anion-cyclopropyl anion reaction.

The ring opening reactions with cyclopropyl anions are rare. The stereoisomeric cyclopropyl anions can easily interconvert under the strongly basic conditions of anion generation, which complicates the ring opening study further.

A kinetic study of ring opening of the cyclopropyl anions (**7.51–7.53**) is shown in Fig. 7.64.⁶⁰ The anions are generated in the presence of LDA in THF. The electron withdrawing CN serves to facilitate the anion formation.

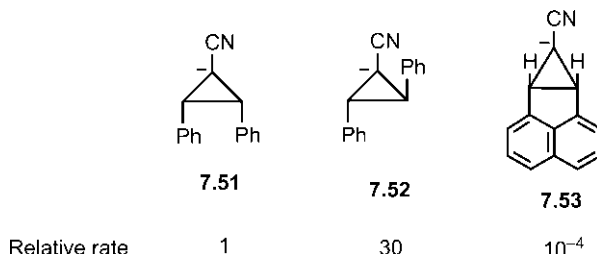


Fig. 7.64 Relative rates of ring opening of cyclopropyl anions generated in the presence of lithium diisopropylamide (LDA).

The relative rates can be explained by the conrotatory ring opening of the cyclopropyl anions (Fig. 7.65). The cyclopropyl anion **7.51** leads to the formation of a sickle-shaped allyl anion **7.54**, which is sterically less stable than a W-shaped allyl anion **7.55** obtained from the cyclopropyl anion **7.52**. Therefore, **7.52** undergoes ring opening faster than **7.51**. For the cyclopropyl anion **7.53**, ring opening by the con mode leads to the formation of an impossibly strained *trans* double bond in a six-membered ring **7.56**. Thus, the reaction is extremely slow (10^4 times slower than **7.51**) and may well proceed by the forbidden path. The cyclopropyl anions are generated as lithium salts which have a limited anionic character; however, it is believed that the electrocyclic process is concerted with the anion-like species.

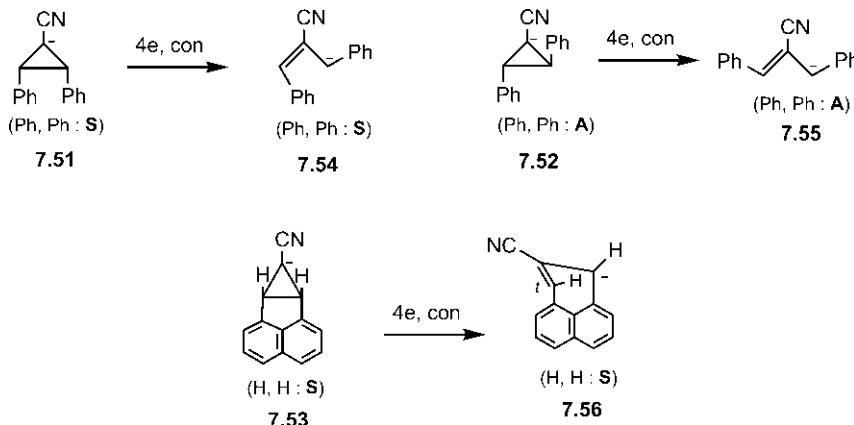


Fig. 7.65 Mechanism of ring opening reactions of cyclopropyl anions in Fig. 7.64.

Aziridines and oxiranes (epoxides) are the heterocyclic analogues of a cyclopropyl anion, which can undergo an ERO to produce an azomethine ylide and a carbonyl ylide, respectively (Fig. 7.66A). The ring opening occurs thermally by the conrotatory process, and photochemically by the disrotatory process, which are illustrated with a *cis* aziridine and a *trans* oxirane (Pr/Ph *trans*) in Fig. 7.66B.

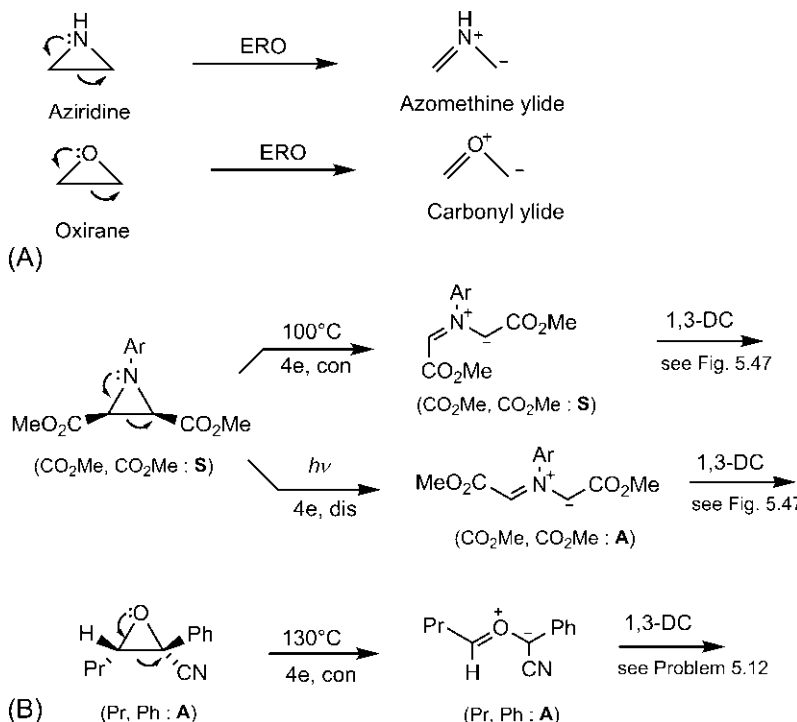
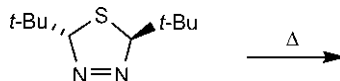


Fig. 7.66 (A) Ring opening of aziridine and oxirane systems; (B) stereochemistry of ring opening of a *cis* aziridine and a *trans* oxirane (Pr/Ph *trans*).

The azomethine ylide and carbonyl ylide dipoles are usually trapped by 1,3-dipolar cycloadditions.

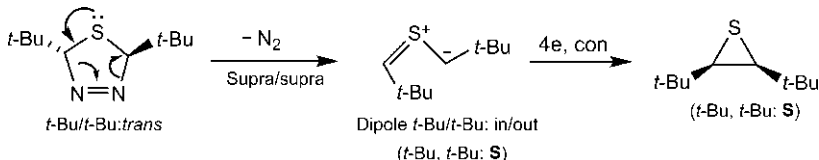
Problem 7.14

Predict the product of the following reaction with mechanism.



Answer⁶¹

The reaction involves a retro-1,3-dipolar cycloaddition with elimination of N₂ to generate a thiocarbonyl ylide dipole which undergoes a 4-electron ring closure by the con mode to give the product *cis*-di-*t*-butylthietane.



7.2.4 6-Electron Electrocyclic Process in Anions

The 6-electron electrocyclic reaction in anions represents a pentadienyl anion-cyclopentenyl anion reaction, which is thermally allowed by the disrotatory process (Fig. 7.67).

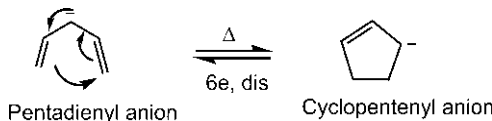


Fig. 7.67 A 6-electron pentadienyl anion-cyclopentenyl anion reaction.

Cycloocta-1,4-diene gives a pentadienyl anion in the presence of BuLi at -78°C . On warming to 35°C , ring closing takes place to form a *cis*-fused 5–5 bicyclic system (Fig. 7.68).⁶²

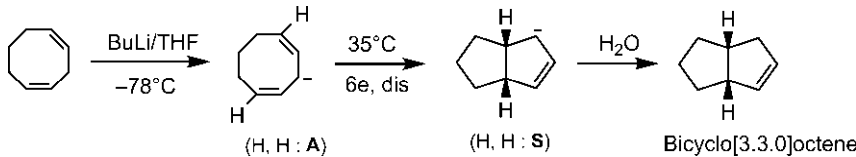


Fig. 7.68 Stereochemistry of ring closing of a pentadienyl anion.

Fig. 7.69 shows a ring opening of a cyclopentenyl anion when a bicyclic system 7.57 on treatment with a base produces a mixture of isomeric cyclohexadienes.⁶³ The ring opening is favourable because of the relief of cyclopropyl strain. The disrotatory reaction is also torquoselective with the formation of a *cis* double bond in a six-membered ring.

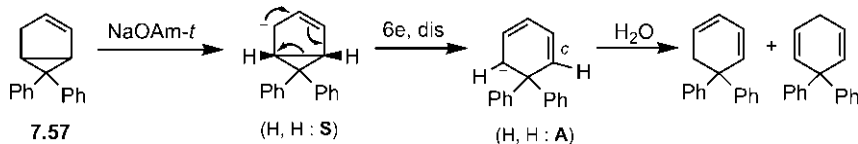


Fig. 7.69 Ring opening of a cyclopentenyl anion.

A heterocyclic analogue **7.58** of the pentadienyl anion, obtained from the treatment of hydrobenzamide with base, undergoes ring closing by the disrotatory process to produce amarine ([Fig. 7.70](#)).⁶⁴ The ring closing is favourable as the negative charge resides on the electronegative nitrogen in the five-membered ring.

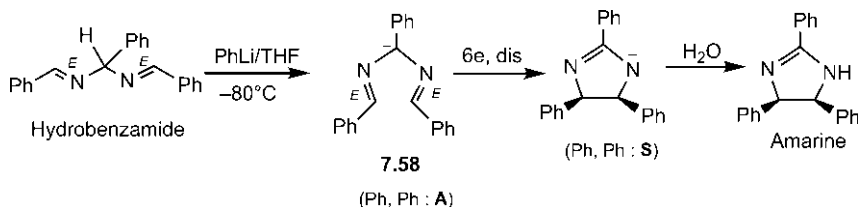


Fig. 7.70 Synthesis of amarine from hydrobenzamide via a 6-electron ring closing reaction.

Another heterocyclic analogue is a nitrile ylide **7.59**, which produces an oxazole by a 6-electron ring closing (Fig. 7.71).⁶⁵ The reaction between an α -acyl carbene (generated from an α -diazocarbonyl compound in the presence of a Rh (II) catalyst) and a nitrile forms the ylide **7.59** *in situ*. The ylide **7.59** is a 1,5-dipole, and the cyclization is also called 1,5-dipolar cyclization.

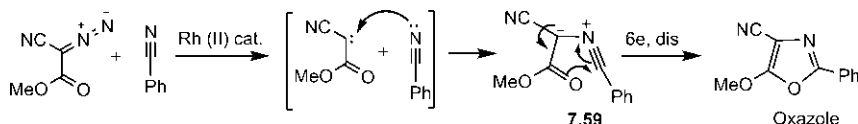
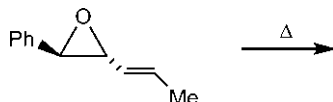


Fig. 7.71 Synthesis of an oxazole via ring closing of a 1,5-dipolar nitrile ylide.

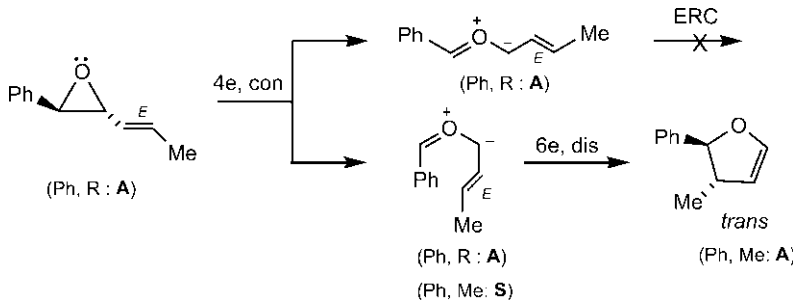
Problem 7.15

Predict the product of the following reaction.

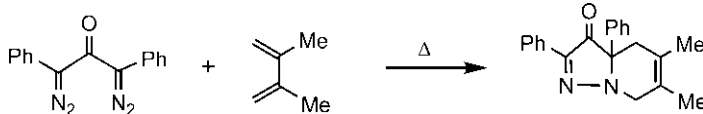


Answer

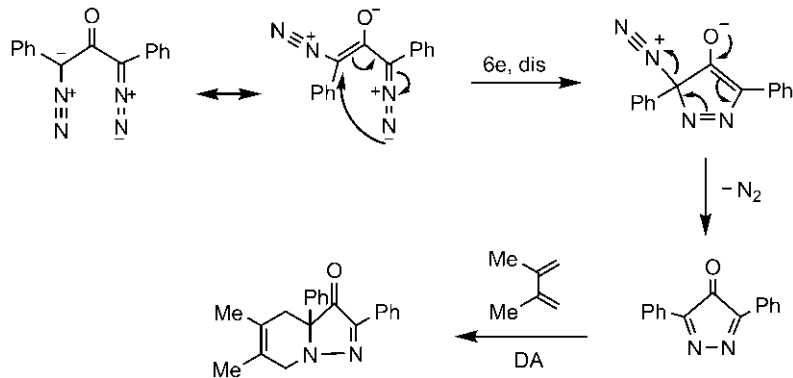
The 4-electron ERO of the oxirane can take place by two possible con modes; however, only the less stable U-shaped intermediate (a heterocyclic analogue of the pentadienyl anion) can undergo a 6-electron ERC by the disrotatory process to give a *trans* dihydrofuran. The more stable W-shaped intermediate cannot undergo electrocyclization as the two ends of the conjugated system are far apart.

**Problem 7.16**

Suggest a plausible mechanism of the following reaction.

**Answer⁶⁶**

The reaction proceeds through a 6-electron ring closing of the diazocarbonyl compound (resembling a pentadienyl anion) followed by loss of nitrogen and the Diels–Alder reaction with the diene.



REFERENCES

1. Marvell, E. N. *Thermal Electrocyclic Reactions*; Academic Press: New York, 1980.
2. Durst, T.; Breau, L. In *Comprehensive Organic Synthesis*; Trost, B. M., Fleming, I., Eds.; Vol. 5; Pergamon Press: Oxford, 1991; p 675.
3. Mandal, D. K. *J. Chem. Educ.* **2012**, *89*, 1041.
4. Funk, R. L.; Vollhardt, K. P. C. *J. Am. Chem. Soc.* **1979**, *101*, 215. *1980*, *102*, 5253.
5. Fleming, I.; Mah, T. *J. Chem. Soc., Perkin Trans. 1* **1975**, 964.
6. Carpenter, B. K. *Tetrahedron* **1978**, *34*, 1877.
7. Kirmse, W.; Rondan, N. G.; Houk, K. N. *J. Am. Chem. Soc.* **1984**, *106*, 7989.
8. Rudolf, K.; Spellmeyer, D. C.; Houk, K. N. *J. Org. Chem.* **1987**, *52*, 3708.
9. Rondan, N. G.; Houk, K. N. *J. Am. Chem. Soc.* **1985**, *107*, 2099.
10. Dolbier, W. R., Jr.; Koroniak, H.; Burton, D. J.; Bailey, A. R.; Shaw, G. S.; Hansen, S. W. *J. Am. Chem. Soc.* **1984**, *106*, 1871.
11. Niwayama, S.; Kallel, E. A.; Spellmeyer, D. C.; Sheu, C.; Houk, K. N. *J. Org. Chem.* **1996**, *61*, 812, 813.
12. Houk, K. N.; Spellmeyer, D. C.; Jefford, C. W.; Rimbault, C. G.; Wang, Y.; Miller, R. D. *J. Org. Chem.* **1988**, *53*, 2125.
13. Bajorek, T.; Werstiuk, N. H. *Chem. Commun.* **2002**, 648.
14. Doorakian, G. A.; Freedman, H. H. *J. Am. Chem. Soc.* **1968**, *90*, 5310.
15. Srinivasan, R. *J. Am. Chem. Soc.* **1968**, *90*, 4498.
16. Schumate, K. M.; Fonken, G. J. *J. Am. Chem. Soc.* **1965**, *87*, 3996. **1966**, *88*, 1073.
17. Goldstein, M. J.; Leight, R. S. *J. Am. Chem. Soc.* **1977**, *99*, 8112.
18. Johnson, R. P.; Daoust, K. J. *J. Am. Chem. Soc.* **1996**, *118*, 7381.
19. Havenith, R. W. A.; Jenneskens, L. W.; van Lenthe, J. H. *Theochem* **1999**, *492*, 217.
20. Corey, E. J.; Streith, J. *J. Am. Chem. Soc.* **1964**, *86*, 950.
21. Criegee, R.; Reinhardt, H. G. *Chem. Ber.* **1968**, *101*, 102.
22. Huntsman, W. D.; Wrists, H. J. *J. Am. Chem. Soc.* **1967**, *89*, 342.
23. Okamura, W. H.; De Lera, A. R. In *Comprehensive Organic Synthesis*; Trost, B. M., Fleming, I., Eds.; Vol. 5; Pergamon Press: Oxford, 1991; p 699.
24. Irie, M. *Chem. Rev.* **2000**, *100*, 1683. *100*, 1685.
25. Blattmann, H.-R.; Schmidt, W. *Tetrahedron* **1970**, *26*, 5885.
26. Schröder, G.; Martin, W.; Oth, J. F. M. *Angew. Chem. Int. Ed. Eng.* **1967**, *6*, 870.
27. Masamune, S.; Seidner, R. T. *Chem. Commun.* **1969**, 542.
28. Trost, B. M.; Gutierrez, A. C. *Org. Lett.* **2007**, *9*, 1473.
29. Laarhoven, W. H. *Org. Photochem.* **1987**, *9*, 129.
30. Maier, G. *Angew. Chem. Int. Ed. Eng.* **1967**, *6*, 402.
31. Warner, P. M.; Lu, S.-L. *J. Am. Chem. Soc.* **1980**, *102*, 331.
32. Gridnev, I. D.; Tok, O. L.; Gridneva, N. A.; Bubnov, Y. N.; Schreiner, P. R. *J. Am. Chem. Soc.* **1998**, *120*, 1034.
33. Huisgen, R.; Konz, W. E. *J. Am. Chem. Soc.* **1970**, *92*, 4102.
34. Brember, A. R.; Freestone, V. C.; Gorman, A. A.; Sheridan, J. B. *Tetrahedron* **1979**, *35*, 2311.
35. Tezuka, T.; Kikuchi, O.; Houk, K. N.; et al. *J. Am. Chem. Soc.* **1981**, *103*, 1367.
36. Jacobs, H. J. C.; Havinga, E. *Adv. Photochem.* **1979**, *11*, 305.
37. Kametani, T.; Tsubuki, M.; Shiratori, Y.; et al. *J. Org. Chem.* **1977**, *42*, 2672.
38. Tiedemann, R.; Turnbull, P.; Moore, H. W. *J. Org. Chem.* **1999**, *64*, 4030.
39. Huisgen, R.; Dahmen, A.; Huber, H. *J. Am. Chem. Soc.* **1967**, *89*, 7130.
40. Dahmen, A.; Huisgen, R. *Tetrahedron Lett.* **1969**, 1465.
41. Fleming, I. *Pericyclic Reactions*, 2nd ed.; Oxford: Oxford University Press, 2015; p.71.
42. Schleyer, P.v.R.; Sliwinski, W. F.; Van Dine, G. W.; Schollkopf, U.; Paust, J.; Fellenberger, K. *J. Am. Chem. Soc.* **1972**, *94*, 125.

43. Sliwinski, W. F.; Su, T. M.; Schleyer, P.v.R. *J. Am. Chem. Soc.* **1972**, *94*, 133.
44. Roberts, J. D.; Chambers, V. C. *J. Am. Chem. Soc.* **1951**, *73*, 5034.
45. Arnold, P. A.; Carpenter, B. K. *Chem. Phys. Lett.* **2000**, *328*, 90.
46. DePuy, C. H. *Acc. Chem. Res.* **1968**, *1*, 33.
47. Schleyer, P.v.R.; Su, T. M.; Saunders, M.; Rosenfeld, J. C. *J. Am. Chem. Soc.* **1969**, *91*, 5174.
48. Reese, C. B.; Shaw, A. *J. Am. Chem. Soc.* **1970**, *92*, 2566.
49. Gassman, P. G. *Acc. Chem. Res.* **1970**, *3*, 26.
50. Greene, F. D.; Selove, D. B.; Pazos, J. F.; Camp, R. L. *J. Am. Chem. Soc.* **1970**, *92*, 7488.
51. Buter, J.; Wassenaar, S.; Kellogg, R. M. *J. Org. Chem.* **1972**, *37*, 4045.
52. Lossing, F. P.; Holmes, J. L. *J. Am. Chem. Soc.* **1984**, *106*, 6917.
53. Cambell, P. H.; Chiu, N. W. K.; Deugau, K.; Miller, I. J.; Sorensen, T. S. *J. Am. Chem. Soc.* **1969**, *91*, 6404.
54. Denmark, S. E. In *Comprehensive Organic Synthesis*; Trost, B. M., Fleming, I., Eds.; Vol. 5; Pergamon Press: Oxford, **1991**; p 751.
55. Habermas, K. L.; Denmark, S. E.; Jones, T. K. *Org. React.* **1994**, *45*, 1.
56. Woodward, R. B.; Lehr, R. Aromaticity. *Chem. Soc. Spec. Publ.* **1967**, *21*, 237.
57. Denmark, S. E.; Wallace, M. A.; Walker, C. B., Jr. *J. Org. Chem.* **1990**, *55*, 5543.
58. Denmark, S. E.; Jones, T. K. *J. Am. Chem. Soc.* **1982**, *104*, 2642.
59. Grant, T. N.; West, F. G. *J. Am. Chem. Soc.* **2006**, *128*, 9348.
60. Newcomb, M.; Ford, W. T. *J. Am. Chem. Soc.* **1974**, *96*, 2968.
61. Sorensen, T. S.; Sun, F. *J. Am. Chem. Soc.* **1997**, *119*, 11327.
62. Bates, R. B.; McCombs, D. A. *Tetrahedron Lett.* **1969**, 977.
63. Sustmann, R.; Dern, H. *J. Chem. Ber.* **1983**, *116*, 2958.
64. Hunter, D. H.; Sim, S. K. *J. Am. Chem. Soc.* **1969**, *91*, 6203.
65. Doyle, K. J.; Moody, C. J. *Tetrahedron* **1994**, *50*, 3761.
66. Trost, B. M.; Whitman, P. J. *J. Am. Chem. Soc.* **1972**, *94*, 8634.

CHAPTER 8

Sigmatropic Rearrangements 1: [1,*j*] Shifts

[1,*j*] Sigmatropic rearrangements involve breaking of an old $1 - 1 \sigma$ bond and formation of a new $1 - j \sigma$ bond with concomitant reorganization of the π bonds (see [Section 3.2.3](#)). The migrating group in a [1,*j*] sigmatropic rearrangement is usually a hydrogen atom or a carbon group.

For [1,*j*] sigmatropic shift in a neutral system, *j* is odd, and the total number of electrons involved = $1 + j$. But in a charged system, *j* is even. For [1,*j*] shift in cations, the total number of electrons involved = $1 + j - 1 = j$, whereas in anions, the total number of electrons mobilized = $1 + j + 1 = 2 + j$.

8.1 [1,*J*] HYDROGEN SHIFTS IN NEUTRAL SYSTEMS (*J*=ODD)

8.1.1 [1,5]H Shifts

A [1,5]H shift involves $1 + 5 = 6$ electrons, and is thermally allowed with suprafacial migration of hydrogen (see [Table 3.4](#)). The reaction shows a very large primary kinetic isotope effect; $k_H/k_D = 5$ at 470K which on normalization to a standard temperature becomes 12.2 at 273K. This signifies that the transition structure **8.1** is highly symmetrical, that is, the migrating hydrogen is almost equally bonded to the two sites in the TS ([Fig. 8.1](#)).

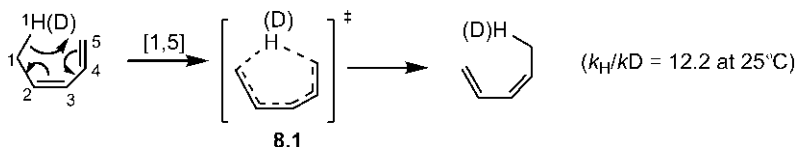


Fig. 8.1 [1,5]H shift shows a large primary kinetic isotope effect.

The suprafacial [1,5]H shifts¹ are geometrically favourable and are very common. These are illustrated with the following examples.

The *(E,R)* isomer of a diene **8.2** on heating gives ~1:1 mixture of two stereoisomeric products, *E,S* **8.3** and *Z,R* **8.4** as shown in Fig. 8.2.²

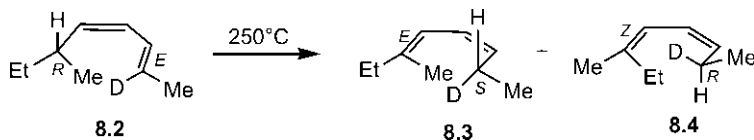


Fig. 8.2 Thermal rearrangement of a diene to a mixture of stereoisomeric products.

The stereochemical outcome can be rationalized based on the [1,5] suprafacial H shift (Fig. 8.3). Diene **8.2** is in conformational equilibrium with the other conformer **8.2'** by rotation about the $\text{Csp}^2\text{--Csp}^3$ bond. Each conformer undergoes a [1,5] suprafacial H shift to give the product mixture: **8.2** gives **8.3** while **8.2'** yields **8.4**. The reaction shows no stereoselectivity; however, the *(E,S)* product may be a major one in other cases if the *(E)* double bond is much more stable than the *(Z)* double bond.

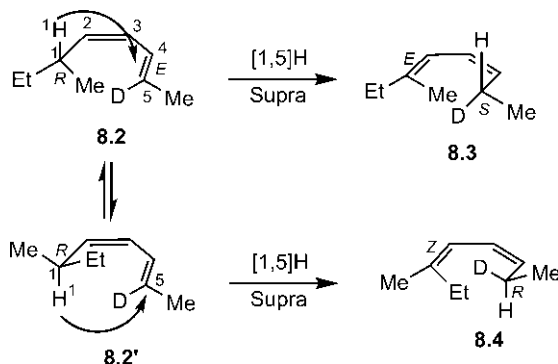


Fig. 8.3 Mechanism of the reaction in Fig. 8.2 in terms of [1,5]H shifts.

The [1,5]H shift is extremely facile in cyclopentadienes because the C-1 and C-5 ends of the pentadienyl system **8.5** are held adjacent to each other. Fig. 8.4 shows that the different constitutional isomers of a substituted cyclopentadiene can be in rapid equilibrium by sequential [1,5]H shifts at room temperature.³ The 5-substituted diene (IUPAC numbering) in which the substituent is not conjugated is less stable than the 1- or 2-substituted isomer with a conjugating substituent, and hence the 5-substituted isomer exists as a minor component in the equilibrium mixture. (Note that the H shift appears to be a [1,2] shift because of the cyclic structure but it is not so; it is mechanistically a [1,5] shift.)

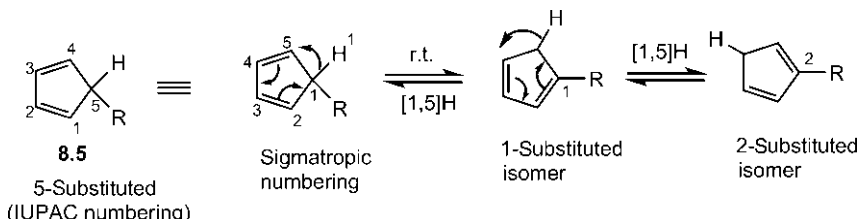


Fig. 8.4 Equilibration of isomers of a substituted cyclopentadiene via [1,5]H shifts.

Thus, the Diels–Alder reaction with 5-methylcyclopentadiene at room temperature involves the more populated and more reactive 1-substituted diene to give the product (Fig. 8.5).

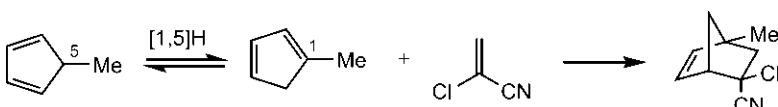


Fig. 8.5 Diels–Alder reaction with 5-methylcyclopentadiene via a 1-substituted isomer.

In Corey's prostaglandin synthesis, an initial step required a Diels–Alder reaction with the 5-substituted isomer of a cyclopentadiene. The reaction was successful at 0°C in a Cu(BF₄)₂-catalysed process (Fig. 8.6).⁴ This is because the rate of isomerization of the 5-substituted isomer through [1,5]H shifts is unaffected by the Lewis acid Cu²⁺, but the rate of Diels–Alder reaction is considerably increased by the coordination of the copper ion with the nitrile group making the dienophile more electrophilic. The substituent CH₂OMe at the bridge adopts a *syn* position with respect to the double bond presumably due to a steric effect from the dienophile substituent.

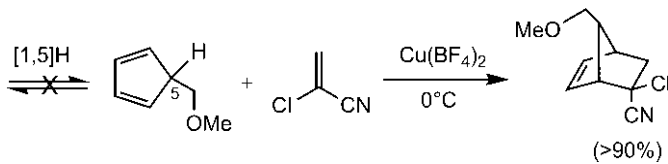


Fig. 8.6 Lewis acid-catalysed Diels–Alder reaction with a 5-substituted cyclopentadiene.

When the deuterium-labelled indene **8.6** is heated, the deuterium is scrambled over the three nonbenzenoid positions (Fig. 8.7).⁵ (Note that

the deuterium scrambling in the product is indicated by placing D within brackets; you can't produce three D's out of one!)

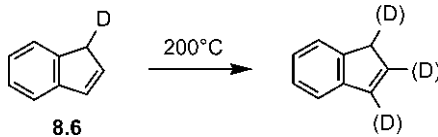


Fig. 8.7 Deuterium scrambling in thermal rearrangement of an indene.

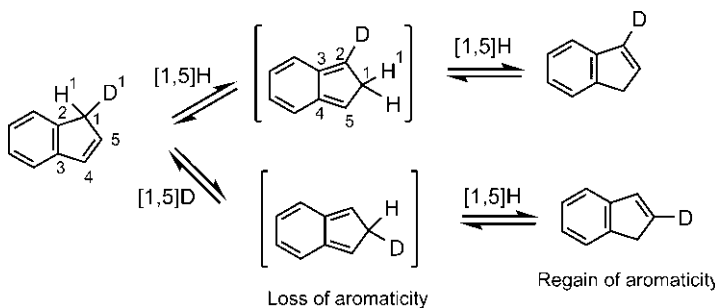
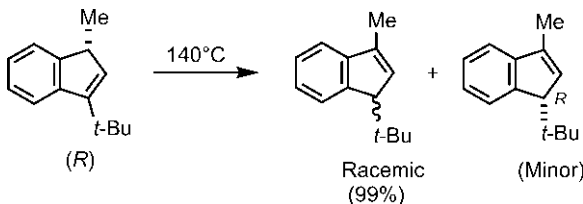


Fig. 8.8 Mechanism of the reaction in [Fig. 8.7](#) involving [1,5]H/D shifts.

The reaction proceeds through a sequence of [1,5]H/D shifts as shown in [Fig. 8.8](#). In the first step, there is loss of aromaticity which is regained in the second step. A [1,5]D shift is however slower than a [1,5]H shift.

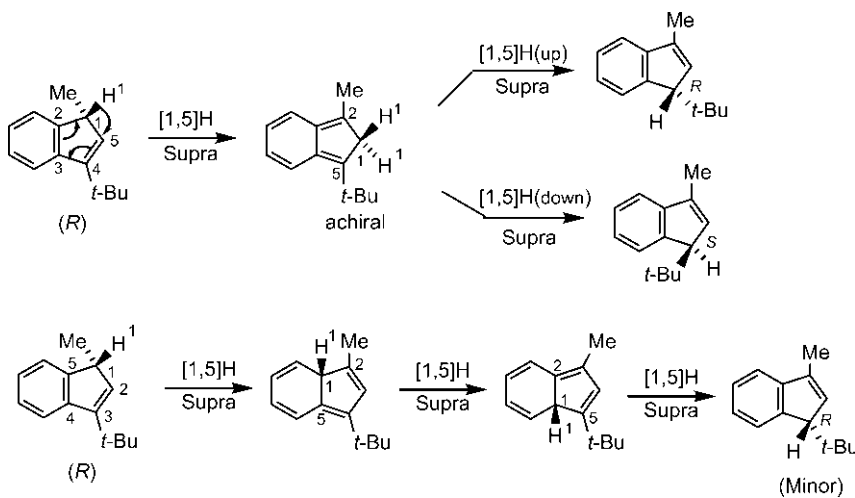
Problem 8.1

Explain the following observation.



Answer⁶

The major racemic product results from [1,5]H shifts via an achiral intermediate. The minor product is obtained by an alternative, less favourable [1,5]H shift on the bridgehead carbon followed by [1,5] shifts until aromaticity is regained.



Thermal [1,5]H shifts also occur in six- and seven-membered rings (Fig. 8.9).^{1,7}

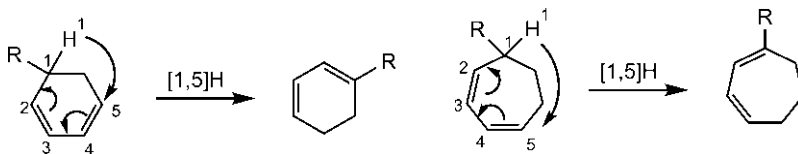


Fig. 8.9 Thermal [1,5]H shifts in cyclohexadiene and cycloheptadiene systems.

Here, the migrating hydrogen at C-1 is not quite close to C-5, and these reactions are slower and occur at higher temperatures. An estimate of energy of activation (E_a) from computational studies^{8–10} shows that E_a for the [1,5] H shift in the cyclopentadiene, cyclohexadiene and the cycloheptadiene system is 27, 41.9 and 35.3 kcal mol⁻¹, respectively. The E_a for the [1,5] shift in cycloheptadiene is somewhat lower than that in cyclohexadiene because of the relatively less distortion of the transition structure for a more flexible seven-membered ring.

As described previously (see Fig. 8.5), the Diels–Alder reaction with a silyloxy-substituted cycloheptadiene shown in Fig. 8.10 also involves a more reactive 1-substituted diene formed via [1,5]H shifts.

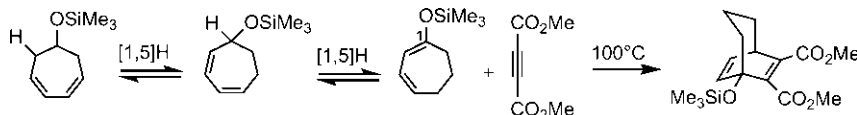


Fig. 8.10 Diels–Alder reaction involving a more reactive 1-substituted isomer of a silyloxy-substituted cycloheptadiene.

Fig. 8.11 shows an example of deuterium scrambling of 7,8-dideuterio-cycloocta-1,3,5-triene in thermal rearrangement.¹¹ It is found that deuterium is scrambled over only four positions 3, 4, 7 and 8 (IUPAC numbering).

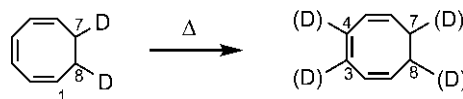


Fig. 8.11 Deuterium scrambling in thermal isomerization of a cyclooctatriene.

Two successive [1,5] shifts explain the result (**Fig. 8.12**). The first [1,5]H shift gives a partially conjugated triene and the second [1,5]H/D shift regenerates the fully conjugated triene. Note that the numbering on the 8-membered ring represents sigmatropic numbering. Two successive [1,5]D shifts however give the starting material.

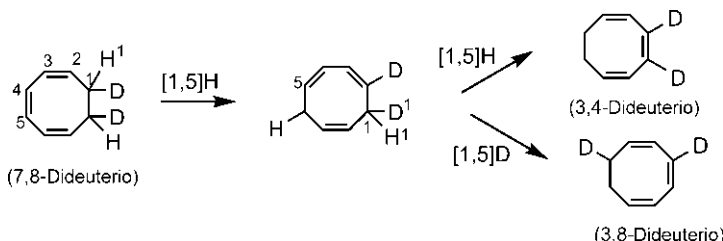


Fig. 8.12 Mechanism of the reaction in **Fig. 8.11** in terms of [1,5]H/D shifts.

The possible [1,3]H or [1,7]H shifts involving antarafacial migration (see below) are geometrically unreasonable for the cyclic molecule. (Check that a series of hypothetical [1,3]H shifts would lead to deuterium scrambling over all eight ring positions.)

Photochemical [1,5]H shifts are symmetry-allowed with antarafacial migration. These antarafacial shifts are geometrically difficult and rare. An example is photoisomerization of photosantonin to neophotosantonin (**Fig. 8.13**).¹² The diene unit of photosantonin is twisted enough (due to severe steric crowding) to make the [1,5] antarafacial H shift possible.

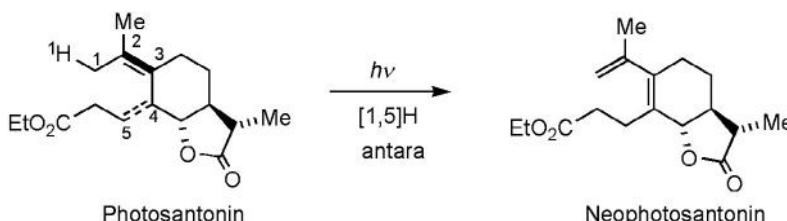
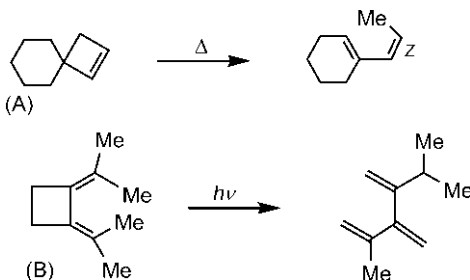


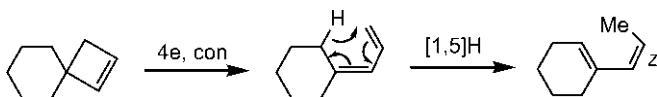
Fig. 8.13 Example of a photochemical [1,5]H shift.

Problem 8.2

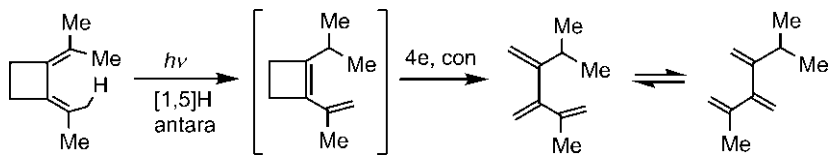
Account for the following observations.

**Answer**

(A) The reaction involves an electrocyclic ring opening followed by a [1,5]H shift. The Z stereochemistry results from the hydrogen shift to the diene unit held in an *s-cis* conformation.



(B) The twisted geometry of the diene unit (due to steric crowding) permits antarafacial [1,5]H shift photochemically. The resulting cyclobutene undergoes an electrocyclic ring opening to give the product.

**8.1.2 [1,3]H Shifts**

A [1,3]H shift is a 4-electron ($4n, n=1$) process, and is allowed thermally with antarafacial migration and photochemically with suprafacial migration (see Table 3.4). However, antarafacial H shift across a small alkene system is geometrically impossible. This is why no thermal [1,3] antarafacial H shift has been observed.

A nonaromatic isomer **8.7** of toluene is thermally stable and has been prepared by pyrolysis of an ester at 350°C (Fig. 8.14). Although the conversion of **8.7** to toluene is highly exothermic, **8.7** does not convert to toluene because of the very high kinetic barrier associated with an impossibly strained transition structure for antarafacial [1,3]H shift. The isomer **8.7** is stable in solution and can undergo Diels–Alder reaction with tetracyanoethylene.¹³ (The nonaromatic isomer is however readily converted to toluene under ionic conditions.)

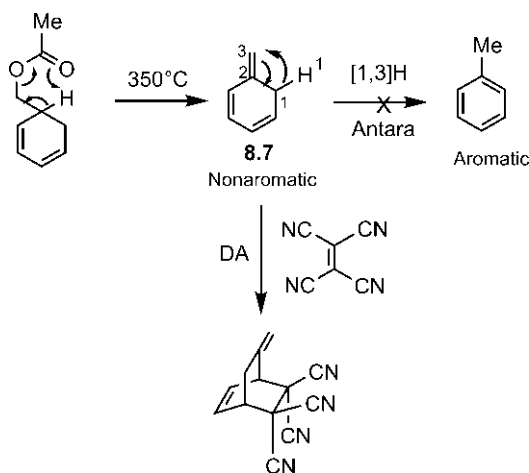


Fig. 8.14 Kinetic stability of a nonaromatic isomer of toluene.

The keto–enol equilibrium by the [1,3]H shift is also not favourable (Fig. 8.15). Thus, the isolation of tautomers is possible, if they are free from any trace of acid or base which catalyses their interconversion by ionic mechanism.

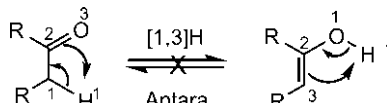


Fig. 8.15 No keto–enol interconversion by [1,3]H shift.

Photochemical [1,3]H shifts can take place suprafacially. Fig. 8.16 shows that an exocyclic alkene is photochemically converted to mainly an endocyclic isomer by the [1,3]H shift.¹⁴

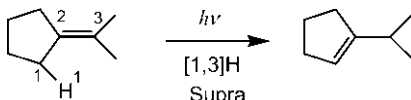


Fig. 8.16 Example of a photochemical [1,3]H shift.

8.1.3 [1,7]H Shifts

The 8-electron [1,7]H shift in a triene system is allowed antarafacially under thermal conditions. Here, in contrast to the [1,3]H shift, antarafacial migration across a longer chain of seven atoms is geometrically favourable. An acyclic triene **8.8** is flexible enough so that H can move from the top face at one end (C-1) to the bottom face of the other end (C-7) (Fig. 8.17A). Fig. 8.17B illustrates [1,7]H and [1,7]D shifts and the primary kinetic isotope effect; k_H/k_D is found to be around 7 which suggests that the transition structure is fairly symmetrical.¹⁵

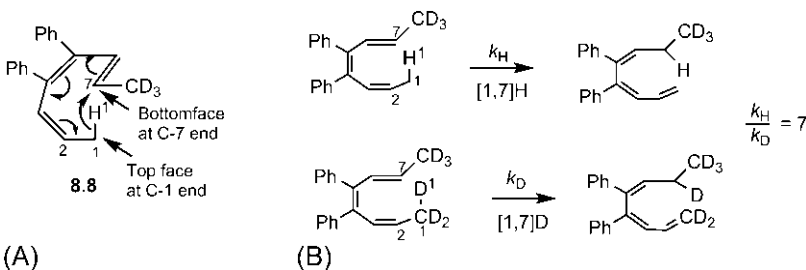


Fig. 8.17 (A) [1,7] Antarafacial H shift; (B) primary kinetic isotope effect for the [1,7]H shift.

The thermal [1,7]H shifts take place only in an acyclic system because in cyclic triene system antarafacial migration of hydrogen requiring overlap to develop on two opposite faces of the ring is geometrically impossible. In an acyclic system, both [1,5] suprafacial H shift and [1,7] antarafacial H shift are possible but the [1,7]H shift takes place in preference to the [1,5]H shift. This shows periselectivity involving the longest conjugated system in [1,j] sigma-tropic shifts.

The thermal [1,7]H shifts are illustrated below with some examples.

Fig. 8.18 shows that an acyclic (*E,S*) triene on heating rearranges to a mixture of (*E,R*) and (*Z,S*) products. No (*E,S*) and (*Z,R*) products are obtained. The stereochemical outcome of the reaction is consistent with a mechanism involving [1,7] antarafacial H shift (cf. Fig. 8.3).

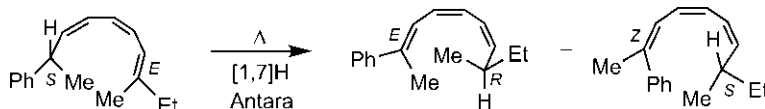


Fig. 8.18 Stereochemistry of a thermal [1,7] sigmatropic rearrangement.

The antarafacial nature of the [1,7]H shift has been clearly demonstrated in the thermal equilibrium of a complex triene **8.9** with two products **8.10** and **8.11** (Fig. 8.19).¹⁶ The antarafacial H shift leads to H (down) in the product **8.10** making H *trans* to OH, while the antarafacial D shift leads to D (up) in **8.11** making D *cis* to OH. Note that the stereochemistry of OH in the starting material serves as a marker to characterize the stereochemistry of H/D migration.

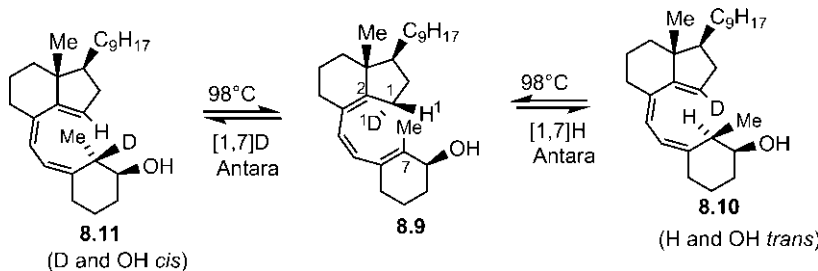


Fig. 8.19 Antarafacial [1,7]H/D shift in thermal equilibrium of a complex triene.

In a vitamin D series, the thermal equilibrium between precalciferol and calciferol (vitamin D₂) involves a [1,7]H shift. The vitamin D₂ synthesis occurs in the human body. When sunlight shines on a baby's skin, photochemical ring opening of ergosterol by the conrotatory process produces precalciferol (see Fig. 7.34, p. 316), which spontaneously isomerizes to vitamin D₂ by the [1,7]H shift (Fig. 8.20).¹⁷



Fig. 8.20 Vitamin D₂ synthesis via the [1,7]H shift.

We have seen earlier (see Fig. 7.17A) that electrocyclic ring closing of (*E,Z,Z*)-hexatriene gives *trans*-5,6-dimethylcyclohexadiene as a major product. The (*E,Z,Z*) triene can however convert into (*Z,Z,Z*) triene

by reversible [1,7]H shifts as shown in Fig. 8.21.¹⁵ In contrast, (*E,Z,E*) isomer **8.12** cannot isomerize through [1,7]H shift because the two ends of the seven-carbon chain are far apart.

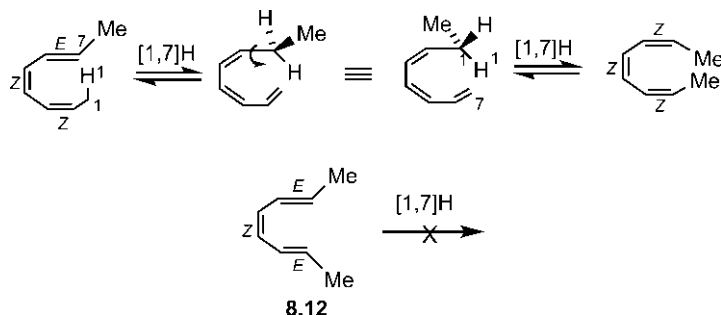
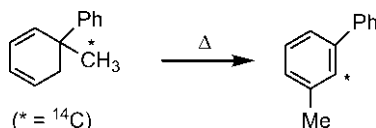


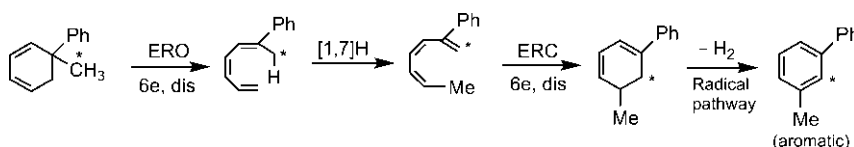
Fig. 8.21 Interconversion of the (*E,Z,Z*)- and (*Z,Z,Z*)-hexatriene by [1,7]H shifts. No [1,7]H shift is possible in (*E,Z,E*)-hexatriene.

Problem 8.3

Suggest a plausible mechanism for the following reaction.

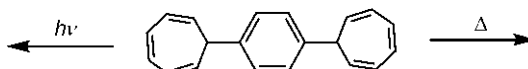


Answer¹⁸



Problem 8.4

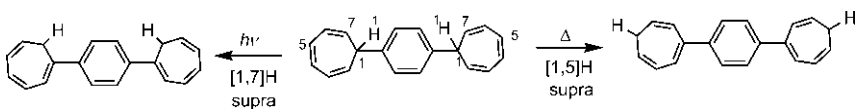
Predict the products of the following reactions.



Answer¹⁹

Only suprafacial H shift is geometrically possible in the terminal cycloheptatriene. Therefore, the product under thermal conditions results

from [1,5]H shifts, whereas, under photochemical conditions, the product arises from [1,7]H shifts.



8.2 [1,J] HYDROGEN SHIFTS IN CHARGED SYSTEMS ($J = \text{EVEN}$)

8.2.1 [1,2]H, [1,4]H and [1,6]H Shifts

[1,2]H shifts are well known in cations, and involve $2 (j=2)$ electrons (Fig. 8.22). Note that one arrow is needed to draw the process. The 2-electron ($4n+2$, $n=1$) rearrangement is thermally allowed with a suprafacial H shift (see Table 3.4), and represents a $[\sigma 2_s + \omega 0_s]$ process (Fig. 8.22). The classical rearrangements of carbocations involving H shifts are the common examples.

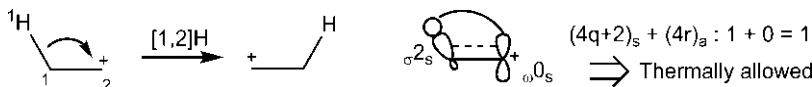


Fig. 8.22 [1,2] Hydrogen shift.

The [1,2]H shift in an anion would involve $j+2=4$ electrons, and will be thermally allowed antarafacially. But this antarafacial migration is geometrically impossible, and concerted [1,2]H shift in an anion does not occur. On the other hand, the [1,4]H shift in anions involves $2+j=6$ electrons, and is thermally allowed with suprafacial migration. This is illustrated with photocyclization of a diarylamine in the synthesis of a carbazole (Fig. 8.23).²⁰ The anionic intermediate 8.13 from a disrotatory electrocyclic ring closure spontaneously undergoes a sigmatropic [1,4]H shift to give carbazole 8.14. The [1,4]H shift is driven by the regeneration of a benzene ring. The suprafacial H shift leads to *trans* Me/H in the product.

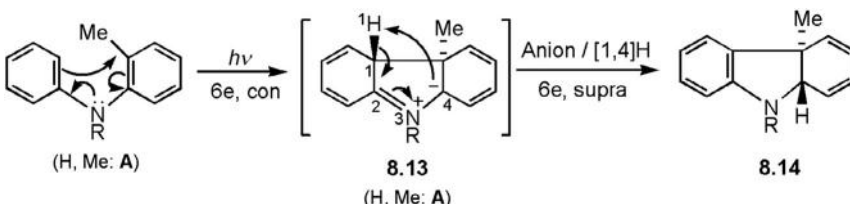


Fig. 8.23 Synthesis of a carbazole via a [1,4]H shift in an anionic intermediate.

The [1,6]H shift in a cation mobilizes $j=6$ electrons and is thermally allowed with a suprafacial shift. Fig. 8.24 shows an acid-catalysed ring opening of an epoxide to give a cyclooctadienyl cation **8.15** which undergoes a [1,6]H shift to form a conjugated cyclooctadienone product. A possible [1,4] H shift is ruled out because the antarafacial H shift is geometrically unattainable. Further, a [1,2] suprafacial H shift is less preferred as it would lead to a less stable unconjugated ketone.

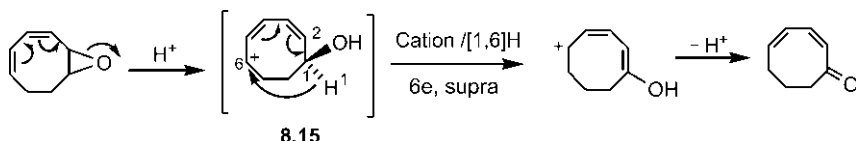


Fig. 8.24 Example of a [1,6]H shift in a cationic intermediate.

8.3 [1,J] CARBON SHIFTS IN NEUTRAL SYSTEMS ($J=ODD$)

8.3.1 [1,5]C Shifts

A thermal 6-electron [1,5]C shift is symmetry-allowed suprafacially with retention of configuration of the migrating group (see Table 3.5). This is illustrated with *cis* and *trans* spirodienes in Fig. 8.25.²¹ As a result of retention of configuration, the relative stereochemistry of two Me groups is retained in the product. The initial product in each case undergoes a rapid [1,5]H shift to give the more stable product.

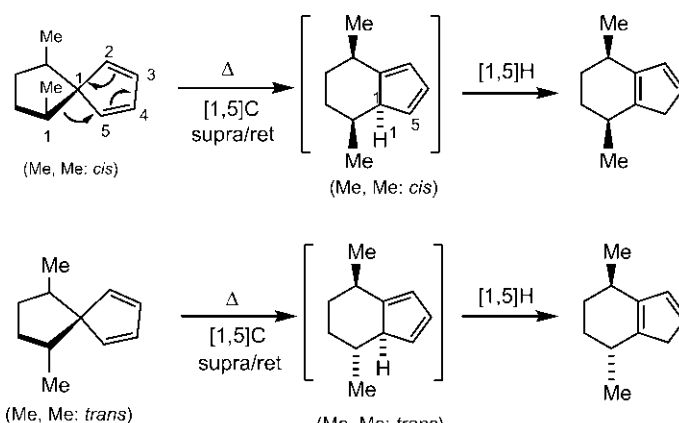
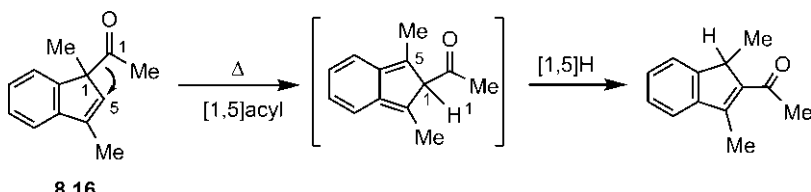


Fig. 8.25 Stereochemistry of [1,5]C shifts in *cis* and *trans* spirodienes.

The unsaturated groups such as carbonyl, vinyl and aryl migrate readily in [1,5]C shift.^{22–24} They are found to be better migrators than saturated alkyl groups. This has been attributed to a favourable secondary orbital interaction in the transition structure between the HOMO of π_4 component and the LUMO of π bond in the migrating group.²² (Recall that the primary frontier orbital interaction involves HOMO of π_4 component with the LUMO of σ_2 component; see Fig. 3.42.) The carbonyl group having a particularly lower energy LUMO with a larger coefficient on carbonyl carbon makes more effective secondary interaction and thus appears to be the best migrators. Fig. 8.26 shows an example of [1,5]C shift where the acyl group migrates in preference to the alkyl group in indene **8.16**.

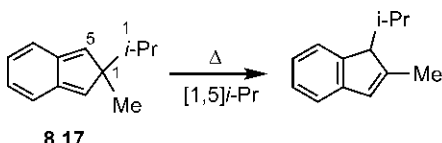


8.16

Fig. 8.26 An example of acyl migration in [1,5]C shift in an indene system.

It has been shown that migratory aptitude decreases in the order $\text{COMe} > \text{H} > \text{CH}=\text{CH}_2 > \text{Me}$.

The migration of alkyl group in the indene system has not been observed. But the [1,5] alkyl shift can occur in isoindene **8.17** or in cyclohexadienone **8.18**, where the rearrangement is facilitated by the formation of an aromatic ring (Fig. 8.27).^{25,26} The higher migratory aptitude of *i*-Pr or Bn than Me is due to a relatively weaker breaking σ bond (isopropyl or benzyl radical is more stable than methyl radical).



8.17

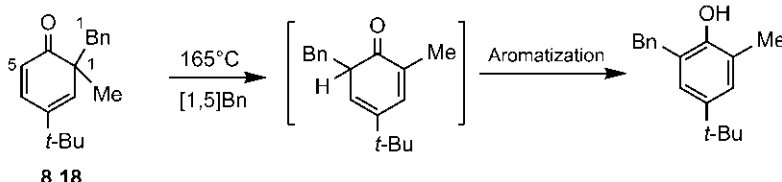


Fig. 8.27 [1,5] Alkyl shifts in isoindene and cyclohexadienone systems.

8.3.2 [1,3]C Shifts

A thermal 4-electron [1,3]C shift is symmetry-allowed suprafacially with inversion of configuration of the migrating group (see Table 3.5). However, the orbital overlap involving the back lobe of the migrating carbon with a lobe of the terminal p orbital (see Fig. 3.43) is difficult to achieve and the transition structure would be highly distorted. As such, the suprafacial [1,3]C shift with inversion is less likely. In some constrained bicyclic systems, thermal [1,3]C shifts of the bridge have been observed (Fig. 8.28).^{27,28} These reactions demonstrate the inversion of configuration of the migrating methylene bridge in conformity with the Woodward–Hoffmann rules. It is of note that an *exo*-substituent remains *exo* as a result of inversion of configuration (see Fig. 2.11). In the [1,3]C shift shown in Fig. 8.28A, *exo*-Me remains *exo*. In Fig. 8.28B, OAc acts as a stereochemical marker; the *trans* relationship of D and OAc changes to *cis* in the product because of inversion at the stereocentre but *exo*-D remains *exo*.

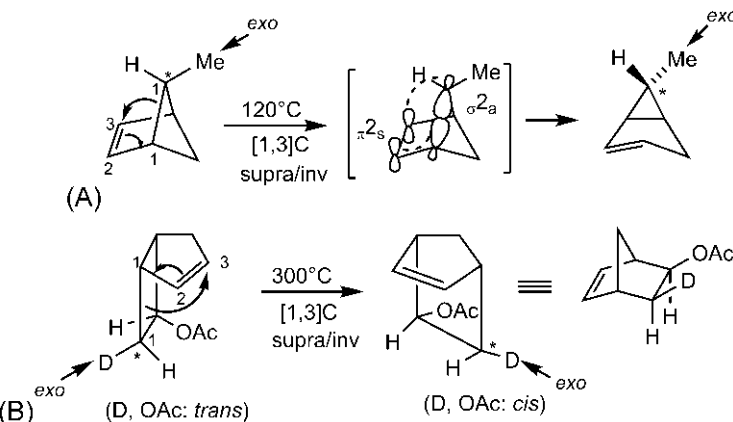


Fig. 8.28 Stereochemistry of the [1,3]C shift in (A) [2.1.1] and (B) [3.2.0] bicyclic frameworks.

As the distorted supra/inversion transition structure entails a high energy barrier, the symmetry-forbidden but geometrically favourable supra/retention pathway may compete with the allowed supra/inversion pathway. (It may be mentioned that a symmetry-forbidden reaction does not imply that the reaction is actually forbidden; it is generally much less likely to take place because it encounters a very high energy barrier.) In the reaction shown in Fig. 8.28B, the product ratio, inv:ret = 19:1. Using Eq. (2.1), this product ratio gives a free energy difference of 3.4 kcal mol^{-1} at 300°C between the allowed and forbidden pathways for the [1,3]C shift. Fig. 8.29 shows

the product composition from the allowed supra/inversion and forbidden supra/retention pathways for the *exo*-Me and *endo*-Me substrates.²⁹ For the *exo*-Me substrate (Fig. 8.29A), the predominant product is the supra/inversion product with the product ratio, inv:ret = 10:1. But, for the *endo*-Me substrate (Fig. 8.29B), the major product is the supra/retention product (inv:ret = 1:7). Since additional steric strain is involved in the supra/inv transition structure for the *endo*-Me substituent, the symmetry-forbidden supra/ret process dominates. The stepwise radical mechanism is a possibility, but is unlikely as this cannot account for the suprafacial migration in preference to antarafacial migration.

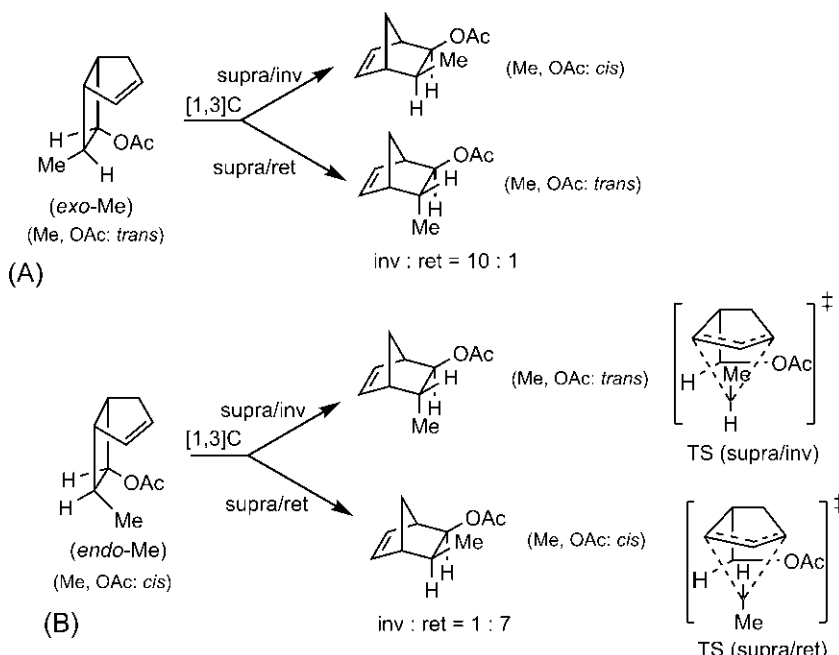


Fig. 8.29 Suprafacial [1,3]C shifts with inversion and retention stereochemistry in [3.2.0] bicyclic systems.

Next, we consider a type of [1,3]C shift known as vinylcyclopropane rearrangement, which is useful for making 5-membered rings (Fig. 8.30).

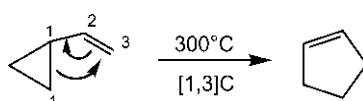


Fig. 8.30 Vinylcyclopropane rearrangement.

Using optically active *trans*, *trans*-2-methyl-1-propenylcyclopropane, a mixture of four products are obtained of which two are consistent with the allowed supra/inv and antara/ret pathways, while the other two correspond to supra/ret and antara/inv products (Fig. 8.31).³⁰

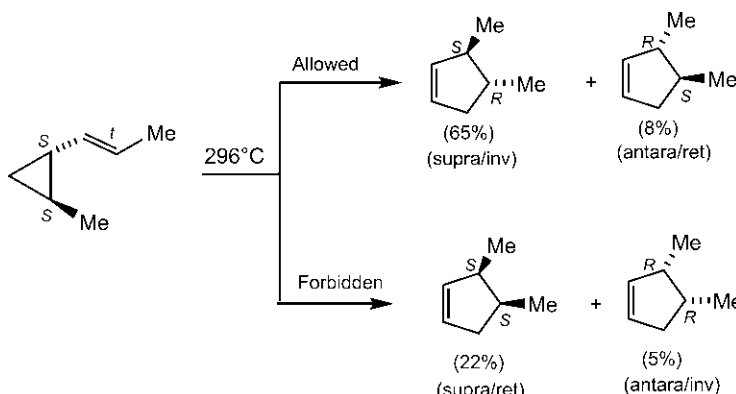


Fig. 8.31 Vinylcyclopropane rearrangement with (1*S*,2*S*)-*trans*, *trans*-2-methyl-1-propenylcyclopropane.

The predominant product is formed by the concerted supra/inv pathway; however, the formation of all four possible stereoisomeric products might suggest a stepwise diradical mechanism involving homolytic cleavage of the migrating σ bond. It has been shown that both pericyclic and radical mechanisms can operate with concerted supra/inversion sigmatropic shift as the major pathway.³¹

Under photochemical conditions, the [1,3]C shift is symmetry-allowed suprafacially with retention of configuration of the migrating group. This is illustrated with an example in Fig. 8.32.^{32,33} The relative stereochemistry of Ph with respect to Me is retained in the product as a result of retention of configuration of the migrating benzylic carbon.

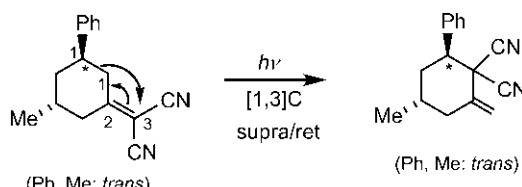
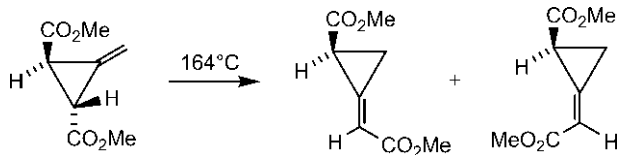


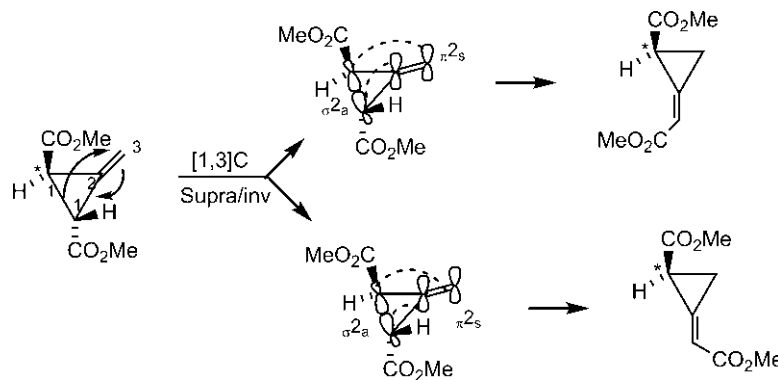
Fig. 8.32 Example of a photochemical [1,3]C shift.

Problem 8.5

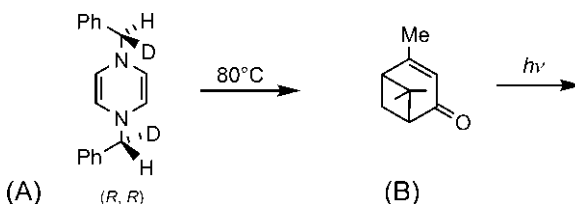
Suggest a mechanism for the thermal rearrangement of the following *exo*-methylene cyclopropane derivative (Feist's ester).

**Answer³⁴**

The reaction involves suprafacial [1,3]C shift with inversion of configuration at the stereocentre (*). The new double bond can have *E*/Z stereochemistry. The orbital interactions leading to inversion of configuration of the migrating centre and double-bond stereochemistry are shown.

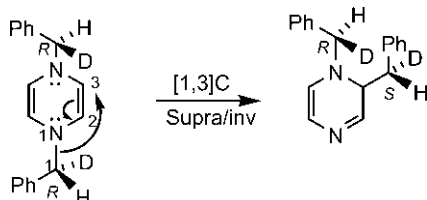
**Problem 8.6**

Predict the products of the following reactions.

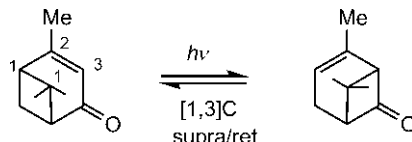


Answer

(A) A [1,3]C shift under the supra/inv mode gives the product. The reaction occurs at a lower temperature because of the loss of antiaromatic character of the substrate (Hückel $4n$ rule, $n=2$).



(B) A photochemical [1,3]C shift by supra/retention pathway gives the product. The reaction is reversible.



8.4 [1,J] CARBON SHIFTS IN CHARGED SYSTEMS ($J = \text{EVEN}$)

8.4.1 [1,2]C Shifts

The 2-electron thermal [1,2]C shifts in cations are the most common rearrangements and proceed suprafacially with retention of configuration of the migrating group (see Table 3.5). (An antarafacial migration with inversion is geometrically impossible.) A schematic representation of a [1,2]C shift and its frontier orbital description for supra/retention mode are shown in Fig. 8.33.

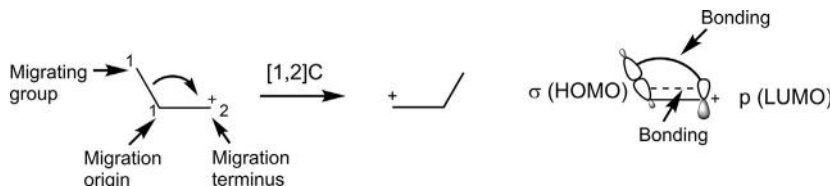


Fig. 8.33 [1,2]C shift and frontier orbital picture for supra/retention pathway.

The migrating centre and migration origin are usually carbons; however, the migration terminus can be carbon (Wagner–Meerwein/pinacol rearrangement), nitrogen (Beckmann/Curtius/Lossen/Schmidt/Hofmann rearrangement) or oxygen (Baeyer–Villiger rearrangement/Dakin reaction).

A Wagner–Meerwein rearrangement for the conversion of α -pinene into bornyl chloride is shown in Fig. 8.34. The reaction proceeds through a [1,2]C shift forming carbocation 8.19, which combines with Cl^- to give bornyl chloride. However, the involvement of the classical carbocation 8.19 cannot explain the stereochemistry of the product. The observed stereochemistry of Cl in the product can be explained by invoking a nonclassical carbocation 8.20.

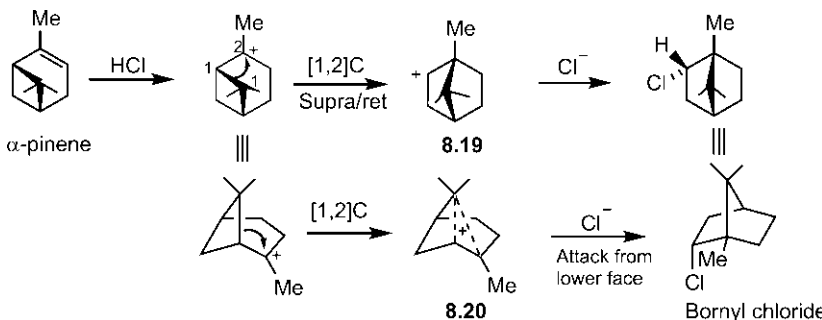


Fig. 8.34 Example of Wagner–Meerwein rearrangement via [1,2]C shift.

The [1,2]C shift in an anion as a 4-electron concerted process is symmetry-allowed suprafacially with inversion of configuration under thermal conditions. But the supra/inversion stereochemistry requiring overlap of the back lobe of the migrating carbon with the lobe of p orbital at the migration terminus is geometrically unattainable.

8.4.2 [1,4]C Shifts

The 4-electron thermal [1,4]C shifts in allyl cations proceed via supra/inversion pathway, which represents an allowed $[\sigma^2_a + \pi^2_s]$ process (Fig. 8.35).

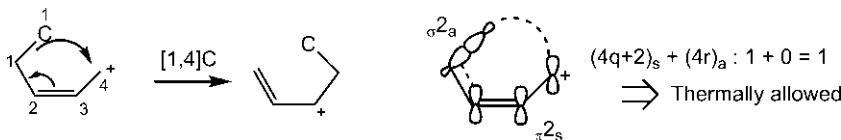


Fig. 8.35 [1,4]C shift and orbital interactions for supra/inversion pathway.

The [1,4]C shift is illustrated in Fig. 8.36 with the rearrangement of a chiral bicyclohexenyl cation **8.21** obtained by treatment of a bicyclic α -bromoketone with a base.³⁵

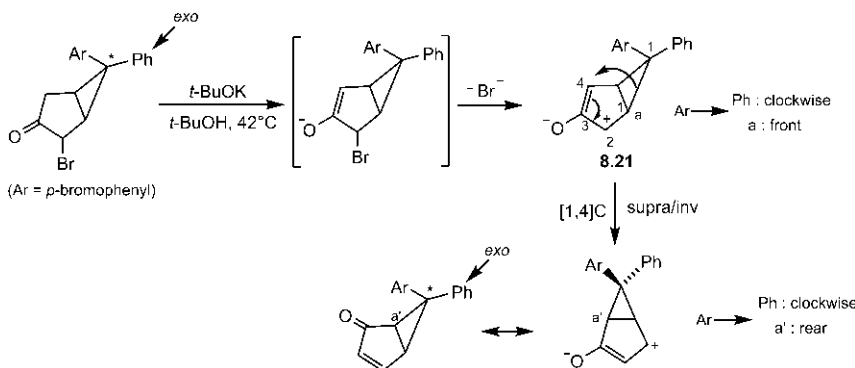


Fig. 8.36 Example of suprafacial [1,4]C shift with inversion of configuration.

The *exo*-Ph remains *exo* as a result of inversion of configuration. See the use of rule (Figs. 2.10 and 2.11) to draw the inversion stereochemistry.

8.5 'WALK' REARRANGEMENTS

In cyclopropane-fused [n.1.0] bicyclic systems, the cyclopropane ring can walk around the periphery of the larger ring as a result of sequential [1,j] C shifts (Fig. 8.37). This is known as 'walk' rearrangement.³⁶

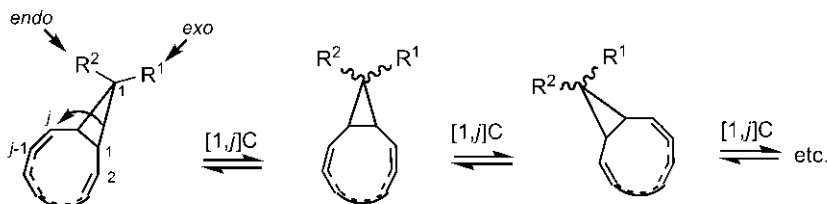


Fig. 8.37 Schematic representation of walk rearrangement.

The methylene bridge revolves round and round the ring and is termed peripatetic cyclopropane bridge. The *exo* and *endo* substituents on the bridge carbon in each step of the rearrangement can either maintain their stereochemical integrity (*exo* remains *exo*; *endo* remains *endo*) or interchange their positions (*exo* becomes *endo* and vice versa) depending on the type of [1,j]C shift involved.

Under thermal conditions, the 4*n*-electron [1,3], [1,4] or [1,7]C shift occurs suprafacially with inversion of configuration of the migrating bridge carbon when the *exo*-substituent remains *exo* and the *endo*-substituent

remains *endo*. A walk rearrangement with a bicyclo[2.1.0]pentenyl system mediated by [1,3]C shifts is shown in Fig. 8.38.³⁷ All four structures 8.22–8.25 in one complete circuit are drawn, in which the movements of the cyclopropane ring are equivalently represented in terms of different positions of Me on the four-membered ring with respect to the cyclopropane ring as it walks around the periphery. The *exo*-CO₂Me remains *exo* in all the structures as a result of suprafacial migration with inversion of configuration. Note that 8.22 is enantiomeric with 8.25. Similarly, 8.23 and 8.24 are enantiomeric. Therefore, if optically active substrate is taken, the rearrangement would lead to racemization.

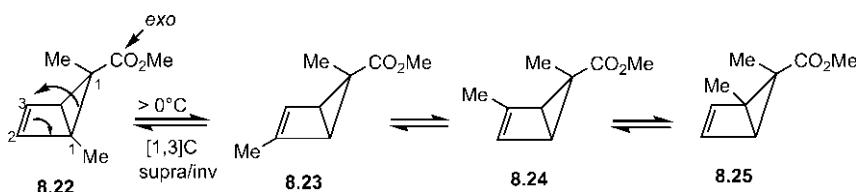


Fig. 8.38 Walk rearrangement of a bicyclo[2.1.0]pentenyl system via [1,3]C shifts.

Photochemical electrocyclic ring closing of a pentadienyl cation 8.27 (generated by protonation of 8.26) at -100°C produces a bicyclic cation 8.28, characterized by four resonance signals in ^1H NMR. On raising temperature from -100°C to -9°C , the bicyclic cation 8.28 undergoes a walk rearrangement involving [1,4]C shifts under the supra/inversion mode when *exo*-Me (shown in bold) remains *exo* and *endo*-Me remains *endo* throughout (Fig. 8.39).³⁸ The movements of the cyclopropane ring change the ring fusion successively to 4–5 in 8.29, 3–4 in 8.30 and so on. As a result of walk rearrangement, all the five starred methyl groups become equivalent on the NMR time scale giving a sharp signal at δ 2.1 (s, 15H). Moreover, the *exo*-Me and *endo*-Me give two signals at δ 1.1 (s, 3H) and -0.6 (s, 3H), respectively. The higher field signal at δ -0.6 for *endo*-Me is due to the shielding effect of π -current of the rotating allyl cation unit. (If there were retention of configuration, *endo* methyl would become *exo* and vice versa, a time-average 6-proton signal would then appear instead of two, 3-proton singlets.) This example beautifully demonstrates the inversion stereochemistry of sigmatropic [1,4]C shifts with an achiral substrate using ^1H NMR.

The walk rearrangement of a bicyclo[6.1.0]nonatriene derivative is shown in Fig. 8.40.³⁹ The rearrangement proceeds through suprafacial [1,7]C shifts with inversion of configuration at the migrating carbon when

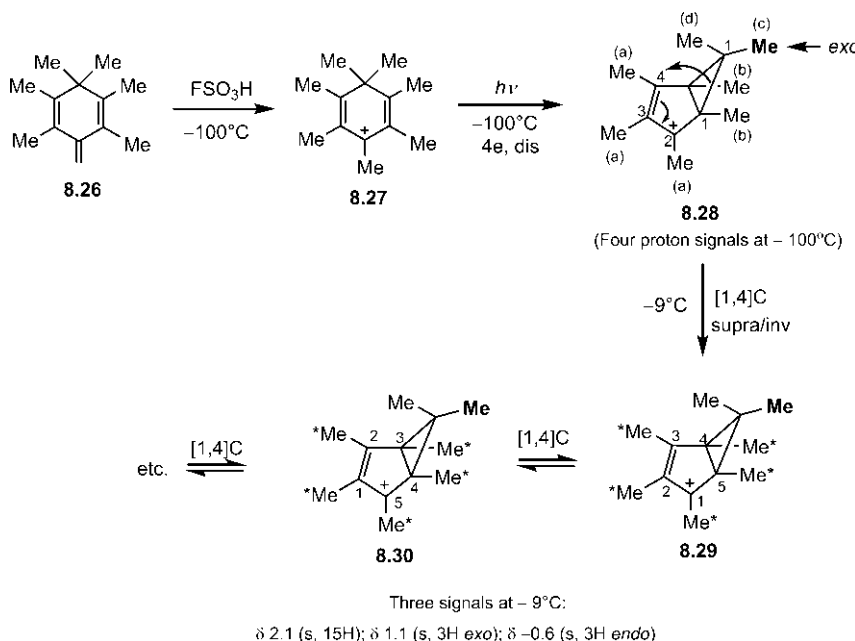


Fig. 8.39 Walk rearrangement of an achiral 5–3 bicyclic cation through [1,4]C shifts. The *exo*-Me in the cation is indicated in bold.

endo-CN remains *endo*. The revolution of the cyclopropane ring can be clockwise or anticlockwise. In Fig. 8.40, clockwise rotation of the cyclopropane ring is equivalently shown as the movement of Me group on the eight-membered ring by one carbon forward anticlockwise at each step of the rearrangement.

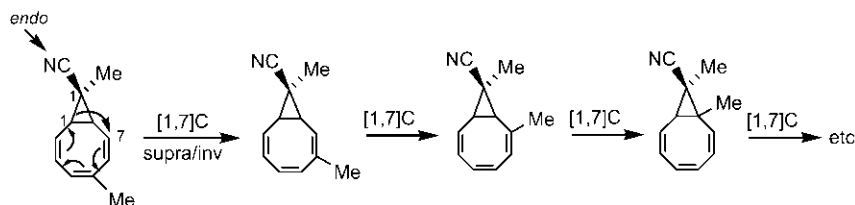


Fig. 8.40 Walk rearrangement of a bicyclo[6.1.0]nonatrienyl system involving [1,7]C shifts.

Thermal [1,5]C shifts involving 6 electrons proceed through supra/retention pathway. As a result of retention of configuration, the *exo* substituent becomes *endo* and vice versa (see Fig. 2.12). Electrocyclic ring closing of a cycloheptatriene **8.31** produces a norcaradiene **8.32** which can undergo

walk rearrangement involving [1,5]C shifts as shown in Fig. 8.41.⁴⁰ The *endo*-Me becomes *exo* in the first step which then goes to the *endo* position in the next step and so on. Owing to the *endo/exo* exchange, no enantiomeric norcaradiene structures are obtained in one full circuit of six structures in the walk rearrangement (cf. Fig. 8.38 where enantiomeric structures result as the stereochemical integrity of the *exo* or *endo* substituent is preserved). Therefore, if optically active cycloheptatriene is used, optical activity will be preserved throughout the rearrangement.

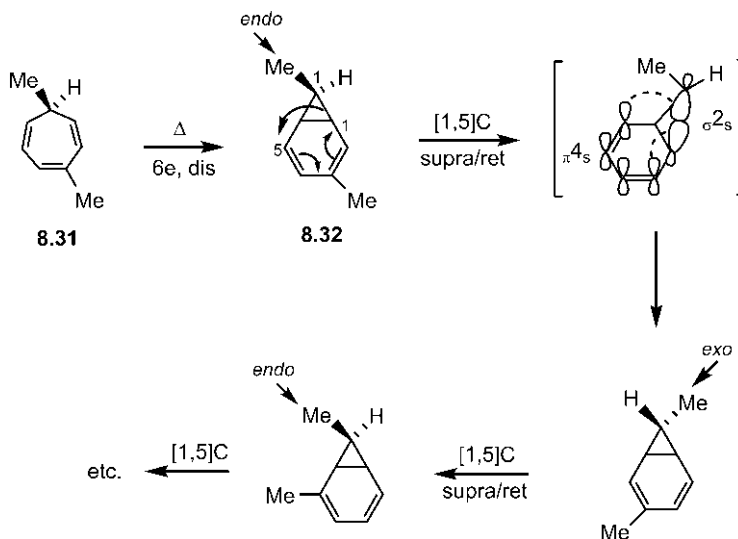


Fig. 8.41 Walk rearrangement in a norcaradiene system mediated by [1,5]C shifts.

To summarize, a cartoon representation (as introduced by Woodward and Hoffmann) for ‘walk’ rearrangement in supra/inversion and supra/retention pathways is shown in Fig. 8.42.⁴¹ The cyclopropane ring is not drawn; the two substituents at the bridge carbon are indicated by open and closed circles. The *endo* and *exo* substituents are drawn, respectively, inside and outside the ring on whose perimeter the cyclopropane ring revolves.

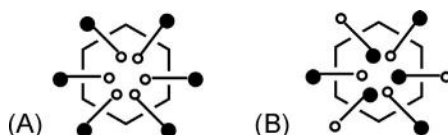
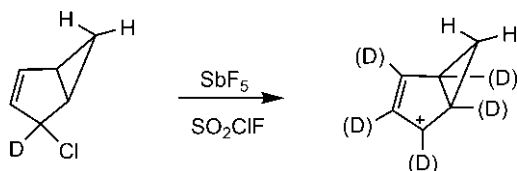


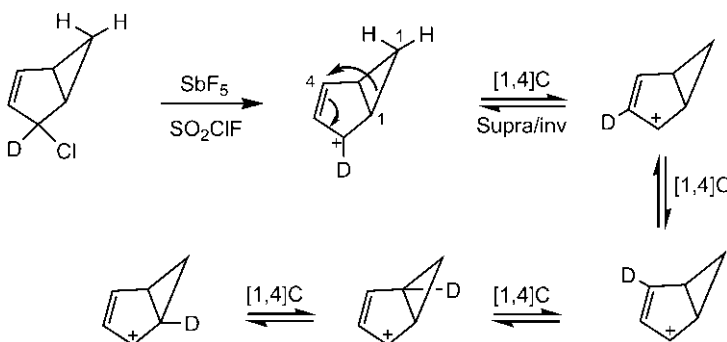
Fig. 8.42 Cartoon representation of walk rearrangement through [1,*j*]C shifts in (A) supra/inversion and (B) supra/retention pathways. Inside the ring: *endo* substituent; outside the ring: *exo* substituent.

Problem 8.7

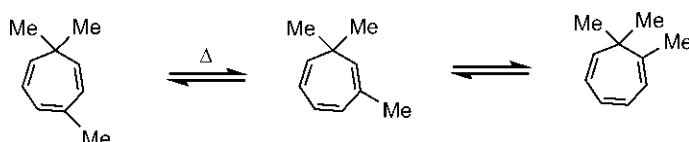
Account for the deuterium scrambling over all five positions of the five-membered ring in the deuterated cation.

**Answer⁴²**

In a superacid medium, an allylic carbocation is generated. A walk rearrangement follows involving [1,4]C shifts under supra/inversion mode. This causes scrambling of deuterium over all positions of the five-membered ring. (As the migrating methylene bridge has no stereochemistry, the inversion stereochemistry of [1,4]C shift is not observable.)

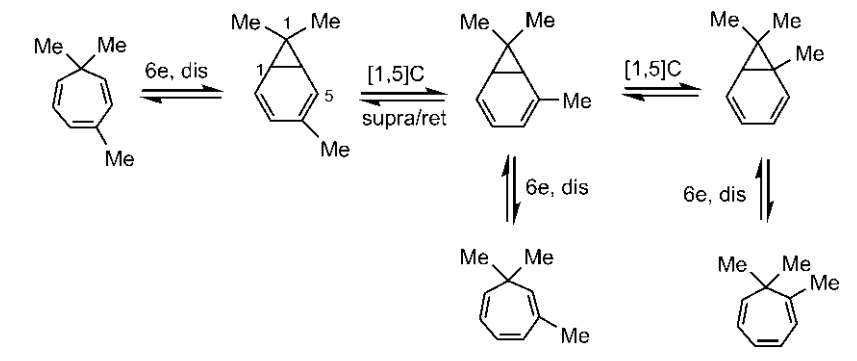
**Problem 8.8**

Give a mechanism for thermal isomerization of 3,7,7-trimethylcycloheptatriene.



Answer⁴³

Thermal isomerization takes place via a sequence of electrocyclic ring closing, walk rearrangement involving [1,5]C shifts and electrocyclic ring opening as shown below. As the migrating methylene bridge has no stereochemistry, the retention stereochemistry of the [1,5]C shift is not observable. There are three possible regioisomeric norcaradienes and cycloheptatrienes.



REFERENCES

1. Spangler, C. W. *Chem. Rev.* **1976**, *76*, 187.
2. Roth, W. R.; König, J.; Stein, W. *Chem. Ber.* **1970**, *103*, 426.
3. Mironov, V. A.; Sobolev, E. V.; Elizarova, A. N. *Tetrahedron* **1963**, *19*, 1939.
4. Corey, E. J.; Weinshenker, N. M.; Schaaf, T. K.; Huber, W. *J. Am. Chem. Soc.* **1969**, *91*, 5675.
5. Berson, J. A.; Aspelin, G. B. *Tetrahedron* **1964**, *20*, 2697.
6. Almy, J.; Cram, D. J. *J. Am. Chem. Soc.* **1970**, *92*, 4316.
7. Mironov, V. A.; Chizhov, O. S.; Kimelfeld, I. M.; Akhrem, A. A. *Tetrahedron Lett.* **1969**, *499*.
8. Alkorta, I.; Elguero, J. *J. Chem. Soc. Perkin Trans. 2* **1998**, 2497.
9. Hess, B. A., Jr.; Baldwin, J. E. *J. Org. Chem.* **2002**, *67*, 6025.
10. Hess, B. A., Jr. *Int. J. Quantum Chem.* **2002**, *90*, 1064.
11. Roth, W. R. *Liebigs Ann.* **1964**, *671*, 25.
12. Burgstahler, A. W. *J. Org. Chem.* **1981**, *46*, 1741.
13. Bailey, W. J.; Baylouny, R. A. *J. Org. Chem.* **1962**, *27*, 3476.
14. Kropp, P. J.; Fravel, H. G., Jr.; Fields, T. R. *J. Am. Chem. Soc.* **1976**, *98*, 840.
15. Baldwin, J. E.; Reddy, V. P. *J. Am. Chem. Soc.* **1987**, *109*, 8051.
16. Hoeger, C. A.; Johnston, A. D.; Okamura, W. H. *J. Am. Chem. Soc.* **1987**, *109*, 4690.
17. Schlatmann, J. L. M. A.; Pot, J.; Havinga, E. *Rec. Trav. Chim.* **1964**, *83*, 1173.
18. Schiess, P.; Dinkel, R. *Tetrahedron Lett.* **1975**, 2503.
19. Murray, R. W.; Kaplan, M. L. *J. Am. Chem. Soc.* **1966**, *88*, 3527.
20. Laarhoven, W. H. *Recl. Trav. Chim. Pays-Bas* **1983**, *102*, 241, 185.
21. Boersma, M. A. M.; Haan, d.J. W.; Kloosterziel, H.; Ven, v.d.L. *J. M. Chem. Commun.* **1970**, 1168.

22. Fields, D. J.; Jones, D. W.; Kneen, G. *Chem. Commun.* **1976**, 873.
23. Miller, L. L.; Greisinger, R.; Boyer, R. F. *J. Am. Chem. Soc.* **1969**, *91*, 1578.
24. Manning, C.; McClary, M. R.; McCullough, J. J. *J. Org. Chem.* **1981**, *46*, 919.
25. Haan, d.J. W.; Kloosterziel, H. *Rec. Trav. Chim.* **1965**, *84*, 1594; **1968** *87*, 298.
26. Miller, B. *Acc. Chem. Res.* **1975**, *8*, 245.
27. Roth, W. R.; Friedrich, A. *Tetrahedron Lett.* **1969**, 2607.
28. Berson, J. A.; Nelson, G. L. *J. Am. Chem. Soc.* **1967**, *89*, 5503.
29. Berson, J. A. *Acc. Chem. Res.* **1968**, *1*, 152; **1972**, *5*, 406.
30. Andrews, G. D.; Baldwin, J. E. *J. Am. Chem. Soc.* **1976**, *98*, 6705.
31. Houk, K. N.; Nendel, M.; Wiest, O.; Storer, J. W. *J. Am. Chem. Soc.* **1997**, *119*, 10545.
32. Cookson, R. C.; Hudec, J.; Sharma, M. *Chem. Commun.* **1971**, 107.
33. Sharma, M. *J. Am. Chem. Soc.* **1975**, *97*, 1153.
34. Doering, W.v.E.; Roth, H. D. *Tetrahedron* **1970**, *26*, 2825.
35. Zimmerman, H. E.; Crumrine, D. S. *J. Am. Chem. Soc.* **1968**, *90*, 5612.
36. Klärner, F.-G. *Top. Stereochem.* **1984**, *1*, 15.
37. Klärner, F.-G.; Adamsky, F. *Angew. Chem. Int. Ed. Eng.* **1979**, *18*, 674.
38. Childs, R. F.; Winstein, S. *J. Am. Chem. Soc.* **1968**, *90*, 7146.
39. Klärner, F.-G.; Wette, M. *Chem. Ber.* **1978**, *111*, 282.
40. Berson, J. A.; Willcott, M. R., III *Rec. Chem. Progr.* **1966**, *27*, 139.
41. Woodward, R. B.; Hoffmann, R. *The Conservation of Orbital Symmetry*. Verlag Chemie/Academic Press: Weinheim/New York, 1971/1970.
42. Swatton, D. W.; Hart, H. *J. Am. Chem. Soc.* **1967**, *89*, 5075.
43. Berson, J. A.; Willcott, M. R., III *J. Am. Chem. Soc.* **1965**, *87*, 2751; **1966**, *88*, 2494.

CHAPTER 9

Sigmatropic Rearrangements 2: [i,j] Shifts

In $[i,j]$ sigmatropic rearrangement, an old $1-1\sigma$ bond is broken and a new $i-j\sigma$ bond is formed with concomitant reorganization of the π bonds (see Section 3.2.3). (The sigmatropic numbering must not be confused with IUPAC numbering.)

9.1 [3,3] COPE REARRANGEMENT

The Cope rearrangement^{1,2} is a thermal $[3,3]$ sigmatropic rearrangement (see Fig. 3.12) of a 1,5-diene to another 1,5-diene. The reaction is reversible and the position of equilibrium is governed by the relative stability of the reactant and the product, which depends on their substitution pattern. For example, the equilibrium of the Cope rearrangement shown in Fig. 9.1 lies in favour of the product 1,5-diene in which a double bond is conjugated.

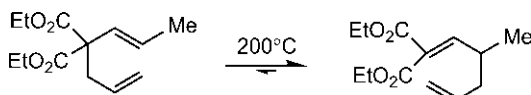


Fig. 9.1 Reversible Cope rearrangement and position of equilibrium.

There are a few variants of Cope rearrangement. When the 1,5-diene possesses a hydroxyl group at C-3 (IUPAC numbering), the rearrangement is known as oxy-Cope rearrangement (Fig. 9.2). Here the initial product is

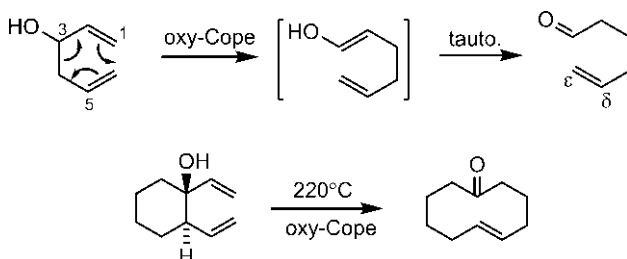


Fig. 9.2 Oxy-Cope rearrangement and an example.

an enol which tautomerizes readily to give δ,ϵ -unsaturated carbonyl compound as the final product. This is illustrated with an example.

The oxy-Cope rearrangement occurs at much lower temperature when a base is added to deprotonate the alcohol substrate. This variant is called anionic oxy-Cope rearrangement (Fig. 9.3A).^{3,4} The increase in the rate of the anionic oxy-Cope rearrangement is dramatic by a factor of 10^{10} – 10^{17} relative to oxy-Cope.⁵ This rate acceleration is attributed to the stabilization of the transition structure relative to the starting material. The presence of the anionic oxygen destabilizes the reactant, and stabilizes the transition structure by the delocalization of the negative charge. Thus raising of reactant free energy and lowering of transition structure free energy for the anionic oxy-Cope system leads to a decrease in free energy barrier ($\Delta\Delta G^\#$), which is estimated to be 15 kcal mol^{−1}. (Draw a free energy profile.)

The base employed in anionic oxy-Cope rearrangement is usually KH because K⁺ is least associated with the anionic oxygen. A crown ether 18-crown-6 is often added to trap the K⁺ ion. The relative rates of oxy- and anionic oxy-Cope rearrangements with an alcohol substrate are shown in Fig. 9.3B.⁵ (In drawing product, ensure that the new σ bond is 3–3 and the new π bonds are 1–2 and 1–2 as per sigmatropic numbering.)

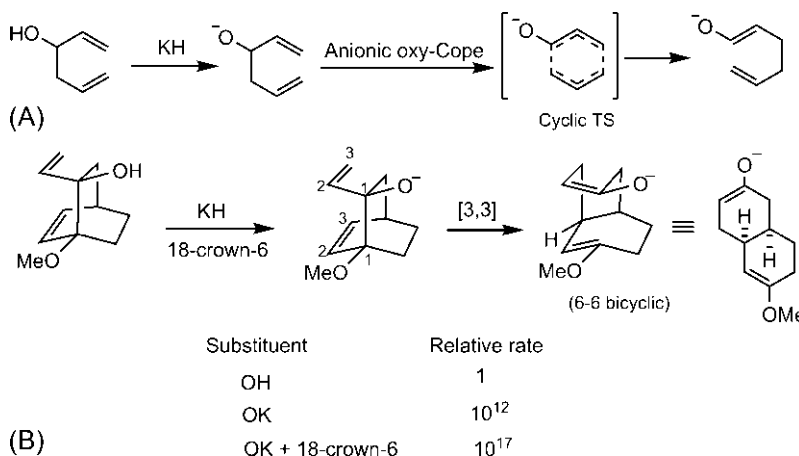


Fig. 9.3 (A) Anionic oxy-Cope rearrangement; (B) relative rates of oxy- and anionic oxy-Cope rearrangements.

The substituent effect on the rate has been explained⁶ by estimating the π -energy difference for the unsubstituted Cope and substituted Cope systems. This analysis is similar to that described previously for electrocyclic

reactions (see [Section 7.1.2.1](#)). The Cope rearrangement involves aromatic Hückel transition structure (TS) (see [Fig. 3.45](#)). The oxy anion substituent (x -substituent) can be modelled as a carbanion centre.

For both unsubstituted and substituted 1,5-dienes,

$$\begin{aligned}\pi\text{-energy} &= \text{energy of four electrons in two isolated double bonds} \\ &= 4(\alpha + \beta).\end{aligned}$$

The π -energy of Hückel TS for the unsubstituted Cope system
= energy of six electrons in completely filled bonding levels (see Fig. 1.30)
 $= 2(\alpha + 2\beta) + 4(\alpha + \beta) = 6\alpha + 8\beta.$

The π -energy of Hückel TS for the x -substituted Cope system⁶

$$= 6\alpha + 8.72\beta$$

These π -energies are shown in an energy diagram ([Fig. 9.4](#)). Clearly, the π -energy difference between the reactant and the Hückel TS for the anionic oxy-Cope rearrangement is less than that for unsubstituted Cope system by 0.72β (in units of β), and hence the rate is increased.

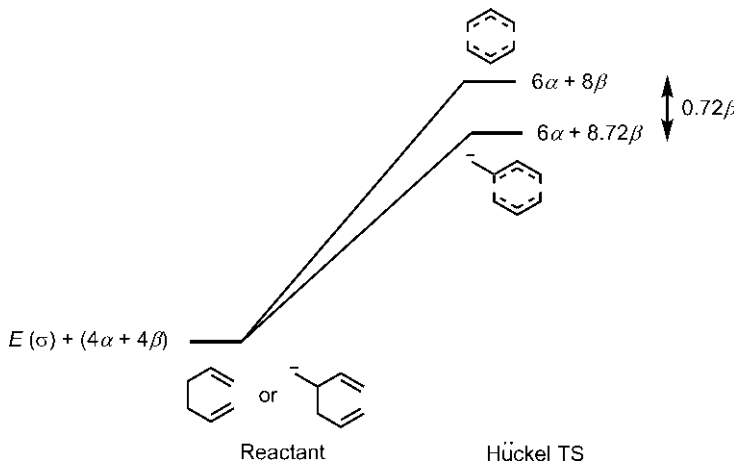


Fig. 9.4 π -Energies of substrates and Hückel transition structures for Cope and anionic oxy-Cope rearrangements.

If a carbocation substituent (z -substituent) is present at C-3, the π -energy of Hückel TS of the z -substituted Cope system will be that of benzyl cation which has the same π -energy as the benzyl anion (a model of Hückel TS for x -substituted Cope system). This is because the two extra electrons in the

anion are in the nonbonding level and do not contribute to π -energy. Therefore a carbocation at C-3 of the 1,5-diene is also expected to accelerate the reaction. This has been observed, for example, in the facile solvolytic Cope rearrangement of a tricyclic substrate as shown in Fig. 9.5.^{7,8}

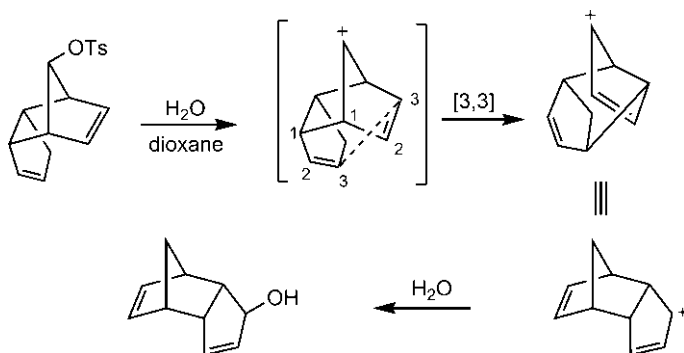


Fig. 9.5 Solvolytic Cope rearrangement of a tricyclic tosylate.

A substituent at C-2 of the 1,5-diene has much smaller effect because delocalization occurs both in the reactant and in the transition structure.

Another variant of Cope rearrangement is the aza-Cope rearrangement (Fig. 9.6).⁹ The substrate in this case is *N*-butenyl-iminium ion which is a heterocyclic analogue of 1,5-diene. When R = OH, the rearrangement is followed by an intramolecular Mannich reaction to provide an excellent route to pyrrolidine synthesis.¹⁰

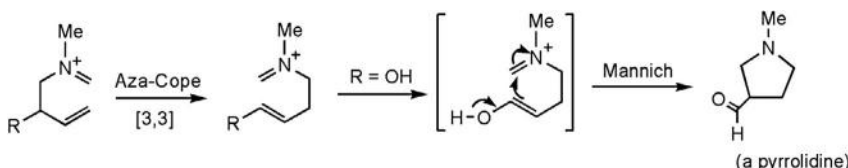
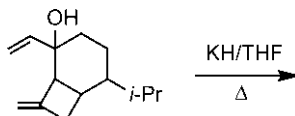


Fig. 9.6 Aza-Cope rearrangement and its use in pyrrolidine synthesis.

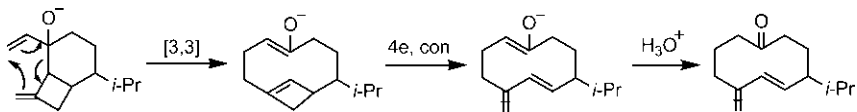
Problem 9.1

Predict the product of the following reaction.



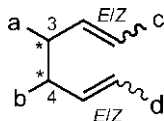
Answer¹¹

The reaction proceeds through an anionic oxy-Cope rearrangement followed by electrocyclic ring opening of the cyclobutene ring to give the product.



9.1.1 Stereochemistry of Cope Rearrangement

The substrate 1,5-diene **9.1** can possess a maximum of two stereocentres at C-3/C-4, and *E* or *Z* stereochemistry of the double bonds.

**9.1**

The 6-electron Cope rearrangement proceeds through supra/supra pathway involving a chair or a boat transition structure (see Fig. 3.46). In general, there are two possible chair and two possible boat conformations, which may lead to four possible stereoisomeric products. However, the chair TS is more stable than boat TS (see Fig. 3.47). An estimate of free energy difference gives $\sim 6 \text{ kcal mol}^{-1}$ in favour of the chair TS. For acyclic 1,5-dienes, when both chair and boat TSs are geometrically accessible, the Cope rearrangement proceeds preferentially through chair TS. If one chair conformation is more stable than the other, the more stable chair TS gives the major product. The Cope rearrangement is thus highly stereoselective. If steric factors make the chair TS prohibitively high in energy, the Cope rearrangement can then proceed through boat TS.

9.1.1.1 Cope Rearrangement via Chair Transition Structure

The chair TS of Cope rearrangement will be drawn as **9.2** (showing all bonds being broken and formed) or **9.3** (a simplified representation showing only the σ bond being formed so as to complete the cycle) (Fig. 9.7).

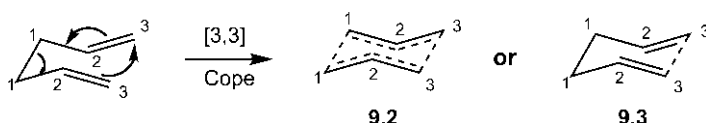


Fig. 9.7 Representation of chair transition structure of Cope rearrangement.

Acyclic Substrate Having Two Stereocentres

Let us consider the Cope rearrangements of the diastereomers of 3,4-dimethylhexa-1,5-diene.¹² The *meso* (*R,S*) diastereomer on heating gives almost exclusively the (*E,Z*) diene (Fig. 9.8). Both stereocentres of the reactant are destroyed in the reaction and a product with new double bond stereochemistry is formed.

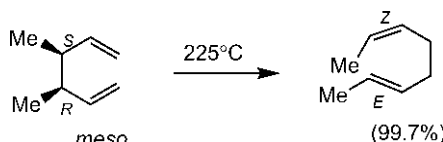


Fig. 9.8 Cope rearrangement of *meso*-3,4-dimethylhexa-1,5-diene.

The stereochemical outcome of the reaction can be rationalized on the basis of the preferred chair conformation of the transition structure as shown in Fig. 9.9. Note that the starting material is drawn in an equivalent sawhorse representation that directly leads to chair TS. One Me is equatorial and the other is axial in the chair TS which gives only the (*E,Z*) isomer.

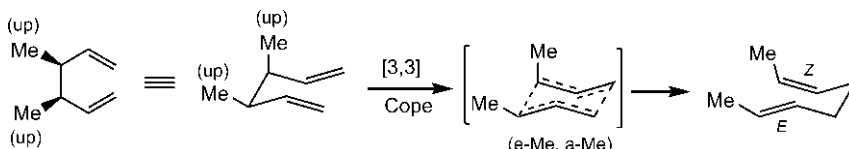


Fig. 9.9 Mechanism of Cope rearrangement shown in Fig. 9.8 involving a chair TS.

The *threo* diastereomer is chiral and racemic (*R,R* + *S,S*), which gives (*E,E*) diene as a major product with a small amount of (*Z,Z*) isomer. This is shown in Fig. 9.10 taking the (*R,R*) enantiomer. The (*S,S*) isomer necessarily gives the same result.

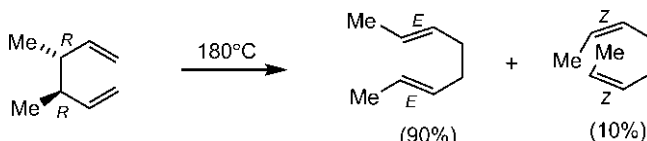


Fig. 9.10 Cope rearrangement of (*R,R*)-3,4-dimethylhexa-1,5-diene.

Here the two products arise from the two possible chair TSs as shown in Fig. 9.11 (see also Fig. 2.6 Method 1). (Note that 3 → 4 is clockwise; be

careful that you do not end up in drawing a wrong enantiomer! The details of drawing are only an aid to understanding; the chair TS can be drawn straightway.) The (e,e) chair conformation, being more stable than (a,a) conformation, leads to the major (*E,E*) product, which explains the stereoselectivity.

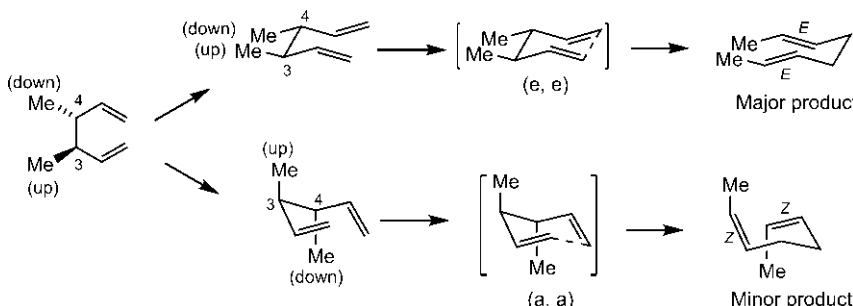


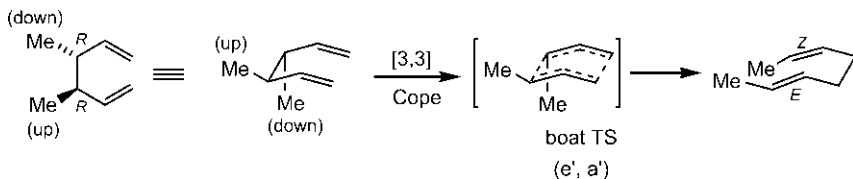
Fig. 9.11 Mechanism of Cope rearrangement of (*R,R*) diene in Fig. 9.10.

Problem 9.2

Draw the product that would arise from the boat TS of Cope rearrangement of (*R,R*)-3,4-dimethylhexa-1,5-diene.

Answer

The starting material is drawn in an equivalent eclipsed sawhorse formula that leads directly to boat TS (see Fig. 2.9). The product is (*E,Z*) isomer.



Acyclic Substrate Having Stereocentre(s) and Double Bond Stereochemistry
Consider the Cope rearrangement of 3-methyl-3-phenylhepta-1,5-diene (Fig. 9.12).

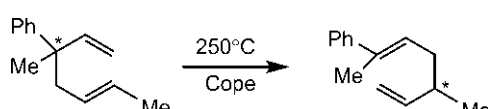


Fig. 9.12 Cope rearrangement of 3-methyl-3-phenylhepta-1,5-diene.

The substrate possesses a stereocentre and is chiral. In the reaction, the old stereocentre is destroyed and a new stereocentre is created to give a chiral product. This is called ‘chirality transfer’. For this stereochemical feature, the [3,3] sigmatropic shifts are very useful in asymmetric synthesis.^{13,14}

Fig. 9.13 shows an asymmetric Cope rearrangement using (*R*) enantiomer of (*E*)-3-methyl-5-phenylhepta-1,5-diene **9.4**.¹⁵ The major product is (*E*) diene **9.5** (87%) with high enantioselectivity for (*S*) enantiomer (ee > 95%). The minor product is (*Z,R*) isomer. The rearrangement proceeds through two possible chair TSs (see also Fig. 2.6 Method 2). The lower energy chair conformation with larger Ph in equatorial position gives the major enantioselective product **9.5**. Note that *E* stereochemistry of the double bond in the starting diene forces Me on the double bond to be equatorial in both chair TSs.

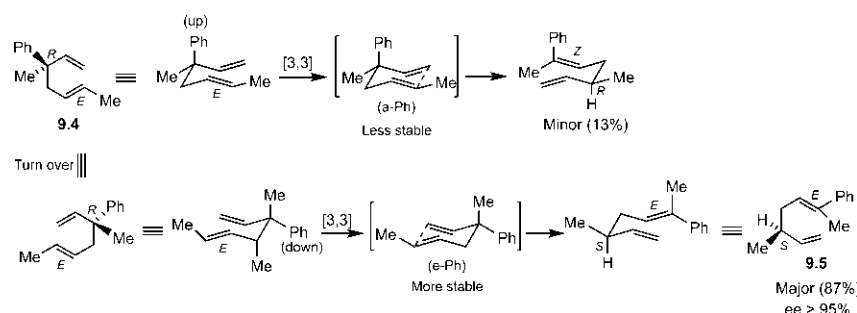


Fig. 9.13 Asymmetric Cope rearrangement using (*R,E*)-3-methyl-3-phenylhepta-1,5-diene.

Anionic Oxy-Cope Rearrangement

The stereochemistry of anionic oxy-Cope rearrangement is illustrated with two diastereomeric substrates **9.6** and **9.7** having *E,E* and *E,Z* stereochemistry of double bonds, respectively (Fig. 9.14).¹⁶ The major diastereomeric product in each case results via more stable chair TS in which Me and O⁻ at the two stereocentres of the substrate occupy less-hindered equatorial positions. Note that *E* stereochemistry in the starting diene forces Me on the double bond to be equatorial while *Z* stereochemistry places Me at axial position. The (*E,E*) diastereomer **9.6** gives a *threo* product whereas the (*E,Z*) diastereomer **9.7** produces an *erythro* product. It should also be noted that the preferred chair TS leads to *E* stereochemistry of new double bond.

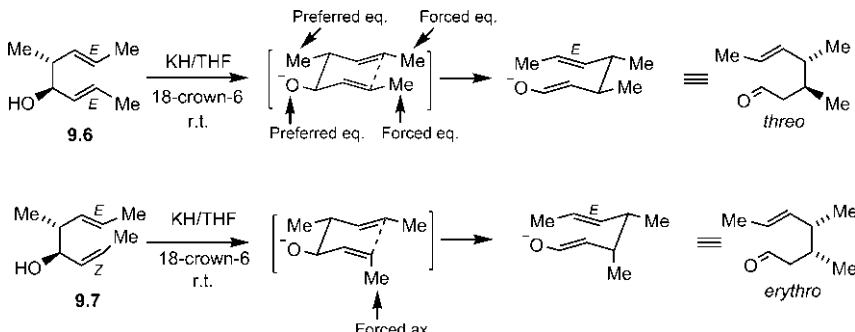


Fig. 9.14 Diastereoselective anionic oxy-Cope rearrangements.

Aza-Cope Rearrangement

The condensation of an amino alcohol **9.8** with acetaldehyde produces an N-butenyl-iminium ion **9.9** which undergoes an aza-Cope rearrangement followed by an intramolecular Mannich reaction to give the pyrrolidine **9.10** (Fig. 9.15). The aza-Cope rearrangement proceeds through chair TS and the subsequent Mannich reaction gives a *cis* stereochemistry at the ring junction of the bicyclic pyrrolidine product. The aza-Cope–Mannich reaction sequence has been employed as a key step in a synthesis of the alkaloid pancracine.¹⁷

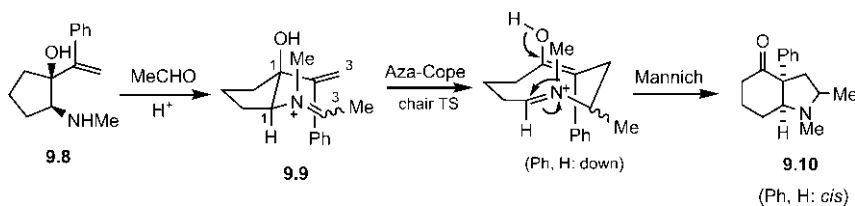


Fig. 9.15 Synthesis of a bicyclic pyrrolidine via aza-Cope rearrangement.

9.1.1.2 Cope Rearrangement via Boat Transition Structure

cis-1,2-Divinylcyclopropane **9.11** undergoes Cope rearrangement to give cyclohepta-1,4-diene (Fig. 9.16).¹⁸ The equilibrium is highly favourable to the product side because of the relief of cyclopropane ring strain. The free energy barrier is also much less compared with that for acyclic diene **9.12**. The enthalpy of activation (ΔH^\ddagger) and entropy of activation (ΔS^\ddagger) for **9.11** and **9.12** are shown. The breaking σ bond in **9.11** is a ‘bent’ bond of cyclopropane which is much weaker than a normal σ bond, and therefore reduces ΔH^\ddagger . The *cis* orientation also facilitates bond formation between the two ends of the vinyl units in **9.11**, and the loss of entropy (ΔS^\ddagger) is therefore

smaller. The Cope rearrangement of a *cis*-1,2-divinylcyclopropane is indeed very fast and occurs at low temperature (-40°C to 20°C).^{19,20} In comparison, *cis*-1,2-divinylcyclobutane undergoes Cope rearrangement at higher temperature (120°C) because the breaking σ bond is stronger than the ‘bent’ bond of cyclopropane.

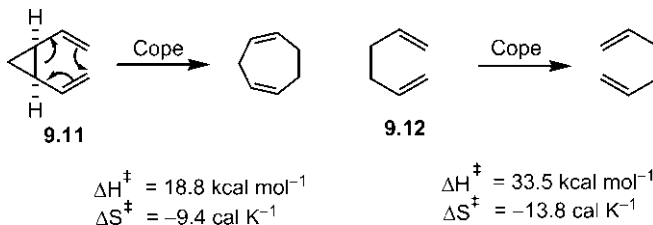


Fig. 9.16 Kinetic parameters of Cope rearrangement of *cis*-1,2-divinylcyclopropane vis-à-vis 1,5-hexadiene.

The Cope rearrangement of *cis*-1,2-divinylcyclopropane proceeds through boat TS via a higher energy *cisoid* conformation **9.13**, instead of a more stable *transoid* conformation **9.14** (Fig. 9.17A). This is because the former leads to favourable *cis* double bonds in the cycloheptadiene **9.15**, while the latter leads to impossibly strained *trans, trans* double bonds in the seven-membered ring **9.16**. The rearrangement through chair TS also does not occur because one double bond would then be unfavourably *trans* in the seven-membered ring (Fig. 9.17B).

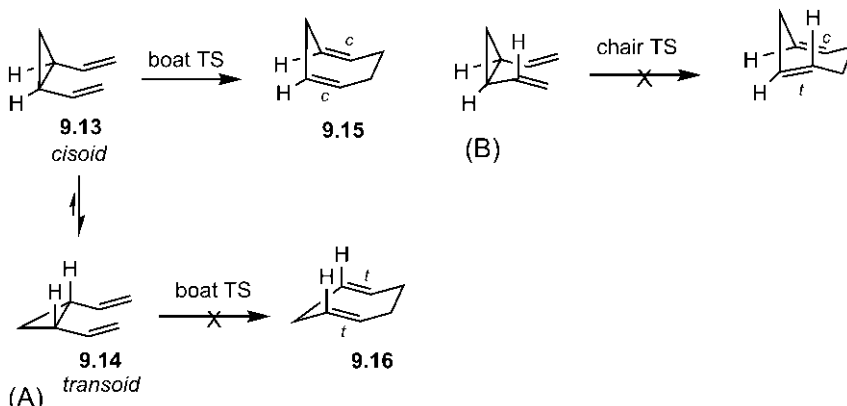


Fig. 9.17 (A) Mechanism of Cope rearrangement of *cis*-1,2-divinylcyclopropane via a preferred boat TS. (B) A chair TS is unfavourable.

The *trans*-1,2-divinylcyclopropane cannot undergo a concerted Cope rearrangement because the termini of the 1,5-diene unit are far apart. However, the *trans* isomer, when heated at 190°C, also gives cyclohepta-1,4-diene. It is possible that the reaction proceeds by a stepwise radical pathway involving the homolysis of cyclopropyl σ bond followed by ring closing of the diradical intermediate (Fig. 9.18).

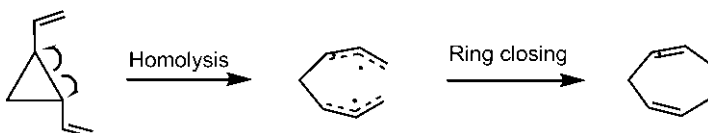
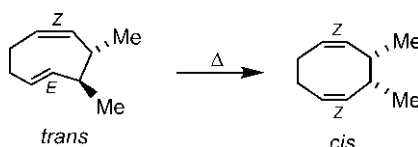


Fig. 9.18 Radical mechanism of rearrangement of *trans*-1,2-divinylcyclopropane.

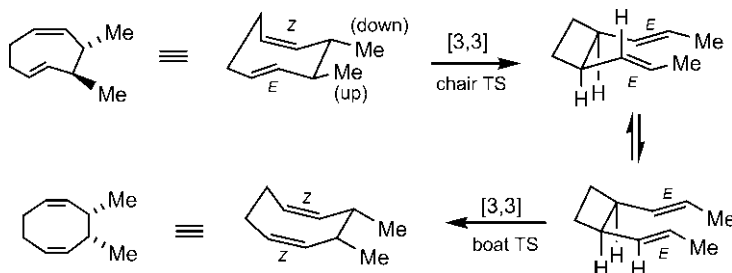
Problem 9.3

Suggest a mechanism for the following rearrangement.



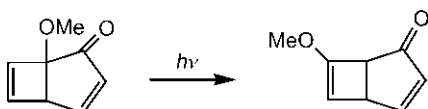
Answer

The reaction involves two consecutive Cope rearrangements. The first Cope rearrangement occurs through chair TS and the second Cope of a *cis*-1,2-divinylcyclobutane proceeds through boat TS.

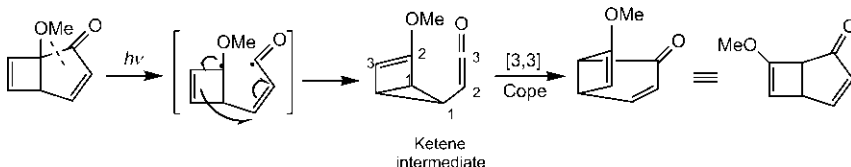


Problem 9.4

The following photochemical reaction proceeds through a ketene intermediate which undergoes a Cope rearrangement to give the product. Draw the mechanism of the reaction.

**Answer**

The ketene intermediate (formed by Norrish Type I photolysis) is a *cis*-divinylcyclopropane which undergoes [3,3] Cope rearrangement.



9.1.2 Degenerate Cope Systems and Fluxional Molecules

We have seen that *cis*-divinylcyclopropane undergoes the Cope rearrangement through boat TS via a *cisoid* conformation. When the two ends of the vinyl groups are linked by a methylene group, a molecule called homotropilidene is obtained. The Cope rearrangement of homotropilidene through boat TS gives the product which is identical to the starting material (Fig. 9.19). A rearrangement in which product and reactant are identical is called a degenerate rearrangement. Thus homotropilidene belongs to degenerate Cope systems. The two degenerate structures represent two identical valence tautomers.

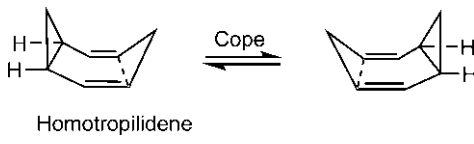


Fig. 9.19 Degenerate Cope rearrangement of homotropilidene. The dashed lines indicate formation of new σ bond in forward and reverse Cope rearrangements.

The degenerate interconversion of homotropilidene has been examined by temperature-dependent ^1H NMR.²¹ The results indicate that the frequency (ν) of interconversion, $\nu = 1 \text{ s}^{-1}$ at -50°C whereas at 180°C , $\nu = 10^3 \text{ s}^{-1}$. Therefore, at higher temperature, homotropilidene has no

single structure, and is described as a time average structure of two identical valence tautomers. This is a fluxional property, and homotropilidene is a fluxional molecule. The term ‘fluxional’ implies that the actual positions of atoms in the molecule fluctuate statistically between their extreme positions in the valence tautomers.

The Cope rearrangement is further facilitated if the *cisoid* form of homotropilidene is locked by a bridging group, when the entropy of activation (ΔS^\ddagger) would be still less negative due to less flexibility imparted by the intervening bridge. Some examples of fluxional molecules²² with different bridging groups are shown in Fig. 9.20.

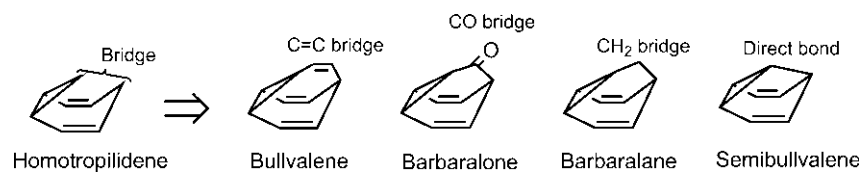


Fig. 9.20 Examples of fluxional molecules.

The rate of Cope rearrangement increases in the order: bullvalene < barbaralone < barbaralane < semibullvalene. The increase in rate is attributed to an increase in ground state energy. As one proceeds from bullvalene to semibullvalene, the molecule becomes more and more strained with progressive rise in ground state energy. Therefore the free energy barrier decreases gradually along the series. The ΔG^\ddagger for the Cope rearrangement of bullvalene, barbaralone, barbaralane and semibullvalene has been estimated to be 12.8, 9.6, 7.8 and 5.5 kcal mol⁻¹, respectively.

Like homotropilidene, the number of fluxional structures is two for barbaralone, barbaralane or semibullvalene. In contrast, bullvalene has 1,209,600 fluxional structures.

Any two of the three vinyl groups in bullvalene can be involved in the Cope rearrangement to give degenerate structures and the process is repeated with the successive structures. To illustrate, three degenerate structures of bullvalene **9.17** involving vinyl groups (1,2), (2,3) and (3,1) are shown in Fig. 9.21A. The three vinyl double bonds must be *cis* in all the degenerate structures. The fluxional behaviour of bullvalene has been established by temperature-dependent ¹H NMR. At -85°C, when the rate of rearrangement is very slow, the structure is ‘frozen’ and the spectrum shows two chemical shift signals at δ 5.65 (6 olefinic protons) and at δ 2.58 (4 nonolefinic protons). At higher temperature of 100°C, the two signals coalesce to give a single sharp peak at δ 4.22 (s, 10H) for an identical averaged environment for all carbons in bullvalene, indicating its fluxional nature.²³

Bullvalene has a C₃ axis passing through the centre of the cyclopropane ring and the other saturated carbon (Fig. 9.21B). Therefore, the number of fluxional structures for bullvalene = (number of ways ten carbons can be arranged)/3 = 10!/3 = 1,209,600.

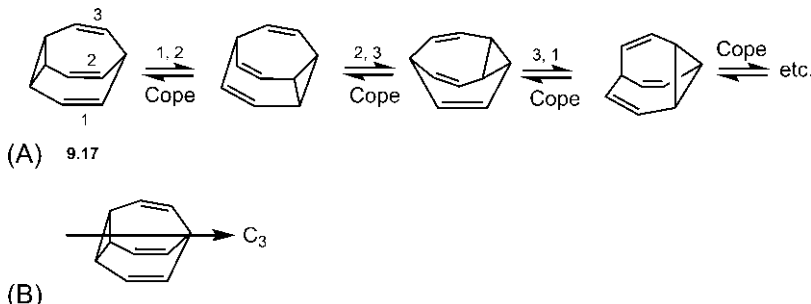


Fig. 9.21 (A) Some fluxional structures of bullvalene; (B) symmetry of bullvalene.

The synthesis of bullvalene involves a good deal of pericyclic chemistry. Two synthetic routes are outlined in Fig. 9.22.^{24,25} The structure of cyclooctatetraene dimer **9.18** in Fig. 9.22A has been established experimentally.

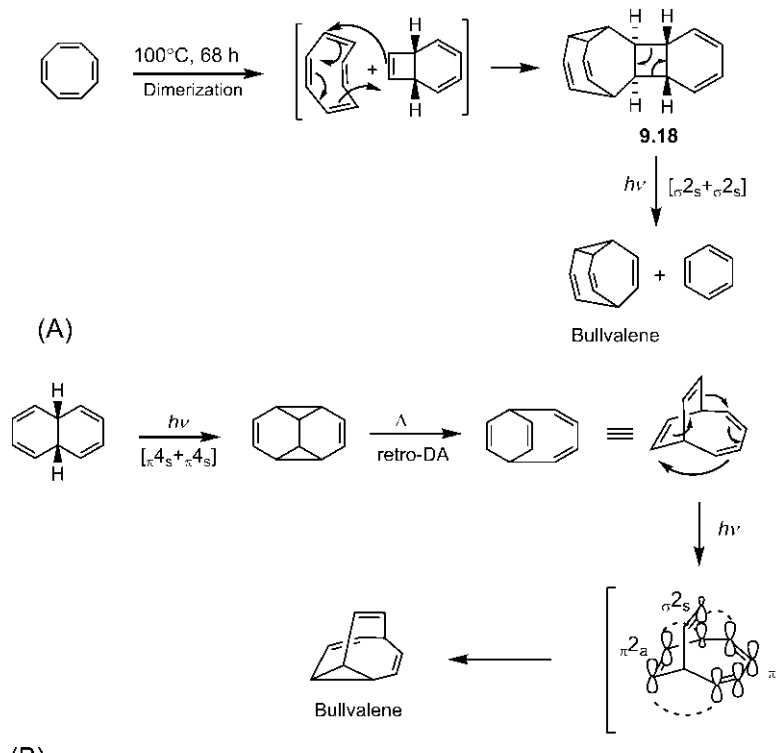
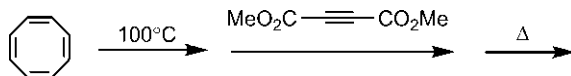
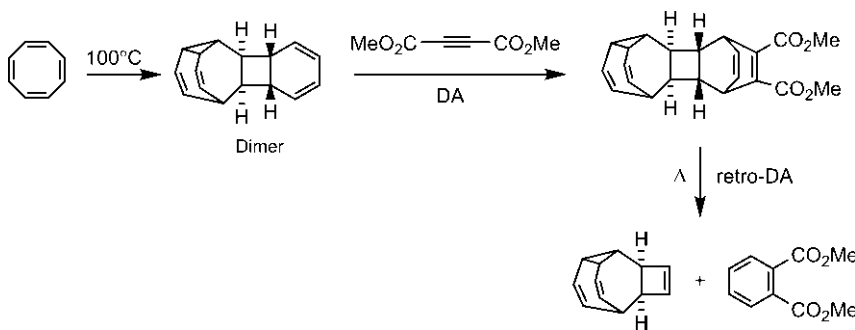


Fig. 9.22 Synthesis of bullvalene from (A) cyclooctatetraene and (B) *cis*-9,10-dihydroronaphthalene.

Problem 9.5

Complete the following scheme.

**Answer****9.1.3 Cope Rearrangement by Antara/Antara Mode**

The Cope rearrangement by antara/antara mode is symmetry-allowed thermally involving a twist transition structure (see Table 3.6, Fig. 3.46). However, geometrically the antara/antara interaction is much less likely and is rare. If the structural constraints of a molecule allow the antara/antara overlap, the Cope rearrangement can occur as shown in Fig. 9.23.²⁶ The bicyclic ketone **9.19** rearranges thermally to the product **9.20** (cf. Problem 9.4).

The twist TS **9.21** represents a thermally allowed $[\sigma_2s + \pi_{2a} + \pi_{2a}]$ reaction. The new σ bond is formed on the bottom side and the breaking σ bond moves towards the top side of the molecule. This picture is equivalent to antara/antara overlap in terms of two allyl components **9.21'**. The *cis* fused bicyclic ketone **9.19** does not undergo electrocyclic ring opening to a tropone because the allowed conrotatory pathway leads to a highly strained *trans* double bond in a seven-membered ring.

The movement of the groups in the rearrangement has been clearly demonstrated using a deuterium/alkyl labelled substrate **9.22** which rearranges to **9.23**.

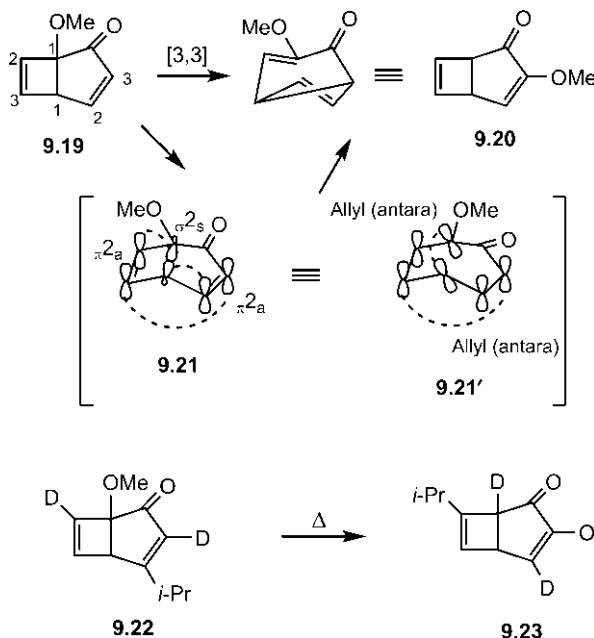


Fig. 9.23 Cope rearrangements by antara/antara mode.

9.2 [3,3] CLAISEN REARRANGEMENT

The Claisen rearrangement^{27,28} is a thermal [3,3] sigmatropic rearrangement of allyl vinyl ether **9.24** to γ,δ -unsaturated carbonyl compound (Fig. 9.24A). The reaction is driven to the product side by the formation of a stable carbonyl π system. This is referred to as aliphatic Claisen rearrangement. If the vinyl unit is a part of an aromatic ring **9.25**, the initial carbonyl product quickly tautomerizes (enolizes) to the more stable aromatic allyl phenol (Fig. 9.24B). This rearrangement of allyl aryl ether **9.25** is called aromatic Claisen rearrangement.²⁹

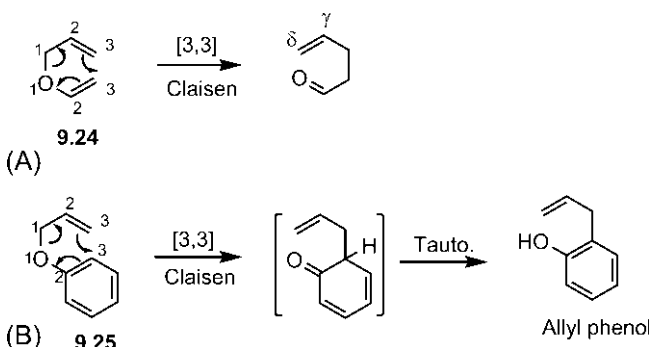


Fig. 9.24 (A) Aliphatic Claisen rearrangement and (B) aromatic Claisen rearrangement.

The aliphatic version is more useful for its scope and stereochemical features. The allyl vinyl ether can be prepared directly from the corresponding allyl alcohol by acid-catalyzed ether exchange (Fig. 9.25A). Another very useful method employs Tebbe's reagent³⁰ which converts a carbonyl compound to the corresponding methylene compound. An example of direct conversion of an ester to a vinyl ether is shown in Fig. 9.25B.³¹

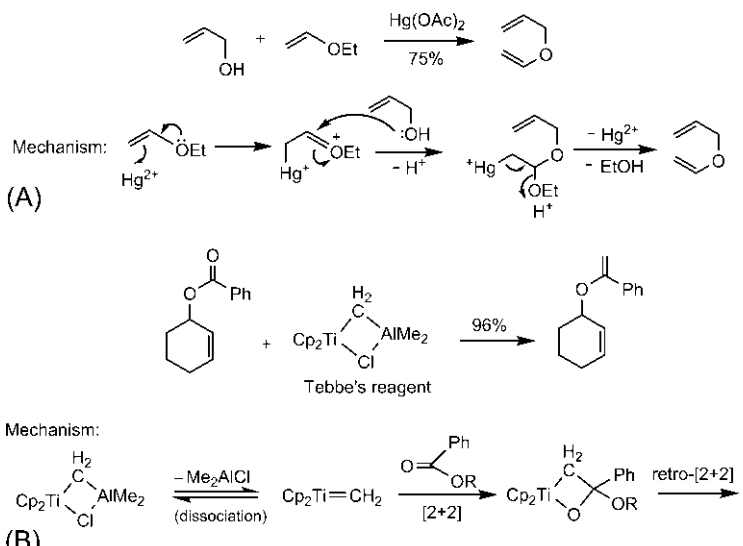


Fig. 9.25 Preparation of allyl vinyl ether using (A) acid-catalyzed ether exchange and (B) Tebbe reaction.

There are some important variants, namely, Johnson–Claisen,³² Eschenmoser–Claisen³³ and Ireland–Claisen³⁴ rearrangements (Fig. 9.26).

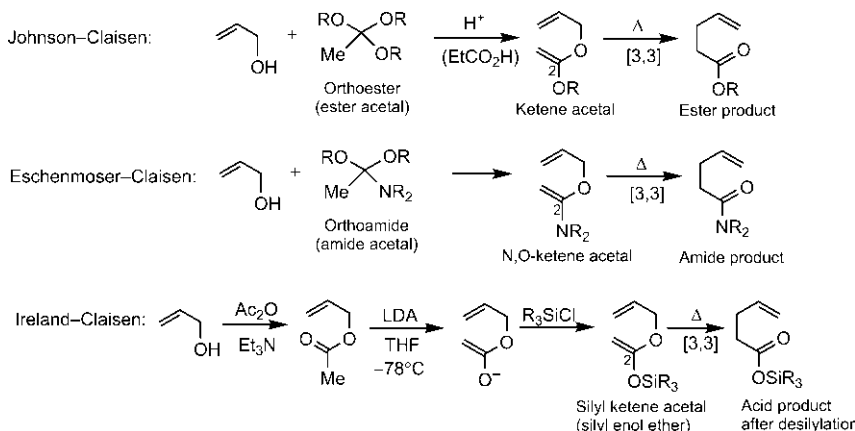


Fig. 9.26 Johnson–Claisen, Eschenmoser–Claisen and Ireland–Claisen rearrangements.

These are useful methods particularly for the stereoselective synthesis of γ,δ -unsaturated carbonyl compounds.

The donor substituent (OR/NR_2) at C-2 of the vinyl unit in Johnson–Claisen/Eschenmoser–Claisen rearrangement increases the rate of the reaction due to ester/amide resonance stabilization in the TS. The silyloxy (OSiR_3) substituent at C-2 in Ireland–Claisen rearrangement is largely accelerating. The temperature of the Claisen rearrangement and its variants lies in the range from 200°C (Claisen) to room temperature (Ireland–Claisen).

There is another variant called Carroll rearrangement³⁵ (also called the Kimel–Cope rearrangement³⁶) which uses an allyl ester of a β -keto acid **9.26**. The reaction proceeds through a [3,3] rearrangement of the enol form followed by loss of CO_2 to give γ,δ -unsaturated carbonyl compound (Fig. 9.27).

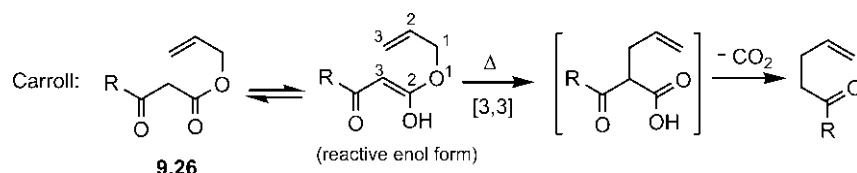
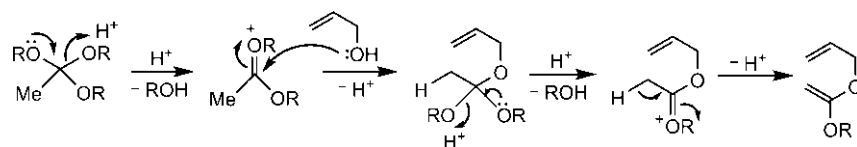


Fig. 9.27 Carroll rearrangement with allyl ester of β -keto acid.

Problem 9.6

Draw a mechanism for the formation of the allyl vinyl ether by Johnson–Claisen procedure.

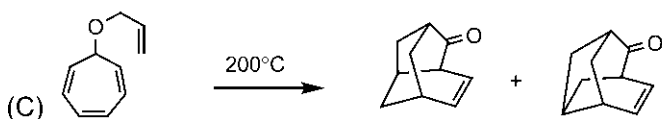
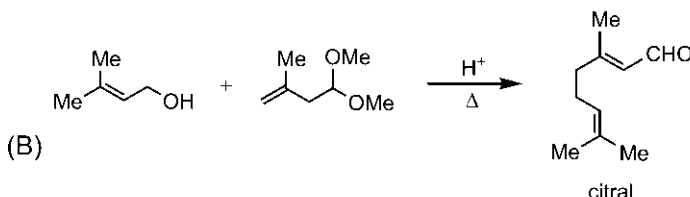
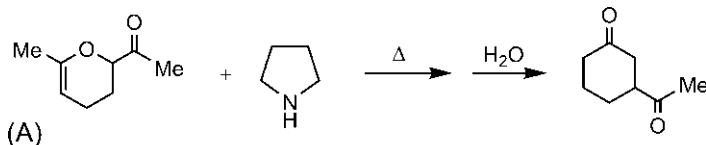
Answer



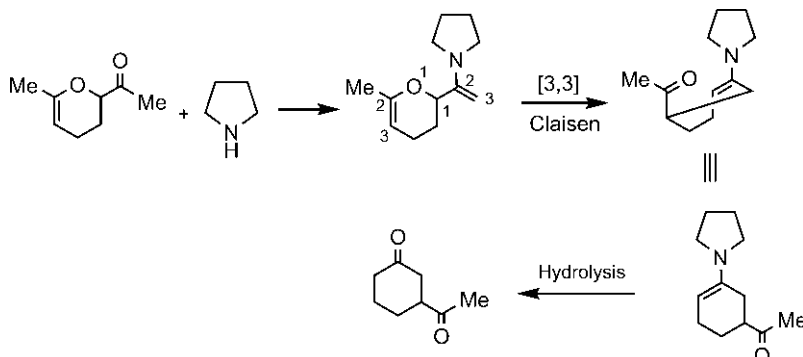
The reaction is reversible; however, the equilibrium is pushed to the right side by distilling off ROH (usually MeOH or EtOH). In the presence of high boiling propionic acid as acid catalyst, the allyl vinyl ether rearranges *in situ* to the Claisen rearrangement product.

Problem 9.7

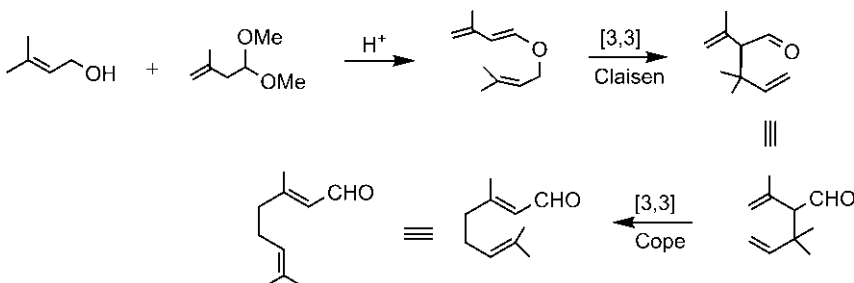
The following reactions involve a Claisen rearrangement besides other steps. Draw a mechanism for each reaction.

**Answer**

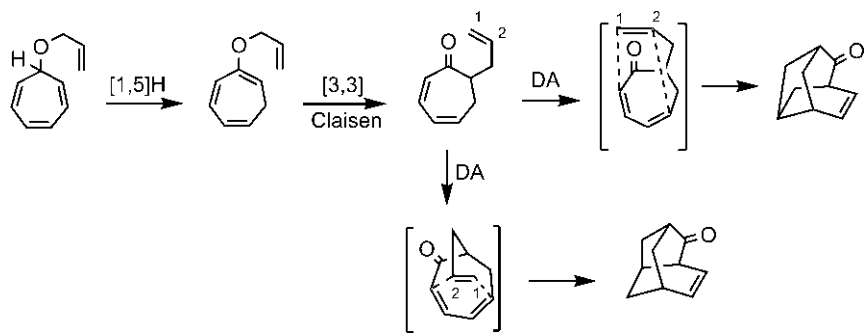
(A) The condensation between the ketone and a secondary amine (pyrrolidine) produces an enamine which undergoes a [3,3] Claisen rearrangement followed by the hydrolysis of the resulting new enamine via imine to give the product.



(B) The reaction proceeds through two successive [3,3] sigmatropic shifts, Claisen and Cope rearrangements to give the product citral.



(C) The reaction proceeds through a sequence of [1,5]H shift, [3,3] Claisen rearrangement and intramolecular Diels–Alder (IMDA) reaction to give the observed products. The two pathways for IMDA reaction indicate the different positions of attachment of alkene to the diene.³⁷



9.2.1 Stereospecificity of Claisen Rearrangement

The stereospecificity of Claisen rearrangement arises from the symmetry-allowed supra-supra interaction between two 3-atom components, allyl (C—C—C) and vinyl ether (C—C—O). To illustrate, we first consider the Johnson–Claisen rearrangement shown in Fig. 9.28. A new C—C bond is formed at the expense of an old C—O bond. The supra/supra pathway leads to the formation of the C—C bond on the same upper face of the breaking C—O bond and thereby determines the stereochemistry of the product.

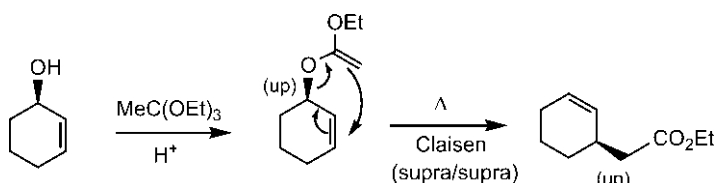


Fig. 9.28 Stereospecificity of a Johnson–Claisen rearrangement.

Next, we consider an Ireland–Claisen rearrangement (Fig. 9.29).³⁸ A [3,3] Claisen rearrangement of the bis silyl enol ether **9.27** generated from the corresponding diacetate produces **9.28** which can undergo a second Claisen rearrangement at a higher temperature. The stereospecificity at each rearrangement step is governed by supra/supra mode with migration occurring on the upper face of the allyl unit. Desilylation of the product after second Claisen rearrangement gives a *cis* dicarboxylic acid **9.29**.

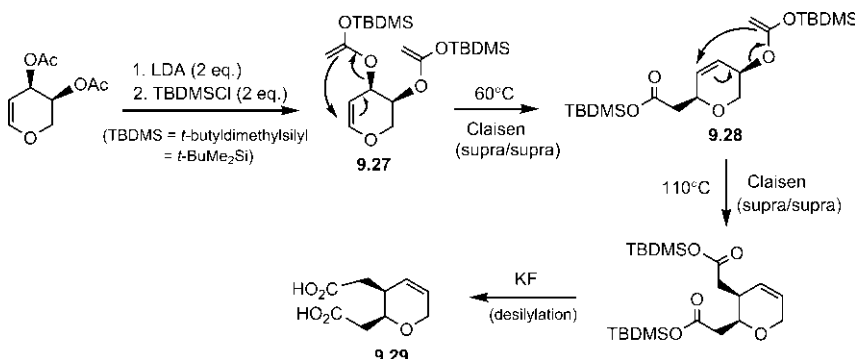
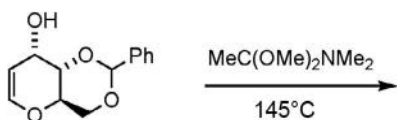


Fig. 9.29 Stereospecificity of an Ireland–Claisen rearrangement.

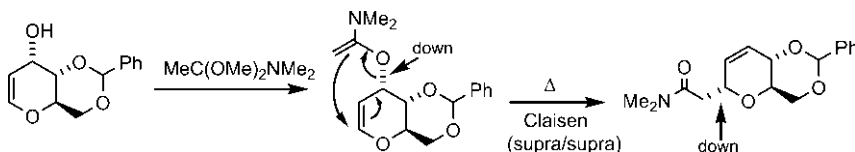
Problem 9.8

Predict the stereochemistry of the product in the following Eschenmoser–Claisen rearrangement.



Answer³⁹

The stereochemistry of the product results from the allowed supra/supra pathway of the Claisen rearrangement.



9.2.2 Stereoselectivity of Claisen Rearrangement

Similar to the Cope rearrangement, the Claisen rearrangement also proceeds through a chair TS or a boat TS. Two possible chair and two possible boat conformations can lead to four possible stereoisomeric products. However, when both chair TS and boat TS are geometrically accessible, the Claisen rearrangement takes place via the preferred chair TS. If one chair conformation is more stable than the other, the more stable chair TS leads to the predominant product. This is the basis of the stereoselectivity. In some sterically constrained systems, the boat TS would be preferred.

9.2.2.1 Claisen Rearrangement via Chair Transition Structure

The chair TS of Claisen rearrangement will be drawn as 9.30 or 9.31 (Fig. 9.30) in a manner similar to that for Cope rearrangement (see Fig. 9.7).

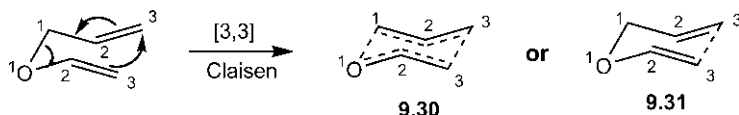


Fig. 9.30 Representation of chair transition structure of Claisen rearrangement.

The substrate allyl vinyl ether can have only one stereocentre, and *E* or *Z* stereochemistry of the double bonds.

To illustrate stereoselectivity, we begin with the Claisen rearrangements of the diastereomeric (*E,E*) and (*E,Z*) substrates (Fig. 9.31).⁴⁰ During the reaction, both double bond stereochemistries are destroyed and two new

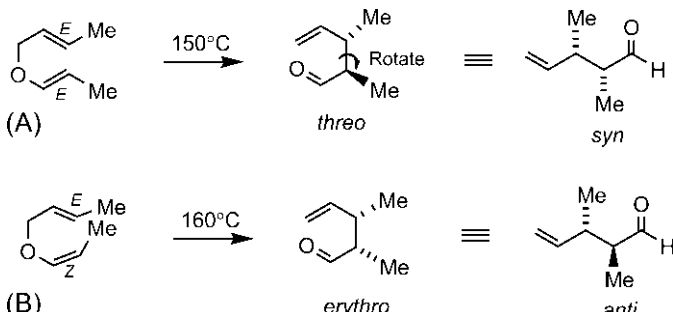


Fig. 9.31 Stereoselectivity of Claisen rearrangement of (A) (*E,E*) and (B) (*E,Z*) allyl vinyl ethers.

stereocentres across the new C—C bond are created in the product. The creation of two stereocentres can give rise to two diastereomeric products (*threo* and *erythro*) in each case. However, the (*E,E*) substrate gives mainly a *threo* or *syn* diastereomer (Fig. 9.31A). The rearrangement is therefore diastereoselective. Similarly, the (*E,Z*) isomer yields an *erythro* or *anti* diastereomer (Fig. 9.31B) (see Section 2.1.2 for descriptors).

The diastereoselectivity has been rationalized on the basis of the preferred chair TS of the rearrangement as shown in Fig. 9.32. As shown in Fig. 9.32A, the racemic *threo* product is obtained from the (*E,E*) isomer via the chair TSs. If the reaction could take place through a boat TS, then an *erythro* product would be obtained (see Problem 9.9). Thus the diastereoselectivity is determined by the preference in favour of the chair TS. Here the two possible chair TSs are of equal energy and enantiomeric, and hence lead to a racemic *threo* product. Similarly, with (*E,Z*) substrate, a racemic *erythro* product is formed, one enantiomer of which is shown in Fig. 9.32B. Also note that the chiral products are obtained as a recemate since the substrates are achiral.

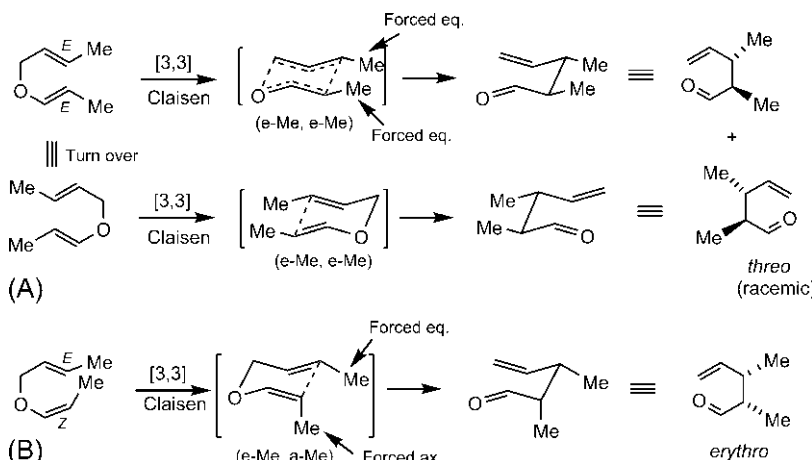


Fig. 9.32 Mechanism of diastereoselectivity of the Claisen rearrangements of (A) (*E,E*) and (B) (*E,Z*) allyl vinyl ethers shown in Fig. 9.31.

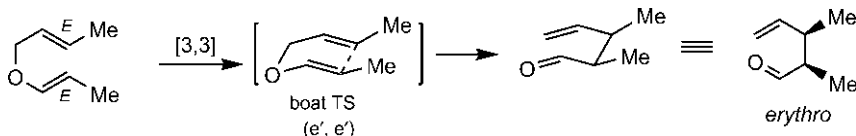
(Note that the (*E,E*) stereochemistry forces both Me's to be equatorial while (*E,Z*) stereochemistry forces one Me to be equatorial and the other Me to be axial. To draw two possible chair TSs easily, see Fig. 2.6.)

Problem 9.9

Give the product that would arise from the boat TS of Claisen rearrangement of (*E,E*) isomer in Fig. 9.31.

Answer

The product is an *erythro* diastereomer.



As shown above, the geometry of the double bonds in the allyl unit and vinyl ether unit of the starting material determines the diastereoselectivity. The stereochemistry of the double bond in the allyl unit is usually provided by an allyl alcohol used for the preparation of the allyl vinyl ether. The formation of a vinyl ether unit with stereochemical purity is however difficult to achieve. In this respect, the Ireland–Claisen procedure provides a suitable method in which the control of enolate geometry can be achieved by judicious choice of enolization conditions. Enolization of an ester with LDA/THF at low temperature favours the formation of a *trans*-enolate whereas, in the presence of the co-solvent HMPA, a *cis*-enolate is favoured (Fig. 9.33).^{41,42}

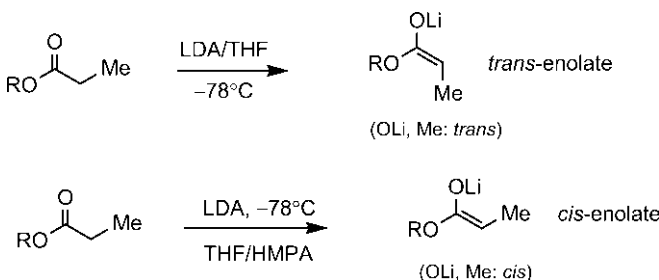


Fig. 9.33 Stereoselectivity in enolate formation.

The stereoselectivity in enolization has been explained as follows. The stereoelectronic requirement for the α -deprotonation of a carbonyl compound by a base to form the enolate is that the breaking C—H bond is

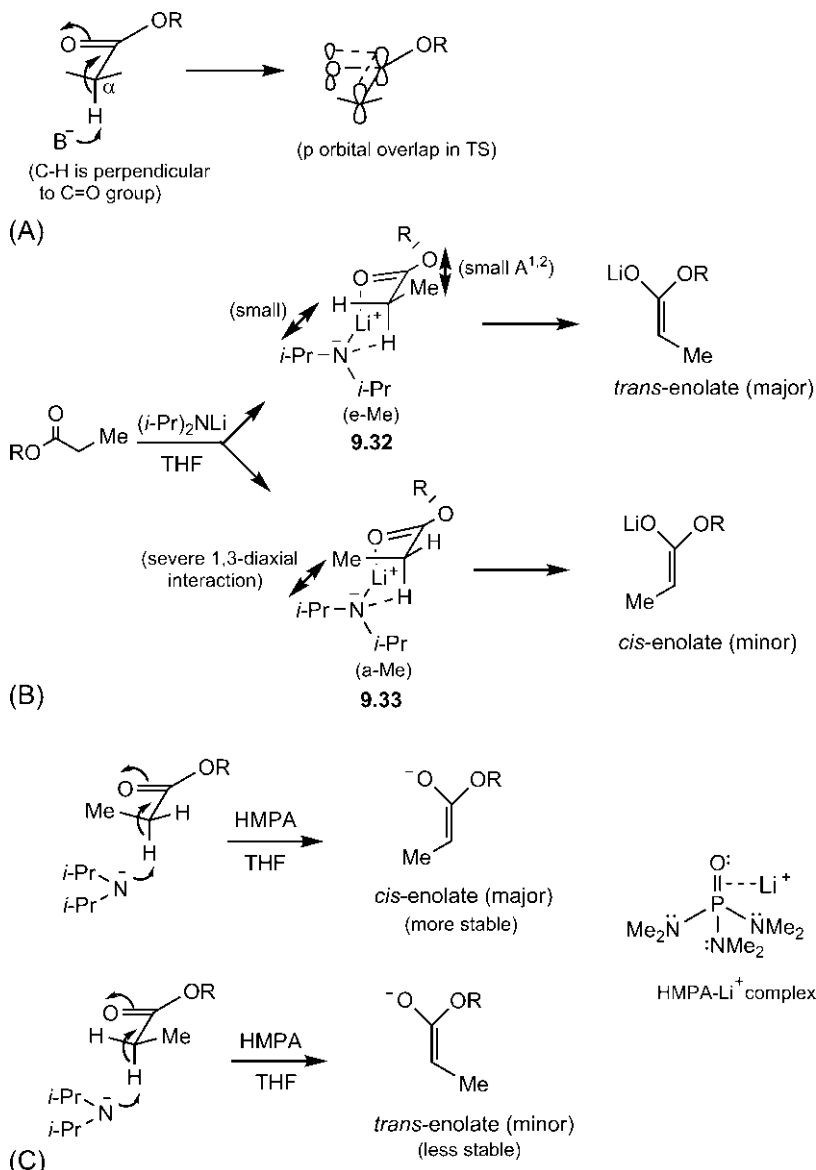


Fig. 9.34 (A) Stereoelectronic requirement for enolization, (B) enolization in THF through cyclic chair transition structure (Ireland model) and (C) enolization in THF/HMPA through open transition structure.

orthogonal to the plane of the carbonyl group. In this conformation, the p orbital on the α -carbon (evolving from the σ C—H orbital) would be parallel to the carbonyl π system, thereby stabilizing the transition structure for the enolate formation (Fig. 9.34A).

In THF alone, the Li^+ cation of LDA is coordinated to the ester carbonyl forming a six-centre cyclic transition structure that is preferably chair-like (Ireland model) (Fig. 9.34B). There are two possible chair transition structures with Me in less-hindered equatorial position 9.32 and in more-hindered axial position 9.33. The α -Me conformation 9.33 suffers from a 1,3-diaxial (*i*-Pr/Me) interaction which is much more severe than the diaxial (*i*-Pr/H) interaction present in ϵ -Me conformation 9.32. There is some allylic ($\text{A}^{1,2}$) strain in 9.32 as the enolate begins to form; however, this is quite small for the steric interaction of Me with the O atom of ester group. Therefore, ϵ -Me chair transition structure is more stable and leads to preferential formation of a *trans*-enolate.

In the presence of HMPA (hexamethylphosphoramide) which can strongly coordinate with Li^+ , the association of Li^+ with ester carbonyl is negligible and the enolization proceeds through an open (non-cyclic) transition structure. The more stable TS (in which the ester OR and Me are far apart) leads to a more stable *cis*-enolate as a major product (Fig. 9.34C). Thus, in THF/HMPA, a thermodynamic enolate is produced whereas in THF alone, a kinetic enolate is formed.

In the Ireland–Claisen rearrangement, the *trans*- or *cis*-enolate is trapped as a silyl enol ether (silyl ketene acetal) which then undergoes a [3,3] sigma-tropic rearrangement to give, after desilylation, a γ,δ -unsaturated carboxylic acid. (The silylation of enolate prior to rearrangement avoids the side reaction by Claisen condensation.) The enolate geometry determines the geometry of the silyl ketene acetal, and hence determines the stereochemistry of the final product.^{34,41,43}

The procedure is illustrated in Fig. 9.35 with an (*E*)-allyl ester 9.34 (obtained from the corresponding (*E*)-allyl alcohol). Enolization in THF followed by silylation with *t*-butyldimethylsilyl chloride (TBDMSCl) produces an (*E*)-silyl ketene acetal which undergoes Claisen rearrangement via the preferred chair TS to give, after desilylation, an *anti* diastereomer of a γ,δ -unsaturated acid. In the presence of HMPA, a (*Z*)-silyl ketene acetal is formed which gives finally a *syn* diastereomer. Therefore, either diastereomeric product can be obtained simply by choice of enolization conditions.

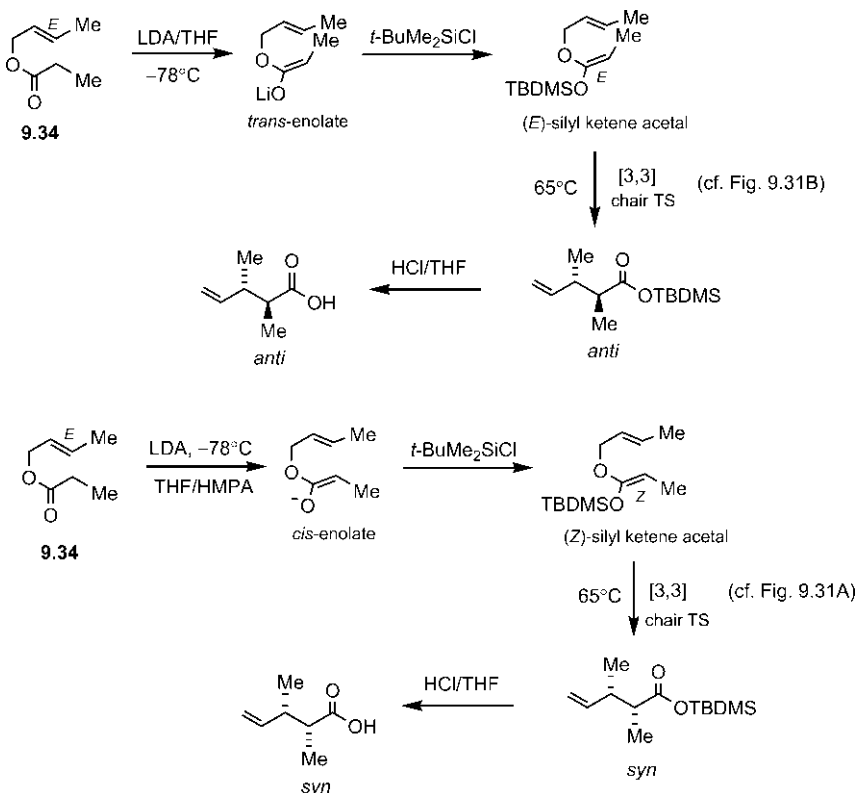


Fig. 9.35 Diastereoselectivity of Ireland–Claisen rearrangement.

Next, we consider the Claisen rearrangement of a chiral substrate with (*E*) stereochemistry of allylic double bond (Fig. 9.36).

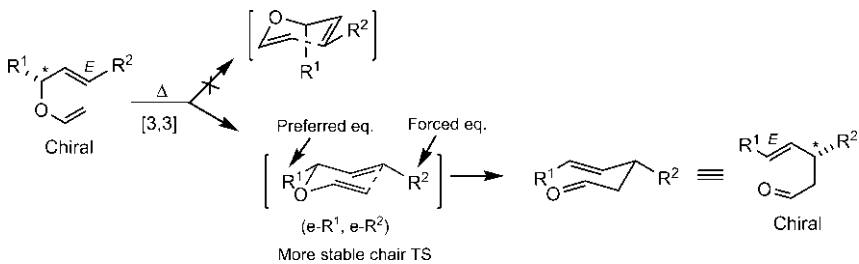


Fig. 9.36 Chirality transfer in Claisen rearrangement.

The old stereocentre is destroyed and a new stereocentre is created giving a chiral product. This is a process of chirality transfer.⁴⁴ The reaction proceeds through a more stable chair TS in which R¹ is equatorial, which

leads to (*E*) configuration of the new double bond. Note that the (*E*) stereochemistry of the old double bond forces R² to be equatorial. If the chiral substrate is used as a single enantiomer, the reaction will be enantioselective.

9.2.2.2 Endocyclic and Exocyclic Substrates

The Claisen rearrangement with endocyclic substrates⁴⁵ shows high diastereoselectivity as shown in Fig. 9.37.

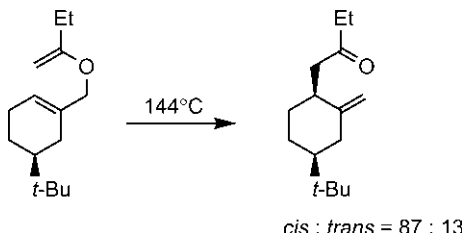


Fig. 9.37 Diastereoselectivity of Claisen rearrangement with an endocyclic substrate.

This has been explained by examining the developing σ and π bonds in the transition structure. As shown in Fig. 9.38, the transition structure is modelled as the interaction between two three-atom radical components in the preferred half-chair conformation of the cyclohexene substrate. The attack of the vinyl ether radical takes place preferentially on the face of the allylic radical which evolves into a favoured chair conformation (path a). The predominant product is therefore a *cis* isomer. The attack of the vinyl ether radical on the other face of the allylic radical leads to a less preferred twist-boat conformation forming the minor *trans* isomer (path b).

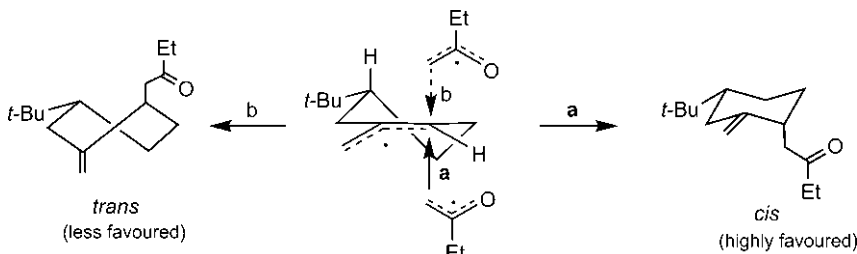


Fig. 9.38 Mechanism of diastereocontrol of the Claisen rearrangement in Fig. 9.37.

For Claisen rearrangement with exocyclic substrate,⁴⁶ the overlap for developing σ and π bonds is almost equally favourable from either alkene diastereoface. As such, both equatorial and axial attacks lead to a mixture of diastereomers (Fig. 9.39). However, steric effects can dominate in other substrates giving a modest preference for equatorial attack.

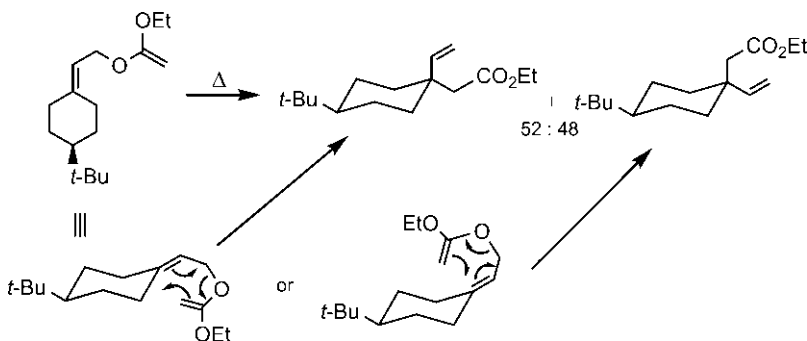


Fig. 9.39 Claisen rearrangement with an exocyclic substrate.

9.2.2.3 Claisen Rearrangement via Boat Transition Structure

For substrates other than simple and acyclic ones, molecular models are usually necessary to determine whether a Claisen rearrangement would occur via a chair TS or a boat TS. In a conformationally constrained system in which three or more atoms of allyl vinyl ether is part of a ring, the Claisen rearrangement proceeds preferably through a boat TS.⁴⁷ To illustrate, let us consider the Johnson–Claisen rearrangement of a cyclic substrate **9.35** in which the three-atom allyl unit is part of the ring (Fig. 9.40). The reaction proceeds through a boat TS to give the product **9.36**. The boat TS is favoured as the chair TS is destabilized by steric interaction.

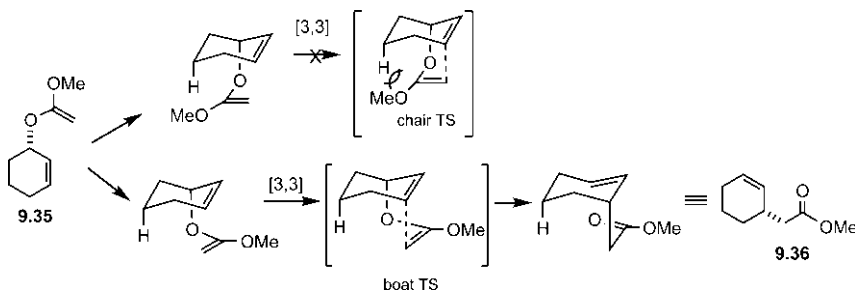


Fig. 9.40 Claisen rearrangement through boat transition structure.

The stereoselectivity of the Ireland–Claisen rearrangements via a boat TS^{48,49} is shown in Fig. 9.41. In Fig. 9.41A, three-atom allyl unit of the substrate is part of the ring. The reaction proceeds through (*E*)-silyl ketene acetal which undergoes Claisen rearrangement via a boat TS to give, after desilylation, a diastereomeric acid. In Fig. 9.41B,⁵⁰ four atoms (including the three-atom vinyl ether unit) are part of a ring and a diastereomeric product results from the Claisen rearrangement via a boat TS.

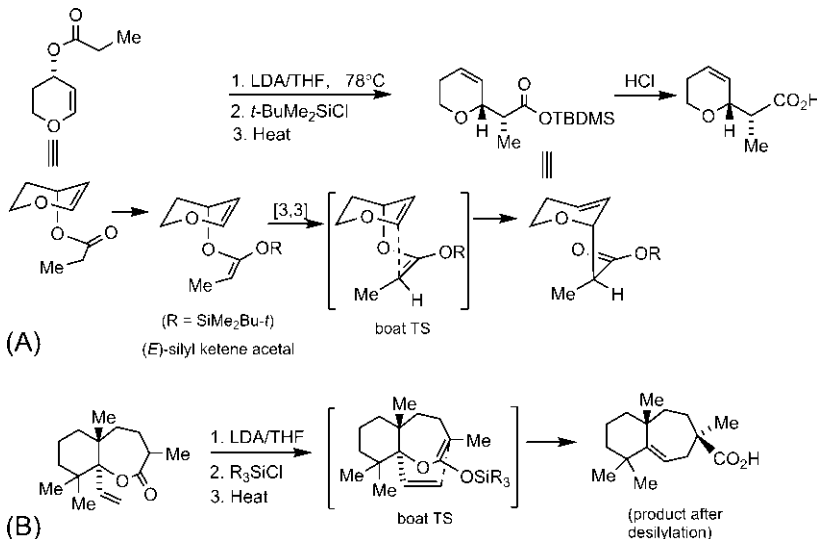
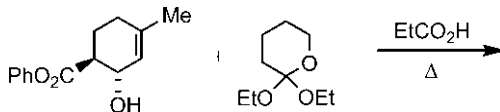


Fig. 9.41 Examples (A and B) of stereoselective Ireland–Claisen rearrangements via boat transition structure.

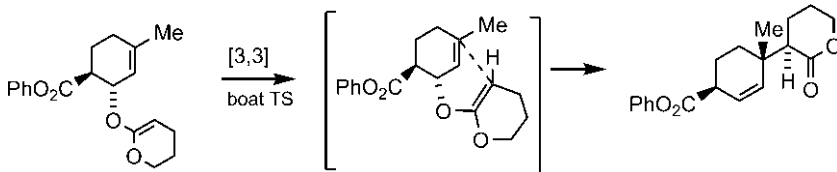
Problem 9.10

Predict the product of the following Johnson–Claisen rearrangement.



Answer

The allyl unit of allyl vinyl ether (formed from the allyl alcohol and orthoester) is part of a ring. The rearrangement proceeds through a boat TS to give the product.



9.2.3 Asymmetric Claisen Rearrangement

Asymmetric Claisen rearrangements^{51,52} have been widely used synthetically. We shall describe here only a few examples in the context of the stereochemistry of the Claisen rearrangement. An asymmetric Claisen rearrangement can be performed using an enantiopure or enantiomerically enriched substrate. This is referred to as ‘substrate control’. An example is shown in Fig. 9.42. Starting with an enantiomerically enriched ester **9.37** (ee 91%), a *syn* product (ee 91%) is obtained. The reaction proceeds through a more stable chair TS (in which Me attached to the old stereocentre is equatorial) to give the enantioselective product. Notice that the silyl derivative is drawn by turning it upside down. (The less preferred chair TS is not shown.)

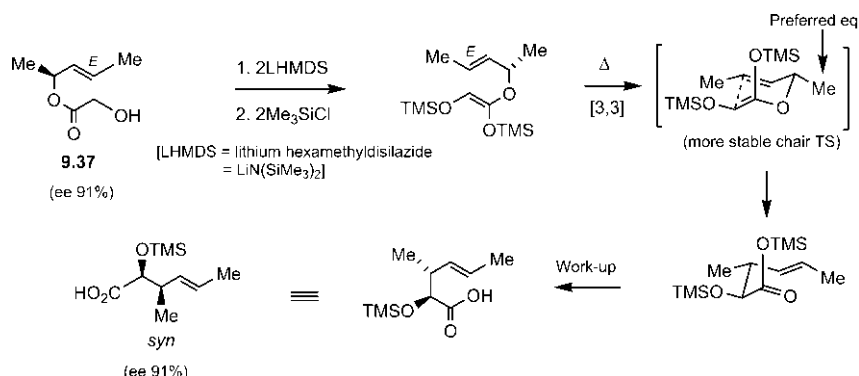


Fig. 9.42 Asymmetric Claisen rearrangement using substrate control.

Usually an enantiomer of a substrate gives a particular enantiomer of the product. It is also possible to convert both enantiomers of a substrate into the same product enantiomer. This is known as ‘enantioconvergent’ synthesis. Fig. 9.43 illustrates an enantioconvergent synthesis using a chiral alcohol.⁵³ Catalytic hydrogenation of (*R*) enantiomer **9.38** gives a (*Z*) alkene by *syn* addition whereas SET reduction of (*S*) enantiomer **9.39** in Na/liquid NH₃ provides a more stable (*E*) alkene. Both (*R,Z*) and (*S,E*) isomers of an allyl alcohol undergo Eschenmoser–Claisen rearrangement to give the same (*S*) enantiomer of the (*E*) product.

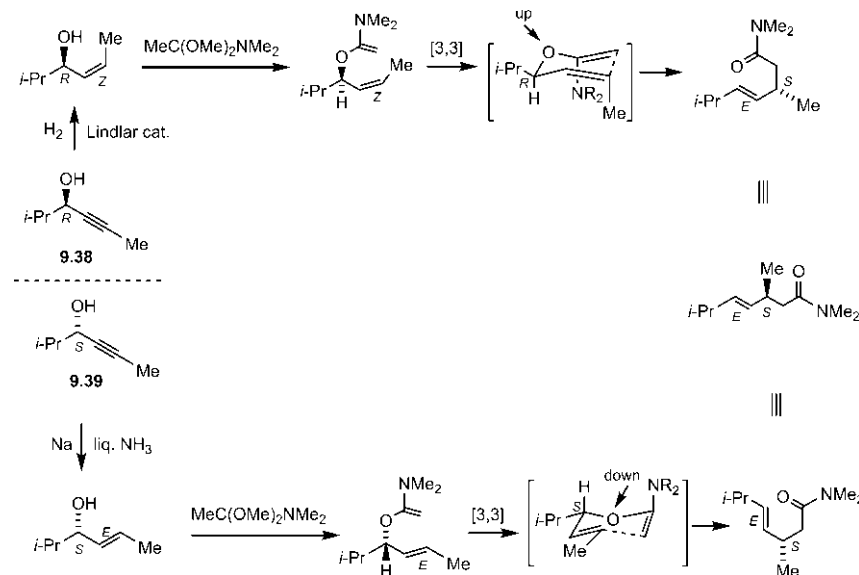
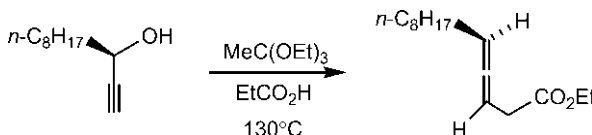


Fig. 9.43 An enantioconvergent synthesis via Eschenmoser–Claisen rearrangement.

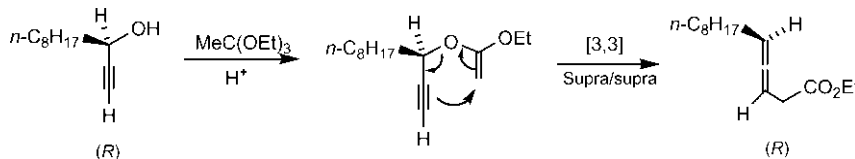
Problem 9.11

The following asymmetric Claisen rearrangement shows a chirality transfer from a substrate with a chiral centre to the product with a chiral axis. Explain this chemical correlation of a chiral centre and a chiral axis.



Answer⁵⁴

The reaction is a Johnson–Claisen rearrangement in which (*R*) enantiomer of the substrate gives (*R*) enantiomer of an allene (for chiral axis descriptor, see [Section 2.2.1](#)). The supra/supra pathway of the rearrangement establishes the correlation of absolute configuration of the chiral centre in the substrate with that of the chiral axis of the allene.



The chiral auxiliary control of asymmetric Claisen rearrangement is an important strategy.¹⁴ Fig. 9.44 illustrates an example using Enders RAMP/SAMP auxiliary. RAMP and SAMP stand for (*R*)- and (*S*)-1-amino-2-methoxymethylpyrrolidine, respectively. The asymmetric reaction is a Carroll rearrangement. An allyl ester of a β -keto acid **9.40** is covalently linked with RAMP, the resulting chiral intermediate with LDA then undergoes a [3,3] sigmatropic shift. The new σ bond is formed on the top face of the cyclopentane ring as its bottom face is sterically shielded. This asymmetric rearrangement with the formation of a new quaternary chiral centre is a key step in the synthesis of an antibiotic malyngolide.⁵⁵

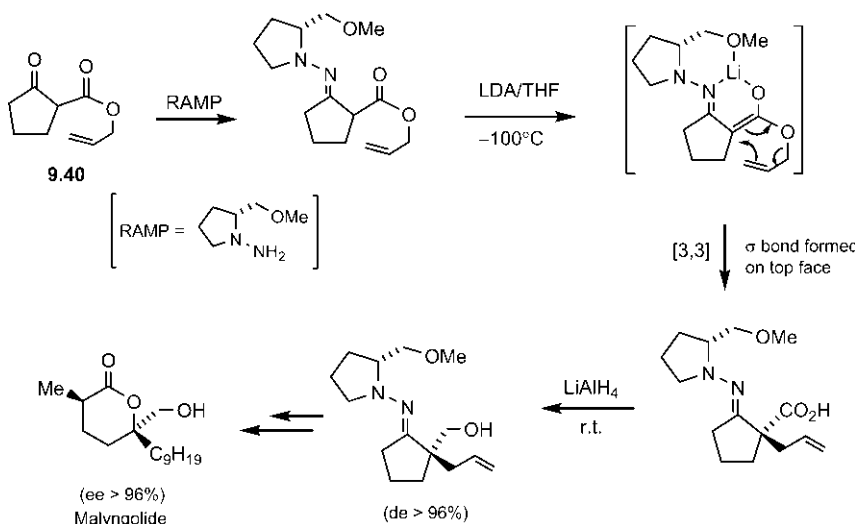


Fig. 9.44 Asymmetric Claisen rearrangement using chiral auxiliary strategy.

Highly enantioselective Claisen rearrangement takes place under reagent control using a chiral boron reagent **9.41** (Fig. 9.45).⁵⁶ The boron enolates are formed stereoselectively depending on the base employed. With the base Et_3N , the *trans*-enolate is formed preferentially whereas in the presence of a more-hindered Hünig's base (*i*-Pr₂N*Et*), the *cis*-enolate is favoured. The boron enolates undergo [3,3] rearrangement to give the products with high enantioselectivity. The *cis*-enolate leads to a *syn* product (ee > 97%) whereas the *trans*-enolate gives an *anti* product (ee 96%) (see Fig. 9.35 for *syn/anti* diastereoselectivity).

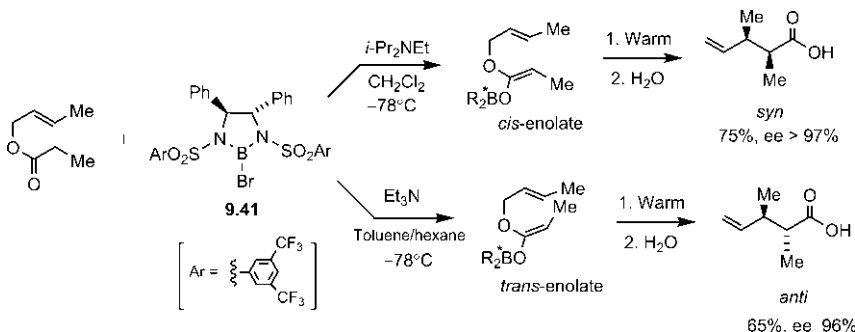


Fig. 9.45 Asymmetric Claisen rearrangement using a chiral boron reagent.

The enantioselectivity arises from the chair TS in which the stereocentres of the chiral boron reagent control the rotational preference of the sulphonyl groups, thereby providing stereodifferentiation at the boron centre.

An example of catalytic asymmetric Claisen rearrangement using box catalyst (see 5.21) is shown in Fig. 9.46.⁵⁷ The ester carbonyl and the vinyl ether oxygen could chelate with the copper forming a well-defined catalyst–substrate complex which directs the stereochemical preference of C–C bond formation to give the enantioselectivity.

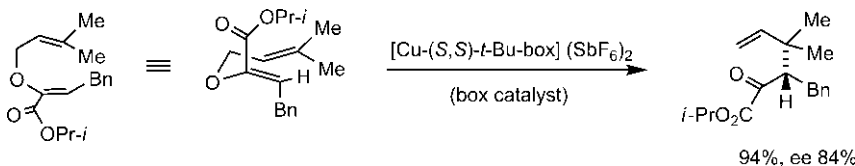


Fig. 9.46 Catalytic asymmetric Claisen rearrangement using box catalyst.

9.2.4 Aromatic Claisen Rearrangement

The aromatic Claisen rearrangement⁵⁸ gives an allyl phenol as the observed product because the initial *ortho*-dienone from [3,3] shift rapidly tautomerizes to a phenolic compound (see Fig. 9.24B). The overall process is termed the *ortho*-Claisen rearrangement. The *ortho*-Claisen rearrangement occurs with inversion (transposition) of the allyl group in the product, as shown with a labelled substrate in Fig. 9.47. The rearrangement proceeds preferentially through a chair TS.

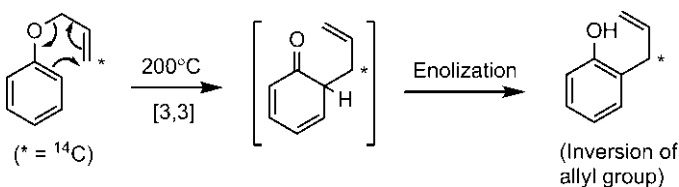


Fig. 9.47 *ortho*-Claisen rearrangement of ^{14}C -labelled allyl phenyl ether.

When both *ortho* positions are substituted (blocked), the initial product of [3,3] Claisen rearrangement cannot enolize and undergoes a [3,3] Cope rearrangement followed by enolization to yield a *p*-allyl phenol. This overall process is known as *para*-Claisen rearrangement. There is no inversion of the allyl group in the product because of two inversions resulting from two consecutive [3,3] shifts, as shown in [Fig. 9.48](#). An evidence of this mechanism also comes from trapping of the intermediate *ortho*-dienone as Diels–Alder adduct with maleic anhydride.

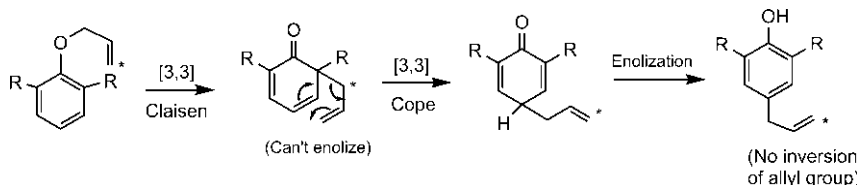


Fig. 9.48 *para*-Claisen rearrangement of *ortho* blocked allyl aryl ether.

[Fig. 9.49](#) shows an aromatic Claisen rearrangement with a substrate **9.42** in which both *meta* positions and the terminal allyl carbon are substituted. Here the enolization of *ortho*-dienone from [3,3] shift will be slowed down due to steric interference between the methyl group on the allylic moiety and the *m*-methyl group of benzene ring. Consequently, enolization of *ortho*-dienone and subsequent [3,3] Cope rearrangement would compete and lead to a mixture of an *o*-allyl phenol and a *p*-allyl phenol.⁵⁹

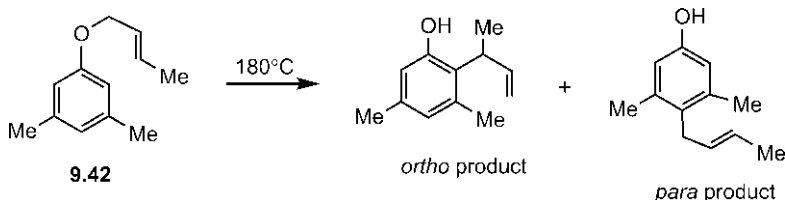


Fig. 9.49 Aromatic Claisen rearrangement giving *ortho* and *para* products.

Since enolization is an ionic step, solvent of low polarity would disfavour enolization to form the *o*-isomer. The ratio of two products is thus solvent dependent. In DMF (more polar solvent), *o*-isomer is major product whereas in decalin (less polar solvent), *p*-isomer is major product.

When phenyl propargyl ether **9.43** is used as a substrate in which a propargyl group replaces the allyl group, the phenolic product from Claisen rearrangement undergoes a [1,5]H shift followed by electrocyclic ring closing to give a chromene ([Fig. 9.50](#)).⁶⁰

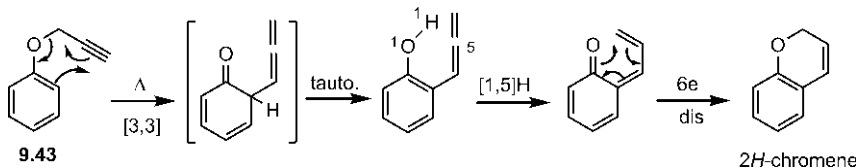
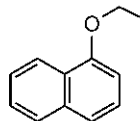
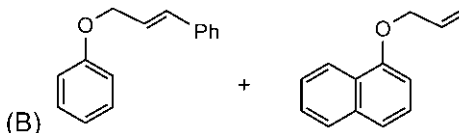
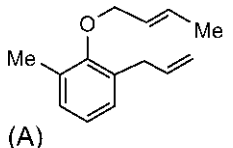


Fig. 9.50 Aromatic Claisen rearrangement of phenyl propargyl ether.

For abnormal aromatic Claisen rearrangement, see [Section 10.1.7](#), [Fig. 10.41](#).

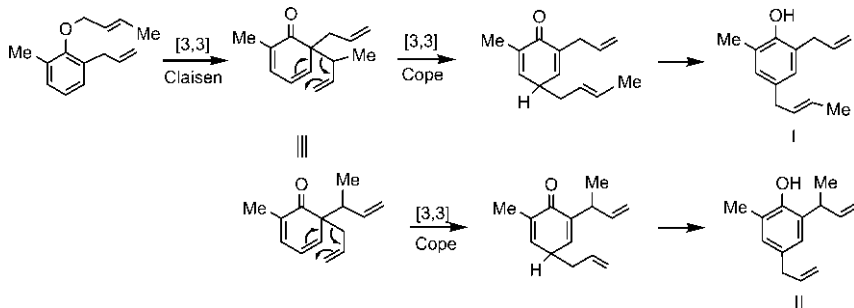
Problem 9.12

Predict the products of the following aromatic Claisen rearrangements.

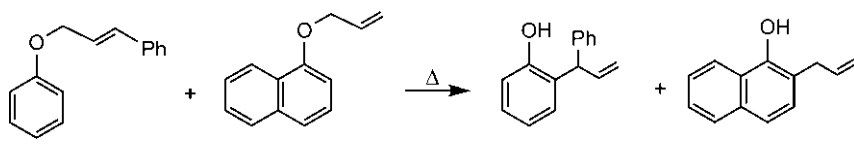


Answer

- (A) As both *ortho* positions are substituted, the reaction proceeds through two consecutive [3,3] Claisen and Cope rearrangements. In Cope rearrangement, both the migrating allyl group and the allyl substituent at *ortho* position participate to give two products (I and II) as shown below. The product I also results via [3,3] Claisen rearrangement involving other *ortho* position bearing Me followed by Cope rearrangement.

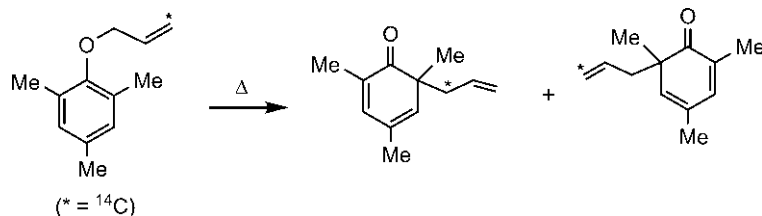


(B) This is a crossover experiment in which no cross products are obtained. This establishes the intramolecular nature of the rearrangement consistent with the pericyclic mechanism.



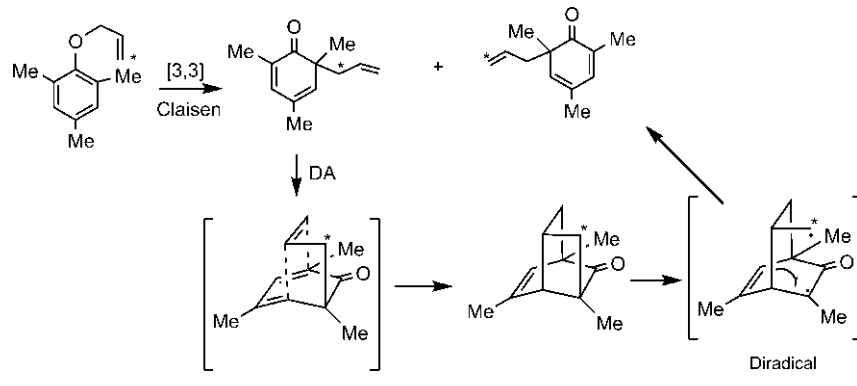
Problem 9.13

Suggest a plausible mechanism for the following rearrangement.



Answer

The first dienone from [3,3] shift can undergo IMDA reaction followed by radical fragmentation of cyclobutane ring to give the second dienone as shown below. The reversibility of the [3,3] shift would cause a scrambling of the ¹⁴C label between C-1 and C-3 of the allyl moiety of the substrate.



9.3 OTHER [3,3] REARRANGEMENTS

Besides Cope and Claisen rearrangements, several heterocyclic analogues of 1,5-diene or allyl vinyl ether can undergo concerted [3,3] sigmatropic rearrangements. Only a few selected are briefly described here.

9.3.1 Aza-Claisen Rearrangement

This is a nitrogen analogue of Claisen rearrangement when oxygen is replaced by nitrogen. For example, the compound **9.44** undergoes a [3,3] aza-Claisen rearrangement to give the product via more stable chair TS in which Me at the stereocentre is preferably equatorial (Fig. 9.51).⁶¹ The reaction also involves a chirality transfer.

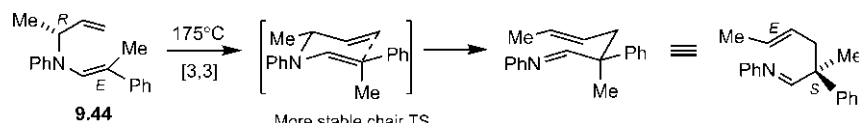


Fig. 9.51 Example of an aza-Claisen rearrangement.

9.3.2 Thia-Claisen Rearrangement

This is a [3,3] sigmatropic rearrangement of allyl vinyl sulphides or sulfoxides, as shown in Fig. 9.52.⁶²

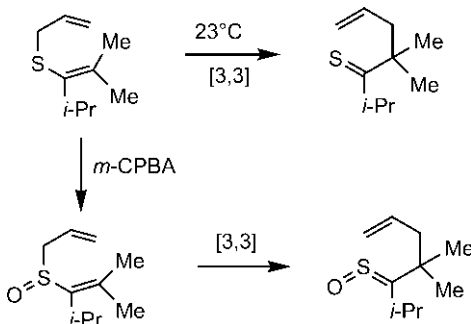


Fig. 9.52 Thia-Claisen rearrangement of allyl vinyl sulphide and sulfoxide.

9.3.3 Overman Reaction

The Overman reaction⁹ provides a very useful method to synthesize allylic amines from allylic alcohols via [3,3] sigmatropic rearrangements of their imidates. As shown in [Fig. 9.53](#), a chiral allyl alcohol is converted to its imidate **9.45** which undergoes a [3,3] shift to give finally a chiral allyl amine. The reaction provides efficient chirality transfer and high stereoselectivity for the (*E*) double bond in the product.

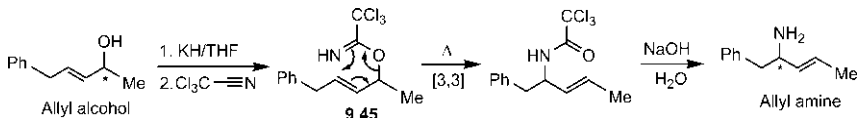


Fig. 9.53 Overman reaction for the synthesis of allyl amine from allyl alcohol via [3,3] sigmatropic rearrangement.

9.3.4 Fischer Indole Synthesis

The synthesis involves the rearrangement of an aryl hydrazone in the presence of a protic or Lewis acid to give an indole ([Fig. 9.54](#)).⁶³ The hydrazone isomerizes to an ene-hydrazine in the presence of acid, which undergoes a [3,3] sigmatropic rearrangement followed by ionic cyclization and elimination of ammonia to form the indole.

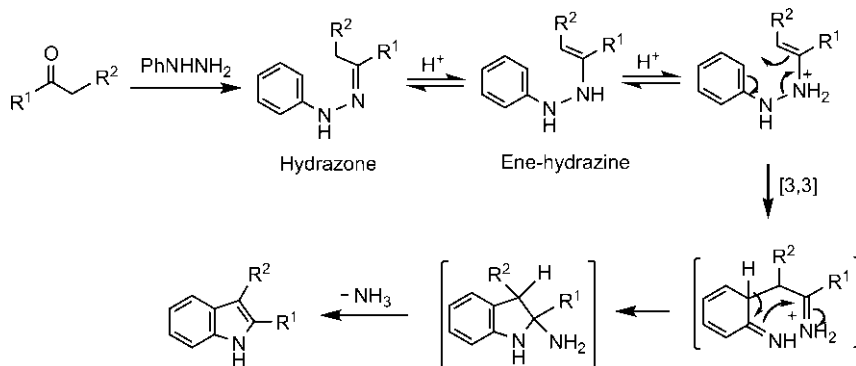
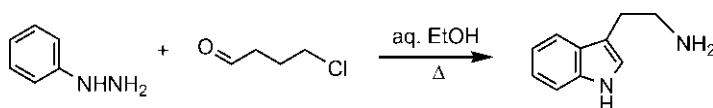


Fig. 9.54 Fischer indole synthesis involving [3,3] sigmatropic rearrangement.

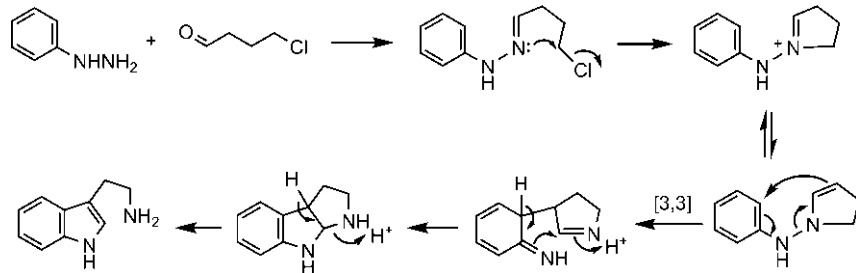
Problem 9.14

Draw a mechanism for the following indole synthesis.



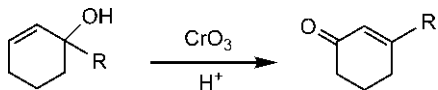
Answer⁶⁴

In this Fischer-type synthesis, nitrogen is not lost as ammonia but is incorporated into the indole side chain. This synthesis is known as Grandberg synthesis of tryptamines.

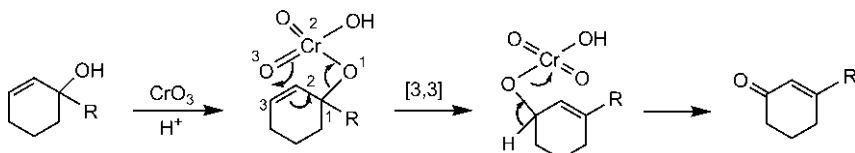


Problem 9.15

Suggest a mechanism for the following Cr(VI) oxidation.

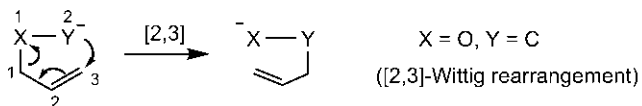
**Answer**

For a 3° alcohol, the intermediate chromate ester cannot lose a proton to give the oxidation product. Here the chromate ester is allylic in nature which can undergo a [3,3] shift to produce a new chromate ester that loses a proton to yield the observed ketone.

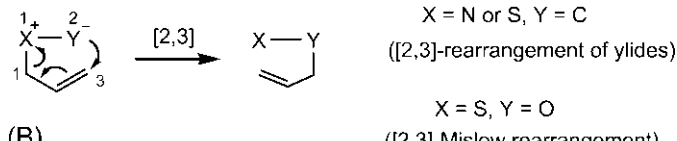


9.4 [2,3] SIGMATROPIC REARRANGEMENTS

A [2,3] sigmatropic rearrangement is a five-atom 6-electron process. There are many variants of [2,3] sigmatropic rearrangements with a variety of substrates containing heteroatoms.⁶⁵ These rearrangements can occur in an anionic system (Fig. 9.55A) as well as in neutral systems (Fig. 9.55B). The most important anionic type is Wittig rearrangement in which the substrate is a carbanion derived from an allyl ether. The neutral systems include ylides (commonly nitrogen and sulphur ylides), and oxides such as sulfoxide when the reaction is called Mislow rearrangement.



(A)



(B)

Fig. 9.55 [2,3] Sigmatropic rearrangements in (A) an anionic system and (B) a neutral system.

9.4.1 [2,3] Wittig Rearrangement

The substrate of the Wittig rearrangement⁶⁶ is a carbanion of allyl ether (alloxycarbanion), which is usually generated by direct deprotonation of allyl ether with a base. The deprotonation can be made in a regioselective manner by incorporating an anion-stabilizing group into the substrate when the base removes the most acidic proton. The anion-stabilizing group is commonly a conjugating substituent (c-type) such as alkenyl, alkynyl or aryl group. (This avoids the side reaction of carbanion condensation with a z-type carbonyl substituent.) In the Wittig rearrangement, a C–C bond is formed at the expense of a C–O bond, and the product is a homoallylic alcohol (Fig. 9.56). Note that Ph, a c-substituent, is the anion-stabilizing group. The stability of the alkoxide provides the driving force for the reaction.

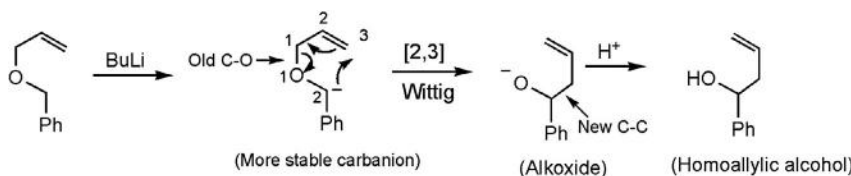


Fig. 9.56 Example of a [2,3]-Wittig rearrangement.

The Wittig rearrangement proceeds suprafacially across the allyl unit via an envelope transition structure (see Fig. 3.48). On the basis of a chair conformation as shown in Fig. 9.57, the envelope TS 9.46 is drawn. Note that *exo* and *endo* substituents in envelope TS correspond to equatorial and axial substituent, respectively, of the chair conformation.

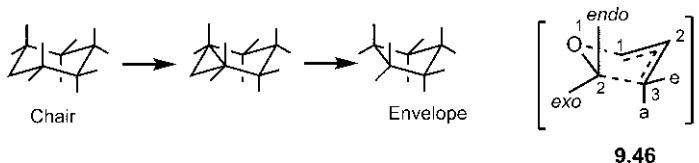


Fig. 9.57 Representation of envelope TS of [2,3] Wittig rearrangement.

The anion-stabilizing c-substituent would preferably occupy the less-hindered *exo* position, away from the fold of the envelope. The Wittig rearrangement is highly stereoselective.^{67,68} Fig. 9.58 illustrates the preference for (*E*) stereochemistry of the new double bond in the product. The rearrangement proceeds through a more stable envelope TS in which Me is equatorial, besides anion-stabilizing Ph being *exo*. The equatorial Me leads to an (*E*) double bond.

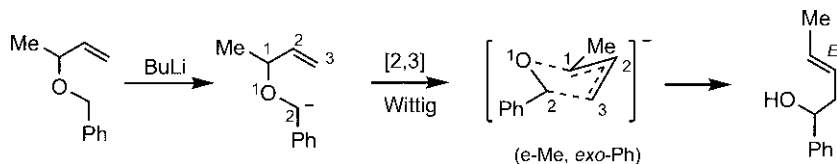


Fig. 9.58 A stereoselective Wittig rearrangement with preference for (*E*) double bond.

The Wittig rearrangement can also create two new stereocentres leading to the formation of two possible diastereomeric products, *syn* and *anti*. Importantly, the rearrangement exhibits high diastereoselectivity as illustrated in **Fig. 9.59** with two (*E*)-substrates. The diastereoselectivity arises from the more stable *exo-c* TS (the *c*-substituent, ethynyl or vinyl being *exo*). Note that Me is forced to be equatorial in the envelope TS due to (*E*) allylic double bond. The *anti* diastereomer is the predominant product in each case (**Fig. 9.59A** and **B**). **Fig. 9.59B** also shows the preference for (*E*) stereochemistry of new double bond as the *i*-Pr group opts for the less-hindered equatorial position in the envelope TS.

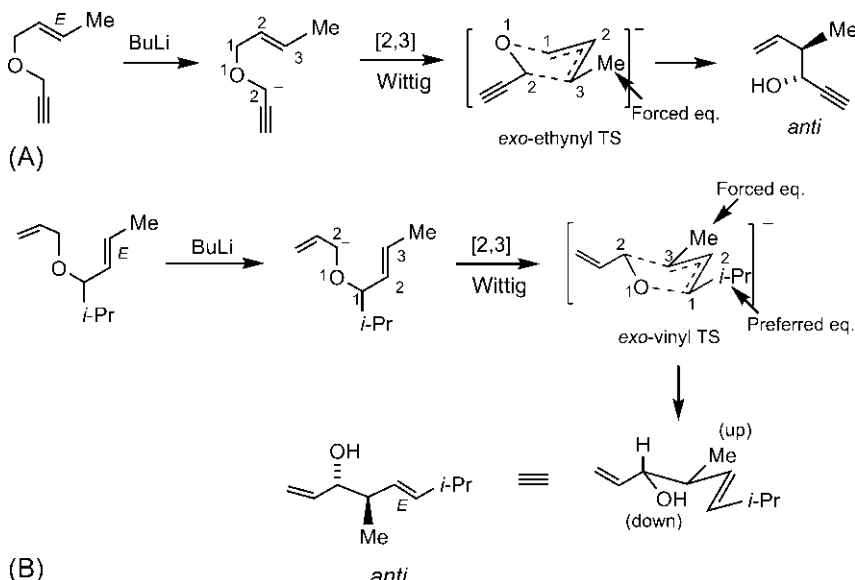


Fig. 9.59 Examples (A and B) of diastereoselectivity of Wittig rearrangement with (*E*)-substrates.

Next, we consider the Wittig rearrangement of a (*Z*)-substrate **9.47**. Here the substrate is also enantiomerically enriched in respect of (*S*)

enantiomer (ee 91%). The rearrangement proceeds through a more stable *exo*-alkenyl TS in which *i*-Pr is preferentially equatorial (Fig. 9.60). Note that (*Z*) allylic double bond forces Me on it to be axial. The product is enantioselectively enriched *syn* diastereomer with (*E*) double bond. The reaction is both diastereoselective and enantioselective (de 94%, ee 91%), and represents an asymmetric Wittig rearrangement.

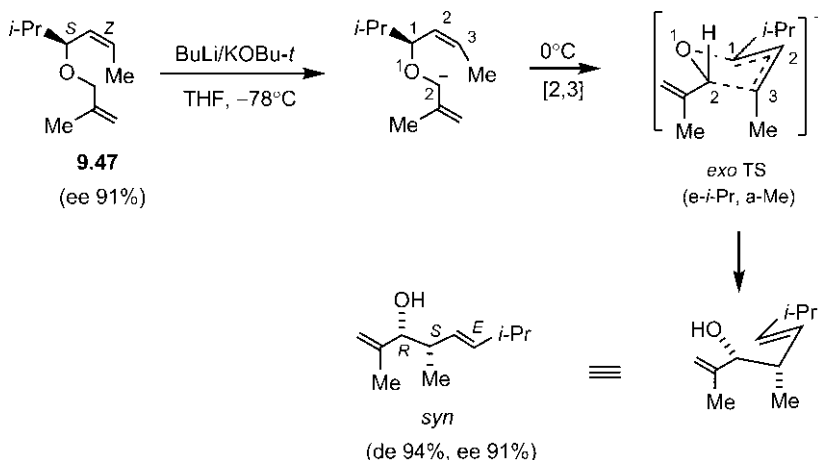


Fig. 9.60 Asymmetric Wittig rearrangement with a (*Z*)-substrate.

The diastereoselectivity of the Wittig rearrangement can be summarized as follows.

- (*Z*) – substrate \rightarrow *exo-c*-TS \rightarrow *syn* product
- (*E*) – substrate \rightarrow *exo-c*-TS \rightarrow *anti* product
- (c = conjugating anion-stabilizing group such as alkenyl, alkynyl or aryl)

It may be mentioned that an enolate-forming carbonyl group is sometimes used as a z-type anion-stabilizing substituent when a reversal of stereoselectivity occurs via a preferred *endo*-z TS.

A variant of the Wittig rearrangement is known as aza-Wittig rearrangement⁶⁹ when oxygen is replaced by nitrogen in the five-atom chain. The substrate is an allyl amine **9.48**. Similar to the Wittig rearrangement, the reaction proceeds through a more stable *exo*-Ph TS to give the *anti* diastereomer (de 90%) (Fig. 9.61).

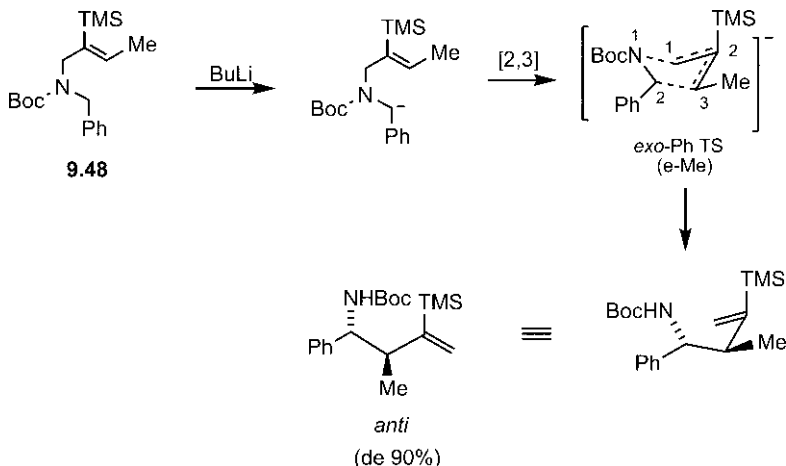
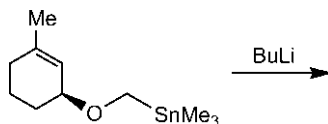


Fig. 9.61 An aza-Wittig rearrangement.

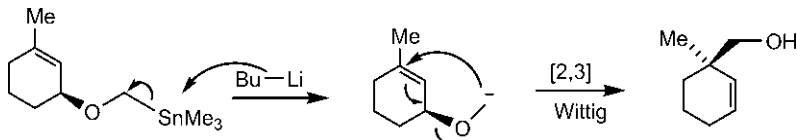
Problem 9.16

Predict the product of the following reaction.



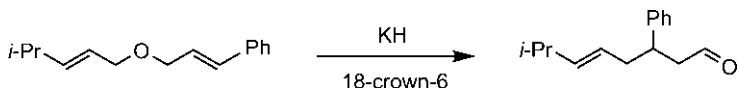
Answer

Treatment with BuLi generates an alloxycarbanion which undergoes a [2,3]-Wittig rearrangement. The suprafacial migration across the allylic unit gives the product.

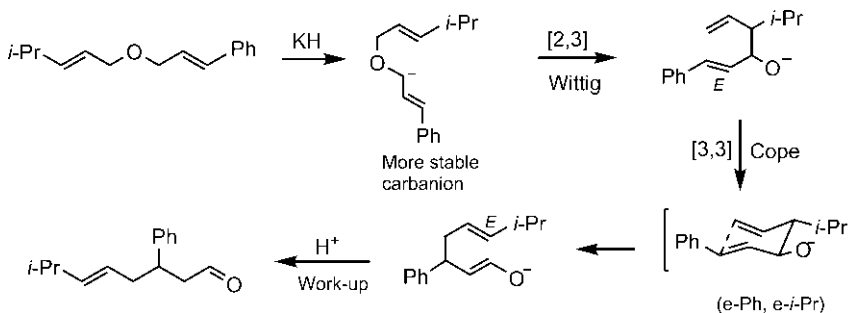


Problem 9.17

Explain the following observation.

**Answer⁷⁰**

The reaction involves a [2,3] Wittig rearrangement followed by [3,3] anionic oxy-Cope rearrangement (18-crown-6 traps the K^+ ion). The (*E*)-stereochemistry of double bond in the product results from a more stable chair TS of Cope rearrangement in which *i*-Pr is preferably equatorial.



9.4.2 [2,3] Sigmatropic Rearrangement of Ylides

9.4.2.1 [2,3] Stevens Rearrangement

Allylic sulphonium and ammonium ylides can readily undergo [2,3] sigma-tropic rearrangement which is referred to as the [2,3] Stevens rearrangement.^{71,72} This is distinct from the 1,2-Stevens rearrangement which involves a radical mechanism.

The sulphur ylide is usually generated by deprotonation of a sulphonium salt with a base. For example, the treatment of a sulphonium salt **9.49** with NaOMe gives the product via a [2,3] sigmatropic rearrangement (Fig. 9.62).⁷³

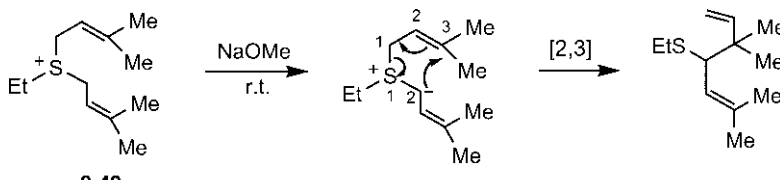


Fig. 9.62 [2,3] Stevens rearrangement of a sulphur ylide.

Sulphonium salts can be readily obtained by alkylation of sulphides. A scheme for the synthesis of γ -cyclocitral via a [2,3] sigmatropic shift is shown in Fig. 9.63.

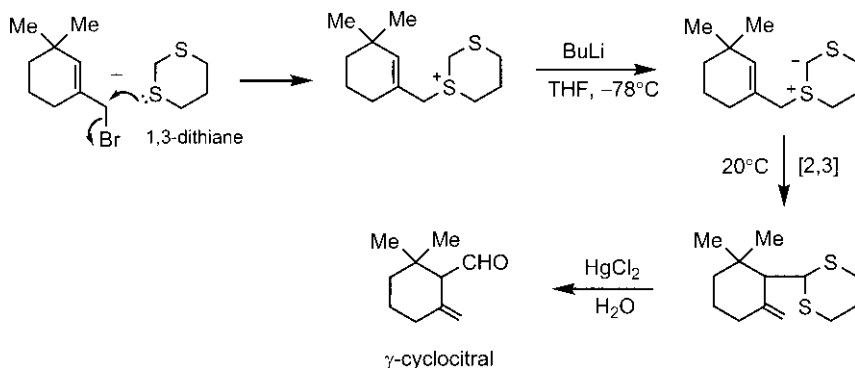


Fig. 9.63 A synthesis of γ -cyclocitral via [2,3] sigmatropic rearrangement.

The [2,3] sigmatropic rearrangement of sulphur ylide can also be used for ring expansion to prepare medium-sized ring (Fig. 9.64).⁷⁴

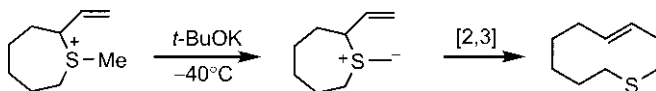


Fig. 9.64 Synthesis of a 10-membered ring using [2,3] rearrangement of a sulphur ylide.

The sulphur ylide can be directly obtained from an allylic sulphide by the addition of a carbene (Fig. 9.65).⁷⁵ The *trans* stereochemistry of the product results from the suprafacial addition across the allyl unit.

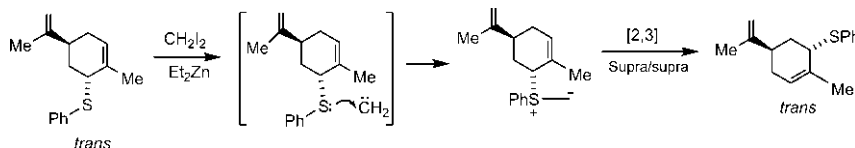
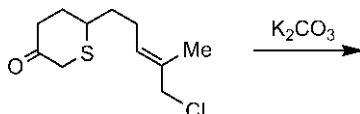


Fig. 9.65 Stereochemistry of [2,3] Stevens rearrangement of a sulphur ylide.

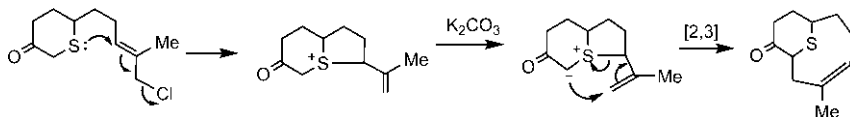
Problem 9.18

Predict the product of the following reaction.

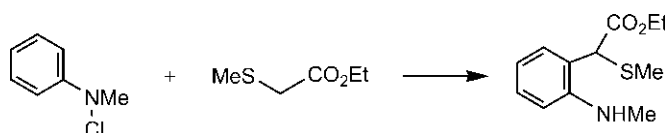


Answer

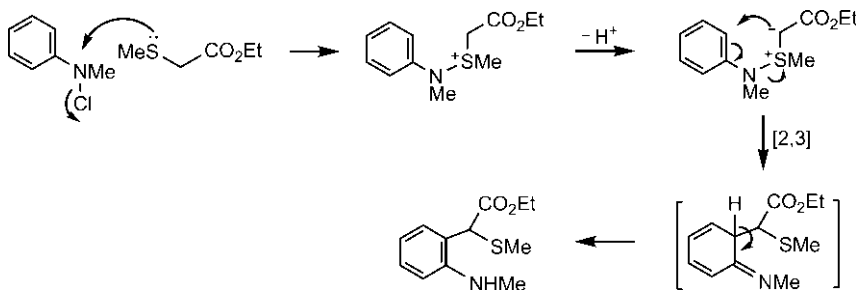
The intramolecular nucleophilic substitution of the allyl chloride (S_N2') produces a sulphonium salt which, after deprotonation, undergoes a [2,3] sigmatropic shift with ring expansion to give the product.

**Problem 9.19**

Draw a mechanism of the following reaction.

**Answer**

Nucleophilic substitution by the sulphur nucleophile and subsequent loss of proton gives an S-anilinosulphonium ylide which undergoes a [2,3] sigmatropic rearrangement to give the product after aromatization.



The nitrogen ylides (obtained by proton abstraction of a quaternary ammonium salt with a base) also undergo [2,3] sigmatropic rearrangement. This is illustrated with two examples in Fig. 9.66.^{76,77} A proton adjacent to

an ester group is abstracted preferentially. Fig. 9.66B shows a ring expansion with the formation of a *trans* double bond in a nine-membered ring.

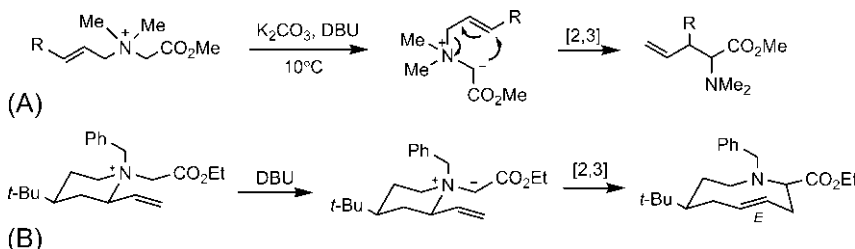


Fig. 9.66 Examples (A and B) of [2,3] sigmatropic rearrangements of nitrogen ylides.

9.4.2.2 Sommelet–Hauser Rearrangement

The Sommelet–Hauser rearrangement⁷⁸ is an aromatic [2,3] sigmatropic rearrangement of a nitrogen ylide generated from a quaternary ammonium salt possessing a benzyl substituent **9.50**. The deprotonation is usually made with a base such as NaNH_2 in liquid NH_3 . The [2,3] shift occurs at the *ortho* position of the aromatic ring and the rearranged isomer rapidly tautomerizes to give the aromatic product (Fig. 9.67). It should be noted that the ylide obtained by the abstraction of a more acidic benzylic proton cannot undergo [2,3] sigmatropic rearrangement; it is in equilibrium with a second ylide which, though being present as a minor species, undergoes the rearrangement. As the reaction progresses, the equilibrium shifts to the side of the reactive ylide.

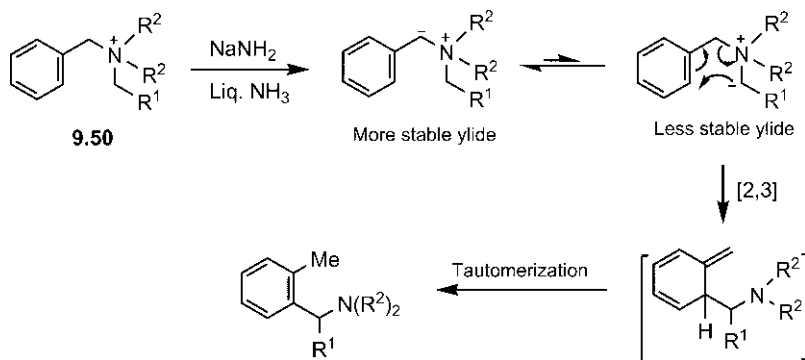


Fig. 9.67 [2,3] Sommelet–Hauser rearrangement.

The reactive nitrogen ylide can also be generated by desilylation. As shown in Fig. 9.68, the ammonium salt **9.51** is desilylated with CsF and the resulting nitrogen ylide rearranges to **9.52** as a major product and **9.53** as a minor product.⁷⁹

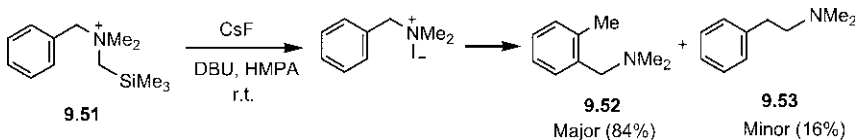


Fig. 9.68 Rearrangement of a nitrogen ylide giving a mixture of products.

Depending on the substrate and reaction conditions, the Sommelet–Hauser rearrangement competes with the 1,2-Stevens rearrangement. In the above reaction, the major product is obtained by Sommelet–Hauser rearrangement whereas the minor product results from the radical pathway of the 1,2-Stevens rearrangement involving homolysis of C–N⁺ bond (Fig. 9.69).

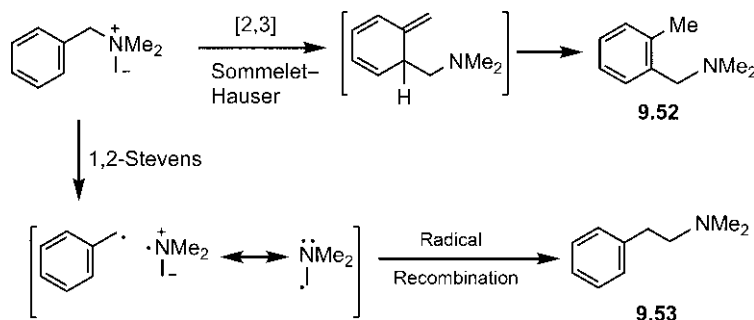
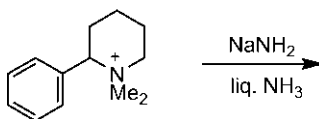


Fig. 9.69 Mechanism of the reaction shown in Fig. 9.68 via Sommelet–Hauser and 1,2-Stevens rearrangements.

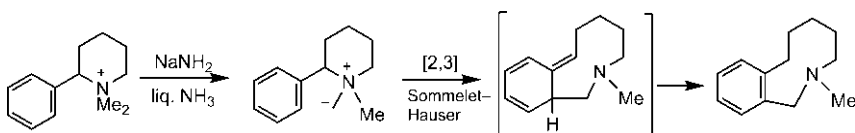
Problem 9.20

Predict the product of the following reaction.



Answer

The reaction is a Sommelet–Hauser rearrangement and involves ring expansion to form a nine-membered ring fused with a benzene ring.



9.4.3 [2,3] Sigmatropic Rearrangement of Oxides

9.4.3.1 Mislow Rearrangement

The [2,3] sigmatropic rearrangement of allyl sulfoxide to allyl sulphenate, in which a new C—O bond is formed, is known as Mislow rearrangement.⁸⁰ The reaction is reversible, and the reverse reaction of allyl sulphenate to allyl sulfoxide is termed a retro-Mislow rearrangement (Fig. 9.70).

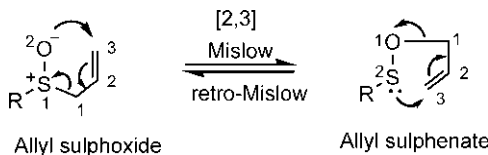


Fig. 9.70 [2,3] Mislow/retro-Mislow rearrangement.

The Mislow rearrangement is thermodynamically unfavourable and the equilibrium lies to the side of the sulfoxide. However, the equilibrium can be pushed towards the sulphenate by cleaving its O—S bond with a thio-philic reagent such as phenyl thiolate, trimethyl phosphite or piperidine to give an allyl alcohol (Fig. 9.71).⁸¹

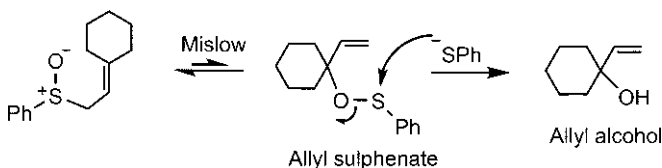
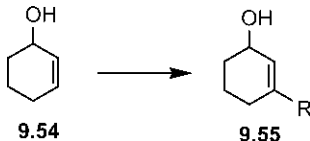


Fig. 9.71 Synthesis of allyl alcohol via a Mislow rearrangement.

A useful application of the Mislow/retro-Mislow rearrangements is alkylation of an allyl alcohol, which is normally difficult to achieve. To illustrate, let us consider the conversion of **9.54** to **9.55**.



The transformation can be performed using retro-Mislow and Mislow rearrangements as shown in Fig. 9.72.

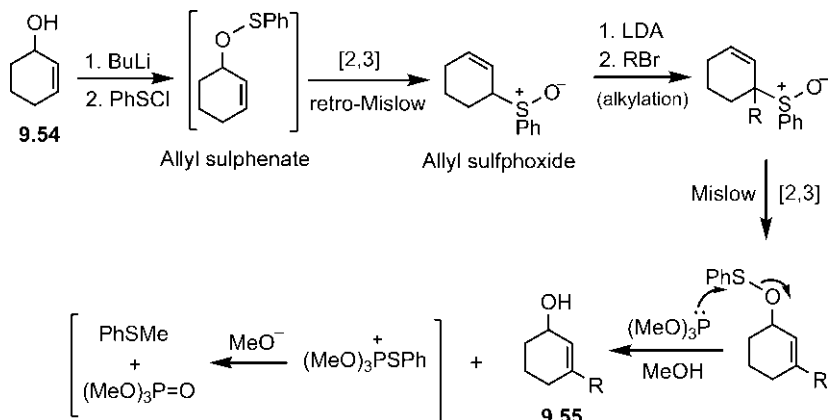


Fig. 9.72 Alkylation of allyl alcohol using retro-Mislow and Mislow rearrangements.

Interestingly, a Mislow/retro-Mislow sequence can transpose the sulphoxide moiety within a π system, as illustrated in Fig. 9.73. Similar to the Wittig rearrangement, the new double bond is *E* resulting from the preferred envelope TS in which bulky R substituent is equatorial.⁸² The substituent Ph on sulphur is preferably *endo*, that is, pointing towards the allylic fragment.⁸³

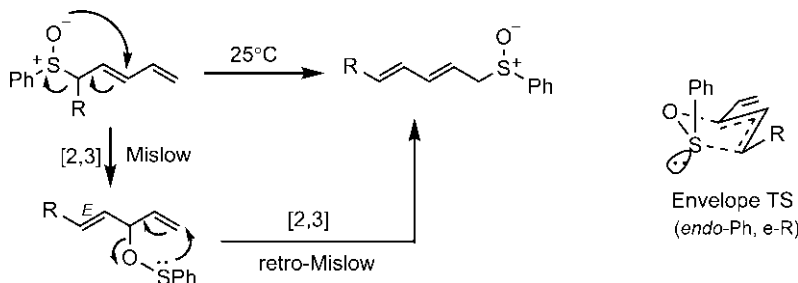


Fig. 9.73 Sulphoxide transposition within a π system and the preferred envelope TS for Mislow rearrangement.

A sulphoxide may be chiral with sulphur as a stereocentre (the lone pair on sulphur being the lowest-priority ligand) whereas a sulphenate is achiral. An optically active allyl sulphoxide can be thermally racemized through an achiral allyl sulphenate involving a Mislow/retro-Mislow sequence. This is shown in Fig. 9.74 with (*S*) enantiomer of an allyl sulphoxide. The allylic sulphoxide–allylic sulphenate rearrangement was discovered by Mislow in connection with this racemization.⁸⁴

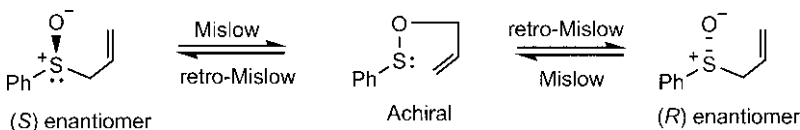


Fig. 9.74 Racemization of optically active allyl sulphoxide.

The Mislow rearrangement of a cyclic allyl sulphoxide **9.56** is found to be highly diastereoselective as the new C—O bond is preferentially formed from the less-hindered equatorial side (Fig. 9.75).^{80,85}

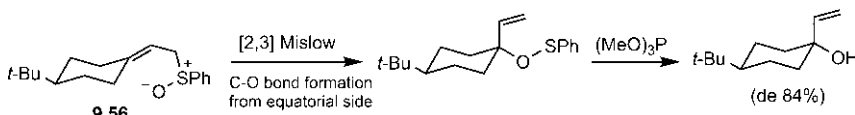


Fig. 9.75 A diastereoselective Mislow rearrangement.

Like other [2,3] shifts, the Mislow rearrangement also proceeds suprafacially with respect to allylic unit. An asymmetric Mislow rearrangement can be performed using a chiral sulphoxide. This is illustrated in Fig. 9.76 using (S) enantiomer of a sulphoxide which undergoes a Mislow rearrangement followed by treatment with a thiophile piperidine to give an (S) allylic alcohol.

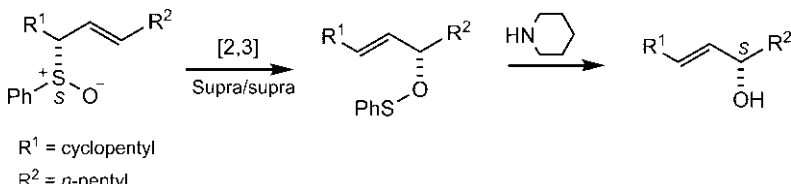


Fig. 9.76 An asymmetric Mislow rearrangement.

Similar to allyl sulphoxides, allyl selenoxides (generated *in situ* by the oxidation of allyl seleno ethers) can undergo [2,3] sigmatropic rearrangements to produce allyl alcohols, as shown in Fig. 9.77.⁸⁶

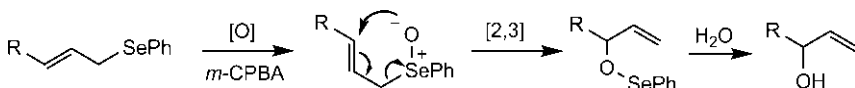


Fig. 9.77 [2,3] Sigmatropic rearrangement of allyl selenoxide.

9.4.3.2 [2,3] Meisenheimer Rearrangement

The [2,3] sigmatropic rearrangement of an allylic N-oxide to a hydroxyl amine is known as Meisenheimer rearrangement.⁸⁷ The cleavage of the N—O bond of the hydroxyl amine product gives an allyl alcohol. This is illustrated with a synthesis of linalool in Fig. 9.78.

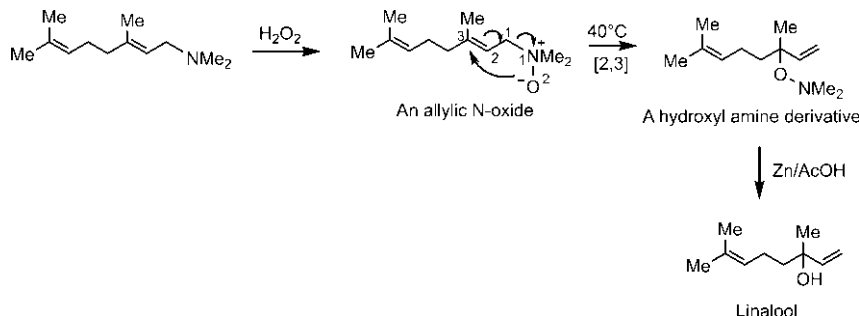


Fig. 9.78 Synthesis of linalool via a [2,3] Meisenheimer rearrangement.

9.5 HIGHER ORDER $[i,j]$ REARRANGEMENTS AND PERISELECTIVITY

When two or more symmetry-allowed and geometrically accessible $[i,j]$ rearrangements are possible in a molecule, a higher order $[i,j]$ shift involving longer conjugated π system(s) would take place preferentially. This indicates periselectivity in sigmatropic rearrangements.

To illustrate, let us consider the aromatic rearrangement of **9.57** in Fig. 9.79.⁸⁸ The major product arises from a higher order, 10-electron $[5,5]$ sigmatropic rearrangement with inversion of pentadienyl group. The product from $[3,3]$ Claisen rearrangement is formed in a smaller amount. A very minor product with no inversion of pentadienyl moiety also results from an overall $[1,5]\text{C}$ shift resulting from two successive $[3,3]$ Claisen

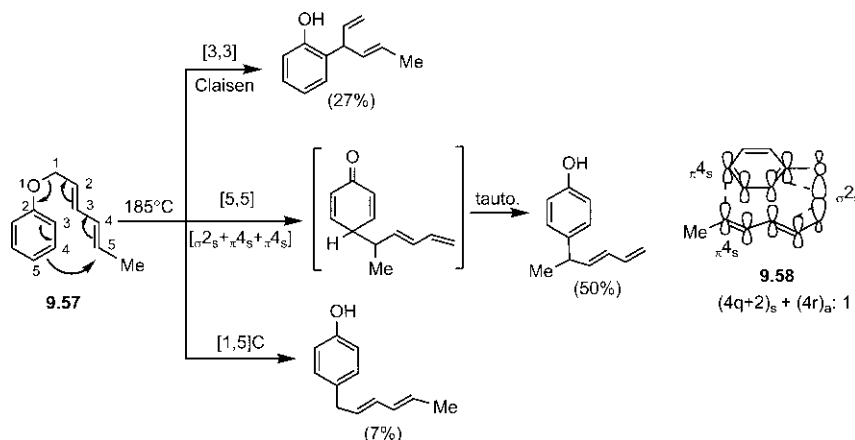


Fig. 9.79 $[5,5]$ Periselectivity in a sigmatropic rearrangement.

and [3,3] Cope rearrangements followed by aromatization to the phenolic compound. The [5,5] rearrangement is a thermally allowed $[\sigma_2 + \pi_4 + \pi_4]$ process **9.58**. Note that two vinyl units are linked to the two ends of [3,3] system to give the longer conjugated systems for [5,5] rearrangement, that is, a [5,5] rearrangement is a bisvinologue of [3,3] rearrangement.

The familiar benzidine rearrangement is another example of [5,5] sigma-tropic shift (Fig. 9.80A).⁸⁹ As shown in Fig. 9.80B, a substrate **9.59** can even undergo an 18-electron [9,9] sigmatropic rearrangement.

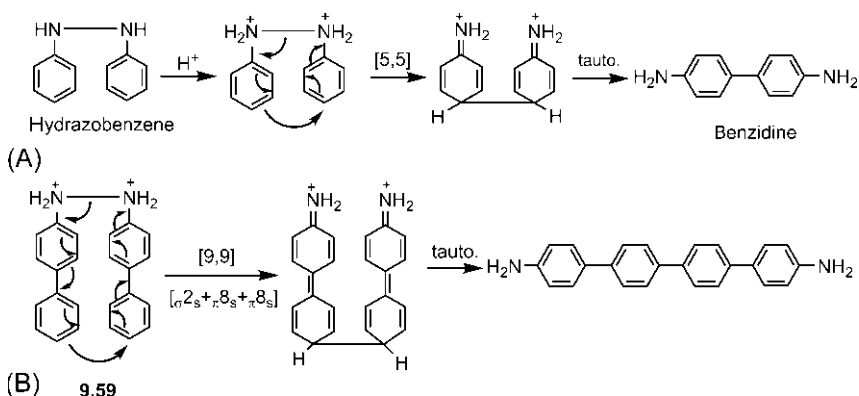


Fig. 9.80 (A) [5,5] Benzidine rearrangement and (B) a [9,9] sigmatropic rearrangement.

The [5,5] rearrangement is also possible in all-carbon systems. An example with a tetrahydroheptalene is shown in Fig. 9.81. The reaction is believed to take place via a tricyclic diradical intermediate.^{90,91}

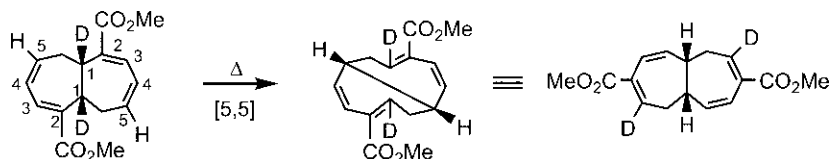


Fig. 9.81 [5,5] Sigmatropic shift in an all-carbon tetrahydroheptalene system.

The higher order $[i,j]$ shifts have also been observed in cations and ylides. For example, a 6-electron [3,4] shift is preferred over a 2-electron [1,2] shift in the cation **9.60** (Fig. 9.82A). Fig. 9.82B shows a 10-electron [4,5] shift of a nitrogen ylide **9.61** in preference to a 6-electron [2,3] rearrangement.⁹² The [4,5] rearrangement is a bisvinologue of [2,3] Stevens rearrangement.

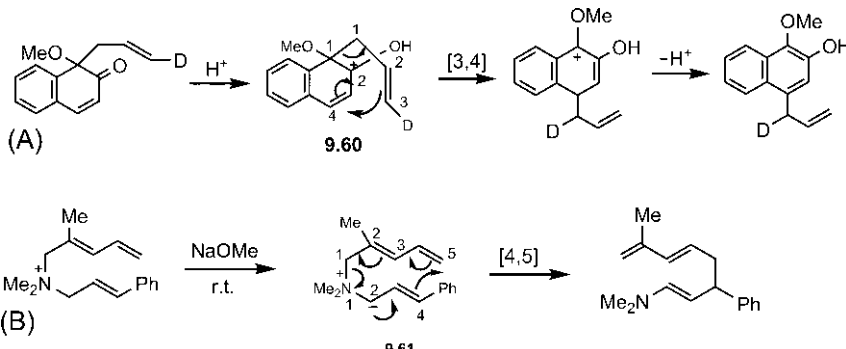
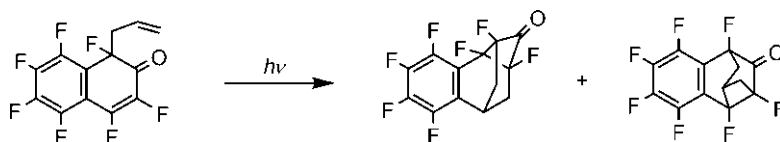


Fig. 9.82 (A) [3,4] Sigmatropic shift in a cation and (B) [4,5] sigmatropic shift in a nitrogen ylide.

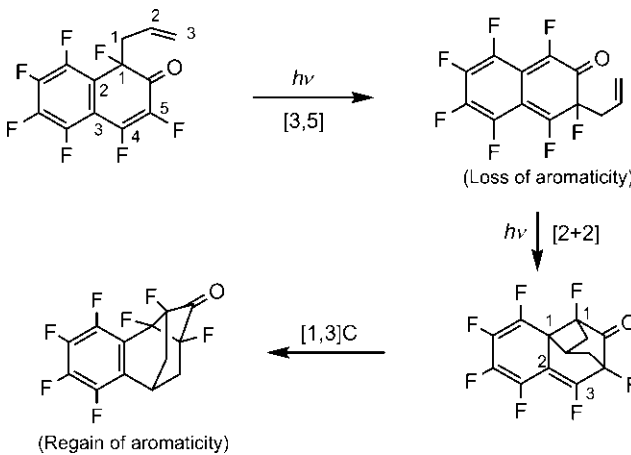
Problem 9.21

Suggest a plausible mechanism for the following transformation.



Answer⁹³

The first product arises from the photochemical 8-electron [3,5] sigmatropic shift followed by an intramolecular [2 + 2] cycloaddition and a [1,3]C shift that re-establishes aromaticity, as shown below. The second product is simply an intramolecular [2 + 2] photoadduct.



REFERENCES

- Hill, R. K. In *Comprehensive Organic Synthesis*; Trost, B. M., Fleming, I., Eds.; Vol. 5; Pergamon Press: Oxford, 1991; p 785.
- Tantillo, D. J.; Hoffmann, R. *Angew. Chem. Int. Ed. Eng.* **2002**, *41*, 1033. *J. Org. Chem.* **2002**, *67*, 1419.
- Wilson, S. R. *Org. React.* **1993**, *43*, 93.
- Paquette, L. A. *Angew. Chem. Int. Ed. Eng.* **1990**, *29*, 609.
- Evans, D. A.; Golob, A. M. *J. Am. Chem. Soc.* **1975**, *97*, 4765.
- Carpenter, B. K. *Tetrahedron* **1978**, *34*, 1877.
- Breslow, R.; Hoffman, J. M., Jr. *J. Am. Chem. Soc.* **1972**, *94*, 2111.
- Yasuda, M.; Harano, K.; Kanematsu, K. *J. Org. Chem.* **1980**, *45*, 2368.
- Overman, L. E. *Acc. Chem. Res.* **1980**, *13*, 218.
- Jacobsen, E. J.; Levin, J.; Overman, L. E. *J. Am. Chem. Soc.* **1988**, *110*, 4329.
- Schreiber, S. L.; Santini, C. *J. Am. Chem. Soc.* **1984**, *106*, 4038.
- Doering, W.v.E.; Roth, W. R. *Tetrahedron* **1962**, *18*, 67.
- Hill, R. K. In *Asymmetric Synthesis*; Morrison, J. D., Ed.; Vol. 4; Academic Press: New York, 1984; p 503.
- Enders, D.; Knopp, M.; Schiffers, R. *Tetrahedron Asymmetry* **1996**, *7*, 1847.
- Hill, R. K.; Gillman, N. W. *J. Chem. Soc. Chem. Commun.* **1967**, 619.
- Wei, S.-Y.; Tomooka, K.; Nakai, T. *Tetrahedron* **1993**, *49*, 1025.
- Overman, L. E.; Shim, J. *J. Org. Chem.* **1993**, *58*, 4662.
- Hudlicky, T.; Fan, R.; Reed, J. W.; Gadamasetti, G. *Org. React.* **1992**, *41*, 1.
- Vogel, E.; Erb, R. *Angew. Chem. Int. Ed. Eng.* **1962**, *1*, 53.
- Brown, J. M.; Golding, B. T.; Stofko, J. J., Jr. *J. Chem. Soc. Chem. Commun.* **1973**, 319.
- Doering, W.v.E.; Roth, W. R. *Angew. Chem. Int. Ed. Eng.* **1963**, *2*, 115.
- Cheng, A. K.; Anet, F. A. L.; Mioduski, J.; Meinwald, J. *J. Am. Chem. Soc.* **1974**, *96*, 2887.
- Schröder, G.; Oth, J. F. M. *Angew. Chem. Int. Ed. Eng.* **1967**, *6*, 414.
- Schröder, G.; Oth, J. F. M.; Merenyi, R. *Angew. Chem. Int. Ed. Eng.* **1965**, *4*, 752.
- Doering, W.v.E.; Rosenthal, J. W. *J. Am. Chem. Soc.* **1966**, *88*, 2078.
- Miyasbi, T.; Nitta, M.; Mukai, T. *Tetrahedron Lett.* **1967**, 3433.
- Wipf, P. In *Comprehensive Organic Synthesis*; Trost, B. M., Fleming, I., Eds.; Vol. 5; Pergamon Press: Oxford, 1991; p 827.
- Ziegler, F. E. *Chem. Rev.* **1988**, *88*, 1423.
- Tarbel, D. S. *Org. React.* **1944**, *2*, 1.
- Pine, S. H. *Org. React.* **1993**, *43*, 1.
- Pine, S. H.; Zahler, R.; Evans, D. A.; Grubbs, R. H. *J. Am. Chem. Soc.* **1980**, *102*, 3270.
- Johnson, W. S.; Wethermann, L.; Bartlett, W. R.; et al. *J. Am. Chem. Soc.* **1970**, *92*, 741.
- Felix, D.; Gschwend-Steen, K.; Wick, A. E.; Eschenmoser, A. *Helv. Chim. Acta* **1969**, *52*, 1030.
- Ireland, R. E.; Mueller, R. H. *J. Am. Chem. Soc.* **1972**, *94*, 5898.
- Carroll, M. F. *J. Chem. Soc.* **1940**, 704 and 1266.
- Kimel, W.; Cope, A. C. *J. Am. Chem. Soc.* **1943**, *65*, 1992.
- Cupas, C. A.; Schumann, W.; Heyd, W. E. *J. Am. Chem. Soc.* **1970**, *92*, 3237.
- Curran, D. P.; Suh, Y. G. *J. Am. Chem. Soc.* **1984**, *106*, 5002. *Tetrahedron Lett.* **1984**, *25*, 4179.
- Tulshian, D. B.; Fraser-Reid, B. *J. Org. Chem.* **1984**, *49*, 518.
- Hansen, H.-J.; Schmid, H. *Tetrahedron* **1974**, *30*, 1959.
- Ireland, R. E.; Mueller, R. H.; Willard, A. K. *J. Am. Chem. Soc.* **1976**, *98*, 2868.
- Ireland, R. E.; Willard, A. K. *Tetrahedron Lett.* **1975**, 3975.
- Chai, Y.; Hong, S.; Lindsay, H. A.; McFarland, C.; McIntosh, M. C. *Tetrahedron* **2002**, *58*, 2905.

44. Goering, H. L.; Kimoto, W. *I. J. Am. Chem. Soc.* **1965**, *87*, 1748.
45. Ireland, R. E.; Varney, M. D. *J. Org. Chem.* **1983**, *48*, 1829.
46. House, H. O.; Lubinkowski, J.; Good, J. *J. Org. Chem.* **1975**, *40*, 86.
47. Khaledy, M. M.; Kalani, M. Y. S.; Khuong, K. S.; et al. *J. Org. Chem.* **2003**, *68*, 572.
48. Ireland, R. E.; MaienFisch, P. *J. Org. Chem.* **1988**, *53*, 640.
49. Ireland, R. E.; Wipf, P.; Armstrong, J. D. *J. Org. Chem.* **1991**, *56*, 650.
50. Danishesky, S.; Funk, R. L.; Kerwin, J. F. *J. Am. Chem. Soc.* **1980**, *102*, 6889.
51. Ito, H.; Taguchi, T. *Chem. Soc. Rev.* **1999**, *28*, 43.
52. Nubbemeyer, U. *Synthesis* **2003**, *7*, 961.
53. Cohen, N.; Lopresti, R. J.; Neukom, C.; Saucy, G. *J. Org. Chem.* **1980**, *45*, 583.
54. Evans, R. J. D.; Landor, S. R.; Regan, J. P. *J. Chem. Soc. Chem. Commun.* **1965**, 397.
55. Enders, D.; Knopp, M. *Tetrahedron* **1996**, *52*, 5805.
56. Corey, E. J.; Lee, D.-H. *J. Am. Chem. Soc.* **1991**, *113*, 4026.
57. Abraham, L.; Czerwonka, R.; Hiersemann, M. *Angew. Chem. Int. Ed. Eng.* **2001**, *40*, 4700.
58. Rhoads, S. J.; Raulins, N. R. *Org. React.* **1975**, *22*, 1.
59. Borgulya, J.; Hansen, H.-J.; Barner, R.; Schmid, H. *Helv. Chim. Acta* **1963**, *46*, 2444.
60. Harfenist, M.; Thom, E. *J. Org. Chem.* **1972**, *37*, 841.
61. Hill, R. K.; Gillman, N. W. *Tetrahedron Lett.* **1967**, 1421.
62. Hwu, J. R.; Anderson, D. A. *J. Chem. Soc., Perkin Trans. 1* **1991**, 3199.
63. Robinson, B. *Chem. Rev.* **1963**, *63*, 373. **1969**, *69*, 227.
64. Grandberg, I. I. *Chem. Heterocycl. Compd. (Engl. Transl.)* **1974**, *10*, 501.
65. Brückner, R. In *Comprehensive Organic Synthesis*; Trost, B. M., Fleming, I., Eds.; Vol. 6; Pergamon Press: Oxford, 1991; p 873.
66. Nakai, T.; Mikami, K. *Org. React.* **1994**, *46*, 105.
67. Hoffmann, R. W. *Angew. Chem. Int. Ed. Eng.* **1979**, *18*, 563.
68. Mikami, K.; Azuma, K.; Nakai, T. *Tetrahedron* **1984**, *40*, 2303.
69. Anderson, J. C.; Smith, S. C.; Swarbrick, M. E. *J. Chem. Soc., Perkin Trans. 1* **1997**, 1517.
70. Greeves, N.; Lee, W.-M. *Tetrahedron Lett.* **1997**, *38*, 6445.
71. Markó, I. E. In *Comprehensive Organic Synthesis*; Trost, B. M., Fleming, I., Eds.; Vol. 3; Pergamon Press: Oxford, 1991; p 913.
72. Clark, J. S., Ed. *Nitrogen, Oxygen and Sulfur Ylide Chemistry, a Practical Approach in Chemistry*; Oxford University Press: Oxford, 2002.
73. Baldwin, J. E.; Hackler, R. E.; Kelly, D. P. *J. Chem. Soc. Chem. Commun.* **1968**, 537.
74. Cere, V.; Paolucci, C.; Pollicino, S.; Sandri, E.; Fava, A. *J. Org. Chem.* **1978**, *43*, 4826.
75. Kosarych, Z.; Cohen, T. *Tetrahedron Lett.* **1982**, *23*, 3019.
76. Coldham, I.; Middleton, M. L.; Taylor, P. L. *J. Chem. Soc., Perkin Trans. 1* **1997**, 2951.
77. Vedejs, E.; Arco, M. J.; Renga, J. M. *Tetrahedron Lett.* **1978**, 523.
78. Pine, S. H. *Org. React.* **1970**, *18*, 403.
79. Tanaka, T.; Shirai, N.; Sugimori, J.; Sato, Y. *J. Org. Chem.* **1992**, *57*, 5034.
80. Evans, D. A.; Andrews, G. C. *Acc. Chem. Res.* **1974**, *7*, 147.
81. Evans, D. A.; Andrews, G. C.; Sims, C. L. *J. Am. Chem. Soc.* **1971**, *93*, 4956.
82. Sato, T.; Otera, J.; Nozaki, H. *J. Org. Chem.* **1989**, *54*, 2779.
83. Reich, H. J.; Yelm, K. E.; Wollowitz, S. *J. Am. Chem. Soc.* **1983**, *105*, 2503.
84. Tang, R.; Mislow, K. *J. Am. Chem. Soc.* **1970**, *92*, 2100.
85. Evans, D. A.; Andrews, G. C. *J. Am. Chem. Soc.* **1972**, *94*, 3672.
86. Nishibayashi, Y.; Uemura, S. *Top. Curr. Chem.* **2000**, *208*, 201.
87. Buxton, J. E. H.; Coldham, I.; Mulholland, K. R. *J. Chem. Soc., Perkin Trans. 1* **1999**, 2327.
88. Frater, G.; Schmid, H. *Helv. Chim. Acta* **1968**, *51*, 190. **1970**, *53*, 269.
89. Cox, R. A.; Buncel, E. In *The Chemistry of the Hydrazo, Azo and Azoxy Groups*; Patai, S., Ed.; Wiley: New York, 1975. Part 2, p. 775.

90. Hafner, K.; Lindner, H. J.; Luo, W.; Meinhardt, K. P.; Zink, T. *Pure Appl. Chem.* **1993**, *65*, 17.
91. Beno, B. R.; Fennen, J.; Houk, K. N.; Lindner, H. J.; Hafner, K. *J. Am. Chem. Soc.* **1998**, *120*, 10490.
92. Laird, T.; Ollis, W. D.; Sutherland, I. O. *J. Chem. Soc., Perkin Trans. 1* **1980**, 2033.
93. Brooke, G. M.; Matthews, R. S.; Robson, N. S. *J. Chem. Soc. Chem. Commun.* **1980**, 194.

CHAPTER 10

Group Transfer Reactions

The two well-known group transfer reactions are ene reaction with a single group transfer, and diimide reduction with a double group transfer (see Section 3.2.4). They resemble the Diels–Alder reaction (Fig. 10.1). In ene reaction, a 4-electron ene component comprising a π bond and a σ bond replaces the diene component, and in diimide reduction, a 4-electron diimide component with two σ bonds replaces the diene component.

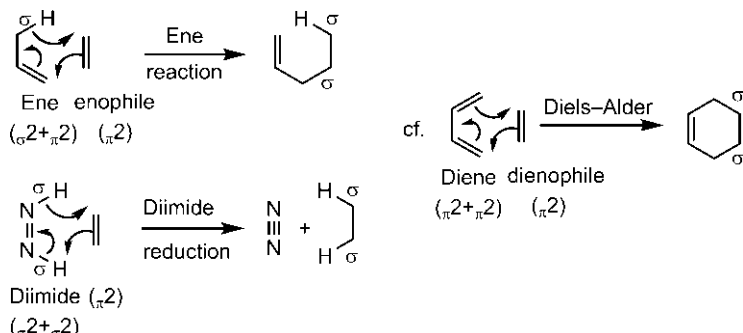


Fig. 10.1 Ene reaction and diimide reduction in analogy with Diels–Alder reaction.

Two new σ bonds are formed in each case. However, no σ bond is broken in Diels–Alder reaction whereas one and two σ bonds are broken in the ene reaction and diimide reduction, respectively. Therefore, the activation energy (ΔG^\ddagger) increases in the order: Diels–Alder < ene < diimide reduction, and the reactions require progressively higher temperatures along the series.

10.1 ENE REACTIONS

The ene reaction^{1–3} was discovered by Kurt Alder co-discoverer of Diels–Alder ‘diene’ reaction, and is referred to as the Alder ‘ene’ reaction. The ene component is usually an alkene bearing allylic hydrogen, and the enophile is a π system similar to the alkene or alkyne dienophile. The ene reaction is

reversible and both ene and retro-ene reactions (Fig. 10.2) are useful in synthesis.

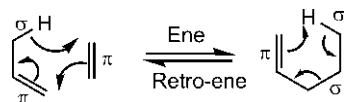


Fig. 10.2 Prototype ene and retro-ene processes.

The hetero-ene reactions with a heteroenophile or a heteroene component are also valuable in synthesis. Some important hetero-ene reactions are represented in Fig. 10.3. In a heteroenophile component, the enophile π system incorporates one or two heteroatoms (Fig. 10.3A). Similarly, a heteroene component includes one or more heteroatoms in the 4-atom ene chain (Fig. 10.3B).

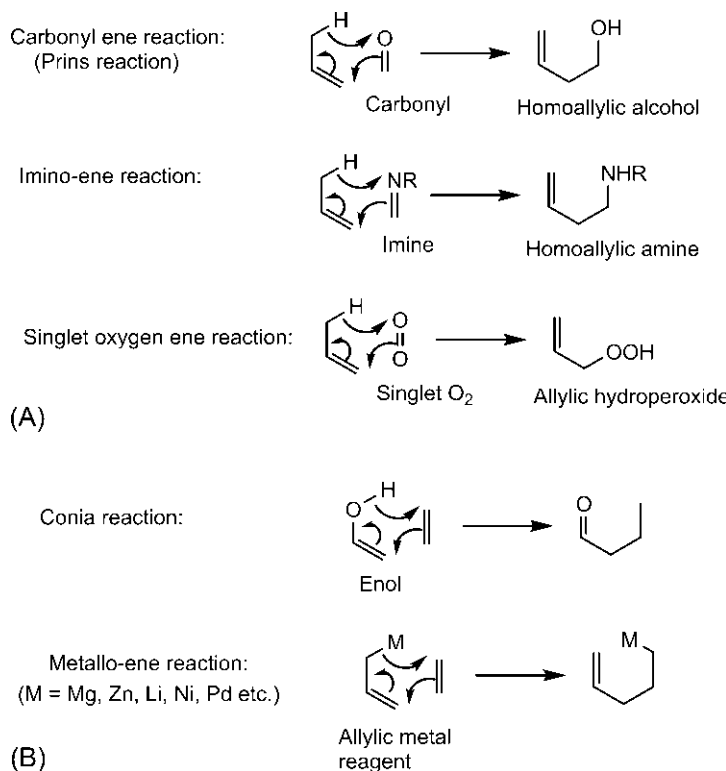


Fig. 10.3 Hetero-ene reactions involving (A) ene and heteroenophile components and (B) heteroene and enophile components.

10.1.1 Frontier Orbital Picture, Reactivity and Regioselectivity

The ene reaction is thermally allowed as a $[\sigma_{2s} + \pi_{2s} + \pi_{2s}]$ process (see Fig. 3.49). The frontier orbital picture of the ene reaction can be represented as $\text{HOMO}_{\text{ene}}/\text{LUMO}_{\text{enophile}}$ interaction 10.1,⁴ similar to $\text{HOMO}_{\text{diene}}/\text{LUMO}_{\text{dienophile}}$ interaction in Diels–Alder reaction as shown in Fig. 10.4A. The HOMO of ene component originates from the linear combination of σ (C—H) and π (C=C) bonds (Fig. 10.4B). The interaction can occur in the π sense as the interacting σ and π orbitals are nearly parallel. The HOMO of ene component is ($\sigma-\pi$) 10.2, which has one node similar to a diene HOMO.

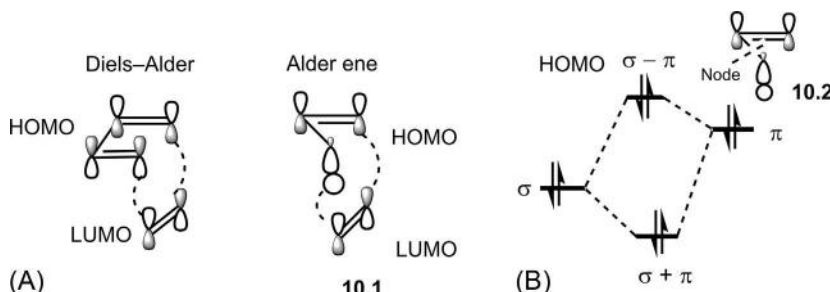


Fig. 10.4 (A) Frontier orbital picture of ene reaction in comparison to Diels–Alder reaction; (B) HOMO of ene component obtained by linear combination.

The all-carbon ene reaction requires a high temperature of 400°C or more. However, like Diels–Alder reaction, the ene reaction is facilitated by electron-withdrawing α -substituent on the enophile which lowers the energy of the LUMO. For example, 2-methylpropene undergoes the ene reaction with maleic anhydride at 170°C (Fig. 10.5).

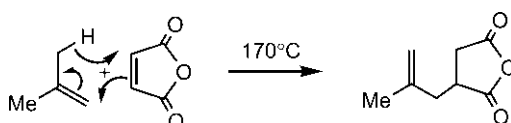


Fig. 10.5 Ene reaction with an activated enophile.

Further, a Lewis acid can catalyse the ene reaction by exerting its effect in further lowering the LUMO energy of the enophile, and the catalysed reactions proceed under relatively mild conditions.⁵

The regioselectivity of the ene reaction arises from the preferential formation of C—C σ bond between the more electron-rich alkene carbon

(large HOMO coefficient) of the ene component and the more electron-deficient β -carbon (large LUMO coefficient) of the enophile. The complexation of enophile with a Lewis acid further polarizes the enophile LUMO leading to an enhanced coefficient on the β carbon. This is illustrated with two examples in Fig. 10.6A and B.^{5,6} It is of note that the reaction under Lewis acid catalysis occurs at room temperature with complete regioselectivity (Fig. 10.6B). In this case, the alkene carbon β to two Me groups in the ene component is more electron rich (large HOMO coefficient).

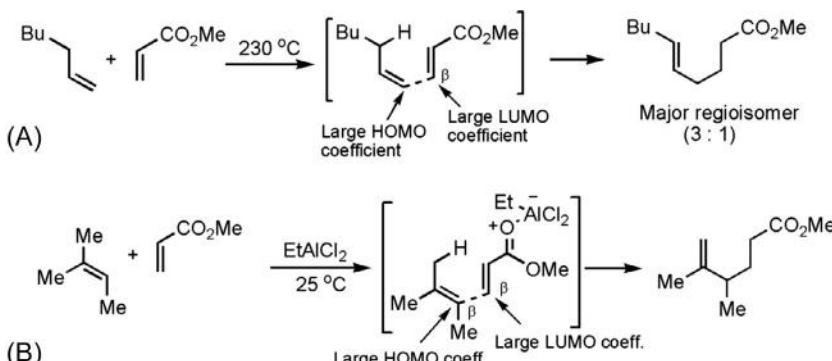
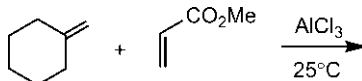


Fig. 10.6 Regioselectivity of ene reactions (A) without Lewis acid and (B) in the presence of Lewis acid.

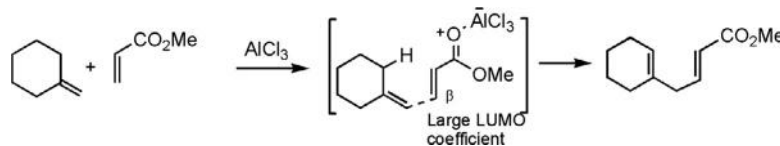
Problem 10.1

Predict the major product of the following ene reaction.



Answer

Under Lewis acid catalysis, the reaction is highly regioselective, and the major product is obtained via preferential formation of C—C bond with the enophile β -carbon having a large LUMO coefficient.



10.1.2 Stereochemistry of Ene Reactions

10.1.2.1 Stereospecificity

The ene reaction proceeds thermally when both the ene and enophile components are suprafacial (see Fig. 10.4A). The new C—H and C—C bonds are therefore formed on the same face of the enophile which gives stereospecificity of the reaction.^{7,8} This is illustrated with three examples in Fig. 10.7. In Fig. 10.7A, the new C—D and C—C bonds formed in the product are *cis*. In Fig. 10.7B, the *trans* D (not *cis* H) of β -pinene is transferred to the benzyne because the *cis* H transfer would involve severe steric interference by the β -pinene bridge.⁹ In Fig. 10.7C, the ene reaction leads to *cis* addition to the triple bond making the two ester groups *cis* in the adduct.

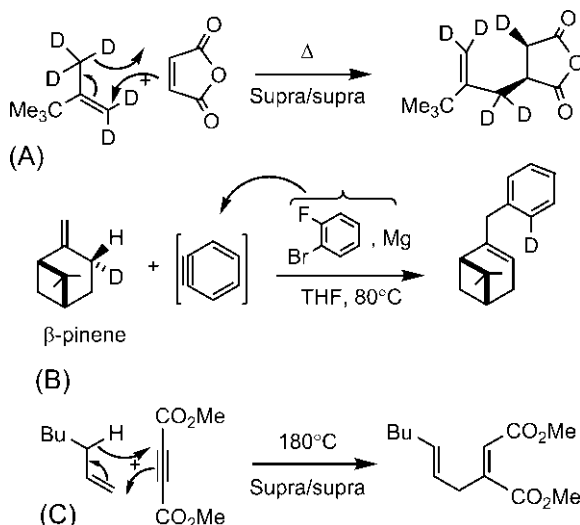


Fig. 10.7 Examples (A–C) of stereospecificity of ene reactions.

10.1.2.2 Stereoselectivity

The ene reaction takes place through an envelope transition structure (see Figs. 3.49 and 10.4). There are two possible envelope transition structures with the *z*-substituent of enophile being *endo* and *exo*, which can lead to a mixture of diastereomeric adducts. However, the ene reaction often leads to an *endo* adduct as a major product.¹⁰ There is a favourable secondary overlap of *z*-substituted enophile with the ene component in the *endo* TS. The ene reaction between (*Z*)-2-butene and maleic anhydride is shown in Fig. 10.8.¹¹ The reaction proceeds preferentially through *endo*-carbonyl TS leading to the major product **10.3** (*endo*:*exo* = 85:15). In this case, the

steric interference between the methyl and a carbonyl group also disfavours the *exo* TS.

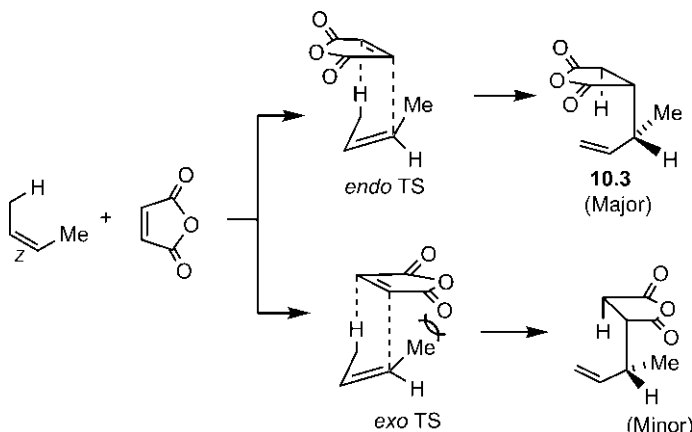
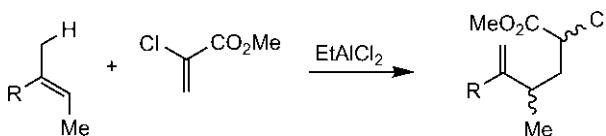


Fig. 10.8 Stereoselectivity of an ene reaction between (Z)-butene and maleic anhydride.

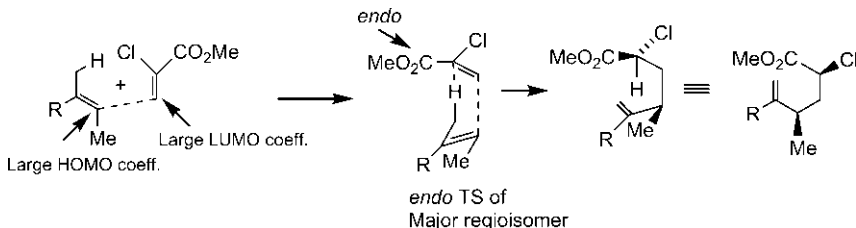
Problem 10.2

Predict the stereochemistry of the product in the following reaction. Also explain the observed regioselectivity.



Answer

Under Lewis acid catalysis, the ene reaction is highly regioselective and diastereoselective. The reaction produces two new stereocentres and the product stereochemistry arises from the preferred *endo*-CO₂Me TS.



10.1.3 Intramolecular Ene Reactions

The intramolecular ene reaction^{3,12,13} which has less negative entropy of activation compared with the intermolecular one can occur with both activated enophile bearing a α -substituent and unactivated enophile lacking a α -substituent. The ene reaction not only resembles Diels–Alder reaction but also shares some characteristics of [1,5] sigmatropic shift (Fig. 10.9A). Note the numbering system for ene reaction: for the ene component, the allylic carbon is labelled 1 and the numbering is continued to 3 while the enophile component is labelled by numbers 4 and 5. The new C–C bond is formed between atoms 3 and 4, and H is transferred from atom 1 to atom 5. The intramolecular ene reactions have been classified into six types^{10,14} of which Oppolzer's classification³ as Type I, Type II and Type III are shown in Fig. 10.9B. The classification is based on the positions of attachment of the ene and enophile components to the tether, which are indicated by the numbering system of [1,5] sigmatropic shift. For Type I, atom 3 of ene unit and atom 4 of enophile are attached to the tether, and is therefore (3,4). Similarly, Type II and Type III are (2,4) and (1,5), respectively. Note that in all types, new C–C bond is 3–4 and H transfer is from 1 to 5.

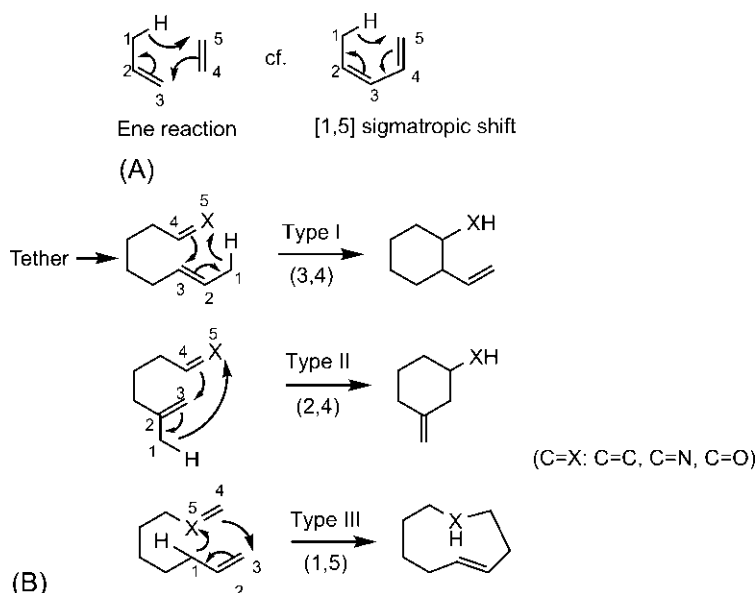


Fig. 10.9 (A) Similarity of ene reaction with [1,5] sigmatropic shift; (B) types of intramolecular ene reactions due to Oppolzer.³

In intramolecular ene reaction, the orbital interaction between the ene component and the enophile component is largely controlled by their geometrical constraints in the molecule. The geometrical constraints imposed by the tether often lead to highly stereoselective reactions. The Type I ene reactions are most common. An example is shown in Fig. 10.10.¹⁵ The reaction proceeds through the transition structure **10.4** governed by the short tether to give a *cis* cyclopentane. Across the new C—C bond being formed, both 3-H on the ene and 4-H on the enophile are down (also seen in an equivalent drawing of the TS **10.4'**.), that is, they are *cis* in the product. The product stereochemistry is also consistent with *Mnemonic 2* (see Fig. 5.7): 3-H(in)/4-H(exo) being *cis*. The TS is called *endo* with respect to the alkyl chain substituent attached to the enophile.

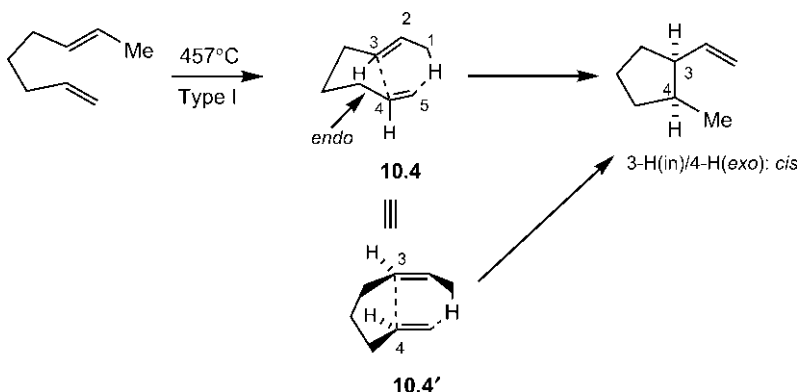


Fig. 10.10 Stereochemistry of an intramolecular ene reaction.

Fig. 10.11 shows another example in which the enophile bears an electron-withdrawing α -substituent and the reaction is a Lewis acid-catalysed reaction.

The stereochemistry of the product arises from the *cis*-decalin chair TS **10.5**. If the H on the six-membered ring in the substrate is up, the C—C bond formation and H transfer from the ene component will take place from the lower face of the enophile due to the short tether.

For Type II reaction, see Sections 10.1.4.4 and 10.1.4.5.

The Type III reactions are few. An example is the thermal equilibrium between 1,7-octadiene and (*Z*)-cyclooctene (Fig. 10.12).^{3,16}

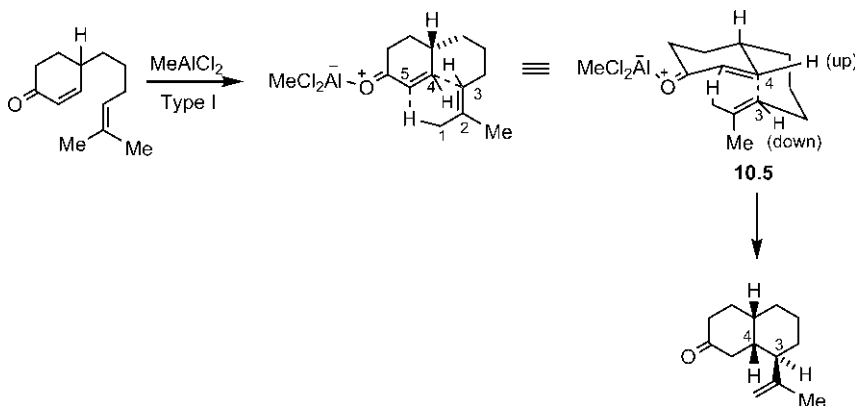


Fig. 10.11 Stereochemistry of a Lewis acid-catalysed intramolecular ene reaction.

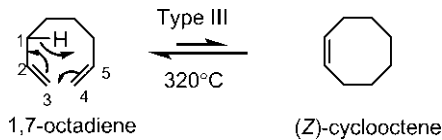


Fig. 10.12 A Type III intramolecular ene reaction.

10.1.4 Hetero-ene Reactions

10.1.4.1 Carbonyl Ene Reaction

The carbonyl ene reaction^{1,17} is more facile than all-carbon ene reaction as the carbonyl enophile has a low energy LUMO. Fig. 10.13 shows a carbonyl ene reaction with ethyl glyoxylate as a carbonyl enophile. This reaction is an efficient method for the synthesis of α -hydroxy esters. Here the ester group (α -substituent) on the enophile lowers the energy of the LUMO further and accelerates the reaction. The formation of aromatic ring in this case also provides the driving force for the reaction.

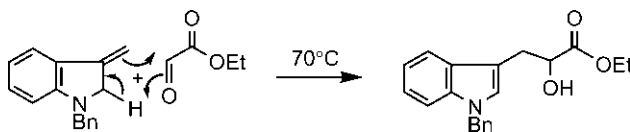


Fig. 10.13 Carbonyl ene reaction with ethyl glyoxylate to form α -hydroxy ester.

The carbonyl ene reaction can give high diastereoselectivity. For example, the reaction between (*Z*)-2-butene and methyl glyoxylate gives *anti*

diastereomer as a major product via the preferred *endo* TS (Fig. 10.14).¹⁸ Similarly, (*E*)-2-butene gives *syn* diastereomer as a major product (*syn:anti*=64:36).

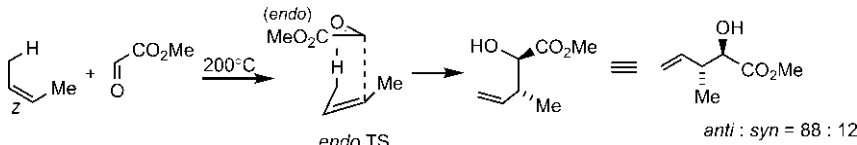


Fig. 10.14 Diastereoselectivity of a carbonyl ene reaction.

If the above reaction with (*Z*)-2-butene is carried out in the presence of a Lewis acid Me_2AlOTf , a reversal of stereoselectivity appears to occur yielding a *syn* isomer as a major product (*syn:anti*=91:9) (Fig. 10.15A). The aluminium reagent complexes with the carbonyl enophile as a monodentate ligand, and the stereochemical outcome can be rationalized on the basis of a chair-like TS.^{10,19} Note that Me is forced to be axial due to (*Z*) double bond. The more stable chair TS leads to a *syn* product. Interestingly, (*E*)-2-butene also gives a *syn* isomer as a major product (*syn:anti*=79:21) (Fig. 10.15B). Thus, with the aluminium reagent as Lewis catalyst, *syn* selectivity is irrespective of the ene stereochemistry.

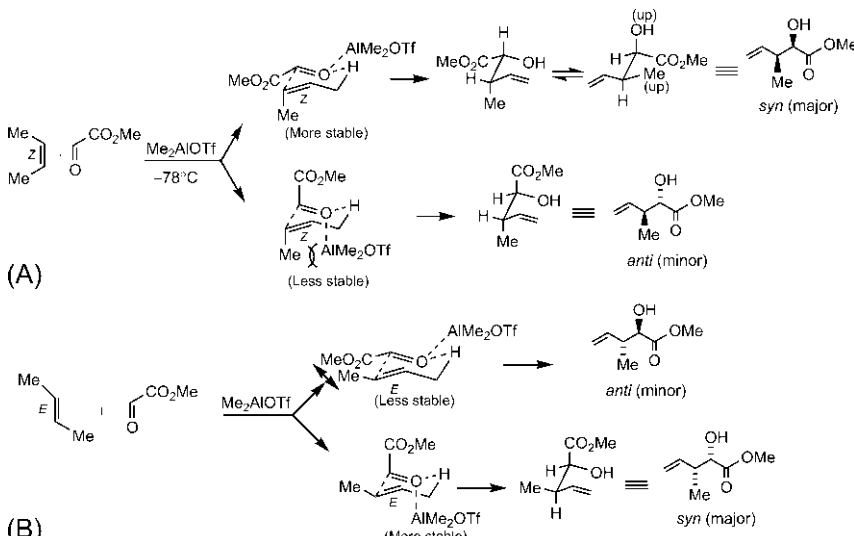


Fig. 10.15 *Syn* selectivity of Lewis acid (AlI_3)-catalysed carbonyl ene reaction with (A) (*Z*)-2-butene and (B) (*E*)-2-butene.

An intramolecular Lewis acid-catalysed carbonyl ene reaction is a key step in the synthesis of (*-*)-menthol from (*R*)-citronellal (Fig. 10.16).²⁰

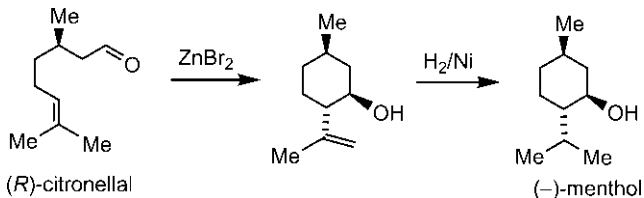


Fig. 10.16 Synthesis of (*-*)-menthol from (*R*)-citronellal.

The stereochemistry of this Type I intramolecular carbonyl ene reaction results from an all-chair bicyclic TS (cf. *trans*-decalin) with methyl group in less-hindered equatorial position as shown in Fig. 10.17.

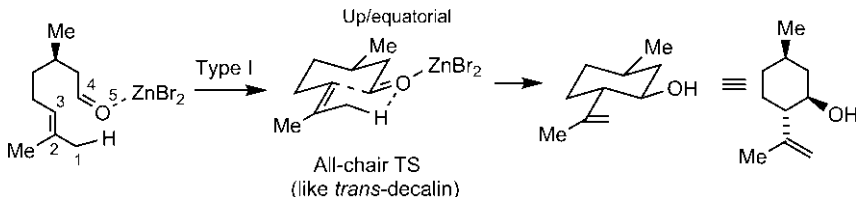


Fig. 10.17 Mechanism of intramolecular carbonyl ene reaction in Fig. 10.16.

10.1.4.2 Imino-ene Reaction

The imino-ene reaction is very facile with the imine enophile bearing a α -substituent. The reaction can also be catalysed by Lewis acid. For example, an N-tosyl imine (obtained from the corresponding glyoxylic ester) reacts readily with an alkene in the presence of a Lewis acid to give a homoallylic amine **10.6** (Fig. 10.18).²¹ The reaction is synthetically useful as the adduct can be easily converted into a γ,δ -unsaturated α -amino acid **10.7**.

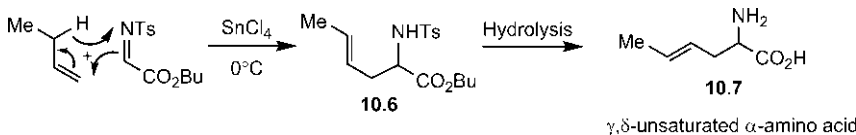


Fig. 10.18 Imino-ene reaction with a synthetic use.

The imino-ene reaction is also stereoselective via the preferred *endo* TS.^{22,23} Fig. 10.19 shows two examples of stereoselective imino-ene reaction with respect to an intermolecular reaction (Fig. 10.19A) and a Type

I intramolecular reaction (Fig. 10.19B).^{24,25} Note that the product stereochemistry is delineated using *Mnemonic 2*.

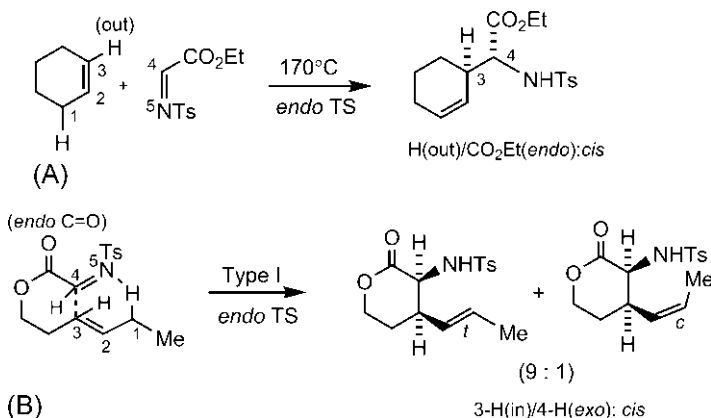


Fig. 10.19 Stereoselectivity of imino-ene reaction with respect to (A) an intermolecular reaction, and (B) a Type I intramolecular reaction.

10.1.4.3 Singlet Oxygen Ene Reaction

The singlet oxygen (see Fig. 4.83) can act as a heteroenophile in ene reaction to give allyl hydroperoxide which can be usefully reduced to allylic alcohol.^{26,27} The stereochemistry of the singlet oxygen ene reaction follows from the suprafacial addition of singlet oxygen to the ene component. This is illustrated with a *cis* substrate **10.8** (Fig. 10.20). When the allylic hydrogen of the ene is sterically hindered, as in the *trans* substrate **10.9**, the approach of the singlet oxygen is prevented and the reaction does not occur. However, like Diels–Alder reaction with singlet oxygen, the ene reaction also takes a highly asynchronous pathway, probably by way of a diradical.²⁸

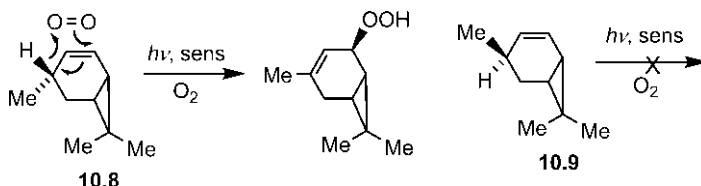
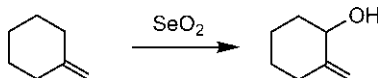


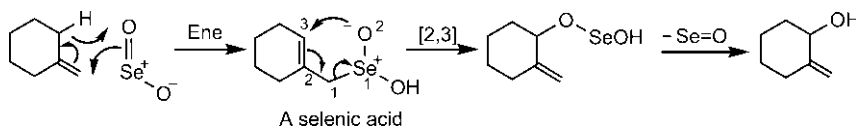
Fig. 10.20 Stereochemistry of singlet oxygen ene reaction.

Problem 10.3

Give a mechanism of the following SeO_2 oxidation of an alkene to an allylic alcohol. Identify the pericyclic steps involved.

**Answer**

SeO_2 hydroxylates an alkene at the allylic position. The reaction involves two pericyclic steps: a hetero-ene reaction followed by a [2,3] sigmatropic rearrangement. The hetero-ene reaction involves $\text{Se}=\text{O}$ unit of SeO_2 as a heteroenophile and produces an intermediate selenic acid which then undergoes [2,3] sigmatropic rearrangement to give a second intermediate that yields the allylic alcohol on cleavage of the $\text{Se}-\text{O}$ bond either in situ or on workup.

**10.1.4.4 Conia Reaction**

The Conia reaction involves a heteroene component which is an enol of a carbonyl compound. (In comparison, a carbonyl group itself is a heteroenophile in carbonyl ene reaction.) The intramolecular Conia reaction is most useful. An example is a synthesis of camphor from dihydrocarvone (Fig. 10.21).²⁹ The dihydrocarvone tautomerizes to enol form which undergoes a Type II intramolecular ene reaction via boat conformation to give camphor.

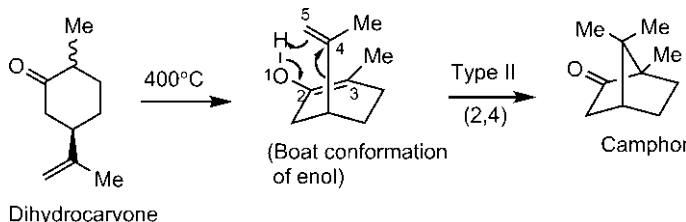


Fig. 10.21 Synthesis of camphor from dihydrocarvone via Conia reaction.

The Conia reaction can proceed under milder conditions with a suitable enolate. For example, the zinc enolate of an ester produces a pyrrolidine at room temperature (Fig. 10.22).³⁰ This is a Type I intramolecular reaction and proceeds through an envelope TS. The stereochemistry of the pyrrolidine product is *cis* (cf. Fig. 10.10). The use of *Mnemonic 2* is also shown.

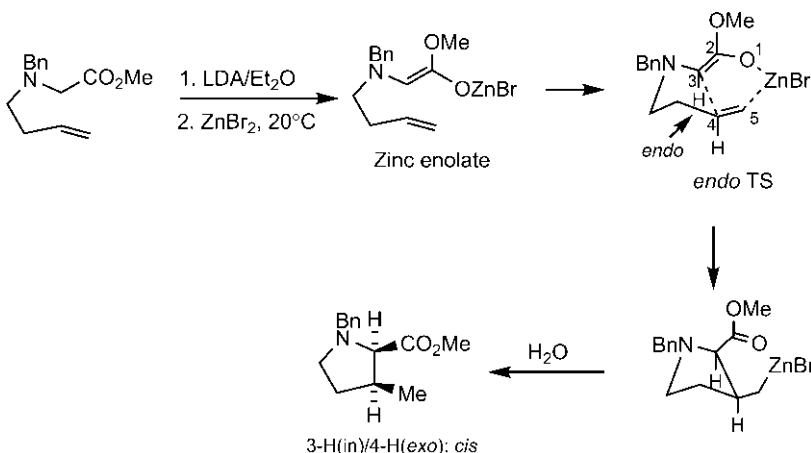
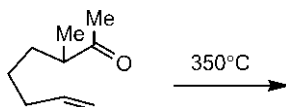


Fig. 10.22 Stereochemistry of a Type I intramolecular Conia reaction with zinc enolate.

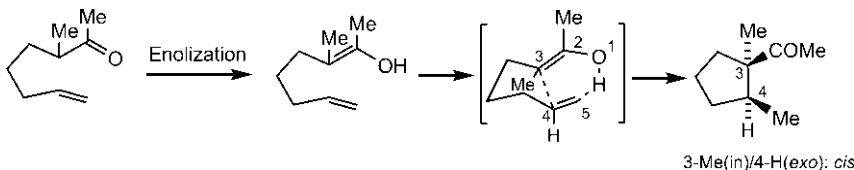
Problem 10.4

Predict the product with stereochemistry of the following reaction.



Answer

This is a Type I intramolecular Conia reaction which proceeds through *endo* TS to give the product.



10.1.4.5 Metallocene Reaction

The ene component of metallocene reaction³¹ is an allylic metal reagent. For example, an allylic Grignard reagent can undergo ene reaction with an alkene enophile to give a new alkene after workup (Fig. 10.23).³² Note the regioselectivity of the reaction.

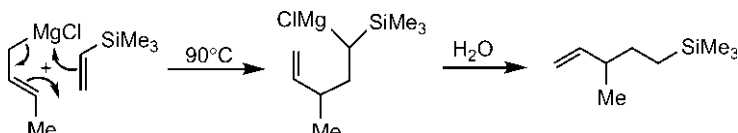


Fig. 10.23 Metallocene reaction with allylic Grignard reagent.

Intramolecular metallocene reactions³³ are more important than intermolecular ones, particularly in natural product synthesis. In Type I metallocene reaction,³⁴ the ease of ring formation is: $5 > 6 \gg 7$. The preferred stereochemistry of a five-membered ring product is *cis* which results from the *endo* envelope TS, as obtained in other Type I reactions (cf. Fig. 10.10). Type I metallocene reactions are very useful in the synthesis of natural products.³³ An example is shown in Fig. 10.24 with respect to a synthesis of the sesquiterpene capnellene.

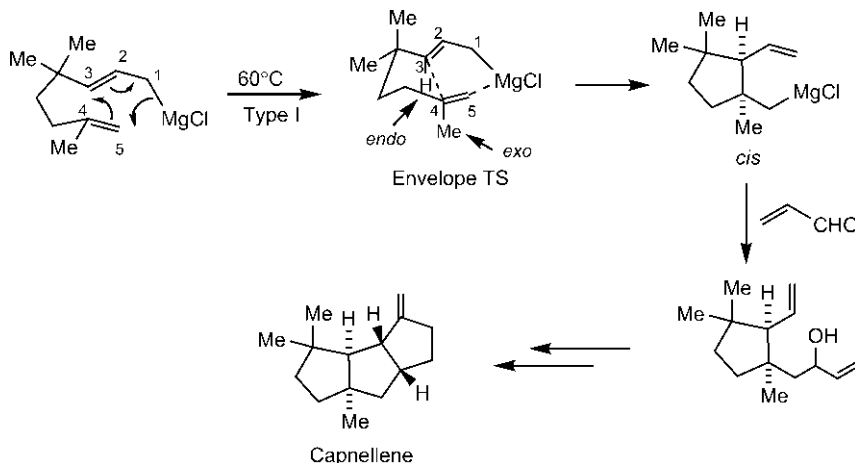


Fig. 10.24 Type I metallocene reaction involved in the synthesis of capnellene.

The scheme shown in Fig. 10.25 involves a Type II metallocene reaction. The ease of ring formation in Type II reaction is: $6 > 5 \approx 7$. The

preferred stereochemistry of the six-membered ring product is *cis* which arises from a bridged bicyclic chair TS **10.10**.

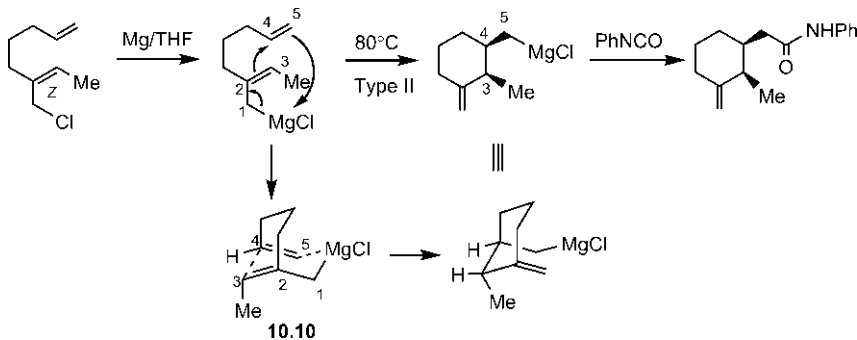


Fig. 10.25 Stereochemistry of Type II metallo-ene reaction.

An example of Type II metallo-ene reaction as a key step in the synthesis of natural product khusimone is shown in [Fig. 10.26](#).³⁵

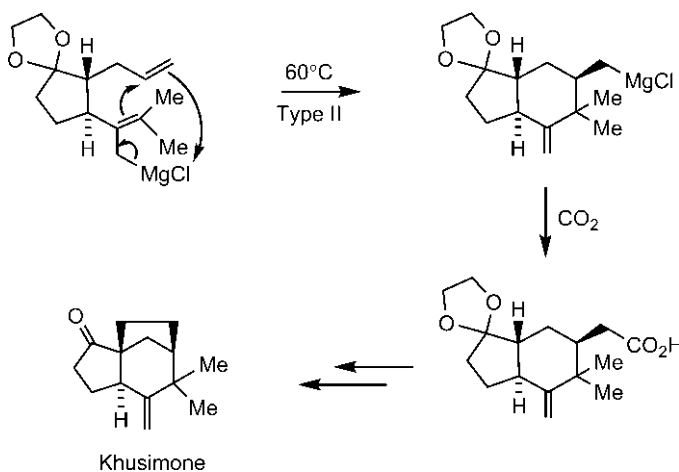


Fig. 10.26 Synthesis of khusimone via Type II metallo-ene reaction.

The diastereoselectivity of the reaction can be explained in terms of more stable TS in which the chair conformation experiences the least steric interaction ([Fig. 10.27](#)). Note that the other less stable TS suffers from severe flagpole interaction of a boat conformation.

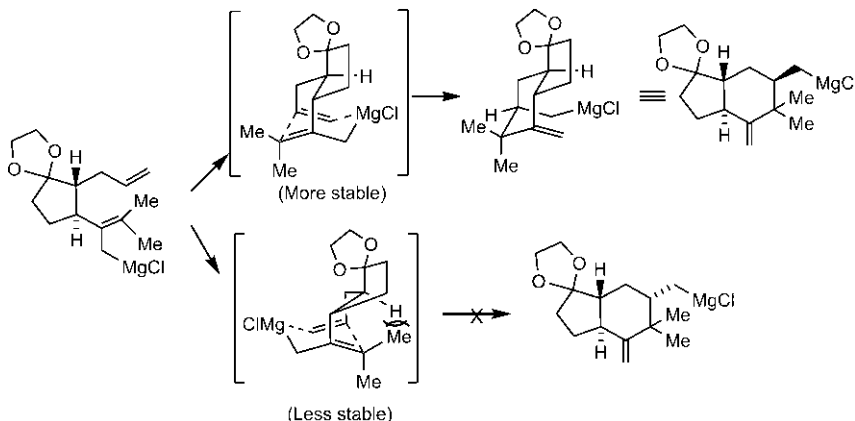


Fig. 10.27 Mechanism of the Type II metallo-ene reaction in Fig. 10.26.

10.1.5 Asymmetric Ene Reactions

We shall briefly describe here the asymmetric version of the ene reaction using chiral Lewis acid catalysts.^{10,36} The chiral catalyst is a metal–chiral ligand complex. The carbonyl ene reaction is particularly efficient for such asymmetric synthesis.

First, we consider a chiral catalyst which is a 2,2'-binaphthol (BINOL) complex of titanium(IV) salt.^{37,38} The catalyst is formed *in situ* from enantiomerically pure (*R*)- or (*S*)-BINOL (for descriptor, see Fig. 2.21, p. 55) and $\text{TiBr}_2(\text{O}i\text{-Pr})_2$. An asymmetric carbonyl ene reaction using methyl glyoxylate is shown in Fig. 10.28.¹⁰ The product is a homoallylic alcohol with high enantiomeric purity (ee 98%). The use of molecular sieves facilitates the alkoxy-ligand exchange for the formation of metal-BINOL catalyst complex.

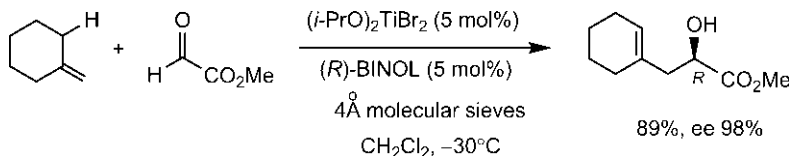


Fig. 10.28 Asymmetric carbonyl ene reaction using (*R*)-BINOL-Ti catalyst.

The enantioselectivity of the reaction can be explained in terms of a model shown in Fig. 10.29.³⁹ The catalyst–enophile complex **10.11** is formed by the coordination of aldehyde oxygen lone pair (*syn* to aldehyde H) to titanium and H...O hydrogen bonding between aldehyde H and

stereoelectronically favourable O of the (*R*)-BINOL ligand. The complex **10.11** has a pentacoordinate trigonal bipyramidal titanium structure. The attack of ene takes place preferentially on the more sterically accessible top (*re*) face of carbonyl enophile (the bottom face being sterically shielded by neighbouring naphthol moiety) to give the (*R*) enantiomer of the product.

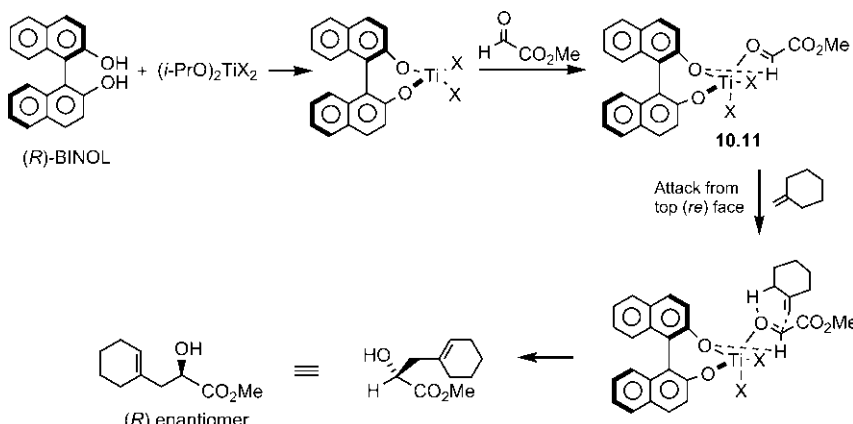


Fig. 10.29 A mechanistic model for asymmetric ene reaction in Fig. 10.28.

As both (*R*)- and (*S*)-BINOL are available in optically pure form, the asymmetric reaction can be used to synthesize each enantiomer of α -hydroxy ester product. Remarkably, this asymmetric glyoxylate-ene reaction exhibits a positive nonlinear effect⁴⁰ wherein the enantioselectivity far exceeds the optical purity of the BINOL. This is attributed to the aggregation of the catalyst. For example, an asymmetric reaction using BINOL of ee 33% gives the ene product with ee 91.4%

Next, we consider a box catalyst, the copper(II) complex of chiral bis-oxazolines **5.21** (see p.219) employed in asymmetric carbonyl ene reaction.⁴¹ An example is shown in Fig. 10.30.

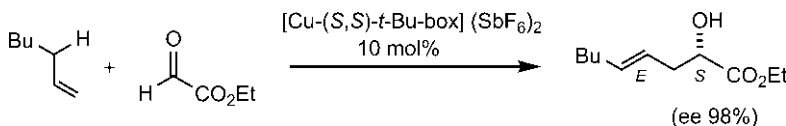


Fig. 10.30 Asymmetric carbonyl ene reaction using a box catalyst.

Here, the two carbonyl groups of the glyoxylate could chelate with the copper forming a well-defined catalyst–enophile complex of square–planar

geometry **10.12** (Fig. 10.31).⁴² The alkene would attack from the bottom face (*si*) of the aldehydic carbonyl enophile (top face being sterically shielded by bulky *t*-Bu group) to give the (*S*) enantiomer of the product. The major diastereomeric product is the more stable (*E*) isomer (*E*:*Z*=96:4).

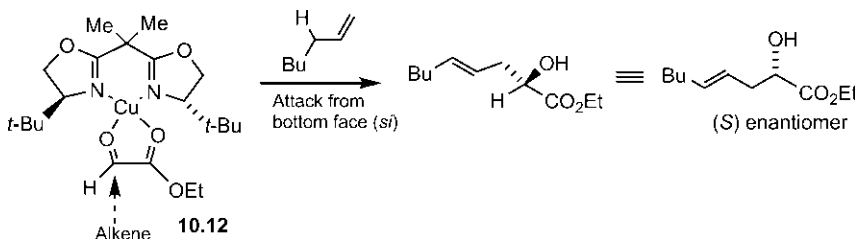


Fig. 10.31 Mechanism of asymmetric carbonyl ene reaction in Fig. 10.30.

10.1.6 Retro-ene Reactions

In retro-ene reaction (Fig. 10.32), a π bond is formed at the expense of a σ bond.

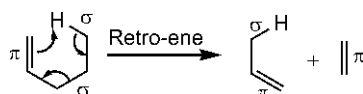


Fig. 10.32 The retro-ene reaction.

However, the reaction is partly driven by the gain in entropy (two species are formed from one species). Further, at the higher temperature needed for retro-ene reaction, the entropic contribution becomes more significant ($\Delta G^\circ = \Delta H^\circ - T\Delta S^\circ$). If the breaking σ bond is weak, the enthalpy factor also contributes to drive the reaction.

The retro-ene reactions are common when the substrate chain contains heteroatom(s), as shown in Fig. 10.33 for pyrolysis of esters and xanthates. The ester pyrolysis requires rather high temperatures (300–500°C) whereas the pyrolysis of xanthate (Chugaev reaction) can be carried out under relatively mild conditions at temperatures of 150–250°C. The reactions proceed by cyclic 1,2-(β -) elimination to give the alkene product. This type of 1,2-elimination is stereospecifically *syn* as the retro-ene reaction is thermally allowed as an all-supra [$\sigma_2s + \sigma_2s + \pi_2s$] process. As shown in Fig. 10.33A, an *erythro* isomer of acetate ester gives mainly a mixture of (*Z*)-butene (undeuterated) and (*E*)-butene (deuterated), each arising from the *syn* elimination.⁴³ The Chugaev reaction (Fig. 10.33B) yields two products from the

elimination of two alternative β hydrogens. The energy gained in the formation of stronger C=O bond at the expense of weaker C=S bond makes the Chugaev reaction more favourable requiring a lower temperature.

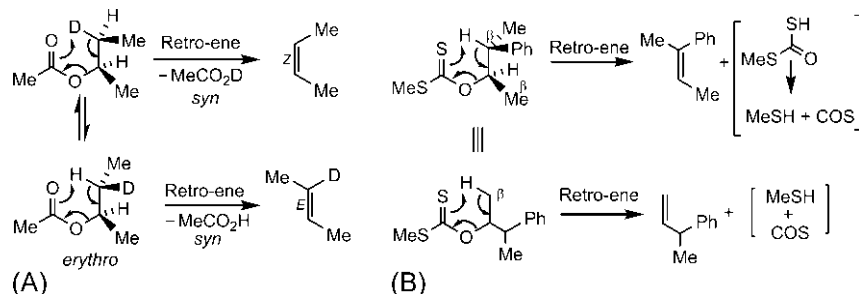


Fig. 10.33 (A) Pyrolysis of an ester and (B) pyrolysis of a xanthate (Chugaev reaction).

The well-known decarboxylation of β -keto acid is another example of retro-ene reaction. The product is an enol which rapidly tautomerizes to carbonyl compound (Fig. 10.34).

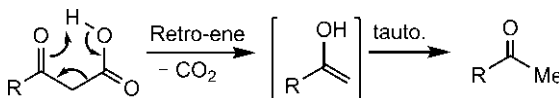
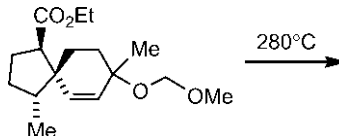


Fig. 10.34 Decarboxylation of β -keto acid through retro-ene reaction.

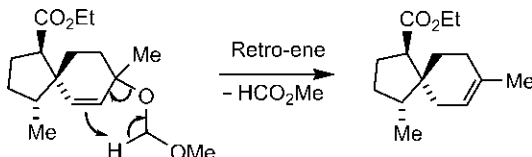
Problem 10.5

Predict the product of the following reaction.



Answer

The pyrolysis of the allylic ether involves a retro-ene reaction, and gives the product by eliminating methyl formate.



The relief of ring strain also favours the retro-ene process (Fig. 10.35A). Two examples showing hydrogen transfer from carbon to carbon and carbon to oxygen are shown in Fig. 10.35B.³ In the conversion of a carene into a menthadiene, an efficient chirality transfer is observed.⁴⁴

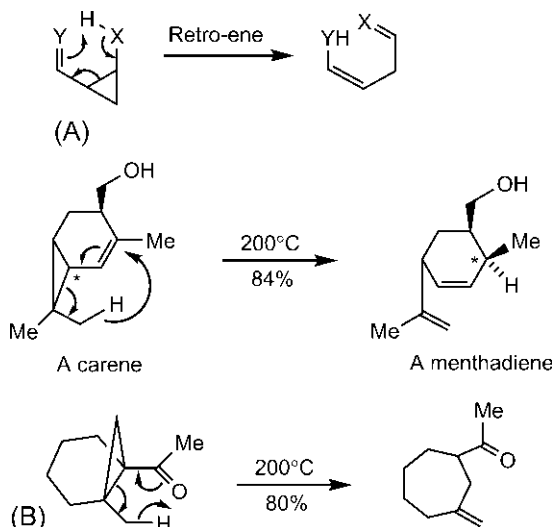


Fig. 10.35 (A) Ring strain effect favouring a retro-ene reaction. (B) Examples of retro-ene reactions favoured by ring strain effects.

10.1.6.1 1,2-Dipolar Retro-ene Reactions

In retro-ene reactions described above, six atoms (including H) are involved and two σ bonds and one π bond mobilize 6 electrons. There are also some important retro-ene reactions which involve a chain of five atoms (including H), when two σ bonds and a lone pair (ω electrons) provide 6 electrons. The substrates in such cases are 1,2-dipoles, usually oxides (N-oxide, sulphoxide or selenoxide) or ylides such as sulphur ylide, which undergo 1,2-elimination. In this text, the cycloelimination of 1,2-dipolar substrates is referred to as 1,2-dipolar retro-ene reaction. A general scheme and the orbital representation of the reaction are shown in Fig. 10.36. As shown, the reaction is a thermally allowed all-supra [$\sigma 2_s + \sigma 2_s + \omega 2_s$] process. Both retro-ene and 1,2-dipolar retro-ene reactions belong to retro group transfer reactions.

The 1,2-dipolar retro-ene reactions are favoured by entropy, charge neutralization and breaking of a weak σ bond ($C-X^+$) and occur at a much

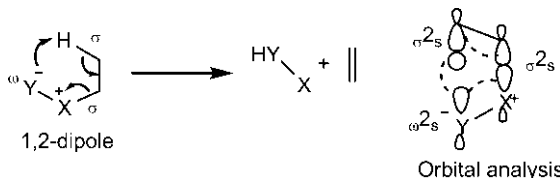


Fig. 10.36 General scheme and orbital representation of 1,2-dipolar retro-ene reaction.

lower temperature. Owing to all-supra mode, the dipolar retro-ene reaction is *syn* stereospecific which is illustrated with an amine oxide (Cope elimination) and a sulphoxide in Fig. 10.37.⁴⁵

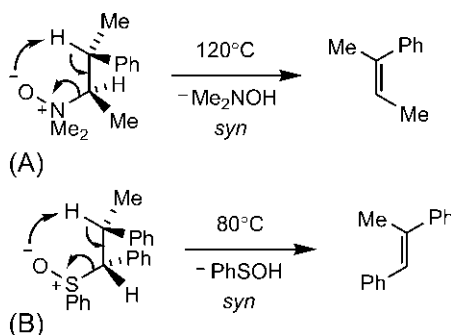


Fig. 10.37 (A) Cope elimination of an amine oxide, and (B) 1,2-cycloelimination of a sulphoxide.

The 1,2-cycloelimination with a selenoxide occurs at room temperature which is used for the synthesis of α,β -unsaturated ketone starting from a ketone (Fig. 10.38).⁴⁶

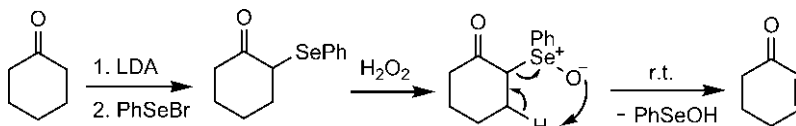
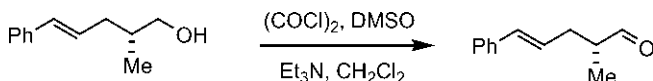


Fig. 10.38 Synthesis of α,β -unsaturated ketone via selenoxide elimination.

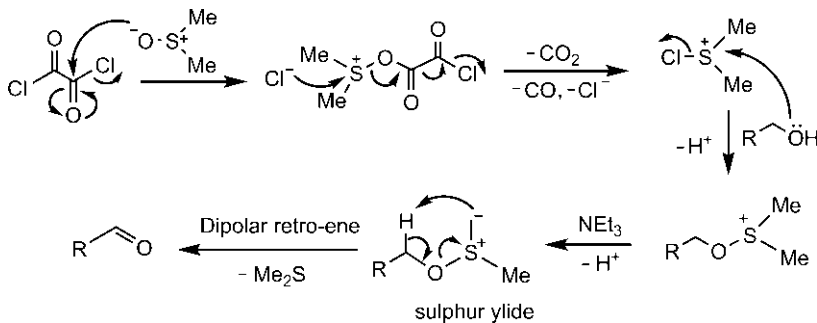
Problem 10.6

Give the mechanism of the following Swern oxidation and identify the pericyclic step involved.



Answer

The reaction of DMSO with oxalyl chloride forms an active species to which the alcohol is added. The nucleophilic attack of the alcohol on the active species followed by deprotonation with NEt_3 gives a sulphur ylide. The final step is pericyclic when the sulphur ylide undergoes a 1,2-dipolar retro-ene reaction to form the aldehyde.



10.1.7 Ene/Retro-ene Sequence in Synthesis and Rearrangement

A sequence of ene and retro-ene reactions is quite useful in synthesis.⁴⁷ For example, β -pinene can be deuterated in a stereospecific manner as shown in Fig. 10.39.⁹ The deuterium transfer takes place from the side opposite to the bridge.

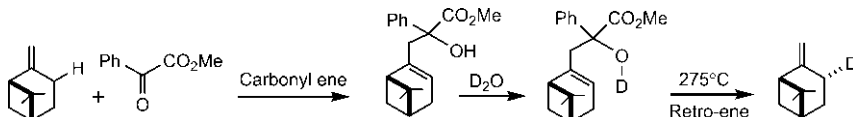


Fig. 10.39 Stereospecific deuteration of β -pinene using ene and retro-ene reactions.

Isotopically labelled chiral acetic acid is a useful reagent in mechanistic studies of enzyme-catalysed reactions. Starting from an (*R*)-alcohol **10.14**, a synthesis of enantiopure isotopically labelled (*R*)-acetic acid **10.15** can be accomplished via ene/retro-ene sequence (Fig. 10.40).⁴⁸ The intramolecular ene reaction involving suprafacial transfer of H atom gives (*Z*) stereochemistry of the T-labelled double bond, and the subsequent retro-ene reaction leads to *syn* transfer of D.

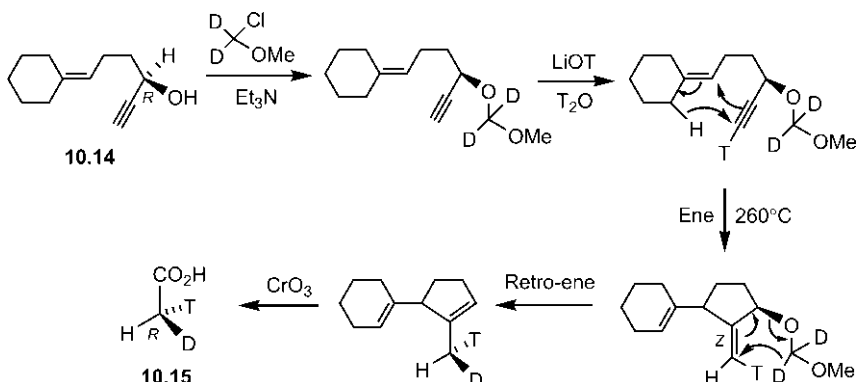


Fig. 10.40 Synthesis of deuterium and tritium labelled (R)-acetic acid via ene/retro-ene sequence.

An aromatic Claisen rearrangement of an allyl vinyl ether **10.13** is shown in Fig. 10.41. Besides the normal [3,3] Claisen product, an abnormal rearranged product is obtained.

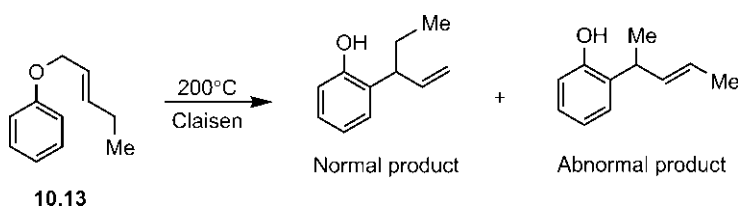


Fig. 10.41 Formation of an abnormal product in aromatic Claisen rearrangement.

The abnormal product is believed to be formed from the normal product via ene/retro-ene sequence as shown in Fig. 10.42.⁴⁹ The ene reaction produces an unstable intermediate which can undergo retro-ene reaction to either revert to the normal product or to give the abnormal product.

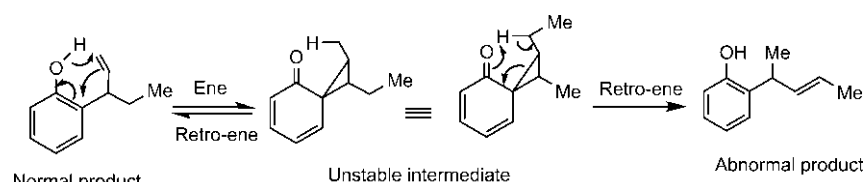
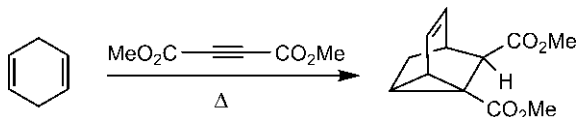


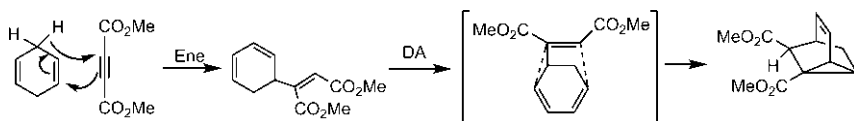
Fig. 10.42 Mechanism of formation of abnormal product in Fig. 10.41.

Problem 10.7

Explain the formation of product in the following reaction.

**Answer⁵⁰**

Cyclohexa-1,4-diene is a nonconjugated diene and cannot undergo Diels–Alder reaction with dimethyl acetylenedicarboxylate (DMAD). An ene reaction produces a conjugated diene which then undergoes an intramolecular Diels–Alder reaction to give the product.



10.2 DIIMIDE REDUCTION AND RELATED REACTIONS

Diimide is usually generated *in situ* either by the oxidation of hydrazine or by didecarboxylation of potassium azodicarboxylate (Fig. 10.43).⁵¹

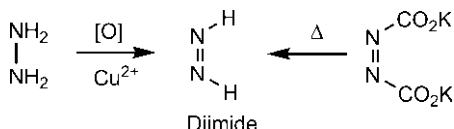


Fig. 10.43 Generation of diimide.

The reduction of alkenes or alkynes by diimide is *syn* stereospecific in an all-supra [$\sigma_{2s} + \sigma_{2s} + \pi_{2s}$] process (see Fig. 3.50, p. 104). The stereospecificity of diimide reduction is illustrated with two examples in Fig. 10.44.^{52,53} The reaction is driven by the formation and loss of a stable N₂ molecule.

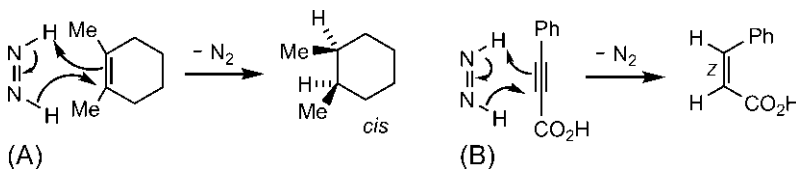


Fig. 10.44 Stereospecificity of diimide reduction with (A) an alkene and (B) an alkyne.

The *syn* hydrogenation by diimide is similar to catalytic hydrogenation; however, while hydrogenation catalysts are poisoned by sulphur compounds, diimide is not. The concerted diimide reduction is more selective for the symmetrical homonuclear C=C double bond over the heteronuclear C=O double bond. It also preferentially reduces the least conjugated double bond as shown in Fig. 10.45.⁵⁴

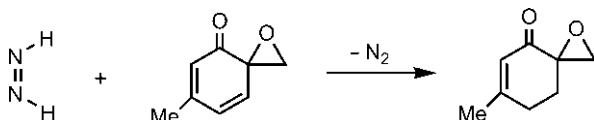


Fig. 10.45 Chemoselectivity of diimide reduction.

Similar to diimide, the pericyclic *syn* delivery of two hydrogens from the dihydroaromatic compound *cis*-9,10-dihydronaphthalene is known (Fig. 10.46).⁵⁵ The formation of aromatic naphthalene provides the driving force for the reaction.

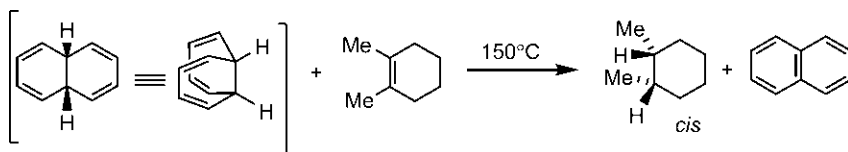


Fig. 10.46 *syn* Hydrogenation by *cis*-9,10-dihydronaphthalene.

Intramolecular *syn* transfer of two hydrogens can also take place in a suitable rigid bicyclic system as shown in Fig. 10.47.⁵⁶ This type of process in which two σ bonds simultaneously migrate intramolecularly is called dyotropic rearrangement.

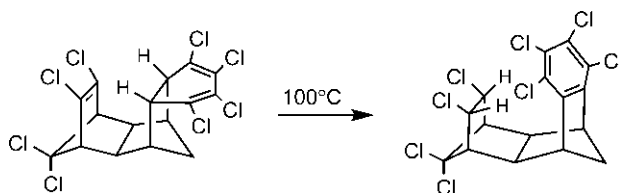


Fig. 10.47 A dyotropic rearrangement involving *syn* transfer of two hydrogens.

10.3 1,4-CYCLOELIMINATIONS

The 1,4-cycloelimination is a retro group transfer reaction, quite distinct from a retro-ene reaction which is a 1,2-cycloelimination. The 1,4-cycloelimination is thermally allowed as an all-supra $[\sigma_2s + \pi 2s + \sigma 2s]$ process (see Fig. 3.51, p. 104). The reaction is thus stereospecifically *syn* involving 1,4-elimination of two *syn* groups. This is illustrated with two examples in Fig. 10.48. Note that the numbers 1 and 4 denote the relative positions of the two groups being eliminated.

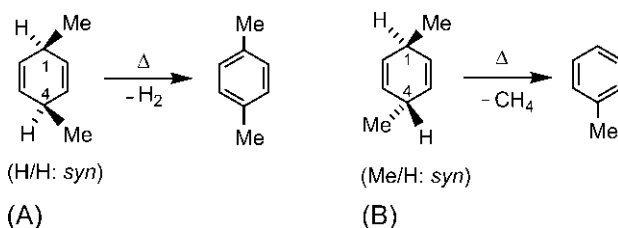


Fig. 10.48 syn Stereospecificity of 1,4-cycloelimination in (A) *cis*- and (B) *trans*-3,6-dimethylcyclohexa-1,4-diene.

The clear evidence of the concerted *syn* elimination comes from the pyrolysis of *trans*-3,6-dideuteriocyclohexa-1,4-diene **10.16** which eliminates HD to give monodeuteriobenzene (benzene-d₁) via boat TS (Fig. 10.49).⁵⁷

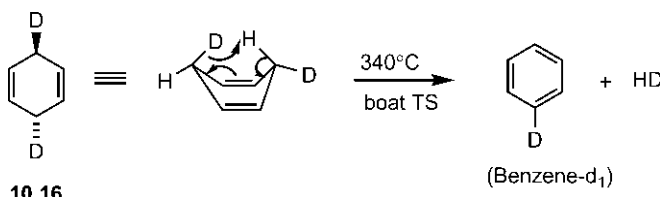


Fig. 10.49 Stereospecific *syn* 1,4-cycloelimination of *trans*-3,6-dideuteriocyclohexa-1,4-diene

In contrast, *cis*-5,6-dideuteriocyclohexa-1,3-diene **10.17** on pyrolysis produces a mixture of benzene, benzene-d₁ and benzene-d₂ (major) (Fig. 10.50). Since the concerted 4-electron $[\sigma_{2s}^2 + \sigma_{2s}^2]$ process **10.18** is thermally forbidden, the reaction proceeds through radical pathway to give a mixture of products. Since C—D bond is stronger than C—H bond, homolytic cleavage of C—H bond occurs more easily resulting in benzene-d₂ as a major product.

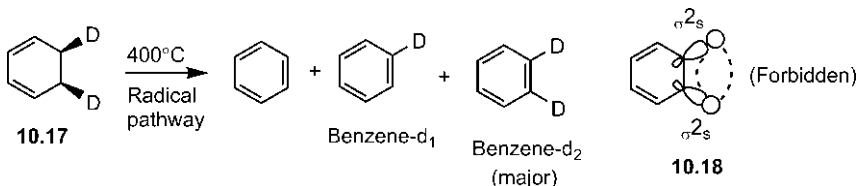


Fig. 10.50 Nonstereospecific 1,2-elimination of *cis*-5,6-dideuteriocyclohexa-1,3-diene.

A synthesis of *trans*-3,6-dideuteriocyclohexa-1,4-diene **10.16** starting from cyclooctatetraene is shown in Fig. 10.51.⁵⁷ The addition of D₂ occurs on the least hindered unconjugated double bond.

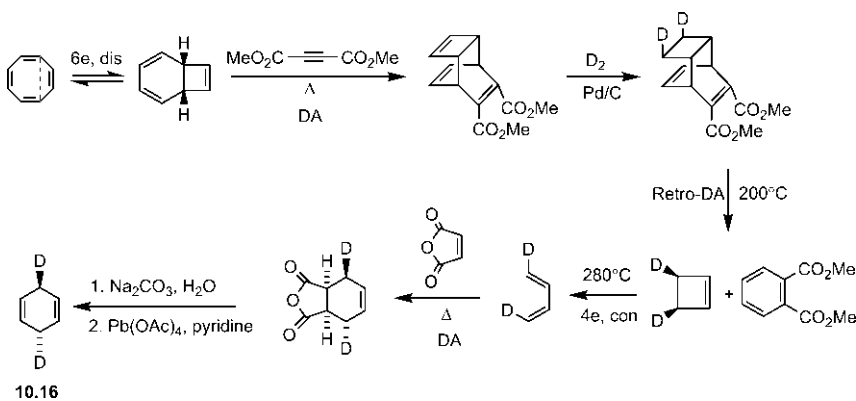


Fig. 10.51 A synthesis of *trans*-3,6-dideuteriocyclohexa-1,4-diene.

We shall end this chapter with a reaction between cycloheptatriene and DMAD in which a potpourri of all four classes of pericyclic processes is involved (Fig. 10.52).

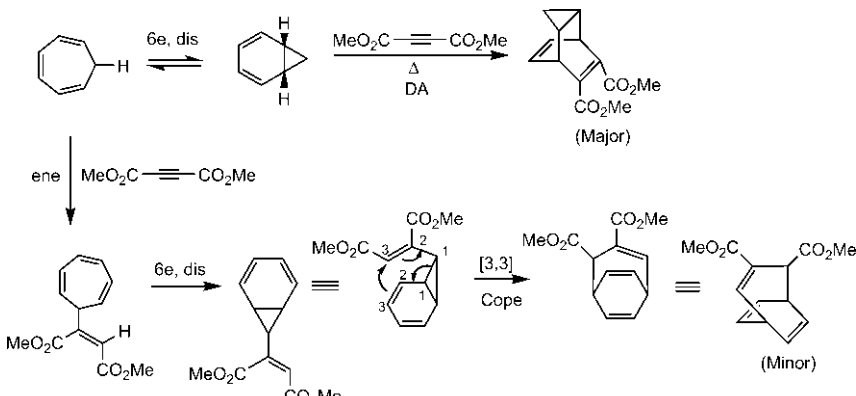


Fig. 10.52 Reaction between cycloheptatriene and dimethyl acetylenedicarboxylate.

The major product arises from electrocyclic ring closing of cycloheptatriene followed by a Diels–Alder reaction with DMAD, and the minor product is formed by ene reaction of cycloheptatriene with DMAD followed by electrocyclic ring closing and [3,3] Cope rearrangement.

REFERENCES

- Snider, B. B. In: *Comprehensive Organic Synthesis*; Trost, B. M.; Fleming, I., Eds.; Vol. 5; Pergamon Press: Oxford, 1991; p 1.
- Hoffmann, H. M. R. *Angew. Chem. Int. Ed. Eng.* **1969**, *8*, 556.
- Oppolzer, W.; Snieckus, V. *Angew. Chem. Int. Ed. Eng.* **1978**, *17*, 476.
- Pederes, G. D.; Jorgensen, W. L. *J. Org. Chem.* **1992**, *57*, 1904.
- Snider, B. B. *Acc. Chem. Res.* **1980**, *13*, 426.
- Alder, K.; von Brachel, H. *Justus Liebigs Ann. Chem.* **1962**, *651*, 141.
- Friedrich, L. E.; Kampmeier, J. A.; Good, M. *Tetrahedron Lett.* **1971**, 2783.
- Stephenson, L. M.; Mattern, D. L. *J. Org. Chem.* **1976**, *41*, 3614.
- Garsky, V.; Koster, D. F.; Arnold, R. T. *J. Am. Chem. Soc.* **1974**, *96*, 4207.
- Mikami, K.; Shimizu, M. *Chem. Rev.* **1992**, *92*, 1021.
- Berson, J. A.; Wahl, R. G.; Perlmutter, M. D. *J. Am. Chem. Soc.* **1966**, *88*, 187.
- Fujita, Y.; Suzuki, S.; Kanehira, K. *J. Synth. Org. Chem., Jpn.* **1983**, *41*, 1152.
- Taber, D. F. *Intramolecular Diels-Alder and Alder Ene Reactions*. Springer Verlag: Berlin, 1984.
- Mikami, K.; Sawa, E.; Terada, M. *Tetrahedron Asymmetry* **1991**, *2*, 1403.
- Huntsman, W. D.; Curry, T. H. *J. Am. Chem. Soc.* **1958**, *80*, 2252.
- Blomquist, A. T.; Taussig, P. R. *J. Am. Chem. Soc.* **1957**, *79*, 3505.
- Adams, D. R.; Bhatnagar, S. P. *Synthesis* **1977**, 661.
- Snider, B. B.; van Straten, J. W. *J. Org. Chem.* **1979**, *44*, 3567.
- Mikami, K.; Loh, T.-P.; Nakai, T. *Tetrahedron Lett.* **1988**, *29*, 6305.
- Nakatani, Y.; Kawashima, K. *Synthesis* **1978**, 147.
- Borzilleri, R. M.; Weinreb, S. M. *Synthesis* **1995**, 347.
- Achmatowicz, O.; Pietraszkiewicz, M. *J. Chem. Soc. Chem. Commun.* **1976**, *484*, *J. Chem. Soc., Perkin Trans 1* **1981**, 2680.
- Tschaen, D. M.; Turos, E.; Weinreb, S. M. *J. Org. Chem.* **1984**, *49*, 5058.
- Bussas, R.; Kresze, G. *Angew. Chem. Int. Ed. Eng.* **1980**, *19*, 732.
- Braxmeier, H.; Kresze, G. *Synthesis* **1985**, 683.
- Frimer, A. A. *Chem. Rev.* **1979**, *79*, 359.
- Stephenson, L. M.; Grdina, M. J.; Orfanopoulos, M. *Acc. Chem. Res.* **1980**, *13*, 419.
- Singleton, D. A.; Hang, C.; Syzmanski, M. J.; et al. *J. Am. Chem. Soc.* **2003**, *125*, 1319.
- Lange, G. L.; Conia, J. M. *Nouveau J. Chim.* **1977**, *1*, 189.
- Lorthiois, E.; Marek, I.; Normant, J. F. *J. Org. Chem.* **1998**, *63*, 2442.
- Lehmkuhl, H.; Reinehr, D. *J. Organomet. Chem.* **1970**, *25*, C47; **1972**, *34*, *1*; **1973**, *57*, 29.
- Lehmkuhl, H.; Hauschild, K.; Bellenbaum, M. *Chem. Ber.* **1984**, *117*, 383.
- Oppolzer, W. *Angew. Chem. Int. Ed. Eng.* **1989**, *28*, 38.
- Felkin, H.; Umpleby, J. D.; Hagaman, E.; Wenkert, E. *Tetrahedron Lett.* **1972**, 2285.
- Oppolzer, W.; Pitteloud, R.; Strauss, H. F. *J. Am. Chem. Soc.* **1982**, *104*, 6476.
- Dias, L. C. *Curr. Org. Chem.* **2000**, *4*, 305.
- Mikami, K.; Terada, M.; Nakai, T. *J. Am. Chem. Soc.* **1990**, *112*, 3949.
- Yuan, Y.; Zhang, X.; Ding, K. *Angew. Chem. Int. Ed. Eng.* **2003**, *42*, 5478.

39. Corey, E. J.; Barnes-Seeman, D.; Lee, T. W.; Goodman, S. N. *Tetrahedron Lett.* **1997**, *37*, 6513.
40. Girard, C.; Kagan, H. B. *Angew. Chem. Int. Ed. Eng.* **1998**, *37*, 2922.
41. Evans, D. A.; Tregay, S. W.; Burgey, C. S.; Paras, N. A.; Vojkovsky, T. J. *Am. Chem. Soc.* **2000**, *122*, 7936.
42. Johnson, J. S.; Evans, D. A. *Acc. Chem. Res.* **2000**, *33*, 325.
43. Skell, P. S.; Hall, W. L. *J. Am. Chem. Soc.* **1964**, *86*, 1557.
44. Ohloff, G. *Chem. Ber.* **1960**, *93*, 2673.
45. Saunders, W. H.; Cockerill, A. F. *Mechanisms of Elimination Reactions*. Wiley: New York, 1973;377.
46. Clive, D. L. J. *Tetrahedron* **1978**, *34*, 1049.
47. Ripoll, J.-L.; Vallee, Y. *Synthesis* **1993**, 659.
48. Townsend, C. A.; Scholl, T.; Arigoni, D. *J. Chem. Soc. Chem. Commun.* **1975**, 921.
49. Hansen, H. J. In: *Mechanisms of Molecular Migrations*; Thyagarajan, B. S., Ed.; Vol. 3; Interscience: New York, 1971; p 177.
50. Huebner, C. F.; Donoghue, E.; Dorfman, L.; Stuber, F. A.; Danieli, N.; Wenkert, E. *Tetrahedron Lett.* **1966**, 1185.
51. Paquette, L. A., Ed.; *Encyclopedia of Reagents for Organic Synthesis*; Vol. 3; Wiley: New York, 1995; p 1892.
52. Corey, E. J.; Mock, W. L.; Pasto, D. J. *Tetrahedron Lett.* **1961**, *11*, 347.
53. Corey, E. J.; Pasto, D. J.; Mock, W. L. *J. Am. Chem. Soc.* **1961**, *83*, 2957.
54. Corey, E. J.; Dittami, J. P. *J. Am. Chem. Soc.* **1985**, *107*, 256.
55. Doering, W.v.E.; Rosenthal, J. W. *J. Am. Chem. Soc.* **1967**, *89*, 4534.
56. Mackenzie, K.; Proctor, G.; Woodnutt, D. J. *Tetrahedron Lett.* **1984**, 977 *Tetrahedron* **1987**, *43*, 5981.
57. Fleming, I.; Wildsmith, E. *J. Chem. Soc. D* **1970**, 223.

CHAPTER 11

Correlation Diagrams

Of the three theoretical approaches advanced for pericyclic reactions (see [Section 3.3](#), p. 74), the orbital symmetry correlation approach^{1–5} is most rigorous, and provides an extremely insightful picture at the molecular level as to which specific reactant molecular orbital is transformed into which product molecular orbital. This picture of correlation of reactant orbitals with product orbitals is presented in a diagram called the orbital correlation diagram. The construction of the orbital correlation diagram is based on a basic premise of *conservation of orbital symmetry*, that is, orbital symmetry is conserved throughout in a concerted process. The orbital correlation clearly predicts which concerted process, under symmetry restrictions, is allowed (favoured) or forbidden (disfavoured). This is termed a symmetry-allowed or symmetry-forbidden reaction. The orbital correlation diagram is applicable to both ground state (thermal) and first excited singlet state (photochemical) processes.

Besides orbital correlation, there is another type of correlation diagram known as the state correlation diagram. The state correlation diagram is based on the state symmetries which are determined from the orbital symmetries. This diagram gives more insight into the energy barrier for the concerted reaction. If the reaction has a symmetry-imposed high-energy barrier, the concerted pathway is highly improbable. An alternative stepwise pathway then may or may not be accessible for the same reaction.

11.1 CONSERVATION OF ORBITAL SYMMETRY

Symmetry plays a pivotal role in the construction of correlation diagrams. Such construction requires that *one or more symmetry elements must persist* throughout the concerted pathway (reactant → TS → product). The wave functions representing molecular orbitals must be either *symmetric (S)* or *antisymmetric (A)* with respect to each persisting symmetry element. A molecular orbital is symmetric (S) if the symmetry operation moves an

orbital lobe to the position of a lobe of the same sign ('+' to '+', '−' to '−'). On the other hand, a molecular orbital is antisymmetric (**A**) if a lobe moves to the position of a lobe of the opposite sign by the operation ('+' to '−' or vice versa).

The principle of conservation of orbital symmetry stipulates that each reactant orbital is transformed into a product orbital of like symmetry. However, such linking of like symmetries is subject to the quantum mechanical *noncrossing rule* which states that levels of like symmetry cannot cross. The origin of the noncrossing rule is electron repulsion.

It is important to note that substituents may formally destroy the symmetry of the basic component(s) of a reaction but the effect of substituents is assumed to be negligible on the symmetry of the molecular orbitals undergoing change. In practice, a symmetry-based correlation using butadiene, for example, will also hold good for the substituted dienes.

11.2 CORRELATION DIAGRAM FOR ELECTROCYCLIC REACTIONS

To construct an orbital correlation diagram, we shall proceed in a practical 'how-to-do-it' manner. The sequence of steps as described below will lead to the correct orbital correlation diagram for an electrocyclic process. A similar step-by-step procedure will be used for setting up orbital correlation diagrams for other classes of pericyclic reactions.

Step 1. Draw the reaction and identify the symmetry element(s) preserved throughout the transformation. The symmetry element chosen must bisect bond(s) formed or broken.

Step 2. Draw an energy level diagram with reactant molecular orbitals on the left and product molecular orbitals on the right. Include all MOs associated with the bonds formed and broken.

Step 3. Sketch the molecular orbitals and classify them as symmetric (**S**) or antisymmetric (**A**) with respect to the persisting symmetry element(s).

Step 4. Invoke the principle of conservation of orbital symmetry to complete the orbital correlation diagram by drawing lines between orbitals of like symmetry (**S—S, A—A**), obeying noncrossing rule.

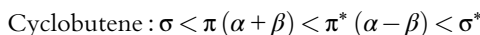
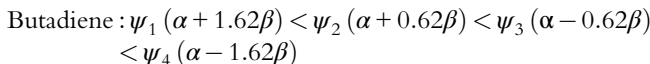
(The noncrossing rule stipulates that crossing of the lines **S—S** and **S—S** or crossing of **A—A** and **A—A** is not permitted; only crossing of **S—S** and **A—A** is permitted.)

11.2.1 Orbital Correlation Diagram for the Conrotatory Process

We begin with conrotatory interconversion of butadiene and cyclobutene.

Step 1. In the conrotatory ring closing (or ring opening), the persisting symmetry element is C_2 (Fig. 11.1). Notice that C_2 lies in the plane of the molecule. The C_2 symmetry is indeed a general feature of the conrotatory electrocyclic process.

Step 2. For the butadiene–cyclobutene interconversion, the relevant MOs of butadiene are $\psi_1 - \psi_4$, and those of cyclobutene are $\sigma, \sigma^*, \pi, \pi^*$. The energy order is



(Note that the Hückel π MO energies are indicated within brackets for a comparison of π MO energies of the reactant and product; however, a qualitative understanding of the relative energy levels is sufficient.)

The MOs of butadiene and cyclobutene are represented in an energy level diagram (energy increases upwards) in Fig. 11.1. With respect to energy, π lies between ψ_1 and ψ_2 , and π^* between ψ_3 and ψ_4 ; σ lies below any bonding π MO and σ^* lies above any antibonding π MO. It may be mentioned that an energy level diagram without comparing the reactant and product energy levels would also suffice.

Step 3. For the purpose of symmetry classification, the simplified sketches of MOs ignoring the difference of coefficients will be used in the construction of correlation diagrams.

With respect to C_2 , each MO of butadiene and cyclobutene is classified as **S** or **A** as shown in Fig. 11.1. It is seen that ψ_1 is classified as **A** (180 degrees rotation about the C_2 axis moves a shaded lobe at C-1 to the position of an unshaded lobe at C-4), and σ is **S** (180 degrees rotation about the C_2 axis moves an unshaded lobe at one end (C-1) of the σ bond to the position of the unshaded lobe at the other end (C-4)). All other MOs are classified similarly.

Step 4. The orbital correlation diagram for the conrotatory process is completed by joining orbitals of like symmetry using the noncrossing rule (Fig. 11.1). It is of note that the orbital correlations are unique and no other correlations exist because of violation of the noncrossing rule.

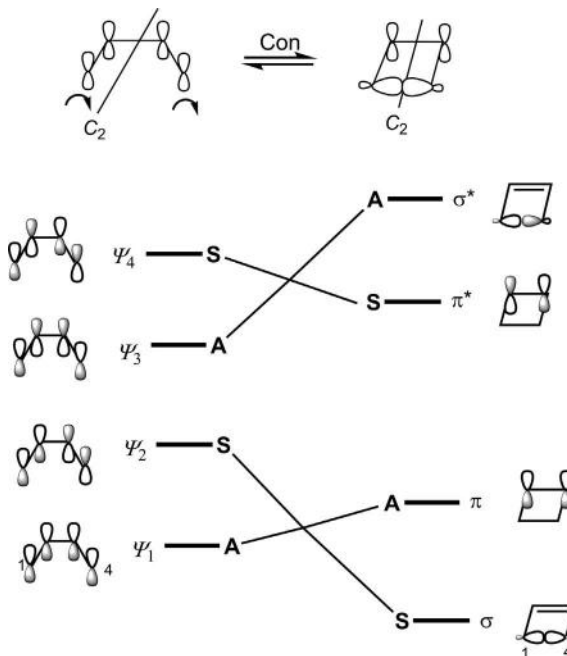


Fig. 11.1 Orbital correlation diagram for the conrotatory butadiene–cyclobutene interconversion.

11.2.1.1 Orbital Correlations in Thermal and Photochemical Reactions

An orbital correlation diagram can be used to find orbital correlations in a ground state (thermal) reaction and also in a first excited state (photochemical) reaction which lead to predictions as to whether a given pericyclic process is symmetry-allowed or symmetry-forbidden thermally or photochemically.

The orbital correlations for the conrotatory ring closing of butadiene to cyclobutene are shown in Fig. 11.2. The electron configuration in the butadiene ground state is $\psi_1^2\psi_2^2$, and in the first excited state $\psi_1^2\psi_2^1\psi_3^1$.

For the ground state process (Fig. 11.2A), all bonding orbitals of butadiene are transformed into all bonding orbitals of cyclobutene ($\psi_1 \rightarrow \pi$; $\psi_2 \rightarrow \sigma$); in other words, the butadiene ground state correlates with the cyclobutene ground state. The conrotatory process is therefore energetically favourable, and is symmetry-allowed thermally. The same is true for the conrotatory ring opening of cyclobutene to butadiene. In contrast, for the first excited state ring closing reaction (Fig. 11.2B), a lower-energy anti-bonding orbital (ψ_3) of butadiene transforms into a very high-energy anti-bonding σ^* orbital of cyclobutene; overall, the first excited state of butadiene correlates with the upper excited state of cyclobutene. The photochemical

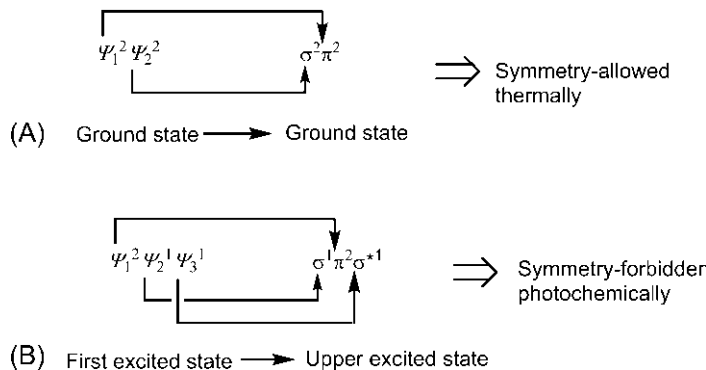


Fig. 11.2 Orbital correlations for the conrotatory ring closing of butadiene to cyclobutene in the (A) ground state thermal process and (B) first excited state photochemical process.

conrotatory reaction would therefore encounter a symmetry-imposed high-energy barrier and is symmetry-forbidden.

11.2.1.2 Physical Correlation of Reactant Orbitals With Product Orbitals

The orbital correlation diagram shows that a particular reactant molecular orbital develops into a specific product molecular orbital. In butadiene MOs, all four carbons have p orbitals, but in a cyclobutene MO (σ or π) only two carbons have orbitals (see Fig. 11.1). This implies that in ring closing, orbitals at two carbons of butadiene are destroyed and in ring opening, orbitals at two carbons have grown during the transformation. The question is: how is this transformation physically possible? Understanding this requires further quantum mechanical manipulation of molecular orbitals along the reaction coordinate. Here we shall describe a simplified and qualitative picture of the physical correlation.

Let us first consider the transformation of ψ_2 into σ in the conrotatory ring closing process. (In the FMO analysis, ψ_2 as HOMO is also involved in developing the σ bond, see Problem 3.3, p.92) During ring closing, all four MOs of butadiene simultaneously undergo the conrotatory change along the reaction coordinate when mixing of orbitals with the same symmetry occurs. Therefore, ψ_2 (**S**) mixes with ψ_4 (**S**) as the reaction proceeds. It is a general quantum mechanical principle that a lower-energy orbital combines with some of the higher-energy orbitals in bonding fashion, whereas a higher-energy orbital mixes with some of the lower-energy orbital in antibonding fashion, as shown for the combination of ψ_2 and ψ_4 in Fig. 11.3A. Along the reaction coordinate, ψ_2 (**S**) thus mixes with ψ_4 (**S**) in bonding fashion as shown in Fig. 11.3B. The ψ_4 contribution reinforces at C-1 and C-4 by the in-phase combination but destroys the lobes at

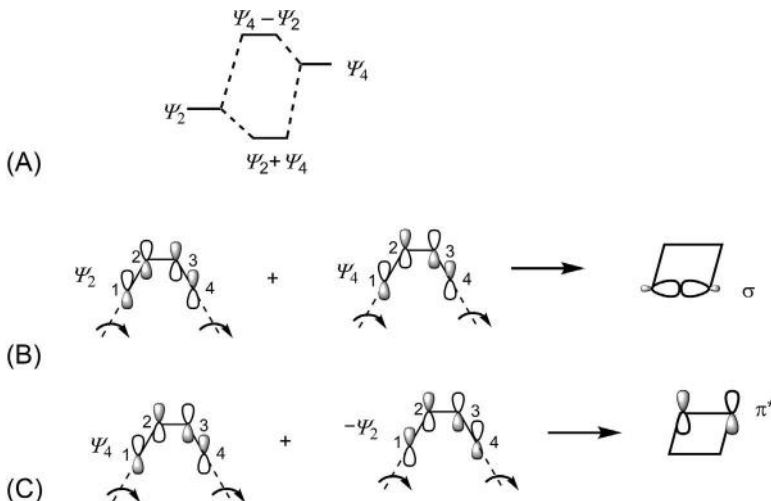


Fig. 11.3 (A) Combination of lower-energy ψ_2 with higher energy ψ_4 . Physical correlation of (B) ψ_2 with σ , and (C) ψ_4 with π^* in the conrotatory ring closing of butadiene to cyclobutene.

C-2 and C-3 by the out-of-phase combination in ψ_2 . The orbitals at C-1 and C-4 of ψ_2 ultimately develop into σ in the conrotatory pathway. Similarly, ψ_4 (**S**) mixes with ψ_2 (**S**) in antibonding fashion, destroying its lobes at C-1 and C-4, and reinforcing the lobes at C-2 and C-3 leading to π^* (Fig. 11.3C). It may be noted that $(\psi_4 - \psi_2) \equiv (-\psi_4 + \psi_2)$. These arguments also apply to the transformation of ψ_1 into π , and ψ_3 into σ^* .

In the conrotatory ring opening, σ is transformed into ψ_2 . Here σ (**S**) mixes with π^* (**S**) in bonding fashion as the reaction proceeds and ultimately develops into ψ_2 , as shown in Fig. 11.4. Mixing of π^* (**S**) with σ (**S**) in antibonding fashion leads to ψ_4 (verify). The transformations of π and σ^* into ψ_1 and ψ_3 , respectively, are obtained by similar arguments.

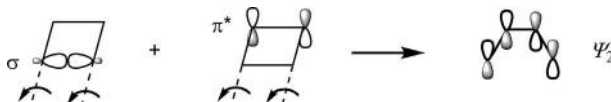


Fig. 11.4 Physical correlation of σ with ψ_2 in the conrotatory ring opening of cyclobutene to butadiene.

11.2.2 Orbital Correlation Diagram for the Disrotatory Process

The orbital correlation diagram for the disrotatory interconversion of butadiene and cyclobutene can be constructed following the step-by-step procedure as described earlier and is shown in Fig. 11.5. The persisting symmetry

element for the disrotatory process is a plane of symmetry (symbolized m instead of σ to avoid confusion with the molecular orbital label). The symmetry plane m is perpendicular to the plane of the molecule. The m symmetry is a general feature of disrotatory electrocyclic reactions. All the MOs are classified as **S** or **A** with respect to m and the correlation diagram is completed using the principle of orbital symmetry conservation and noncrossing rule.

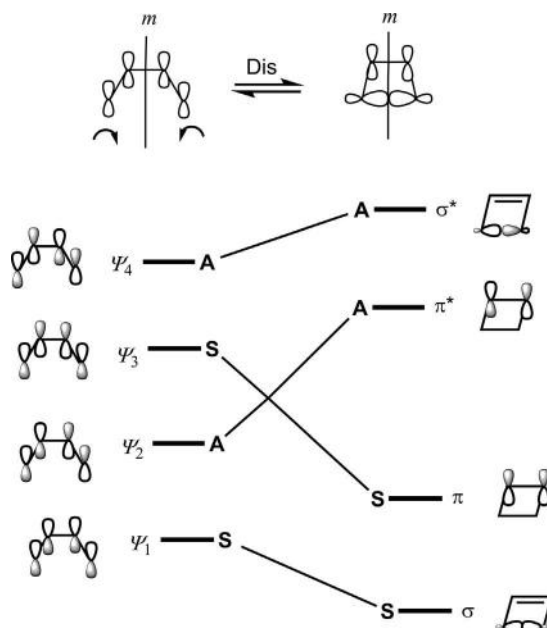


Fig. 11.5 Orbital correlation diagram for the disrotatory butadiene–cyclobutene interconversion.

11.2.2.1 Orbital Correlation

For the thermal ring closing process, a bonding orbital (ψ_2) transforms into an antibonding orbital (π^*) and the butadiene ground state correlates with a doubly excited state (2 electrons promoted to π^*) of cyclobutene (Fig. 11.6A). In the ring opening reaction, the cyclobutene ground state correlates with a doubly excited state of butadiene. Doubly excited states are of very high energy. The thermal disrotatory reaction would therefore encounter a symmetry-imposed high-energy barrier and is symmetry-forbidden. However, for the photochemical reaction, the first excited state of butadiene correlates with the first excited state of cyclobutene (Fig. 11.6B) and vice versa. This is a favourable process and the disrotatory reaction is symmetry-allowed photochemically.

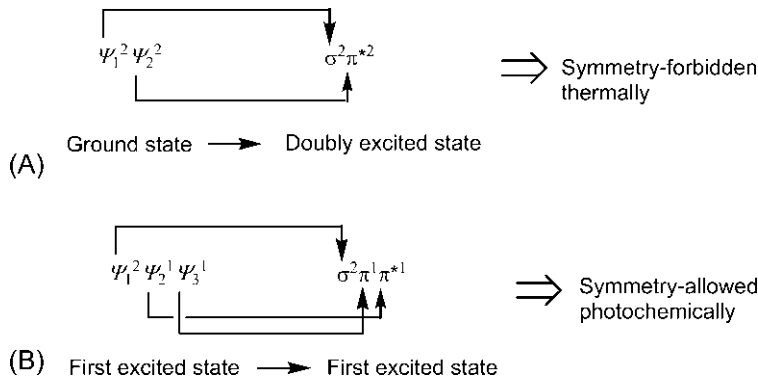


Fig. 11.6 Orbital correlations for the disrotatory ring closing of butadiene to cyclobutene in the (A) thermal process and (B) photochemical process.

In the FMO analysis of the photochemical disrotatory ring closing process, the singly occupied excited state LUMO (ψ_3) of butadiene is involved in developing the σ bond. However, the correlation diagram shows that ψ_1 (not ψ_3) is transformed into σ . ψ_1 and ψ_3 have a similar phase relationship at the terminal carbons. This is why the FMO picture using ψ_3 gives a valid conclusion as to whether the photochemical process is allowed or not. Actually, it is ψ_1 which is transformed into σ .

Problem 11.1

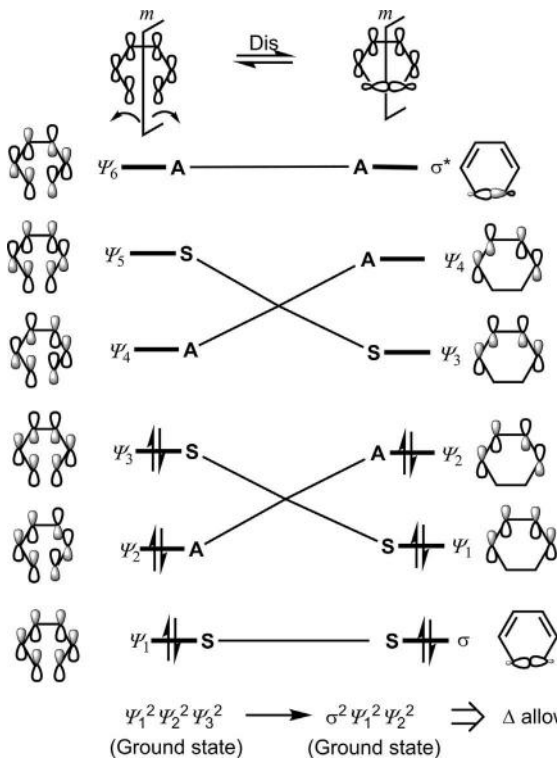
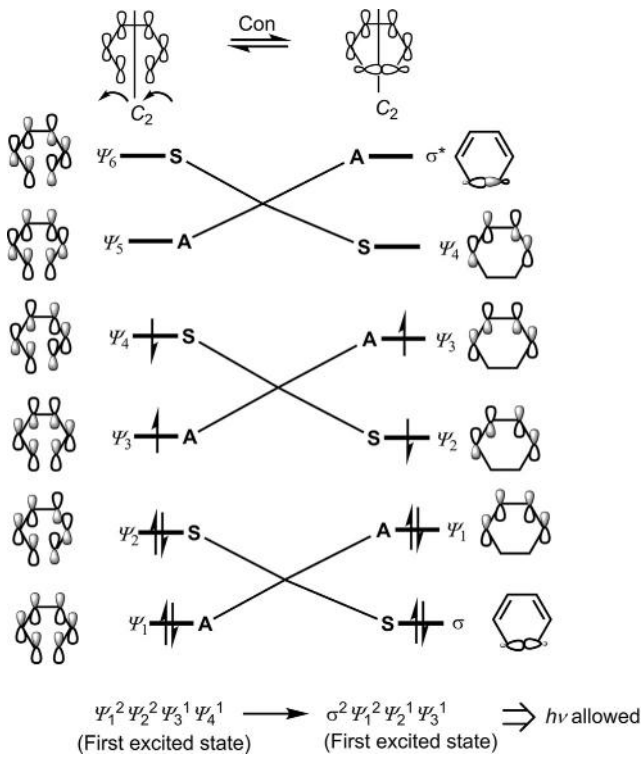
Draw orbital correlation diagrams for the conrotatory and disrotatory ring closing of hexa-1,3,5-triene to cyclohexa-1,3-diene. Predict which process is symmetry-allowed thermally or photochemically.

Answer

For the conrotatory process, the persisting symmetry element is C_2 , and the disrotatory process has m symmetry. The orbital correlations from the respective orbital correlation diagram show that the conrotatory process is symmetry-allowed photochemically as the first excited state of hexatriene correlates with the first excited state of cyclohexadiene, and the disrotatory process is symmetry-allowed thermally because the hexatriene ground state correlates with the cyclohexadiene ground state. Note that in the diagram, the reactant and product energy levels are not compared. However, the product energy levels in comparison to the reactant energy levels can be drawn using the energy order given below.

$$\begin{aligned} \text{Hexatriene : } & \psi_1 (\alpha + 1.8\beta) < \psi_2 (\alpha + 1.25\beta) < \psi_3 (\alpha + 0.45\beta) \\ & < \psi_4 (\alpha - 0.45\beta) < \psi_5 (\alpha - 1.25\beta) < \psi_6 (\alpha - 1.8\beta) \end{aligned}$$

$$\begin{aligned} \text{Cyclohexadiene : } & \sigma < \psi_1 (\alpha + 1.62\beta) < \psi_2 (\alpha + 0.62\beta) < \psi_3 (\alpha - 0.62\beta) \\ & < \psi_4 (\alpha - 1.62\beta) < \sigma^* \end{aligned}$$



11.2.3 Orbital Correlation Diagram for Electrocyclic Reactions in Charged Systems

An important electrocyclic reaction in a charged system is the Nazarov cyclization which involves the ring closing of the pentadienyl cation to the cyclopentenyl cation. The orbital correlation diagram of the process can be easily constructed following the steps as described previously. The persisting symmetry element for the conrotatory process is C_2 , whereas a plane of symmetry (m) is maintained throughout the disrotatory pathway. The correlation diagrams for the conrotatory and disrotatory processes are combined in Fig. 11.7. The MO energy levels for the cyclopentenyl cation relative to those for the pentadienyl cation are drawn using the MO energy order given below.

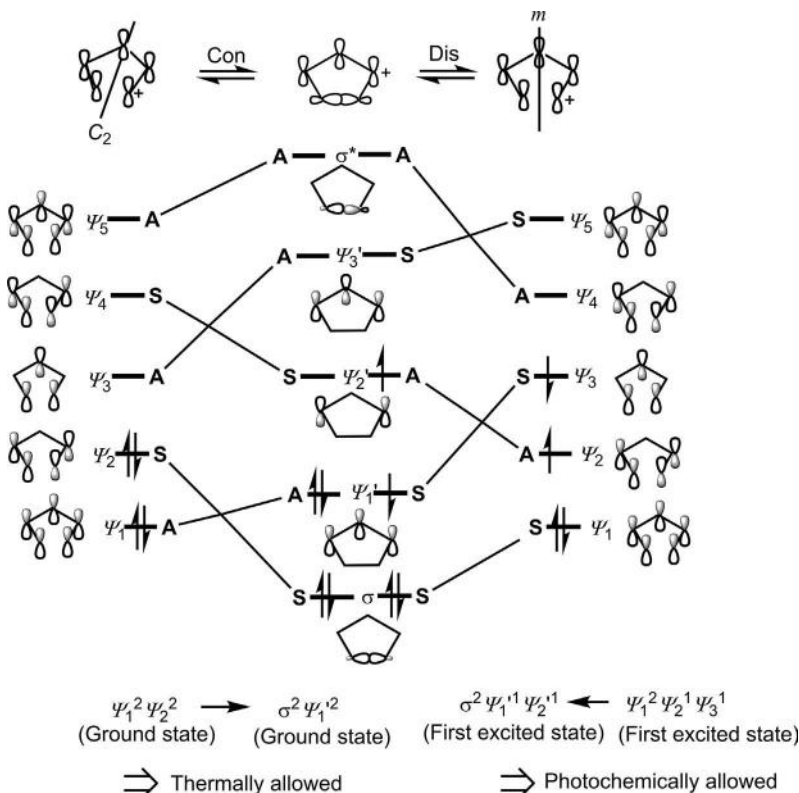
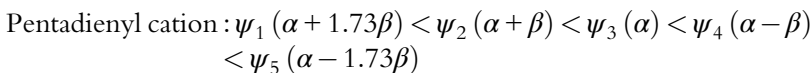


Fig. 11.7 Combined orbital correlation diagram for the conrotatory and disrotatory electrocyclic closure of the pentadienyl cation to the cyclopentenyl cation.

The orbital correlations clearly show that the conrotatory process is symmetry-allowed thermally, whereas the disrotatory process is symmetry-allowed photochemically. Note that the electrocyclic conversion of the pentadienyl cation to the cyclopentenyl cation is a 4-electron process and the same conclusions as derived for the 4-electron process in a neutral system (butadiene–cyclobutene conversion) are obtained.

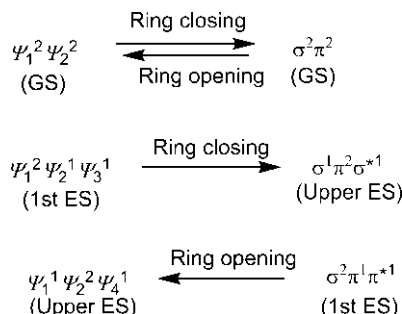
The orbital correlation diagrams shown in Fig. 11.7 also hold good for the conversion of the pentadienyl anion to the cyclopentenyl anion because the same sets of molecular orbitals are involved in cation/anion systems. However, the pentadienyl anion–cyclopentenyl anion reaction is a 6-electron process. Here the conrotatory process is symmetry-allowed photochemically and the disrotatory process is allowed thermally.

11.2.4 State Correlation Diagram for Electrocyclic Reactions

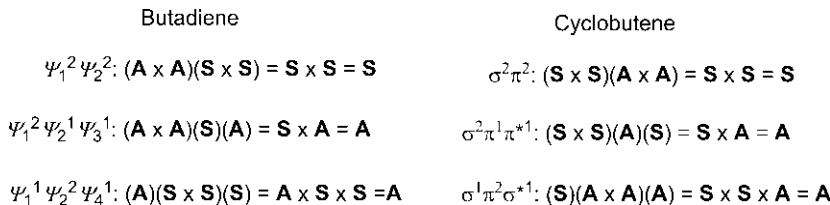
The state correlation diagram is based on state symmetry, and is formed by linking states of like symmetry. The state symmetry for the electronically ground state or excited state of a molecule is derived from orbital symmetries. An orbital symmetry refers to the symmetry of a 1-electron orbital. Thus, a state symmetry is determined by multiplying together the symmetries for all electrons in various orbitals of an electronic state, using the direct product rules: $\mathbf{S} \times \mathbf{S} = \mathbf{S}$; $\mathbf{A} \times \mathbf{A} = \mathbf{S}$; $\mathbf{S} \times \mathbf{A} = \mathbf{A}$; $\mathbf{A} \times \mathbf{S} = \mathbf{A}$. We will illustrate the construction of the state correlation diagram for an electrocyclic reaction using the butadiene–cyclobutene interconversion by conrotatory and disrotatory modes.

11.2.4.1 State Correlation Diagram for the Conrotatory Butadiene–Cyclobutene Interconversion

The orbital correlations for the conrotatory ring closing and ring opening for the butadiene–cyclobutene interconversion (see Fig. 11.1) are



The state symmetries for the ground state (GS), first excited state (1st ES) and upper excited state (upper ES) of butadiene and cyclobutene are determined from orbital symmetries as follows.



A state correlation diagram is then constructed using relative energies of butadiene and cyclobutene states, specifying their state symmetries and linking states of like symmetry as shown in Fig. 11.8.

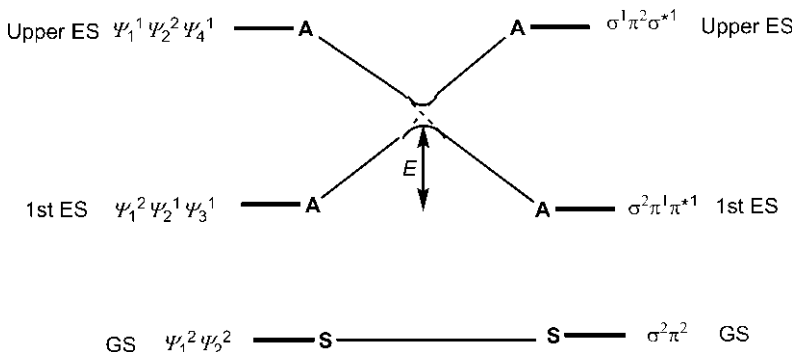
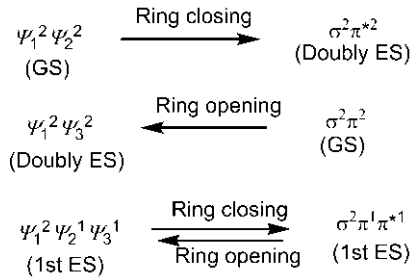


Fig. 11.8 State correlation diagram for the conrotatory butadiene–cyclobutene interconversion.

The state correlation diagram clearly shows a ground state–ground state symmetry correlation, and confirms the earlier conclusion that the conrotatory process is symmetry-allowed in the ground state. Interestingly, the **A** to **A** state correlation between the first excited state of butadiene and upper excited state of cyclobutene and vice versa cannot occur because of the non-crossing rule. This contradicts the direct orbital correlation obtained from the orbital correlation diagram. Therefore, the correlation between the 1st ES and upper ES signifies an attempted correlation but not actual correlation. The state correlation diagram provides that the actual correlations of the **A** states are obtained by curved lines (Fig. 11.8). Being unable to cross, the first excited **A** state on each side is correlated, involving a high-energy barrier (*E*), and the conrotatory photochemical reaction is therefore forbidden.

11.2.4.2 State Correlation Diagram for the Disrotatory Butadiene–Cyclobutene Interconversion

The orbital correlations for the disrotatory ring closing and ring opening are as follows (see Fig. 11.5).



The state symmetries for the above states can be determined from orbital symmetries in a similar manner as described before. For instance, the symmetry of the ground state butadiene $\psi_1^2 \psi_2^2$ is $(\mathbf{S} \times \mathbf{S})(\mathbf{A} \times \mathbf{A}) = \mathbf{S} \times \mathbf{S} = \mathbf{S}$. The state correlation diagram for the disrotatory process is shown in Fig. 11.9.

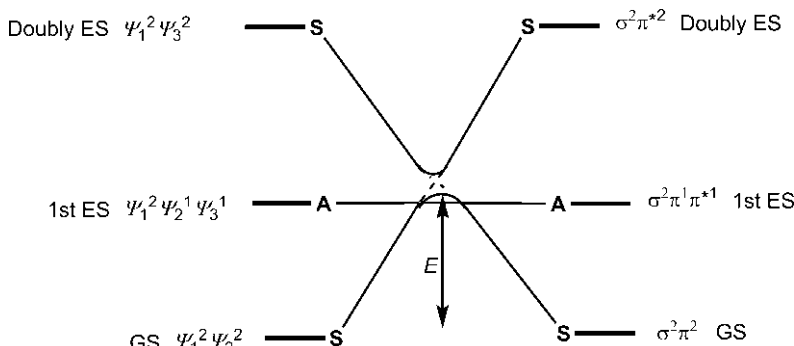


Fig. 11.9 State correlation diagram for the disrotatory butadiene–cyclobutene interconversion.

The diagram shows that the disrotatory process is photochemically allowed with **A** to **A** correlation between the first excited states. The actual cyclobutene product, however, is not the excited state product; the excited molecule must drop to the ground state by $\pi^* - \pi$ demotion. The diagram also reveals the high-energy barrier (E) for the forbidden ground state (thermal) reaction. The **S** to **S** state correlation between the ground state of the reactant and the doubly excited state of the product violates the noncrossing

rule. Therefore, the ground state (**S**) of the reactant tends to proceed towards the doubly excited state (**S'**) of the product (as required by orbital correlation) but, being unable to cross, returns to the ground state with the same symmetry. Evidently, for the ground state reaction, the energy barrier E is very high, similar to the energy requirement of an electronic excitation.

11.3 CORRELATION DIAGRAM FOR CYCLOADDITION REACTIONS

Here we shall describe the correlation diagrams for the [4 + 2] Diels–Alder reaction, cheletropic cycloadditions, [2 + 2] cycloadditions including *ortho*- and *meta*-additions of ethylene to benzene, and [2 + 2 + 2] cycloadditions including prismane to benzene conversion.

11.3.1 Correlation Diagram for the [4 + 2] Diels–Alder Reaction

The orbital correlation diagram of the Diels–Alder [$\pi 4_s + \pi 2_s$] cycloaddition of butadiene with ethylene can be constructed following the step-by-step procedure described in [Section 11.2](#). The only persisting symmetry element is a plane of symmetry (m) bisecting both reactants as shown in [Fig. 11.10](#).

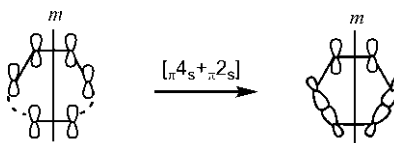
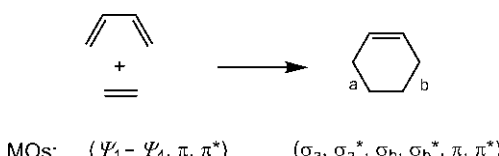
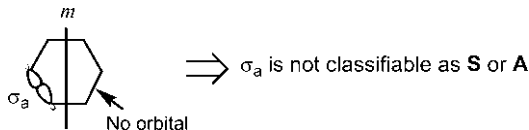


Fig. 11.10 Persisting symmetry plane (m) in the $[\pi 4_s + \pi 2_s]$ Diels–Alder reaction.

The reactant and product molecular orbitals associated with the bonds formed or broken are given below. Notice that the two equivalent σ bonds are labelled a, b.



The construction of the correlation diagram requires that all the MOs must be symmetric (**S**) or antisymmetric (**A**) with respect to m . However, unlike an electrocyclic reaction, the four localized σ MOs (σ_a , σ_a^* , σ_b , σ_b^*) cannot be classified as **S** or **A**, as shown for σ_a below.



Therefore, for symmetry classification, we need to generate a new set of delocalized σ MOs by linear combination. Note that the two σ bonds can interact in a π sense. The formation of four new σ MOs (σ_1 , σ_2 , σ_3^* , σ_4^*) is shown in Fig. 11.11. σ_a and σ_b combine to produce $\sigma_1 = \sigma_a + \sigma_b$ and $\sigma_2 = \sigma_a - \sigma_b$. Similarly, a combination of σ_a^* and σ_b^* gives σ_3^* and σ_4^* .

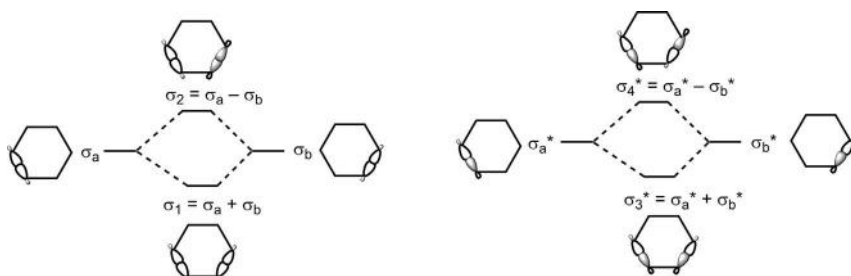


Fig. 11.11 Generation of new σ MOs for analysis of the Diels–Alder reaction.

The relative energies of the reactant MOs and those of the product MOs are

$$\begin{aligned} \psi_1 &< \pi < \psi_2 < \psi_3 < \pi^* < \psi_4 \\ \sigma_1 &< \sigma_2 < \pi < \pi^* < \sigma_3^* < \sigma_4^* \end{aligned}$$

The orbital correlation diagram of the Diels–Alder reaction is shown in Fig. 11.12. Note that the product energy levels are drawn in comparison to the reactant energy levels.

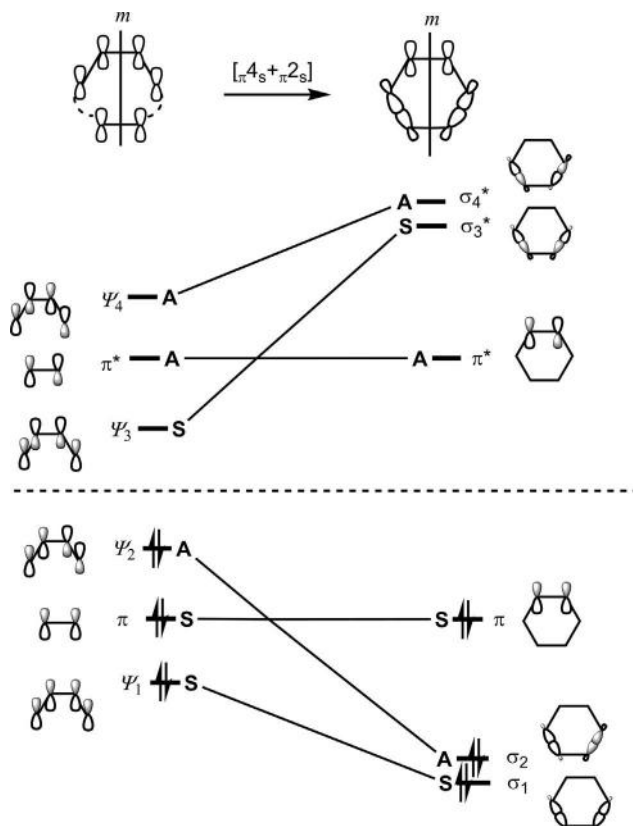


Fig. 11.12 Orbital correlation diagram for the $[\pi 4s + \pi 2s]$ Diels–Alder reaction.

For the ground state (thermal) reaction, the orbital correlations are

$$\Psi_1^2 \pi^2 \Psi_2^2 \rightarrow \sigma_1^2 \sigma_2^2 \pi^2$$

Thus, all bonding orbitals of reactants are directly correlated with all bonding orbitals of the product and the thermal reaction does not encounter a symmetry imposed barrier. This does not imply that no activation energy is required for the cycloaddition. The energy changes associated with rehybridization, bond length changes and distortion in the bond angles will contribute to the activation energy for the reaction. The orbital correlations indicate that there is no unfavourable rise in energy along the reaction coordinate and the reaction is symmetry-allowed thermally. This conclusion is further supported by the correlation of the reactant ground state (**S**) directly with the product ground state (**S'**) as shown in Fig. 11.13. Note that only the relevant

part of the state correlation diagram is shown. The state symmetry is determined from the orbital symmetries using direct product rules (see Section 11.2.4).



Fig. 11.13 The ground state to ground state correlation in the Diels–Alder reaction.

11.3.1.1 Physical Correlation

The orbital correlation diagram shows that π MO of ethylene is transformed into π MO of cyclohexene. In view of the frontier orbital picture, this might appear to be surprising; however, this is what happens eventually. This π to π correlation can be realized physically as follows.

Along the reaction coordinate, $\pi(\mathbf{S})$ mixes with orbitals of like symmetry, that is, $\psi_1(\mathbf{S})$ and $\psi_3(\mathbf{S})$. The mixing of $\pi(\mathbf{S})$ with the lower-energy orbital $\psi_1(\mathbf{S})$ occurs in bonding fashion, whereas it occurs with a higher-energy orbital $\psi_3(\mathbf{S})$ in antibonding fashion as shown in Fig. 11.14. The superposition of such bonding and antibonding mixings leads to cancellation at C-1 and C-4 of the diene. On the other hand, there is reinforcement at C-2 and C-3 of the diene moiety. The ethylene π orbital is essentially divided between the diene and ethylene in the transition structure, and is ultimately transformed into the π orbital of cyclohexene.

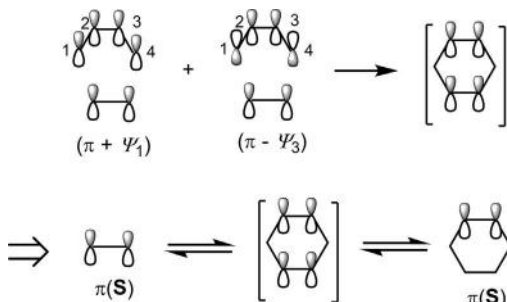


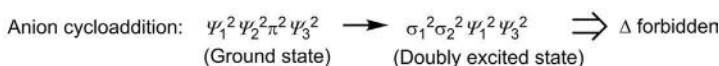
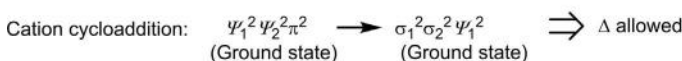
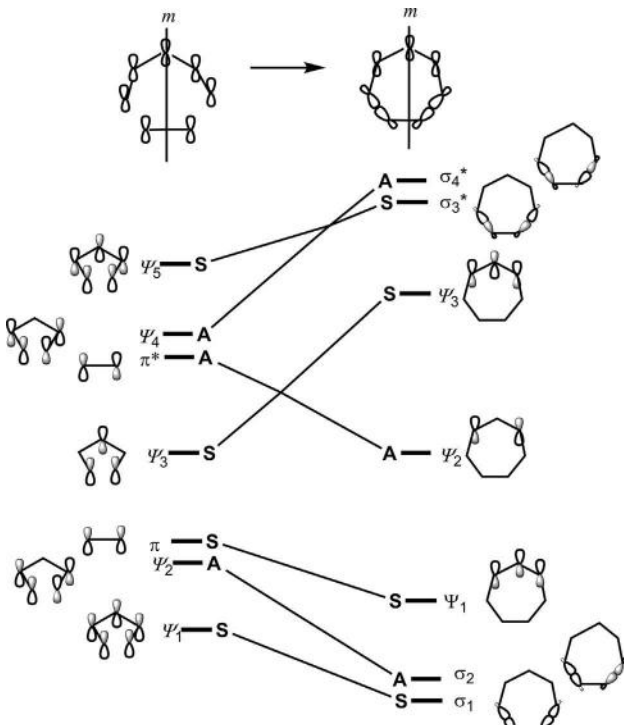
Fig. 11.14 Physical correlation of ethylene π with cyclohexene π in the Diels–Alder reaction.

Problem 11.2

Draw an orbital correlation diagram for cycloaddition of the pentadienyl cation (or anion) with ethylene by suprafacial/suprafacial addition. Hence, predict which reaction is symmetry-allowed or symmetry-forbidden thermally.

Answer

The cycloaddition of the pentadienyl cation with ethylene is a $[\pi^4_s + \pi^2_s]$ cycloaddition while the cycloaddition of the pentadienyl anion with ethylene indicates a $[\pi^6_s + \pi^2_s]$ process. In the supra/supra pathway, the persisting symmetry element is a mirror plane (m). The orbital correlation diagram of the pentadienyl system (cation/anion) with ethylene is shown below. Note that the product MOs constitute four new σ MOs generated by linear combination and three π MOs of the allyl system. The orbital correlations show that the 6-electron cycloaddition of the pentadienyl cation with ethylene is symmetry-allowed thermally, whereas the 8-electron reaction of the pentadienyl anion with ethylene is symmetry-forbidden thermally.

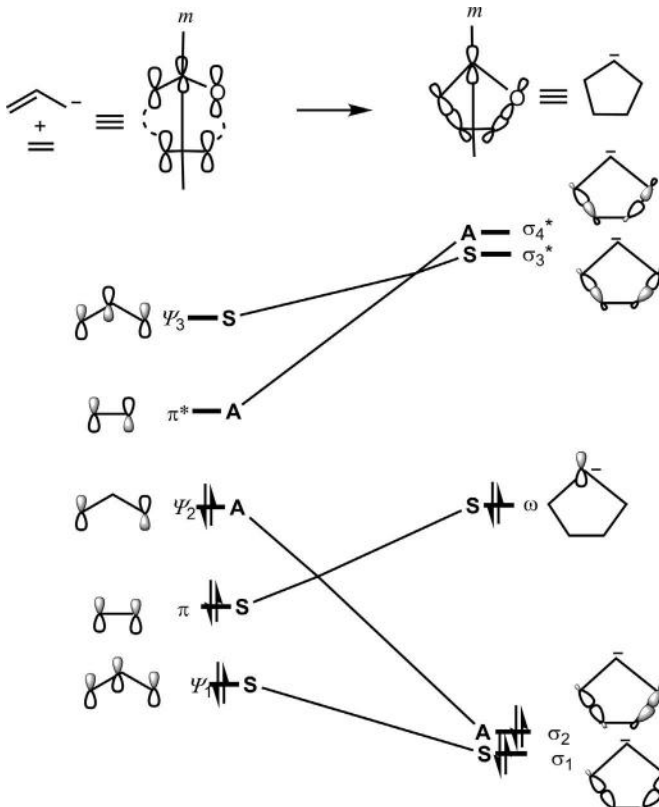


Problem 11.3

Draw an orbital correlation diagram for the $[\pi 4_s + \pi 2_s]$ 1,3-dipolar cycloaddition using a model cycloaddition between the allyl anion and ethylene and hence predict that the reaction is symmetry-allowed thermally.

Answer

A 1,3-dipole is isoelectronic with an allyl anion. The correlation diagram of the 1,3-dipolar cycloaddition therefore resembles that of the cycloaddition between the allyl anion and ethylene. The persisting symmetry element is a mirror plane (m) passing through the central atom of the allyl anion and bisecting the alkene. The reactant MOs have the relative energies $\psi_1 < \pi < \psi_2 < \pi^* < \psi_3$ (ψ_2 is nonbonding). The product MOs constitute four σ MOs and a nonbonding ω orbital (p). For symmetry classification, the new product σ MOs are generated by the linear combination procedure as done for the Diels–Alder reaction. The orbital correlations show that the reactant bonding and nonbonding orbitals are correlated with the bonding and nonbonding orbitals of the product. Therefore, there is no unfavourable rise in energy as the reaction proceeds and the cycloaddition is symmetry-allowed thermally.



11.3.2 Correlation Diagram for Cheletropic Cycloadditions

A cheletropic cycloaddition can proceed through linear and nonlinear pathways (see Section 6.1, p. 269). The persisting symmetry element for a linear cheletropic cycloaddition is a mirror plane (*m*) as illustrated by the reaction between butadiene and SO₂ in Fig. 11.15.

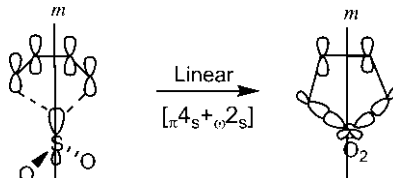


Fig. 11.15 Persisting symmetry plane (*m*) in a linear cheletropic reaction.

The orbital correlation diagram can be constructed in a similar manner as described for the Diels–Alder reaction, and is shown in Fig. 11.16. The reactant orbitals are four π MOs (ψ_1 – ψ_4) of butadiene and two nonbonding orbitals $\omega(\text{sp}^2)$ and $\omega(\text{p})$ of SO₂. Their energy order is

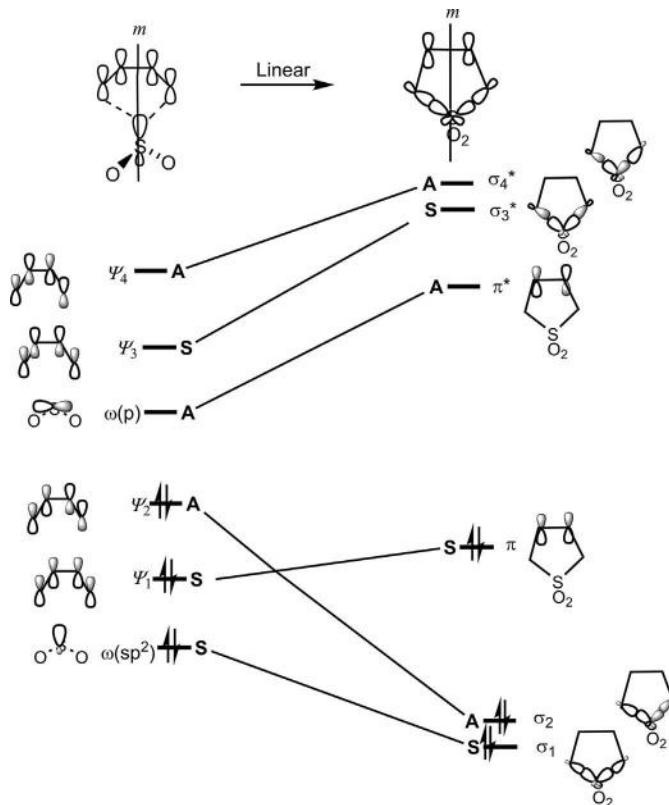


Fig. 11.16 Orbital correlation diagram for a linear cheletropic reaction between butadiene and SO₂.

$\omega(sp^2) < \psi_1 < \psi_2 < \omega(p) < \psi_3 < \psi_4$. The product orbitals are four σ MOs ($\sigma_1, \sigma_2, \sigma_3^*, \sigma_4^*$) generated by linear combination and two π MOs (π, π^*) of the ring double bond.

For thermal reaction, the orbital correlations are $(sp^2)^2\psi_1^2\psi_2^2 \rightarrow \sigma_1^2\sigma_2^2\pi^2$ which indicate that the lowest energy nonbonding orbital and all bonding orbitals of reactants are correlated with all bonding orbitals of the product. The linear cheletropic cycloaddition of SO_2 with butadiene is therefore symmetry-allowed thermally.

In contrast, the orbital correlation diagram for the linear cheletropic cycloaddition of the singlet carbene to ethylene (Fig. 11.17) shows that the linear singlet carbene cycloaddition is symmetry-forbidden thermally since a bonding reactant orbital (π) is correlated with an antibonding product orbital (σ_3^*) and the reactant ground state is correlated with a doubly excited state of the product.

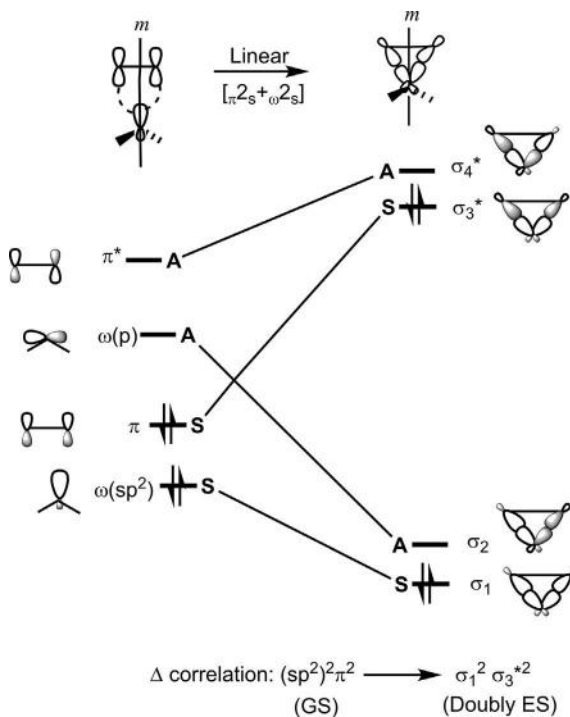


Fig. 11.17 Orbital correlation diagram for the linear singlet carbene cycloaddition.

It was shown in Chapter 6 that the singlet carbene cycloaddition by the nonlinear pathway is thermally allowed. The nonlinear pathway, however, involves rotation of the carbene plane through 90 degrees as the product is

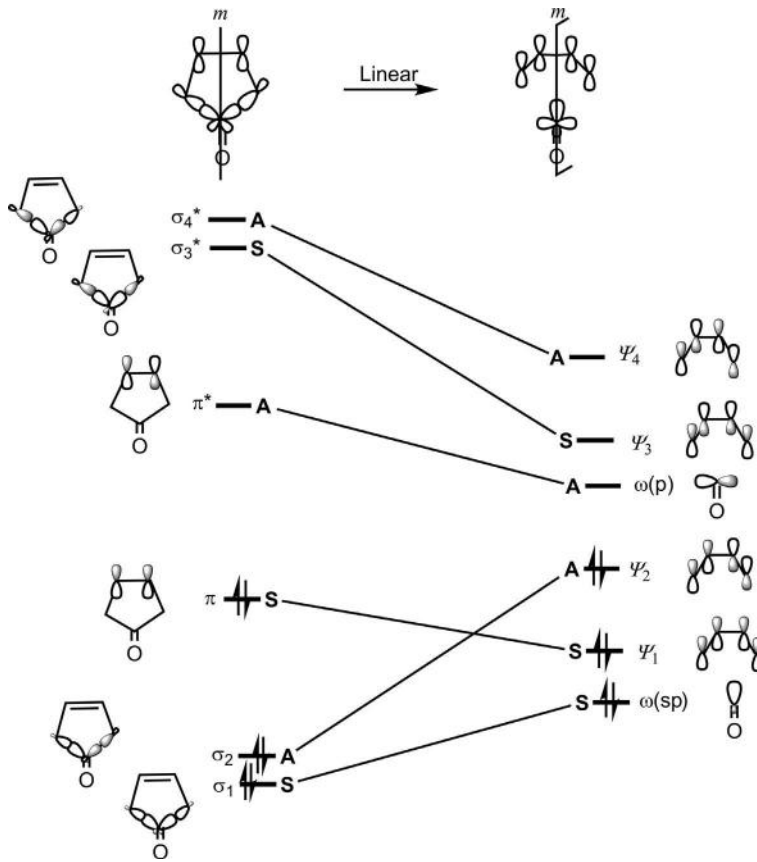
reached (see Fig. 6.6, p. 273). As a result, the nonlinear pathway lacks a persisting symmetry element and the correlation diagram is not relevant in this case.

Problem 11.4

Draw an orbital correlation diagram for the linear cheletropic extrusion of carbon monoxide from 3-cyclopentenone and hence predict that the reaction is symmetry-allowed thermally.

Answer

The cheletropic extrusion of CO is similar to that of SO₂, which is the reverse of the cheletropic cycloaddition of SO₂. The linear CO molecule has a filled sp orbital and a vacant p orbital on carbon. For linear extrusion of CO, the persisting symmetry element is a mirror plane (*m*) bisecting the C=C bond and passing through the C=O bond of cyclopentenone. The orbital correlation diagram is shown below. The extrusion reaction is symmetry-allowed thermally since all bonding orbitals of the reactant are correlated with all bonding orbitals of butadiene and the lowest energy nonbonding $\omega(sp)$ orbital of CO.



11.3.3 Correlation Diagram for [2 + 2] Cycloadditions

11.3.3.1 Correlation Diagram for the [2 + 2] Cycloaddition of Two Ethylene Molecules

The $[\pi_{2s} + \pi_{2s}]$ cycloaddition of two ethylene molecules (Fig. 11.18) shows that three symmetry planes, namely mirror plane 1 (yz plane), mirror plane 2 (xz plane) and mirror plane 3 (xy plane), can persist throughout the transformation.

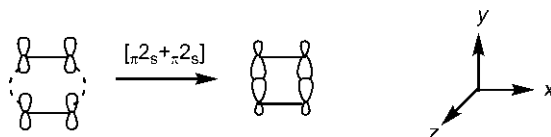


Fig. 11.18 $[\pi_{2s} + \pi_{2s}]$ Cycloaddition of two ethylene molecules. All atomic orbitals lie in the xy plane.

However, since all atomic orbitals lie in the xy plane (plane 3), all the σ and π MOs will be necessarily symmetric (**S**) with respect to this plane. As such, the mirror plane 3 is of no use and is ignored. The persisting symmetry elements for the purpose of analysis are then mirror plane 1 (m_1) and mirror plane 2 (m_2), each of which bisects bonds formed or broken as shown in Fig. 11.19.

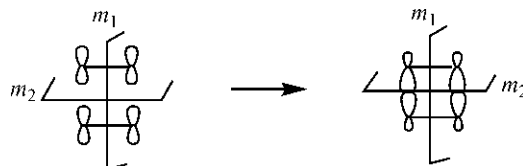
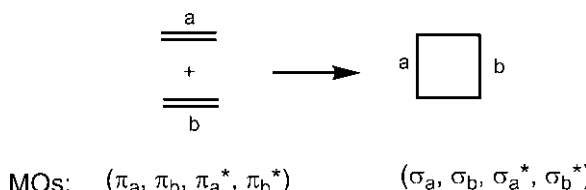


Fig. 11.19 Persisting symmetry planes (m_1 and m_2) for analysis of $[\pi_{2s} + \pi_{2s}]$ cycloaddition.

The reactant and product molecular orbitals associated with bonds made or broken are given below. The two π bonds or two σ bonds are labelled a, b.



However, none of these π MOs and σ MOs can be classified as **S** or **A** with respect to both symmetry planes m_1 and m_2 . Therefore, using the procedure of linear combination, new sets of π MOs and σ MOs are obtained as shown in Fig. 11.20. It should be understood that at finite distances of approach of the two π systems, the interaction can develop into a new set of π MOs.

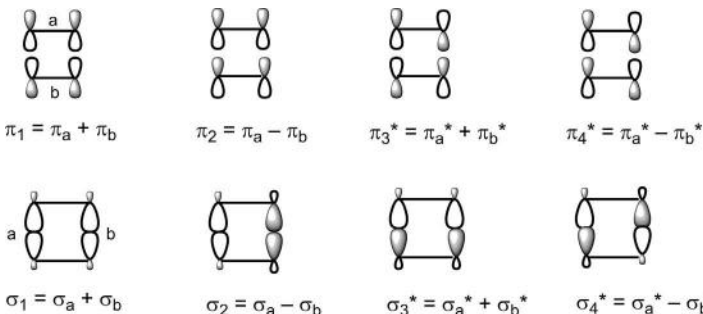


Fig. 11.20 Generation of new sets of π and σ MOs for analysis of $[\pi 2_s + \pi 2_s]$ cycloaddition.

In symmetry classification, each MO is designated by two symmetry labels, one with respect to m_1 and the other with respect to m_2 . Thus, π_1 is classified as **S₁S₂** (symmetric with respect to m_1 , symmetric with respect to m_2). Similarly, π_2 is **S₁A₂** (symmetric with respect to m_1 , antisymmetric with respect to m_2) and so on. Linking the orbitals of like symmetry using the noncrossing rule gives the orbital correlation diagram (Fig. 11.21). Notice that the energy levels of σ MOs are drawn in comparison to those for π MOs.

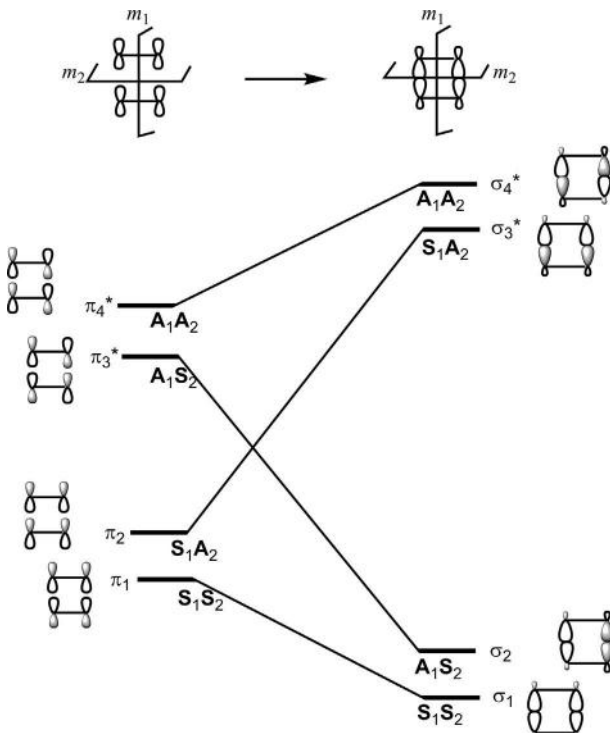
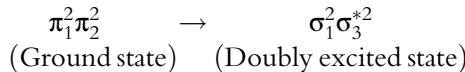


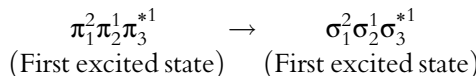
Fig. 11.21 Orbital correlation diagram for the $[\pi 2_s + \pi 2_s]$ cycloaddition of two ethylene molecules.

The orbital correlations for thermal reaction are



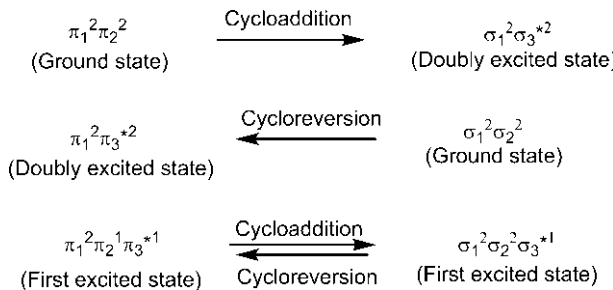
Since a bonding orbital (π_2) is transformed into a high-energy antibonding orbital (σ_3^*) and the reactant ground state correlates with the doubly excited state of the product, thermal $[\pi 2_s + \pi 2_s]$ cycloaddition would suffer from a symmetry-imposed high-energy barrier and hence is symmetry-forbidden. (An idea of the magnitude of the high-energy barrier can be obtained from the state correlation diagram, see below.)

For the photochemical reaction, the orbital correlations indicate that the reactant first excited state is correlated with the first excited state of the product, and hence the photochemical $[\pi 2_s + \pi 2_s]$ cycloaddition is symmetry-allowed.



State Correlation Diagram

The orbital correlations for the $[\pi 2_s + \pi 2_s]$ cycloaddition and $[\sigma 2_s + \sigma 2_s]$ cycloreversion, as obtained from the orbital correlation diagram, are



The state symmetries for the above reactant and product states are determined from the orbital symmetries using the direct product rules as follows.

$$\begin{aligned} \pi_1^2 \pi_2^2 : & (\mathbf{S}_1 \mathbf{S}_2 \times \mathbf{S}_1 \mathbf{S}_2)(\mathbf{S}_1 \mathbf{A}_2 \times \mathbf{S}_1 \mathbf{A}_2) = (\mathbf{S}_1 \times \mathbf{S}_1 \times \mathbf{S}_1 \times \mathbf{S}_1)(\mathbf{S}_2 \times \mathbf{S}_2 \times \mathbf{A}_2 \times \mathbf{A}_2) \\ & = \mathbf{S}_1 \mathbf{S}_2 \equiv \mathbf{S} \end{aligned}$$

$$\begin{aligned} \pi_1^2 \pi_2^1 \pi_3^{*1} : & (\mathbf{S}_1 \mathbf{S}_2 \times \mathbf{S}_1 \mathbf{S}_2)(\mathbf{S}_1 \mathbf{A}_2)(\mathbf{A}_1 \mathbf{S}_2) = (\mathbf{S}_1 \times \mathbf{S}_1 \times \mathbf{S}_1 \times \mathbf{A}_1)(\mathbf{S}_2 \times \mathbf{S}_2 \times \mathbf{A}_2 \times \mathbf{S}_2) \\ & = \mathbf{A}_1 \mathbf{A}_2 \equiv \mathbf{A} \end{aligned}$$

$$\begin{aligned} \pi_1^2 \pi_3^{*2} : & (\mathbf{S}_1 \mathbf{S}_2 \times \mathbf{S}_1 \mathbf{S}_2)(\mathbf{A}_1 \mathbf{S}_2 \times \mathbf{A}_1 \mathbf{S}_2) = (\mathbf{S}_1 \times \mathbf{S}_1 \times \mathbf{A}_1 \times \mathbf{A}_1)(\mathbf{S}_2 \times \mathbf{S}_2 \times \mathbf{S}_2 \times \mathbf{S}_2) \\ & = \mathbf{S}_1 \mathbf{S}_2 \equiv \mathbf{S} \end{aligned}$$

$$\sigma_1^2 \sigma_2^2 : (\mathbf{S}_1 \mathbf{S}_2 \times \mathbf{S}_1 \mathbf{S}_2)(\mathbf{A}_1 \mathbf{S}_2 \times \mathbf{A}_1 \mathbf{S}_2) = (\mathbf{S}_1 \times \mathbf{S}_1 \times \mathbf{A}_1 \times \mathbf{A}_1)(\mathbf{S}_2 \times \mathbf{S}_2 \times \mathbf{S}_2 \times \mathbf{S}_2)$$

$$= \mathbf{S}_1 \mathbf{S}_2 \equiv \mathbf{S}$$

$$\sigma_1^2 \sigma_2^1 \sigma_3^{*1} : (\mathbf{S}_1 \mathbf{S}_2 \times \mathbf{S}_1 \mathbf{S}_2)(\mathbf{A}_1 \mathbf{S}_2 \times \mathbf{S}_1 \mathbf{A}_2) = (\mathbf{S}_1 \times \mathbf{S}_1 \times \mathbf{A}_1 \times \mathbf{S}_1)(\mathbf{S}_2 \times \mathbf{S}_2 \times \mathbf{S}_2 \times \mathbf{A}_2)$$

$$= \mathbf{A}_1 \mathbf{A}_2 \equiv \mathbf{A}$$

$$\sigma_1^2 \sigma_3^{*2} : (\mathbf{S}_1 \mathbf{S}_2 \times \mathbf{S}_1 \mathbf{S}_2)(\mathbf{S}_1 \mathbf{A}_2 \times \mathbf{S}_1 \mathbf{A}_2) = (\mathbf{S}_1 \times \mathbf{S}_1 \times \mathbf{S}_1 \times \mathbf{S}_1)(\mathbf{S}_2 \times \mathbf{S}_2 \times \mathbf{A}_2 \times \mathbf{A}_2)$$

$$= \mathbf{S}_1 \mathbf{S}_2 \equiv \mathbf{S}$$

(For any reactant or product state, the state symmetry $\mathbf{S}_1 \mathbf{S}_2$ or $\mathbf{A}_1 \mathbf{A}_2$ is labelled as **S** or **A** for simplicity.) The state correlation diagram is shown in Fig. 11.22. The energy levels of the product states are drawn in comparison to those of the reactant states.

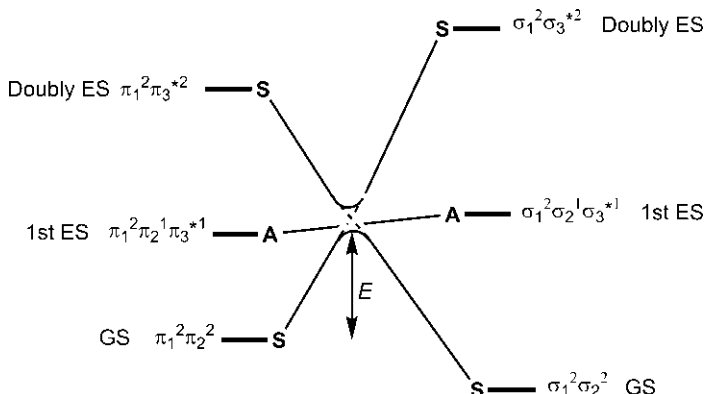


Fig. 11.22 State correlation diagram for the $[\pi_{2s} + \pi_{2s}]$ cycloaddition of two ethylene molecules.

The state correlation diagram shows that the photochemical reaction is symmetry-allowed as a result of direct **A** to **A** correlation, and thereby confirms the earlier conclusion. It may be mentioned that the excited state product must drop to the ground state by $\sigma_3^* \rightarrow \sigma_2$ demotion to give the cyclobutane. Importantly, the diagram reveals the high-energy barrier (E) for the ground state reaction. As shown in Fig. 11.22, the reactant ground state (**S**) tends to correlate with the doubly excited state (**S**) of the product (as required by orbital correlation) but this cannot occur because of the violation of the noncrossing rule. The crossing is therefore avoided and the reactant ground state is forced to correlate with the product ground state of like symmetry. This evidently involves a high-energy barrier (E) which is similar to the energy required for an electronic excitation. The ground state (thermal) reaction is therefore symmetry-forbidden.

11.3.3.2 Correlation Diagram for the Ortho- and Meta-addition of Ethylene to Benzene

Here we shall see what will happen if a π_2 component in [2 + 2] photocycloaddition is part of an aromatic ring. It seems that the $[\pi_{2s} + \pi_{2s}]$ photocycloaddition of ethylene to benzene across adjacent carbons (*ortho*-addition) will be an allowed pericyclic reaction. However, surprisingly, an orbital correlation diagram (Fig. 11.23) shows that the reaction is symmetry-forbidden.⁶ The persisting symmetry element is a mirror plane (m) bisecting both molecules. The reactant orbitals are the six π MOs ($\psi_0, \psi_1, \psi_{-1}, \psi_2, \psi_{-2}, \psi_3$) of benzene (see Fig. 1.31, p. 32) and two π MOs (π, π^*) of ethylene. The product orbitals are four σ MOs ($\sigma_1, \sigma_2, \sigma_3^*, \sigma_4^*$) similar to those described in Fig. 11.20 and four π MOs ($\psi_1 - \psi_4$) of the diene unit of bicyclooctadiene. All the orbitals are classified as **S** or **A** with respect to m .

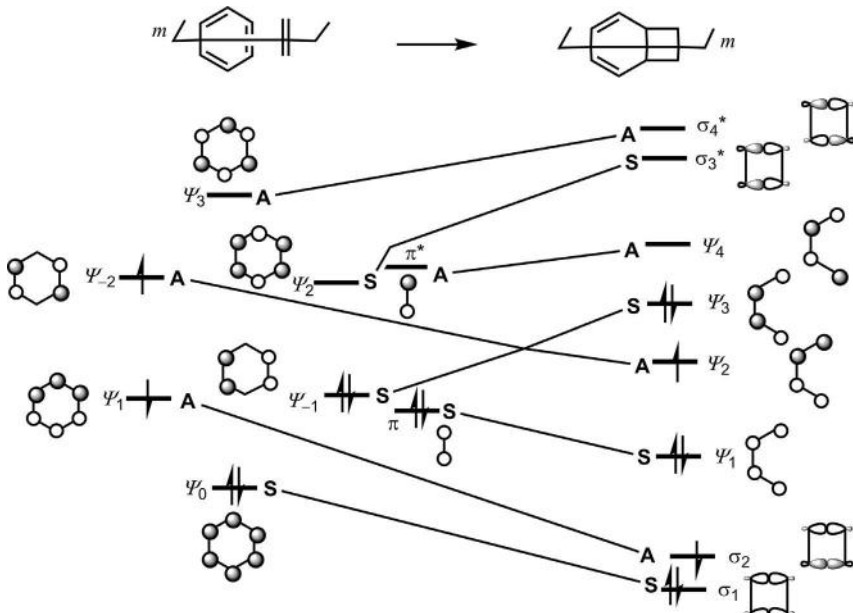
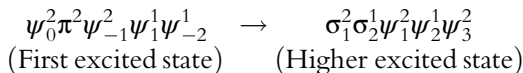


Fig. 11.23 Orbital correlation diagram for the [2 + 2] *ortho*-addition of ethylene to benzene.

The first singlet excited state (S_1) of benzene arises from a forbidden transition at 254 nm (responsible for a low-intensity absorption band), which involves the promotion of an electron from ψ_1 (or ψ_{-1}) to ψ_{-2} (or ψ_2). Both configurations contribute to the wave function of S_1 benzene (the ${}^1B_{2u}$ state)

and therefore one of them, ψ_1 to ψ_{-2} , is chosen for the correlation. The orbital correlations in the first excited singlet state are



Clearly, the reactant first excited state is correlated with the higher excited state of the product, and photochemical *ortho*-addition is therefore symmetry-forbidden.

In sharp contrast, the *meta*-addition of ethylene to benzene is an allowed process as the correlation diagram (Fig. 11.24) shows.⁶ *meta*-addition involves initial bonding to *meta* positions in the singlet excited state to give a prefulvene-type diradical, which is used for the construction of the correlation diagram. The diradical is probably not an intermediate, and it begins to form the second bond in the transition structure so that the reaction is concerted but highly asynchronous. The persisting symmetry element in this case is also a mirror plane (*m*) which passes through C-1 and C-4 of the benzene ring and bisects the ethylene (cf. *ortho*-addition). The reactant orbitals are the same as for *ortho*-addition but the product orbitals are not the same set. Instead of four π MOs for diene in *ortho*-addition, there are three π MOs ($\psi_1 - \psi_3$) for the allyl radical and one p orbital for a radical centre in *meta*-addition.

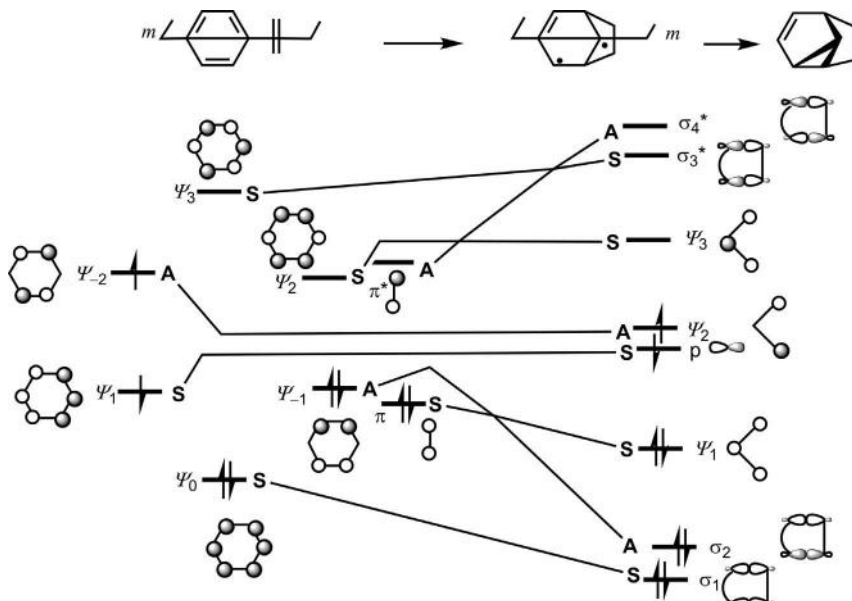
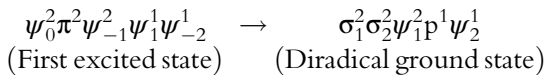


Fig. 11.24 Orbital correlation diagram for the *meta*-addition of ethylene to benzene.

The orbital correlations shown below indicate that the photochemical *meta*-addition is symmetry-allowed.



The *meta*-additions are more common and show stereospecificity for a concerted process.⁷ The *ortho*- and *meta*-additions are exemplified in Fig. 11.25. The photocycloaddition of benzene with maleic anhydride gives an *ortho*-adduct as an intermediate which undergoes a Diels–Alder reaction with a second molecule of maleic anhydride to form finally a 1:2 adduct (Fig. 11.25A).^{8,9} The reaction is initiated by excitation of a weak charge-transfer complex between maleic anhydride and benzene and proceeds through a stepwise ionic pathway. The photocycloaddition of cyclopentene with benzene gives a *meta*-adduct (Fig. 11.25B).^{10,11} The reaction also exhibits stereoselectivity in favour of the *endo* isomer (*endo*:*exo* = 88:12). The preferred *endo* addition has been accounted for by secondary orbital interactions.¹²

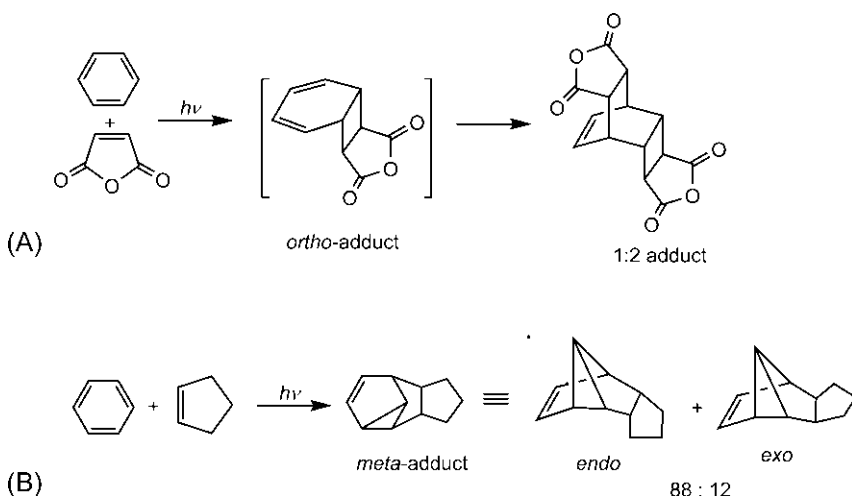


Fig. 11.25 Cycloaddition of alkenes to benzene: (A) *ortho*-addition; (B) *meta*-addition.

11.3.3.3 Correlation Diagram for the $[\pi 2_s + \pi 2_a]$ Cycloaddition of Two Ethylene Molecules

Now we consider the $[\pi 2_s + \pi 2_a]$ cycloaddition of two ethylene molecules involving a crossed transition structure. The orbital correlation diagram is shown in Fig. 11.26. The persisting symmetry element is C_2 (perpendicular to the plane of the paper). The π MOs can be classified as symmetric (**S**) or

antisymmetric (**A**) with respect to C_2 , but for classification of σ MOs, a new set is constructed by the linear combination procedure.

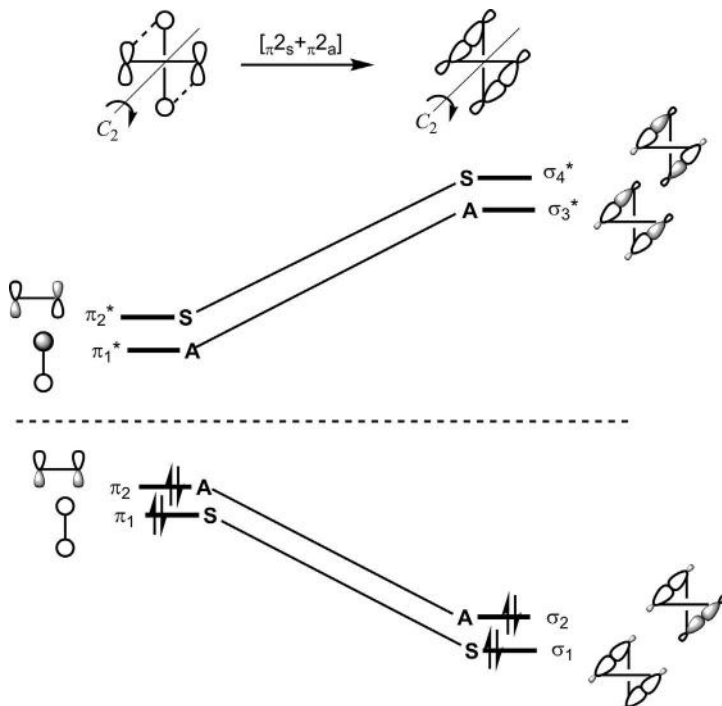


Fig. 11.26 Orbital correlation diagram for the $[\pi_{2s} + \pi_{2a}]$ cycloaddition.

For the thermal reaction, the orbital correlations are

$$\pi_1^2 \pi_2^2 \rightarrow \sigma_1^2 \sigma_2^2$$

Thus, all bonding orbitals of reactants are directly correlated with all bonding orbitals of the product and the $[\pi_{2s} + \pi_{2a}]$ process is symmetry-allowed in the ground state.

11.3.4 Correlation Diagram for the [2+2+2] Cycloadditions

Let us consider the cycloreversion of cyclohexane into three ethylene molecules. Assuming a boat transition structure, the reaction can be described as an all-suprafacial $[\sigma_{2s} + \sigma_{2s} + \sigma_{2s}]$ process (Fig. 11.27). The three σ bonds broken and the three π bonds formed are labelled by the numbers

1, 2, 3. A disrotatory motion is indicated for the breaking σ bond 3 for π interaction in the transition structure. The persisting symmetry element is a mirror plane (m).

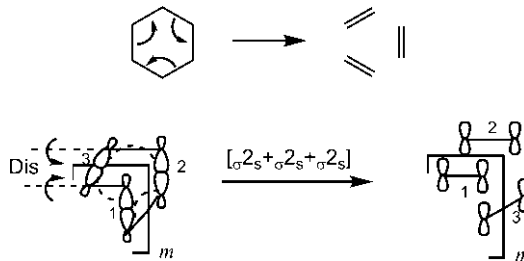


Fig. 11.27 Persisting symmetry plane (m) in the $[\sigma_2 + \sigma_2 + \sigma_2]$ cycloreversion of cyclohexane.

The reactant MOs are σ_1 , σ_1^* , σ_2 , σ_2^* , σ_3 , σ_3^* while the product MOs are π_1 , π_1^* , π_2 , π_2^* , π_3 , π_3^* . Of these, only σ_3 , σ_3^* and π_3 , π_3^* are classifiable as **S** or **A** with respect to m . Therefore, four new σ MOs and four new π MOs are generated by the linear combination method. The symmetry classification of the reactant and product MOs is shown in Fig. 11.28.

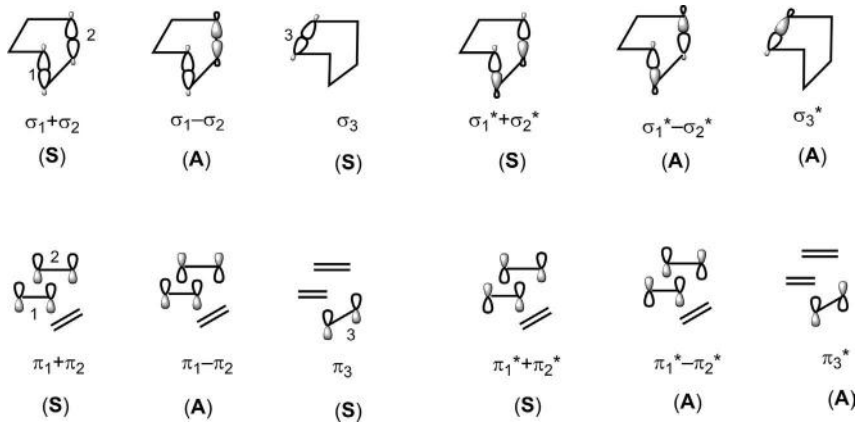


Fig. 11.28 Reactant σ MOs and product π MOs, and their symmetry classification.

The orbital correlation diagram is constructed by linking orbitals of like symmetry obeying the noncrossing rule, and is shown in Fig. 11.29.

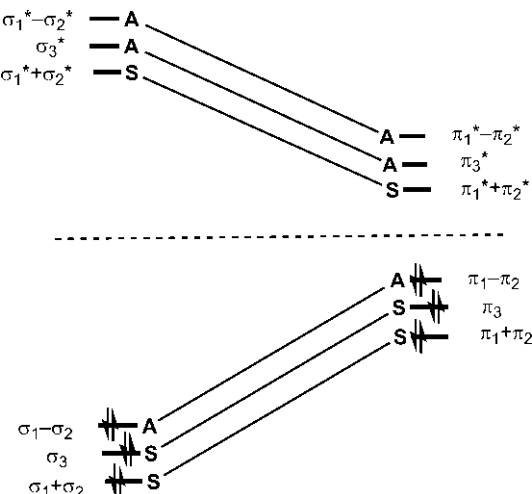


Fig. 11.29 Orbital correlation diagram for the $[\sigma_{2s} + \sigma_{2s} + \sigma_{2s}]$ cycloreversion of cyclohexane.

The orbital correlations indicate that, for a thermal reaction, all bonding molecular orbitals of cyclohexane are correlated with all bonding molecular orbitals of ethylenes. The $[\sigma_{2s} + \sigma_{2s} + \sigma_{2s}]$ cycloreversion of cyclohexane is therefore symmetry-allowed thermally.

11.3.4.1 Correlation Diagram for the Prismane–Benzene Conversion

The conversion of prismane to benzene is also a $[2+2+2]$ cycloreversion when three σ bonds of prismane are broken to form three π bonds of benzene as shown in Fig. 11.30.

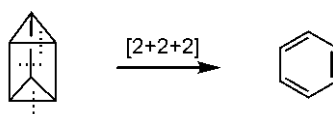


Fig. 11.30 Cycloreversion of prismane to benzene.

Prismane is a three-dimensional molecule with a prism-like structure, whereas benzene is a planar cyclic molecule. Therefore, prismane to benzene transformation requires that the breaking of σ bonds leads to a planar arrangement of six carbons as well as rotation of the breaking σ orbitals to allow overlap for π bond formation, as shown in Fig. 11.31.

The transformation is a $[\sigma_{2s} + \sigma_{2s} + \sigma_{2s}]$ process. (Note that in prismane the 1–4 σ bond lies right below the plane of 2–6 and 3–5 bonds.) To illustrate, the transformation is applied to a prismane molecular orbital **11.1**, which gets transformed into a specific molecular orbital **11.2** of benzene.

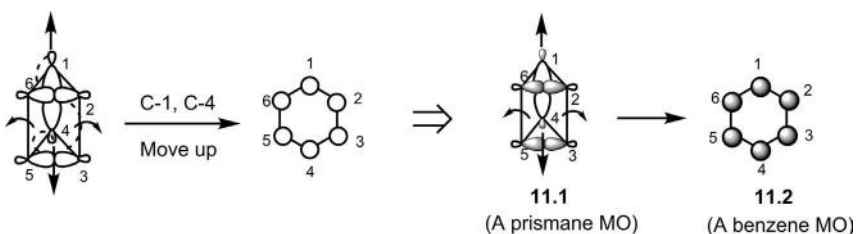


Fig. 11.31 Orbital picture for conversion of three-dimensional prismane to planar benzene and the transformation of a prismane molecular orbital.

Prismane is a highly strained molecule while benzene is aromatic and very stable. Thus, thermodynamics is strongly in favour of the transformation which is exothermic by 91 kcal mol⁻¹. The $[\sigma_{2s} + \sigma_{2s} + \sigma_{2s}]$ transformation is also expected to be symmetry-allowed. However, surprisingly, prismane once formed can exist and is not readily converted to benzene. (Hexamethylprismane is converted to hexamethylbenzene above 60°C via a Dewar benzene or a benzvalene.) It appears that the prismane–benzene conversion is distinct from the general class of symmetry-allowed [2 + 2 + 2] reactions. We shall see below that the prismane–benzene conversion is actually symmetry-forbidden, arising from the symmetry restrictions imposed by the geometry of the prismane molecule. The kinetic stability of prismane thus stems from the symmetry-forbiddenness of the transformation.

[Fig. 11.32](#) shows that there are two persisting symmetry planes (m_1 and m_2) imposed by the geometry of prismane. This is in contrast to the presence of one symmetry plane in the cycloreversion of boat cyclohexane (see [Fig. 11.27](#)). For the purpose of symmetry classification, the three bonding σ MOs (**11.3–11.5**) and three antibonding σ MOs (**11.6–11.8**) are obtained in a similar manner as described for cycloreversion of cyclohexane. The symmetry labels of six σ MOs are given with respect to m_1 and m_2 . The symmetry classification of three bonding π MOs ($\psi_0, \psi_1, \psi_{-1}$) and three anti-bonding π MOs ($\psi_2, \psi_{-2}, \psi_3$) of benzene (see [Fig. 1.31](#), p. 32) is also performed with respect to m_1 and m_2 .

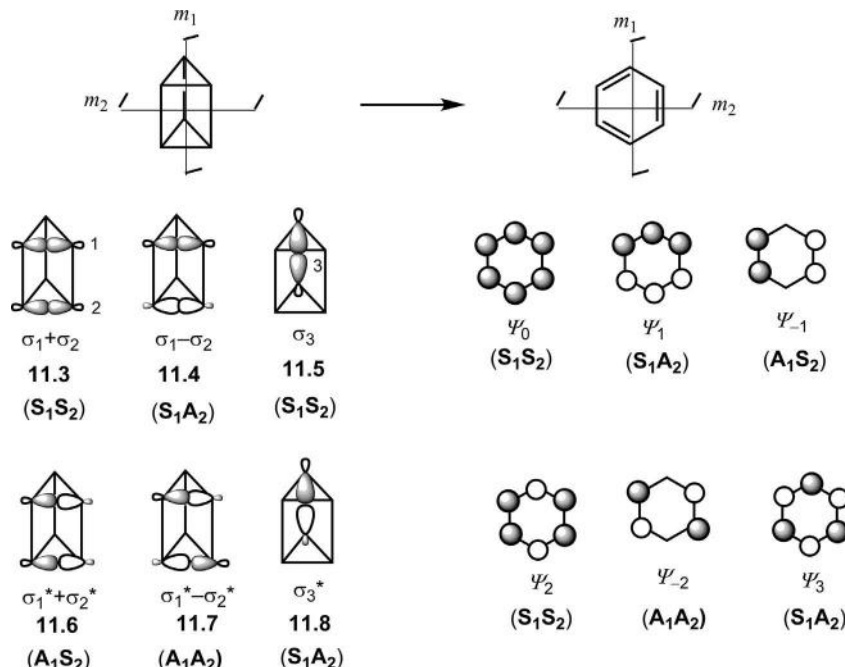


Fig. 11.32 Prismane σ MOs and benzene π MOs and their symmetry classification.

The orbital correlation diagram is constructed by linking orbitals of like symmetry obeying the noncrossing rule, and is shown in Fig. 11.33. For benzene, ψ_1 , ψ_{-1} are degenerate bonding π MOs, and ψ_2 , ψ_{-2} are degenerate antibonding π MOs.

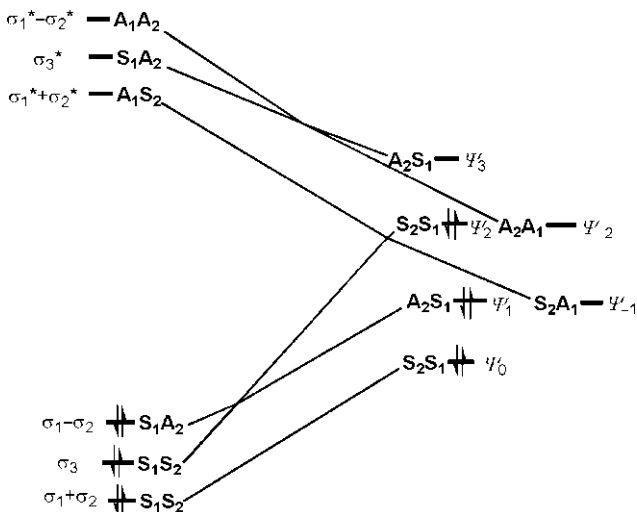
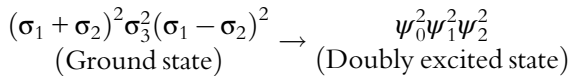


Fig. 11.33 Orbital correlation diagram for the prismane–benzene conversion.

The orbital correlations for the ground state (thermal) reaction are



The correlations indicate that one bonding orbital (σ_3) of prismane is correlated with an antibonding orbital (ψ_2) of benzene, and the prismane ground state correlates with the doubly excited state of benzene. The transformation is therefore symmetry-forbidden.

Physical Correlation

We shall now see how the σ orbitals of prismane are physically transformed into the π orbitals of benzene. As the reaction proceeds, mixing of orbitals of the same symmetry takes place along the reaction coordinate. A combination of $(\sigma_1 + \sigma_2)$ with σ_3 of the same symmetry S_1S_2 gives the two generalized orbitals **11.9** and **11.10** which are transformed, as described in Fig. 11.31, into ψ_2 and ψ_0 , respectively (Fig. 11.34). (Notice that **11.1** = **11.10** and **11.2** = ψ_0 .) The mixing of bonding ($\sigma_1 - \sigma_2$) with antibonding σ_3^* of S_1A_2 symmetry produces the generalized bonding orbital **11.11** and antibonding orbital **11.12** that are transformed into bonding ψ_1 and antibonding ψ_3 , respectively. It is clearly seen that two of the bonding σ orbitals of prismane (**11.10** and **11.11**) are transformed into two bonding orbitals of benzene (ψ_0 and ψ_1), but the third bonding σ orbital **11.9** transforms into an antibonding orbital of benzene (ψ_2) which makes the transformation of prismane to benzene symmetry-forbidden. The transformations of $(\sigma_1 + \sigma_2)$ and $(\sigma_1 - \sigma_2)$ into ψ_{-1} and ψ_{-2} are also shown in Fig. 11.34.

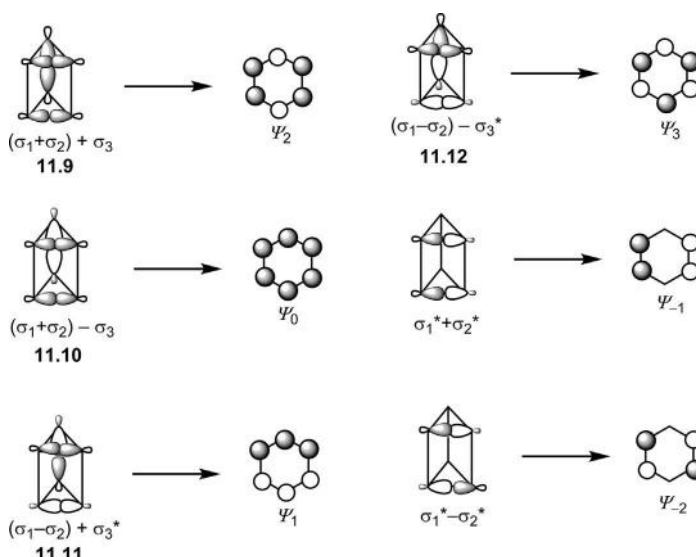


Fig. 11.34 Physical correlation of σ orbitals of prismane with π orbitals of benzene.

11.4 CORRELATION DIAGRAM FOR SIGMATROPIC REARRANGEMENTS

The correlation diagrams are not relevant for analysis of $[1,j]$ and $[i,j]$ ($i \neq j$) sigmatropic rearrangements. This is because no persisting symmetry element is present throughout the transformation; the reactant or the product does not possess a proper symmetry element but the transition structure may possess. For example, in a $[1,5]$ sigmatropic H shift, no nontrivial symmetry element persists throughout the transformation (Fig. 11.35).

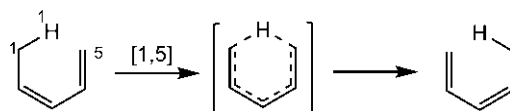


Fig. 11.35 No persisting symmetry element in the $[1,5]$ sigmatropic rearrangement.

The correlation diagram can, however, be constructed for $[i,j]$ ($i=j$) sigmatropic rearrangements such as the $[3,3]$ Cope rearrangement, in which a symmetry element can persist throughout the process. The Cope rearrangement is a $[\pi_2s + \sigma_2s + \pi_2s]$ process and can proceed through a chair or a boat transition structure.

First, we consider the Cope rearrangement via a chair transition structure. The persisting symmetry element is C_2 which bisects the σ bond broken or formed as shown in Fig. 11.36

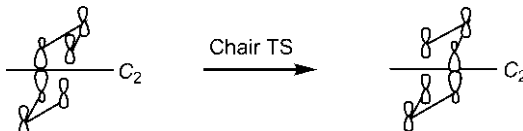


Fig. 11.36 Persisting C_2 symmetry in the Cope rearrangement via a chair transition structure.

It should be noted that the set of molecular orbitals is the same for the reactant and the product. The σ and σ^* orbitals can be classified as **S** or **A** with respect to C_2 . However, to classify π MOs with respect to C_2 , new π MOs are created by the linear combination method. The orbital correlation diagram is shown in Fig. 11.37. In the ground state (thermal) reaction, all reactant bonding MOs are transformed into all product bonding MOs, and the reaction is therefore symmetry-allowed thermally.

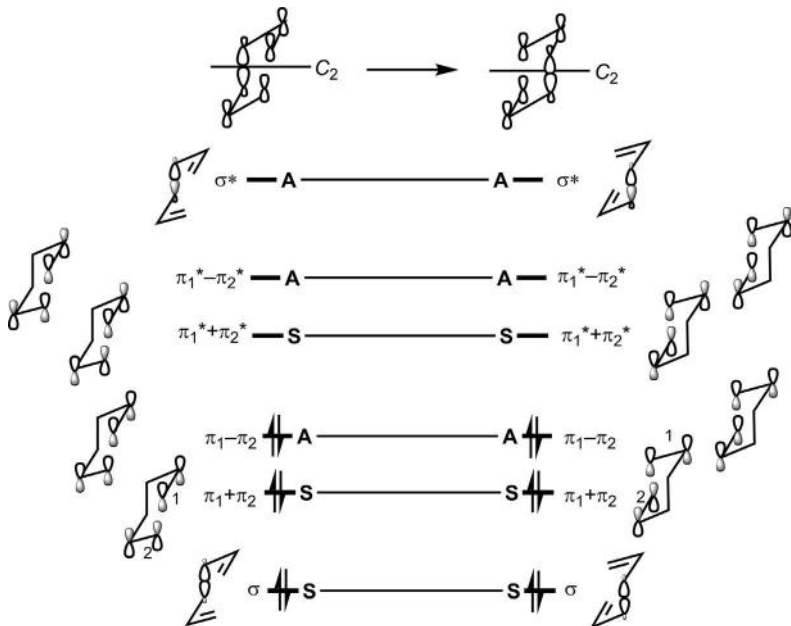


Fig. 11.37 Orbital correlation diagram for the Cope rearrangement via a chair TS.

Next, we consider the Cope rearrangement via a boat transition structure. Here the persisting symmetry element is a mirror plane (m). The orbital correlation diagram is shown in Fig. 11.38. The orbital correlations indicate that the reactant ground state is correlated with the product ground state for a symmetry-allowed thermal reaction.

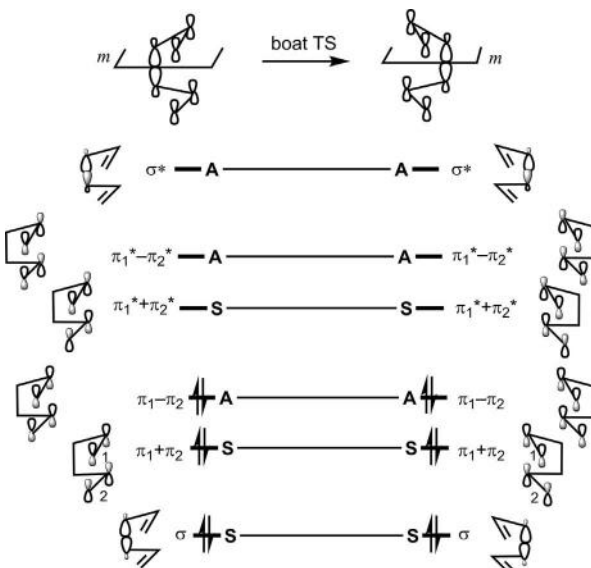


Fig. 11.38 Orbital correlation diagram for the Cope rearrangement via a boat TS.

The correlation diagram for the [3,3] Claisen rearrangement is similar because the presence of oxygen does not fundamentally alter the MO pattern and symmetry.

11.5 CORRELATION DIAGRAM FOR GROUP TRANSFER REACTIONS

The correlation diagram is not relevant for analysis of the ene reaction for the same reason as mentioned for the [1,5] sigmatropic rearrangement (see Fig. 11.35). However, the correlation diagram can be constructed for the double group transfer reaction such as diimide reduction. For the purpose of analysis, we shall consider an all-carbon version in terms of the suprafacial transfer of two hydrogens from ethane to ethylene (Fig. 11.39). The reaction is a $[\sigma_2s + \sigma_2s + \pi_2s]$ process.

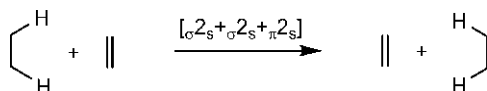


Fig. 11.39 An all-carbon model of the double group transfer reaction.

The persisting symmetry element is a mirror plane (m) bisecting each component. The set of molecular orbitals is the same for the reactants and the products. To classify C—H σ MOs with respect to m , new σ MOs are generated by the linear combination method. The orbital correlation diagram is shown in Fig. 11.40. In the ground state (thermal) reaction, all bonding MOs of reactants are transformed into all bonding MOs of the products, and the reaction is symmetry-allowed thermally.

Problem 11.5

Draw an orbital correlation diagram for a suprafacial transfer of two hydrogens from ethane to butadiene at its termini. Hence, predict whether the reaction is symmetry-allowed or symmetry-forbidden thermally.

Answer

The reaction is a $[\sigma_2s + \sigma_2s + \pi_4s]$ process. The persisting symmetry element is m , bisecting each molecule. The orbital correlation diagram is shown below. (Sketch the orbitals.) For thermal reaction, a reactant bonding orbital (ψ_2) is transformed into an antibonding orbital (π^*) of the product. The reaction is therefore symmetry-forbidden thermally.

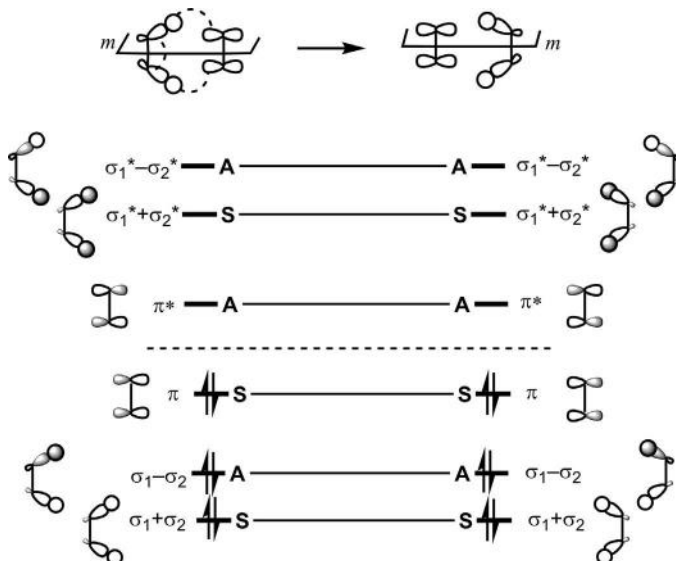
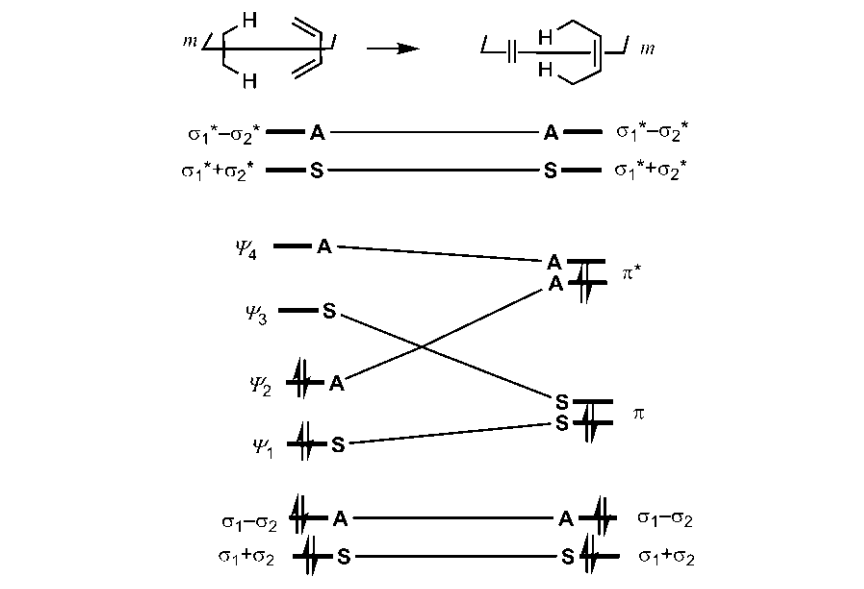


Fig. 11.40 Orbital correlation diagram for the group transfer reaction involving a suprafacial transfer of two hydrogens from ethane to ethylene.



11.6 CONCLUDING REMARKS

In principle, any reaction must conform to the requirements of quantum theory and symmetry restrictions but the explicit analysis is exceedingly complex in general. However, for concerted pericyclic reactions, symmetry considerations can be applied in a straightforward manner and the analysis can be made in a more or less pictorial fashion. Based on the persisting symmetry element(s), the entire reacting system belongs to a symmetry group, and the consequent analysis can be made using group theory when the symmetry designations of orbitals are obtained from the character table for the relevant symmetry group. For the sake of simplicity, the terms relating to the symmetry group/character table are not used here. The correlation diagram provides a profound insight into the mechanism of a pericyclic reaction but it is not for routine use. In view of this, Woodward and Hoffmann formulated ready-to-use generalized rules for pericyclic reactions (see [Section 3.3.1](#), p. 75) based on their results of analyses of a wide range of concerted reactions.

REFERENCES

1. Longuet-Higgins, H. C.; Abrahamson, E. W. *J. Am. Chem. Soc.* **1965**, *87*, 2045.
2. Hoffmann, R.; Woodward, R. B. *J. Am. Chem. Soc.* **1965**, *87*, 2046.
3. Hoffmann, R.; Woodward, R. B. *Acc. Chem. Res.* **1968**, *1*, 17.
4. Woodward, R. B.; Hoffmann, R. *Angew. Chem. Int. Ed. Eng.* **1969**, *8*, 781.
5. Woodward, R. B.; Hoffmann, R. *The Conservation of Orbital Symmetry*; Verlag Chemie/Academic Press: Weinheim/New York, 1971/1970.
6. Bryce-Smith, D.; Gilbert, A.; Mattay, J. *Tetrahedron* **1977**, *33*, 2459. **1986**, *42*, 6011.
7. Bryce-Smith, D.; Foulger, B.; Forrester, J.; Gilbert, A.; Orger, B. H.; Tyrrell, H. M. *J. Chem. Soc., Perkin Trans. 1* **1980**, 55.
8. Angus, H. J. F.; Bryce-Smith, D. *J. Chem. Soc.* **1960**, 4791.
9. Bryce-Smith, D.; Vickery, B.; Fray, G. I. *J. Chem. Soc. C* **1967**, 390.
10. Merritt, V. Y.; Cornelisse, J.; Srinivasan, R. *J. Am. Chem. Soc.* **1973**, *95*, 8250.
11. Osselton, E. M.; van Dijk-Knepper, J. J.; Cornelisse, J. *J. Chem. Soc. Perkin Trans. 2* **1988**, 1021.
12. Houk, K. N. *Pure Appl. Chem.* **1982**, *54*, 1633.

INDEX

Note: Page numbers followed by *f* indicate figures, *t* indicate tables and *b* indicate boxes.

A

- Abnormal product, formation of, 454–455, 454*f*
Absolute stereochemistry
 Mandal's approach, 49–51
 R/S descriptor assignment, 51–54
 α,β -unsaturated carbonyl compound, photocycloaddition of, 243–248
Achiral axis descriptor, 54–55*f*, 56
Acyclic conjugated π system, 7–18
Acyclic diastereomer, 43
Acyclic dienes
 stereospecific reaction, 193, 193*f*
 s-trans conformation, 111
Acyclic triene, 351, 351–352*f*
Acyl migration, in indene, 356, 356*f*
[2+2] Alkene cycloaddition, 79–80
Alkene dipolarophiles, 158–160, 163
Alkene metathesis, 265, 265*f*
Alkyl shifts
 in cyclohexadienone, 356, 356*f*
 in isoindene, 356, 356*f*
Alkyne π system, 25
[2+2] Allene cycloaddition
 regioselectivity, 262*f*
 stereospecificity, 262*f*
Allyl anion cycloaddition, 235–237
 regioselectivity, 236*f*
 stereoselectivity, 236*f*
 stereospecificity, 236*f*
Allyl cation cycloaddition, 231–234
Allyl cation–cyclopropyl cation reaction, 322, 322*f*
Allylic Grignard reagent, 445, 445*f*
Allyl system, 15–17
Allyl vinyl ether, 387, 387*f*
 acid-catalyzed ether exchange, 387, 387*f*
 Tebbe's reagent, 387, 387*f*
 α -chloro enolates, disrotatory ring closing, 330, 330*f*
 α -hydroxy ester, 439, 439*f*
Amarine synthesis, 338*f*
Amine oxide, Cope elimination of, 451–452, 452*f*
Anionic oxy-Cope rearrangement, 372, 372*f*
Antara/antara interaction, 79
Antarafacial migration, 95–97, 351
Antarafacial ω component, 76, 76*f*
Antarafacial π component, 76, 76*f*
Antarafacial σ component, 76, 76*f*
Aromatic Claisen rearrangement
 allyl aryl ether, 404, 405*f*
 ^{14}C -labelled allyl phenyl ether, 405, 405*f*
 ortho, 404, 405*f*
 para, 405, 405*f*
 of phenyl propargyl ether, 406, 406*f*
Arylacetylenes, 150–151
Asymmetric Claisen rearrangement
 box catalyst, 404, 404*f*
 chiral auxiliary strategy, 403, 403*f*
 chiral boron reagent, 403, 404*f*
 substrate control, 401, 401*f*
Asymmetric Diels–Alder reaction
 chiral auxiliaries, 215–219, 215–216*f*
 chiral catalyst, 219–221
 endo stereochemistry, 217*f*
Asymmetric 1,3-dipolar cycloaddition, 229–230, 229–230*f*
 chiral vinyl sulphoxide, 230*f*
Asymmetric ene reactions
 2,2'-binaphthol (BINOL), 447
 box catalyst, 448, 448*f*
 catalyst–enophile complex, 447–448
 chiral Lewis acid catalysts, 447
 mechanism, 448–449, 449*f*
 mechanistic model, 447–448, 448*f*
Asymmetric synthesis, 58–59, 213
Atomic orbital (AO), 2*f*
 nitrogen, 3
 oxygen, 3
 s, p and hybrid orbitals, 1–2
2-Aza-allyl anions, 236
Aza-Claisen rearrangement, 408, 408*f*

- Aza-Cope rearrangement, 374–375, 374*f*
 bicyclic pyrrolidine synthesis via, 379,
 379*f*
- Azepine, 177*f*
 dimerization, 176*f*, 284
 HOMO/LUMO coefficient, 176–177
- Azide–alkyne cycloaddition, 171–172, 171*f*
- Aziridine, 328
 ring opening of, 336, 336*f*
- Azomethine imine cycloaddition, 160–161
- B**
- Basis set, 3
- Basketene synthesis, 240*f*
- Benzene
 cycloaddition of alkenes, 489*f*
 cycloreversion of prismane, 492*f*
 derivatives, 149
meta-addition of ethylene, 487–489, 488*f*
ortho-addition of ethylene, 487–489, 487*f*
 photocycloaddition, 248, 248*f*
 π MOs, energy diagram, 31*f*, 32–33
 schematic diagram, 32*f*
- Benzidine rearrangement, 425, 425*f*
- Benzocyclobutene, 297
 electrocyclic ring opening, 211
 with methyl acrylate, 321, 321*f*
 pyran synthesis, 318–319, 318*f*
 synthesis, 280, 281*f*
- Benzocyclopropene synthesis, 149–150,
 149*f*
- Benzoquinone epoxide synthesis, 149–150,
 149*f*
- β -keto acid
 Carroll rearrangement, 388–390, 388*f*
 decarboxylation of, 450–451, 450*f*
- β -lactam antibiotics, 259
- β -pinene, 435
 stereospecific deuteration of, 453, 453*f*
- 5–3 Bicyclic cyclopropyl tosylates
 solvolysis, 325, 325*f*
 thermal isomerizations, 326, 326*f*
 torqueoselectivity, 325, 326*f*
- Bicyclic decalin system, 46
- Bicyclo[3.2.0]hept-6-en-2-one, thermal
 ring opening of, 301, 301*f*
- 2,2'-Binaphthol (BINOL), 55, 447
- Box catalyst, 404, 404*f*, 448, 448*f*
- Bromocyclooctatetraene, thermal
 conversion of, 310–311, 310–311*f*
- Bullvalene
 Cope rearrangement, 383
 fluxional structures of, 383, 384*f*
 symmetry, 384, 384*f*
 synthesis, 384–385, 384*f*
- Butadiene, 11–13, 12*f*
 Diels–Alder cycloaddition, 111*f*
 dimerization, 248, 248*f*
 disrotatory interconversion, 466–467,
 467*f*
 ring closing of, 65, 65*f*
- C**
- Camphor synthesis, 443, 443*f*
- Capnellene synthesis, 445, 445*f*
- Carbazole synthesis, 354, 354*f*
- [1, *j*] Carbon shifts
 in charged systems (*j*=even)
 [1,2]C shifts, 361–362, 361–362*f*
 [1,4]C shifts, 362–363, 362–363*f*
 in neutral systems (*j*=odd)
 [1,3]C shifts, 357–361, 357–359*f*
 [1,5]C shifts, 355–356, 355–356*f*
- Carbonyl ene reaction
 α -hydroxy ester, 439, 439*f*
(*E*)-2-butene, 440, 440*f*
(*Z*)-2-butene, 440, 440*f*
diastereoselectivity, 439–440, 440*f*
with ethyl glyoxylate, 439, 439*f*
intramolecular, 441, 441*f*
(–)-menthol synthesis, 441, 441*f*
- Carbonyl π system, 18–19
 π MOs, energy diagram, 18*f*
- Carroll rearrangement, 388–390, 388*f*
- Catalyst–enophile complex, 447–448
- Catalytic asymmetric 1,3-dipolar
 cycloaddition, 229*f*
- Catalyzed azide–alkyne cycloaddition, 172*f*
- C–C σ bond, 6–7, 7*f*
- Chair *vs.* boat TS, 101
- C–H bond, 6–7, 7*f*
- Cheletropic cycloadditions
 extrusions of nitrogen and carbon
 monoxide, 280, 281*f*

- linear singlet carbene, 481, 481*f*
 orbital correlation diagram, 480–481,
 480*f*
 persisting symmetry plane, 480, 480*f*
 selection rules, 271, 271*t*
 with singlet carbenes, 271–275, 271*t*,
 271–274*f*
 with sulphur dioxide, 275–280, 276–278*f*
- Cheletropic extrusions
 of carbon monoxide, 280, 281*f*
 of nitrogen, 280, 281*f*
 seven-membered ring sulphones, 277,
 278*f*
- Chiral auxiliaries
 advantage, 219
 asymmetric Diels–Alder reaction, 216*f*
 (R)–(+)- α -terpineol synthesis, 217*f*
 Grignard reaction, 216
 oxazolidinone preparation, 215*f*
- Chiral axis descriptor, 54–55*f*, 55
- Chiral catalyst
 asymmetric Diels–Alder reaction, 220*f*
 shikimic acid synthesis, 220–221, 221*f*
- Chirality transfer, 378, 397–398
- Chiral Lewis acid catalysts, 447
- Chugaev reaction, 449–450, 450*f*
- cis*-5,6-dideuteriocyclohexa-1,3-diene, 457,
 458*f*
- cis* dienophiles, stereospecific reaction, 193*f*
- cis*-9,10-dihydronaphthalene, 456, 456*f*
 intramolecular [4+4] photocycloaddition
 of, 282, 283*f*
- cis*-3,4-dimethylcyclobutene, 293, 294*f*
- Claisen rearrangement, 45, 72–73, 99–100,
 258*f*
 aliphatic, 386, 386*f*
 aromatic, 386, 386*f*
 chirality transfer in, 397, 397*f*
 diastereoselectivity, 393, 393*f*, 398, 398*f*
 with endocyclic substrate, 398, 398*f*
 with exocyclic substrate, 398, 399*f*
 stereoselectivity, 392–400
 stereospecificity, 390–391
 via boat transition structure, 399–400,
 399*f*
 via chair transition structure, 392–398,
 392*f*
- Click chemistry, 171–172
- Conia reaction, 443–444, 443–444*f*
 camphor synthesis, 443, 443*f*
 dihydrocarvone, 443, 443*f*
 stereochemistry, 444–445, 444*f*
 type I intramolecular reaction, 444–445,
 444*f*
 zinc enolate, 444–445, 444*f*
- Conrotatory butatadiene–cyclobutene
 interconversion
 orbital correlation diagram for, 463, 464*f*
 state correlation diagram for, 472, 472*f*
- Cope elimination, amine oxide, 451–452,
 452*f*
- Cope rearrangement, 45, 72–73, 99–100,
 100*f*
 anionic oxy-Cope rearrangement, 378,
 379*f*
 asymmetric, 378, 378*f*
 aza-Cope rearrangement, 379, 379*f*
 chair TS, 376, 376*f*
cis-1,2-divinylcyclopropane, 379–380,
 380*f*
 of (R,R) diene, 376–377, 377*f*
 of (R,R)-3,4-dimethylhexa-1,5-diene,
 376, 376*f*
 equilibrium of, 371, 371*f*
 homotropilidene, 382
 of *meso*-3,4-dimethylhexa-1,5-diene,
 376, 376*f*
 of 3-methyl-3-phenylhepta-1,5-diene,
 377, 377*f*
 orbital correlation diagram, 496, 497*f*
trans-1,2-divinylcyclopropane, 381–382,
 381*f*
 two-component FMO analysis, 100*f*
 via boat transition structure, 379–382,
 380–381*f*
 via chair transition structure, 375–379,
 375*f*
- Corey's synthesis, of caryophyllene, 244
- Correlation diagrams
 for [2+2] cycloadditions, 483–490
 [4+2] Diels–Alder reaction, 474–479,
 474–477*f*
 for electrocyclic reactions, 462–474
 for group transfer reactions, 498–499

- Correlation diagrams (*Continued*)
 orbital, 461–462
 for sigmatropic rearrangements, 496–498
- C-substituent, perturbation, 19–20
- Cubane synthesis, 240*f*
- Cyclic conformation, 45–47
- Cyclic conjugated π system, 30–38
 Hückel system, 30–35
 Möbius system, 36–38
- Cyclic dienes, 201, 231
 stereospecific reaction, 193*f*
- Cyclic hexatrienes
 cycloheptatriene, 308–309
 frontier orbital interaction, 309–310,
 310*f*
 norcaradiene structure, 309–310,
 309–310*f*
 valence tautomerism, 308–309, 309*f*
- Cycloaddition, 69–71
 alenes, 260–262
 allene with acrylonitrile, 262*f*
 8 electrons, 282, 282–283*f*
 with allyl anions, 235–237
 with allyl cations, 231–234
 atom convention, 69, 70*f*
 butadiene, 116
 characteristics, 69*f*
 [2+2] cycloaddition reaction, 237–265
 cyclopentadiene to dichloroketene, 257*f*
 cyclopropanone, 232*f*
 [4+2] Diels–Alder reaction, 191–223
 electron convention, 69, 70*f*
endo selectivity, 228*f*
exo selectivity, 228*f*
 extrusions of nitrogen and carbon
 monoxide, 280, 281*f*
 ionic and radical pathway, 67*f*
 isocyanates, 260–262
 of ketenes, 250–260
 metal alkylidenes, 264–265
 more than 10 electrons, 285–287,
 286–288*f*
 multicomponent, 287–291, 288–290*f*
 1,3-dipolar cycloaddition, 223–230
 with pentadienyl cations, 235
 periselectivity, 176–182
 selection rule, 80, 80*t*
- with singlet carbenes, 271–275, 271*t*,
 271–274*f*
 singlet oxygen and ozone, 182–188
 singlet vinyl carbenes, 263
 with sulphur dioxide, 275–280, 276–278*f*
 10 electrons, 283–285, 283–286*f*
 vinyl cations, 260–262
- [2+2] Cycloaddition, 238*f*
 alkenes, 84–85
 alkenes to benzene, 489, 489*f*
 β -lactam formation, 261*f*
 of metal alkylidene, 264*f*
 orbital correlation diagram
 meta-addition of ethylene to benzene,
 487–489, 488*f*
 ortho-addition of ethylene to benzene,
 487–489, 487*f*
 of two ethylene molecules, 484, 484*f*
 persisting symmetry planes, 483, 483*f*
 photochemical [2+2] cycloaddition,
 237–248
 π and σ MOS analysis, 483, 484*f*
 product π MOs, 491, 491*f*
 reactant σ MOs, 491, 491*f*
 state correlation diagram, 485–486, 486*f*
 stereochemical mode, 79*f*
 thermal [2+2] cycloaddition, 248–265
 of two ethylene molecules, 483–486, 483*f*
- [2+2+2] Cycloaddition
 cyclohexane, cycloreversion, 490–491,
 491*f*
 prismane–benzene conversion, 491*f*,
 492–495, 493–495*f*
- [4+2] Cycloaddition, 231–237
 allyl cation with cyclopentadiene, 231*f*
 with cations and anion, 231*f*
- Cyclobutadiene
 π MOs, energy diagram, 33*f*
 structure, 34–35
- Cyclobutene
 conrotatory ring opening of, 298, 298*f*,
 300–301
 π -energy of Möbius TS, 298, 299*f*
 torquoselectivity, 299–301, 299*f*
- 1,4-Cycloelimination, 104, 104*f*, 457–459
cis-5,6-dideuteriocyclohexa-1,3-diene,
 457, 458*f*

- cycloheptatriene, 458, 458/
dimethyl acetylenedicarboxylate, 458,
458/
syn stereospecificity, 457, 457/
trans-3,6-dideuteriocyclohexa-1,4-diene,
457–458, 457–458/
Cycloheptadiene, 347, 347/
Cycloheptatriene, 458, 458/
carbene cycloaddition, 274–275, 274/
1,4-cycloelimination, 458, 458/
geometry and sudden polarization in
excited state, 312–313, 313/
norcaradiene structure, 308–309, 309/
photochemical ring closing of, 312, 312/
regioselectivity of photocyclization,
312–315, 313–314/
valence tautomerism, 308, 309/
Cyclohexadiene, 347, 347/
Cyclohexadienone, alkyl shifts in, 356, 356/
Cyclohexane
boat conformation, 47/
chair conformation, 45/
cyclic conformation, 45
cycloreversion of, 490–491, 491/
Cyclooctatetraene
basketene synthesis, 240–241, 240/
bullvalene synthesis, 384–385, 384/
photocyclization of, 315, 315/
thermal conversion, 223/
valence tautomerism, 308, 309/
Cyclooctyne, 112, 113/
Cyclopentadiene, 200/
with chlorosulphonyl isocyanate, 260
[4+2] cycloaddition of allyl cation, 231,
231/
Diels–Alder cycloaddition, 111/
dimerization, 201–204, 201/
with tropone, 283, 283/
Cyclopentenyl anion, 337, 338/
Cyclopentenyl cations, 331, 331/
Cyclopropane, 271, 271/
Cyclopropanones
cyclopropyl cation-allyl cation reaction,
328, 329/
disrotatory ring opening, 328, 329/
electrocyclic ring opening, 232, 232/
Cyclopropyl tosylate, 335, 335/
cyclopropyl anions, ring opening, 335,
335/
cyclopropyl cations, ring opening, 322,
324, 325/
nucleophilic attack, 322
solvolytic, 322, 322/
torquoselectivity, 323, 324/
Cycloreversion
cyclohexane, 490–491, 491/
of prismane, 492/
sulphur dioxide, 277
- D**
- Danishefsky diene, 125–127, 127/
Dehydro-Diels–Alder (DDA) reaction,
150–153, 151–152/
Dehydrohalogenation, 162
Deuterium scrambling
in thermal isomerization of
cyclooctatriene, 348, 348/
in thermal rearrangement of indene,
345–346, 346/
Dewar benzene
electrocyclic ring opening, 303, 303/
synthesis, 303–305, 304/
Diastereoselectivity
of carbonyl ene reaction, 440/
of Claisen rearrangement with endocyclic
substrate, 398, 398/
of Ireland–Claisen rearrangement, 396,
397/
of Wittig rearrangement, 414
Diazoalkane cycloaddition, 156–159
Diazomethane, 155/
1,4-Dibromocyclooctatetraene, thermal
transformation of, 312, 312/
Dichlorocarbene, 275
site selectivity, 275
stereospecific addition of, 271, 271/
Dichloroketene, 251
Diels–Alder cycloaddition, 34, 113/
butadiene, 111/
cyclopentadiene, 111/
Danishefsky diene, 125–127, 127/
dehydro-Diels–Alder reaction, 150–153
frontier orbital control and reactivity,
112–122

- Diels–Alder cycloaddition (*Continued*)
 heterocyclic synthesis, 144–150
 hetero Diels–Alder reactions, 134–138
 inverse electron demand, 118–121
 Lewis acid catalysis, 140–144
 normal electron demand, 116–118
 2-pyridone synthesis, 148*f*
 regioisomer formation, 122*f*
 regioselectivity, ‘ortho/para’ orientation, 122–134, 126*f*
 schematic representation, 110*f*
 with singlet oxygen, 183–185, 184*f*
 site selectivity, 138–140, 139*f*
 valence bond, 134*f*
- Diels–Alder (DA) reaction, 58, 63, 63*f*, 191
 curved arrow representation, 64*f*
 diastereoselectivity, 197*f*
 $4n+2$ electron system, 78–79
 electrostatic interaction, 207*f*
endo and *exo* cycloaddition, 194*f*
 ground state correlation, 476–477, 477*f*
 ionic mechanism, 66*f*
 with 5-methylcyclopentadiene, 345, 345*f*
 orbital correlation diagram, 475, 476*f*
 pericyclic mechanism, 66*f*
 persisting symmetry plane, 474, 474*f*
 physical correlation of ethylene π with cyclohexene π , 477–479, 477*f*
 radical mechanism, 66*f*
 schematic representation, 191*f*
 secondary orbital interaction, *endo* addition, 196–197, 196*f*
 σ MOs for, 475, 475*f*
 silyloxy-substituted cycloheptadiene, 347, 347*f*
 stereocentres in, 198–199*f*
 stereochemical feature, 191
 stereoselectivity, Lewis acid, 204*f*
 stereospecificity, 192*f*
 with 5-substituted cyclopentadiene, 345, 345*f*
 tetracyanoethylene, 350
 thermodynamic control, 205–206, 206*f*
 valence isomer trapping of, 311, 311*f*
- [4+2] Diels–Alder reaction, stereochemistry asymmetric, 213–221
 intramolecular, 208–213
- $[\pi 4_a + \pi 2_a]$ Diels–Alder cycloaddition, 223
 photochemical, 221–222
 stereoselectivity, *endo* rule, 194–208
 stereospecificity, *cis* principle, 191–194
- Diels–Alder/retro-Diels–Alder sequence, 145*f*, 149–150
 heterocyclic synthesis, 144–148
- Dienes, 112*f*, 192–204
 photochemical ring closing, 302, 303*f*
 thermal isomerization of, 301–302, 302*f*
 thermal rearrangement of, 344, 344*f*
 thermal ring closing, 302, 303*f*
- Dienophile, 193–204, 214*f*
 Lewis acid complex, 140*f*
- Dihydrocarvone, 443, 443*f*
- Dihydropthalic anhydride, photocycloaddition of, 288–289, 289*f*
- Diimide
cis-9,10-dihydronaphthalene, 456, 456*f*
 dyotropic rearrangement, 456, 456*f*
 generation, 455, 455*f*
 hydrazine oxidation, 455
 potassium azodicarboxylate, didecarboxylation of, 455
 reduction, 455–456, 455–456*f*
syn hydrogenation, 456, 456*f*
- Dimerization
 azepine, 176*f*, 284
 butadiene, 248, 248*f*
 cyclopentadiene, 201–204, 201*f*
 N-carbethoxyazepine, 284, 284*f*
- Dimethyl acetylenedicarboxylate (DMAD), 148–149, 193, 458, 458*f*
- Dimethyldihydropyrene, photochromism of, 306–307, 306*f*
- 5,7-Dimethylenecyclohepta-1,3-diene, cycloaddition of, 285, 285*f*
- Dimethylfulvene, 30*f*, 179–180, 179*f*
- Dimethyl phthalate synthesis, 149*f*
- Dimide reduction, 104
- 1,3-Dipolar cycloaddition (1,3-DC)
endo/exo stereochemistry, 224
 frontier orbital interactions, 157*f*, 162*f*, 186*f*
- HOMO/LUMO energy separation, 157*f*
- Huisgen cycloaddition, 153–154

- osmium tetroxide, 187–188
 ozone and related dipole, 185–188
 pyrrole synthesis, 172–173, 173*f*
 regioselectivity, 155–174
 schematic representation, 224*f*
 stereoselectivity, 227–230
 stereospecificity, 224–227, 226*f*
1,3-Dipole, 65
 Disrotatory butatadiene–cyclobutene interconversion
 orbital correlation diagram for, 466–467, 467*f*
 state correlation diagram, 473–474, 473*f*
 Divinyl ketone, Nazarov cyclization of, 331, 331*f*
 Diyl cycloaddition, 174–175
DMAD. *See* Dimethyl acetylenedicarboxylate (DMAD)
 Dynamic stereochemistry, 41
 Dyotropic rearrangement, 456, 456*f*
- E**
- Electrocyclic isomerization,
 dimethyldihydropyrene, 306–307, 306*f*
 Electrocyclic reactions, 71, 71*f*
 butadiene, ring opening, 91*f*
 in charged systems, 322–339, 325–327*f*, 329–338*f*
 conrotatory, 88
 cyclobutene, ring opening, 90–92, 90*f*
 disrotatory, 88
 8-electron electrocyclic process, 319–320, 321–322*f*
 4-electron electrocyclic process, 297–305, 298–299*f*, 301–305*f*
 4-electron *vs.* 6-electron electrocyclic process, 312–319, 314–320*f*
 hexatriene, ring closing, 88–89, 90*f*
 Mandal's stereochemical rule, 294–297, 295–297*f*
 mixed electrocyclic and cycloaddition reactions, 321, 323–324*f*
 in neutral systems, 293–321
 selection rule, 92, 92*t*
 Woodward–Hoffmann generalized rule, 89*f*
- Electrocyclic ring closing (ERC), 293
 of hexatriene to cyclohexadiene, 305, 305*f*
 of octatetraene to cyclooctatriene, 319, 319*f*
 Electrocyclic ring opening (ERO)
 of cyclobutene, 293, 294*f*
 Dewar benzene, 303, 303*f*
 Mandal's stereochemical rule, 296–297, 296*f*
 Electrostatic repulsion, 207
 Enantioconvergent synthesis, 401–403, 402*f*
 Enders RAMP/SAMP auxiliary, 403
 Endoperoxide, 184
 Ene reactions, 103–104
 with activated enophile, 433, 433*f*
 asymmetric, 447–449
 β -pinene, stereospecific deuteration of, 453, 453*f*
 diimide reduction, 431, 431*f*
 ene/retro-ene sequence, 453–455
 frontier orbital picture, 433, 433*f*
 hetero, 432, 432*f*, 439–446
 HOMO, 433
 intramolecular, 437–438, 437–439*f*
 LUMO, 433
 regioselectivity, 433–435, 434*f*
 retro, 432*f*, 449–453
 stereoselectivity, 435–436, 436*f*
 stereospecificity, 435, 435*f*
 Ene/retro-ene sequence
 abnormal product, formation of, 454–455, 454*f*
 tritium labelled (R)-acetic acid synthesis, 453, 454*f*
 Enolization
 ester, 394, 395*f*
 stereoselectivity, 394–396
 in THF, 396
ERC. *See* Electrocyclic ring closing (ERC)
ERO. *See* Electrocyclic ring opening (ERO)
 Eschenmoser–Claisen rearrangement, 387–388, 387*f*
 enantioconvergent synthesis via, 401–403, 402*f*
 Ethylene, 8–10, 9*f*
 E/Z descriptor, 56, 56*f*

F

- Favorskii rearrangement, 240, 330
 Fischer indole synthesis, 409–411, 410f
 Fischer projection, 52f
 Fluxional molecules, 382–383, 383f
 Frank–Condon principle, 10
 Free energy diagram, of stereoselective reaction, 59f
 Frontier molecular orbital (FMO), 196–197
 defined, 85–86
 photochemical [2+2] cycloaddition, 87f
 photochemical $[\pi_{2_s} + \pi_{2_s}]$ reaction, 87f
 $[\pi_{2_s} + \pi_{2_s}]$ and $[\pi_{2_s} + \pi_{2_a}]$ cycloaddition, 86, 87f
 $[\pi_{4_s} + \pi_{2_s}]$ Diels–Alder reaction, 86f
 Frontier orbital analysis
 of ene reaction, 291b, 291f
 of multicomponent systems, 289–291, 289f
 of Wittig rearrangement, 291b, 291f
 Frontier orbital coefficient pattern, 125f
 Frontier orbital control and reactivity
 alkenes and dienes, 114f
 Diels–Alder reaction, 115f, 116–118
 HOMO/LUMO energy separation, 113, 117f, 121–122
 Frontier orbital energy, 9f, 10, 13f
 allyl system, 15–16
 butadiene, 13f
 dimethylfulvene, 30f
 ethylene, 9f
 hexatriene, 14
 nodal properties, 18f
 orbital symmetry, 13
 substituent effect, 19–28, 24t
 Frontier orbital interaction, 123f
 Diels–Alder reaction, regioselectivity, 131f
 1,3-dipolar cycloaddition, 157f, 162f, 186f
 inverse electron demand Diels–Alder reaction, 127f
 nitrone regioselectivity, 166f
 Salem–Klopman equation, 109f
 Fulvene, 179f
 azulene synthesis, 181f
 interaction energy diagram, 29f
 periselectivity, 178–182, 179f
 π MOs, 29

G

- Grandberg synthesis, tryptamines, 410
 Grignard reaction, 216
 Group transfer reaction, 73–74, 73f
 correlation diagrams, 498–499, 498–499f
 1,4-cycloelimination, 104, 457–459
 diimide reduction, 104, 455–456
 ene reaction, 103–104, 431–455
 selection rule, 104, 104t
 Gymnomitrol synthesis, 235f

H

- Heptafulvene, cycloaddition of
 with dimethyl acetylenedicarboxylate, 285, 286f
 with tetracyanoethylene, 286–287, 287f
 Hetero Diels–Alder reaction, 137f
 heterodienes, 136–138
 heterodienophiles, 135–136
 regioselectivity, 137f
 Heterodienes, 136–138
 Heterodienophiles, 135–136
 Hetero-ene reactions
 carbonyl, 439–441, 439–441f
 Conia reaction, 443–444, 443–444f
 imino, 441–442, 441–442f
 metallo, 445–446, 445–447f
 singlet oxygen, 442–443, 442f
 Hexadehydro-Diels–Alder (HDDA) reaction, 150
 Hexamethylphosphoramide (HMPA), 396
 Hexaphenylbenzene synthesis, 280, 281f
 Hexatriene, 13–14
 interconversion, 352–354, 353f
 ring closing of, 88–89
 Highest occupied molecular orbital (HOMO), 7, 85–86
 LUMO interaction, 89
 1-substituted dienes, 25–27, 26f
 2-substituted dienes, 27–28, 27f
 Homotropilidene, degenerate Cope rearrangement, 382–383, 382f
 Houk’s data, 21, 24
 Hückel molecular orbital (HMO) theory, 82–83
 linear conjugated system with even number of p orbitals, 8–14

- linear conjugated system with odd number of p orbitals, 15–18
- Hückel π system, 36*f*
- Hückel rule, 33–34
- Hückel transition structure (TS), 372–373
- Huisgen cycloaddition, 153–154, 171–172
- Hybrid orbital, 2, 2*f*
- Hydrazine oxidation, 455
- [1, *j*] Hydrogen shifts
- in charged systems (*j*=even), 354–355, 354–355*f*
 - in neutral systems (*j*=odd)
 - [1,3]H shifts, 350–351*f*
 - [1,5]H shifts, 343–348*f*
 - [1,7]H shifts, 351–353*f*
- I**
- Imino-ene reaction
- N-tosyl imine, 441
 - stereoselectivity, 441–442, 442*f*
 - with synthetic use, 441, 441*f*
- Indolizine, cycloaddition of, 285, 286*f*
- Intramolecular carbonyl ene reaction, 441, 441*f*
- Intramolecular cycloaddition, 233*f*
- 2-oxyallyl cations, 233, 233*f*
 - pentadienyl cation, 235*f*
- Intramolecular DDA reaction, 152*f*
- Intramolecular Diels–Alder (IMDA) reaction
- bridged-ring system, 211*f*
 - exo* steroid product, 211*f*
 - regioselectivity, 210*f*
 - stereochemistry, 210*f*
 - type I substrate, 208–209, 209–210*f*
 - type II substrate, 211*f*
- Intramolecular 1,3-dipolar cycloaddition, 168*f*, 229
- unsaturated nitrone, 229*f*
- Intramolecular ene reactions
- Lewis acid-catalysed reaction, 438, 439*f*
 - Oppolzer's classification, 437, 437*f*
 - sigmatropic shift, 437, 437*f*
 - stereochemistry, 438, 438*f*
 - type I reaction, 437
 - type II reaction, 437
- type III reaction, 438, 439*f*
- Intramolecular Mannich reaction, 374–375
- Intramolecular nitrone cycloaddition, 167–168
- Intramolecular photochemical Diels–Alder reaction, 222*f*
- vitamin D₂, 222*f*
- Intramolecular photocycloaddition, 239, 239*f*, 246–248, 246*f*
- Inverse electron demand Diels–Alder (IEDDA) reaction, 118–121, 119*f*, 128*f*, 197
- Inversion stereochemistry, 357–358, 358*f*
- Ireland–Claisen rearrangement, 387–388, 387*f*
- diastereoselectivity of, 396, 397*f*
 - stereospecificity of, 391–392, 391*f*
 - via boat transition structure, 399–401, 400*f*
- Isocyanate cycloaddition, 260–262
- Isoindene, alkyl shifts, 356, 356*f*
- Isoxazole/isoxazoline/isoxazolidine synthesis, 162–163*f*
- intramolecular nitrone cycloaddition, 167–168
 - nitrile oxide cycloaddition, 162–165
 - nitrone cycloaddition, 165–168
- J**
- Jahn–Teller Distortion. *See* Cyclobutadiene
- Johnson–Claisen rearrangement, 387–388, 387*f*
- stereospecificity of, 390, 390*f*
- K**
- Ketene cycloaddition, 251*f*
- mechanistic analysis, 250–251
 - periselectivity, 257–259
 - regioselectivity, 252–255, 252–254*f*
 - stepwise mechanism, 259–260
 - stereoselectivity, 255
 - stereospecificity, 251–252, 252*f*
- Ketenophile, 250
- Keto–enol equilibrium, 350
- Khusimone, 446, 446*f*

L

- Lewis acid
effect of, 204–205
intramolecular reaction, 210
- Lewis acid catalysis, Diels–Alder
cycloaddition, 141*f*
solvent effect, 143–144
- Ligand priority order, 49–51, 50–51*f*
- Linalool synthesis, 423, 424*f*
- Linear combination of atomic orbital (LCAO), 2
- Lithium diisopropylamide (LDA), 233
- Lowest unoccupied molecular orbital (LUMO), 7, 85–86
1-substituted dienes, 25–27, 26*f*
2-substituted dienes, 27–28, 27*f*
- Luciduline synthesis, 168*f*
intramolecular nitrone cycloaddition, 168*f*

M

- Maleic anhydride, 200*f*
- Mandal’s approach, to ligand priority, 49–51, 52*f*
- Mandal’s stereochemical rule
in cheletropic cycloaddition, 296*f*, 297
in cheletropic extrusion, 296*f*, 297
electrocyclic reactions, 294–297,
295–297*f*
in electrocyclic ring opening, 296–297,
296*f*
syn/anti designation, 295–296, 295*f*
- Meisenheimer rearrangement, 423, 424*f*
- (–)-Menthol synthesis, 441, 441*f*
- Metal alkylidenes, 264–265
- Metallo-ene reaction
with allylic Grignard reagent, 445, 445*f*
capnellene synthesis, 445, 445*f*
intramolecular, 445
khusimone, 446, 446*f*
type I, 445, 445*f*
type II, 445–446, 446–447*f*
- Mislow rearrangement
allyl selenoxides, 423, 423*f*
allyl sulphoxide, 421, 421*f*, 423, 423*f*
diastereoselectivity, 423, 423*f*
- Möbius π system, 36–38, 36*f*

MO energy diagram, 37–38, 37–38*f*

Möbius TS, 88–89, 95–96, 98

Molecular orbital (MO)

- atomic orbital, 1–3
bonding and antibonding, 6*f*
carbonyl π system, 18–19
C–H and C–C σ bond, 6–7
cyclic conjugated π system, 30–38
defined, 3
energy diagram, 5–6, 5*f*
fulvene system, 28–30
Hückel molecular orbital theory, 7–18
 π system, 19–28
trimethylenemethane, 28–30

Molecular orbital theory, 74–75.

See also Perturbational molecular orbital (PMO) theory

N

- Nazarov cyclization, 470
- asymmetric synthesis, 332, 332*f*
- divinyl ketone, 331, 331*f*
- regioselectivity, 332–334, 333*f*
- silicon-directed cyclization, 332–334,
332*f*
- N-carbethoxyazepine, thermal
dimerization, 284, 284*f*
- Next-lowest unoccupied molecular orbital (NLUMO), 30
- Nitrile imine cycloaddition, 160
- Nitrile oxide cycloaddition, 162–165, 162*f*,
224*f*
- Nitrogen, atomic orbital, 3
- Nitrene cycloaddition, 165–168, 165*f*
- N-methylmorpholine-N-oxide (NMO), 188
- Noncrossing rule, 462–463
- Norbornene, photodimerization, 241*f*
- Normal electron demand Diels–Alder
reaction, 116–118, 118*f*, 121–122,
126*f*
- N-tosyl imine, 441

O

- Octatetraene
with dimethyl acetylene dicarboxylate,
321, 321*f*
- electrocyclic ring closing, 319, 319*f*

- Oppolzer's classification, 437, 437*f*
- Orbital correlation diagram
butadiene–cyclobutene
interconversion, 463, 464*f*
for conrotatory process, 463–466
conrotatory ring closing of butadiene to cyclobutene, 464–466, 465–466*f*
for Cope rearrangement via chair TS, 496, 497*f*
for disrotatory process, 466–469, 467–468*f*
disrotatory ring closing of butadiene to cyclobutene, 467, 468*f*
electrocyclic conversion of pentadienyl cation to cyclopentenyl cation, 470*f*, 471
for electrocyclic reactions in charged systems, 470–471, 470*f*
FMO analysis, 468–470
noncrossing rule, 463
physical correlation of reactant orbitals with product orbitals, 465–466, 466*f*
in thermal and photochemical reactions, 464–465, 465*f*
- Orbital symmetry, 10
allyl system, 16*f*
butadiene, 13*f*
conservation, 461–462
correlation approach, 74
ethylene, 10*f*
frontier orbitals, 13
1,3,5-hexatriene, 14*f*
- Ortho*–Claisen rearrangement, 404, 405*f*
- Ortho* regioselectivity, 194–195
- Osmium tetroxide (OsO_4), 187–188, 187*f*
- Overman reaction, 409, 409*f*
- Oxazole synthesis, 338–340, 338*f*
- Oxirane, ring opening of, 336, 336*f*
- 2-Oxyallyl cation cycloaddition, 232
cyclopropanone, 232*f*
formation of regiosomeric adducts, 234*f*
- intramolecular cycloaddition, 233, 233*f*
stereospecificity of cycloaddition, 232*f*
- Oxy–Cope rearrangement, 371–372, 371*f*
- Oxygen, atomic orbital, 3
- Ozone (O_3), 185–188
- Ozonide decomposition, by dimethyl sulphide, 187*f*
- Ozonide formation, 185–186*f*
- Ozonolysis, 185, 187
- P**
- Para*–Claisen rearrangement, 405, 405*f*
- Paterno–Büchi reaction, 241, 241–242*f*
- Pentadienyl cation–cyclopentenyl cation reaction, 330, 330*f*
- Perezone–pipitzol conversion, 235*f*
- Periselectivity
carbene cycloaddition, 273–274, 274*f*
fulvene cycloaddition, 178–182, 179*f*
ketene cycloaddition, 257–259
- Perturbation
by *c*-substituent, 19–20
by *x*-substituent, 22–24
by *z*-substituent, 20–22
- Perturbational molecular orbital (PMO) theory, 82–83
- Diels–Alder cycloaddition, 110–153
diyl cycloaddition, 174–175
1,3-dipolar cycloaddition, 153–174
periselectivity, 176–182
Salem–Klopman equation, 107–110
- 2-Phenylallyl anion, 236
- Photochemical [2+2] cycloaddition
alkenes, 237
 α,β -unsaturated carbonyl compound, 243–248
intramolecular photocycloaddition, 239
[$\pi 2_s + \pi 2_s$] cycloaddition, 237
- Photochemical Diels–Alder reaction, 221–222
intramolecular cycloaddition, 221, 222*f*
[$\pi 4_s + \pi 2_a$] and [$\pi 4_a + \pi 2_s$] modes, 221*f*
- Photochemical pericyclic reaction, 75, 83
- Photochemical retro-cycloaddition, 238
- Photochemical ring closing, cycloheptatriene, 312, 312*f*
- Photochromism, dimethyldihydropyrene, 306–307, 306*f*
- Photodimerization
of anthracene, 282, 282*f*
of cyclopentenone, 244*f*

- Photodimerization (*Continued*)
 of norbornene, 241*f*
 of 2-pyridone, 282, 282*f*
 of 2-pyrone, 282, 282*f*
 of tropone, 285–286, 286*f*
- Photosantonin, photoisomerization of, 348–349
- π -energy, of Hückel transition structure (TS), 373–374, 373*f*
- PMO. See Perturbational molecular orbital (PMO) theory
- π molecular orbital, 4*f*, 17–18
 allyl system, 16*f*
 benzene, energy diagram, 31*f*, 32–33
 butadiene, 11*f*
 cyclobutadiene, energy diagram, 33*f*
 1,3,5-hexatriene, 14*f*
 substituted alkenes, HOMO/LUMO energies and coefficients, 19–25
 substituted dienes, HOMO/LUMO energies and coefficients, 25–28
 trimethylenemethane, 29*f*
- p orbital
 end-on approach, 3–4
 orthogonal approach, 4
 side-on approach, 4
- Potassium azodicarboxylate, didecarboxylation of, 455
- Primary kinetic isotope effect, 343, 343*f*, 351, 351*f*
- Prismane–benzene conversion, 491*f*, 492–495, 493–495*f*
- Pyran synthesis, 318–319, 318*f*
- Pyrazolidine synthesis
 azomethine imine cycloaddition, 160
- Pyridine synthesis, 148–149, 151*f*
- Pyrolysis
 of ester, 449–450, 450*f*
 of xanthates, 449–450, 450*f*
- Pyrrole synthesis, 173*f*
 1,3-dipolar cycloaddition, 172–173
- hetero Diels–Alder reaction, 134–138
 isoxazole/isoxazoline/isoxazolidine synthesis, 162–168
- nitrile imine cycloaddition, 160*f*
- 1,3-dipolar cycloaddition, 155–174
- ‘ortho/para’ orientation, 122–134
- pyrazoline synthesis, 156–161, 158*f*
- regioisomer formation, 122*f*
- tetramethylenemethane cycloaddition, 175*f*
- 1,2,3-triazole/triazoline synthesis, 169–172
- Relative stereochemistry
 and descriptor, 42–44
 in reaction, 47–49
- Retention stereochemistry, 357–358, 358*f*
- Retro-Claisen rearrangement, 258–259, 258*f*
- Retro-cycloaddition, 80–82, 205–207, 265*f*
- Retro-Diels–Alder reaction, 80, 81*f*, 144–145
- Retro-ene reactions, 74
- α,β -unsaturated ketone synthesis via selenoxide elimination, 452–453, 452*f*
- amine oxide, Cope elimination of, 451–452, 452*f*
- β -keto acid, decarboxylation of, 450–451, 450*f*
- β -pinene, stereospecific deuteration of, 453, 453*f*
- 1,2-dipolar, 451–453, 452*f*
- pyrolysis
 of ester, 449–450, 450*f*
 of xanthates, 449–450, 450*f*
- ring strain effects, 451, 451*f*
- sulphoxide, 1,2-cycloelimination of, 451–452, 452*f*
- Retro group transfer reaction, 74*f*
- Retro-Mislow rearrangement, 421, 421*f*
- Ring strain effects, 451, 451*f*
- R/S descriptor, 51–54, 53*f*

R

- Regioselectivity, 135*f*
 azomethine imine cycloaddition, 161*f*
 ene reactions, 433–435, 434*f*
 frontier orbital interaction, 123*f*

S

- Salem–Klopman equation, 6
 antibonding effect, 108
 Coulombic repulsion, 108

- cycloaddition applications, 108–110
 defined, 107
 frontier orbital interaction, 109*f*
 Sawhorse representation, 43*f*
 Sedridine, 228*f*
 SeO_2 oxidation, 443
 Sigmatropic rearrangement, 71–73, 71*f*
 [1, *j*] carbon shifts, 96–98, 99*t*
 in charged systems (*j*=even), 361–363
 in neutral systems (*j*=odd), 355–361
 Claisen rearrangement, 386–408,
 386–388*f*
 aromatic, 404–408, 405–406*f*
 asymmetric, 401–404, 401–404*f*
 aza-Claisen, 408, 408*f*
 Fischer indole synthesis, 409–411, 410*f*
 Overman reaction, 409, 409*f*
 stereoselectivity, 392–400, 392–395*f*,
 397–400
 stereospecificity, 390–391, 391*f*
 Thia-Claisen, 408, 409*f*
 Cope rearrangement
 by antara/antara mode, 385, 386*f*
 via boat transition structure, 379–382,
 380–381*f*
 via chair transition structure, 375–379,
 375–379*f*
 correlation diagrams, 496–498, 496–497*f*
 degenerate Cope systems and fluxional
 molecules, 382–385, 382–384*f*
 higher order $[I, J]$ rearrangements,
 424–426, 424–426*f*
 [1, *j*] hydrogen shifts, 93–96, 96*t*
 in charged systems (*j*=even), 354–355
 in neutral systems (*j*=odd), 343–354
 Mislow rearrangement, 421–423,
 421–424*f*
 Sommelet–Hauser rearrangement,
 419–420, 419–420*f*
 Stevens rearrangement, 416–419,
 416–417*f*, 419*f*
 walk rearrangements, 363–368
 Wittig rearrangement, 412–416,
 412–415*f*
 Sigmatropic shift, 425, 425*f*, 437, 437*f*
 benzidine rearrangement, 425, 425*f*
 in cation, 425–427, 426*f*
 in nitrogen ylide, 425–427, 426*f*
- Singlet carbenes
 cheletropic reactions, 271–275, 271*t*,
 271–274*f*
 cycloheptatriene, cycloaddition with,
 274–275, 274*f*
 dichlorocarbene, stereospecific addition
 of, 271, 271*f*
 frontier orbital interactions, 272–273,
 272*f*
 HOMO, 271–272, 274–275
 LUMO, 271–272, 274–275
 nonlinear pathway, 272, 273*f*
 orbital picture, 269, 270*f*
 periselectivity and site selectivity,
 273–275, 274*f*
 three-component analysis, 272–273,
 273*f*
- Singlet oxygen cycloaddition, 183*f*
cis-1,4-diol formation, 185*f*
 Diels–Alder reaction, 183–185, 184*f*
 Singlet oxygen ene reaction, 442–443, 442*f*
 Singlet vinyl carbenes, 263, 263*f*
 $[\pi_{2a} + \pi_{2s}]$ cycloaddition, 263*f*
 Singly occupied molecular orbital (SOMO),
 16–17
- Site selectivity
 carbene cycloaddition, 274–275, 274*f*
 diazoalkane cycloaddition, 158*f*
 Diels–Alder cycloaddition, 138–140, 139*f*
 frontier orbital theory, 139–140
 Smirnov–Zamkow reaction, 261
 Solvent effect, 143–144
 Solvolysis
 5–3 bicyclic cyclopropyl tosylates, 325,
 325*f*
 of cyclopropyl tosylate, 322, 322–323*f*
 Solvolytic Cope rearrangement, tricyclic
 tosylate, 373–374, 374*f*
 Sommelet–Hauser rearrangement
 desilylation, 419
 nitrogen ylide, 419, 419–420*f*
 SOMO/SOMO interaction, 94*f*
 State correlation diagram
 for conrotatory butadiene–cyclobutene
 interconversion, 471–472, 472*f*
 [2+2] cycloadditions, 485–486, 486*f*
 for disrotatory butadiene–cyclobutene
 interconversion, 473–474, 473*f*

- Static stereochemistry, 41
 Staudinger reaction, 258–260*f*, 260
Stereocentre. *See also* Stereogenic centre
 absolute stereochemistry, 49
 configuration, 41–42, 42*f*
 Stereochemical idiosyncrasies, 66–67
Stereochemistry
 β-lactam, 260*f*
 [2+2] cycloaddition reaction, 237–265
 cyclobutadiene iron tricarbonyl via a
 photochemical electrocyclic
 reaction, 304*f*
 delineation, 199–200*f*, 218*f*
 Dewar benzene
 electrocyclic ring opening, 303, 303*f*
 synthesis, 303–305, 304*f*
 diastereotopic face, 56–57
 [4+2] Diels–Alder reaction, 191–223
 dienes
 photochemical ring closing, 302,
 303*f*
 thermal isomerization of, 301–302,
 302*f*
 thermal ring closing, 302, 303*f*
 1,3-dipolar cycloaddition, 223–230
 enantiotopic face, 56–57
exo adduct of reaction, 199*f*
 4-electron electrocyclic process, 300–301
 (*E,E*)-2,4-hexadiene, photochemical ring
 closing of, 302, 302*f*
 6-electron electrocyclic process, 305, 306*f*
 stereoaxis (*see* Stereogenic axis)
 stereogenic centre, 41–54
 stereoselective reaction, 58–60
 stereospecific reaction, 58–60
Stereogenic axis
 achiral axis descriptor, 56
 chiral axis descriptor, 55
Stereogenic centre
 absolute stereochemistry and descriptor,
 49–54
 cyclic conformation, 45–47
 relative stereochemistry, 42–44, 47–49
 stereocentre configuration, 41–42
 Stereoselective Diels–Alder reaction, 59*f*
 Stereoselective ketene cycloaddition, 256*f*
 Stereoselective reaction, 58–60
 Stereoselectivity, 60*t*
 Claisen rearrangement, 392–400
 diene and dienophile, 194–204
 ene reactions, 435–436, 436*f*
 in enolate formation, 394, 394*f*
 force, roles, 207–208
 free energy diagram, 59–60
 imino-ene reaction, 441–442, 442*f*
 ketene cycloaddition, 255–257
 Lewis acids, effect of, 204–205
 1,3-dipolar cycloaddition
 asymmetric cycloaddition, 229–230
 intramolecular cycloaddition, 229
 thermodynamic control, 205–206
 Stereospecific Diels–Alder reaction, 58*f*
Stereospecificity
cis principle, 191
 dienes, 192–193
 dienophile, 193–194
 ene reactions, 435, 435*f*
 of Ireland–Claisen rearrangement,
 391–392, 391*f*
 of Johnson–Claisen rearrangement, 390,
 390*f*
 ketene cycloaddition, 251–252, 252*f*
 1,3-dipolar cycloaddition, 224–227,
 226*f*
 photochemical [2+2] retro-
 cycloaddition, 239*f*
 Stereospecific reaction, 58–60
 Stevens rearrangement, of suphfur ylide,
 416, 416*f*
 γ-cyclocitral, 417, 417*f*
 stereochemistry, 417–418, 417*f*
 10-membered ring, synthesis of, 417,
 417*f*
 Sulphoxide, 1,2-cycloelimination of,
 451–452, 452*f*
 Sulphur dioxide (SO₂)
 cycloreversion, 277
 with diene, 276, 276*f*
 five-membered ring sulphones,
 photochemical extrusions of, 277,
 277*f*
 (2E,4E)-hexadiene, 275–276, 276*f*
 linear/dis pathway, 276, 276*f*
 orbital picture, 269, 270*f*

- seven-membered ring sulphones, thermal cheletropic extrusions of, 277, 278*f*
stereospecificity of cheletropic cycloadditions, 276, 277*f*
three-membered ring sulphones, thermal extrusions of, 278, 278*f*
- Suprafacial ω component, 76, 76*f*
Suprafacial π component, 76, 76*f*
Suprafacial σ component, 76, 76*f*
Supra/inversion pathway, 362, 362*f*
Supra/retention pathway, 361, 361*f*
Supra/supra mechanism, 195
syn hydrogenation, 456, 456*f*
- T**
- Tetrahydro-Diels–Alder (TDDA) reaction, 150
- Tetramethylenecyclooctane, cycloaddition of, 288, 288*f*
- Tetramethylenemethane (TMM), 174, 175*f*
- Thermal [2+2] cycloaddition
isocyanates, vinyl cations and allenes, 260–262
ketene cycloaddition, 250–260
singlet vinyl carbenes, 263
- Thermal decarboxylation, 240
- Thermal pericyclic reaction, 75, 83
- Thermal transformation
bromocyclooctatetraene, 310–311, 310–311*f*
of *cis* 4–8 bicyclic system into *trans* 6–6 bicyclic system, 316–317, 317*f*
deuterium labelled *cis* 4–6 bicyclic system, 317–318, 318*f*
of four-membered ring into six-membered ring, 315, 316*f*
- Thia–Claisen rearrangement, 408, 409*f*
- TMM. *See* Tetramethylenemethane (TMM)
- Toluene, nonaromatic isomer of, 350, 350*f*
- Torquoselectivity
7–3 bicyclic bromides, 326, 327*f*
5–3 bicyclic cyclopropyl tosylates, 325, 326*f*
- cyclopropyl tosylate, 323, 324*f*
4-electron electrocyclic process, 299–301
- trans*-3,6-dideuteriocyclohexa-1,4-diene, 457, 457*f*
- trans*-9,10-dihydronaphthalene, 307–308, 307*f*
- trans*-3,4-dimethylcyclobutene, 293, 294*f*
- trans*-1,2 disubstituted cyclohexane, 45*f*
- Transition metal alkylidene, 264
- Transition structure aromaticity approach, 99*f*
- Triazines, 146
- 1,2,3-Triazole/triazoline synthesis, 169–172
- Tricyclic tosylate, solvolytic Cope rearrangement, 373–374, 374*f*
- Triplet state photocycloaddition, 243*f*
- Tritium labelled (R)-acetic acid synthesis, 453, 454*f*
- Tryptamines, Grandberg synthesis of, 410
- Two-chair bicyclic transition structure, 46*f*
- Type I intramolecular reaction, 444–445, 444*f*
- V**
- Vinyl cation cycloaddition, 260–262, 261*f*
FMO interaction, 261*f*
- Vinylcyclopropane rearrangement, 358–359, 358–359*f*
- Vitamin D series, electrocyclic reactions in, 315, 316*f*
- Vitamin D₂ synthesis, 352, 352*f*
- W**
- Wagner–Meerwein rearrangement, 361–362, 362*f*
- Walk rearrangement
of achiral 5–3 bicyclic cation, 364, 365*f*
of bicyclo[6.1.0]nonatrienyl system, 364–365, 365*f*
of bicyclo[2.1.0]pentenyl system, 363–364, 364*f*
in norcaradiene system, 365–366, 366*f*
supra/inversion pathways, 366–368, 366*f*
supra/retention pathways, 366–368, 366*f*
- Wittig rearrangement, 72–73, 102
allyl ether, carbanion of, 412
anion-stabilizing group, 412

Wittig rearrangement (*Continued*)

asymmetric, 414*f*
aza-Wittig rearrangement, 414–416, 415*f*
diastereoselectivity, 413–414, 413*f*
for (*E*) double bond, 412, 413*f*
envelope transition structure, 412, 412*f*
homoallylic alcohol, 412, 412*f*
with (*Z*)-substrate, 413–414, 414*f*

Woodward–Hoffmann generalized rule,
75–76, 95*f*, 107, 270–272
[2+2] alkene cycloaddition, 79–80
cycloaddition reaction, 76–88
Diels–Alder reaction, 78–79
electrocyclic reaction, 88–92
group transfer reaction, 103–104
retro-cycloaddition reaction, 80–82
sigmatropic rearrangement, 93–102
suprafacial/inversion pathway, 98*f*

X

X_{ab}
con/dis motion, 271
dis motion, 271
linear process, 269–270, 270*f*
nonlinear process, 269–270, 270*f*
orbital picture, 269, 270*f*
 π system, 271
Woodward–Hoffmann generalized rules,
270

Xanthates, pyrolysis, 449–450, 450*f*
X-substituent, perturbation, 22–24

Z

Zinc enolate, 444–445, 444*f*
Z-substituent, perturbation, 20–22

Pericyclic Chemistry

Orbital Mechanisms and Stereochemistry

Dipak K. Mandal

Formerly of Presidency College/University, Kolkata, India

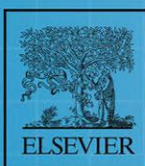
Pericyclic Chemistry: Orbital Mechanisms and Stereochemistry is a complete guide to the topic, ideal for graduate and advanced undergraduate students as well as researchers in organic chemistry. An introduction to molecular orbital theory and relevant stereochemical concepts are provided as background to the following chapters on pericyclic chemistry. The qualitative perturbation molecular orbital theory is incorporated as the most accessible and useful approach to understanding many aspects of reactivity and selectivity. Included are chapters on cycloadditions, the most versatile class, as well as electrocyclic reactions, sigmatropic rearrangements and group transfer reactions. A separate chapter on the construction of correlation diagrams is also included, emphasizing a practical, hands on approach. The four classes of pericyclic reactions are discussed and illustrated with unifying mechanistic approaches, stereochemical features and synthetic applications. Author Dipak Kumar Mandal brings over 20 years of teaching experience to the topic and illuminates pericyclic chemistry with a clear and fresh perspective.

Key Features

- Comprehensive guide featuring unifying mechanistic approaches, stereochemical details including asymmetric versions, and novel rules and mnemonics to delineate product stereochemistry
- Includes two background chapters on molecular orbitals and stereochemical concepts
- Emphasizes a theoretical understanding using perturbation theory (Salem-Klopman equation) and physical insights from orbital and state correlation analyses
- Provides problems with detailed worked solutions within the chapters, reinforcing principal themes in the text.

About the Author

Dipak K. Mandal is a former professor of chemistry at Presidency University, Kolkata, India. He completed his PhD thesis under the supervision of Professor N. K. Sinha at the Bose Institute, Kolkata and carried out postdoctoral work in the USA from 1990-1993 with Professor C. Fred Brewer at Albert Einstein College of Medicine, New York. He has been passionately involved in teaching undergraduate and graduate level organic chemistry for about 35 years, and his keen interest in chemical education resulted in three publications in the Journal of Chemical Education. His research interests include protein folding, structure and dynamics, and peptide synthesis.



elsevier.com/books-and-journals

ISBN 978-0-12-814958-4

9 780128 149584